DEPARTMENT OF CIVIL AND ENVIRONMENTAL ENGINEERING

UNIVERSITY COLLEGE LONDON

AN EXPERIMENTAL INVESTIGATION OF THE STATIC AND DYNAMIC BEHAVIOUR OF MASONRY ASSEMBLAGES USING SMALL SCALE MODELS

by

Spiros Alexandropoulos

A thesis submitted to the University of London

for the degree of Doctor of Philosophy

June 1996

To my parents

Abstract

The last 10 years has seen a renewed interest in the behaviour of unreinforced masonry panels under earthquake loading. Research on full scale structures requires massive, expensive test equipment, is time consuming and costly in manpower. Full scale testing therefore, has been limited to specific, very narrow investigations. Modelling at a reduced scale offers immense savings with wider possible fields of study. The first stage of the author's work was aimed therefore at developing prototype materials for 1:4 scale models, and establishing their fundamental mechanical properties. A complete description of the material properties should provide all the parameters for numerical and analytical predictions and for static and dynamic testing of prototype replicas at the small scale. The parameters investigated in the static testing phase included compressive, tensile and shear strength, Young's modulus and Poisson's ratio, shear modulus and brick-mortar interface bond among others. The second stage involved the development of a shaking table and the investigation of six low-aspect, confined, infill panels subjected to sinusoidal cyclic loading. The study investigated their dynamic behaviour and energy dissipation capacity with progressive damage. Parametric studies were conducted with respect to the brick, mortar and masonry strength. The damage was photographically documented and the cracking propagation is detailed from the initial stages up to collapse. Classic full scale cracking patterns and failure modes were observed which gave the author considerable confidence in the model results. Shear-ductile failures were recorded for panels confined by low axial compressive forces which seems in part to contradict some current opinion, but reference is also given to similar findings published recently in scientific journals. The final component of the work was concerned with a numerical assessment using a commercially available finite element program incorporating a non-linear concrete constitutive material model. This numerical model was fine-tuned by using the previously obtained experimental data to simulate cracking patterns of small masonry specimens under static load.

Acknowledgements

I would like to take this opportunity to express my sincere gratitude to my supervisor Dr. Richard H. Bassett, for his support, guidance and encouragement throughout this work.

Thanks are also due to Messrs. M. Saytch, O. Bourne, J. Ford and L. Wade for the excellent and often miniature work they were called upon to produce. The shaking table set-up was manufactured, assembled and operated by Mr. M. Hayes whose involvement and dedication is greatly acknowledged.

The PFA used in this study, was kindly donated by POWERGEN at the Kingsworth Power Station and the co-operation of Mr. S. Bowler is appreciated.

Thanks also to Mr. Alan Hoy from EQE International Ltd., who generously supplied several field reconnaissance reports from recent destructive earthquakes.

I would also like to extend my appreciation to the staff and in particular Mr. M. Chrimes at the library of the Institution of Civil Engineers who went to great lengths to satisfy numerous requests for technical literature.

Finally I am indebted to Kalli whose patience, support and optimism (not forgetting the sandwiches), sustained me for the course of this study.

Table of contents

Page

List of Figures

List of Tables

List of Photos

Notation

f_{bc}	brick compressive strength
f_{mc}	mortar compressive strength
f_{Mc}	masonry compressive strength
f_{bt}	brick tensile strength
f_{mt}	mortar tensile strength
f_{Mt}	masonry in-plane diagonal tensile (shear) compressive strength
E_b	brick modulus of elasticity
ν_b	brick Poisson's ratio
E_m	mortar modulus of elasticity
ν_m	mortar Poisson's ratio
E_M	masonry modulus of elasticity
ν_M	masonry Poisson's ratio
G_M	masonry shear modulus
γ	shear strain
A	cross-sectional area
l	length of wall
h	height of wall
t	thickness of wall
I	second moment of area
K	uncracked lateral stiffness
V	lateral (shear) force
f_n	natural frequency of vibration
T_n	natural period of vibration
ζ	equivalent viscous damping factor
g	acceleration of gravity
S_l	length scale factor
S_σ	stress scale factor
ρ	mass density

τ shear strength (interface bond test)

τ_o shear strength at zero precompression (interface bond test)

σ_n precompression normal to the bed joint

μ coefficient of friction for unit/mortar interface

r regression analysis correletion coefficient

Chapter 1

Introduction

1.1 Problem definition.

The vulnerability of unreinforced masonry elements to seismic induced damage has been documented extensively in field investigation reports. This is usually attributed to the lack of any agreed seismic resistant design procedures. Furthermore, neither experimental nor analytical research on masonry are widespread in industry or academia compared to steel and reinforced concrete. Consequently its use is limited to simple applications such as infilling frames to form internal or external partitions. In a few places like South America and the Mediterranean region, unreinforced masonry is occasionally partly considered in seismic codes but is still principally used for infilling reinforced concrete frames of skeletal residential and commercial buildings without any design specifications apart from the quality of the mortar and the compressive strength of the units. This lack of full consideration has resulted in catastrophic earthquake induced failures. The cause is often attributed to the presence and plan configuration of infill walls which in reality modify the stiffness and dynamic properties of the structure. A shift in opinion is currently taking place, with attempts being made to incorporate the masonry into code provisions as elements which require special considerations with regard to design, detailing and its anchorage to the surrounding frame. For example in-plane confinement and out-of-plane stability is prescribed for certain height panels in the new Italian and Peruvian Seismic Codes; revised storey drift limitations are imposed by Mexican and Greek Codes. However, due to the lack of consistent experimental data, most code procedures simply recommend reduction factors for the ultimate in-plane shear strength in an effort to account for and prevent brittle post-cracking behaviour which has at least been repeatedly observed as the most dangerous response

in past earthquakes. In this respect masonry can be safely used as a non-structural element in seismic prone regions but actually assessing its real contribution to the energy dissipation capacity of a properly designed and detailed structure remains controversial. With the European Community, Japan and the United States involved in major research programs, this perception is set to change since a number of recently published experimental investigations concluded that unreinforced masonry infill panels can be ductile, and have a long life after initial cracking even in cases where shear dominated failures prevail, provided certain design rules are followed.

The behaviour of masonry structures subjected to seismic loads is very difficult to analyse and predict since no comprehensive theoretical or analytical models exist. Research developments were held back in the past due to the complexity in accessing the composite behaviour, based on the properties of the constituent materials, namely brick or block units, mortar and reinforcement when applicable. Analytical modelling has also been limited due to lack of consistent experimental data. Tests on full scale structures are not usually economically feasible with just a handful of research laboratories around the world having adequate funds and facilities to conduct such tests. Small scale models offer an indisputable alternative and have been successfully used on a number of occasions for modelling concrete and steel assemblages and to a much lesser extent masonry systems.

This study was concerned in the first instance with producing a 1:4 scale moulded brick unit, using easily available materials and establishing its suitability for use in static and dynamic tests. During the planning stage it was decided that to successfully implement a model study, the time and economic costs involved should be minimal throughout, from unit mass production to model fabrication and to the eventual testing stages.

The experimental investigation carried out was planned as a reference (pilot) study and was not related to any particular full scale structural assemblage. Nevertheless the behaviour and response of a model can be correlated to larger similar structures, by using similarity conditions. Correct similarity conditions result in the

deformation characteristics and cracking patterns being representative of both and under these circumstances model data can be relied on to indicate and even to predict prototype behaviour. Correct application of similarity conditions was the author's aim, as the success of the tested 1:4 scale models would enable further research to extend their general applicability to more complex modelling investigations of masonry structures.

1.2 Research objectives.

General objectives

- To: - develop bricks and mortar whose properties and physical qualities will enable them to be incorporated in 1:4 scale physical models of masonry structural assemblages.
- To: - provide an understanding of all the aspects relating to the applicability of small scale modelling techniques for masonry systems.
- To: - develop a simple, robust one-directional shaking table for the 1:4 model masonry assemblages.
- To: - observe and record the elastic and inelastic response of model masonry panels subjected to static and dynamic loads.
- To: - evaluate the possibility of using analytical methods to simulate masonry cracking, failure modes and ultimate strength.

Scope

- By using trial and error procedures develop appropriate mixes based on the design parameters for bricks and mortar, as dictated by similarity conditions when applied to static (strength and stiffness) and to dynamic loading (unit density) of masonry structures. Mass-produce moulded bricks from the appropriate mixes.
- Perform parametric studies on the constituent materials and masonry assemblages to establish their fundamental mechanical properties.
- Perform shaking table tests on low-aspect, (shear) infill walls, using the various types of bricks developed.

- Measure their dynamic properties and response with particular attention to the post-cracking stages and photographically record the progressive cracking and collapse.

1.3 Outline of the thesis.

Since this research study is entirely based on reduced scale physical models a general description of the *similarity conditions* derived from the theory of *dimensional analysis* is given in chapter 2. This includes scale factors for static and dynamic modelling of masonry systems as well as a brief summary of the parameters that govern the interpretation of the results and their relation to full scale structures. An extensive literature review is included in chapter 3 with details of the experimental and theoretical studies that have been reported in technical publications from various countries and research laboratories. Chapters 4 and 5 describe the static and dynamic experimental investigations that were carried out on model masonry assemblages. Chapter 6 is concerned with the results of an analytical investigation that was performed using a commercially available finite element system. Finally chapter 7 summarises the conclusions and observations drawn from the author's work and identifies areas of research that require further consideration.

1.4 Terminology.

Assemblage: A matrix of different materials that forms a composite system and in this case masonry, consisting of a number of units and mortar joints.

Sub-assemblage: A smaller system consisting mainly of 2 or 3 brick units and the corresponding amount of mortar joints.

Wallette: An assemblage of rectangular shape which represents a reduced size masonry panel, 2 to 3 units long by 6 to 10 units high.

Microconcrete: Concrete consisting of cement paste and reduced size aggregates.

Chapter 2

Modelling Theory and Similarity Principles

2.1 Introduction.

The purpose of physical modelling is to provide repeatable cost effective items in which carefully controlled variations can be included so as to investigate their influence on the behaviour and thus to be able to predict the response of prototype structures. This prediction may include all pertinent response parameters or it may be limited to selected parameters such as natural frequencies. The range of prediction may be limited to the linear elastic response or it may constitute the complete response history to failure. Material and geometric nonlinearities can be investigated. In the cases of single parameter and elastic response prediction several model design requirements can be relaxed. This makes model analysis a simpler but a less powerful tool. The set of scaling laws defining the model prototype relationship is developed by the theory of similitude based on dimensional analysis.

2.2 Dimensional Analysis.

Dimensional analysis is based on the assumption that every physical phenomenon can be expressed by a dimensionally homogeneous equation of the type

$$q_1 = \Phi\,(q_2, q_3, \ldots\ldots q_n) \qquad (2.1)$$

where n is the total number of physical quantities involved in the phenomenon, q_1 is a dependent quantity and q_2 to q_n are the parameters on which q_1 depends [Ref. 1]. The

form of the function involves the magnitudes q_2 to q_n in some way but not necessarily in the form of a product. The Buckingham's Pi theorem, states that any dimensionally homogeneous equation can be reduced to a functional relationship between a complete set of n-N independent dimensionless products (π-factors), taking the form

$$\Pi_1 = \phi\,(\Pi_2, \Pi_3, \ldots \Pi_{n-N}) \tag{2.2}$$

where Π_1 to Π_{n-N} are independent dimensionless products of powers of the physical quantities q_1 to q_n. The number N is the rank of the dimensional matrix and is usually equal to the number of basic units needed to describe the physical quantities.

Equation (2.2) is a dimensionless form of equation (2.1), and it must be equally valid for prototype and model if similitude is to be achieved. A condition for complete similitude is

$$(\Pi_1)_p = (\Pi_1)_m \tag{2.3}$$

and

$$(\Pi_2)_p = (\Pi_2)_m$$

$$(\Pi_{n-N})_p = (\Pi_{n-N})_m \tag{2.4}$$

where the subscripts *p* and *m* refer to prototype and model, respectively. Equation (2.3) is referred to as the prediction equation and equations (2.4) constitute the design conditions for the model.

Equation (2.1) is the starting point of any dimensional analysis. Extreme caution must be exercised when specifying the right number of physical quantities which enter (2.1). This is reflected when equation (2.4) impose the design conditions for the reproduction of the prototype at model scales. The input of the parameters and quantities in the right hand side of equation (2.1) requires a preliminary study of the

physical problem in order to fully understand the behaviour of the prototype and the laws which govern it.

It is often the case that direct simulation of certain quantities, such as material properties and loading conditions, are very difficult if not impossible to achieve. This can be a result of either economic or technological constraints. This leads to the design and fabrication of *distorted models* in which some of the design conditions are violated. Distorted models are commonly used as an alternative and according to the literature reviewed in chapter 3, have produced results that despite distortion replicate the key behaviour of the prototype modelled.

A model that satisfies all the similitude requirements set forth by a dimensional analysis, is called a *true model* and it maintains complete similarity. In many situations the design of such a model is impossible, forcing the analyst to resort to alternative models by altering carefully selected quantities, and ensuring that the range of response prediction investigated is not affected by an excessive amount of error. By maintaining '*first-order*' similarity and neglecting second-order effects, the *valid or adequate model* can be adopted [Ref. 1]. In these models, the prediction equation is not directly affected. Design conditions may be violated but investigation of the physical response reveals that the results will not be significantly dependent on the violated design condition. A direct example with particular importance to this research, is the case of dynamic loading of masonry walls where the effects of gravitational forces are small compared to those of inertia forces and may be neglected.

The physical quantities involved in a structural problem usually belong to one of the following groups.

- ► Geometric properties.
- ► Material properties.
- ► Initial conditions.
- ► Environmental effects.

A more detailed account of the above will be given in sections 2.3 and 2.4 when equations (2.1) and (2.2) will be utilised to derive appropriate similitude relationships for masonry components and assemblages investigated in this thesis.

2.3 Similitude requirements.

Determination of the necessary similitude requirements is the first step in the successful implementation of the modelling process. A set of physical quantities commonly found in engineering mechanics and their dimensional measures under the *gravitational system* is presented in Table 2.1. The basic independent quantities (e.g. length, force) can be used as components for all other physical quantities. Their dimensions can be expressed as products of powers of fundamental quantities.

This forms the basis of the similitude theory. Once the dimensionless products have been developed, the equality between prototype and model can be established, and subsequently the scaling laws are formed which will dictate the whole experimental procedure. The scales are selected arbitrarily to match the fundamental quantities needed to describe the phenomenon. Limitations almost always arise due to physical constraints, as mentioned in section 2.2.

In a static problem force [F] and length [L] are the fundamental quantities where in a dynamic problem, mass [M] length [L] and time [T] provide a choice of three arbitrarily selectable scales. By examining models with complete similarity equation (2.3) can be expanded into

$$\frac{\Pi_{1p}}{\Pi_{1m}} = \frac{\phi(\Pi_{2p}, \Pi_{3p}, ..., \Pi_{np})}{\phi(\Pi_{2m}, \Pi_{3m}, ..., \Pi_{nm})} = 1 \qquad (2.5)$$

once for the model and once for the prototype. For true modelling problems the formulation of scaling relations can be formed by translation of the Pi (Π) terms into

required scale factors. Pi terms can be formulated in several different ways and this can be a result of personal preference or expertise in solving problems of similar nature.

Table 2.1 List of physical quantities

Quantity		Units
l	Length	l
Q	Force	F
M	Mass	$FL^{-1} T^2$
σ	Stress	FL^{-2}
ε	Strain	-
a	Acceleration	LT^{-2}
δ	Displacement	L
ν	Poisson's ratio	-
E	Modulus of elasticity	FL^{-2}

Violation of a similitude requirement leads to departure from complete similarity. The ratio in equation (2.5) is no longer unity and differences are observed in the results which are commonly labelled *size effects*. Models that lack complete similarity may be generally called *distorted models*. However a distinction can be made between models with first-order similarity (valid models) and truly distorted models. First order similarity is a direct result of the need to use the same material for the model as for the prototype, although the use of different materials (section 2.4) is an inevitable and often preferred solution. By neglecting the difference from the actual value of the ratio ϕ_p / ϕ_m and unity, departure from true modelling is permitted and distortions arise. In first-order similarity the ratio might only be approximate to 1 as a direct result of second-order deviations from complete similarity. On the other hand, if first-order

deviations are permitted (true distorted models), the resulting ratio will in general be unknown and subsequently the model-prototype prediction equation (2.3) will no longer be correct. This type of distortion can arise due to discrepancies in boundary and initial conditions, geometry or material properties. An important aspect of this type of modelling is the possibility of allowing distortion in the reproduction of the prototype material stress-strain characteristics, referred to as *'strain distortion'*.

Figure 2.1 displays the behaviour of a model material in complete similarity with regard to uniaxial stress state, (ε_p / ε_m). If an alternative material were to be used following the stress-strain laws displayed in figures 2.2 and 2.3, the strains would be smaller or larger than the prototype respectively. As a result the model displacements which are a function of strain times length, would be different than those of the prototype. The magnitude of the strain distortion is indicated by the factors a_1 and a_2 in the figures.

Other types of model distortions may arise caused by inadequate material simulation such as distortions in Poisson's ratio, strain rate effects etc. These distortions can be labelled as unintentional, and the errors that they produce can be accounted for by modifications in the dimensionless functional relationship of the problem. It should be noted though that such alterations cannot correct an erroneous preliminary assessment of the structural behaviour and expected response of the model under investigation.

Table 2.2 Dimensionless products encountered in engineering problems

$\rho v^2 / E$ *	v^2 / lg **	$\rho gl / E$	a / g	σ / E	$l\omega^2 / g$	aT	$\sigma l^2 / P$	$t/l \sqrt{E/\rho}$

* Cauchy Number ** Froude Number

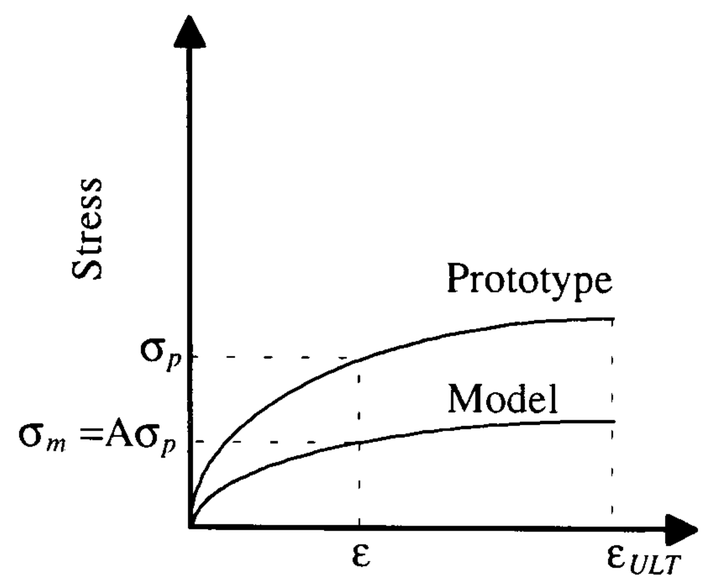

Figure 2.1 Completely similar model material

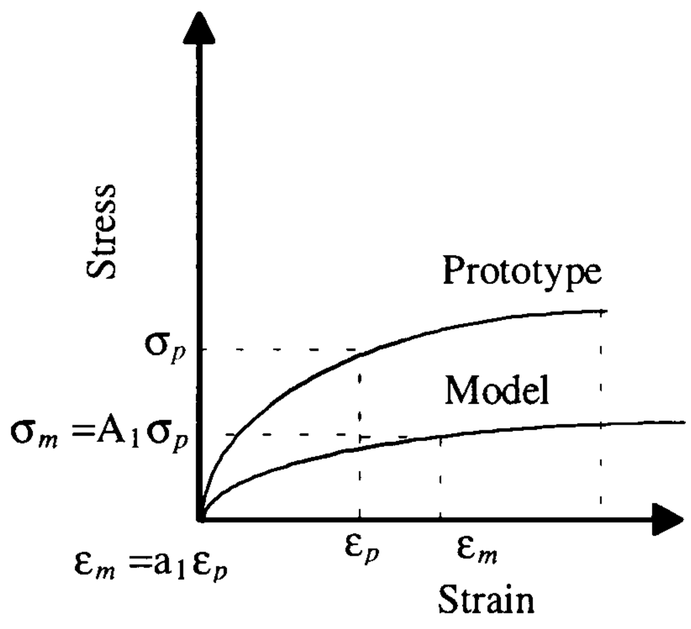

Figure 2.2 Distorted model materials - case 1

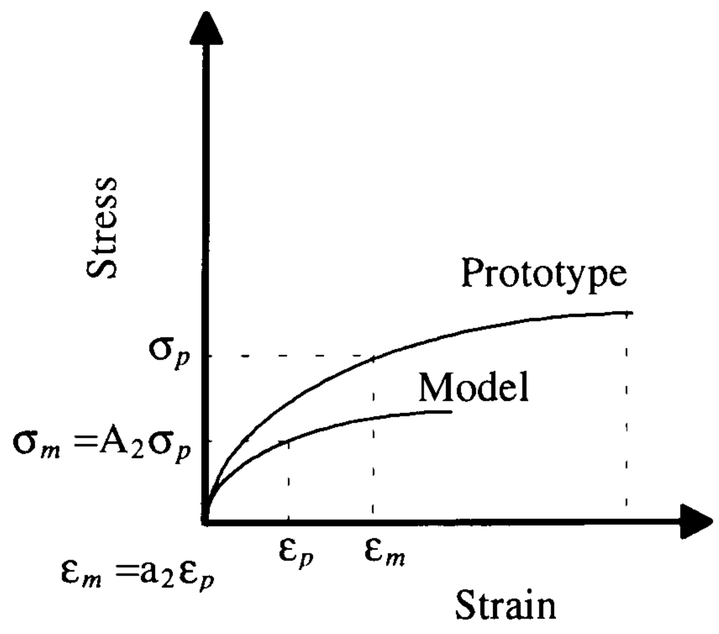

Figure 2.3 Distorted model materials - case 2

2.4 Masonry models for static and dynamic loading studies.

2.4.1 Structures under static loading.

The modelling techniques used in design and analysis of masonry structures, subjected to static and dynamic loads, should in general be able to predict elastic as well as inelastic behaviour. The mode of failure as well as the damage patterns of masonry elements obtained during model testing, should exhibit the same characteristics as in a prototype structure. A similarity in these mechanisms will be the most important measure of the accuracy of the experimental procedure and modelling method.

Static loading usually includes dead and live loads, but it could also include equivalent static loads for the dynamic effects of earthquakes or other abnormal loads. Based on the assumption that there are no significant time-dependent effects that could influence structural behaviour, the parameters dominating the modelling process are shown in Table 2.3 column (3). For complete similarity of structural behaviour including inelastic effects of cracking and yielding, the scale factors are as shown in Table 2.3 column (4). All dimensionless quantities such as Poisson's ratio must be equal for model and prototype. If it is assumed that the working stresses caused by the self-weight of the structure are not significant (which is often the case in most load-bearing masonry buildings, or the walls acting as infills in concrete and steel structures) then the scale factors shown in Table 2.3 column (5), will be adequate for modelling. Although these factors constitute a practically true modelling procedure, difficulties arise in the fabrication stage due to the small size of the composite elements (bricks, mortar joints and reinforcement when applicable), and in the modelling of stress-strain curves for the components and masonry assemblages.

Group	Quantity	Dimension	True model	Practical true model
1	2	3	4	5
Loading	Concentrated load	F	S_σ/S_l^2	S_l^2
	Line load	FL^{-1}	S_σ/S_l^2	S_l
	Pressure	FL^{-2}	S_σ/S_l^2	1
	Moment	FL	S_σ/S_l^2	S_l^3
Geometry	Linear dimension	L	S_l	S_l
	Displacement	L	S_l	S_l
	Angular displacement	-	S_l	1
	Area	L^2	S_l^2	S_l^2
Material properties	Masonry unit stress	FL^{-2}	S_σ	1
	Masonry unit strain	-	1	1
	Modulus of elasticity of masonry unit	FL^{-2}	S_σ	1
	Unit Poisson's ratio	-	1	1
	Specific weight	FL^{-3}	S_σ/S_l	$1/S_l$
	Mortar stress	FL^{-2}	S_σ	1
	Mortar strain	-	1	1
	Modulus of elasticity of mortar	FL^{-2}	S_σ	1
	Mortar Poisson's ratio	-	1	1
Design	Assemblage compressive strength	FL^{-2}	S_σ	1
	Assemblage strain	-	1	1
	Modulus of elasticity of assemblage	FL^{-2}	S_σ	1
	Tensile strength normal to bed joints	FL^{-2}	S_σ	1
	Tensile strength parallel to bed joints	FL^{-2}	S_σ	1
	Shear strength of bed joints	FL^{-2}	S_σ	1
$S_l = L_p / L_m$ = length scale factor $S_\sigma = \sigma_p / \sigma_m$ = stress scale factor				

Table 2.3 Scale factors for masonry under static loading [Ref. 1]

		Scale Factors				
		Dimension	**True Replica Model**	**Artificial Mass Simulation**	**Gravity Forces Neglected Prototype Material**	**Strain Distortion**
1	**2**	**3**	**4**	**5**	**6**	**7**
Loading	Force, Q	F	$S_E S^2$	$S_E S_l^2$	S_l^2	$S_E S_l^2 S_\varepsilon$
	Acceleration, α	LT^{-2}	1	1	S_l^{-1}	1
	Gravitational acceleration, g	LT^2	1	1	Neglected	1
	Velocity, υ	LT^{-1}	$S_l^{1/2}$	$S_l^{1/2}$	1	$(S_\varepsilon S_l)^{1/2}$
	Time, t	T	$S_l^{1/2}$	$S_l^{1/2}$	S_l	$(S_\varepsilon S_l)^{1/2}$
Geometry	Linear dimension, l	L	S_l	S_l	S_l	S_l
	Displacement, δ	L	S_l	S_l	S_l	$S_\varepsilon S_l$
	Frequency, ω	T^{-1}	$S_l^{-1/2}$	$S_l^{-1/2}$	S_l^{-1}	$(S_\varepsilon S_l)^{1/2}$
Material properties	Modulus of elasticity, E	FL^{-2}	S_E	S_E	1	S_E
	Stress, σ	FL^{-2}	S_E	S_E	1	$S_E S_\varepsilon$
	Strain, ε	-	1	1	1	S_ε
	Poisson's ratio, ν	-	1	1	1	-
	Mass density, ρ	$FL^{-4}T^2$	S_E / S_l	*	1	$S_\varepsilon S_E S_l^{-1}$
	Energy, EN	FL	$S_E S_l^3$	$S_E S_l^3$	S_l^3	$S_E S_l^3 S_\varepsilon^2$

*$(g\rho l / E)_m = (g\rho l / E)_p$

Table 2.4 Scale Factors for Earthquake Response of Structures

2.4.2 Masonry under dynamic loading.

The use of small scale replica models in structural engineering has long been an alternative to full scale modelling but has often been viewed with scepticism with regards to scale effects and use of materials. Using full-scale structures to investigate dynamic-related phenomena such as rate of loading effects, dynamic response characteristics under realistic seismic excitations, failure mechanisms, torsional effects, stiffness and mass irregularities and soil-structure interaction, is practically impossible. Replica models however can be very versatile when specific phenomena are studied as the choice of scale and configuration can be carefully chosen. Physical modelling of structures under dynamic loading, is more complex due to the non-linear response resulting from the imposed time-dependent forces. These forces are the inertia forces that are the product of mass and acceleration, the resisting forces that are a function of the stiffness of the structure in the particular direction in which motion is occurring, and the energy dissipation of material or construction related damping forces. There are also cases where gravity-induced stresses have to be considered, affecting modelling profoundly. Since two different types of models have been developed for this study, a more detailed account of the types of models introduced in section 2.2, is necessary. It should be noted that several types of dynamic loads encountered in structural engineering (e.g. blast and impact loads), can be studied using one of the models described below, but the present research work is mainly concerned with masonry structural elements and assemblages under static loading conditions imposed by standard laboratory testing equipment and seismic loading generated by shake table sinusoidal excitations.

2.4.2.1 True models.

Table 2.4 column 4, shows the scale factors for a true replica model [Ref. 2]. Such a complete observation of similitude requirements is considered to be impossible in earthquake engineering. Exact duplication of the prototype material properties is required, if the model is to simulate the elastic and nonlinear, inelastic behaviour of the

structural system up to and including failure. The single major difficulty in this type of modelling, is the selection of an appropriate model material and it will be shown that since in nature no two materials are the same, inevitable errors are always introduced during the simulation process. As mentioned before, in a dynamic problem which may be described by mass (M), force (F), length (L) and time (T) three scales can be selected arbitrarily. The three independent variables typically chosen in such a study are the gravitational acceleration g, the linear dimension l, and the modulus of elasticity E. The gravitational acceleration scale factor S_g has to be equal to unity unless a centrifuge is used. For normal circumstances this reduces the choice of selectable arbitrary scales to two. Exact material modelling implies that simultaneous duplication of inertial (F_I), gravitational (F_G) and restoring (F_R) forces according to the Froude and Cauchy scaling requirements has to be achieved. Their relationships to material density, stiffness, length and applied acceleration may be expressed as

$$F_I \sim \rho l^3 a$$

$$F_G \sim \rho l^3 g$$

$$F_R \sim \sigma l^3 = \varepsilon E l^2$$

where ρ σ and ε are measures of density stress and strain. Independent of scale F_I and F_G must bear a fixed ratio as also must F_I and F_R. The following parameters result from this requirement

$$\frac{F_I}{F_G} \sim \frac{\rho l^3 a}{\rho l^3 g} \sim \left\{ \begin{array}{l} \frac{a}{g} \\ \frac{v^2}{lg} \end{array} \right. \qquad \text{Froude's Number}$$

$$\frac{F_I}{F_R} \sim \frac{\rho l^3 a}{\varepsilon E l^2} \sim \left\{ \begin{array}{l} \frac{\rho l a}{E} \\ \frac{\rho v^2}{E} \end{array} \right. \qquad \text{Cauchy's Number}$$

Since S_G is unity, the dimensionless product a / g (Froude's number usually written as v^2/lg), dictates that

$$S_a = S_G = 1 \qquad (2.6)$$

In dynamic loading studies where gravitational forces play a significant role in the stress history of the structure, all dimensionless terms (Table 2.2) that contain *g* must be accounted for. From the ratio of Froude's and Cauchy's numbers, the necessary condition for simultaneous replication of gravitational, inertia and restoring forces under fixed gravitational acceleration is derived,

$$\frac{S_E}{S_\rho} = S_l \tag{2.7}$$

where S_E is the ratio of modulus of elasticity between prototype and model, S_l and S_ρ ratios of length and mass density respectively. Equation (2.7) clearly demonstrates the limitations described before, with regard to material modelling. For a true model, stress and stiffness scale factors are taken equal or near to unity and as a result the density scale factor is inversely proportional to the chosen length scale factor ($S_\rho = 1 / S_l$). In this study where the length scale factor was chosen as 4, the mass density of the model material had to be increased by the same amount, if true similarity was to be accomplished. Section 4.2 describes in detail the scale factors considered for the masonry under investigation together with the steps and procedures adopted for true and distorted scale modelling.

2.4.2.2 Distorted models.

All physical models that violate any of the conditions set in section 2.4.2.1 are called distorted models. A distinction between truly distorted and valid models has already been established in a previous section. When an important design condition is violated resulting in a truly distorted model, it becomes very difficult if not impossible to apply corrections to the other physical quantities and for this reason such types of models are rarely used in dynamic studies of nonlinear problems. One exception could be the case where modelling of identical strains is required and the use of alternative materials results in *strain distortion* (Table 2.4, column 7). For such a distortion, model displacements velocities and accelerations would be different than those of the prototype and the errors induced would be proportional to the factors a_1 and a_2 ($\varepsilon_m = a\varepsilon_p$), in figures 2.2 and 2.3 respectively. If on the other hand a *second-order* distortion is

permitted, and no adjustments are necessary with respect to the other dimensionless products, models are classified as valid or adequate. There are two types of models commonly used in general dynamic loading experimental investigations offering different types of distortion with respect to mass similitude.

2.4.2.2.1 Artificial mass simulation models.

Complete model similarity laws and equations developed in the preceding sections, clearly demonstrated that the choice of model materials is the most difficult step during a small scale model investigation. While attempting to reduce strength and Young's modulus during development of the material, the specific weight is inevitably reduced. Since the mass characteristics (inertia forces) are very important for structures subjected to dynamic loading, mass density distortion can be minimised by employing a technique termed as artificial mass simulation. Additional mass in the form of lead bricks or steel ingots is added and securely fixed to selected locations on the structure, in a manner such that its contribution to the overall strength and stiffness of the model is negligible [Ref. 2].

This type of distorted simulation can be applied to any model structure or structural assemblage overcoming material difficulties, and it has been widely used by many if not all the researchers in this field. There are two ways to implement the procedure described above depending on the type of structural system under investigation. The most common case encountered is that of lumped mass systems which are essentially two-dimensional (frames and walls), when the added seismically effective mass is lumped at the floor levels or fixed on the top of a wall or panel (under the precautions mentioned above), and is decoupled from the density of the model material effectively relaxing the specific weight dimensional requirement that S_E/S_ρ must be equal to S_l. If a material is used that has the same strength and modulus of elasticity as the prototype the stress scale factor is unity $S_\sigma = 1$, or

$$(S_\sigma)_m = (S_\sigma)_p \tag{2.8}$$

and since $\sigma = m\ a / l^2$

$$S_\sigma = S_m\ S_a\ S_l^{-2} = 1 \tag{2.9}$$

The acceleration scale factor will be unity since $(g)_m = (g)_p$ as explained earlier, so from equation (2.9)

$$S_m = S_l^2 \tag{2.10}$$

In the equation above m represents the entire mass of the model and can be used to calculate the amount of additional mass needed for simulation purposes. The above would also satisfy Cauchy's requirement for simulation of inertial and restoring forces. If the material used is not identical to the prototype ($S_E \neq 1$), then equation (2.10) would be

$$S_m = S_E\ S_l^2 \tag{2.11}$$

When correct simulation of the mass distribution in space is required (distributed mass systems, accounting for three-dimensional effects such as slab-frame interaction), the procedure of lumping masses at floor levels or wherever appropriate is not accepted, since this interaction is important in simulating the dynamic response of the model. In this case discrete masses must be distributed over the floor slab area in a manner that permits simulation of both gravitational and inertial effects. As a result the mass density of the structurally effective material (ρ_0) needs to be decoupled by an additive mass of density (ρ_1) which is to be built into the model but has no counterpart component in the prototype. The prototype density would be $(\rho_0)_p$ and the model density $(\rho_0)_m + \rho_1$. From Table 2.2 the term $al\rho / E$ can be used to derive the mass density ρ_1.

$$\left[\frac{gl(\rho_0 + \rho_1)}{E}\right]_m = \left[\frac{gl\rho_0}{E}\right]_p \tag{2.12}$$

but with testing for 1g (m/sec^2) for model and prototype as is always the case (except for experiments involving a centrifuge) the relation becomes

$$\rho_1 = \left[\frac{S_E}{S_l} - (S_{\rho_0}) \right] (\rho_0)_p \qquad (2.13)$$

where S_{ρ_0} is the density of the material $((S_{\rho_0})_m / (S_{\rho_0})_p)$. For a model constructed by using prototype materials ($S_E = S_{\rho_0} = 1$) with a scale factor of 1, the density according to equation (2.13) will have to be increased by a factor of 3.

For models with artificial mass simulation using prototype materials the similitude requirements summarised in Table 2.3, column 5 are applied with the exception of the mass density where equations (2.10) to (2.13) are applied appropriately. This type of modelling has been extensively used for reinforced microconcrete and masonry applications (section 3.2), usually providing a good prediction of prototype behaviour and response under dynamic loading conditions.

There are cases however when for certain types of structural configurations the gravity stresses are small compared to stresses induced by dynamic motions generated through a shaking table facility or a cyclic loading history. In such a case the gravitational acceleration can be omitted allowing more freedom in the selection of the scaling parameters without the need for artificial mass simulation. For models made with prototype materials these factors are summarised in Table 2.3, column 6.

In post-elastic tests where gravity effects are always present, true model distortion should be accounted for, while for linear elastic testing the gravitational effects can safely be neglected and effectively decoupled from seismic effects, thus allowing dynamic response characteristics to be simulated in the model without regard to the scaling of the gravitational acceleration.

The possibilities of dynamic modelling using one of the methods described above are subject to the limitations of the individual problem. If the inaccuracy caused by neglecting gravity forces is unacceptable, an intermediate solution can be applied by adding artificial mass to minimise the effect. This method of partially neglecting gravity forces as well as the strain distortion method described earlier, are rarely used due to complications in the simulation process and the errors that these induce that are very

difficult to account for and interpret. This experimental investigation features two of the aforementioned modelling techniques, namely the true replica and the artificial mass simulation model.

2.5 Scale effects and accuracy of small scale models.

Throughout this study the examination of small scale structural models was performed using simulation techniques described in the previous section, but as mentioned earlier the models did not represent any real full-scale structure or assemblage. Therefore scale effects cannot be quantitatively described. Nevertheless a brief description is provided in order to establish the limitations and feasibility of the model materials, fabrication techniques and testing procedures used in the experimental investigation.

2.5.1 Scale effects.

Size or scale effects in the physical properties of the model material are defined as the change in the indicated unit strength due to a change in specimen size. When direct comparison to a prototype or prediction of prototype properties is required, size effects play a significant role and can provide inaccurate information if they are not accounted for or eliminated altogether. Several theoretical studies of size effects have been developed with the approach being based on a thorough statistical treatment of experimental results. In small scale masonry models, the heterogeneity of the constituent materials produces inevitable scale effects as model size decreases. These effects which can produce significant variations in the strength of masonry specimens are dependent on several factors which are introduced during the various stages of specimen preparation, construction and testing and are summarised below. The procedures and techniques adopted in an effort to minimise such scale effects and reduce inaccuracies such as dimensional tolerances for example, are detailed in chapter 4.

2.5.1.1 Compaction and density.

Compaction of the ingredients during the moulding process cannot be scaled and can affect the strength properties significantly. As a result when smaller moulds are used for casting, the degree of compaction is higher, resulting in higher density and strength due to better filling of the internal voids and release of entrapped air bubbles. The effects can be partly minimised by compacting the specimens in a uniform manner (model and prototype, different specimens of the same model).

2.5.1.2 Curing and water evaporation.

Curing of the cast specimens is highly dependent on the size, especially the surface area-volume ratio that increases with a corresponding decrease in size, effectively speeding up the curing process. This has a direct effect on compressive strength which generally increases depending on specimen size and laboratory environmental conditions (wet or dry curing, temperature, humidity). Evaporation of water (moisture loss) in small scale specimens which is also dependent on its surface area-volume ratio (smaller flow gradients), results in higher strength.

2.5.1.3 State of stress.

The state of stress and the strain gradient can influence the strength of the specimen. Different stress states (compression, tension), depend on different parameters such as parallelism at the opposite loading faces for a specimen subjected to uniaxial compression.

2.5.1.4 Strain rate.

Higher strain or loading rates result in higher strength and this effect is further amplified during the dynamic loading stage. As specimen size decreases the head

movement (load application rate) of the testing machine should also be decreased. This is not always applicable and depends on the operating limitations of the loading apparatus, in particular the displacement and/or loading control method available to the operator.

2.5.1.5 Testing machines.

The properties of the machine to be used for testing, can play a significant role in introducing scale effects on test results. The stiffness characteristics, size and shape of the loading platens are the most important parameters. A more uniform strain condition is applied to the specimen through stiff loading platens, while thinner flexible platens tend to apply a more uniform state of stress. Size is also very important and a proper scaling of the platen surface area will result in more accurate readings with respect to the specimen's property measured, although this scaling does not need to conform to strict similitude requirements. The end (top and bottom) platens, can restrain lateral movements at the end faces of the specimen during loading, inducing artificial stresses which result in higher apparent compressive strength. This effect was observed during the early stages of this experimental study concerned with the development of the prototype units, and subsequently a technique was devised and applied for the remainder of the investigation (section 4.4), with the intention of minimising the erroneous contribution of such effects to the end results.

2.5.2 Accuracy.

Accuracy in small scale modelling is also dependent on several factors, since errors can be introduced as early on as the planning stage and up to the analysis and interpretation of the final test results. The most important of these are summarised below and are further examined in the chapters 4 and 5 as these were encountered during casting, construction and testing of the models.

2.5.2.1 Errors during fabrication.

As size decreases the fabrication process becomes more and more difficult since the dimensional tolerances become smaller. Construction of a model with a scale beyond a certain limit becomes practically impossible. The geometry has to be reproduced very accurately in order to minimise errors and any subsequent analysis of the results should be based on actual dimensions measured after fabrication. The moulds used for casting should be manufactured by materials that are easy to machine and maintain their dimensions in time when subjected to harsh laboratory conditions. Perspex, steel and brass moulds have been successfully used during this study, although it should be noted that perspex was discovered to be a superior material for general masonry components fabrication (bricks and blocks), while steel or brass can be used for control specimens (cubes, cylinders and prisms).

2.5.2.2 Material properties.

When testing models in the inelastic range, material properties such as compressive and tensile strength become very significant. By using prototype (or nearly prototype) materials most of the properties are simulated properly and small variations and distortions (strain scale distortion) can be accounted for, in most cases. In masonry modelling where bricks are connected together with mortar at the joints and at regular intervals, the problem becomes more complicated and the bond between the constituent materials has to be modelled accordingly or errors could be introduced which will affect the test results.

2.5.2.3 Accuracy during testing and data recording.

Accuracy during testing small scale specimens is dependent on the testing and measurement set-up and the loading technique applied. The loads applied should be represented as truly as possible and should resemble the techniques used for loading

their larger counterparts. In most cases standard laboratory testing machines can be used successfully by applying small modifications to their loading set-up (section 4.4). There are cases though when purpose-built types of loading systems are necessary due to limitations of the existing equipment. It is then where care should be taken in order to design a system that will apply the prescribed loading history as close as possible. A prime example is the small shake table for seismic loading studies, which is usually purpose-built, designed to comply to the specific needs of the testing laboratory. In addition to loading, instrumentation of the specimen should be carefully planned and executed. Placing measuring devices and sensors at improper locations, will affect the accuracy and interpretation of the test results with further implications arising when adequate bonding or mounting of the sensing elements is not exercised with care. Measurements that apply to this study range from strains, deflections, loads, accelerations and cracking location. The selection of any such device depends on its working range, degree of accuracy and ease of use. The calibration constant for most of the transducers can be verified and applied to all subsequent test readings. Loads are often measured using load cells which can be accurate up to 0.5% of their linear range while accelerometers which are essentially very sensitive seismic transducers exhibiting very low damping ratios and high natural frequencies, are used to measure accelerations. Mechanical devices such as dial gauges can be used for measuring deflection although electrical transducers (LVDTs), are becoming more common in modern laboratories. Their accuracy varies between 0.025 mm and 0.00025 mm and readings can be fed directly to a data logging device. In the measurement of strains and curvatures, electrical resistance strain gauges are widely used, although strain values can be extrapolated by displacement readings using LVDTs as it was done in this study (section 4.4). Electrical resistance strain gauges are susceptible to errors associated with bonding of the gauge element to the face of the specimen, temperature variations etc. Finally crack detection methods such as microscopic examination may be needed if crack width and spacing are to be simulated. For this study a simple form of crack detection (section 4.4) was used in order to study crack formation and propagation. Another area where errors can be introduced, is during the stage of data acquisition and reduction. The system to be used should be able to convert, collect and store data from all the sensors with a high degree of accuracy and speed, two factors which are dependent entirely on the cost of the equipment. A fairly accurate data acquisition board

was used in the static and dynamic experimental stages of this study and its specifications and limitations will be described in detail in a later section.

2.5.2.4 Interpretation of test results.

The final step in any model investigation involves interpretation of the results obtained during the various testing stages and comparison to some available theory or similar experimental evidence, especially in cases such as masonry where the relevant theory is not very well established. Failures modes and cracking histories can always be verified by photographic evidence present in textbooks or research reports and papers. For example, photographic records exist showing failure modes of masonry infill panels in buildings subjected to real earthquake loading and these can be used as evidence for verifying failure patterns in model masonry infill walls subjected to similar loading excitations under controlled laboratory conditions.

2.6 Conclusions.

Dimensional analysis could be applied to derive modelling laws for various types of model tests of structures subjected to different types of loading. Exact duplication of all parameters during an experimental study is impossible to achieve even if using prototype materials for model construction. By careful planning and consideration most of the errors can be accounted for and minimised thus providing a sufficient degree of accuracy. Since modelling is an approximate scientific technique and theory can only account for some of its aspects, practical experience plays a vital role in achieving the goal of better understanding of the physical phenomena under investigation. Models do not need to be replicas of actual prototype structures in order to provide physical data on the behaviour and response of structural systems and develop a better understanding of the mechanisms that govern their behaviour. There are numerous examples in literature (chapter 3) where experimental model investigations have provided a wealth of information that was subsequently used to fine-tune and calibrate computational

models and design codes. It was shown that the true replica model is the ideal choice once a suitable material is available. Reasonably accurate results on the dynamic behaviour of structural systems can be obtained by testing models with artificial mass simulation thus allowing the use of prototype materials. Discretely distributed additional mass or lumped mass can be added to the model depending on the type of structural system and the influence of mass distribution on the response under dynamic loading. When testing models under static loading the case is simplified and accurate modelling is easier to achieve. Size effects can enter the modelling process during various stages and could lead to erroneous results which in turn can be identified by examining and comparing modes of failure, ultimate load predictions and overall model behaviour. Careful consideration of all the parameters that might affect accuracy and proper planning during the early stages (e.g. calibration and static check prior to testing), can provide a useful and reliable experimental technique.

Chapter 3

Literature Review

3.1 Introduction.

The first phase of this research work was devoted to the examination of the possibility of using small scale models for testing brick masonry assemblages under a variety of loading conditions. Feasibility and reliability of the models was considered vital if further research was to continue successfully. The second phase which was dependent on the success of the first one, involved testing model brick masonry shear walls confined by a special steel frame, subjected to sinusoidal shake table excitations and examining their behaviour and response. As a result a large number of publications, research papers and conference proceedings dealing with all aspects of experimental modelling in small scale, were reviewed and evaluated. This review though, was not limited to clay brick masonry alone but was extended to concrete block unreinforced and reinforced masonry as well as microconcrete. Since research in small scale brickwork especially clay unreinforced masonry is rather limited, this review had to be expanded to cover other areas of small scale modelling as well as full scale testing, in order to draw information and knowledge that would prove useful if applied to the specific problem dealt with in this thesis. The first part of the review is concentrated on experimental testing of models of various sizes including masonry shear walls, infilled concrete and steel frames as well as masonry component and assemblage testing. The second part of this review briefly examines the various theories that have been developed in the last 40 years, as well as the analytical procedures that have been adopted since the introduction of powerful mainframe computers that has greatly simplified the numerical process.

3.2 Review of experimental work.

Use of small scale models in engineering dates back many hundreds of years, although those were used primarily for demonstration and planning purposes. Since experimental stress analysis became available at the turn of this century as a tool in structural engineering among other sciences, measurements of strains and forces were used to predict structural behaviour. When this could not be achieved on actual structures, models were constructed resembling the original as closely as possible and thus allowing the engineers to study behaviour more closely than ever before. An excellent example is the fabrication of a three dimensional 1:240 scale model of the Hoover Dam in the United States in the early 30's [Ref. 1]. Recent advances in digital computers along with the progress made in experimental techniques have assisted greatly in the understanding of the behaviour of structural systems subjected to various loading conditions in the nonlinear range and at failure. In earthquake engineering the use of hydraulic actuators and earthquake simulators such as shake tables have provided answers to many situations where theory could not be established owing to the complexity of the problem. At first elastic models using modern materials such as plastics were extensively used in order to study behaviour within the elastic range giving rise to limitations when used to predict any inelastic behaviour of a loaded structural system. Material such as concrete, steel and masonry which exhibit nonlinearity in the post yield phase, require the use of inelastic models in order to reproduce their characteristic behaviour up to failure. Steel, concrete and masonry structures have been successfully modelled in the past 30 years using prototype or near-prototype materials.

3.2.1 Masonry - an introduction.

Masonry has been widely used in building construction especially in developing countries where local resources can be utilised in the manufacturing of the constituent components. The range of materials used in construction consists of masonry units that differ greatly from country to country, mortar, grout and reinforcement. Mediterranean,

African and South American countries use unreinforced masonry for low-cost housing, single storey load-bearing buildings, multi storey shear wall systems and infill partitions. In countries such as Canada, Australia and North America reinforced and prestressed masonry systems are used as complete building configurations even in areas of high seismicity. Due to the different approaches of construction techniques, different materials have to be used in order to accommodate the needs for special requirements such as reinforcement or local design codes and manufacture processes. Typical clay brick units are shown below (dimensions are approximate).

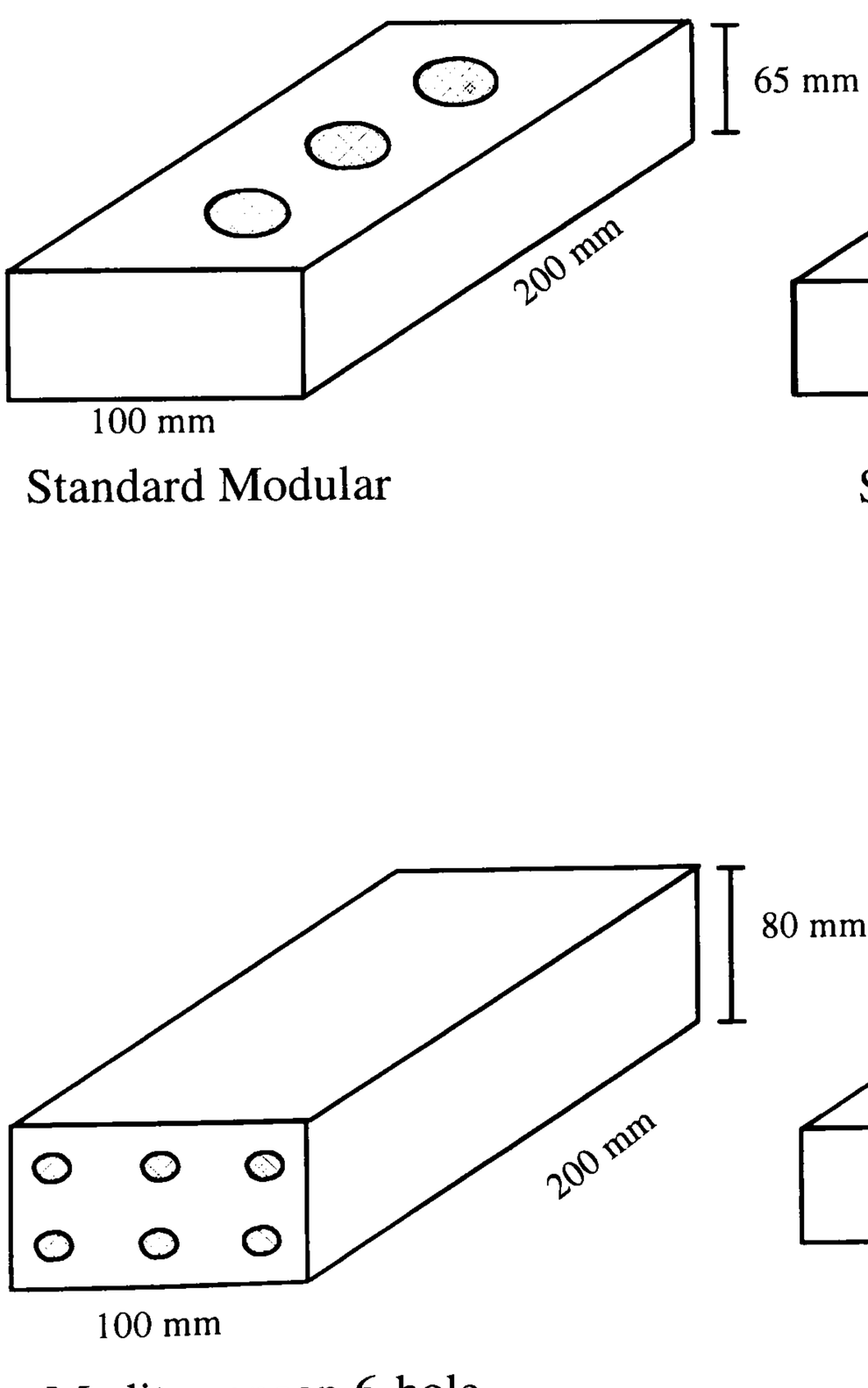

Figure 3.1 Clay units used in unreinforced masonry construction.

Concrete masonry units come in various shapes and sizes. The standard concrete block has nominal dimensions of 200 x 400 x 400 mm. Typical concrete masonry blocks are shown in figure 3.2.

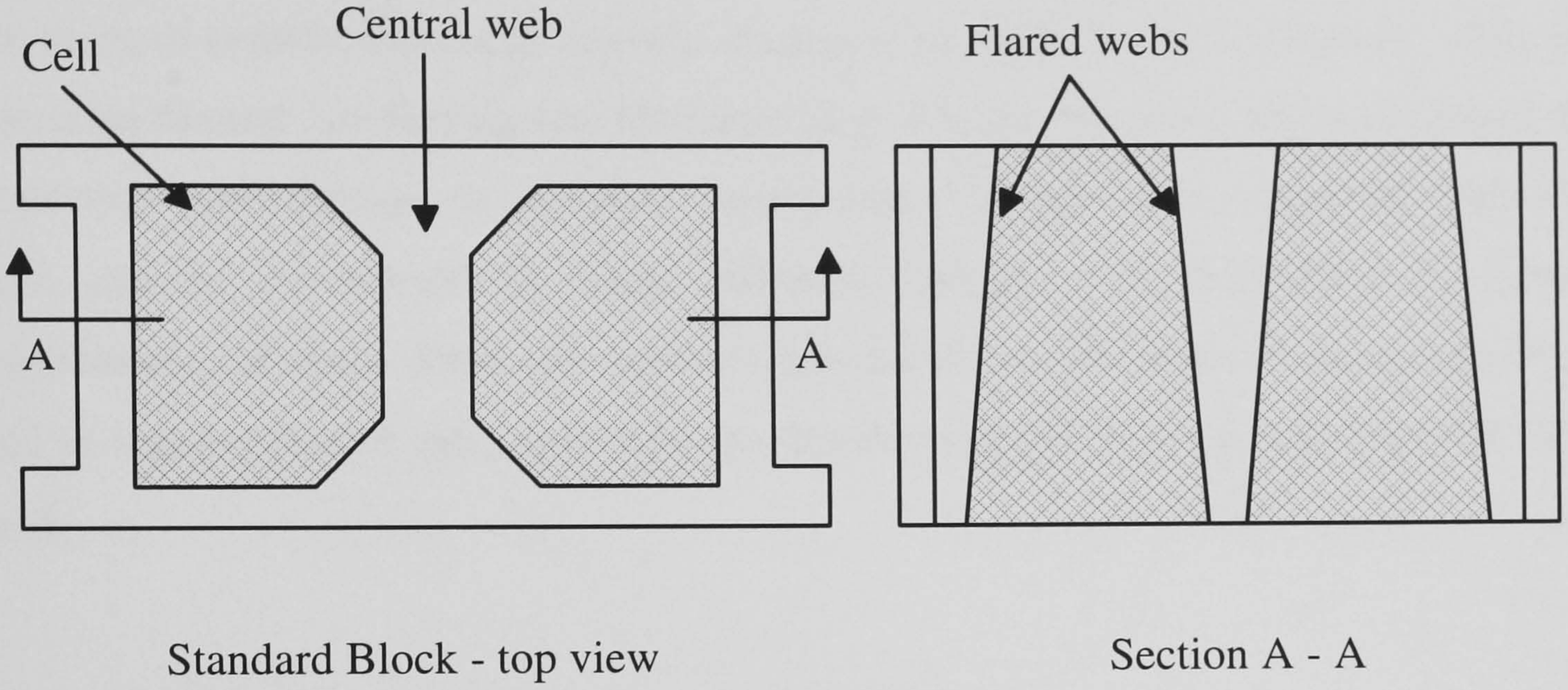

Figure 3.2 Typical concrete masonry units.

Typical clay and concrete units described in the two preceding figures represent just a small selection of the forms available for masonry construction. These represent however the units most frequently used by researchers in small scale modelling. Mortar which acts as a medium in bonding individual units into a composite assemblage is a combination of cement, lime, sand and water. British Standards [Ref. 82a], specifies five types of cement-lime-sand mortars identified by proportion specification, while the American Society for Testing and Materials [Ref. 83] specifies four types identified by proportion specification or property specification (compressive strength). Masonry walls can be constructed in many different configurations depending on design requirements, aesthetic form and cultural considerations. The patterns most commonly used in construction of solid or composite masonry elements include *running* and *stack* bond.

3.2.2 Small scale masonry modelling.

Direct small scale modelling techniques were first applied to nonlinear problems of reinforced concrete structures in the mid 1950s. The amount of work devoted exclusively to unreinforced masonry with particular reference to infill frames under dynamic (seismic or cyclic) loading is limited with publications and research papers on the subject surfacing once every few years, and as a result in an attempt to examine experimental techniques and procedures that could be used for the purposes of this research work and to assess if possible the state-of-the-art in physical modelling of masonry assemblages using small scale specimens, the literature review was narrowly expanded to areas covering reinforced masonry and microconcrete.

Plaster of Paris and gypsum combined with sand aggregate and steel wire reinforcement were first investigated as potential mixes for simulating concrete, (Brock, White et. al., Ranganathanm et. al., Preece, [Ref. 3] among others). Sabnis and White [Ref. 4], investigated the use of high strength gypsum mixes as cementing agents for concrete modelling and produced satisfactory results with respect to compressive and tensile strength and simulation of stress-strain characteristics of prototype concrete.

The need for exact modelling of prototype concrete in the inelastic range eventually led to the development of microconcrete (Johnson, Mirza, [Ref. 3]).

Aldridge and Breen [Ref. 5], worked extensively on the design of a model concrete mix (1:8 scale replica of the prototype mixture) using different aggregate sizes, smooth black annealed wire for reinforcement and small size cylinders for moulded control specimens. In the following years microconcrete was researched extensively producing a variety of different mixes with respect to the fundamental properties of prototype concrete. Different techniques have been applied to solve the problems arising when scale is reduced, especially with respect to the aggregate cement matrix, reinforcement, tensile strength, bond behaviour and size of control specimens. Although aggregate size have been successfully reduced to satisfy similitude requirements, many of the properties of concrete have not been reproduced as expected. The choice of a suitable design mix depends primarily on the model scale and the properties of the prototype to be modelled, depending on the specific problem under investigation. Cement is the same in model and prototype mixes although size gradation has been reported in literature at the early stages of microconcrete development (Oberti [Ref. 3]). Aggregate is the next constituent material and the one where research has concentrated for a long time since it plays a vital role in concrete properties such as tensile and microstructure bond strength. As a model material aggregate is a combination of carefully graded sand designated as fine or coarse depending on sieve-passing ratios. Since no minimum or maximum allowable sizes are specified by codes the thickness of the particle sizes is entirely dependent on the model scale factor chosen. Sizes as small as 4 mm and as large as 10 mm have been reported in literature. Depending on the size of the model, admixtures are often used in order to improve workability during casting.

Commercially available wire reinforcement was introduced in model concrete in the early stages of material development but proved to be inadequate in developing bond strength and subsequently in 1966 at Cornell University (Harris et. al. [Ref. 6]) a technique was developed to cold deform wire for use as reinforcement. The principle of this technique is still in use, although due to technological development it has become a

become a more advanced process (Noor [Ref. 7]), and it is based on a simple device that deforms the wire while it is forced through two pairs of grooved gears driven manually or by a mechanical motor.

Recent developments in microconcrete include replacement of portland cement with equal amount of fly-ash (Swamy and Falih [Ref. 8]), producing a so called small aggregate concrete with improved water retention and scaling of fine aggregates. Noor [Ref. 9], describes a different microconcrete mix where part of the aggregate is replaced with glass beads in an attempt to improve tensile strength modelling. In the same paper a set of trial mixes were produced where coarse sand particles were coated with silicon base agent in an attempt to reduce tensile strength, a procedure described also by Müller [Ref. 10]. Another casting mix with particular reference to this work is reported by Clough and Niwa [Ref. 11], while attempting to model a 1:150 scale concrete arch dam on an earthquake simulator facility. The mix consisted of plaster, celite, sand and some lead powder which was added in the final stages of development in order to achieve the desired unit weight dictated by similarity laws. Although the material density was partly increased by adding lead powder to the mixture, the investigation was not taken any further due to the distortion of the compressive strength and elastic modulus in the material which according to the authors could not be overlooked. They concluded that this procedure could provide satisfactory results if used for larger model scales.

Direct modelling of concrete structures using small scale models has become an advanced experimental technique used by many researchers around the world in situations where behaviour of complex structural systems cannot be fully understood and analysed using a theoretical approach. The experience and knowledge gained from research into microconcrete has been successfully used in small scale modelling of masonry structures. Work on this subject is surprisingly limited despite the fact that masonry is quite a common construction material in many countries and has been used as such for hundreds of years. The University of Edinburgh in Scotland, Illinois and Drexel in the United States, the Institute for Testing and Research in Materials and Structures (ZRMK) in Slovenia and with limited contribution the Aristotle University in

northern Greece have by far been the most established research centres in small size clay brick and concrete block masonry modelling.

The first attempt to model masonry structures known, was performed in 1956 at the Building Research Station in England by Vogt [Ref. 12]. Although only qualitative results were obtained by using 1:4 and 1:10 scale bricks, this signalled the start of an ongoing investigation into small scale brickwork initiated at the University of Edinburgh in the mid 60s under the direction of Professor A. W. Hendry that was set to continue for the next 20 or so years and in the process establishing small scale modelling as a feasible and reliable alternative to full scale experimental testing.

From early investigations by Hendry and Murthy [Ref. 13-14], who performed basic static tests on 1:3 and 1:6 scale model walls and piers with respect to the compressive strength of masonry, it was evident that small scale models could reproduce the behaviour of the full scale prototypes. Sinha, Sinha et. al. and Hendry [Ref. 15-16-17-18] carried out tests on 1:2 and 1:3 axially loaded model brick walls stiffened along their vertical edges by returns, as well as 1:6 scale shear walls subjected to lateral loading using wire cut bricks and 1:1/4:3 cement-lime-sand mortar. A series of tests on full scale structures was also performed and the authors concluded that although small differences in model and prototype stiffness were observed the behaviour of the model specimens closely resembles that of the prototype and in particular the failure mode and cracking patterns.

Kadir [Ref. 19] performed model-scale tests on brick masonry infill panels with the aim of developing an approximate solution for the calculation of strength and stiffness of infilled frames. Tests included 2 and 3 storey infilled frames where Kadir investigated the effects of aspect ratio, openings and lack of fit between the wall and the surrounding frame, on the behaviour of the model masonry. The results showed a fairly good correlation with his approximate analytical solution considering the reliability of the model tests.

Work on small scale modelling has been pursued for the past two decades at the Institute for Testing and Research in Materials and Structures (ZRMK) in Slovenia, former Yugoslavia. Research commenced in the early 70s after NATO donated and financed a one degree of freedom (horizontal) earthquake simulator which was installed at ZRMK and used for the dynamic modelling of unreinforced and reinforced masonry structures [Ref. 20 to 31].

Tomazevic [Ref. 27], gives a description of the various materials that have been used at ZRMK for the construction of small scale masonry buildings. By considering the limitations of the shaking table with respect to the maximum acceleration, operating frequency range and model-platform weight, scale factors and laws of similarity (section 2.2), 4 different types of bricks have been produced and used so far. The first one which according to the authors satisfies the laws of complete model similarity, was a purpose made unit (figure 3.3) consisting of pulverised fuel ash, perlite, fire clay, corundum dust and kalven (sodium tripolyphosphate), hand pressed in a special mould and kiln burned at 805^0C for one hour. These 1:7 scale units represented prototype light-weight ceramic hollow blocks (390x290x190 mm) and were used in the construction of four-storey plain masonry buildings [Ref. 20].

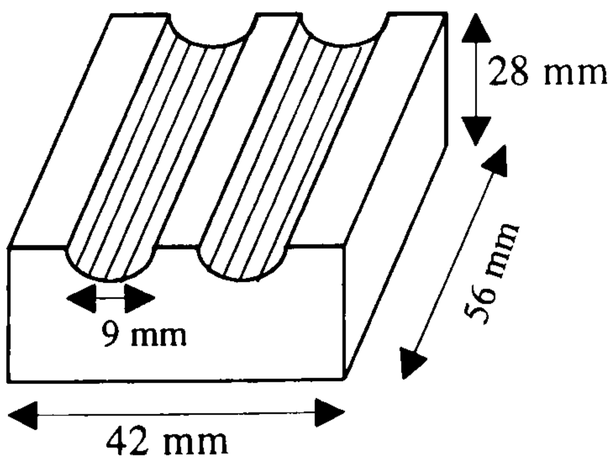

	Compressive strength (MPa)		Specific mass kg/m³	
Model bricks	1.90		11.30	
Model mortar	1.03			
	Compressive strength (MPa)	Tensile strength (MPa)	Elastic modulus (MPa)	Shear modulus (MPa)
Model masonry	1.25	0.11	532	87

Figure 3.3 ZRMK brick [Ref. 20] **Table 3.1 Mechanical properties [Ref. 20]**

The mechanical properties of the units and model masonry determined by standard tests are shown in Table 3.1. The authors used a mortar consisting of quartz sand and fire

clay which could retain its mechanical properties constant after drying. The semi-circular channels on the upper side of the units (figure 3.3), were used in later stages to accommodate reinforcement made out of aluminium wire of 1.0 mm diameter. Tests on prototype masonry assemblages (e.g.. specific mass $\gamma = 1.5$ kg/m^3, compressive strength f_c = 5 MPa), revealed that the complete model similarity laws set out at the planning stage, were not fully satisfied. The dimensions of the four storey model building which was composed of two wall panels in each storey pierced with door and window openings, were 712x427 mm in plan and 1392 mm in elevation, with walls being 42 mm thick and the reinforced microconcrete floor slabs 30 mm thick. Additional mass was fixed onto the slabs consisting of four 10 kg lead bricks on each storey, providing a total of 160 kg of additional weight in an attempt to simulate the mass distribution along the height of the model.

One more additional fixture employed in the experimental testing performed at ZRMK was the prestressing of the walls with steel ropes. According to Tomazevic and Velechovsky [Ref. 27] if a model which does not comply to the complete model similarity laws (*true model* - section 2.3) is required to reproduce the correct failure mechanisms when subjected to simulated seismic loading, then the working stresses in the walls should be reproduced as adequately as possible. Additional mass which is fixed on the slabs is not always enough to complement self-weight and any further addition of extra weight will affect the similarity in mass distribution. In order to overcome this problem they used a technique which involves prestressing of the walls with flexible steel ropes fixed to the top slab and anchored into the foundation of the model. Soft springs are used at the top end of the ropes to keep the prestressing forces virtually constant while the model is subjected to shake table horizontal displacements. In the case of the model described above and tested by Tomazevic [Ref. 20], twenty ropes of 1.5 mm diameter induced a total prestressing force of 10 kN, which increased the level of normal stresses in the ground storey walls to 20 per cent of their compressive strength. Calculations and testing showed that this technique does not alter the dynamic behaviour of the model or the magnitude of base shear developed during the shaking tests. A preliminary study involved testing individual walls under constant vertical and cyclic lateral loading with the aim to reproduce similar cracking patterns

and failure mechanisms (shear, flexure), and according to the published results a satisfactory correlation on the load-deflection relationships and hysteresis envelopes has been observed. Finally the complete model building was tested under simulated earthquake loading. The ZRMK shake table is driven by means of a two-way acting programmable hydraulic actuator with a static capacity of ±160 kN and displacement capacity of ±125 mm. Displacements and accelerations were measured by means of LVDTs and accelerometers located at each storey level (LVDTs mounted on a reference frame, accelerometers mounted on the concrete slabs). Small amplitude sinusoidal excitations were applied and the shape and frequency of the first natural mode were obtained. The input motion was programmed in the shape of the El Centro 1940 earthquake (N-S component) but due to limitations on the driving power of the actuators the El Centro ground accelerations could not be reproduced accurately. Moreover the simulator could not cause collapse of the model by means of earthquake excitations. As a result sinusoidal excitations with a frequency which followed the decaying natural frequency of the model were applied in an attempt to cause collapse of the structure. Throughout testing two S-8 movie cameras were used to record failure mechanisms and to provide a photographic history of the collapse for publication purposes. The building was modelled by means of a four degree of freedom shear system with masses concentrated at floor levels and storey hysteresis envelopes (storey mechanism model - shear walls with pier action, [Ref. 25 and 26]) defining the non-linear behaviour of the system. By adopting this procedure the seismic resistance analysis of any masonry building can be reduced to the problem of calculating the lateral load-lateral displacement hysteresis envelope of the critical storey of the building which is the sum of the idealised hysteresis envelopes of all the walls in the critical storey. The validity of the storey mechanism model, which is greatly dependent on strength and stiffness deterioration phenomena, was demonstrated during this test. Further work to validate this model is continuing.

Another type of brick used at ZRMK for several experimental investigations [Ref. 21-22-23], has the shape of the 6-hole block shown in figure 3.2 and follows the laws of simple model similarity (section 2.2). Prototype light-weight perforated blocks were cut into corresponding 1:5 scale model blocks and used for construction of plain

and reinforced masonry models. The modelling factors adopted in these studies are presented in table 3.2.

Physical quantity	**Modelling factor**
Strength (f)	1
Strain (ε)	1
Equiv. viscous damping (ν)	1
Displacement (d)	5
Force (F)	25
Time (t)	5
Frequency (ω)	0.2
Velocity (v)	1
Acceleration (a)	0.2
Specific mass (γ, kg/m^3)	0.73 (1.0)
Compressive strength (f_c, MPa)	0.84 (1.0)
Tensile strength (f_t, MPa)	1.25 (1.0)

Table 3.2 Modelling factors (1:5) [Ref. 21]

The mortar used for construction of the walls and for grouting of the reinforcement was a 1:2:9 mixture of ordinary portland cement lime and fine sand (aggregate size 0-2 mm). Microconcrete with 1:3 cement-sand (aggregate size 0-4 mm) proportions together with commercially available fully annealed wire was used for construction of the concrete members. These materials with properties shown in Table 3.3, were used in the construction of 8, three storey to a 1:5 scale masonry buildings.

Tomazevic and Modena [Ref. 21] tested two of the models, studying the seismic behaviour of reinforced masonry systems. The first represented a mixed structural system with peripheral masonry walls and a central reinforced concrete column. The second model, which was used for comparison, had a centrally placed cruciform-shaped masonry wall instead of an r.c. column. Models were augmented by an additional 300 kg mass at each floor level, and a prestressing force of 48 kN was induced on the walls by steel ropes via soft springs, in order to satisfy similarity conditions as

explained earlier. Three different sets of synthetic numerically generated accelerograms (derived from Eurocode 8 response spectra) were used to program the earthquake simulator. The results confirmed the behaviour of mixed masonry building systems subjected to simulated earthquake loading and conclusions were drawn on ductility demands, flexural capacity and out-of-plane resistance of reinforced masonry walls. In summary the authors conclude that vertical and horizontal reinforcement of the walls improves and enhances ductile behaviour and eliminates out-of-plane phenomena. For peak ground accelerations not exceeding 0.25g such buildings will behave elastically, whereas for accelerations up to 0.4g limited damage without collapse is anticipated.

Mechanical properties	**Model**	**Prototype**
Compressive strength of blocks (MPa)	9.45	(not available)
Compressive strength of mortar (MPa)	1.8-2.7	5-7.5
Compressive strength of concrete (MPa)	23-28	25-30
Compressive strength of masonry (MPa)	6.33	5.3
Tensile strength of masonry (MPa)	0.4	0.5
Modulus of elasticity of masonry (MPa)	6,450	4,500
Tensile strength of reinforcing steel	382 (ϕ 6 mm)	450-540 (ϕ 6-12 mm)
Tensile strength of reinforcing steel	448 (ϕ 4.2 mm)	

Table 3.3 Mechanical properties of model materials (average values) [Ref. 21, 22]

Modena and Tomazevic [Ref. 22] and Tomazevic et. al. [Ref. 23 and 24], tested the remaining masonry building models. These differed in their construction from the first two. Four of the models were tested [Ref. 22] as a continuation of the co-operative research program described above, and confirmed that the procedures adopted were satisfactory. The conclusions of this block of work were aimed at validating the effectiveness, reliability and accuracy of small scale model testing. The authors claim the results were more than satisfactory.

The final two models were similar to the ones described earlier, number 7 incorporating a mixed structural system of horizontally and vertically reinforced

masonry walls with a central r.c. column and number 8 using the same structural system but with unreinforced masonry walls. Only the main characteristic details of the prototype building were modelled in order to simplify the construction process. The brittle behaviour of the unreinforced masonry building model under seismic loading was evident both visually and with respect to the measured quantities (hysteresis loops). Some irregularities appeared in the failure mechanisms which were thought to be a result of the simplifications introduced in the construction and modelling process. The model with reinforced masonry walls behaved much more consistently demonstrating increased ductility under repeated severe shaking. This was also evident from the hysteresis loops obtained for the model at the ultimate state.

The third type of material used by ZRMK researchers [Ref. 28 and 29] to replicate stone masonry buildings in accordance with model similarity laws was local natural stone. It was crushed and cut into small size pieces (6 - 8 cm in diameter). Low strength mortar (f_c=1.23 MPa) consisting of portland cement, lime and sand (aggregate size 0 - 2 mm) in the proportion of 0.5:4:12 was used to construct stone-masonry buildings to a 1:4 scale.

In the first study Tomazevic et. al. [Ref. 28] constructed and tested 2, two-storey stone masonry building models, in order to investigate the influence of floor rigidity on the seismic behaviour of historic masonry buildings. In the first model wooden floors without tie-beams were used while in the second one, these were replaced by massive reinforced concrete slabs. At the scale of 1:4 the driving capacity of the actuators proved to be not enough to reproduce the complete loading history, so the weight of the models was reduced by modelling only part of the building. The layout of the two models was identical and also the configuration was similar to two larger models tested by Benedetti and Castoldi [Ref. 31]. The properties of the model masonry obtained from standardised testing procedures are shown in table 3.4 together with the corresponding prototype ones obtained by in-situ and laboratory tests on existing masonry walls in both original and strengthened state. According to the authors these in-situ and laboratory tests cannot be considered reliable. Uniaxial compression as well as cyclic lateral loading tests were performed on small specimens (prisms-walls), to

obtain stress strain curves and load-deflection hysteresis loops for both model and prototype. Although differences between model and prototype material properties precluded complete model similarity, the authors concluded that since the shear strength of the model masonry (which greatly influences the failure mechanism under such loading conditions) was successfully modelled, the similarity laws could be applied regardless. The models were instrumented with LVDTs, accelerometers and SVHS cameras. They were subjected to a simulated earthquake loading history based on the modified N-S component (peak ground acceleration 0.43g) of the Petrovac record. Modes of vibration, storey stiffness and seismic resistance were calculated for both models and their response was correlated in order to observe the differences in the behaviour under shake table testing caused by structural configuration characteristics.

Quantity	**Model**	**Prototype 1:4 scale**	**Prototype - actual**	
			Original	**Cement-grouted**
f_c (MPa)	0.77	3.08	0.3-0.9	0.6-3.7
f_t (MPa)	0.049	0.25	0.02-0.19	0.19-0.33
E (MPa)	489	1,956	200-1000	800-3000
G (MPa)	168	672	70-90	100-450
Γ (MPa)	2,143	2,143	2,200	2,200

Table 3.4 Mechanical properties of model and prototype materials [Ref. 31]

In the second study by Tomazevic et al [Ref. 29], 4 additional models were tested in order to enhance the experimental findings of the above two tests. Models 3 and 4 were identical to the ones described earlier (Tomazevic et. al. [Ref. 28]) while the second two models 5 and 6 had a different floor system. Model 5 had wooden floors which this time were tied to the peripheral walls and model 6 had a brick vault ground floor with a wooden floor on the second storey. Results verified the conclusions drawn in the previous study and further recommendations were made with regards to the rigidity of the floor system in use. Methods for assessing the influence of floor rigidity on the seismic response of historic stone-masonry buildings were proposed.

The final brick type was used by ZRMK researchers in an extensive recent study [Ref. 30] on 1:2 scale reinforced masonry walls. This was a concrete unit very similar in shape to the Standard block shown in figure 3.2. The blocks had a flatwise compressive strength of 15 MPa and were used in conjunction with a similar perforated block (same strength but much smaller cell dimensions), for the construction of 32 reinforced masonry model walls. A 1:3.5 cement-sand mortar (compressive strength f_c=14.4 MPa) was used for laying the blocks and grouting the model reinforcement. The reinforcement consisted of 10 mm and 6 mm diameter deformed steel bars (*yield stress* f_y=522 MPa and 253 MPa respectively) placed in the vertical holes of the perforated blocks and on each horizontal mortar bed-joint. Masonry prisms were loaded uniaxially and a value of f_c=5.2 MPa was obtained for the compressive strength of reinforced masonry. The walls (figure 3.4) were tested as simple cantilevers anchored to heavy reinforced concrete foundation blocks. The tests involved application of lateral load generated by a programmable hydraulic actuator acting at mid-height of the bond beam, while constant vertical load was applied by means of another one-way hydraulic actuator of 500 kN capacity. Both of the hydraulic jacks were fixed to an adjacent stiff steel frame. This reduced vibrations to the recording instruments during testing.

Four different types of lateral displacement time-histories and two different levels of constant vertical load (which are described below), were applied to the models both statically and dynamically in an attempt to compare and evaluate the differences observed in the seismic behaviour of the reinforced walls and study the influence each of the components had on the test results:

- monotonically increased displacements,
- cyclic lateral displacements with increased amplitudes (in 3 intervals),
- cyclic lateral displacements with uniformly increased displacement amplitudes,
- simulated displacement response of a masonry building to an earthquake.

Shear and bending were the basic failure conditions observed on the walls. Diagonal cracks originated first in the mortar joints and propagated into the concrete blocks as loading increased. The final failure involved splitting and crushing of the blocks and buckling of vertical reinforcement took place at the top edge of the walls (vertical load

of 60 kN), and shearing and crushing of the blocks within the weakest course of the wall (vertical load 120 kN).

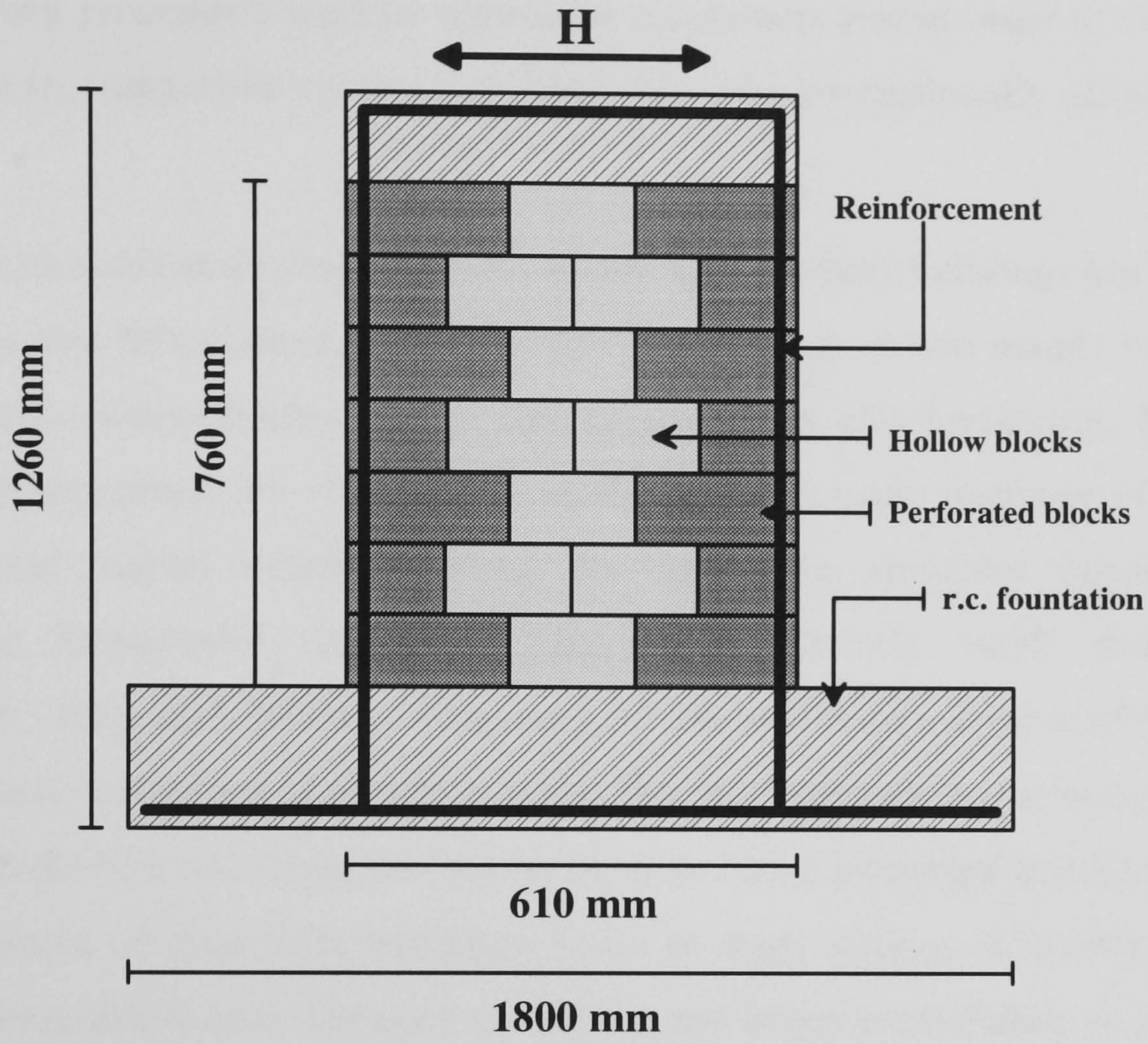

Figure 3.4 Physical description of model reinforced masonry walls [Ref. 30]

Although results obtained from this work are only applicable to the specific type of masonry used, the authors underline the fact that qualitative conclusions described below are valid in general:

► The vertical load applied to the models which simulates the working stresses induced in prototype walls in buildings, determine the type of failure mechanism and the lateral resistance and ductility of the walls.

► Monotonic and cyclic loading histories produce different results, with an increase observed in the lateral resistance and ductility in monotonic tests (both static and dynamic).

► When cyclic loading procedures are applied, lower values of lateral resistance and higher ductility factors are obtained statically than dynamically.

According to the authors, design methods based on experimental results are dependent on the loading procedures used by individual researchers and in order to compare and correlate these, compatible testing procedures should be internationally adopted.

Work on small scale modelling of concrete and masonry buildings has been going on since the mid 80's at the Aristotle University in Greece. It was mainly concentrated on reinforced concrete frames infilled with typical Greek clay brick units. Manos et al [Ref. 32-33] examined the influence of infills on the seismic response of reinforced microconcrete framed structures, using the earthquake simulator installed at the Engineering Department laboratory. This is a relatively small shaking table (1.2 x 1.2 m - max. load 1000 kg - frequency 0.1 Hz to 100 Hz), capable of reproducing one horizontal component of ground motion. The test structure shown in figure 3.5 is a 1:7 scale model of a two storey reinforced concrete frame prototype building which is a typical example of residential buildings found in many regions in Greece. Buildings like these were extensively damaged during the last major earthquakes, (e.g. Kalamata earthquake with a magnitude of 6.2 on the Richter scale and peak ground horizontal acceleration of 0.27g). Two models with identical geometry were constructed, one with plain bars used as reinforcement and one reinforced with cold-deformed bars manufactured in the workshop. Bars of 2.9, 2.4 and 0.8 mm diameter were used respectively to reinforce the columns, beams and slabs of the model. Model solid clay bricks, with average dimensions of 20x30x40 mm and compressive strength of 5.3 MPa, were supplied by a local manufacturer and used for infilling the frames of the first model in both storeys. For the second model only the top storey had brick walls but with additional door openings. In this part of the study the bricks were secured in place using special wedges and not mortar, since the authors needed to reuse the units for subsequent tests. Additional weight was fixed to the slabs of the models in order to fulfil the similitude requirements for mass density and dead load. The model was instrumented by mounting accelerometers and displacement transducers at various points on the structure depending on the type of loading applied. First a *static tilt test* was performed, where the model rests on a platform that can be rotated around a

horizontal axis thus introduced static lateral loads at the two slab levels where the lead mass was anchored. A *low level impulse loading* was also applied using a hammer at various positions on the model. A *sweep test* was later introduced to the model which involved fixed amplitude and varying frequency sinusoidal excitations. Finally *simulated earthquake motions* were applied derived from prototype ground motion records (El Centro 1940, Kern County 1952 and Parkfield 1966), and scaled with respect to time by a factor of 2.706. Frequencies, displacements, accelerations and failure mechanisms, were recorded for both models and were used to define their response to the various loading histories.

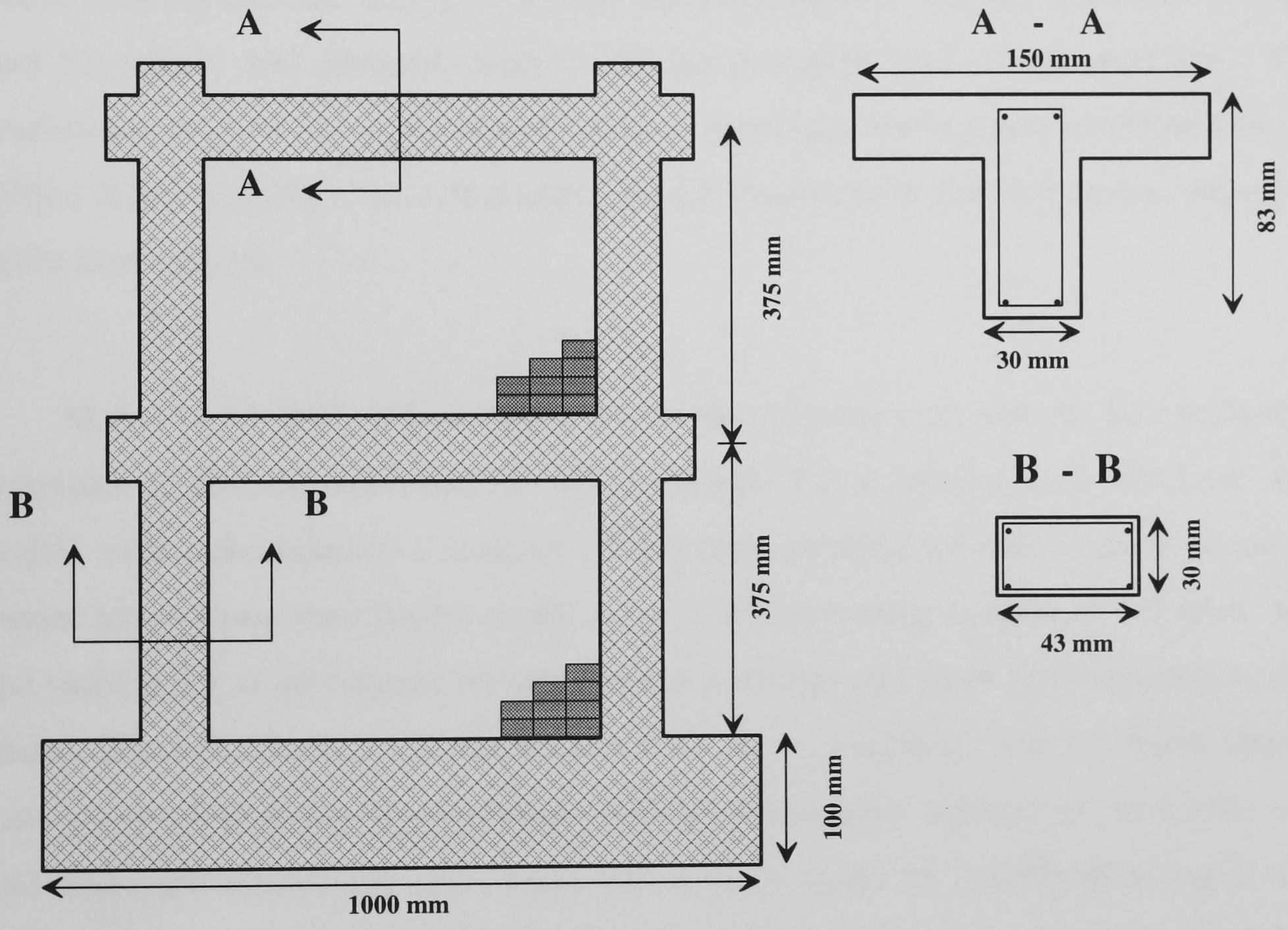

Figure 3.5 Model details [Ref. 32]

Since the models were constructed with many different configurations (asymmetric placement of masonry, wide openings, removal of walls at various stages and repair of damaged walls) using mortarless masonry and not tested up to collapse, valuable information with regards to their behaviour and response up to failure is not available

although the authors mention that this will be dealt with in a future study. Nevertheless, a substantial increase was noticed with respect to the stiffness of the structural system and is attributed to the masonry infills which improved the seismic resistance in general. After the experimental procedure was completed, a numerical study was performed on a four storey prototype r.c. building with similar building configurations to the models in an attempt to verify the conclusions drawn from the laboratory tests. The building was severely damaged during the Kalamata earthquake with damage concentrated mainly on the r.c. columns and shear walls of the ground floor (open air garage with no infills), as well as the external masonry infills of the first storey. The ETABS and DRAIN2D/85 computer programs which replicate masonry infills with a special 'bracing element' incorporating the compression strut method (section 3.3), were used for elastic and inelastic analysis of the prototype and model structures. The conclusions verified the experimental findings, especially the increase in stiffness of the infilled frame and the extent of damage on r.c. members in the first storey where no infills were present.

Manos et. al. [Ref. 34] continued where the previous work left off, by conducting experimental tests on individual r.c. infilled frames but in smaller scale this time. The models were constructed to a scale of 1:9 but were identical in other respects to model frames tested some time before at the same laboratory using a scale of 1:3 [Ref. 35]. The latter acted as prototypes for comparison purposes and were in themselves scaled models of actual prototype frames of typical Greek r.c. buildings. The 1:9 model frames were constructed using microconcrete with a compressive strength of 19.6 MPa and cold deformed reinforcing steel bars with a yield stress of 232.45 MPa. Solid clay bricks (20x30x40 mm as before) were used for infilling the frames, (6-hole horizontally perforated clay bricks were used in the 1:3 scale study which represent common units used in Greece). Three unit course prisms and 172 mm square panels were used to determine compressive (0.93 MPa) tensile (0.18 MPa) and shear (0.35 MPa) strength of the model masonry. Although the target was to accurately reproduce the 1:3 scale models major discrepancies were observed. Firstly the 1:3 model masonry was 50 percent stronger in compression and 24 percent stronger in tension. The mortar bed joints were also modelled incorrectly according to the authors. Discrepancies like these were also present in the 1:3 scale model infilled frames [Ref. 35] where for example the

brick units and reinforcing bars were not modelled according to the laws of similitude applicable to a scaling factor of 1:3 (relative to prototype walls 1:1). Dimensions in the 1:9 scale models were reproduced quite accurately, and the same can be said for the microconcrete and reinforcement used in the construction of the models (figure 3.6). This accuracy is reflected in the damage patterns and hysteresis loops obtained for both 1:3 and 1:9 bare frame models when subjected to a cyclic response history applied horizontally at the top by means of a hydraulic actuator. The infilled frames were subjected to the same loading procedure as the bare frames and the cracks distribution at ultimate load visibly confirmed the consequences of deviation from model similarity laws. The cyclic shear capacity of the 1:9 masonry infill frames exceeded by 15 to 30 percent the corresponding 'prototype' behaviour and this according to the authors is caused by the 23 percent deviation on the shear strength between the models and the thickness and geometry of the mortar joints. It should be noted that modelling concrete and especially masonry in such a small scale (1:9) is very difficult to achieve without consequently sacrificing accuracy.

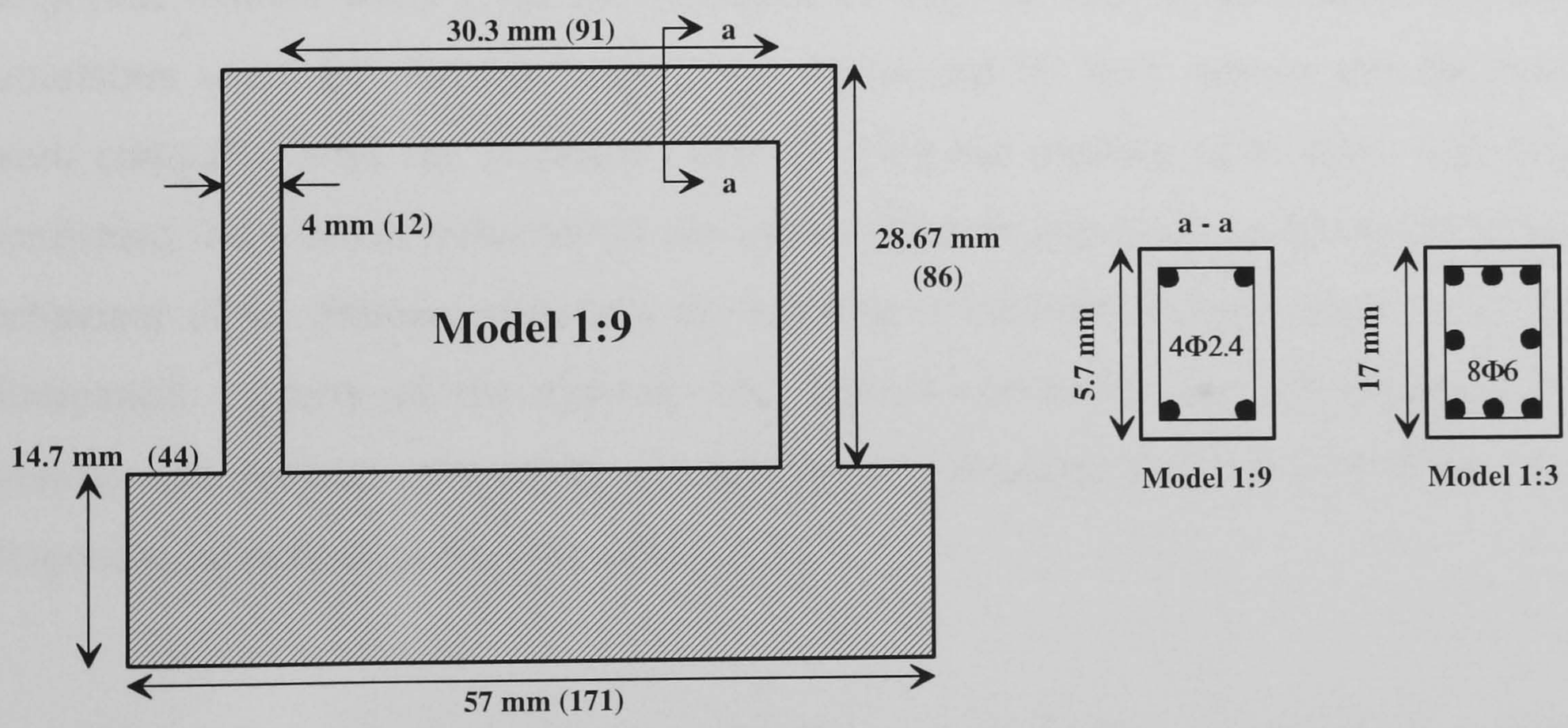

(Numbers in parentheses indicate corresonding dimensions for 1:3 scale model)

Figure 3.6 Details of reinforced concrete model wall [Ref. 34]

In a further study conducted by Manos et. al. [Ref. 36] model frames like the ones used before ([Ref. 32] and figure 3.5) were tested to verify the diagonal strut theory for masonry walls acting as infills in reinforced concrete frames, a theory which is explained in more detail in section 3.3. Two 2-storey, 1:7 scale reinforced microconcrete model frames were constructed, both having identical configurations. The first one had actual diagonal struts installed on the main diagonals of the frame bays, whereas the second one had infill walls with the same clay bricks used in the previous two studies. For the first model 3 different configurations were investigated, one where 8 prestressed struts (4 for each storey-two in each bay) were installed on the bays laying on the axis of the excitation, one with 8 unprestressed struts as before and one with 4 prestressed struts (2 for each storey-one in each bay). The models were then subjected to shaking table base motion which represented the El Centro 1940 N-S record, properly scaled to conform with similitude requirements. The second model had clay brick infill walls in line with the axis of motion and contrary to the previous study these were constructed with a cement-lime mortar. This model was subjected to low amplitude random white noise and simulated earthquake loading histories. A numerical simulation using ETABS (as before), was performed for both models and the results were compared with the response obtained from the shaking table tests. The study confirmed the positive influence of the infills (either masonry or struts) on the seismic behaviour of r.c. frames, especially the increase in stiffness and the improved energy dissipation capacity of the system. The authors concluded that the diagonal strut analogy can provide reasonably accurate results, provided that the properties of the diagonals are defined correctly (section 3.3).

The earliest reported work on small scale masonry in the United States is reported by Benjamin and Williams [Ref. 37] and Yorulmaz and Sozen [Ref. 38]. Benjamin and Williams conducted a series of tests using small scale specimens with standard solid and 1:4 scale bricks, including two-brick shear couplets, model brick masonry cantilever walls and brick walls built into strong frames in order to examine the shear strength of masonry with and without precompression. Yorulmaz and Sozen performed similar tests using 13.5 x 21.8 x 47.5 mm bricks. About 10 years later, Drexel University started investigating small scale masonry within the framework of a research program that still continues today. This research program is devoted exclusively to hollow

concrete block masonry using 1:4 scale units which were supplied initially by the US Masonry Association and later manufactured in-house. The methodology for direct small scale modelling was developed by Harris and Becica [Ref. 39] in the late 70s, when based on their limited preliminary tests they concluded that direct modelling of concrete masonry is feasible.

An extensive research programme was initiated a few years later by applying the techniques developed in Ref. 39, to masonry assemblages under various loading conditions. Hamid et al [Ref. 40] investigated the behaviour of concrete block masonry under axial compression. They tested 49 model prisms and the results were correlated to full scale tests performed a few years back at two different laboratories. The technique of *true modelling* was applied, following a dimensional analysis study. The units (average compressive strength of 25 MPa) were manufactured in-house by a block-making machine, to a scale of 1:4 in respect to actual prototype units (figure 3.7).

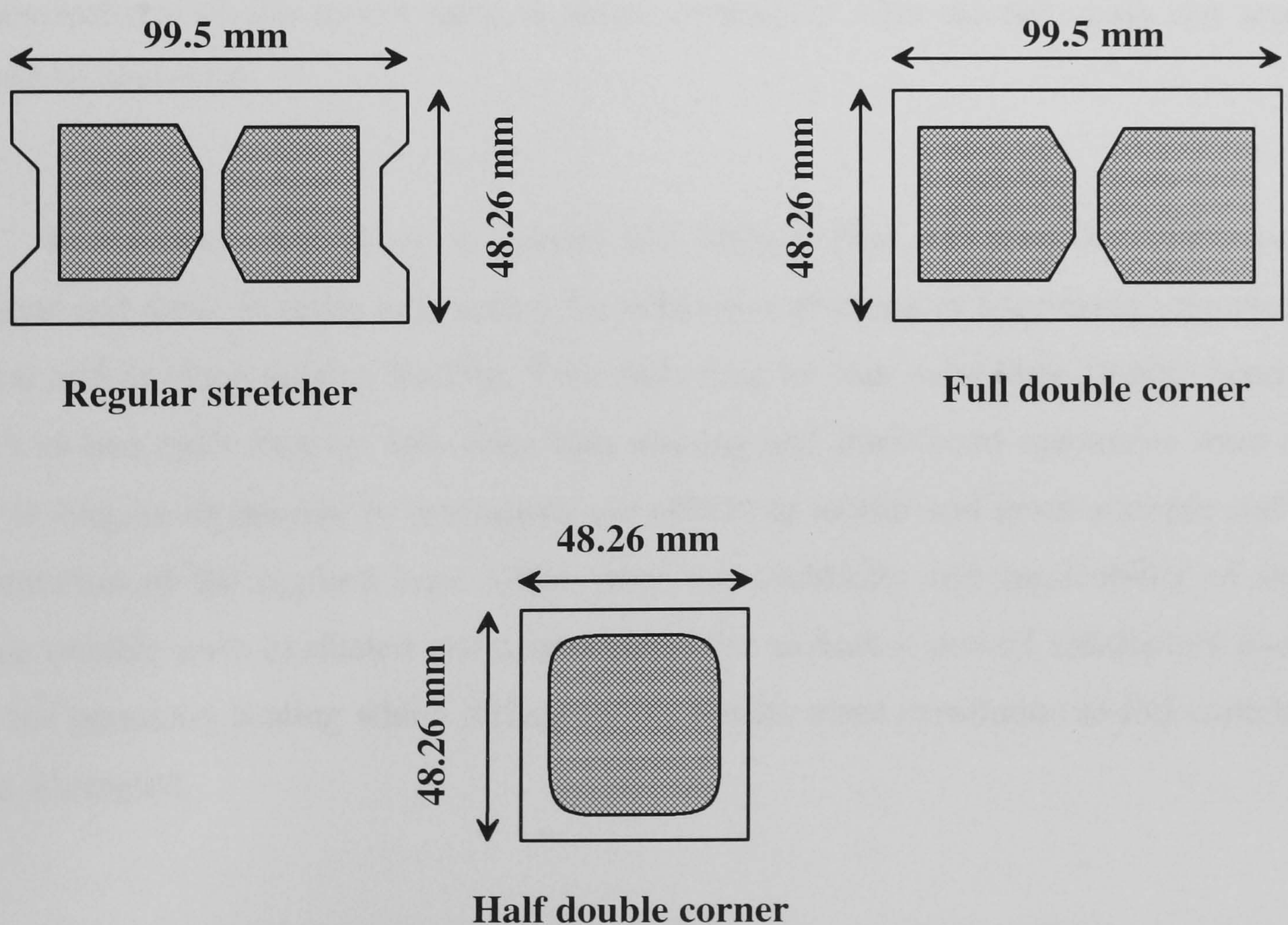

Figure 3.7 Configurations of model blocks [Ref. 40]

In order to scale down the joint thickness to 2.5 mm, three different mortar mixtures consisting of fine sand, cement and lime were used, having a compressive strength of 6.2-11.9 MPa (based on 51 mm air-cured cubes). Three different grout mixtures were also used in order to fill the block cells as required for this type of masonry construction. Masonry assemblages consisting of three courses high by one course wide prisms made out using the half block units, and two three and five courses high by one course wide assemblages, made out using the other two units shown in figure 3.7, were cast in order to examine the influence and effect of the aspect ratio. The effect of bond type was also examined (running versus stack), as well the effect of mortar and grout strength. The results revealed many parameters that could influence the compressive strength of concrete masonry small scale prisms, such as the modelling of the joint thickness and the effects of platen restraint. Correlation to full scale specimens showed discrepancies that were attributed to the fact that the geometry of the blocks was not modelled accurately due to the difficulties in fabricating the units. The authors conclude that this type of modelling is feasible and with a more refined scaling of the geometry characteristics of the model units, a better correlation with the full scale test results could be achieved.

In a follow up publication, Hamid and Abboud [Ref. 41] used the same blocks, mortar and grout in order to examine the behaviour of masonry specimens subjected to shear and in-plane tension loading. Two units long by four units high running bond, as well as two units long by two units high running and stack bond specimens were cast for testing, in an attempt to investigate the effects of mortar and grout strength and the orientation of the applied load. Once more the feasibility and applicability of small scale models were evaluated and according to the authors it proved satisfactory except for the geometry scaling which influences the results when correlation to full scale tests was attempted.

In a later study by the same authors [Ref. 42], the block-making machine was modified and as a result, accurately 1:4 scaled units were fabricated. The same assemblages used in the previous two studies were again constructed and tested under identical loading conditions. A better correlation was observed this time, which was

also attributed to the improved workmanship techniques used during construction and testing, providing the authors with a more reliable method for examining the complex behaviour of concrete masonry using small scale specimens.

Abboud, et. al. [Ref. 43 and 44] continued investigating small scale modelling techniques, by performing a series of tests on masonry wall-to-floor connections under gravity loading and slender reinforced masonry walls under monotonic and cyclic out-of-plane loading, using the same materials as in the previous studies. An excellent correlation between model and prototype results was observed.

Further investigation in direct small scale modelling at Drexel University continued when Larbi and Harris [Ref. 45 and 46], tested nine 1:3 scale rectangular block masonry shear walls, under in-plane monotonically increased and reversed cyclic loads. All the specimens were also subjected to an axial precompression of 1.9 MPa. The walls had two boundary elements consisting of a top reinforced concrete beam and a bottom reinforced concrete footing, which both served to connect the walls to the test set-up. The behaviour of the specimens was governed by diagonal tensile cracking or flexural failure depending on the amount of vertical and horizontal reinforcement. The modelling technique was verified by comparing model and prototype results which were in good agreement. The advantages of using small scale models, such as reduced capacity loading equipment and reduced space requirement for setting-up the experiments, were according to the authors "the biggest assets in small scale modelling".

Under the same research objective, Ghanem et al [Ref. 47] tested fourteen, 1:3 scale partially reinforced masonry shear walls under in-plane lateral loads with and without precompression in order to study the effects of axial precompression on the behaviour of the walls.

The same masonry blocks manufactured by the block-making machine at Drexel, were used by Harris et. al. [Ref. 48] in an investigation on the seismic retrofitting of

lightly reinforced concrete frames using masonry infills. Microconcrete model reinforcement was used for the construction of the three storey model. The frames were cast horizontally in order to eliminate the procedure of beam-column joint construction. The frames were infilled 60 days after casting, and subjected to lateral loads by means of a "Whiffle tree" arrangement where a hydraulic jack is connected to a distribution network of beams that applies the loading to all three stories evenly. Vertical loads were also applied to the columns at the top storey by means of gravity loading and a beam multiplication system. An inelastic analysis was performed on the building using the IDARC program, which is capable of modelling among others, infill shear walls, cracking in concrete members and inelastic deformations caused by yielding of the reinforcement. The infills greatly increased the lateral resistance and reduced the drift of the concrete frames, although an undesirable catastrophic mode of failure occurred in one of the columns attributed to the strength of the infill materials. The authors concluded that the masonry infill should be anchored to the bounding frame to force failure to take place in the masonry, without a premature shear/flexure failure in the columns. According to the authors, the reduced scale models were successful in modelling infilled frames and therefore should be investigated further.

Research into small scale modelling with applications to the seismic response of concrete masonry buildings was initiated at the University of Illinois in 1985 as part of the "U.S. Co-ordinated Program for Masonry Building Research" [Ref. 49 and 50]. It was Task 7.1 of the program, which involves physical modelling of masonry components and building systems. Abrams, Paulson et. al. [Ref. 51-52-53] tested a number of 1:4 scale three storey structures (figure 3.8), using reduced scale reinforced masonry and reinforced microconcrete. The units used (2″x2″x4″), were exactly one-quarter of the size of a typical 8-in. (203.2 mm) standard block shown at the top of figure 3.2, and were manufactured by a local supplier using a model press machine in the manner used for full-scale blocks. Mortar and grout were also scaled down with respect to aggregate size. Reinforcement was scaled down by using 3.07 mm diameter gage wire. The mechanical properties of the model masonry were established by standard tests but were not of primary importance, since no prototype was represented in this study. Nevertheless the properties were essential in the design of the structure and the interpretation of the test results. Compressive strength and modulus of elasticity

of the model masonry were measured using three-course high prisms, while a flat-wise compression test was performed to determine compressive strength of the blocks.

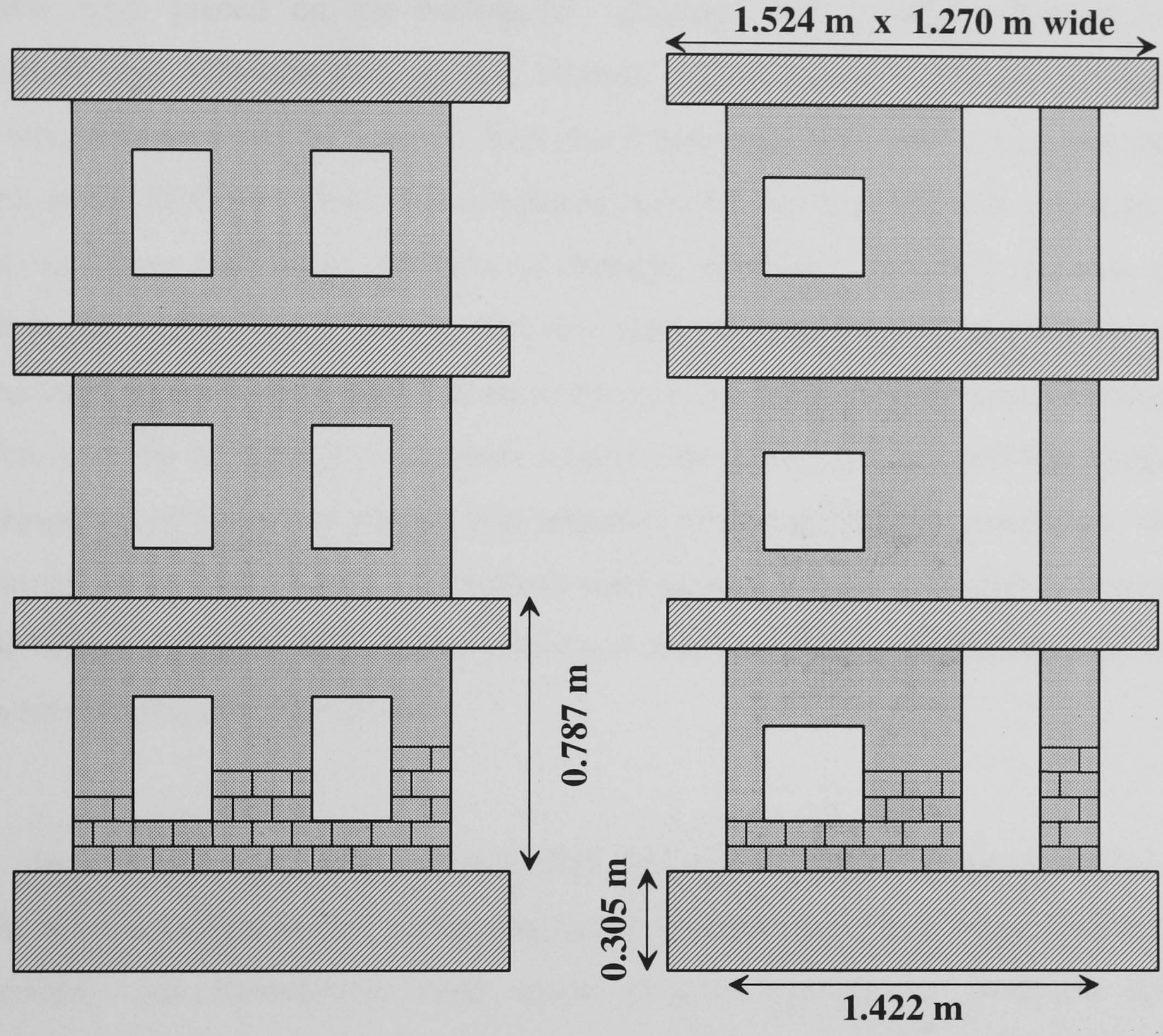

(All dimensions in metres, both models identical except window openings)

Figure 3.8 Structural configuration of 1:4 models [Ref. 53]

Square reinforced masonry panels were placed in a testing machine and subjected to compressive forces applied along a diagonal axis based on ASTM E 519-74 [Ref. 88]. Using this method plots of nominal shear stress versus shear strain can be obtained thus allowing the determination of the shear modulus of model masonry. According to the authors this test was used to estimate the shear capacity of the central pier of the building, since it is non-representative of the type of strain of such a pier particularly

after cracking. Weights were added to each of the three storey levels to simulate inertia forces. The time scale and the amplitude of the input motions were scaled down, but not in accordance with the scaling of the building components. The authors claimed that this was not necessary as no prototype was available for comparison. The two identical models were placed on the earthquake simulator and initially subjected to low amplitude free vibration tests so that changes in the natural frequency and apparent viscous damping could be detected. This was followed by simulated earthquake motions based on the El Centro 1940 N-S component record. The intensity was varied to cause light, moderate and heavy amounts of damage. From the observed response of the models the authors point out the fact that crack patterns are visual evidence of the correctness of small scale models even in the case where no prototype tests exist against which to verify it. Aspects of dynamic response measurements can provide insights for development of numerical models and adoption of strength design procedures. Overall the acceptability and precision of reduced scale models have been demonstrated even in such complex cases as three storey perforated masonry building structures subjected to simulated earthquake excitation.

In a more recent study Abrams [Ref. 54], tested a series of unreinforced brick walls in order to demonstrate the assumption that unreinforced masonry elements do not necessarily fail immediately after cracks develop even under sustained loading. Although the tests were performed on full scale walls extracted from an old building the results are thought to be of value to this research project. The walls had a low aspect ratio and were constructed with unreinforced brick and strong mortar. Lateral forces were applied in-plane while a constant vertical compressive strength was maintained throughout. Another two walls were constructed using reclaimed common bricks and subjected to cyclic lateral loading for comparison purposes. The walls exhibited a substantial deformation capacity beyond initial cracking up to three times their ultimate strength. The results were correlated with an evaluation procedure proposed by the author that uses an analytical solution to estimate the post-cracking ultimate strength of masonry flexural elements.

Research work on the subject of small scale masonry (assemblages, shear walls and infill panels) is not limited to the aforementioned academic institutions. A few more scientific papers and research reports with some relevance to this work will be presented below, in an attempt to provide a global view of recent and current research activity on the subject.

Maidstone [Ref. 55] performed tests on 1:6 scale microconcrete and brick infilled frames subjected to monotonically increased lateral loading applied in-plane to the corners of one of the main diagonals (racking loads). Empirical equations were proposed for estimation of the stiffness and strength of masonry infilled frames based on the equivalent diagonal strut concept.

Klinger and Bertero [Ref. 56] tested reinforced concrete infilled frames in a 1:3 scale under quasi-static loads, in the first stage of a research program initiated at the University of California at Berkeley studying the effects of infills on the seismic resistance of reinforced concrete frames. An analytical investigation using the ANSR-I computer program, was used to predict the behaviour of the models and to compare with the experimental results. An additional element was written and incorporated in the program based on the equivalent strut concept to predict the behaviour of the infill and surrounding frame. It should be noted that the authors used the strut concept using formulas proposed by Maidstone [Ref. 55], to determine the width of the equivalent strut.

Brokken and Bertero [Ref. 57] tested 18, 3 1/2-storey by 1 1/2-bay reinforced concrete frames to a scale of 1:3, infilled with panels constructed from various types of infilling materials, thus continuing the research program set out in the previous reference. The frames were loaded axially at the columns by two hydraulic jacks that simulated the dead and live loading present in a prototype. A horizontal jack that provided monotonic and cyclic loading histories, was attached to the top storey of the frame. In the report an extensive review of the behaviour and response of each of the 18 tested frames is included together with accompanying figures. Conclusions were directed towards the behaviour of infilled frames compared to bare frames, the

influence of the loading history and the overall seismic resistance of infilled concrete buildings.

Page [Ref. 58] and Dhanasekar et. al. [Ref. 59-60-61] tested a total of 186 (360 mm) square panels constructed by half scale bricks laid in stretcher bond with a 1:1:6 cement, lime and sand mortar. A special loading rig was manufactured consisting of a set of flexible steel brush platens acting as bearing surfaces and two hydraulic jacks placed in orthogonal directions, in order to subject the panels to a state of biaxial stress under monotonically increased loads. The failure modes of panels with different bed joint orientations were studied under biaxial compression and combined compression-tension states of stress. It was found that the mortar joints influence the failure mode of the masonry panels, and that in order to properly define failure under the states of stress commonly found in masonry infill walls, a three-dimensional failure surface was required. The failure surface proposed by the authors together with the basic stress-strain relations (normal, parallel and shear) derived from the tests were incorporated into an iterative finite element model capable of predicting displacements stresses and failure of brick infilled frames. The adequacy of the numerical model was verified by testing a series of half scale model infilled frames (dimensions of 1495 mm long by 995 mm high), consisting of cold formed steel channel sections welded in such a way as to form an I section surrounding brickwork with 5 mm mortar joints all cast horizontally (mortar joint between frame and infill-8 mm). A monotonically increasing racking load was applied until consistent cracks formed in the infill. The excellent correlation between the experimental and the analytical investigation gave the authors the confidence to propose that the finite element model could be more widely used in parametric studies of brick infilled frames.

Dawe et al [Ref. 62] tested ten 1:3 scale models of masonry infilled steel frames, under shake table sinusoidal excitations. A typical test model consisted of a welded steel portal frame made from 50 mm wide flat bar stock enclosing a clay brick masonry panel. The panels were 943 mm long by 929 mm high and 60 mm thick. The concrete base consisted of 1:1.5:3 cement, sand and course aggregate mixture. The model masonry consisted of reduced size clay bricks measuring 90 x 60 x 55 mm

(compressive strength not available) and ASTM S-type mortar with a compressive strength of 21 MPa (51 mm cubes) and tensile strength of 1.4 MPa (*briquettes*). The joints were modelled with a scale factor of 2 (5 mm) due to fabrication difficulties. Two lead bricks of 100 kg each were placed on the two top corners of the frame to simulate according to the authors the mass of the supported floor. In addition, the authors connected the two masses with a rigid timber bar in order to apply rotational rigidity to the upper corners of the frame. A sinusoidal motion was applied to the frame with increasing frequency and acceleration until the wall was destroyed. For the walls with restrained rotations at roof level (timber beam) a shear mode of failure was observed together with sliding of the units. For the walls with no timber beam on top a flexural mode of failure with cracks mainly at the base and local failure at the top corners was observed. An analytical study was performed for the walls based on three simple models and programmed for use on a digital computer. The first one was a single degree of freedom model, the second one was based on the compression strut theory and the third on the braced frame model (these are described in section 3.3). The authors concluded that the first (SDOF) and third (braced frame) models perform reasonably well while the compression strut model could not provide satisfactory results with respect to the linear and nonlinear response of the frame. This contradicts the conclusions drawn by other researchers [Ref. 36], on the performance of the equivalent strut theory in the elastic range of response.

Liauw and Kwan [Ref. 63] tested two 1:3 scale four storey high reinforced concrete frames infilled with concrete and brick walls in order to compare their responses. Although the individual response of each model is apparently consistent with that of other researchers, a comparison between the two model configurations failed to produce any conclusive results due to the limited number of the experiment.

Jurukovski, Alessi et. al. [Ref. 64 and 65] constructed and tested three 1:3 scale models of reinforced concrete frames infilled with brick walls, under various simulated earthquake histories. The 4 storey models were designed according to the laws of *complete-model* similarity, using reduced scale bricks (80x80x40 mm) which were produced by a local manufacturer. Reinforced concrete, steel reinforcement and mortar

were also modelled using the 1:3 scale factor. Simulated earthquake loading was applied by two hydraulic actuators on a biaxial 5x5 m shake table. The purpose of this work was to investigate two different strengthening techniques, (r.c central core and r.c. jackets applied to the external walls). The building replicated typical Italian concrete-masonry structures located in earthquake prone regions. The authors conclude that both the two techniques used during the experiments could provide a cost effective solution and would increase seismic safety because of their high energy absorption capacity.

3.3 Review of analytical methods.

The behaviour of masonry under different states of stress ranging from the most simple case of uniaxial compression to the more complex one of dynamic lateral loading is far from understood. All the failure theories developed so far are based on the fundamental properties of the constituent materials. Brick masonry under compression fails due to an interaction of the bricks and mortar joints which have different deformation characteristics, while failure of masonry under tensile or shear stresses is related to the bond between the two materials. The interaction of units and mortar in brick masonry has been the subject of many investigations. However the experimental procedures adopted by the various researchers could by no means could considered consistent. This incompatibility in the laboratory testing to determine the fundamental properties of the materials, is reflected in design codes which vary greatly from country to country. Theory of elasticity and finite element models have been proposed but there seems to be a disagreement as to their ability to predict the behaviour of masonry assemblages subjected to independent compression, tension, or shearing stresses. Based on the above it is difficult if not impossible, to predict the behaviour of brick infilled frames where masonry is subjected to combined, complex states of stress. Applying the theory of elasticity using finite element analyses, has been adopted but its success is limited by the uncertain boundary conditions between the infill and the surrounding frame. These limitations have led investigators to adopt empirical and approximate solutions to define the behaviour and to determine the strength and stiffness of masonry walls. What

follows is essentially a descriptive survey of the various analytical methods currently available. The basic concepts and assumptions of these methods are outlined. Introduction and comments are also made on the failure and resistance mechanisms of masonry assemblages.

3.3.1 Masonry assemblages.

3.3.1.1 Stack bond prisms.

A stack of bricks bonded together with mortar represents the most basic subassemblage and should demonstrate the behaviour of masonry under compressive stress. When a masonry prism is loaded with a uniaxial compressive force the constituent materials having different properties (strength, stiffness) tend to expand laterally which results in triaxial compressive stresses in the mortar joints and bilateral tensile coupled with axial compressive stresses in the bricks. This rather complicated state of stress [Ref. 66] shown in figure 3.9, eventually results in a tensile vertical splitting failure with cracks passing though the bricks and mortar at the narrow faces of the masonry prism. Although the exact characteristics of this failure mechanism are still debated upon [Ref. 68 and 69], the final mode of failure of masonry prisms is widely accepted and has been proved experimentally to be consistent from both small and full scale tests. Computational models have been developed [Ref. 67-68-70-71] with the more recent ones [Ref. 68] taking into account the effects of non-linearity of the mortar.

3.3.1.2 Masonry panels.

Infill panels subjected to in-plane loads are intended to primarily resist shear forces (assuming that correct detailing was taken into account during the design process, which is rarely the case). Real shear walls have to develop resistance mechanisms which account for axial load and bending as well as shear forces. The

mechanism of failure observed in infilled frames, reveals that like shear walls the masonry in infill walls is in a state of biaxial stress.

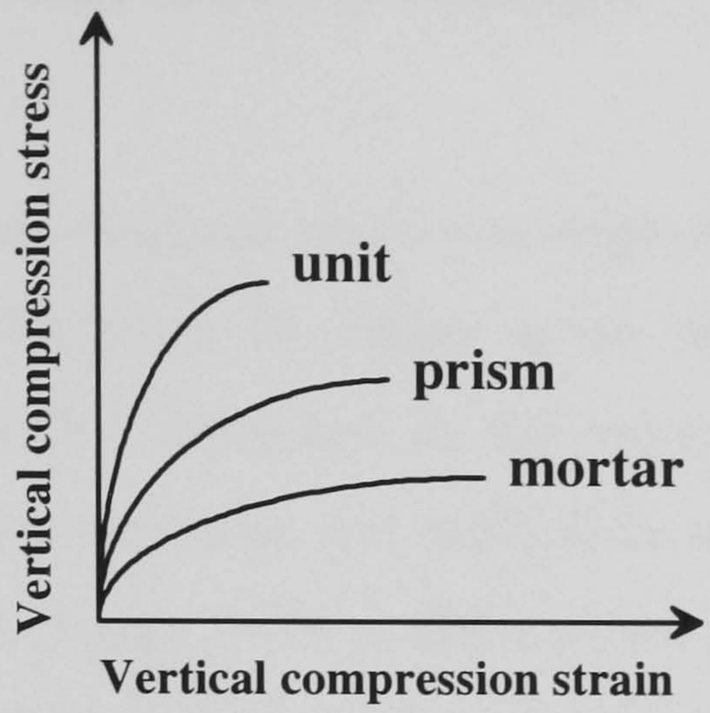

Stress strain relationship for prism and constituent materials

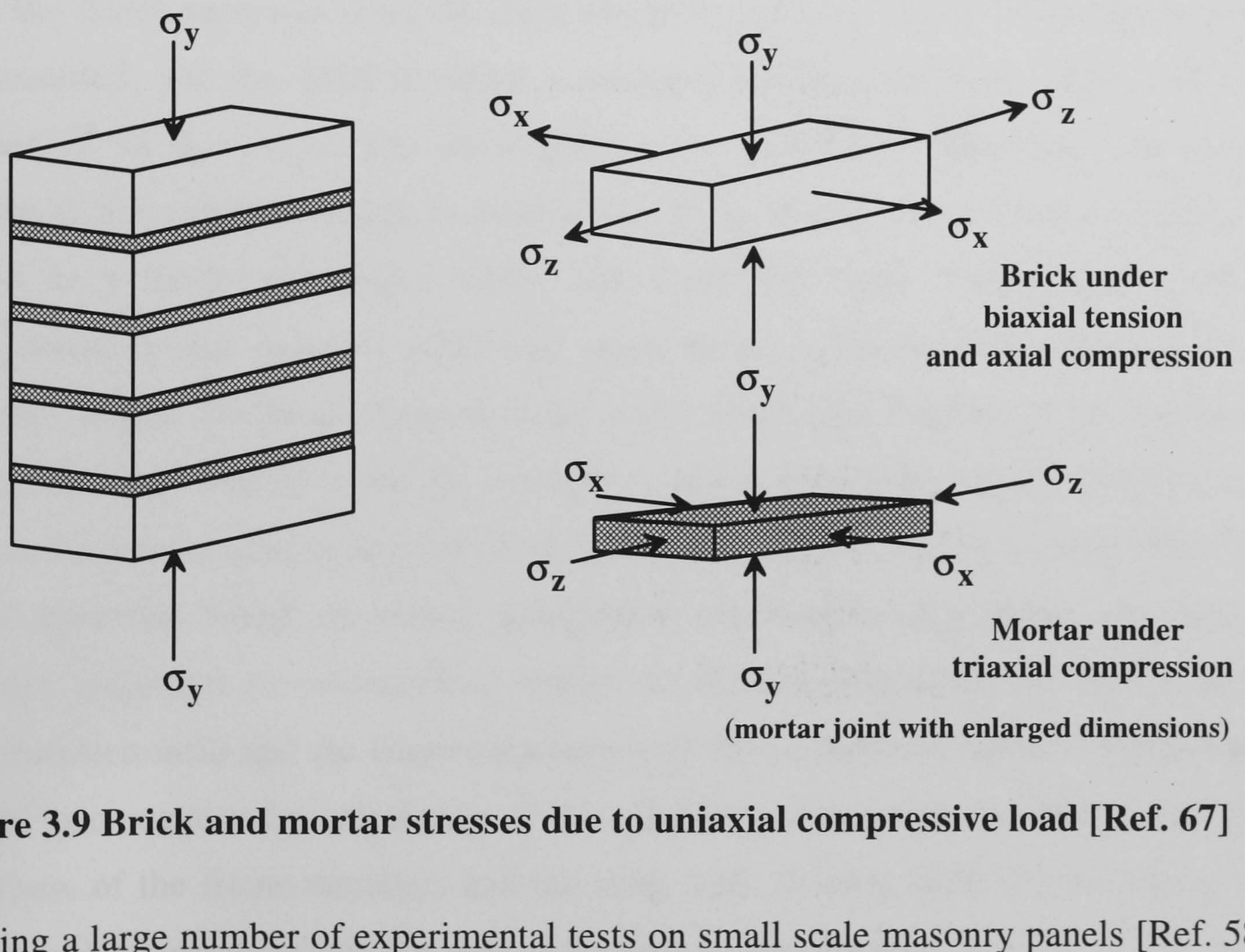

Figure 3.9 Brick and mortar stresses due to uniaxial compressive load [Ref. 67]

Following a large number of experimental tests on small scale masonry panels [Ref. 58 and 59], Page et. al. have developed three-dimensional failure surfaces for solid brick masonry stressed in orthogonal tension-compression, in terms of stresses normal and parallel to the bed jointing planes. A finite element model based on this general failure criteria for brick masonry has been written and implemented with very promising results [Ref. 60].

3.3.2 Infilled frames.

3.3.2.1 Equivalent diagonal strut concept.

The concept of equivalent diagonal struts was originally proposed in the mid 50s by Polyakov and later investigated by many other researchers. It provides an approximate solution but is highly dependent on the properties of the equivalent strut and the contact provisions between frame and infill. Considering a masonry infill wall under repeated lateral loading (figure 3.10) in full contact with the surrounding frame, the concept can be explained and its limitations identified. For low levels of loading a composite action between the frame and the infill wall takes place where the infill contributes at its maximum to the stiffness of the system. At increasing levels of lateral loading the frame separates from the infill except in the two corners where the forces are transmitted, and the infill develops a diagonal compression zone which can be converted to an equivalent strut having the same geometric properties. The strut according to the original concept is idealised as being pinned at the corners (frame is idealised as a pin-jointed truss), whilst effectively the frame beam-column joints restrain rotations thus inducing additional shear forces at the columns. Shear cracks appear that reduce the lateral stiffness of the wall and the effectiveness of the diagonal compression strut. Failure could be a result of many parameters which are directly related to the fundamental properties of the masonry materials. Stafford-Smith [Ref. 72 and 73] used the 'beam on elastic foundation' formulation (free beam on elastic foundation subjected to concentrated loads), to develop equations for the contact lengths between infill and the frame members near the compressed corners. Maidstone [Ref. 55] also suggested a calculation of the effective width based on observations of the stiffness of the frame members and the infill wall. Smolira [Ref. 74] introduced a braced frame approach where the only difference to the previous concept is that the frame members are connected rigidly. The author performed a limited number of tests to verify his approach but he concludes that further tests would have to be performed for the method to be used with confidence for analysis of infilled walls. Dawe et. al. (section 3.2.2 [Ref. 62]) successfully used the approach by Smolira to predict the response of flexible steel infilled frames up to the initial stages of nonlinear response.

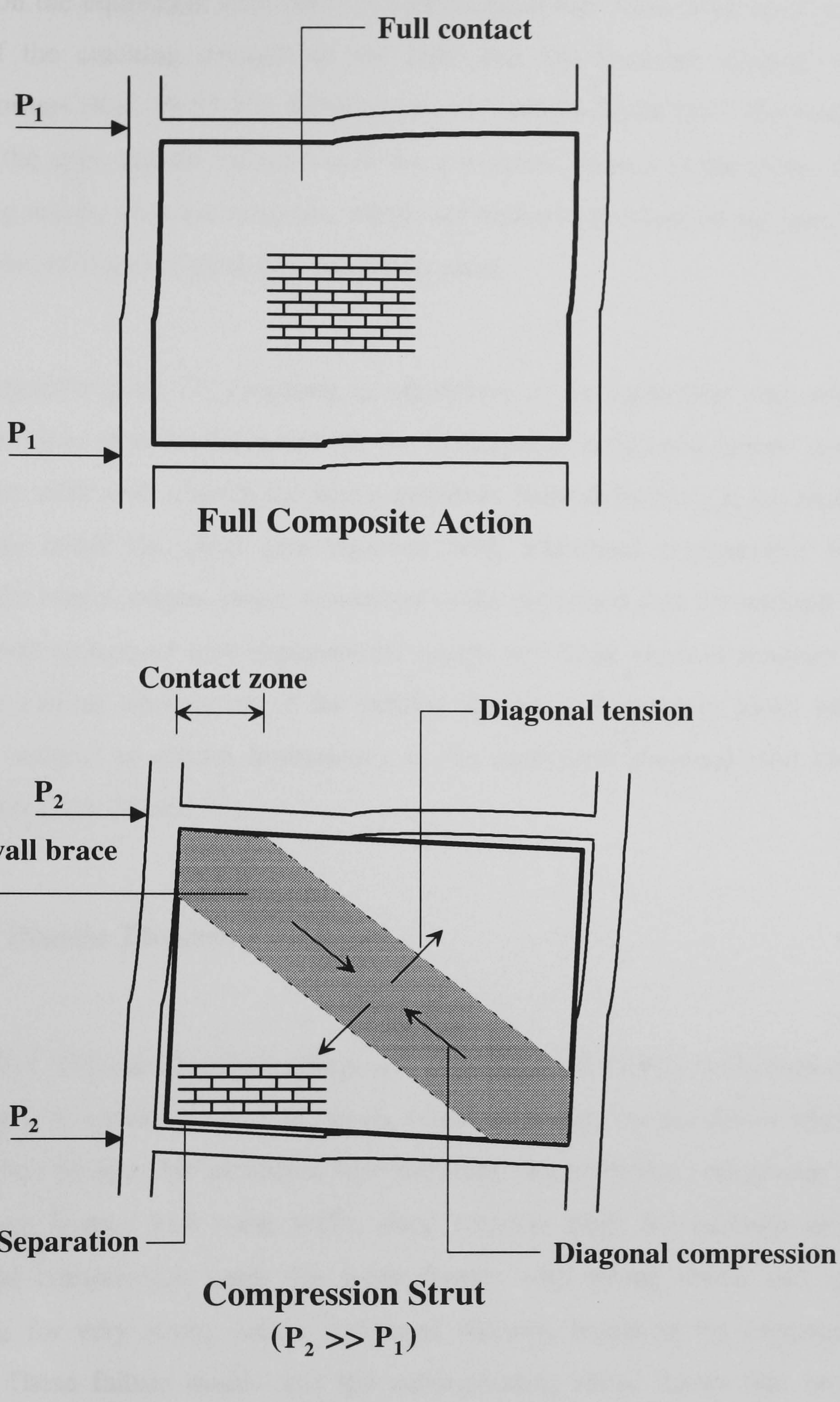

Figure 3.10 Compression strut concept [Ref. 78]

Based on the equivalent strut concept various equations have been proposed for calculation of the cracking strength of the infill and the crushing strength at the compressed corners [Ref. 19-55-75]. Riddington and Stafford-Smith [Ref. 76] produced equations for the approximate calculation of the maximum stresses at the centre of the infill following results of stress analyses, which are highly dependent on the geometric properties of the infill and in particular the aspect ratio.

Thiruvengadam [Ref. 77] proposed an alternative to the equivalent strut method namely the multiple strut model based on the assumption mentioned before that the forces from the infill wall restrain the frame members from deforming at the zones of contact and as result the infill gets confined with additional compressive forces generated by the beam-column joints. According to the published data the multiple strut model is in good agreement with experimental results and finite element analyses with respect to the natural frequencies of the infilled frames and certainly looks like an improvement (subject to certain limitations), to the equivalent diagonal strut models described earlier [Ref. 55 and 73].

3.3.2.2 Plastic Theory.

Wood [Ref. 79] was the first to propose a plastic theory for the evaluation of the ultimate strength of unreinforced infill panels, based on results by Maidstone [Ref. 55] on model infilled frames. He identified four different failure modes (composite shear mode for strong frames with weak walls, shear rotation mode for medium strength walls, diagonal compression mode for weak frames with strong infills and corner crushing mode for very strong panels and weak frames), based on his experimental observations. These failure modes and the corresponding shear forces that produce collapse can be evaluated in terms of the frame bending strength and the crushing stress of the wall. The theoretical predictions however show a large scatter when compared to experimental results by different researchers on full and model scale frames and according to Wood this is due to a lack of plasticity of the masonry infills. Liauw and Kwan [Ref. 80], suggested that the discrepancies arising in Woods' theory might be a result of the excessive friction assumed at the interface and the neglect of separation in

the composite shear mode. The authors identify three failure modes for single storey frames depending on the stiffness of the frame elements and the infill wall (corner crushing with failure in columns for strong infill and weak columns, corner crushing with failure in beams for strong infill and weak beams and diagonal crushing at the corners with subsequent failure at the joints in the frame for weak infill and strong frame). The predictions of this theory agree rather well with experimental results on model brickwork, and a similar simplified method according to the authors could be applied in multi-storey infilled frames.

3.4 Finite element method.

Analytical investigations using the finite element method can be divided into two main categories. The first one includes dedicated computer codes written and used primarily as research tools to study the behaviour of masonry assemblages following an experimental investigation. The second is based on commercially available packages with in-built or user-supplied constitutive material models. The main advantage of a commercial finite element package is that it is widely available and can be employed by a number of researchers for comparison purposes. Since such a program (chapter 6) was used for computer simulations performed in this thesis, more emphasis is placed on these rather than the first type described. Most of this type of analytical research work has been produced during the past 6 to 8 years and this has to be attributed to the wealth of experience now available from computational predictions of reinforced concrete which are now at an advanced stage.

Two of the most important modelling problems in finite element analyses are the uncertain boundary conditions for the masonry infill and the brick-mortar interface bond at the head and bed joints. In purpose-written programs these parameters are mainly derived from experimental testing of masonry assemblages where in commercial packages concrete constitutive models are sometimes used with user modified properties. In most cases Mohr-Coulomb elastic-plastic constitutive models are used for modelling the bricks and mortar joints. The bond between the panel and the

surrounding frame is usually modelled with *gaps* or joint elements having linear or nonlinear properties. Chiostrini and Vignoli [Ref. 92] performed a nonlinear analysis of masonry walls under horizontal loads using the commercially available ANSYS package (Swanson Analysis Systems Inc.). Bricks were modelled individually while mortar was represented using gap-elements and in a second attempt a larger structure was modelled with elements that included many bricks and mortar joints, for reasons of simplifying the mesh discretisation.

Saadeghvaziri and Mehta [Ref. 93] modelled an unreinforced masonry wall subjected to axial compressive loads and in-plane horizontal loads applied along the full length at the top of the panel, under displacement control with the main research objective concentrated on the modelling of the crack sensitive mortar joints. A user-supplied model based on a set of shear and normal spring joints was incorporated into ANSYS and the authors concluded that the model was reliable enough to be used for further parametric studies in cases where experimental results are not available.

Rots and Lourenco [Ref. 94] used results from assemblage tests (prisms, wallettes, couplets) to evaluate the masonry mechanical properties for subsequent modelling of masonry shear walls using the DIANA finite element package developed and marketed by the Dutch Building and Construction Research Centre-TNO. Each brick of the shear wall was modelled using eight 8-noded plane stress elements while the mortar joints were modelled using 6-noded line interface elements. The authors state that the component properties are detrimental to the success of analytical modelling in complex systems such as masonry structures where behaviour is governed by so many different parameters which cannot be overlooked or simplified.

Vermeltfoort et. al. [Ref. 95 and 96] employed the UDEC finite element program (Itasca Consulting Group Inc.) for modelling square masonry shear walls. As before small scale assemblages were used for the determination of the material properties together with full scale tests on walls subjected to horizontal loads applied along the top edge. The fundamental properties of the masonry components and assemblages (compressive and tensile strength, modulus of elasticity and Poisson's ratio, bond

strength and finally fracture energy which is defined as the amount of energy to create one unit of area of a crack along the brick-mortar interface - chapter 6), were considered as the most important input parameters to the program if successful simulation of cracking patterns, failure modes and ultimate strength was to be achieved. Preliminary conclusions indicated similarity in the cracking patterns and load displacement curves between experimental tests and finite element analyses with the only discrepancy found in the ultimate shear load the walls were able to resist (twice the experimental value) but this was attributed to the material modelling of the brick units which did not include strain softening effects (chapter 6).

Molyneaux [Ref. 97] used the DYNA3D finite element package (marketed by Oasys - Ove Arup Computer Systems) to study the behaviour of non-structural masonry walls under impact loading. In this investigation bricks and mortar were modelled separately and since failure was expected at the joints, these were modelled as interface elements with a tension and shear cut-off criterion and post-cracking friction properties. The cracking patterns were represented successfully but no results were provided with regards to ultimate strength. The author argues that the dynamic strength of mortar which is greater than the corresponding static strength, should be measured experimentally for inclusion in any further analytical studies.

Cerioni et. al. [Ref. 98] used the ADINA finite element package together with a purpose-written computer program with quadrilateral elements and elastic-plastic linear materials properties to study the dynamic behaviour of unreinforced masonry panels and to compare the results between the two programs. In the first instance the authors analysed a masonry panel that was experimentally tested by Mengi and McNiven (University of Californa at Berkeley-1987). Although the experimental testing involves two identical walls connected at the base and the top where the additional mass was attached the finite element model was based on a single panel. It was divided into quadrilateral symmetrical elements with no provision for mortar joints. Separations between adjacent nodes were formulated for the brick elements allowing the modelling process to employ a denser mesh. Furthermore Cerioni et. al. assumed the constituent materials properties of the experimentally tested walls, due to lack of appropriate

information but at the end a very good correlation was observed with regards to the time-displacement and acceleration histories of the walls in comparison.

Finally, Combescure et. al. [Ref. 99] used the CASTEM 2000 (developed by the French Atomic Energy Commission) finite element code to study the behaviour of masonry infilled frames under cyclic horizontal loading, based on experimental test results available and in progress in several European laboratories, under the objective set-out by the recent European Commission funded research project HCM-PREC8. This involved individual masonry infilled frames as well as complete three-bay, four-storey structures. More emphasis is placed on the contact modelling between panels and frame members (perfect and unilateral frictionless contact). This is not in line with experimental results which demonstrate that the contact length is influenced by the relative stiffness of the panel and frame, the overall size and the applied loading pattern (monotonic or cyclic). These in their turn, affect the strength, cracking and failure mode of the composite system. The masonry walls were modelled as a homogeneous media governed by elastic or non-linear constitutive relationships. Strain softening effects were included in the formulations based on modification of the shear stiffness value (chapter 6) once cracking occurs. Although the authors acknowledge the simplifications of the frame-panel contact hypothesis, they recommend further developments to improve the modelling and in particular to account for the deterioration of strength and stiffness in masonry panels subjected to cyclic loading histories.

3.5 Conclusions.

This review has attempted to cover the whole spectrum of small scale masonry research and testing under seismic (quasi-static and dynamic) loading with a few examples of masonry subassemblages tested under static loading. The procedures commonly used involve tests under cyclic load provided by hydraulic, manual or programmable actuators. The loading is applied to masonry assemblages such as cantilever walls and infill panels of reinforced and unreinforced clay brick and concrete block masonry. Shake table studies are not common mainly due to their complexity and relatively high

cost. Cyclic loading testing although not representative of more general seismic action, can provide meaningful information regarding the detailed response and behaviour of masonry systems. Masonry research is not widespread, just a few academic institutions and research centres are devoted entirely to experimental and analytical studies. As a consequence the methods and techniques used, vary significantly and this tends to preclude useful comparisons.

The scale of the models investigated is dependent on the testing equipment available to the researchers. In general square and rectangular (but with high aspect ratio h/l) walls and infill panels in a scale of 1:3 to 1:5 are preferred, although construction in the Mediterranean region, South America and other parts of the world consists mainly of low aspect ($h/l < 0.8$) rectangular unreinforced masonry walls with relatively low strength compared to the surrounding reinforced concrete frames. Infill panels in these countries are rarely taken into account in the design and are considered only for interior partitions with no special construction consideration being given to the beam/column-wall connections. A poorly laid bed of mortar cannot be considered as a medium for integrating the wall to the frame or for allowing the flexibility of the wall to deform in combination or even independently to the frame members.

The physical modelling of masonry using the theory of dimensional analysis has at times provided satisfactory results, despite the fact that complete similarity has not been achieved. The artificial mass simulation technique used by all the researchers so far has proved to be an excellent way of conforming to similarity laws (inertia forces), by augmenting the mass density of the brick units when masonry is subjected to dynamic loads. The literature review failed to discover a case where a different approach has been used and subsequently no comparison can be made. An alternative was investigated as part of the experimental testing carried out in this research work (chapter 4).

The literature review revealed some more questionable points in the experimental determination of the fundamental properties of masonry both for full and small scale testing. There are still many tests performed on masonry materials and assemblages

around the world that employ different procedures and testing methods, thus revealing the diversities in current opinion with respect to the adoption of the fundamental properties in design calculations. One distinct example is the diagonal tensile test on small masonry panels and the degree of accuracy and representation it provides with respect to the prediction of the wall shear strength under in-plane horizontal loading (chapter 4).

The computer programs available for the analysis of masonry infill walls can only provide approximate solutions with respect to their cracking pattern, ultimate strength and energy dissipation capacity when subjected to seismic excitations. Modelling of the constituent materials has proved to be an immensely laborious task, mainly due to the differences in the deformation characteristics between bricks and mortar jointed together as a result of a chemical reaction that develops a bond at the interfaces and whose behaviour depends on many parameters that are complex to identify and measure. Research at experimental level can provide information and data that would improve, calibrate and enhance analytical constitutive relationships. This would increase the possibility of successfully modelling and simulating the behaviour of masonry when subjected to dynamic loading. In particular the behaviour following initial cracking as in this situation infill walls, are not considered to have reached their ultimate performance.

Chapter 4

Material Development and Static Tests

4.1 Introduction.

Experimental investigation of masonry infill walls functioning as frame partitions or shear resisting elements, has been conducted by a number of researchers using full or reduced scale physical models with different techniques for static-cyclic or dynamic load application. Work of this kind at full scale requires greater effort and large test facilities and can become very time consuming. A wide range of testing would be financially prohibitive. Small scale models offer significant advantages in both economic and technical terms as described earlier. These advantages should act as incentives to attracting more funding for research in masonry, which in turn will establish the material as a reliable structural element even in earthquake prone areas where masonry has long been excluded from use or not taken into account during the design process. Experimental results are required in order to access the performance characteristics of masonry systems as well as to develop and calibrate analytical models capable of predicting the complex behaviour beyond the elastic range. The constituent components must be characterised by properties established by using unified, standard test procedures. So far most, if not all, of the properties of masonry materials and subassemblages have been approximated using formulae derived from experimental observations and statistical analyses. The first part of the authors' work described in this thesis was concerned with the development of a prototype material for use in the subsequent testing program on model masonry shear walls. A comprehensive laboratory programme was devised and carried out to establish the properties of the constituent masonry materials and of the assemblages, the ideal model dimensions and the overall feasibility of the models for laboratory testing.

4.2 Modelling of masonry components.

4.2.1 Development and description of prototype bricks.

The development of a prototype small scale brick was carried out by a trial and error procedure. Different mixes were evaluated based on strength characteristics, unit weight and water absorption. The principal ingredients were ordinary portland cement, fine grading Leighton Buzzard sand, pulverised fuel ash and fine to medium lead shot. Sand was the major ingredient mainly due to its ability to provide a highly porous mix. The grading is shown in figure 4.1.

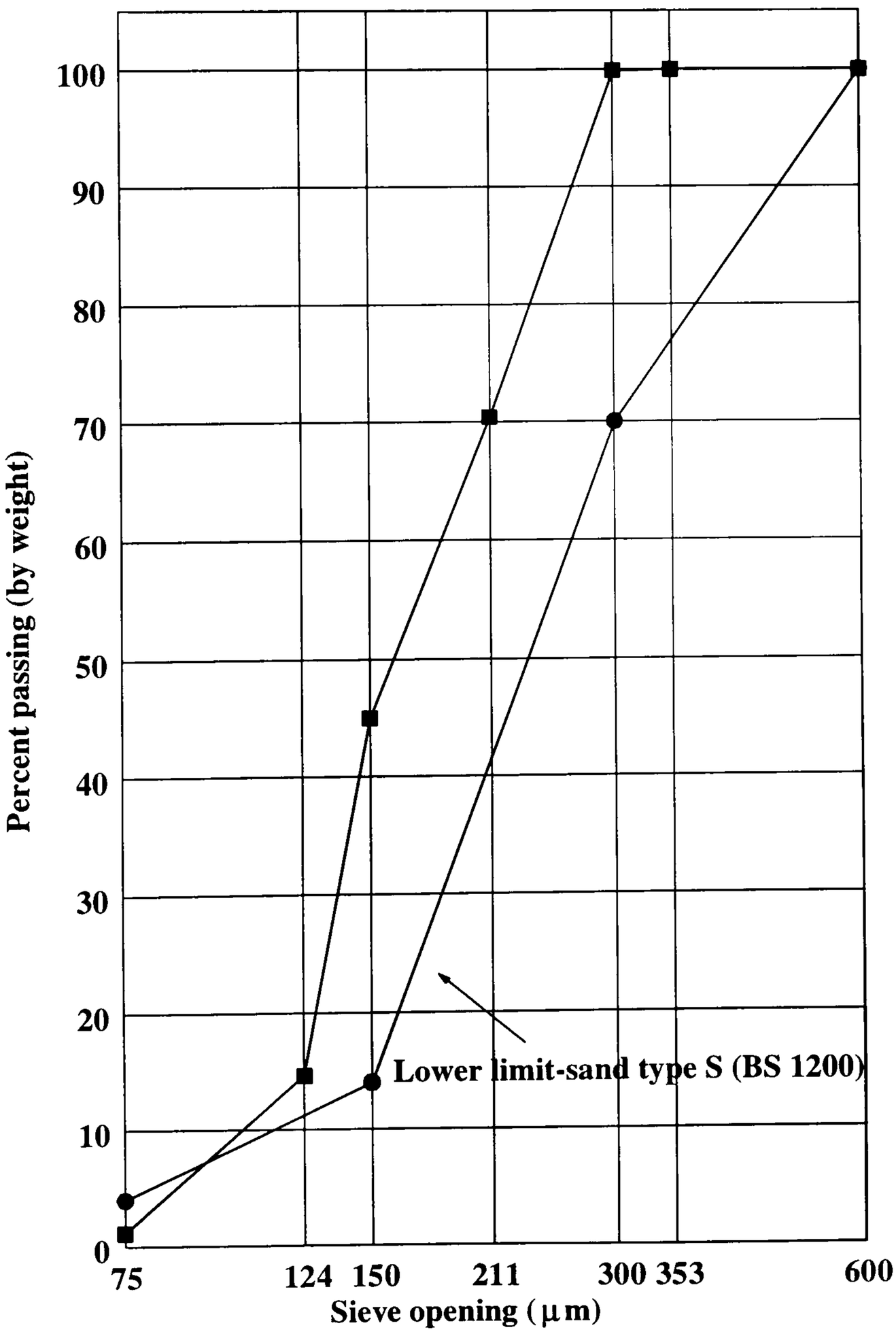

Figure 4.1 Grading envelope for sand used in brick and mortar making

Pulverised fuel ash (Pfa) was added to replace an equivalent amount of cement to produce the required low strength mixes. Cement was used as the main binding agent being the prime contributor to the development of strength. Finally lead shot was utilised in the second part of the material development to produce bricks with a significantly increased mass, while maintaining the same unit strength properties.

Altogether 16 different mixes were produced and these are summarised in table 4.1. Groups 1 to 9 represent the trial compositions for the ordinary brick mix while groups 10 to 16 for the alternative mix which included lead shot. The final two groups labelled as B6 and B15 (based on the previous groups 6 and 15 respectively), represent the two mixes that were chosen as the most suitable for subsequent mass brick production. The water/cement ratio does not follow any concrete mix design rules and was mainly determined upon workability during mixing and casting. Due to the large quantity of Pfa used, the water/cement-ash ratio is also given as an indicator. Several variations of the Pfa and sand content were made during the first experimental phase to achieve the two most suitable mixes for mass brick production. The tests also provided valuable information regarding the effects of increased ash and sand contents on the workability, bleeding or water retention and strength and stiffness properties of the specimens. For each trial mix nine 50 mm cubes and six 150x50x50 mm prisms were cast following the recommendations of British Standards (concrete mix design and mortar specifications) and other relevant publications regarding mixing, casting, demoulding and curing. The cube and prism dimensions were considered as the most appropriate for determining the strength and stiffness properties of 1:4 scale model bricks (section 2.5). The specimens were tested at 3, 7 and 21 days after casting, in order to establish the pattern for strength development with these unusual mix compositions. The cubes were tested under uniaxial compression using a CONTEST testing machine (table 4.2), while the prisms were predominantly used for the determination of the dynamic modulus of elasticity using the resonance frequency method. The density was calculated (figure 4.2) for all hardened specimens since brick unit weight was one of the basic requirements set out by the dimensional similitude theory (section 2.4) for masonry assemblages tested under dynamic loading conditions (table 4.3). When the finalised mixes were established, a displacement-control testing machine (DENISON) together with a computerised data acquisition system, were used

for the determination of the strength and stiffness properties of the model masonry materials.

GROUP 1	PFA/OPC : **1/1**	PFA-OPC/SAND : **3/1**	W/C : **0.73** W/CA : **0.36**
GROUP 2	PFA/OPC : **2/1**	PFA-OPC/SAND : **5/1**	W/C : **1** W/CA : **0.33**
GROUP 3	PFA/OPC : **3/1**	PFA-OPC/SAND : **7/1**	W/C : **1.71** W/CA : **0.34**
GROUP 4	PFA/OPC : **4/1**	PFA-OPC/SAND : **4/1**	W/C : **2.28** W/CA : **0.33**
GROUP 5	PFA/OPC : **6/1**	PFA-OPC/SAND : **1/1**	W/C : **1.67** W/CA : **0.33**
GROUP 6	PFA/OPC : **4/1**	PFA-OPC/SAND : **1/2**	W/C : **2.75** W/CA : **0.55**
GROUP 7	PFA/OPC : **4/1**	PFA-OPC/SAND : **1/2.5**	W/C : **2.50** W/CA : **0.50**
GROUP 8	PFA/OPC : **4/1**	PFA-OPC/SAND : **1/3**	W/C : **3** W/CA : **0.60**
GROUP 9	PFA/OPC : **4/1**	PFA-OPC/SAND : **1/4**	W/C : **3.57** W/CA : **0.71**
GROUP 10	PFA/OPC : **4/1**	PFA-OPC/SAND : **1/2.5** SAND/LEAD : **5/1**	W/C : **2.37** W/CA : **0.47**
GROUP 11	PFA/OPC : **4/1**	PFA-OPC/SAND : **1/3** SAND/LEAD : **3/1**	W/C : **2.75** W/CA : **0.55**
GROUP 12	PFA/OPC : **4/1**	PFA-OPC/SAND : **1/2** SAND/LEAD : **2/1**	W/C : **1.87** W/CA : **0.37**
GROUP 13	PFA/OPC : **4/1**	PFA-OPC/SAND : **1/3** SAND/LEAD : **2/1**	W/C : **3.2** W/CA : **0.64**
GROUP 14	PFA/OPC : **4/1**	PFA-OPC/SAND : **1/2** SAND/LEAD : **2/1**	W/C : **3.71** W/CA : **0.52**
GROUP 15	PFA/OPC : **4/1**	PFA-OPC/SAND : **1/1** SAND/LEAD : **1/2**	W/C : **2.71** W/CA : **0.38**
GROUP 16	PFA/OPC : **6/1**	PFA-OPC/SAND : **1/1.5** SAND/LEAD : **1/2**	W/C : **2.5** W/CA : **0.50**
GROUP B6	PFA/OPC : **4/1**	PFA-OPC/SAND : **1/2**	W/C : **2.51** W/CA : **0.50**
GROUP B15	PFA/OPC : **4/1**	PFA-OPC/SAND : **1/1** SAND/LEAD : **1/2**	W/C : **2.89** W/CA : **0.40**

OPC : Ordinary Portland Cement **PFA :** Pulverised Fuel Ash

W/C : Water / Cement ratio **W/CA :** Water / Cement and Ash ratio

Table 4.1 Mix compositions (proportions by weight)

GROUP	3 DAYS	7 DAYS	21 DAYS	28 DAYS
Group 1	28	32.6	50	-
Group 2	13.8	17.9	28.2	-
Group 3	6.2	9.7	13.6	-
Group 4	4.2	6.7	9.2	-
Group 5	5.2	7	10	-
Group 6	2.2	4.2	6.8	-
Group 7	2.6	4.7	7	-
Group 8	1.1	2	3.5	-
Group 9	0.7	1.6	3.8	-
Group 10	2.4	4.6	7.6	-
Group 11	1.5	3.2	5.5	-
Group 12	5	8	N/A	-
Group 13	0.6	1.5	6.2	-
Group 14	1.1	1.8	7.5	-
Group 15	2.1	3.5	8.5	-
Group 16	2.4	4.1	10.7	-
Group B6	-	-	-	4.4
Group B15	-	-	-	6.2

Tests for groups 1 to 16 performed on the Contest (model GD-10A)

Tests for groups B6 and B15 performed on the Denison (model T42-B4)

Results for G12-21 days not available due to equipment malfunction

Based on the average of 3 specimens for each test period

Table 4.2 Mean compressive strength results (MPa)

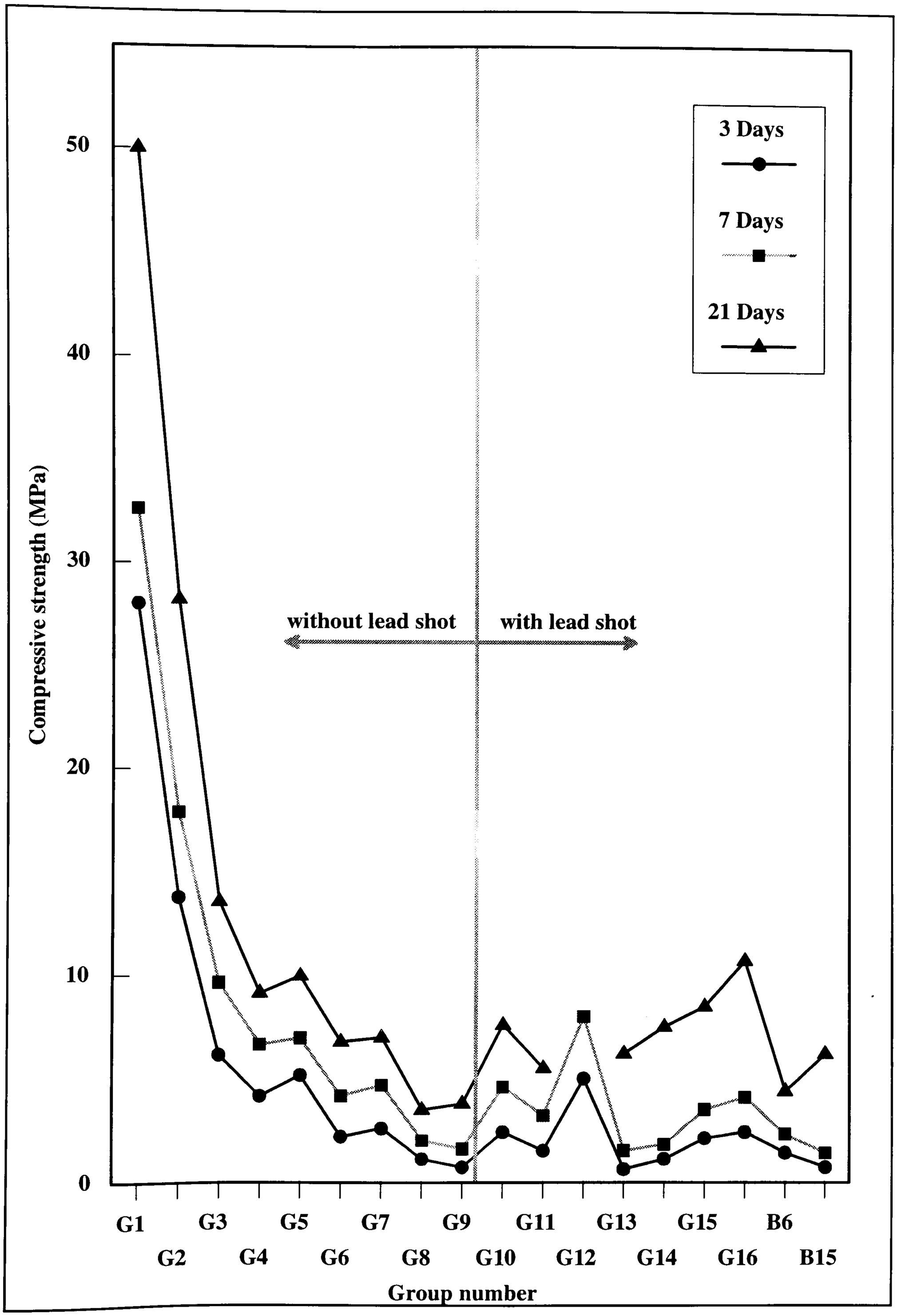

(Groups B6-B15 tested only at 28 days and the values for the 3 and 7 day compressive strength were obtained by statistical calculations). Based on average of 3 specimens.

Figure 4.2 Compressive strength development

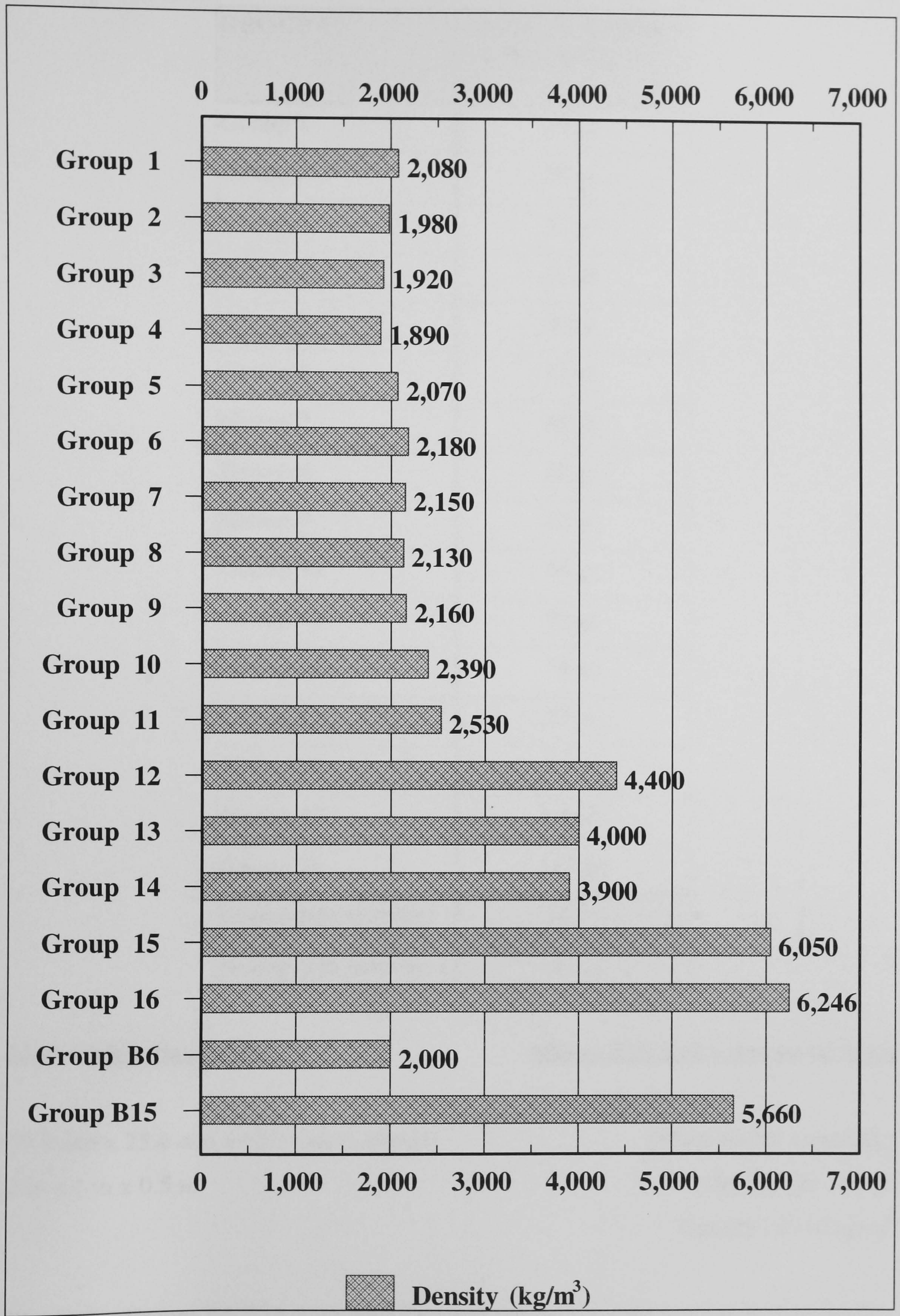

(Measured by the water replacement method and based on the average of 6 specimens)

Figure 4.3 Density variation for the trial mixes

GROUP #	MODEL BRICK UNIT WEIGHT
Group 1	40 gr.
Group 2	38 gr.
Group 3	37 gr.
Group 4	37 gr.
Group 5	40 gr.
Group 6	42 gr.
Group 7	43 gr.
Group 8	40 gr.
Group 9	42 gr.
Group 10	46 gr.
Group 11	50 gr.
Group 12	75 gr.
Group 13	73 gr.
Group 14	71 gr.
Group 15	110 gr.
Group 16	114 gr.
Group B6 (average)	34 gr.
Group B15 (average)	117 gr.

Model brick dimensions

50.8 mm x 25.4 mm x 12.7 mm (LxWxH)

2 in x 1 in x 0.5 in

Milton Hall Red commercial brick

(Machine cut specimen)

Dry weight : 32 gr.

Density : 2310 kg/m^3

(Bricks for Groups B6-B15 were manufactured and their weight accurately measured)

Table 4.3 Unit weight of model brick units

4.2.2 Model masonry mortar.

Once the prototype bricks were developed and produced, the model mortar could be developed based on relative strength properties. The aim was to produce a very low strength mortar using prototype materials if possible. British Standards BS 5628 [Ref. 81] as well as BS 4551 [Ref. 82a], give compositions of standard designated types of mortars based on basic properties such as strength and durability. Mortar types (iv) and (v) with a composition of ordinary portland cement, lime and fine sand, where chosen as the most appropriate due to their improved mortar-brick adhesion capabilities and very low compressive strength. Four trial mixes were prepared (table 4.4) using the same fine Leighton Buzzard sand (figure 4.1), in order to comply with modelling requirements (similitude) especially with regards to the width of the horizontal and vertical mortar joints, as explained later in this chapter.

Mortar Group	Cement : lime : sand	Mortar designation
Group M1	1 : 2 : 9	(iv)
Group M2	1 : 3 : 10	(v)
Group M3	1 : 3 : 11	(v)
Group M4	1 : 3 : 12	(v)

Table 4.4 Mortar mix compositions - BS4551:Table 3 (proportions by volume)

For all the mixes in table 4.4 a series of specimens were prepared in order to determine the strength and stiffness properties of the model mortar. As before a set of three 50 mm cubes and the same number 150x50x50 mm prisms were cast and cured for 7 and 28 days. Table 4.5 summarises the results of the compression tests performed on a DENISON tension-compression machine (model T42-B4), using a purpose-built steel rig with scaled upper and lower platens. Recommendations regarding mixing, compaction, curing and testing were extracted from British and American Standards.

One important point to note is that the mortar control specimens were air-cured but covered tightly with polythene sheets in a controlled temperature chamber.

Mortar Group	Cement:lime:sand	W/C	Compressive strength	Workability
Group M1	1 : 2 : 9	3.29	1.06	Medium
Group M2	1 : 3 : 10	3.33	0.94	Low
Group M3	1 : 3 : 11	2.54	0.76	High
Group M4	1 : 3 : 12	3.95	0.69	Medium

Table 4.5 Mean 28-day compressive strength (MPa) of 50 mm cubes and workability assessment for preliminary model mortar mixes

The mix for group M1 was the first selection for the model mortar while group mix M3 could act as an alternative choice to be used in circumstances when mortar strength had to be even lower. All of the above (table 4.5), is just an indication of the type of mortar mix to be used when constructing the masonry model specimens. While the basic guidelines would be followed, the water/cement ratio could be adjusted at any time to improve workability and compensate for water loss due to evaporation during the bricklaying process. For each masonry specimen a series of cubes and prisms were cast, consisting of the same mortar mix used for laying the bricks, cured under the same environmental conditions and tested at the same date as the corresponding masonry assemblages.

4.3 Fabrication techniques and procedures.

In order to achieve mass brick production purpose-made moulds were designed and manufactured in the workshop. In total 4 moulds were made each with a capacity of 112 bricks. A drawing showing a disassembled mould is presented in figure 4.4. The steel parts are connected together to form the upper body of the mould which in turn is screwed down on to a heavy rectangular steel plate. Finally machine-cut perspex partitions identical in size can be easily slotted into position.

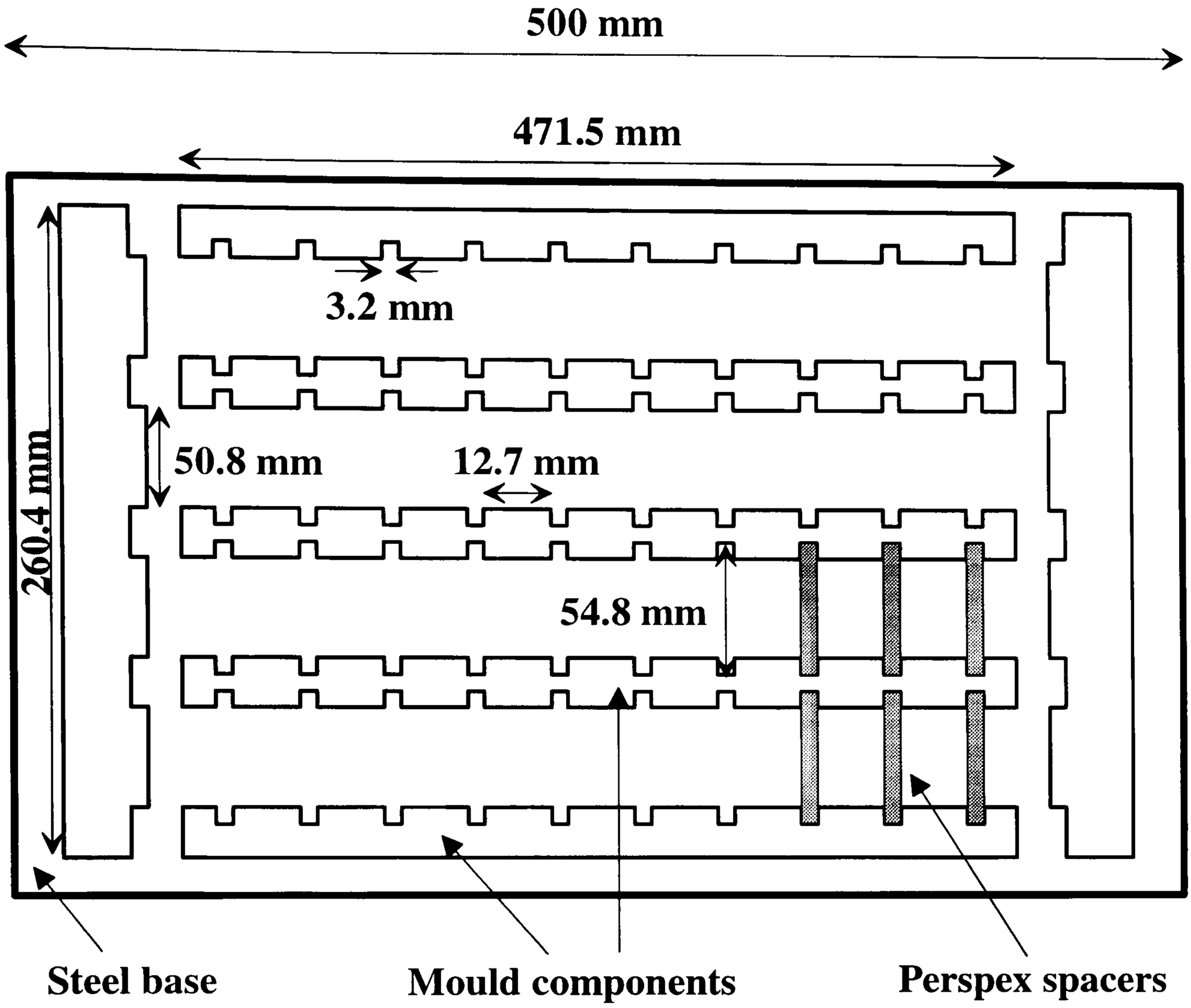

(Height of all mould components-excl. base is 25.4 mm)

Figure 4.4 Plan of a mould used for brick production

For each of the two mixes chosen as the most suitable for brick production enough material was prepared to fill the four moulds as well as brass moulds for cubes and prisms to be used as control specimens (photo 4.1). The perspex spacers do not need any particular attention with regards to oiling or lubrication due to their smooth non-adhesive surface. The steel mould components are heavier in weight, demanding a higher frequency of vibration in order to produce a well compacted mix which in turn forced the perspex spacers to vibrate violently.

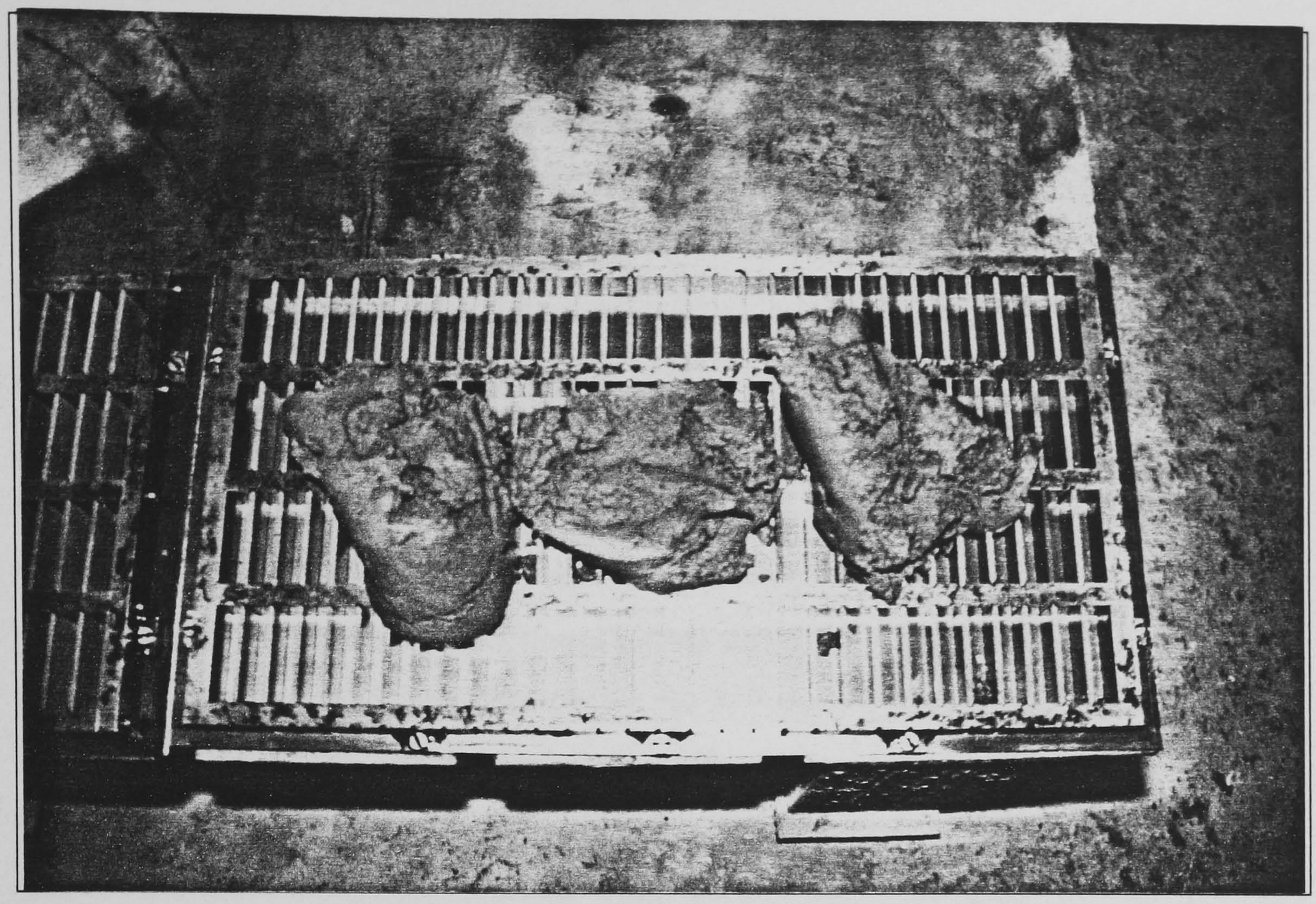

Photo 4.1 Brick moulds with mix ready for compaction

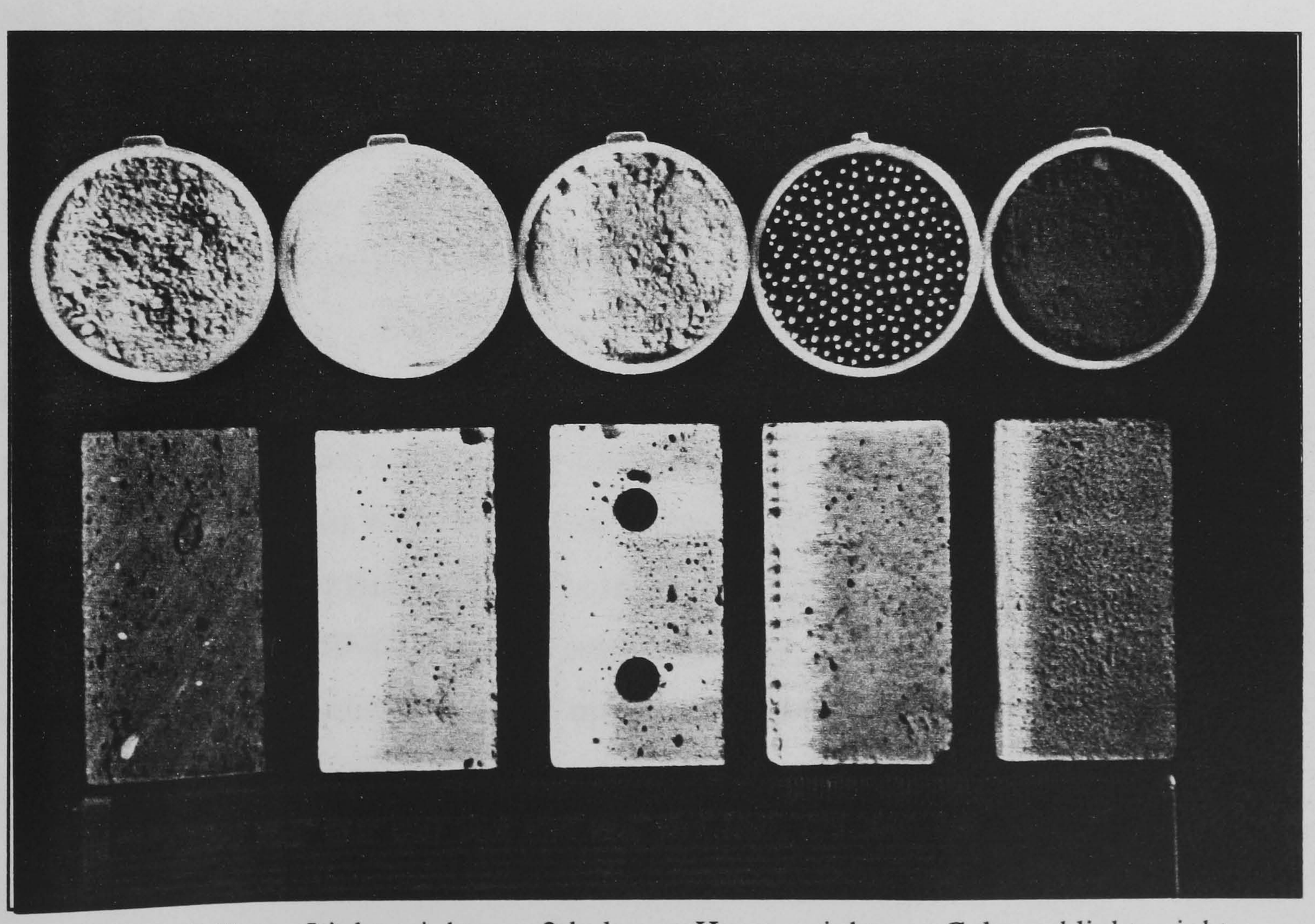

Milton Hall Lightweight 2-hole Heavyweight Coloured lightweight

Photo 4.2 Model brick units and material samples

As a result, steps were taken in order to restrain and keep them in position while at the same time allowing the moulds to vibrate gently. During the demoulding procedure an average of 3% to 5 % of the model bricks were damaged and discarded.

Bricks that were investigated for production are shown in photo 4.2, which includes a Milton Hall commercially available clay brick, machine-cut to the same dimensions as the model units. Also in the photo third from the left a brick is shown with two holes for installing reinforcement as well as samples of Pfa, sand, cement, lead shot and red pigment that was used for colouring. For each batch of brick units produced, a series of control specimens (cubes and prisms with dimensions as before), were also prepared and tested after curing for 3, 7 and 21 days in lime saturated water in order to determine the strength and stiffness properties (compressive strength, stress-strain characteristics, Young's modulus, Poisson's ratio) of the model material. In order to minimise the errors occurring while testing small scale specimens on machines that are not designed for such a purpose, a special rig was designed to minimise the so called "platen effects". Figure 4.5a provides a schematic description of the apparatus which was manufactured in the workshop and was implemented for the testing of cubes and prisms as well as masonry subassemblages such as 5-unit high brick prisms and 2x6 unit square masonry wallettes. Individual components were made out of mild polished steel except the upper plate which is described later on. Discrepancies attributed to "platen effects" were observed while testing 50 mm cubes (without the aid of the device mentioned above), on a CONTEST (model GD-10A, platen diameter 180 mm) and a DENISON (model T42-B4, platen diameter can be easily adjusted using additional supports) under uniaxial compressive load. During the first experimental phase a series of trial cubes were cast with half of them tested on the CONTEST and the rest on the DENISON under identical loading procedures (e.g. rate of loading). Results from tests performed on the DENISON were consistently 15 to 20% lower verifying earlier suspicions about the unsuitability of machines with fixed, large diameter platens for tests on small size specimens.

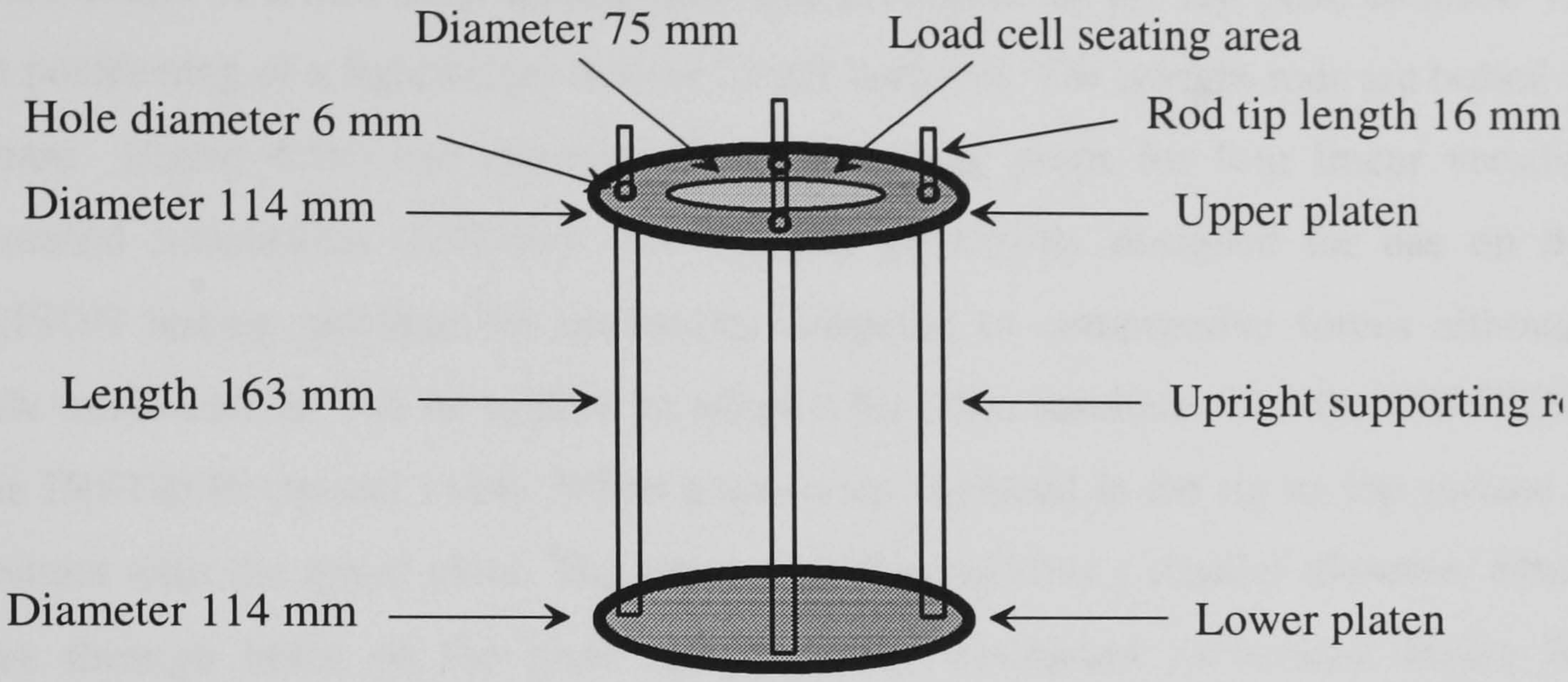

Figure 4.5a Rig used for tests on control specimens

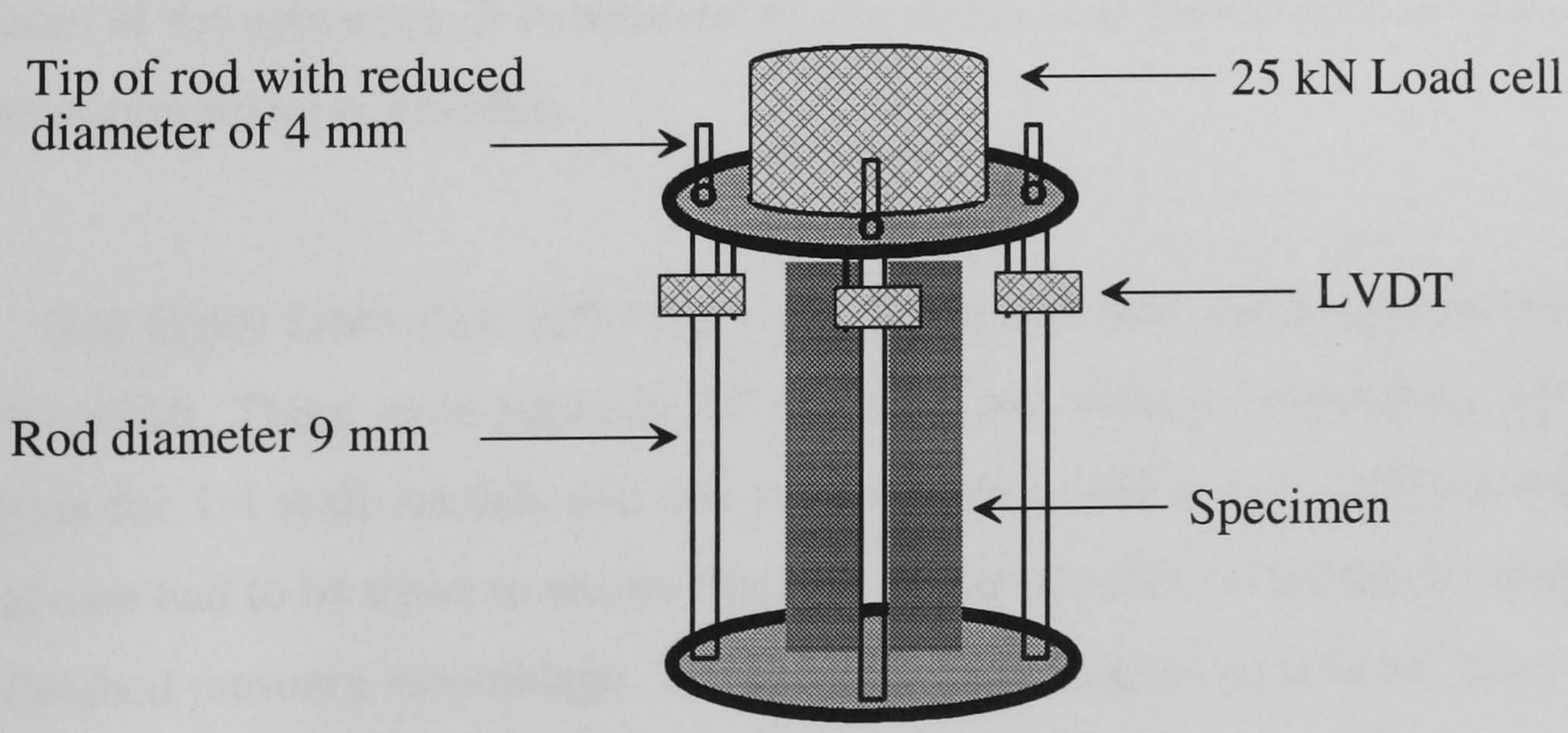

Figure 4.5b Drawing showing specimen and instrumentation arrangement

Two circular plates, part of the rig described previously, were manufactured, one made out of thick (8 mm) perspex and the second one (same thickness) from duraluminium. A 2 mm deep seating area was machined on the top plate to allow for exact positioning of a lightweight hollow 25 kN load cell. The upright rods are bolted to the base (figure 4.5b) and can be used as mounting props for four linear variable differential transducers (LVDTs). The rig was principally designed for use on the DENISON testing machine for specimens subjected to compressive forces although simple modifications can be applied to adapt it for other machines like the CONTEST or the INSTRON (model 1114). When a specimen is placed in the rig its top surface is in contact with the upper plate. The top part of the rods has a smaller diameter which passes through holes on the plate thus allowing downward movement during the loading process. The transducers are protected from accidental damage since the upper plate cannot fall below a certain height. Although the rig was designed for a specific specimen height, other shorter specimens can also be accommodated, by adding spacers (e.g. steel cubes) to the bottom plate.

To further minimise the platen restraining effects on the lateral expansion of the top and bottom surfaces of the test specimens, greased Teflon pieces machine-cut to the dimensions of the specimens were inserted between the rig platens and the loaded surfaces of the specimen. It is believed by the author that Teflon reduced platen effects to the minimum level possible.

One major fabrication difficulty was encountered with the horizontal and vertical mortar joints. These were between 2.5 mm to 3 mm wide as dictated by dimensional analysis for 1:4 scale models and this joint thickness had to be consistent throughout. Great care had to be taken to ensure that this would not alter or disturb the alignment of the finished masonry assemblage. The final solution adopted to achieve this was to lay the bricks horizontally with the aid of a drawn grid and pour the mortar in from above. This process of course, deviates from standard construction methods used initially which required the bricks to be laid in layers vertically with the aid of a casting frame built from steel angles, employing string and weights as plumb lines. Although this resembled the standard bricklaying method, it was time consuming and very sensitive to

workmanship dependent and led to significant errors (e.g. misalignment and resulting eccentricities).

4.4 Static tests for model masonry assemblages.

As mentioned previously a series of tests was devised in order to establish the suitability of the masonry constituent materials through their fundamental properties. The brick and mortar properties were essential for the subsequent static and dynamic testing of masonry assemblages and could also be used for the formation or calibration of constitutive relations for analytical calculations. Information and guidelines regarding testing were extracted from the British, European and American standards although no firm specifications appear to exist for many of the tests described later. In cases where they do appear (e.g. diagonal tension for masonry square panels-ASTM E519-74 [Ref. 88]), these were followed as closely as possible. Table 4.6 provides a summary of all the tests that are needed in order to provide a complete parametric description of the masonry constituent materials and assemblages. This table is the a result of a literature survey with regards to experimental testing procedures adopted by different researchers for evaluating the basic characteristic properties of model masonry assemblies. Some of these test procedures have been investigated in this study and are described in the following sections.

	MATERIAL	DIMENSIONS	SPECIMEN TYPE	AGE	TEST TYPE	LOADING SYSTEM	MEASURED QUANTITY	MEDIUM	INSTRUMENTATION
1	Brick mix	50mm	Cube	28 days	Uniaxial compression	CONTEST	Compressive strength	None (cast-in side)	None
2	Brick mix	150mm*50mm*50mm	Prism	28 days	Splitting tensile	CONTEST	Split/Tensile stren.	Teflon	None
3	Brick mix	150mm*50mm*50mm	Prism	28 days	Direct tensile	INSTRON-1144/HOUNSF.	Direct Tensile str.	Brush platens	None
4	Brick mix	150mm*50mm*50mm	Prism	28 days	2 point flex/tensile	CONTEST	Modulus of Rupture	None (cast-in side)	None
5	Brick mix	150mm*50mm*50mm	Prism	28 days	Uniaxial compresion	DENISON	Static Mod. Elast.	None (cast-in side)	LVDT
6	Brick mix	150mm*50mm*50mm	Prism	28 days	Uniaxial compression	DENISON	Poisson's Ratio	None (cast-in side)	Strain gages(lon+tr)
7	Brick unit	50.8mm*25.4mm*12.7mm	Unit	28 days	Uniaxial compression	DENISON	Compressive strength	Teflon+steel sheet	None
8	Brick unit	50.8mm*25.4mm*12.7mm	Unit	Any	5 Hour Boiling test	---	Initial Rate Absor.	None (cast-in side)	Electronic Balance
9	Brick unit	50.8mm*25.4mm*12.7mm	Unit	Any	24 Hour Immersion	---	Water Absorption	None (cast-in side)	Electronic Balance
10	Brick unit	50.8mm*25.4mm*12.7mm	Unit	28 days	Direct tensile	INSTRON-1144/HOUNSF.	Direct Tensile str.	Brush platens	None
11	Mortar	50mm	Cube	28 days	Uniaxial compression	DENISON	Compressive strength	None (cast-in side)	None
12	Mortar	150mm*50mm*50mm	Prism	28 days	Splitting tensile	CONTEST-DENISON	Split/tensile str.	Teflon	None
13	Mortar	38mm*102mm(1.5"*4")	Cylinder	28 days	Splitting tensile	DENISON-CONTEST	Split/tensile str.	Teflon	None
14	Mortar	150mm*50mm*50mm	Prism	28 days	Uniaxial compression	DENISON	Static Mod. Elast.	None (cast-in side)	LVDT
15	Mortar	150mm*50mm*50mm	Prism	28 days	Uniaxial compresion	DENISON	Poisson's Ratio	None (cast-in side)	Strain gages(lon+tr)
16	Mortar	38mm*102mm	Cylinder	28 days	Uniaxial compression	DENISON	Static Mod. Elast.	Teflon+Capping	LVDT
17	Mortar	38mm*102mm	Cylinder	28 days	Uniaxial compresion	DENISON	Poisson's Ratio	Teflon+Capping	Strain gages(lon+tr)
18	Masonry (l*w*h)	50.8mm*25.4mm*44.1mm	3-brick prism	28 days	Uniaxial compression	DENISON	Compressive strength	Teflon+steel sheet	LVDT
19	Masonry	50.8mm*25.4mm*75.5mm	5-brick prism	28 days	Uniaxial compresion	DENISON	Compressive strength	Teflon+steel sheet	LVDT
20	Masonry	50.8mm*25.4mm*75.5mm	5-brick prism	28 days	Uniaxial compression	DENISON	Static Mod. Elast.	Teflon+steel sheet	LVDT
21	Masonry	50.8mm*25.4mm*75.5mm	5-brick prism	28 days	Uniaxial compression	DENISON	Poisson's Ratio	Teflon+steel sheet	LVDT/Rosette
22	Masonry	50.8mm*25.4mm*106.9	7-brick prism	28 days	2 point flex/tensile	CONTEST	Modulus of Rupture	None	None
23	Masonry	50.8mm*25.4mm*28.4mm	2-brick prism	28 days	Eccentrical compr.	DENISON	Flexural Bond str.	Teflon+steel sheet	None
24	Masonry assem.	93mm*25.4mm*93mm	Square wallette	28 days	Diagonal compression	DENISON	Shear modulus	Corners+capping	LVDT/Rosette
25	Masonry assem.	93mm*25.4mm*93mm	Square wallette	28 days	Diagonal compression	DENISON	Shear strains	Corners+capping	LVDT/Rosette
26	Masonry assem.	93mm*25.4mm*93mm	Square wallette	28 days	Uniform compression	DENISON	Compressive strength	Teflon+steel sheet	Strain gage
27	Masonry assem.	(not uniform)	3 or 4 unit assembly	28 days	Axial Shear	DENISON	Shear Bond strength	Teflon+steel sheet	None
28	Masonry assem.	78mm*25.4mm*73mm	Rectangular panel	28 days	2 point flex/tensile	CONTEST	Modulus of Rupture	None	None
29	Masonry assem.	50.8mm*25.4mm*75.5mm	Rectangular Prism	28 days	Uniaxial compression	DENISON	Compressive strength	Teflon+steel sheet	None
30	Sand	---	Loose sand	---	Sieving		% pass (sand type)	None	Balance

Table 4.6 Tests for masonry materials and assemblages

4.4.1 Water absorption properties for brick units.

Together with the strength results presented in table 4.2, two of the most important tests that had to be conducted as early as possible, were tests numbers 8 and 9 (column 1-table 4.6), which would provide results regarding the rate of absorption of water for the brick units. If these values are not within limits recommended by the codes then the bricks could turn out to be unusable, since water absorption is the characteristic quality which demonstrates how bricks will adhere and bond with the mortar at the joints. The above test procedures involved placing brick units for 5 hours in boiling water suspended from a steel frame and as with almost all the other tests summarised in table 4.6, dimensions given in the codes (e.g. immersion depth of unit in water-BS 3921:1985, [Ref. 82b]) are scaled down by a factor of 4 to comply with similitude requirements. Table 4.7 shows results from the initial rate of suction/absorption (I.R.S.) test conducted for bricks of the first group (B6 - high sand content) while table 4.8 presents results from the water absorption tests on bricks from both groups. All the bricks used in these tests were randomly selected from a batch of about 400 units and oven dried for about 20 hours. The code specifications for test procedures and quality control, were followed throughout. I.R.S. values generally range between 0.25 and 2.05 kg/min./m^2 with the range of 0.3 to 0.8 kg/min./m^2 presented in technical literature as ideal [Ref. 78 and 104].

Brick #	**Wet weight (gr.)**	**Dry weight (gr.)**	**I.R.S. kg/min./m²**
1	30.71	29.93	0.6
2	32.59	31.93	0.5
3	32.22	31.24	0.8
4	31.73	30.77	0.7
5	31.93	30.98	0.7
6	32.38	31.73	0.5

Mean initial rate of absorption (I.R.S.) is **0.63 (kg/min./m²).**

Bricks taken from **group B6.**

Based on specifications of **BS 3921:1985, appendix H.**

Table 4.7 Initial rate of suction/absorption test results

The following table summarises results for the water absorption test of oven dried bricks immersed for 24 hours in cold and 5 hours in boiling water.

Brick type	Dry weight (gr.)	Wet weight (gr.)	Mean Water
B6 unit (light)	30.68	35.12	**14.5% (by mass)**
B15 unit (heavy)	99.57	102.43	**3% (by mass)**

Dry weight measured from oven dried specimens.

Absorption values are based on average from **6 units**.

Based on specifications of **BS 3921:1985, appendix E.**

Table 4.8 Water absorption tests results

Tests for strength and absorption were the only experimental procedures not requiring detailed electrical and electronic data collection and acquisition equipment. Most of the tests on materials and components involved instrumentation such as strain gauges, transducers and load cells among others and these are described in the following sections.

4.4.2 Strength characteristics of individual masonry components.

The following sections deal with the experimental investigation of the fundamental properties of the individual masonry components such as stress-strain characteristics. In total 4 series of tests were performed but for the sake of simplicity these are all classified as one experimental stage and comparisons are drawn and analysed at the end of this chapter. For most of these tests electronic instrumentation and data collection was essential in order to obtain information on the behaviour of the tested specimens up to failure. The literature review presented in chapter 3 revealed that there is a consistent lack of knowledge with regards to the behaviour and performance of masonry assemblages at the ultimate stage. In the following section a description is given of the instrumentation and data acquisition system as well as the techniques that were employed in order to ensure that accuracy of the final results was within acceptable limits.

4.4.2.1 Instrumentation and data acquisition.

Definition of strain dictates that measurements based on electrical resistance strain gauges are taken at finite lengths along the face of the specimens and in line with the load applied. Such requirements can be easily followed for materials like steel for example which are relatively homogeneous, but with masonry assemblages that consist of a matrix of brick units and mortar joints this would require attaching gauge elements on to the brick unit and the mortar joint separately and in combination and measuring their individual and combined deformation characteristics in order obtain strain values for the composite material. This difficulty can be overcome by using linear variable differential transducers (LVDTs) that extend across several units and mortar joints of

the masonry specimen. This ensures that the results correspond as close as possible to the true masonry behaviour and are not over-influenced by the individual behaviour of one of the components. A further advantage arising from the use of LVDTs as deformation measuring devices, is that when used in the experimental set-up they can be located in such a way as to be protected during the failure process.

4.4.2.1.1 Instrumentation.

All of the tests that are described in the following sections were conducted on a tension-compression DENISON machine (model GD-10A). This test facility operates under displacement control with a manual selection of load ranges (10 kN to 5000 kN). A commercial load cell was attached to the upper platen of the machine and carried a purpose-built seating plate to load the top face of the specimen. Readings from the load cell transducer had to be amplified before been processed and stored in the data acquisition system. Due to the very low voltage output (maximum of 1.0 V) from the load cell a 'high and low gain-low drift D.C. amplifier' with adjustable settings, was designed and assembled by the electronics workshop staff to amplify the cell output and to filter unwanted signal noise. The system is shown in figure 4.6. This procedure minimised the low level signal problems to a certain degree, and additional steps, described in section 4.4.2.1.2 had to be taken to further improve the transducer signal. The source of the additional electrical noise was thought to be the instrumentation itself, the computerised data acquisition system (internal bus card) and the power supply.

LVDTs (model RDP-D5200H - adjustable linear range ±2.5 and ±5.0 mm) were used for measuring displacement over a predefined length on the face of the specimen. The rig described earlier (figure 4.5) was initially used for mounting the transducers however after initial testing it was decided that greater reliability could be achieved by attaching the mountings to the specimens. Small aluminium corners (12 mm x 12 mm) with tapped mounting points were glued on to the faces of the specimen using high-strength fast-cure epoxy. The transducers were then secured to these with screws, aligned and connected to the data acquisition system. Since specimen size varied considerably for the various tests, miniature cylindrical steel extensions (diameter 2 mm, lengths 15-35-70-90 mm) were designed, which increased the working length

(20 mm) of the original transducer's sensing element. The extensions were equipped with a two way coupling sleeve that allowed a secure connection between the sensing element and the extension arm; (details of the items described above can be observed in the numerous photographs included in the following sections). For most of the experimental tests presented in this chapter, identical sets of displacement transducers were mounted in pairs on opposite sides of the test specimen and the output signals were averaged before final collection by the data logging device, to improve the quality of the results.

4.4.2.1.2 Data acquisition.

Signals generated by the load and displacement transducers were collected by an internal bus data acquisition and control system based on an IBM 286 compatible personal computer. Initially signals from the external devices (load cell, LVDTs) were amplified and conditioned and these in turn were connected to an 8-channel differential input interface device (Burr-Brown PCI-20010T-2). An analog to digital conversion board (Burr-Brown PCI-20089W-1) was installed in one of the internal computer expansion slots. This accepted the signals and after digitisation stored them in virtual memory for further processing, graphical on-line output and hard disk storage. This process was controlled using a dedicated software program (Labtech Notebook version 4.1, [Ref. 100]), covering the starting and stopping of the acquisition process, the number and type of channels acquired (unipolar-bipolar) as well as the speed of data acquisition and subsequent data conversion and archiving. Once in storage the signals were converted to appropriate engineering units (mm-kN) and processed using the program's in-built functions together with purpose written subroutines for digital signal processing (Appendix A). Graphical output was available in real time during data acquisition through the computer monitor. Figure 4.6 shows the computerised data acquisition system in diagrammatic form as it was set and used throughout the static experimental testing stage.

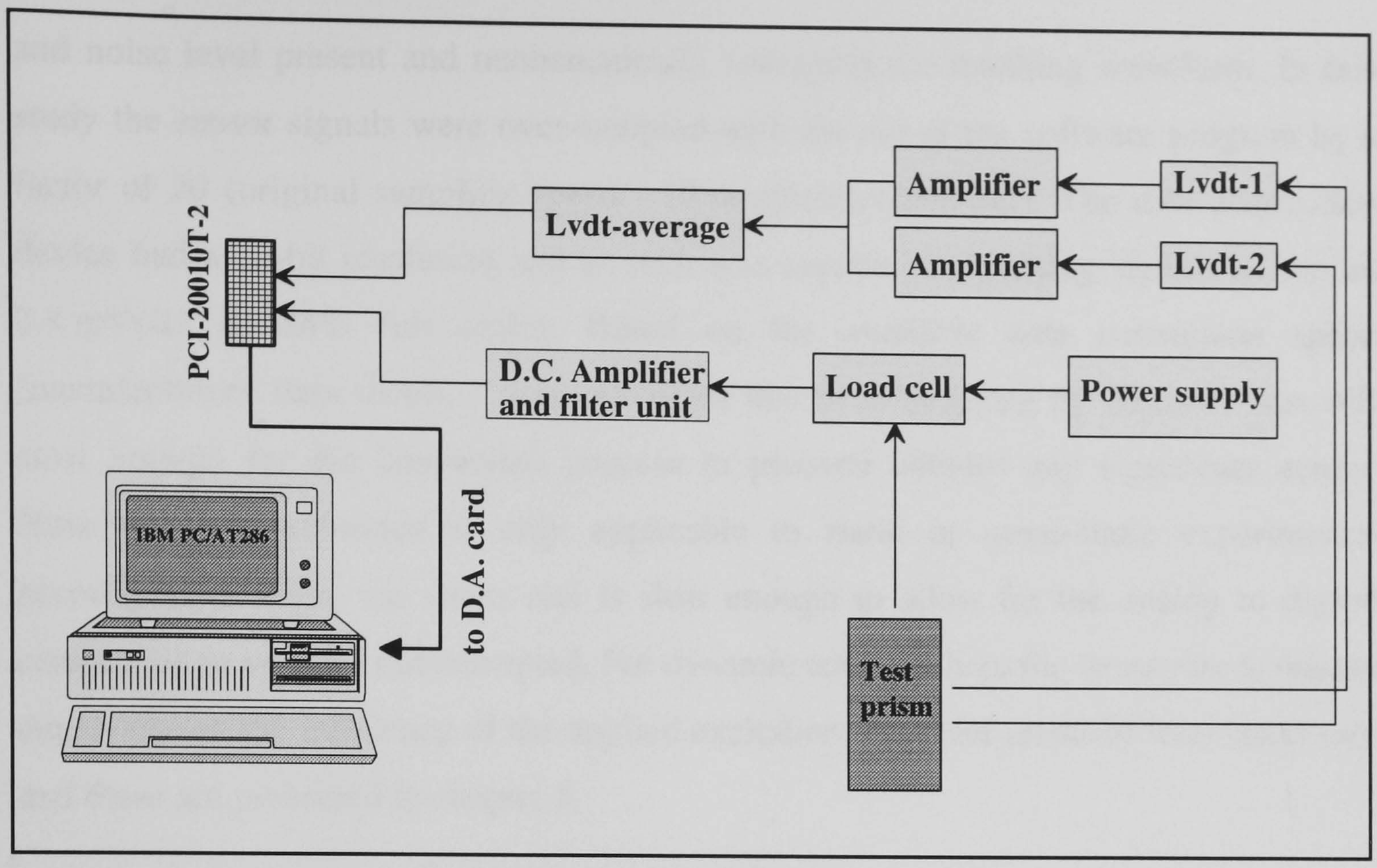

Figure 4.6 Instrumentation arrangement and internal bus data acquisition system

As indicated earlier electrical noise proved to be a major problem during data collection. Output from the transducers was consistently polluted by unwanted noise that affected the accuracy of the test results. The steps taken in order to minimise noise to the lowest level possible included [Ref. 101,102]:

► Use of twisted-pair cables for all the electrical connections and in particular for the load cell set-up.

► Use of differential instead of single-ended connections as inputs to the interface device.

► Design, manufacture and use of a purpose-built load cell amplifier that incorporated a low-pass analogue filter for signal conditioning.

► Use of a dedicated mains filter for all power supply connections.

► And finally digital over-sampling of the transducer signals. This technique which is simple, inexpensive and easy to implement involves increasing the sampling rate by a factor (any multiple of twice the original sampling rate), depending on the application

and noise level present and mathematically averaging the resulting waveform. In this study the sensor signals were over-sampled with the aid of the software program by a factor of 20 (original sampling speed - 10 samples/sec/channel). The data acquisition device had a 12-bit resolution and as such was capable of detecting signals as low as 2.4 mVolts (0.024% full scale). Based on the available data conversion speed (manufacturers' data sheet), it was calculated that over-sampling by 20 times was still slow enough for the conversion process to proceed without any significant errors. However, this technique is only applicable to static or quasi-static experimental investigations where the stress rate is slow enough to allow for the analog to digital conversion to proceed uninterrupted. For dynamic testing where the stress rate is mainly dependent on the frequency of the applied excitation, different methods were necessary and these are presented in chapter 5.

4.4.2.2 Model brick units.

As mentioned, 6 or more control specimens were prepared for each batch of bricks produced including cubes, prisms and cylinders. These were cured for 7, 14 and 28 days in lime saturated water, under the same laboratory conditions as the model brick units. After curing these were taken out of the wet tank, allowed to surface dry and the aluminium support corners glued on. Next day the LVDTs were attached and the specimens mounted in the testing machine. Before testing each specimen, an initial load of 200N was applied in order to test the fixity and overall operation of the instrumentation. The tests proceeded by applying the prescribed loading using a displacement control at a constant rate between 0.4 to 1.2 mm/min. The rate was based on the assessed specimen strength at failure.

Table 4.9 presents a summary of the test results for specimens made of various brick mixes. The compressive strength is included for cubes, prisms as well as individual brick units for comparison purposes and was calculated by dividing the ultimate load by the cross sectional area. The modulus of elasticity is derived from the stress-strain graphs and is the secant modulus at 45% of the ultimate prism compressive strength; the same procedure was adopted for the axial-lateral strain graphs to measure the specimen's Poisson's ratio, while strain values were obtained from LVDT data

divided by the effective gauge length. Reduced size cylinders were used for the determination of the tensile strength f'_{bt} (split cylinder test).

B-I	**Compressive strength**	**Tensile strength**	**Modulus of elasticity**	**Peak strain**	**Ultimate strain**	**Poisson's ratio**
Cube	7.22	-	-	-	-	-
Brick unit	9.01	-	-	-	-	-
Prism	5.83	-	4551.3	0.0022	0.0109	0.09
Cylinder	-	0.69	-	-	-	-
Cube dimensions: 50 mm Brick unit dimensions: 50.8x25.4x12.7 mm Prism dimensions: 150x50x50 mm Cylinder dimensions: 135x38 mm						
B-II	**Compressive strength**	**Tensile strength**	**Modulus of elasticity**	**Peak strain**	**Ultimate strain**	**Poisson's ratio**
Cube	7.275	-	-	-	-	-
Brick unit	9.18	-	-	-	-	-
Prism	5.9	-	6148.8	0.0035	0.0053	0.05
Cylinder	-	0.58	-	-	-	-
Modulus of elasticity and Poisson's ratio obtained as secant values at 45% of ultimate compressive strength						
B-III	**Compressive strength**	**Tensile strength**	**Modulus of elasticity**	**Peak strain**	**Ultimate strain**	**Poisson's ratio**
Cube	7.413	-	-	-	-	-
Brick unit	10.3	-	-	-	-	-
Prism	6.998	-	6600.4	0.0016	0.0017	0.1
Cylinder	-	0.67	-	-	-	-
Cylinder tensile splitting strength calculated from: $T = 2P/\pi ld$ Test results represent average of 6 specimens						
B-IV	**Compressive strength**	**Tensile strength**	**Modulus of elasticity**	**Peak strain**	**Ultimate strain**	**Poisson's ratio**
Cube	7.766	-	-	-	-	-
Brick unit	9.8	-	-	-	-	-
Prism	6.631	-	5968.8	0.0019	0.0104	0.12
Cylinder	-	0.65	-	-	-	-
Compressive f'_{bc}, tensile strength f'_{bt} and modulus of elasticity E_b units in **MPa**						

Table 4.9 Summary of brick test results

Brick compressive strength is usually determined by testing capped units or drilled cylindrical cores under uniaxial compression. The latter can produce highly scattered results due to the inherent variability of the material properties, while the former can only provide qualitative information due to the fact that the failure mode is significantly influenced by the 'platen effects' compared to the true material behaviour. Brick units under compression as components of a masonry matrix (section 4.4.3), exhibit a vertical splitting mode of failure (photo 4.14), which so far has been successfully reproduced only in tests that incorporate 'brush platens' [Ref. 78] for compressive load application. Photos 4.3, 4.4, 4.5 and 4.6 show failed specimens as well as one of the LVDTs complete with an extension arm and mounting sleeve. The brick unit shown in photo 4.3 demonstrates a typical shear failure mode influenced by the low specimen aspect ratio (h/l = 0.25) which relates to the increased transverse confining stresses at the loading faces. Although reduced scale platens and greased Teflon packing were used, it was unsuccessful in influencing the final failure mode and subsequently this led to the adoption of 50 mm cast cubes for the determination of the brick compressive strength. A statistical analysis of the results obtained from testing brick units and cubes cast from the same mix was carried out and the findings are presented in section 4.5.

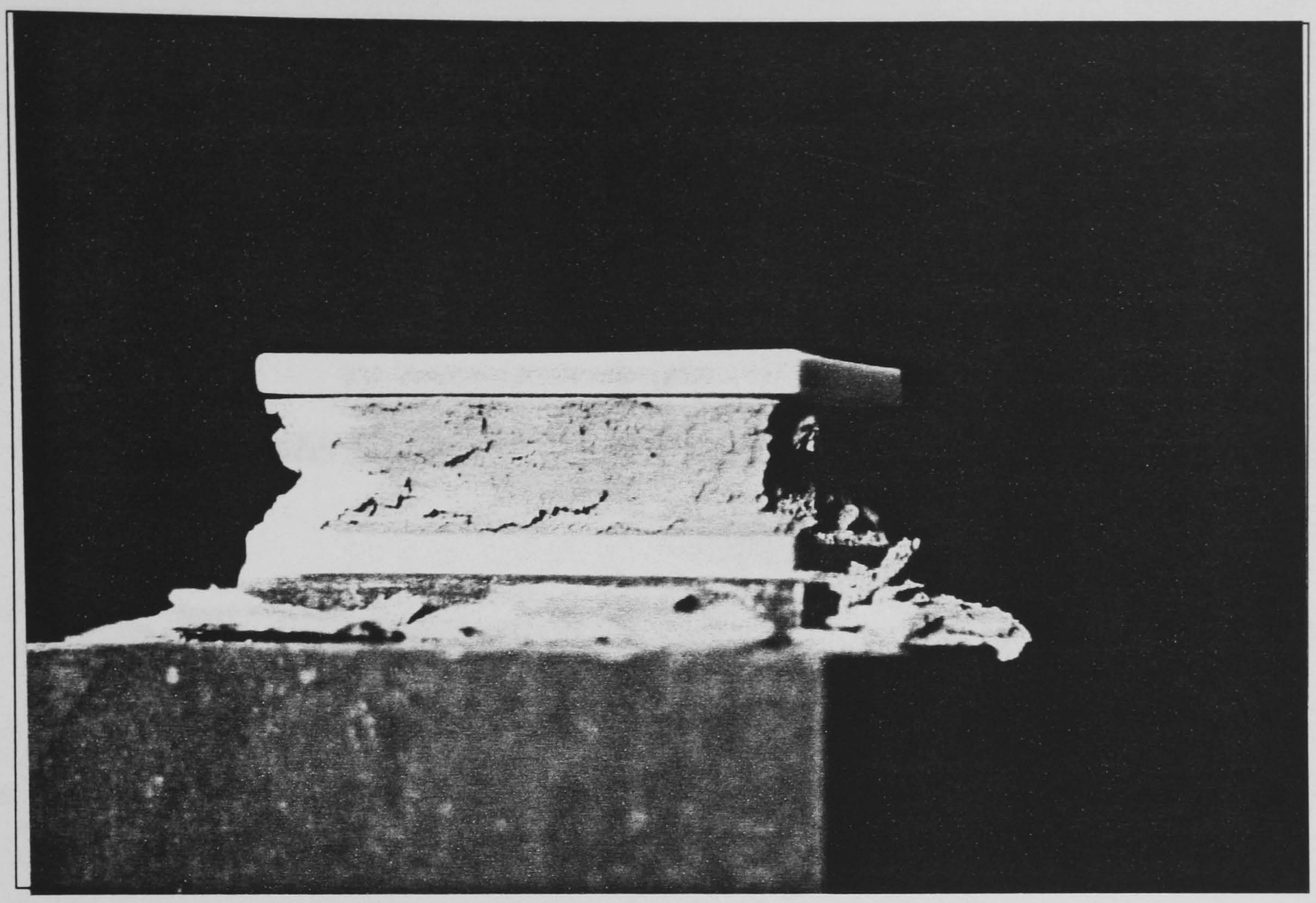

Photo 4.3 Failure mode of brick unit under uniaxial compression

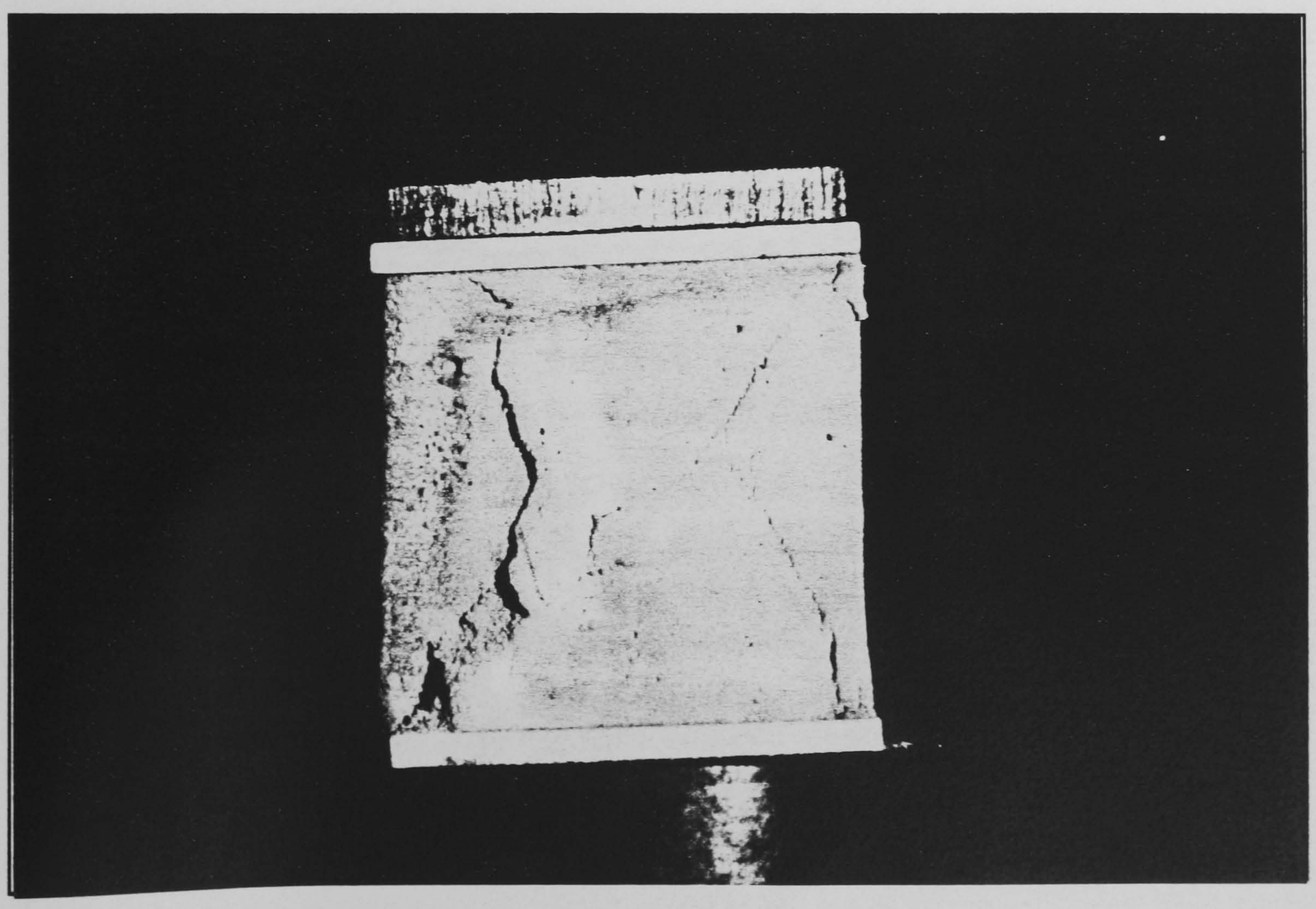

Photo 4.4 Brick-mix cast cube and compression failure mode

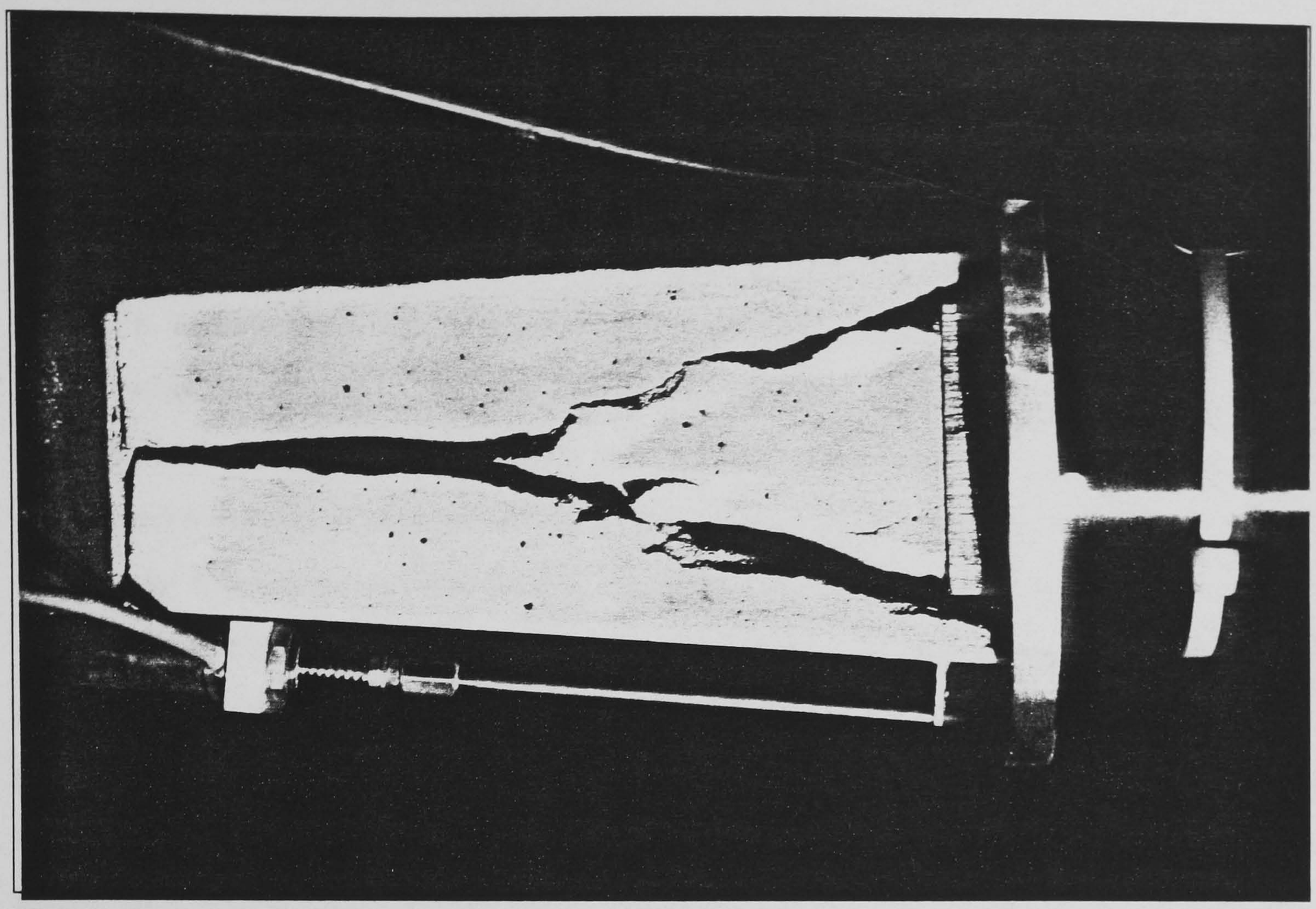

Photo 4.5 Brick-mix cast prism and compression failure mode

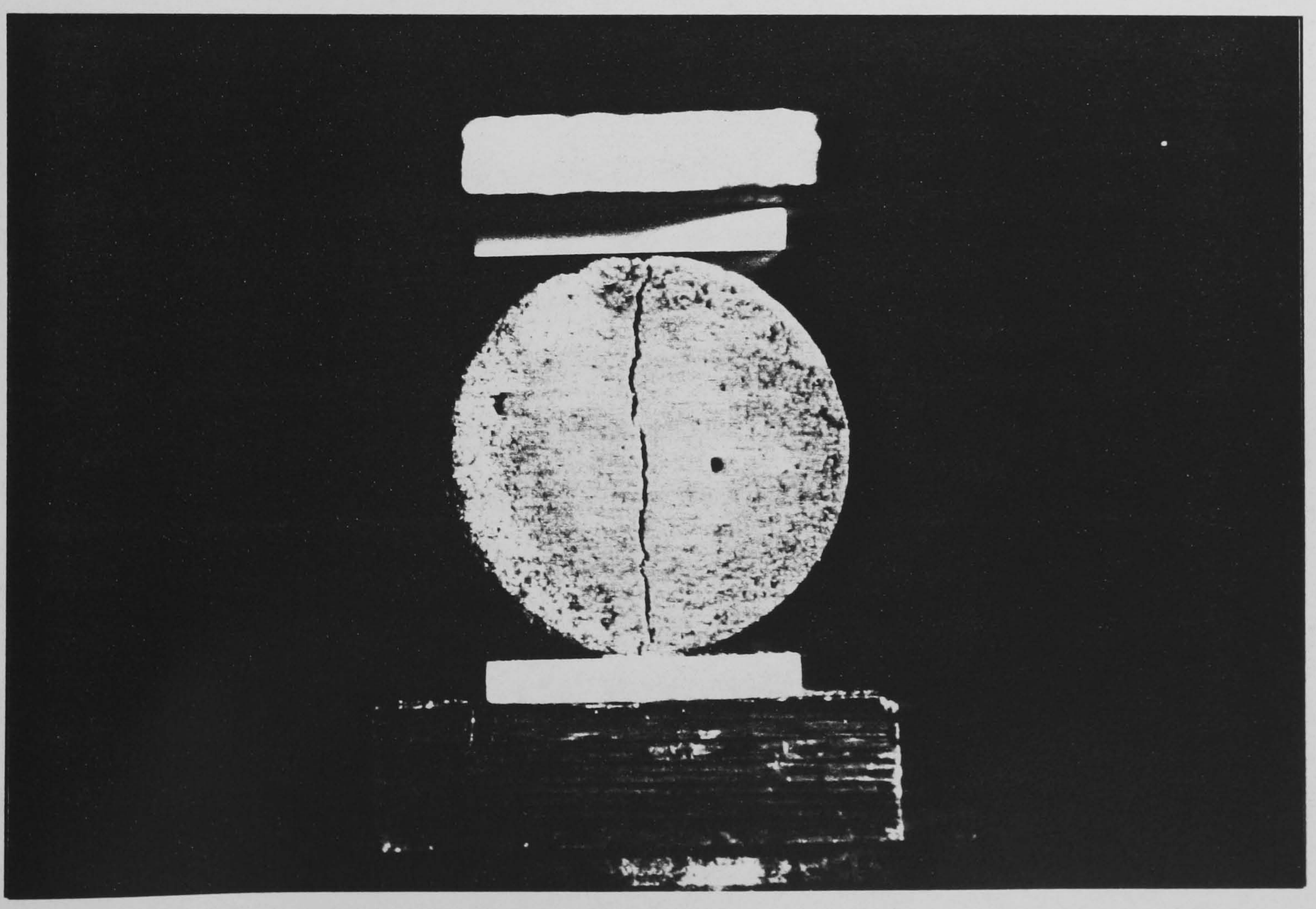

Photo 4.6 Brick-mix cast cylinder and tensile splitting failure mode

4.4.2.2.1 Stress-strain relationships.

The advantage of casting control specimens for each batch of bricks produced, became evident when the values for the Young's modulus and Poisson's ratio had to be measured. British, American and the new RILEM (International Union of Testing and Research Laboratories for Materials and Structures) standards, do not include or recommend a procedure for measuring the modulus of elasticity of brick units. Nevertheless limited examples can be found in technical literature. These were dominated by research interests, in particular cases involving analytical calculations that are highly dependent on information regarding the behaviour of individual masonry components. For the purposes of this study the basic concrete technology procedures were followed regarding the determination of the elastic modulus and Poisson's ratio as that of a homogeneous cast specimen under compressive load. An attempt was made to try and obtain the descending (strain softening) branch of the resulting load-displacement curve but this was not always possible mainly due to the fact that the transducer mountings were often dislocated by the initial cracking. 28 brick prisms were tested as part of this experimental investigation.

Figures 4.7 to 4.14 show selected stress-strain and lateral-longitudinal strain diagrams for 4 different brick-mix prisms (table 4.9). The curves are composed of a few hundred points each and digital as well as analogue filtering was successful in eliminating noise only in certain cases depending on individual circumstances. When this was not possible, key sections of the curves were reproduced by using only selected points. A nonlinear ascending (mostly above 50% of the ultimate compressive strength), as well as a descending softening branch beyond the ultimate limit is evident in the diagrams, and in particular in figure 4.13. It is interesting to note in figures 4.7 and 4.9 the initial region of the curves, where for low stress levels, the tangent is steep indicating an apparent increase in the elastic modulus. This has been observed by a number of researchers and in particular for masonry built with weak lime-mortars [Ref. 104]. Deformations in the mortar bed area resulting from workmanship, uneven bedding and characteristics of the chemical and mechanical bond between bricks and mortar, have been suggested as possible explanations.

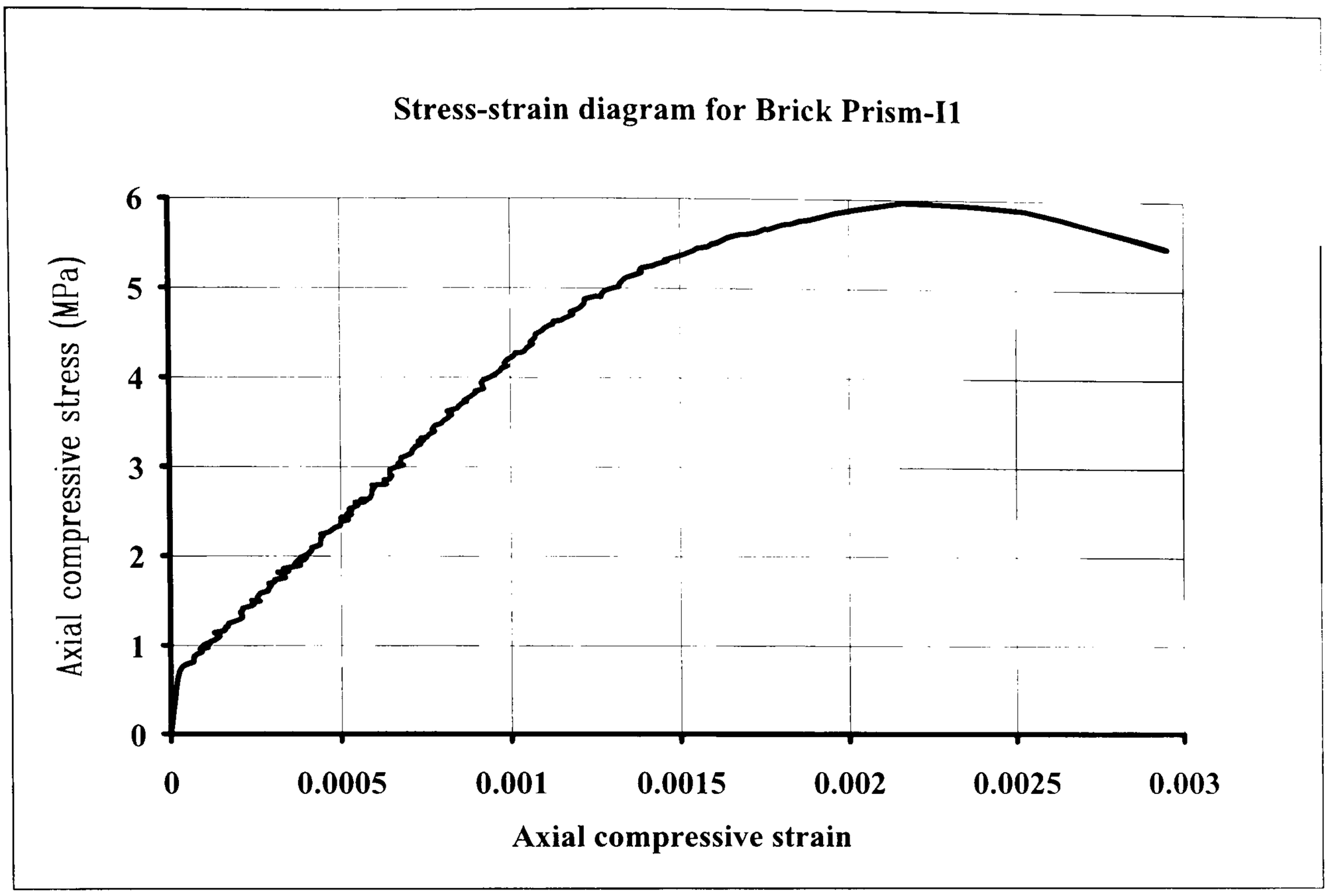

Figure 4.7 Brick I1 stress-strain diagram

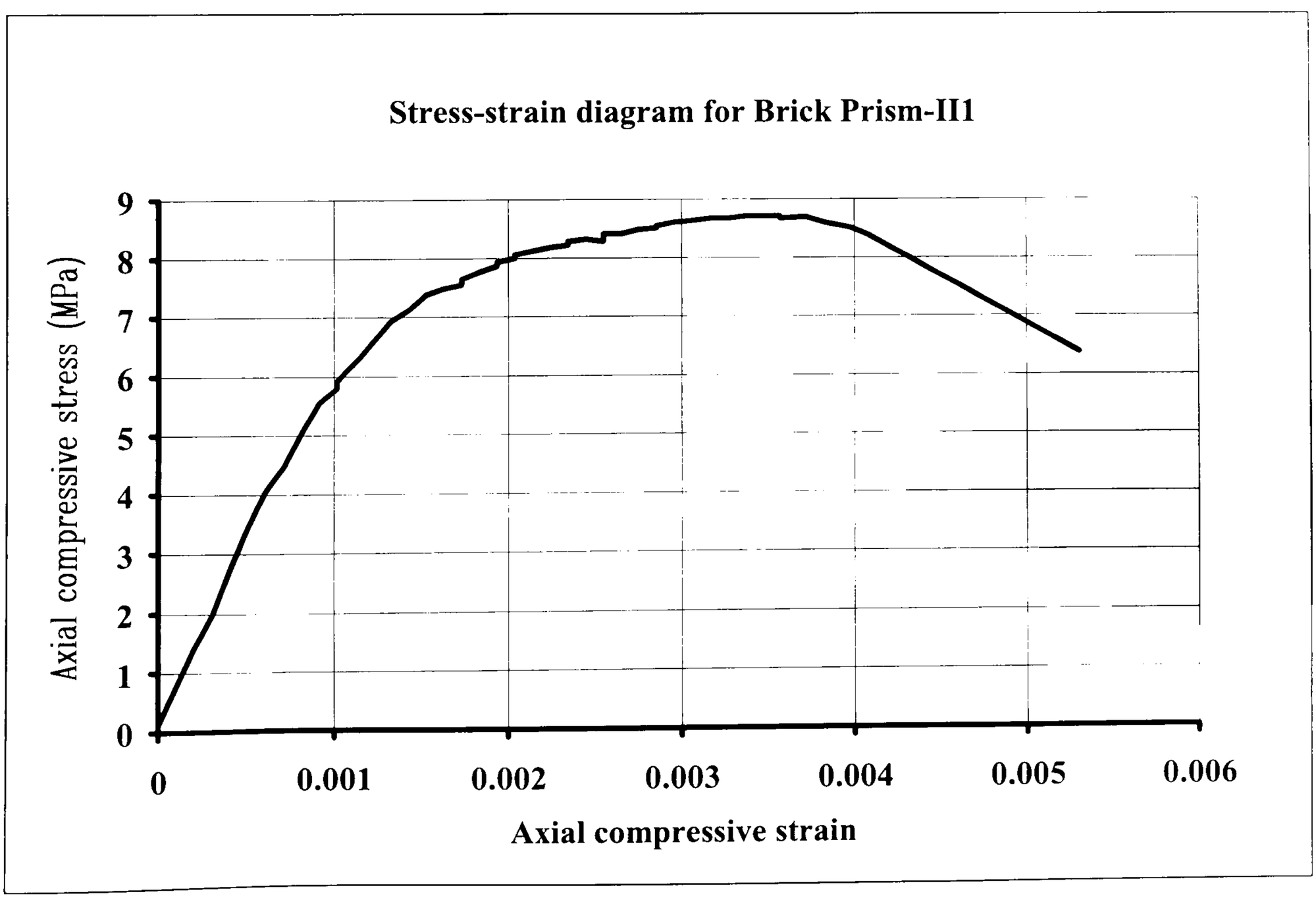

Figure 4.8 Brick II1 stress-strain diagram

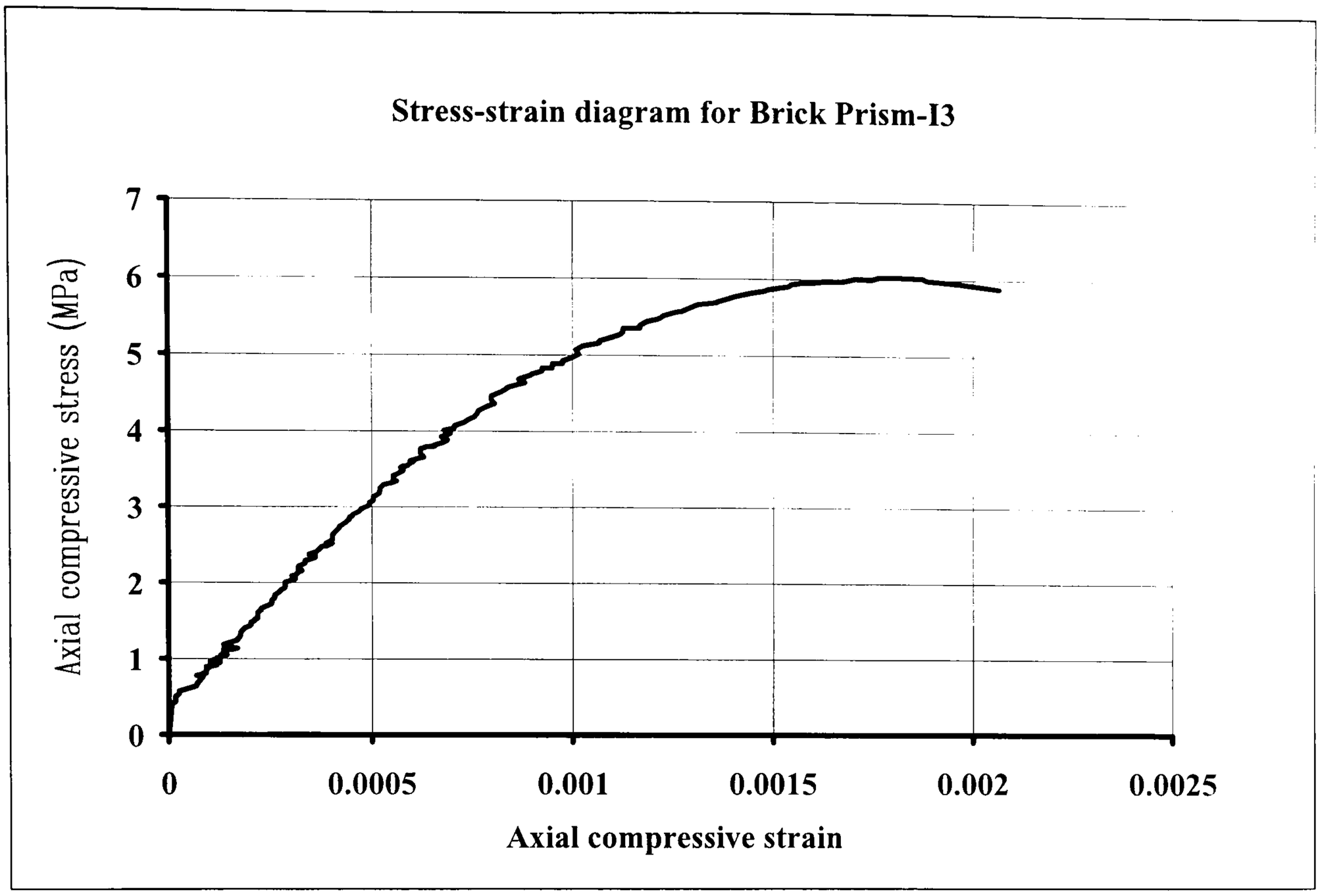

Figure 4.9 Brick I3 stress-strain diagram

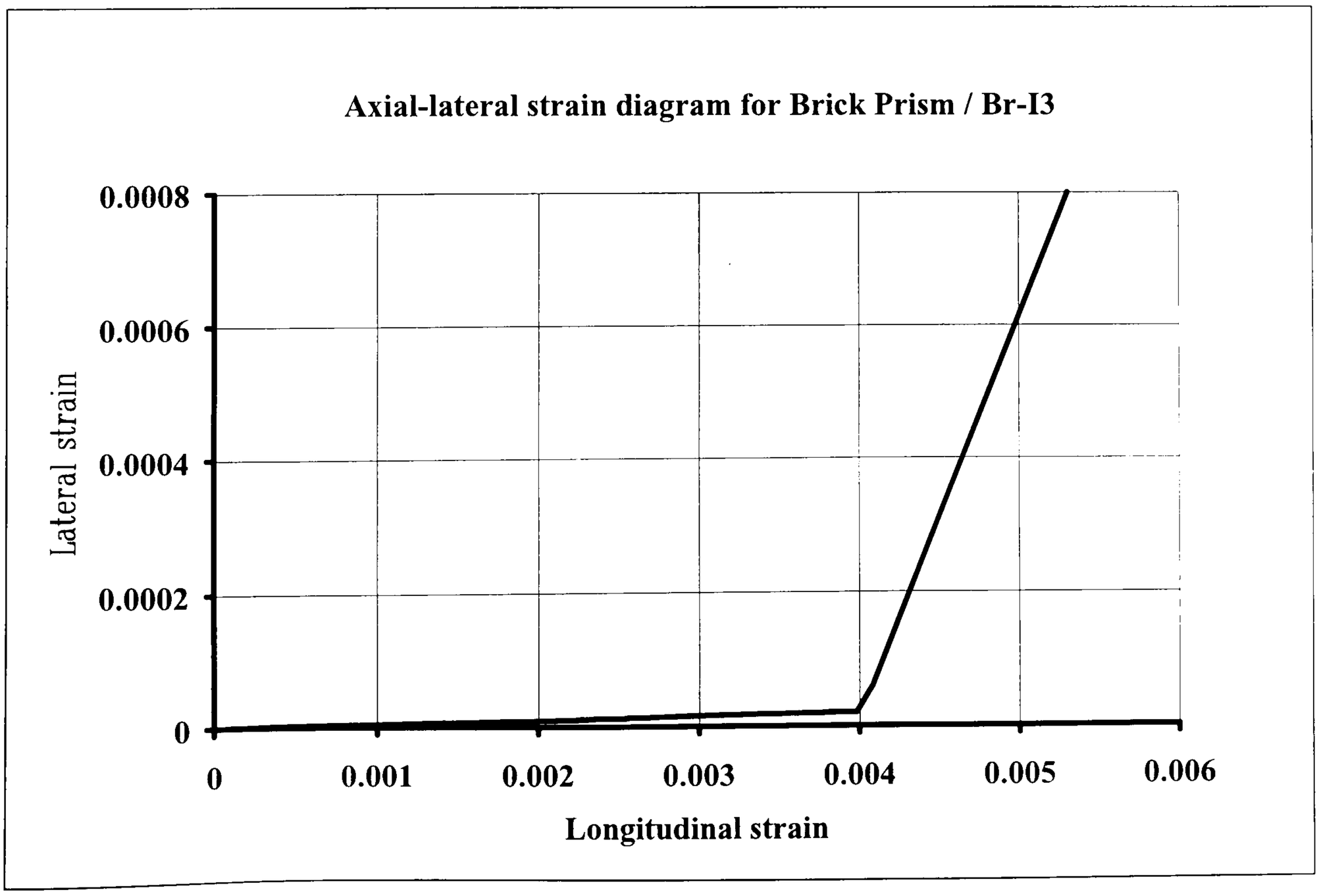

Figure 4.10 Brick I3 axial (longitudinal)-lateral strain diagram

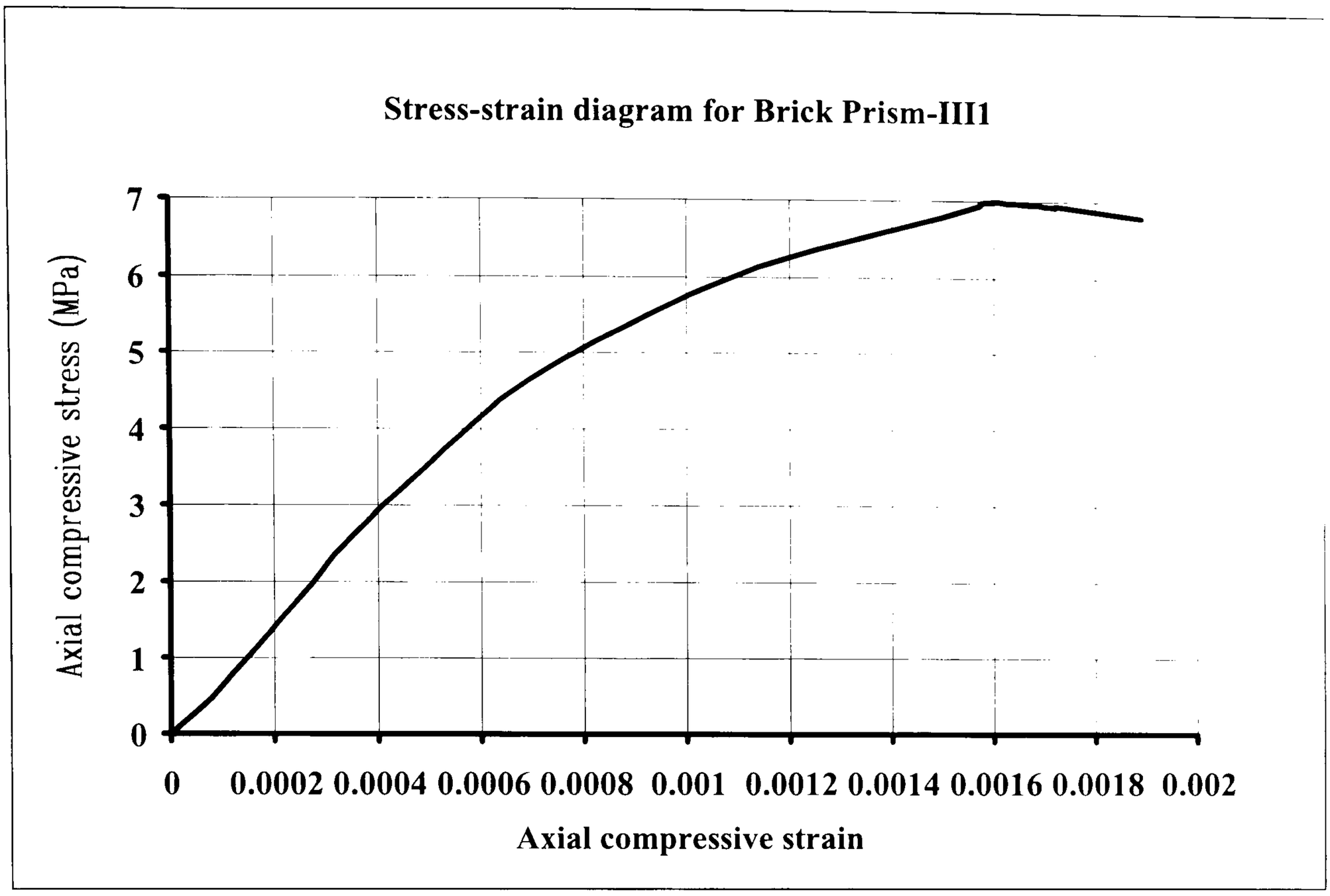

Figure 4.11 Brick III1 stress-strain diagram

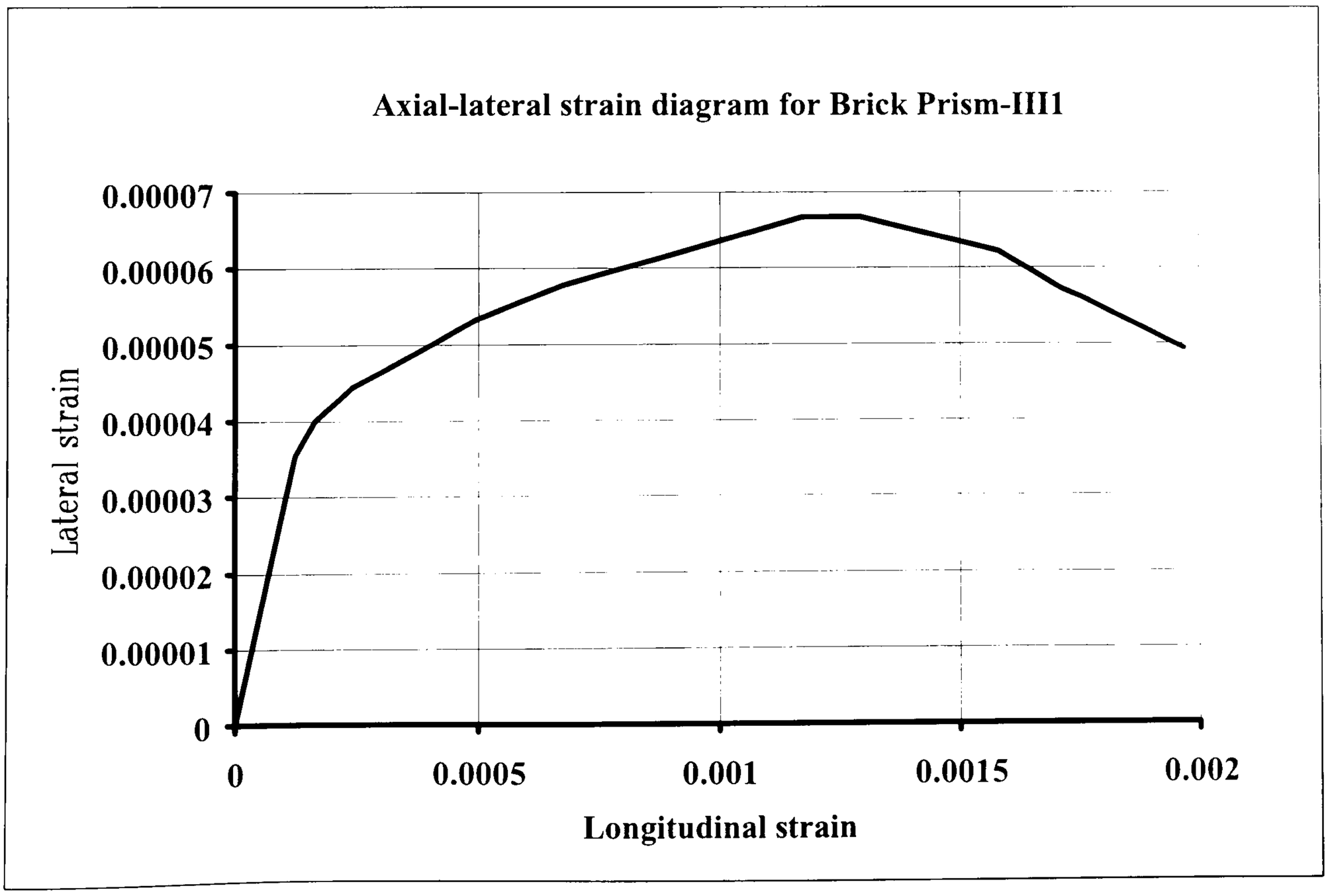

Figure 4.12 Brick III1 axial (longitudinal)-lateral strain diagram

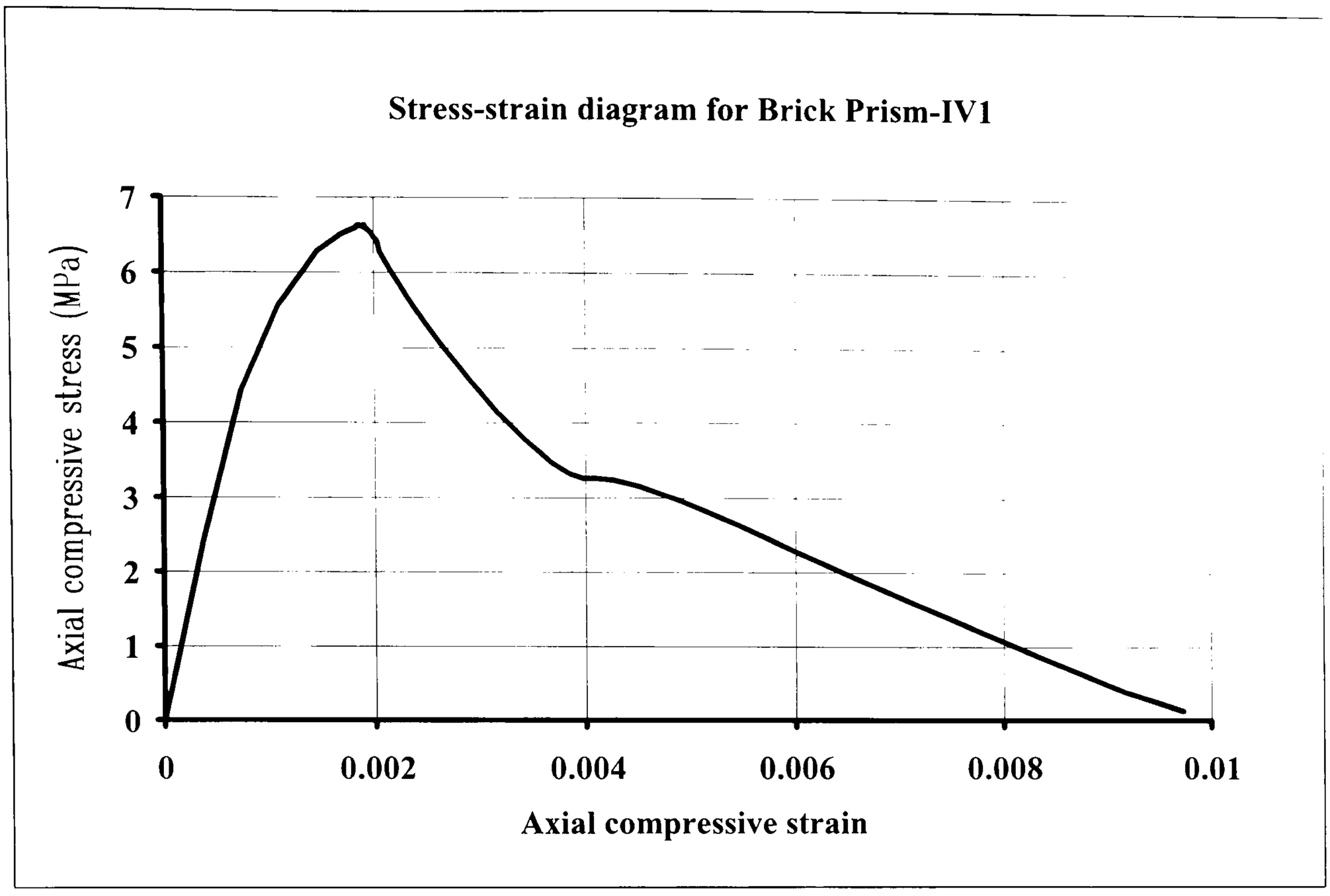

Figure 4.13 Brick IV1 stress-strain diagram

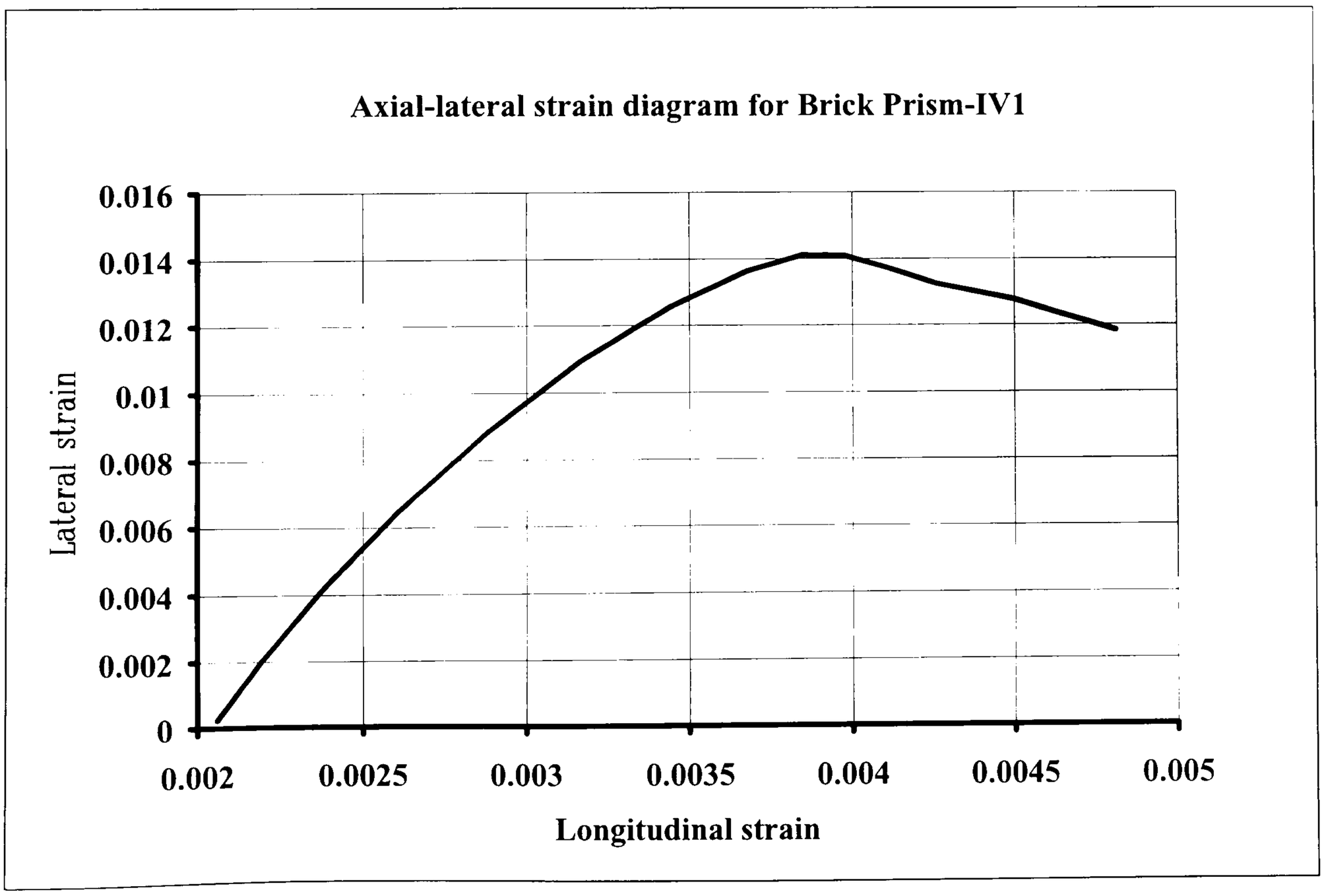

Figure 4.14 Brick IV1 axial (longitudinal)-lateral strain diagram

4.4.2.3 Model mortar test results and stress-strain diagrams.

Table 4.10 presents a summary of the test results for mortar control specimens. Figures 4.15 to 4.20 show selected stress-strain and axial-lateral strain diagrams from tests on mortar prisms M-I/II/III/IV (table 4.10). In contrast to brick specimens, mortar control specimens were air-cured, but covered with tight polythene sheets and stored under a controlled temperature environment.

M-I	**Compressive strength**	**Tensile strength**	**Modulus of elasticity**	**Peak strain**	**Ultimate strain**	**Poisson's ratio**
Cube	1.78	-	-	-	-	-
Prism	1.645	-	1965.8	0.0023	0.0035	0.15
Cylinder	-	0.171	-	-	-	-
Cube dimensions: 50 mm Cylinder dimensions: 135x38 mm Prism dimensions: 150x50x50 mm						
M-II	**Compressive strength**	**Tensile strength**	**Modulus of elasticity**	**Peak strain**	**Ultimate strain**	**Poisson's ratio**
Cube	1.762	-	-	-	-	-
Prism	1.497	-	1685.6	0.0028	0.0141	0.18
Cylinder	-	0.178	-	-	-	-
Modulus of elasticity and Poisson's ratio obtained as secant values at 45% of ultimate compressive strength						
M-III	**Compressive strength**	**Tensile strength**	**Modulus of elasticity**	**Peak strain**	**Ultimate strain**	**Poisson's ratio**
Cube	1.85	-	-	-	-	-
Prism	1.506	-	2014.9	0.0038	0.0107	0.17
Cylinder	-	0.168	-	-	-	-
Cylinder tensile splitting strength calculated from: $T = 2P/\pi ld$ Test results represent average of 6 specimens						
M-IV	**Compressive strength**	**Tensile strength**	**Modulus of elasticity**	**Peak strain**	**Ultimate strain**	**Poisson's ratio**
Cube	2.782	-	-	-	-	-
Prism	2.485	-	2844.9	0.0033	0.0057	0.19
Cylinder	-	0.217	-	-	-	-
Compressive f'_{mc}, tensile strength f'_{mt} and modulus of elasticity E_m units in **MPa**						

Table 4.10 Summary of model mortar test results

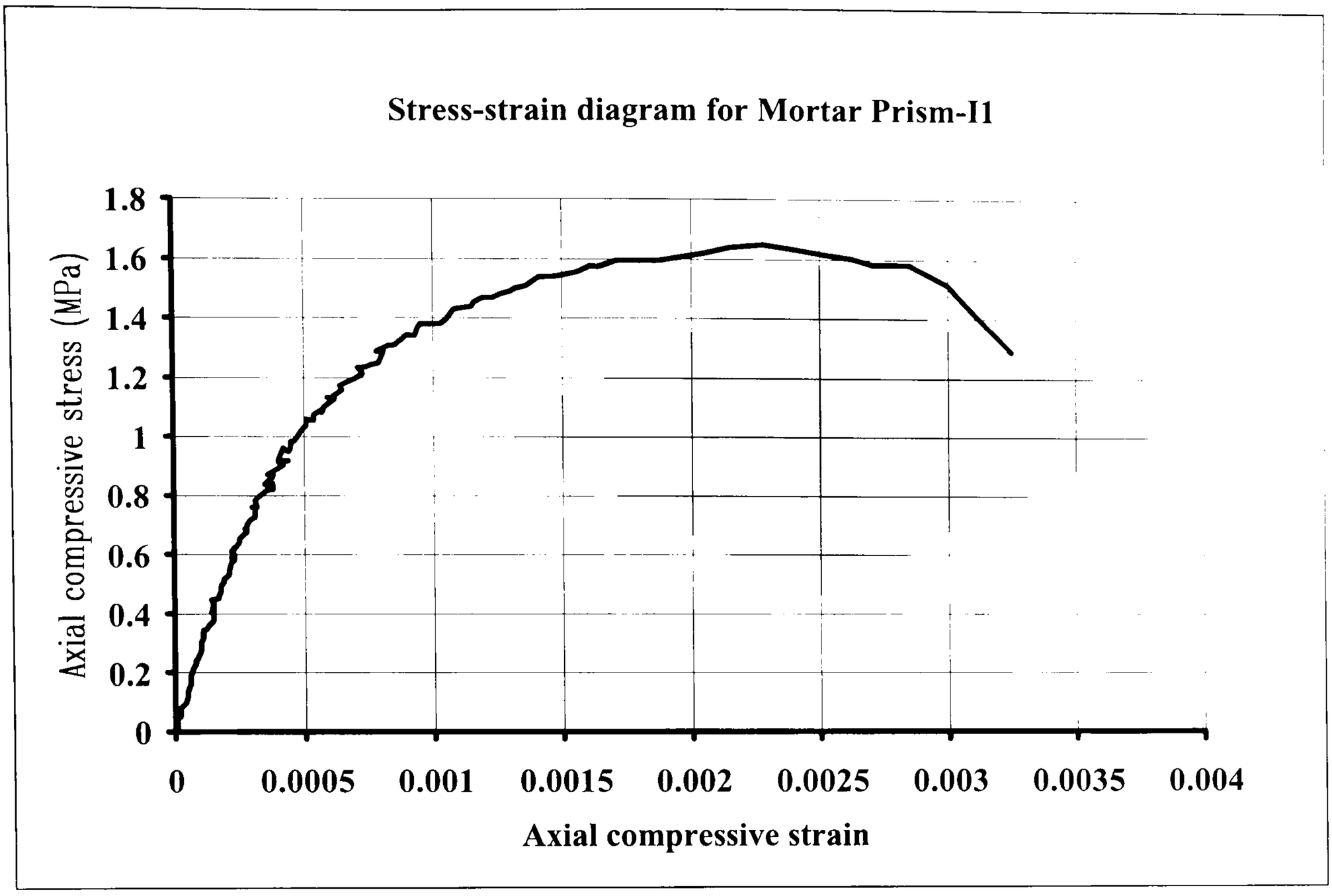

Figure 4.15 Mortar I1 stress-strain diagram

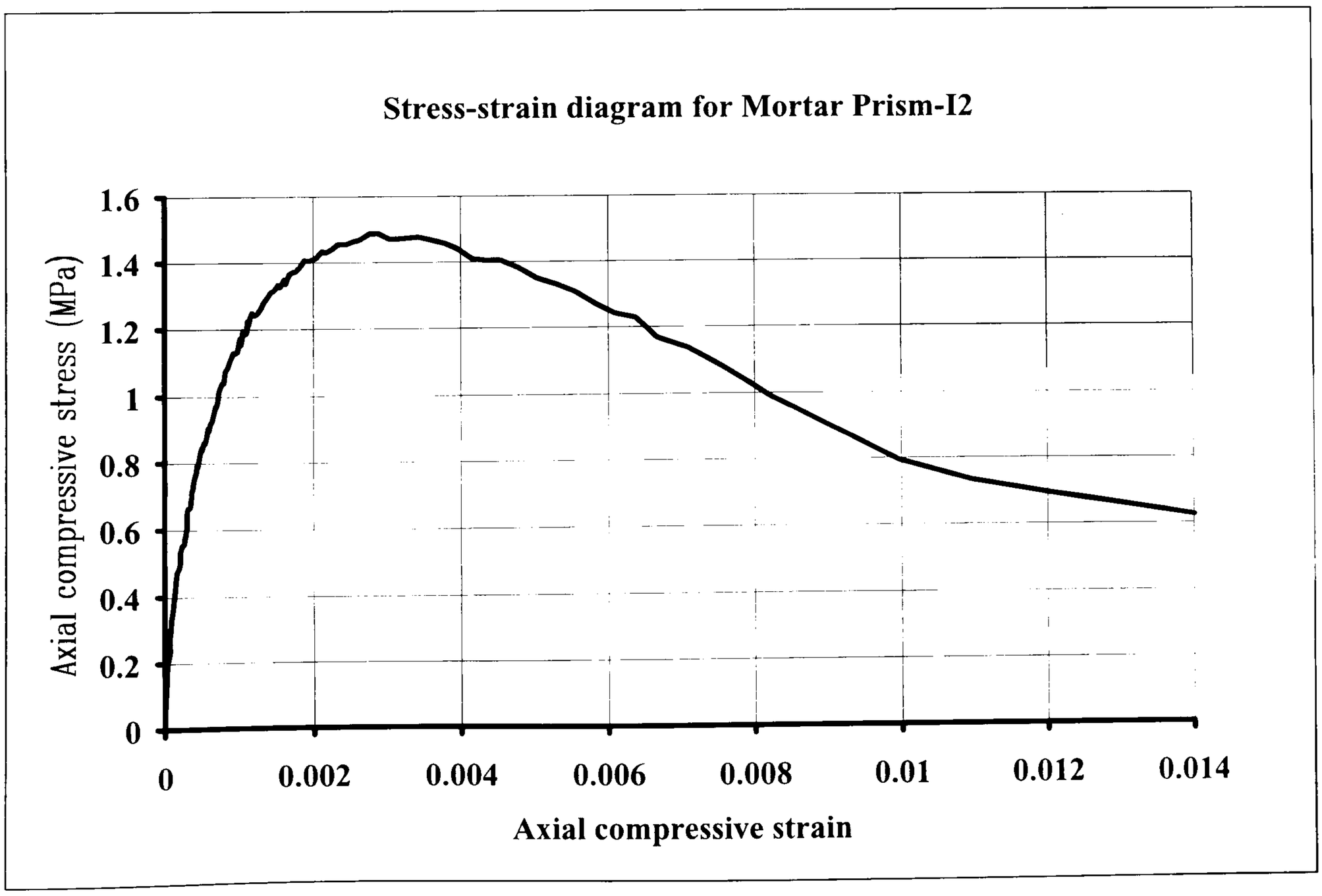

Figure 4.16 Mortar I2 stress-strain diagram

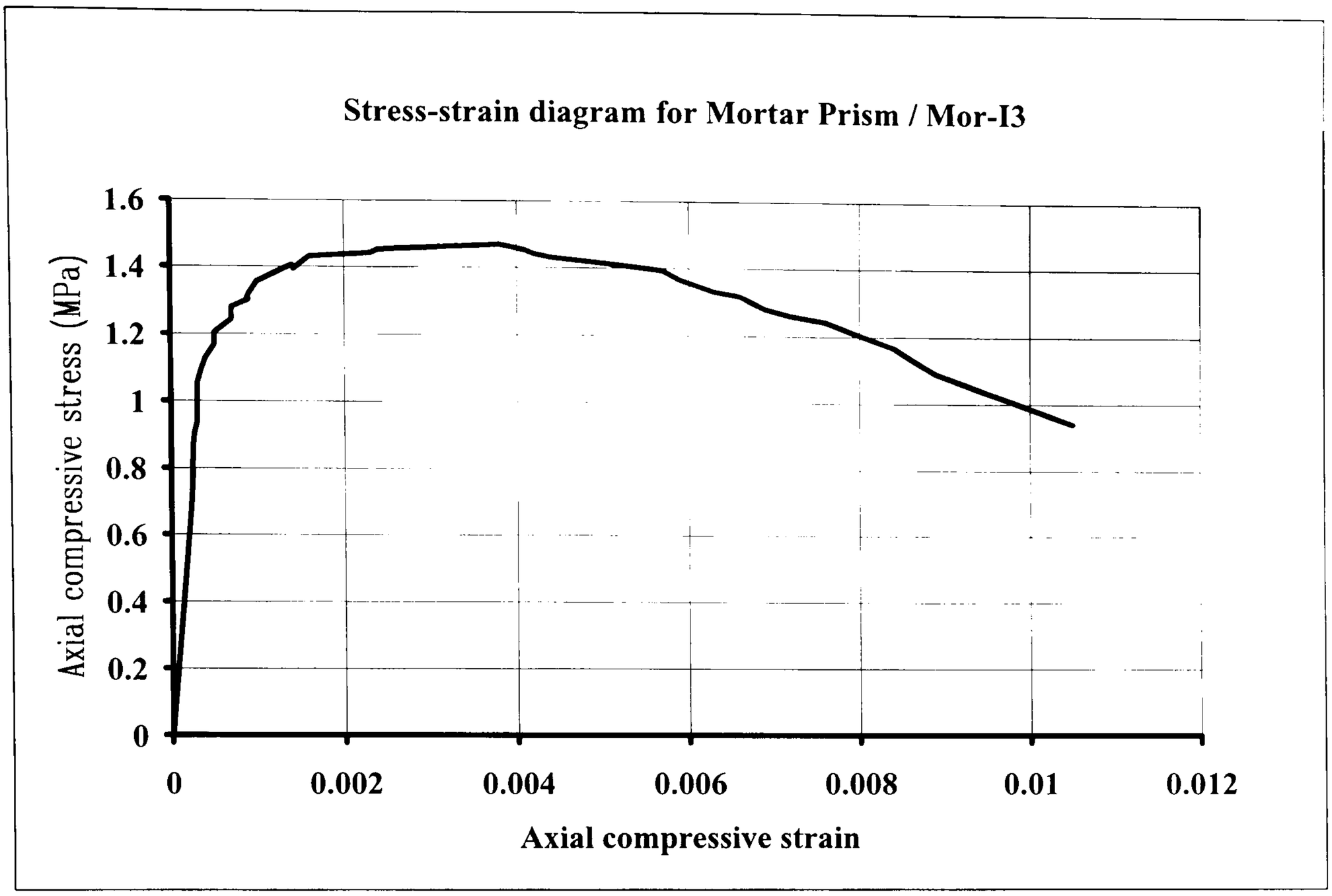

Figure 4.17 Mortar I3 stress-strain diagram

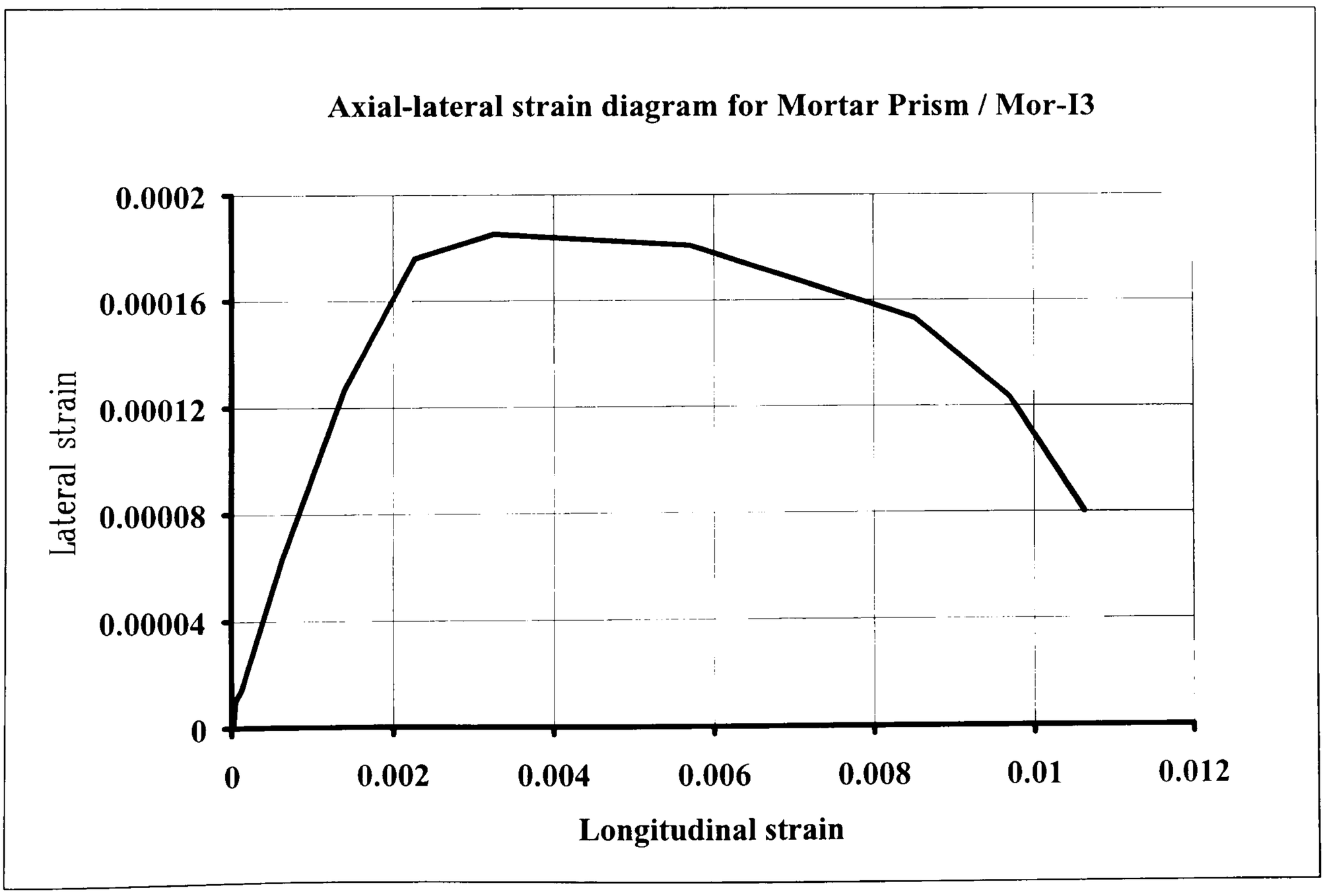

Figure 4.18 Mortar I3 axial (longitudinal)-lateral strain diagram

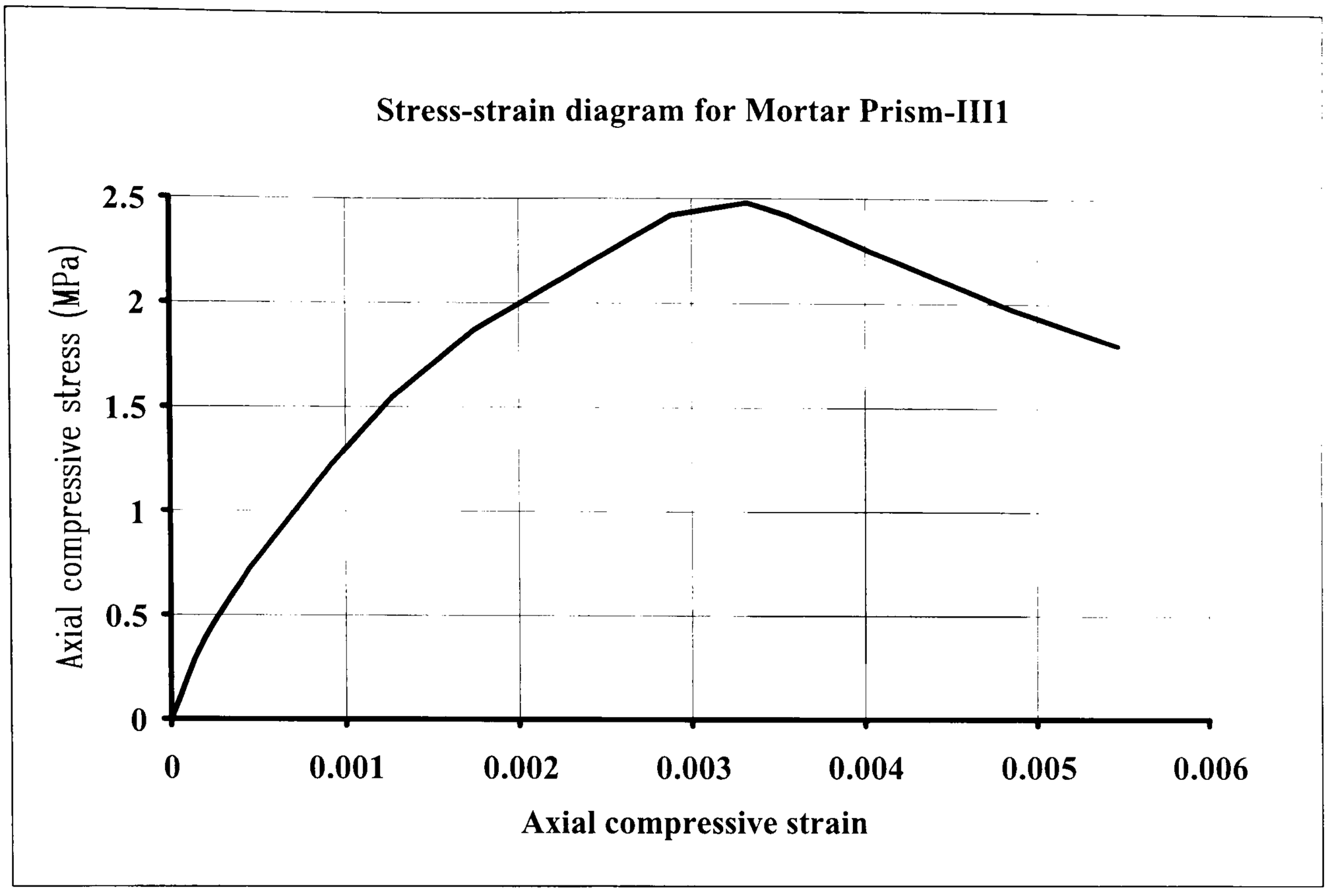

Figure 4.19 Mortar III1 stress-strain diagram

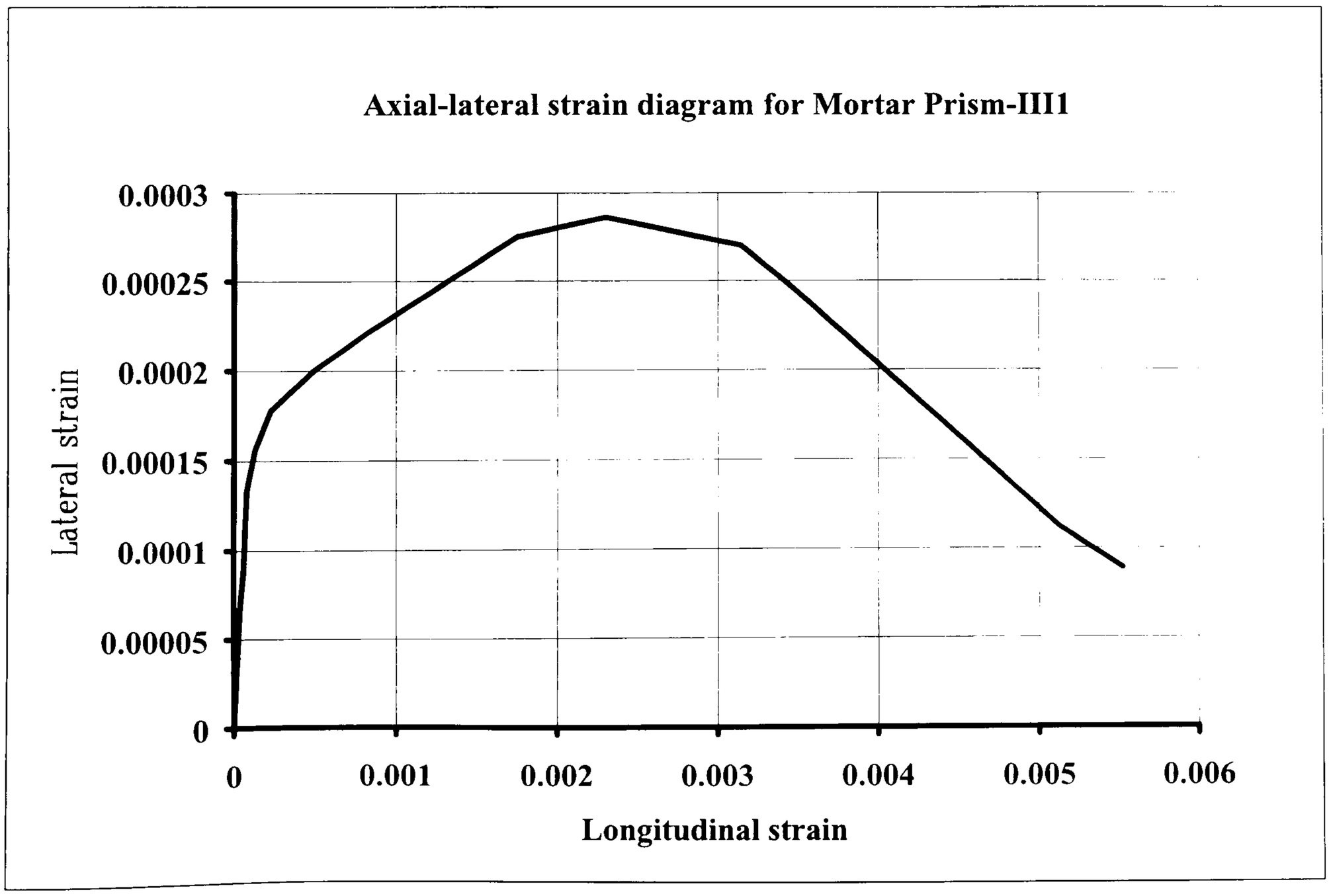

Figure 4.20 Mortar III1 axial (longitudinal)-lateral strain diagram

4.4.3 Masonry compressive strength.

The determination of the model masonry compressive strength f'_{Mc} was obtained by testing reduced scale brick masonry assemblages under uniaxial compressive load. Figure 4.21 shows the layout of some of the specimens together with their dimensions.

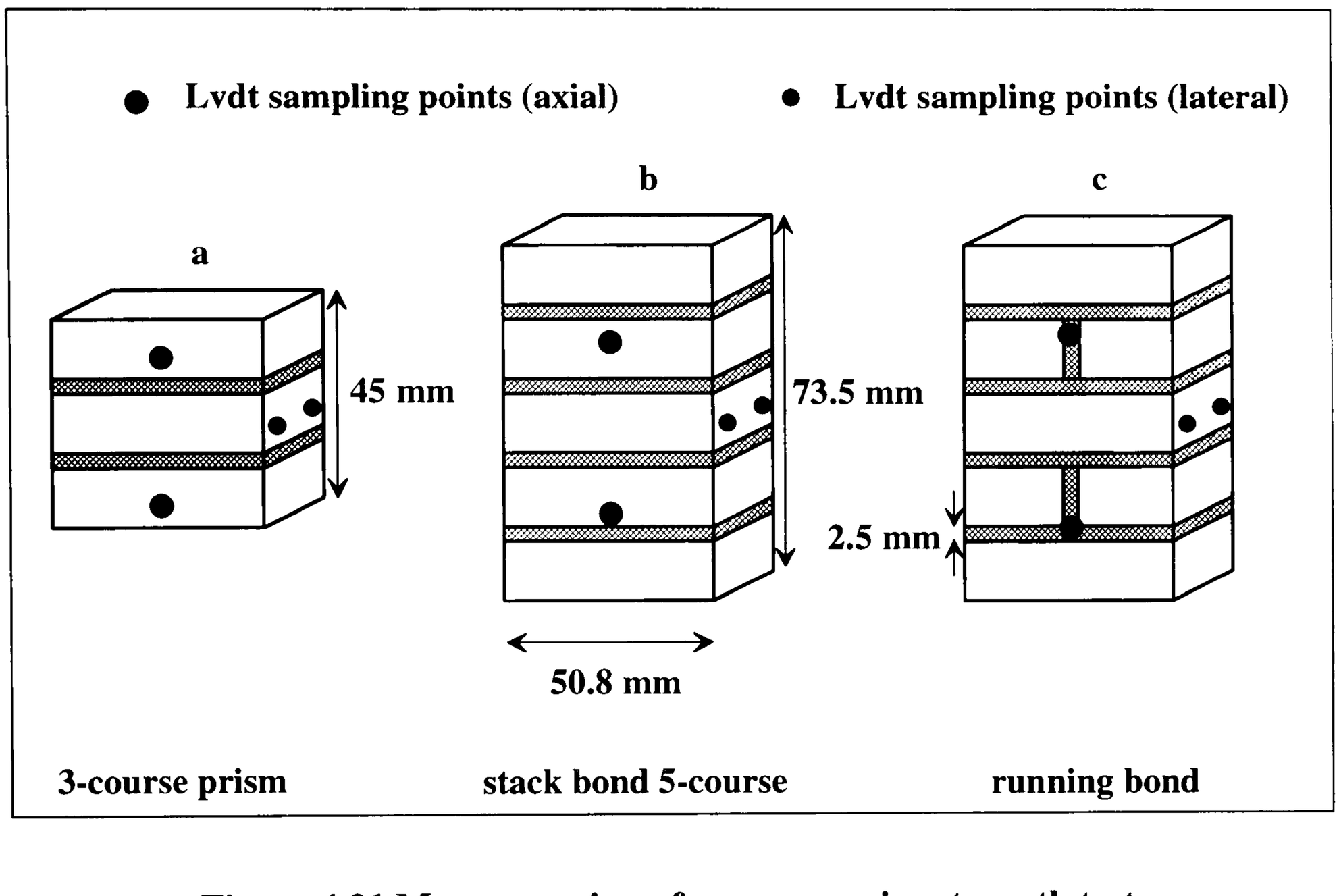

Figure 4.21 Masonry prisms for compressive strength tests

Test ASTM E447-74 [Ref. 86] suggests using prisms with length equal to or greater than the thickness of the bricks and height at least twice the brick thickness. RILEM LUMB1-1991 [Ref. 89] recommends wallettes with a height to thickness ratio between 3 and 5 (2 unit lengths width), or simple stack bonded prisms of three or more units. In the preliminary stages two sets of masonry assemblages based on the RILEM recommendations were constructed and tested for compressive strength (photos 4.7 and 4.8) but due to the number of units necessary for their production, it was decided to revert to the above shown 5-course prism configuration (figure 4.21 b,c) where the same number of components (mainly brick units) would produce more test specimens and improve the overall statistical analysis of the results. The three course assemblage (figure 4.21a) was dismissed early on in the investigation since conical failures were observed as a result of the low aspect ratio (h/t = 1.78).

Photo 4.7 Two by four by one unit wallette

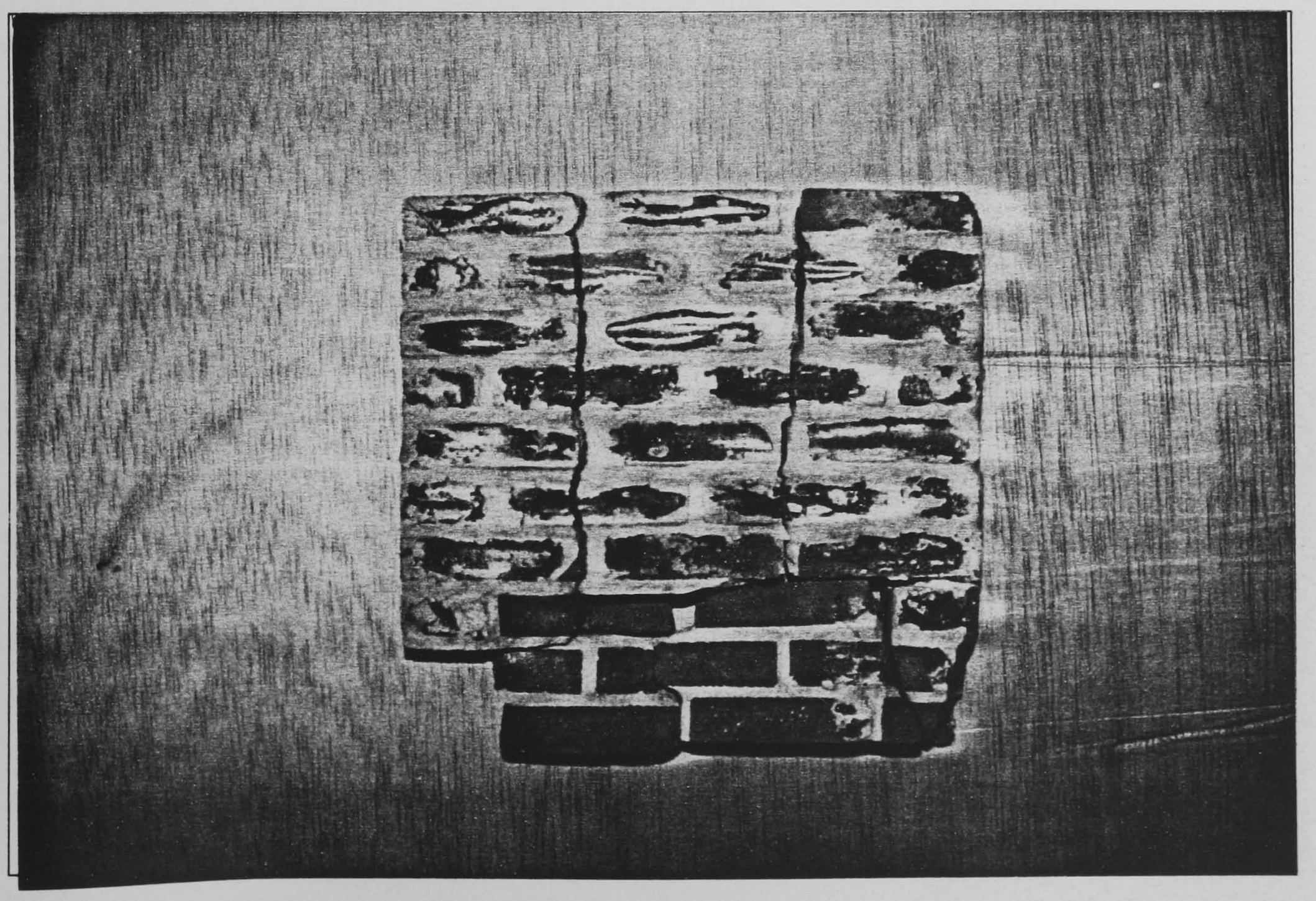

Photo 4.8 Three by ten by one unit wallette

The final configuration of a 5-course stack and running bond prism had a 2.9 (h/t) aspect ratio which permitted the correct mode of failure to happen. The prisms were constructed horizontally (section 4.1.3.3) thus ensuring uniformity in the joint thickness and satisfying the similarity conditions set out in chapter 2 (photo 4.9). Immediately after casting these were covered with polythene sheets and air-cured for 7 and 28 days together with mortar control specimens. Photos 4.10 and 4.11 show a selection of control specimens and masonry assemblages that includes wallettes and couplets which will be explained further in the following sections. One day before testing the specimens were uncovered and the aluminium support corners were glued on to the faces with quick cure (3 hour full strength) epoxy resin.

Masonry properties can vary significantly over the height of a specimen and as a result deformation measurements (figure 4.21) were taken over a gauge length that included at least three brick units and two mortar joints in order to provide combined results. The top and bottom units were excluded from deformation measurements so as to minimise any influences produced by the confining effects of the end platens. Lateral deformation readings were simultaneously obtained from transducers mounted midheight on the side faces of the prism. It should be noted that these were attached on to the middle brick of the assemblage (figure 4.21) and therefore were primarily influenced by the deformation characteristics of the unit rather than the masonry. Teflon packing was placed between the specimen and the platens for reasons explained previously. A thick circular steel bearing plate was manufactured with a spherical head for accurate positioning and alignment with the hollow load cell which in turn was fixed to the testing machine's moving platform (photo 4.12). Cracking patterns and failure modes were recorded photographically at the end of each test. The model prisms exhibited a consistent vertical splitting type of failure with cracks that originated near the centre brick and with increased loading extended to the full height of the specimen (photos 4.13 and 4.14). No crushing of either the brick units or mortar joints took place in any of the prisms. This failure pattern was also observed and documented by other investigators on tests of full and small masonry prisms of the same (or nearly the same) aspect ratio [Ref. 1, 40, 68 - photo 4.23].

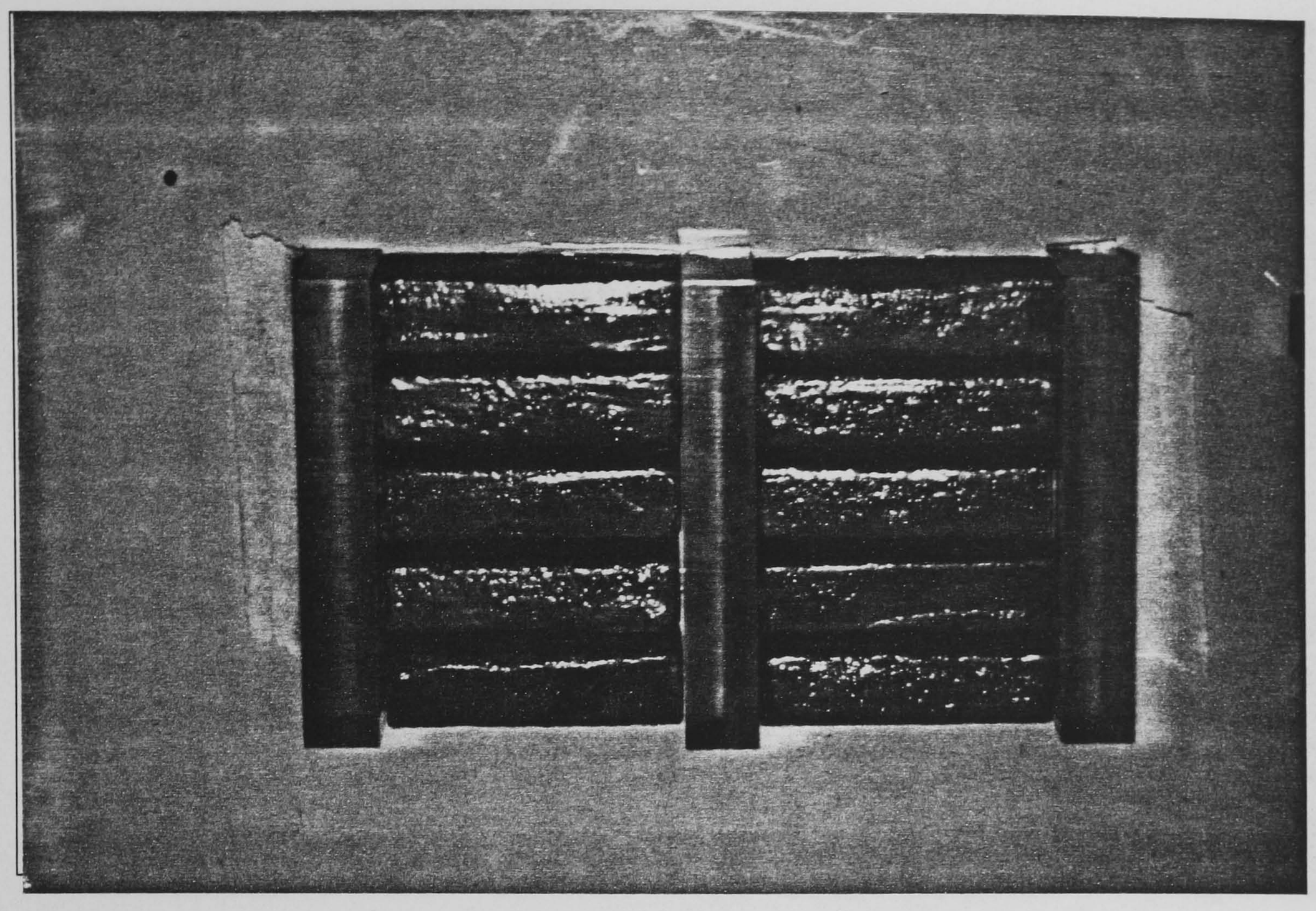

Photo 4.9 Masonry running bond prisms ready for mortar placement

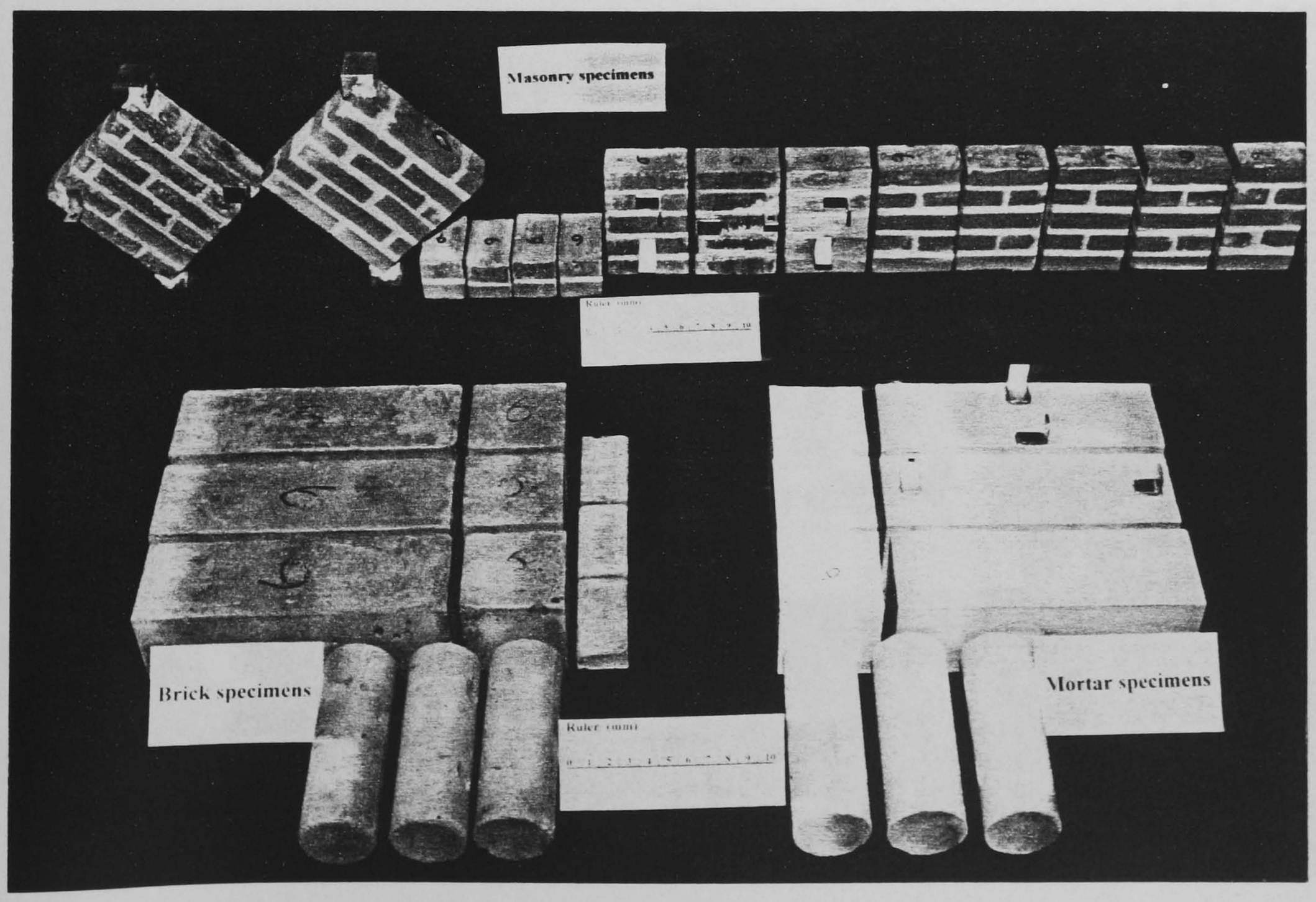

Photo 4.10 Masonry control specimens and assemblages

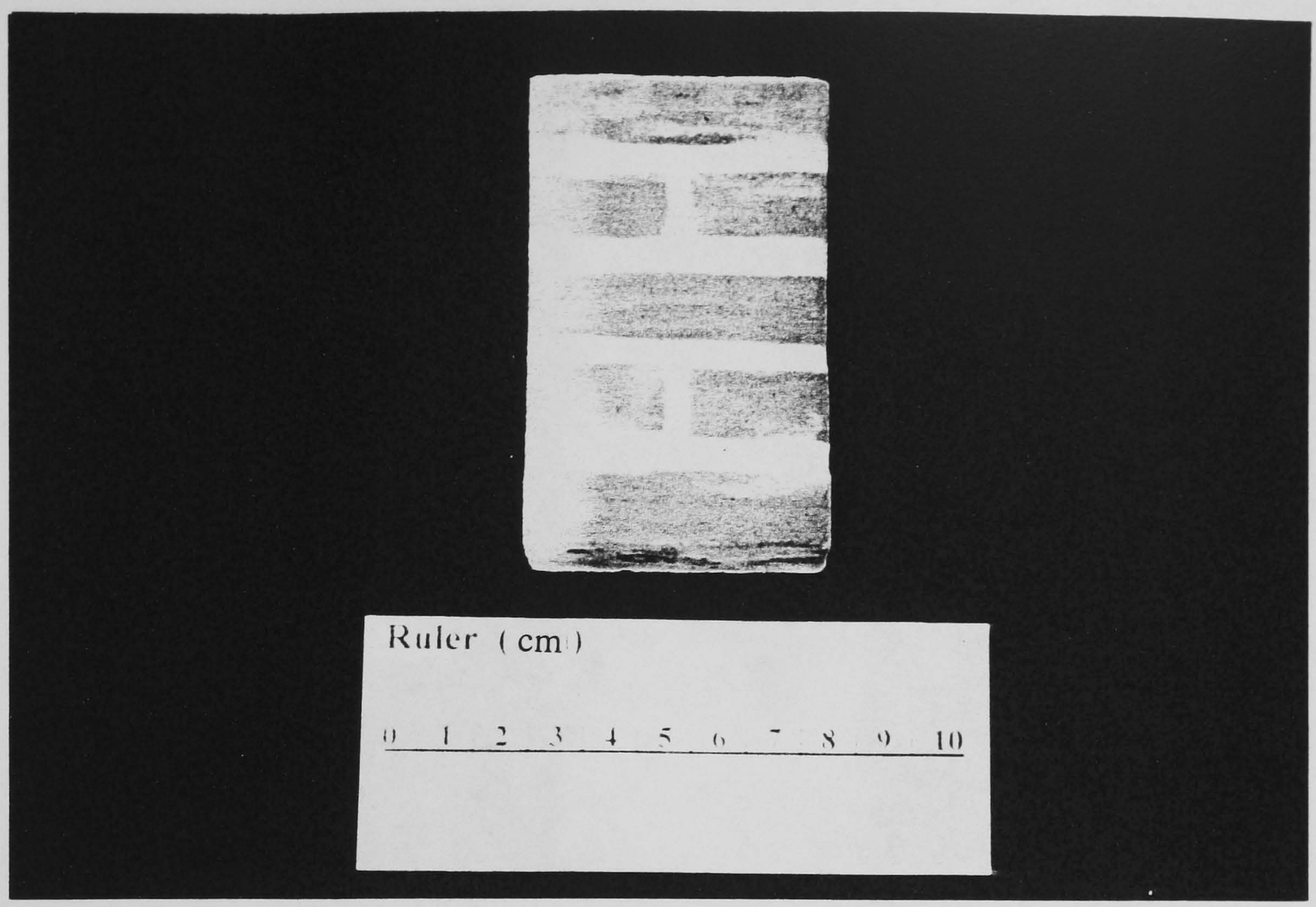

Photo 4.11 5-course running bond model prism

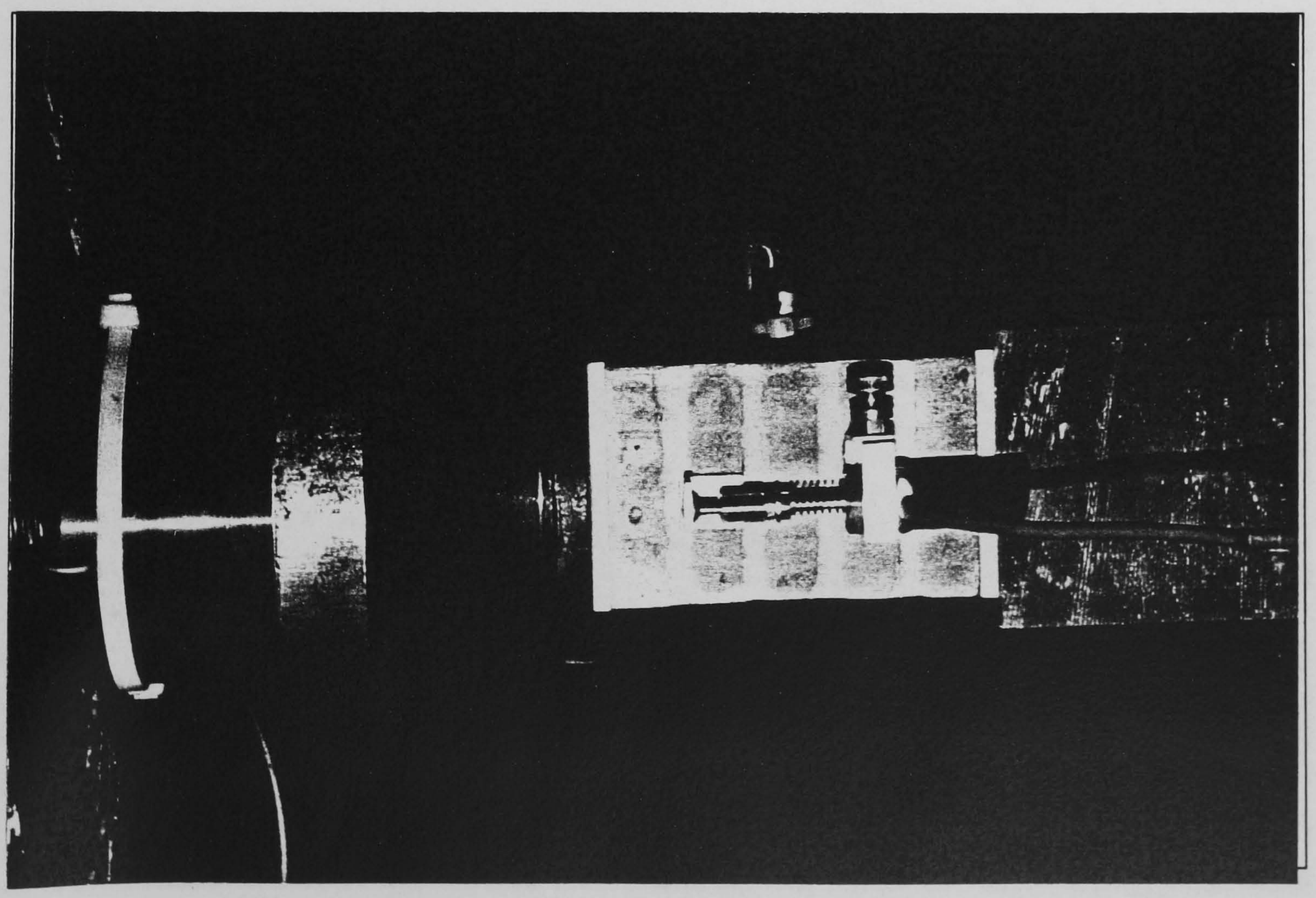

Photo 4.12 Masonry prism ready for compressive strength testing

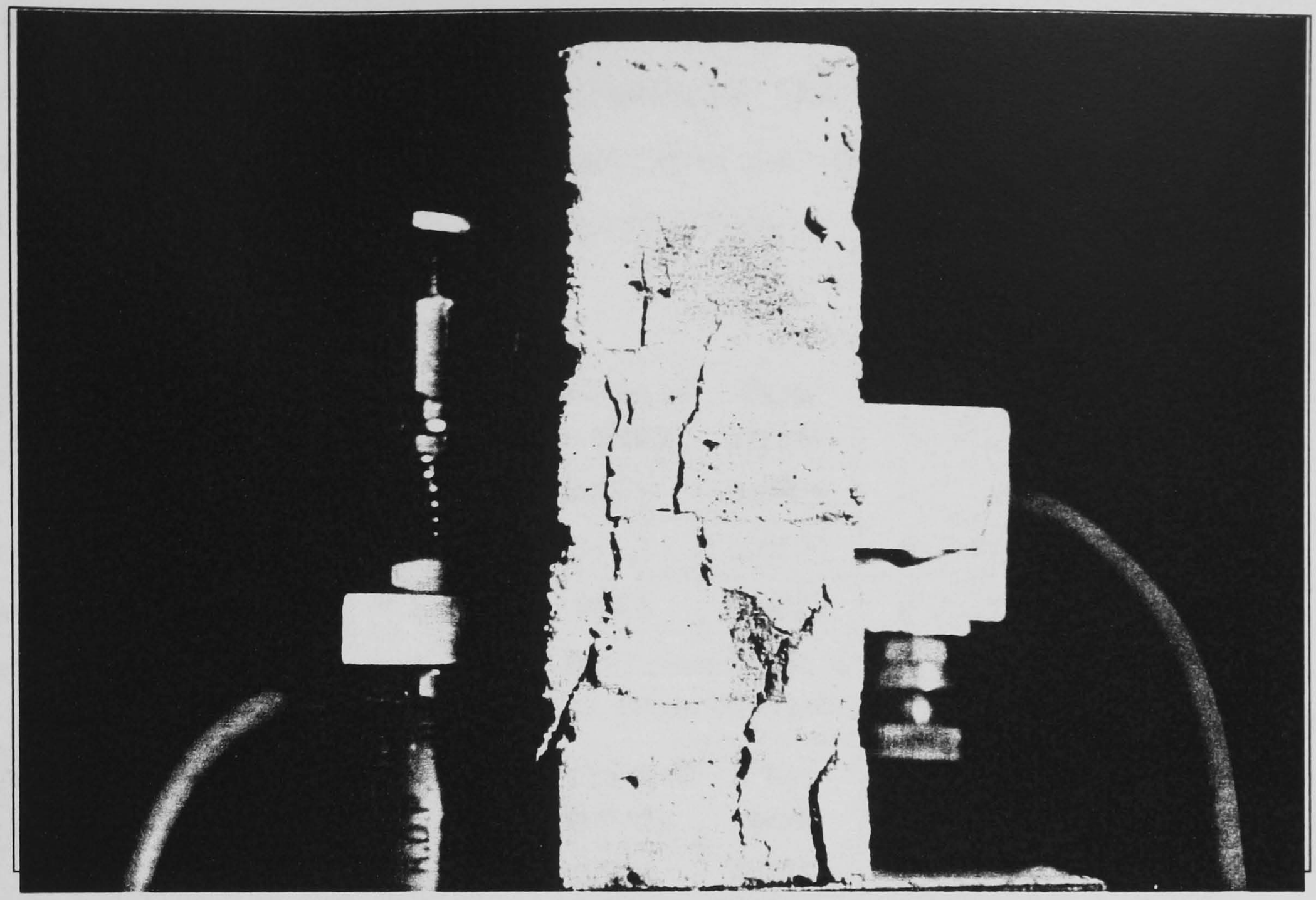

Photo 4.13 Close-up of vertical splitting failure mode for model prism

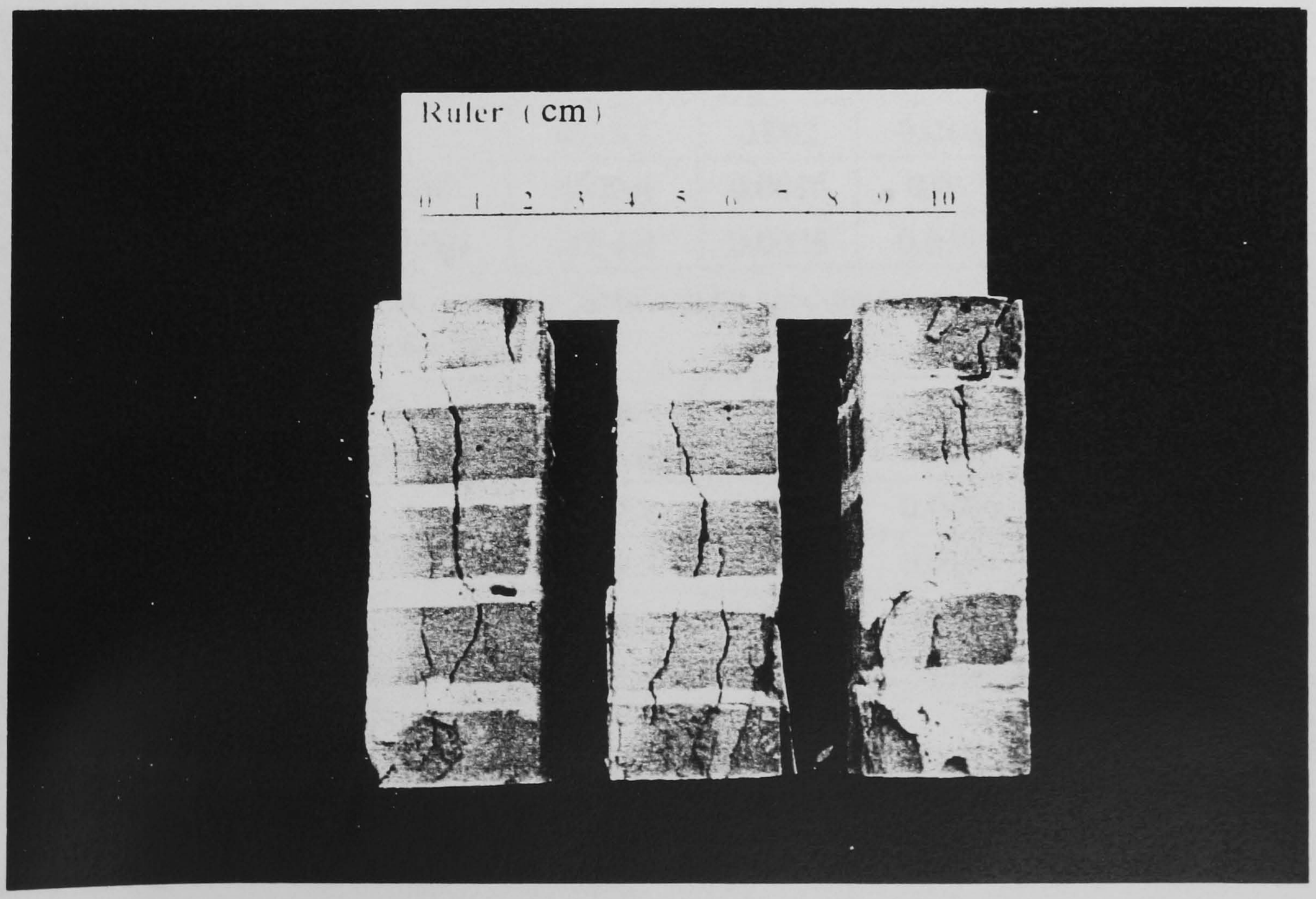

Photo 4.14 Further failure modes for model prisms

Table 4.11 presents test results for 5-course masonry prisms, including results for the brick units and mortar used for their construction. Figures 4.22 to 4.26 show a selection of stress-strain and axial-lateral strain curves obtained for the masonry prisms tested using the procedures and techniques described before.

MP-I	**Compressive strength**	**Tensile strength**	**Modulus of elasticity**	**Peak strain**	**Ultimate strain**	**Poisson's ratio**
Mas. prism	4.853	-	3698.2	0.0026	0.0041	0.13
Brick	7.22	0.69	4551.3	0.0022	0.0109	0.09
Mortar	1.78	0.171	1965.8	0.0023	0.0035	0.15
Cube dimensions: 50 mm Cylinder dimensions: 135x38 mm Prism dimensions: 150x50x50 mm Mas. prism dimensions: 73.5x50.8x25.4 mm						
MP-II	**Compressive strength**	**Tensile strength**	**Modulus of elasticity**	**Peak strain**	**Ultimate strain**	**Poisson's ratio**
Mas. prism	3.26	-	2862.4	0.0017	0.0078	0.12
Brick	7.275	0.58	6148.8	0.0035	0.0053	0.06
Mortar	1.762	0.178	1685.6	0.0028	0.0141	0.18
Modulus of elasticity and Poisson's ratio obtained as secant values at 45% of ultimate compressive strength						
MP-III	**Compressive strength**	**Tensile strength**	**Modulus of elasticity**	**Peak strain**	**Ultimate strain**	**Poisson's ratio**
Mas. prism	5.24	-	4323.6	0.002	0.0148	0.19
Brick	7.413	0.67	6600.4	0.0016	0.017	0.11
Mortar	1.85	0.168	2014.9	0.0038	0.0107	0.17
Brick and mortar strength values based on 50 mm cube specimens Test results represent average of 6 specimens						
MP-IV	**Compressive strength**	**Tensile strength**	**Modulus of elasticity**	**Peak strain**	**Ultimate strain**	**Poisson's ratio**
Mas. prism	3.01	-	2207.8	0.0019	0.0086	0.15
Brick	7.766	0.65	5968.8	0.0019	0.0104	0.12
Mortar	2.782	0.217	2844.9	0.0033	0.0057	0.19
Compressive f'_{Mc}, tensile strength f'_{Mt} and modulus of elasticity E_M units in **MPa**						

Table 4.11 Summary of test results for masonry prisms and control specimens

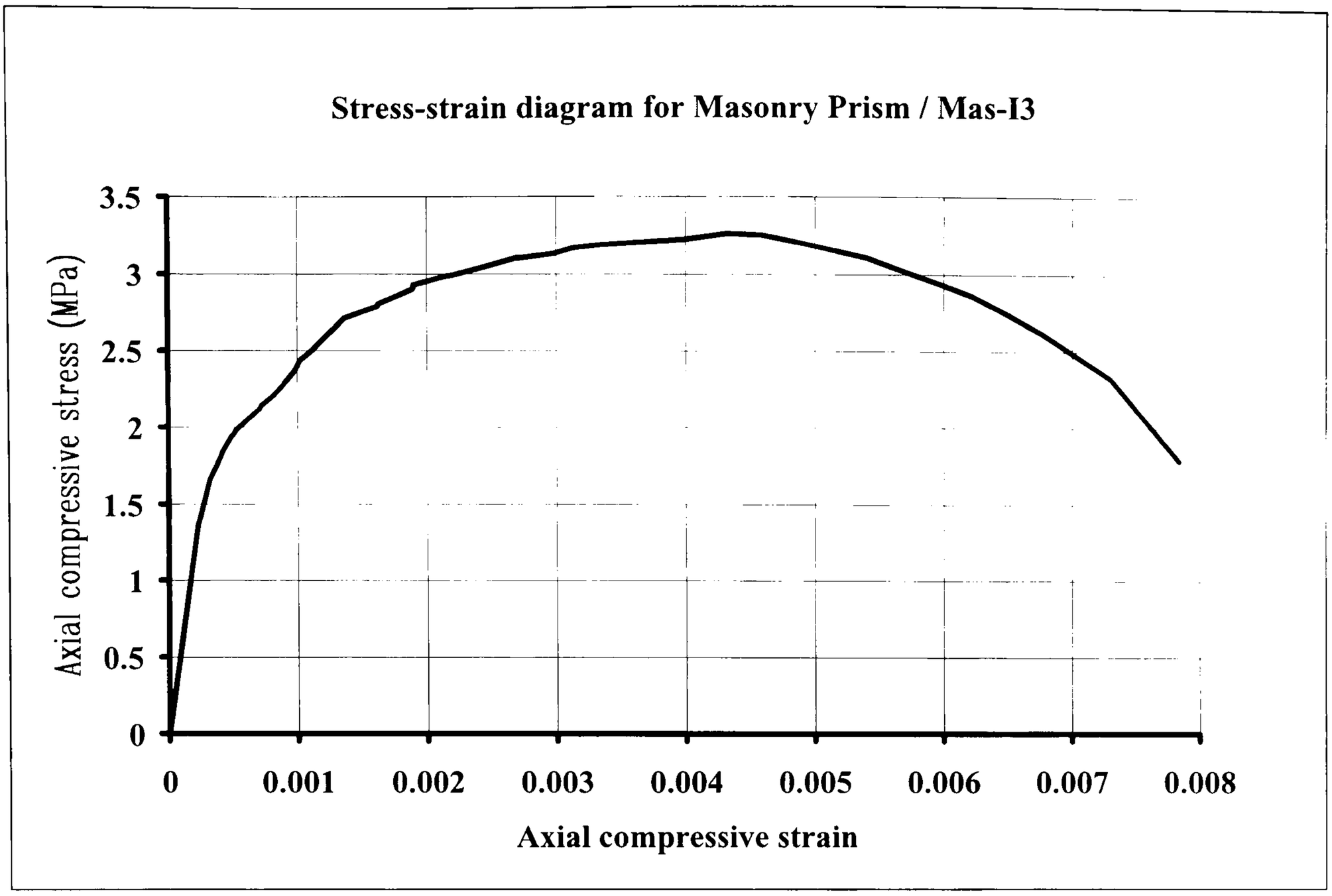

Figure 4.22 Masonry stress-strain diagram (I3)

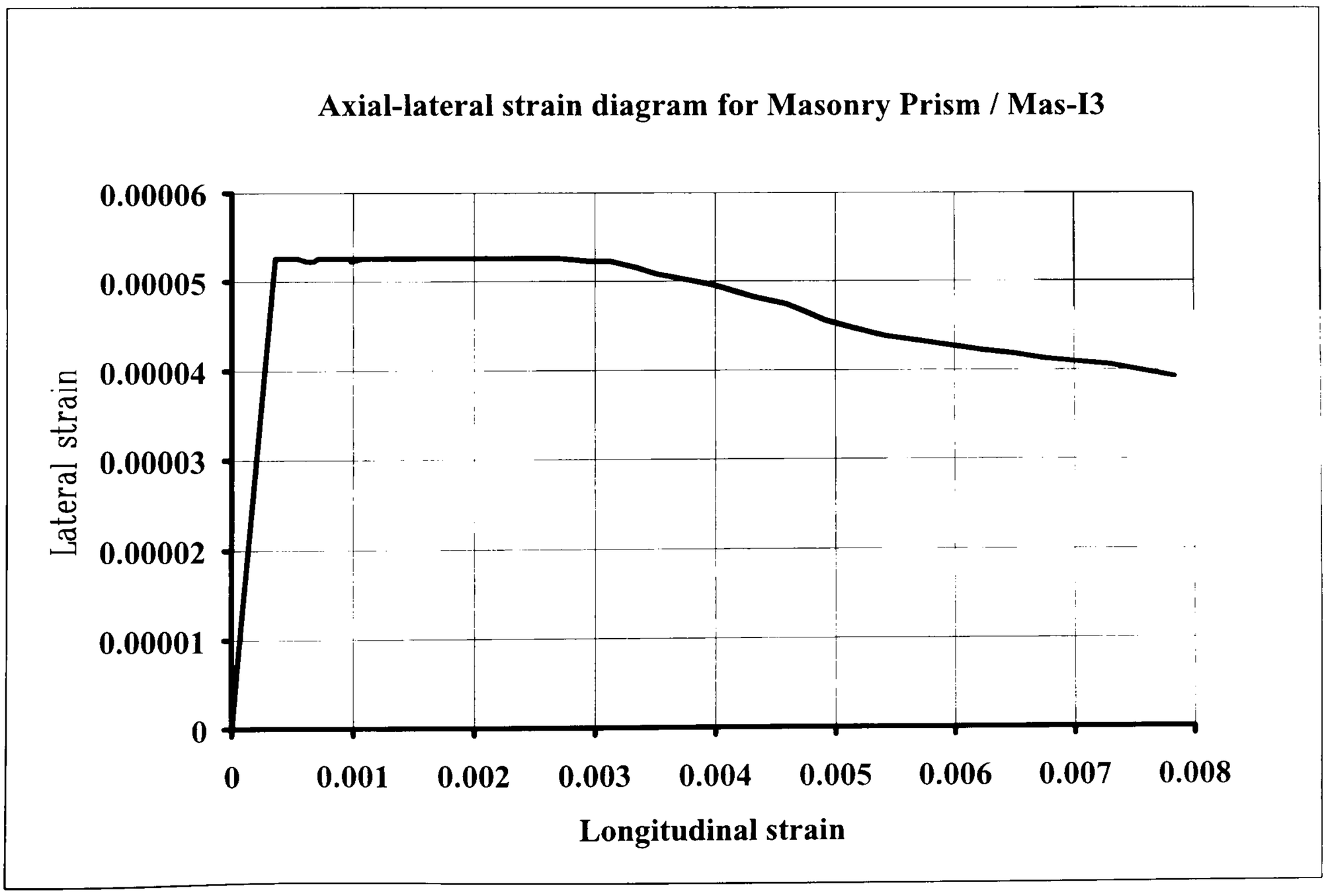

Figure 4.23 Masonry axial (longitudinal)-lateral strain diagram (I3)

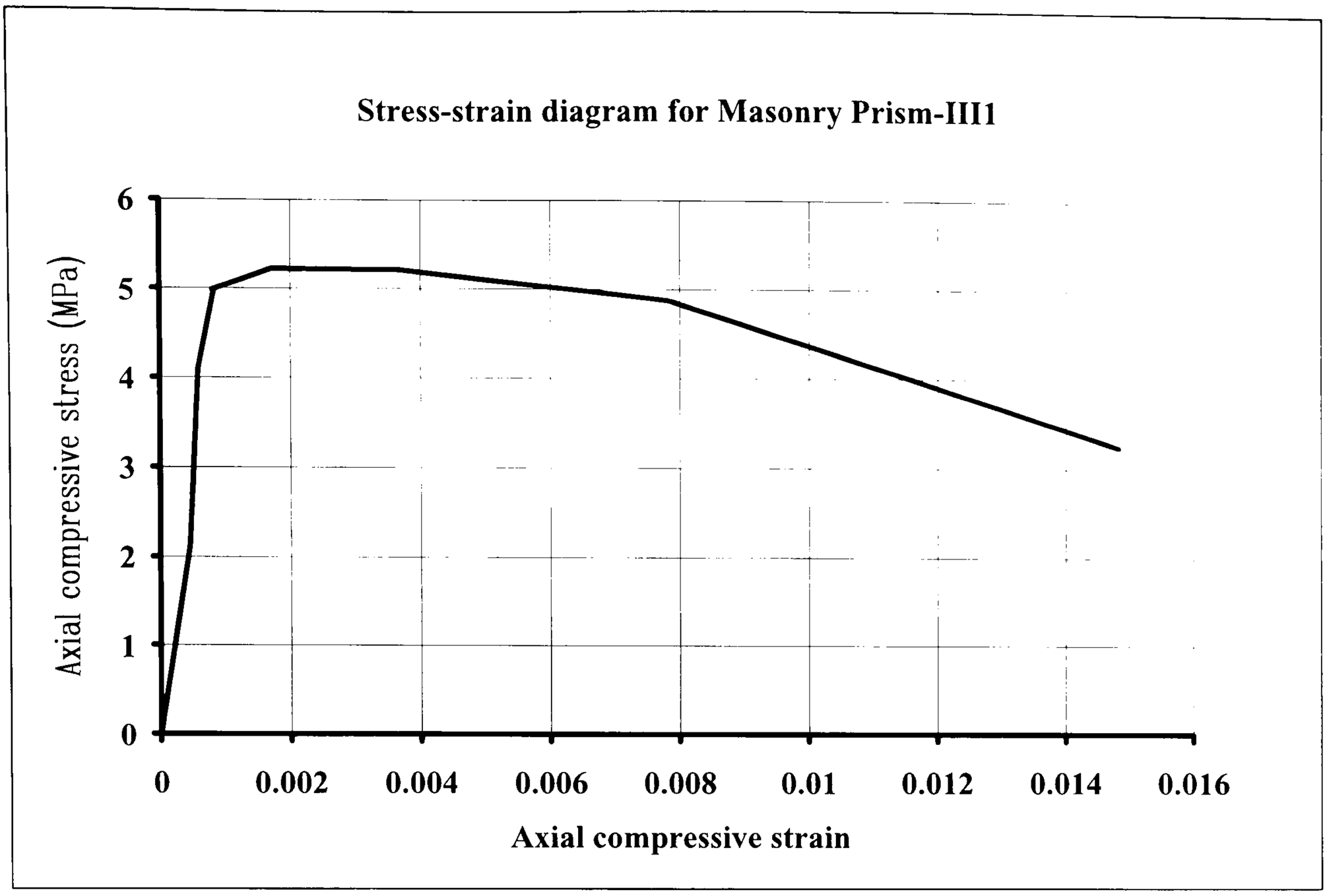

Figure 4.24 Masonry stress-strain diagram (III1)

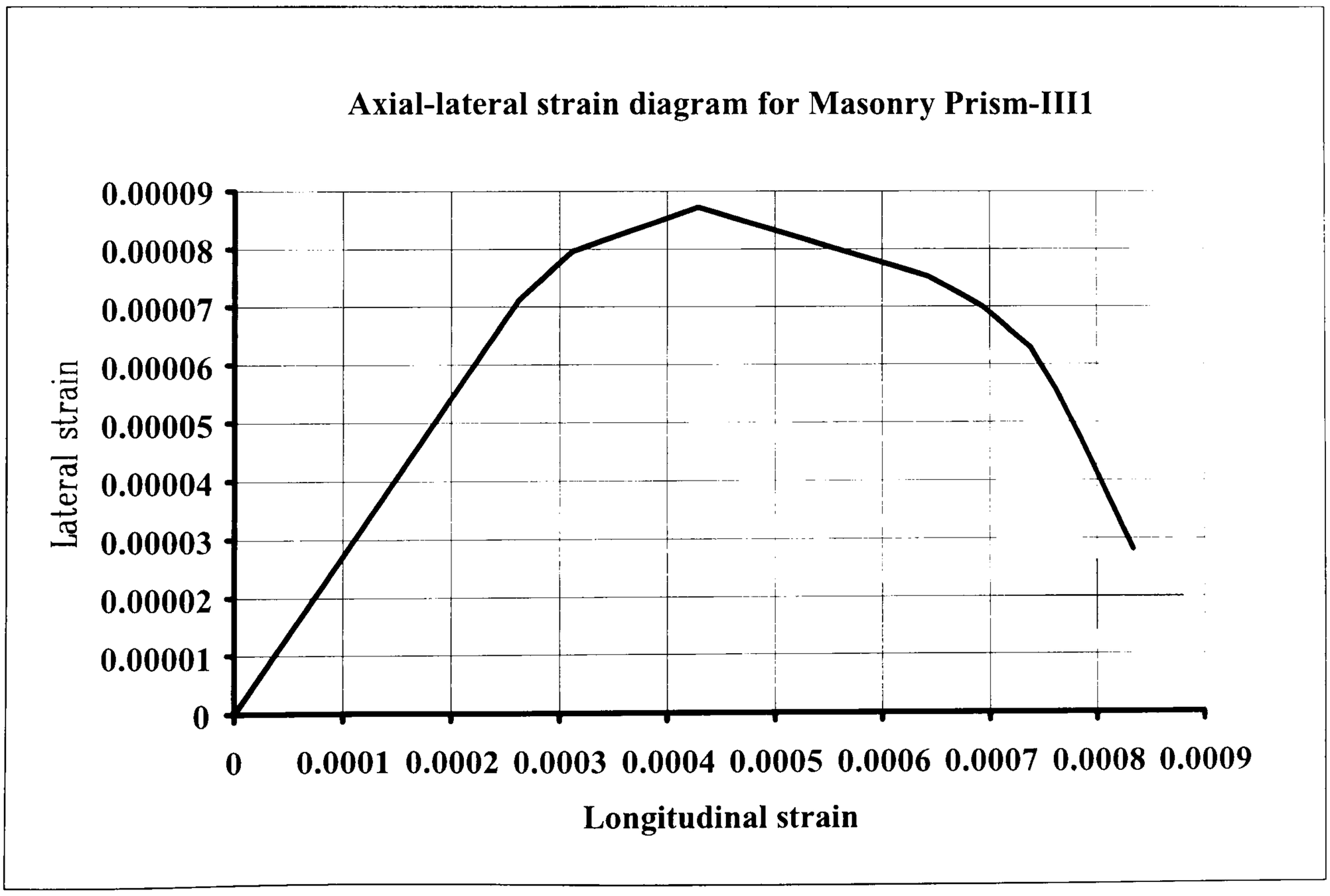

Figure 4.25 Masonry axial (longitudinal)-lateral strain diagram (III1)

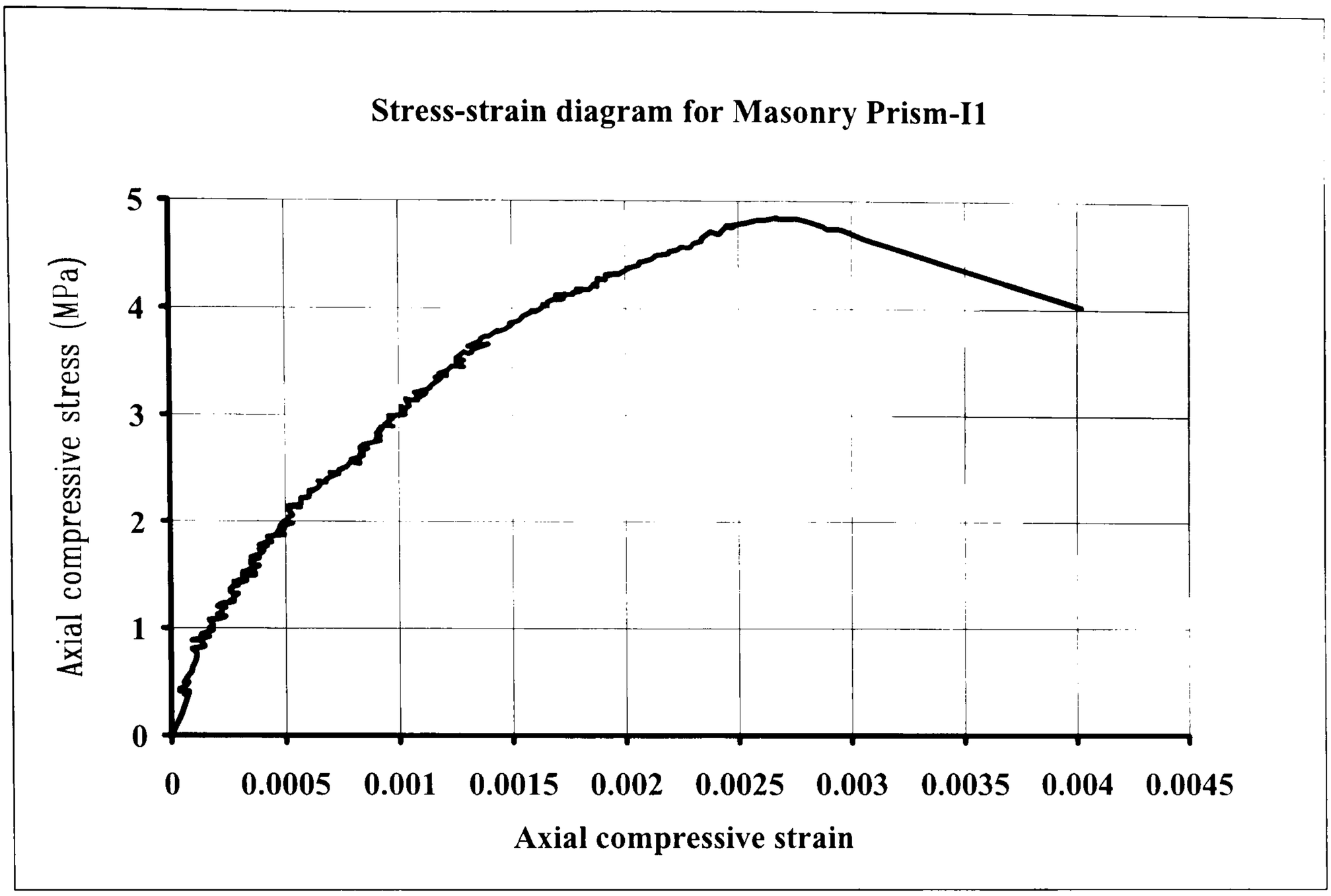

Figure 4.26 Masonry stress-strain diagram (I1)

4.4.4 Masonry shear strength.

The determination of overall masonry shear strength f'_{Md} has long been a subject of intense debate and disagreement due mainly to the difficulty in reproducing reasonable boundary conditions for specimens tested in the laboratory. In-plane shear resistance of masonry is an important characteristic that determines the behaviour of masonry particularly when subjected to various types of lateral loads (wind, seismic). To distinguish between tests conducted on full scale panels and small structural assemblages the purpose of the test should be clarified beforehand. Laboratory experiments on small wallettes (full or reduced scale), that include square masonry specimens consisting of just a few courses are usually conducted with the aim of providing a prediction of the in-plane diagonal tensile strength as well as examining the various parameters that influence the behaviour and strength properties, such as individual brick and mortar compressive and tensile strength. On the contrary full scale masonry panels can be subjected to static or cyclic in-plane shear load in an attempt to

verify or establish new design methods based on failure modes, ultimate strength, stiffness degradation and hysteretic behaviour.

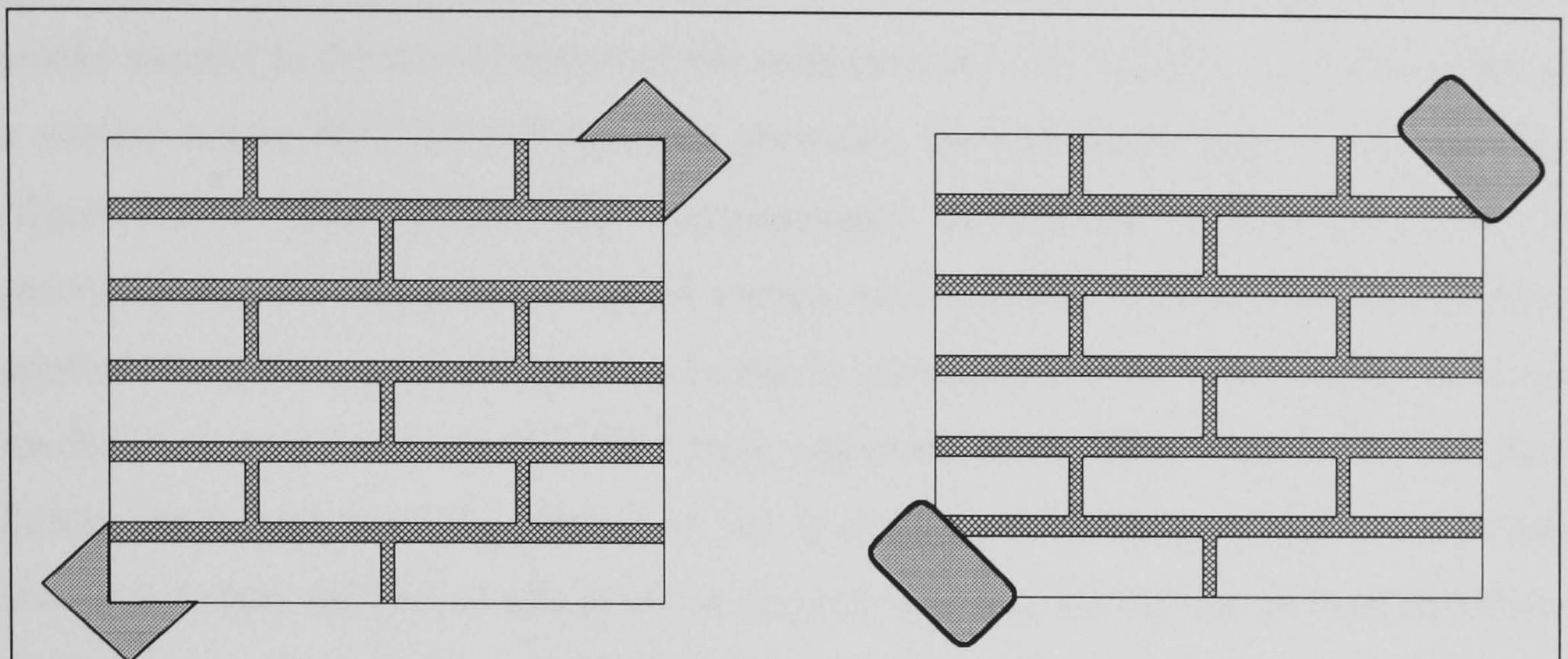

a. Square masonry wallette (RILEM-LUMB6/91) with corner loading shoes

b. Square masonry wallette (ASTM-E519/74) with corner loading shoes

Dimensions: (shown) 104x104 mm (small-2 units x 6 units)
(not shown) 158x158 mm (large -3 units x 10 units)

Figure 4.27 Masonry assemblages for in-plane tensile splitting tests

ASTM describes two methods that are solely intended to induce diagonal tensile cracking on the test specimen. The principal differences between the two are the size of

the assemblage and the way the load is applied. In the first case (ASTM-E519) a square wallette is subjected to a diagonal compression load (figure 4.27b) through steel loading shoes at the two opposite corners and it is recommended as a research test method for parametric studies only. The usual mode of failure consists of a pattern of diagonal cracks parallel to the line of action of the compressive load. RILEM (LUMB6) suggests a similar test to ASTM-E519 but with provision for a different type of loading shoe (figure 4.27a). The second test recommended by ASTM (E72-racking test) is recommended for larger scale square panels, that involves a horizontal lateral force applied along the top of the panel while this is restrained from overturning by tie-down mechanisms (e.g. steel ropes). The main argument in all these tests is that the final failure mode and cracking pattern of the specimen are influenced and subsequently forced to follow the line of action of the applied load and not the line of least resistance in the panel which is quite difficult to predict. They may therefore not represent the critical behaviour in shear. Nevertheless the strength information and the behaviour characteristics derived from such tests are in their own way consistent and therefore can be used as relative criteria in the design of masonry elements (infill panels and shear walls) that are required to resist lateral forces as part of their principal structural function.

For the purposes of this investigation where it was necessary to evaluate the feasibility of such tests using small scale models and to predict the shear strength (diagonal tensile strength) of complete masonry panels for any subsequent dynamic testing, the square wallette was chosen as the most suitable specimen for diagonal compression tests. Sets of loading shoes scaled down from sizes recommended both by the ASTM and RILEM test procedures, were designed and manufactured in the workshop. The first type was made out of 1.5 mm thick steel hollow tube while the second was manufactured from duraluminium. Two different size wallettes where investigated (dimensions shown in figure 4.27), since it was intended to use the smallest size that could still provide reliable results. After casting the specimens in the laboratory using perspex moulds and a drawn bottom grid to ensure consistency in the mortar joint thickness, the wallettes were air cured for 3, 7 and 28 days covered tightly with plastic sheets together with mortar control specimens cast from the same mix. One day before testing these were uncovered, the instrumentation aluminium supports were

glued on and the loading shoes put in position using dental plaster (plaster 24 hour compressive strength, f'_{pc}= 12 MPa). Table 4.11 presents a summary of the tests performed on model wallettes, with average values taken out of 3 specimens in each group.

WT-I	**Compressive strength**	**Tensile cylinder strength**	**In-plane wallette tensile strength**	**Shear modulus**	**Peak shear strain**	**Ultimate shear strain**
Wallette	-	-	0.382	1646.45	0.0002	0.002
Brick	7.22	0.69	-	-	-	-
Mortar	1.81	0.179	-	-	-	-
Wallettes - I/II dimensions: 159x159x25.4 mm Wallettes - III/IV dimensions: 104x104x25.4 mm						
WT-II	**Compressive strength**	**Tensile strength**	**In-plane tensile strength**	**Shear modulus**	**Peak strain**	**Ultimate strain**
Wallette	-	-	0.242	1105.2	0.00023	0.0128
Brick	7.275	0.58	-	-	-	-
Mortar	1.762	0.162	-	-	-	-
Shear modulus obtained as a secant value at 45% of ultimate in-plane tensile strength Tensile strength taken as f'_{Md}= 0.707 P/A (P-applied load, A-cross sectional area)						
WT-III	**Compressive strength**	**Tensile strength**	**In-plane tensile strength**	**Shear modulus**	**Peak strain**	**Ultimate strain**
Wallette	-	-	0.449	1952.8	0.00023	0.0148
Brick	7.413	0.67	-	-	-	
Mortar	1.97	0.189	-	-	-	
Brick and mortar strength values based on 50 mm cube specimens Test results represent average of 3 specimens						
WT-IV	**Compressive strength**	**Tensile strength**	**In-plane tensile strength**	**Shear modulus**	**Peak strain**	**Ultimate strain**
Wallette	-	-	0.124	N/A	N/A	N/A
Brick	7.766	0.65	-	-	-	-
Mortar	0.45	0.057	-	-	-	-
Compressive, tensile strength and shear modulus G'_M units in **MPa**.						

Table 4.12 Summary of test results for masonry wallettes and control specimens

Specimens for group WT-IV (table 4.12) were tested at 3 days and failed too quickly (sliding along the horizontal mortar joints close to the loaded corners) for any consistent data to be available so these were excluded altogether. LVDTs with extensions rods were mounted on the faces of the wallettes along the two diagonal axes and at some distance away from the corners. The gauge measuring length was identical for both transducers which coupled with a second pair mounted on the opposite side, were used to provide average values (photo 4.16). Measured data of load and deformation for both axes (parallel and transverse) were converted to shear stress and shear strain values using formulas included in ASTM-E519. Based on these values the modulus of rigidity (shear modulus) was also calculated.

Photo 4.16 show a larger size wallette (159x159x25.6 mm) before testing with the LVDTs mounted as well as the RILEM prescribed loading shoes, while photo 4.17 shows one of the smaller size wallette specimens for visual comparison of size. As mentioned before the ultimate strength and mode of failure in this test are mainly dependent on the tensile strength of the individual components. Secondary parameters that may influence the behaviour include water absorption characteristics of the brick units and the overall size of the specimens. It was observed that between the 7 and 28 day specimen test period the mode of failure changes from a combined shear and sliding mode (photo 4.18) to a diagonal tensile splitting one (photo 4.19). This clearly demonstrates the dependence of this test on the tensile strength of the brick units and particularly of the mortar joints which is also highly influenced by the shear bond strength and interface friction (section 4.4.5). Figures 4.28 and 4.29 present shear stress -shear strain diagrams for masonry wallettes taken from groups WT-I and WT-II respectively.

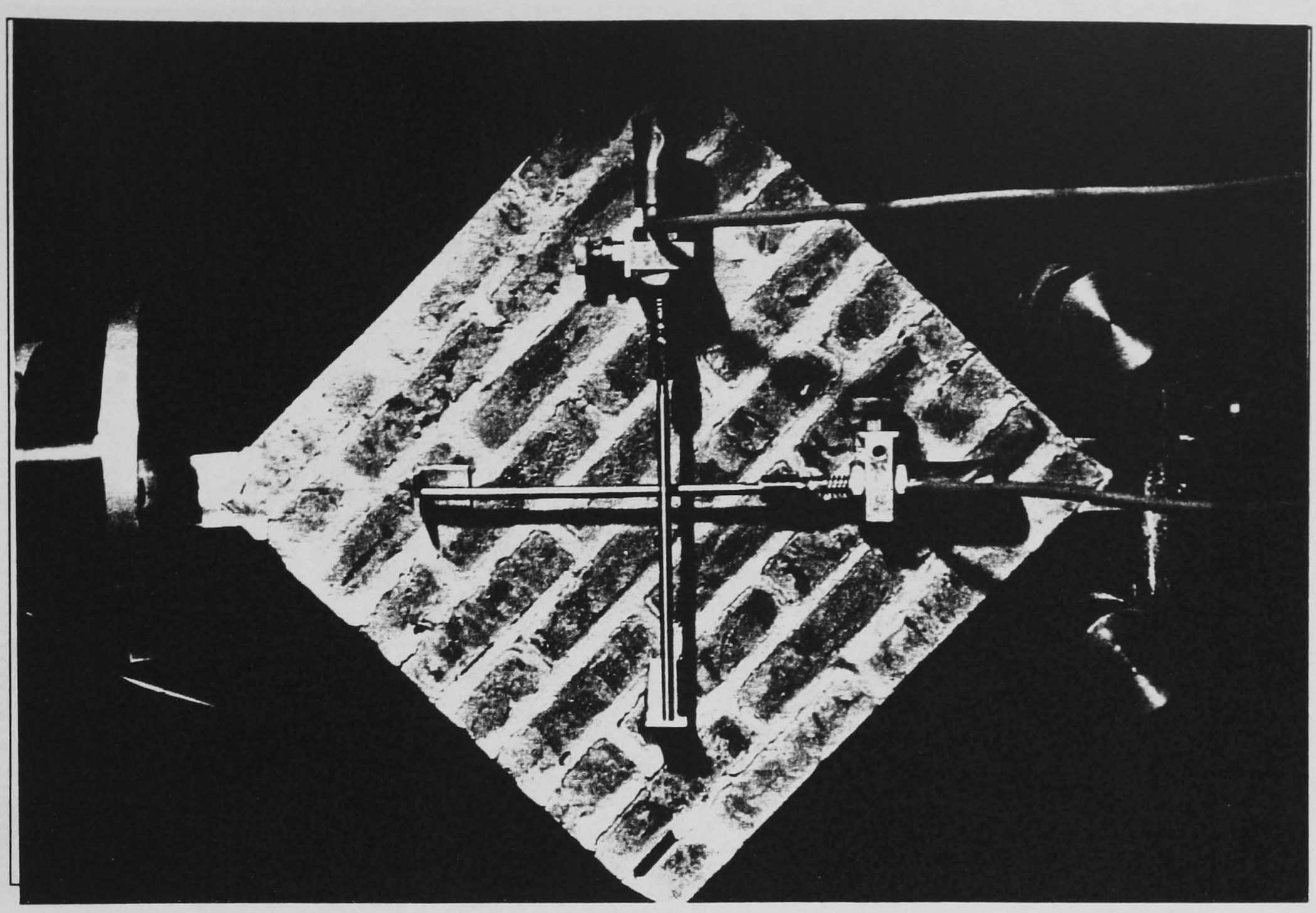

Photo 4.16 Larger size model masonry wallette ready for testing

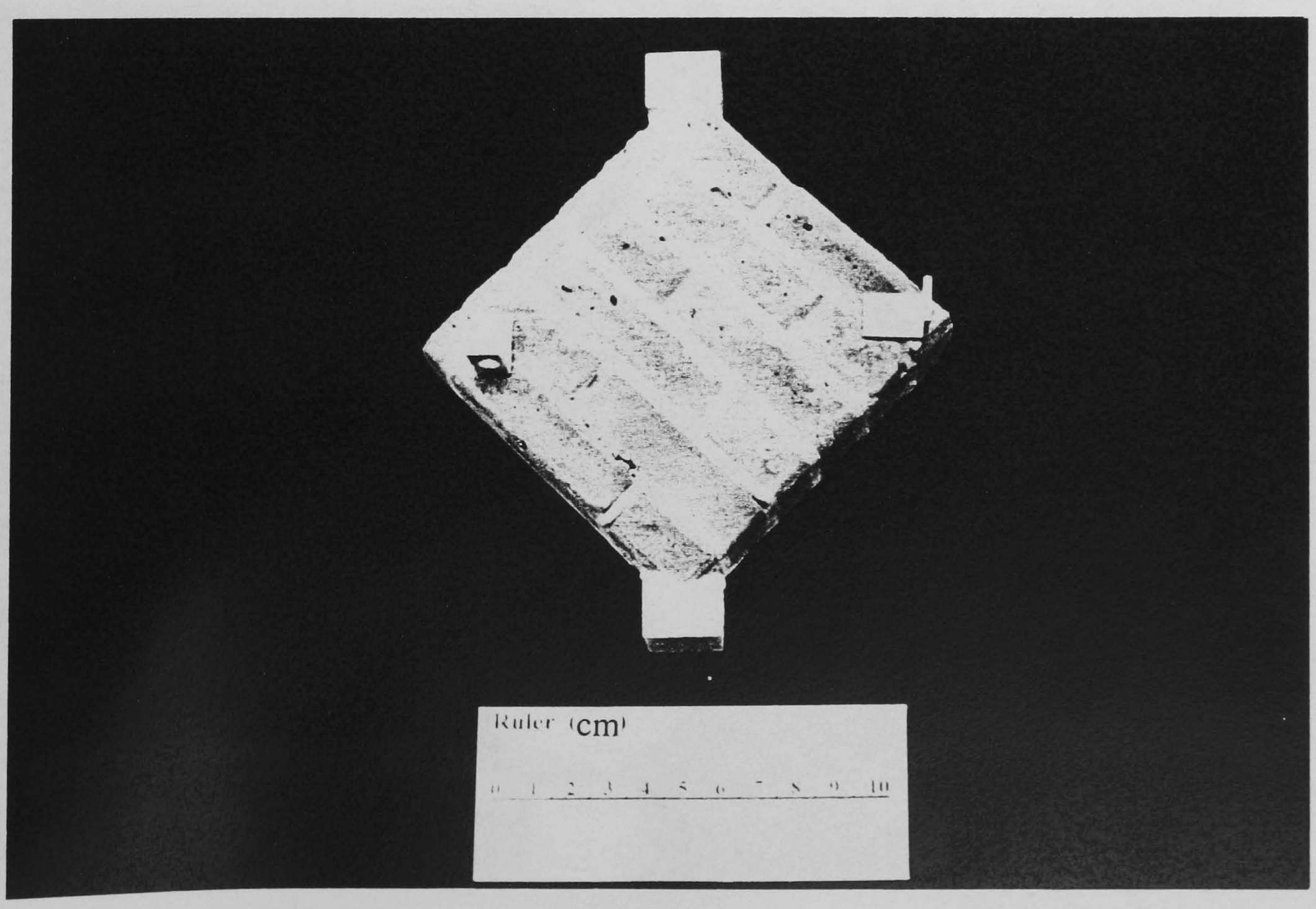

Photo 4.17 Small size masonry wallette

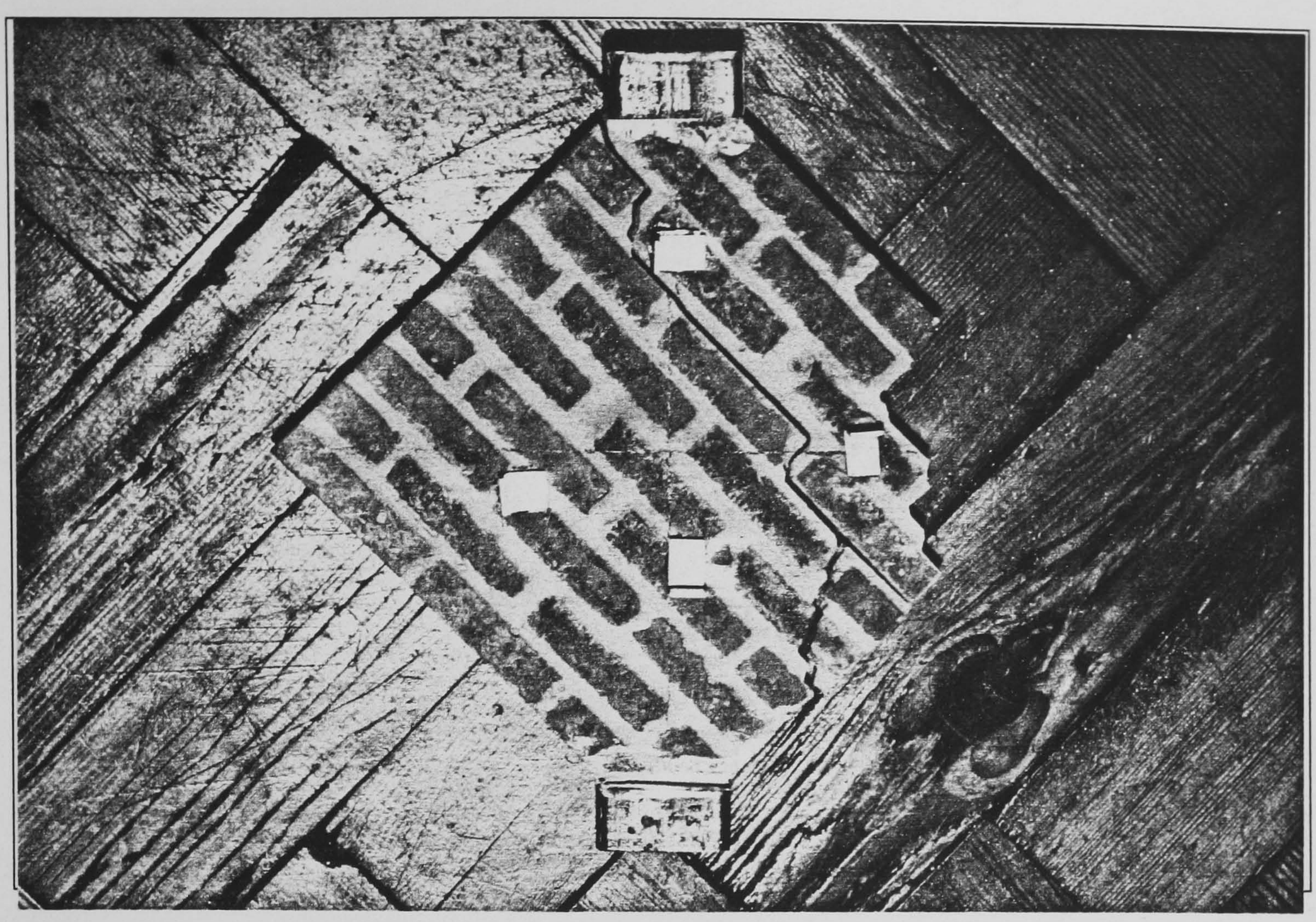

Photo 4.18 Shear-sliding mode of failure for 7-day large wallette

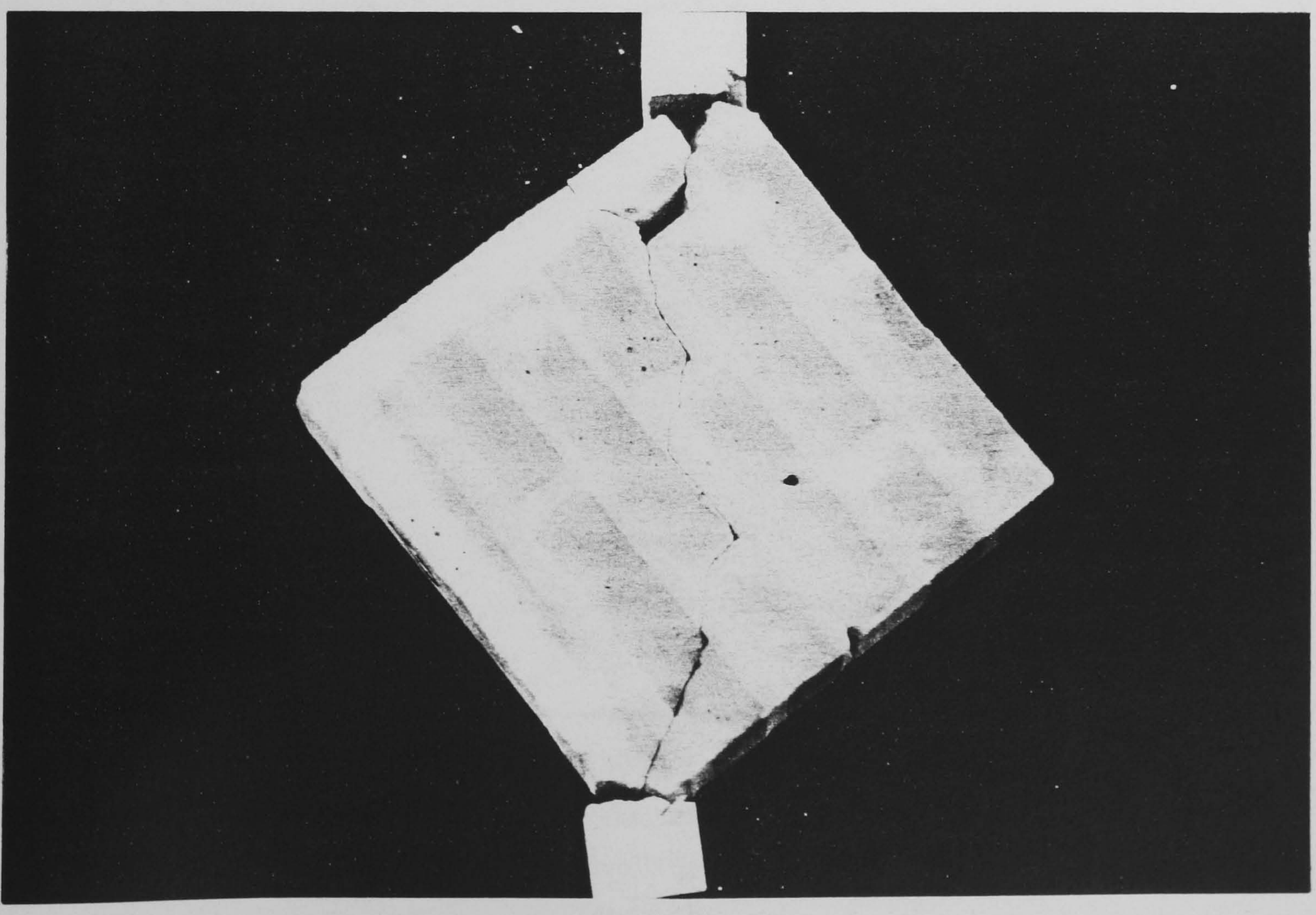

Photo 4.19 Diagonal tensile splitting cracking in small masonry wallette

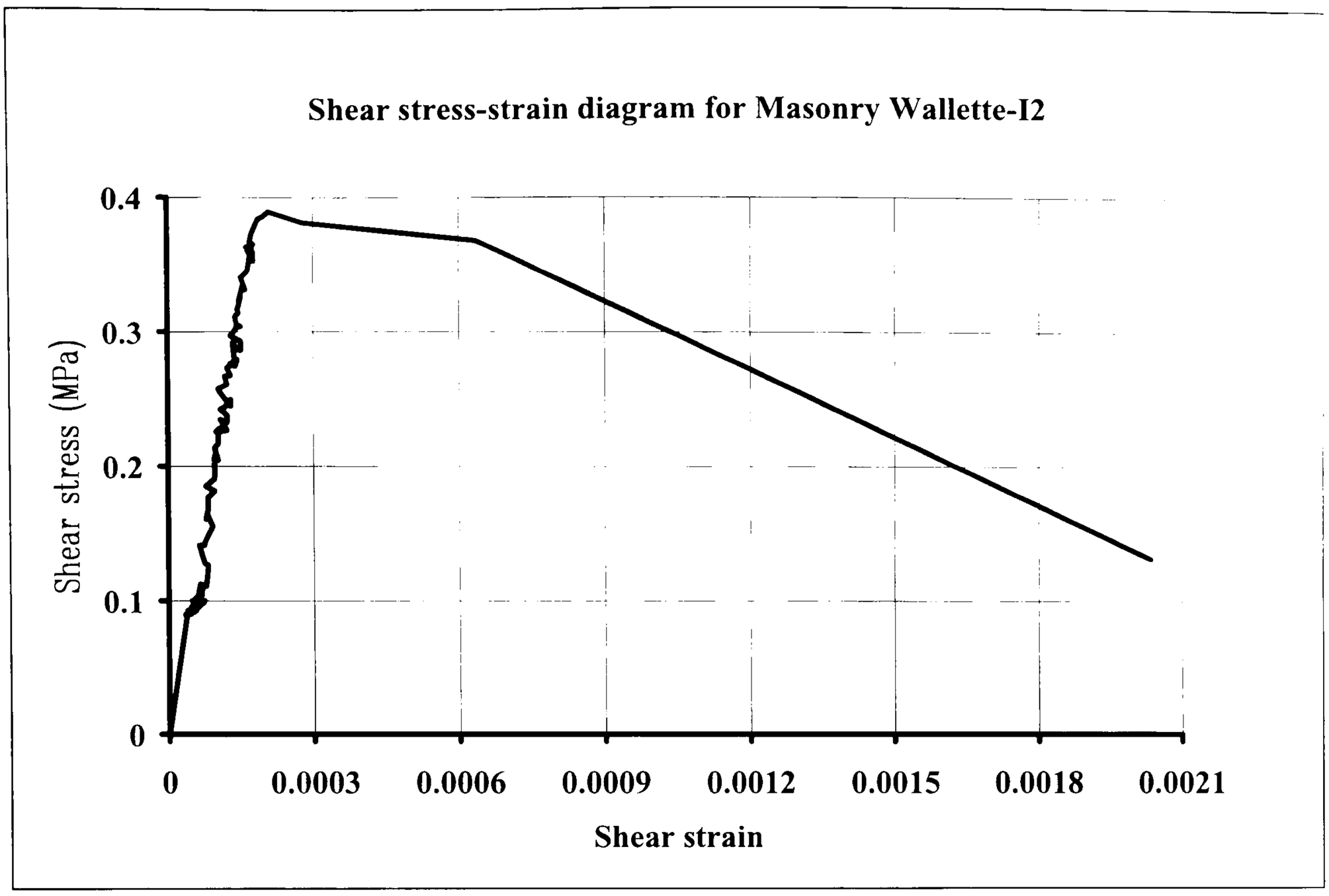

Figure 4.28 Masonry wallette shear stress - shear strain diagram (I2)

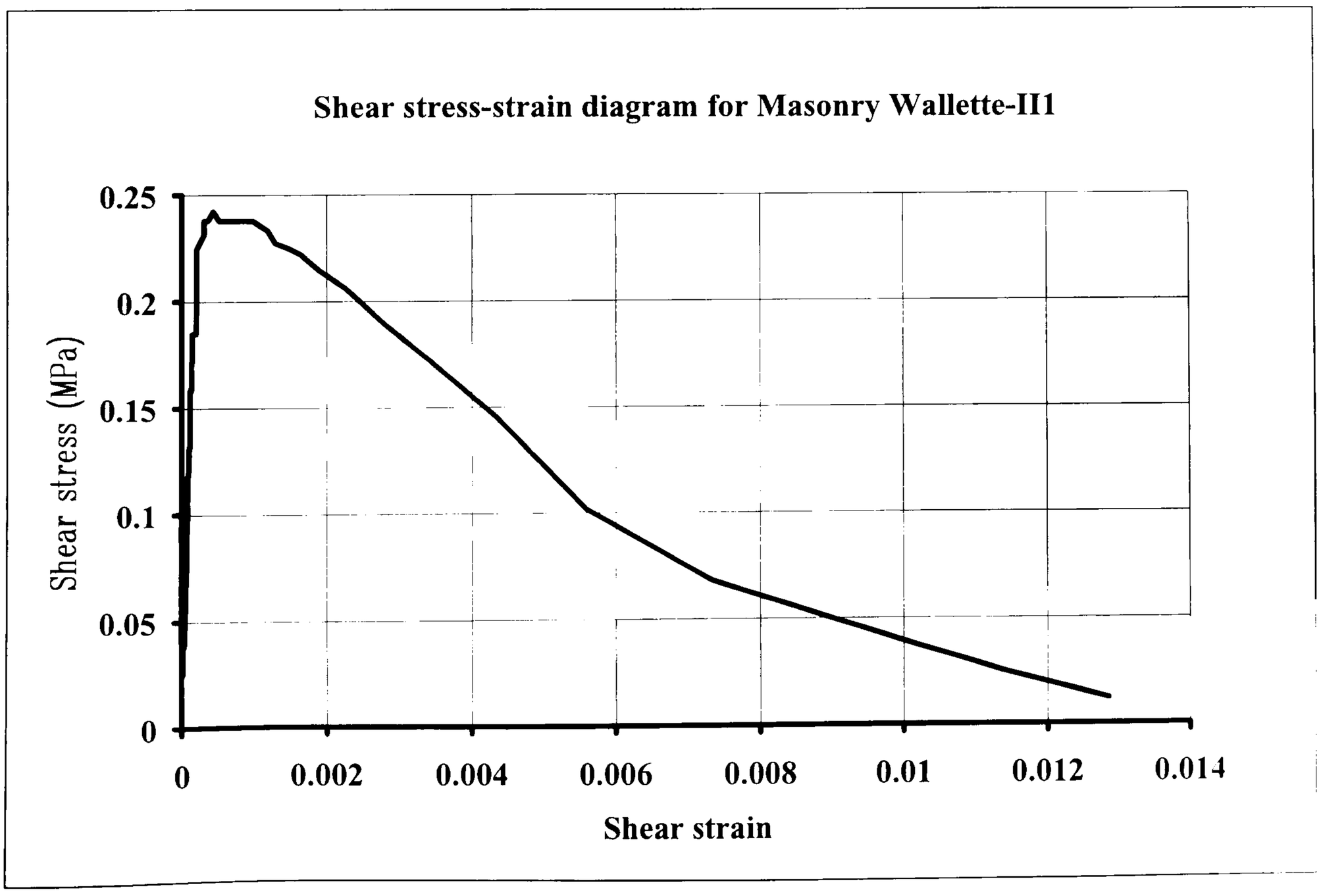

Figure 4.29 Masonry wallette shear stress - shear strain diagram (II1)

4.4.5 Masonry shear bond strength.

Another test that is not universally standardised is the mortar bed joint bond strength test, which is primarily used in research experimental investigations that concentrate on parametric studies for calibration of analytical models. Many different variations for the test set-up exist in literature [Ref. 90, 104, 106] with the aim of measuring the shear and friction strength at the interface of the mortar joint and the brick bedding area. The mode of failure is usually a form of shear slip along the interface which is primarily dependent on the interface bond strength. Although not clearly understood, the water absorption characteristics of the units during construction combine with the chemical reactions (capillary actions involved in the exchange of moisture between mortar and brick and cement hydration) that take place during curing of the specimens, to form a bond between the two masonry components and account for much of the joint strength. Since vertical as well as horizontal joints exist in a normal masonry assemblage the bond strength is known to consist of a tensile component, a shear bond component and usually an interface friction component. This strength is highly influenced by the normal load acting at various angles with respect to the lateral load, and as a result an experimental test procedure should incorporate provisions to account for confinement applied by external compressive forces. The first bond strength experimental set-up that was investigated by the author involved a masonry assemblage (photo 4.20) that was loaded through a compressive force acting in line with the horizontal bed mortar joints. The resulting cracking pattern shown in photo 4.21 which is parallel to the line of action of the applied compressive force, is a tensile splitting mode of failure resulting from stress concentration at the interface from lateral confinement of the bed joints by the adjoining brick units. It was decided to adopt a different procedure where the confining force could be controlled in order to observe any relationships between the compressive and shear stresses with respect to the joint bond strength. This involved placing a brick couplet in a typical shear box arrangement (figure 4.30) and repeating the procedure for different levels of compressive load. Resulting shear slip failure modes along the brick mortar interface are shown in photo 4.22. A variation of this test set-up (figure 4.30) has been previously used by Hendry et. al. [Ref. 90] among others, for the study of shear bond strength in relation to the moisture content of 1:6 model brick couplets.

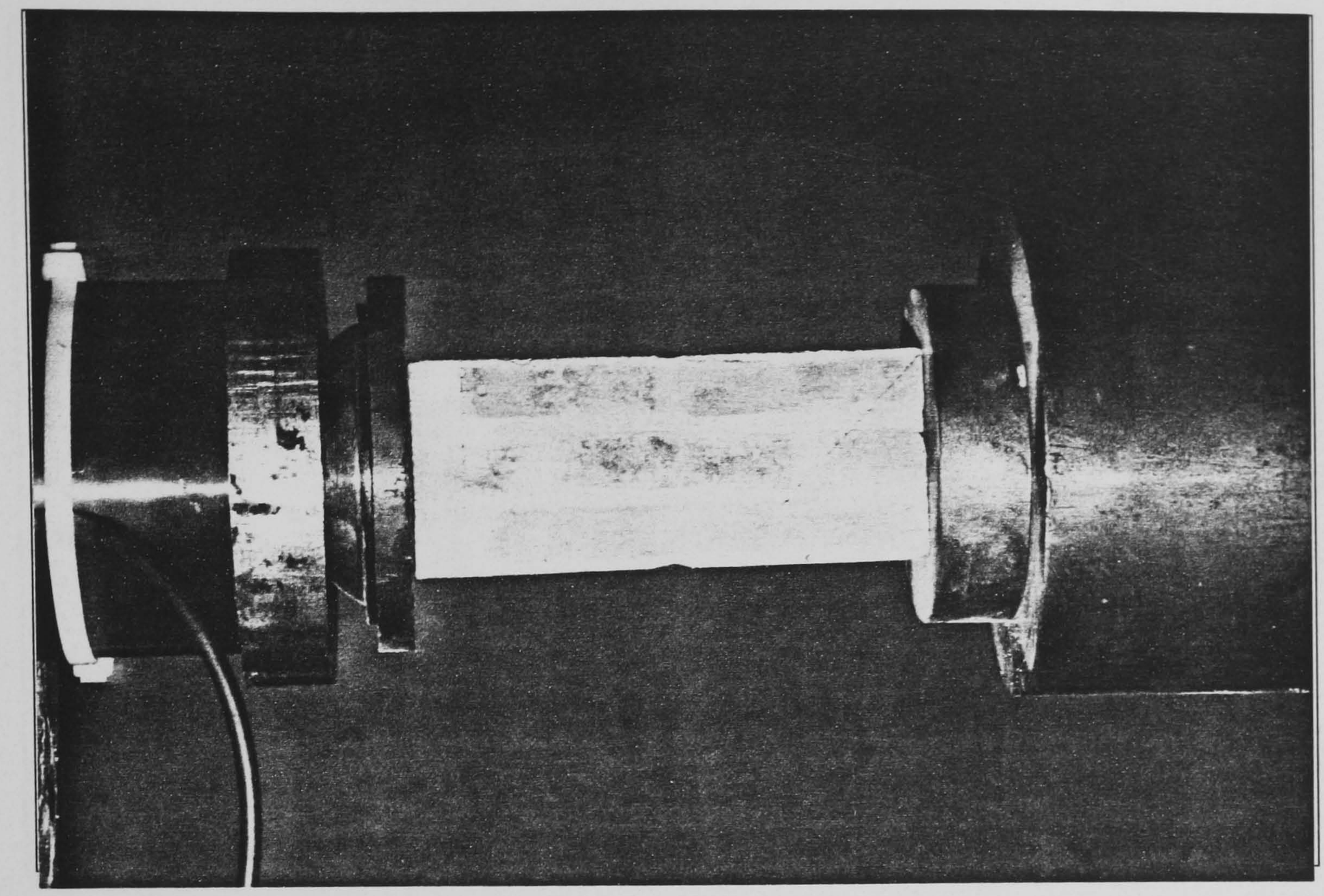

Photo 4.20 Masonry assemblage for bond strength

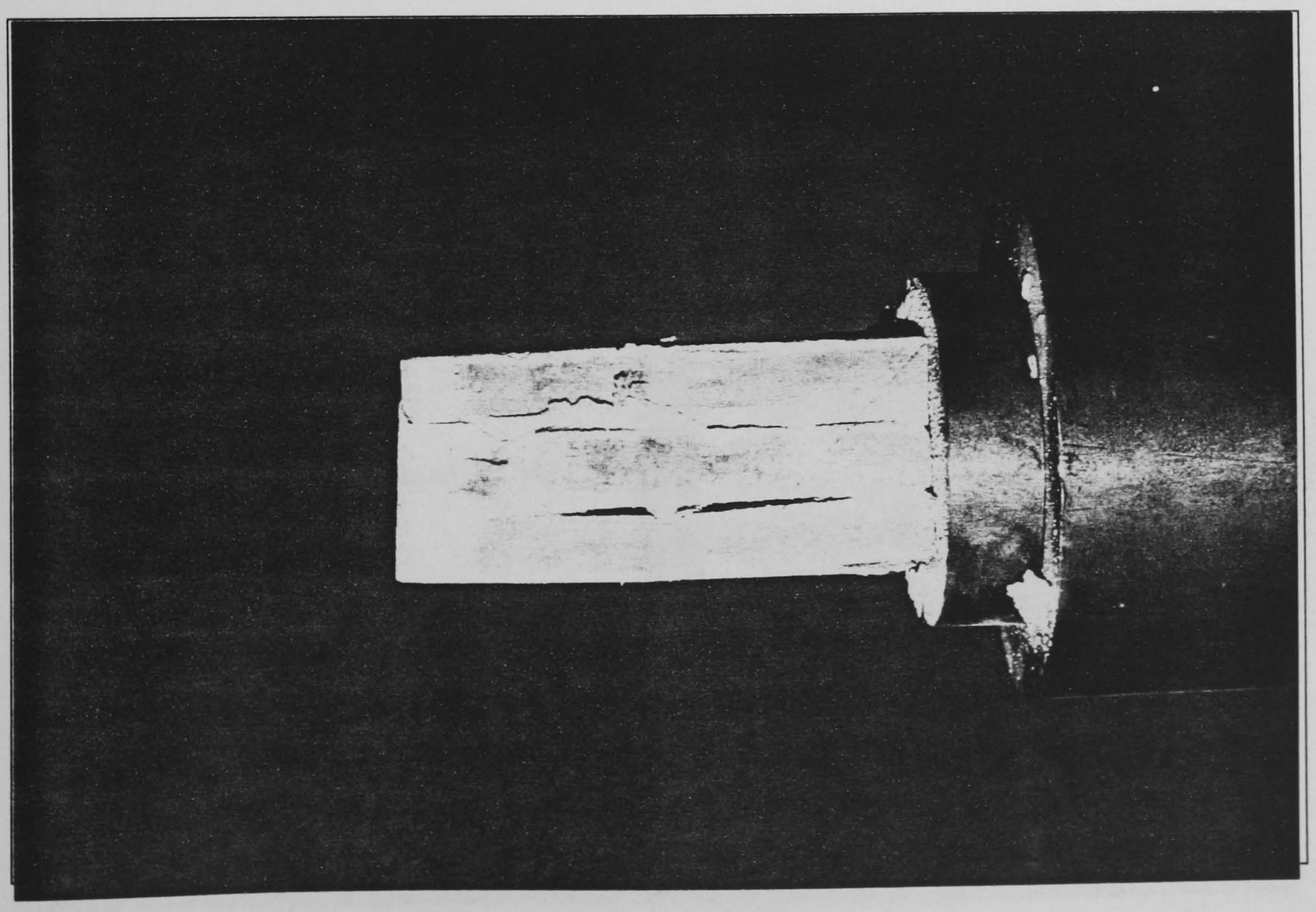

Photo 4.21 Mortar joint bond failure mode

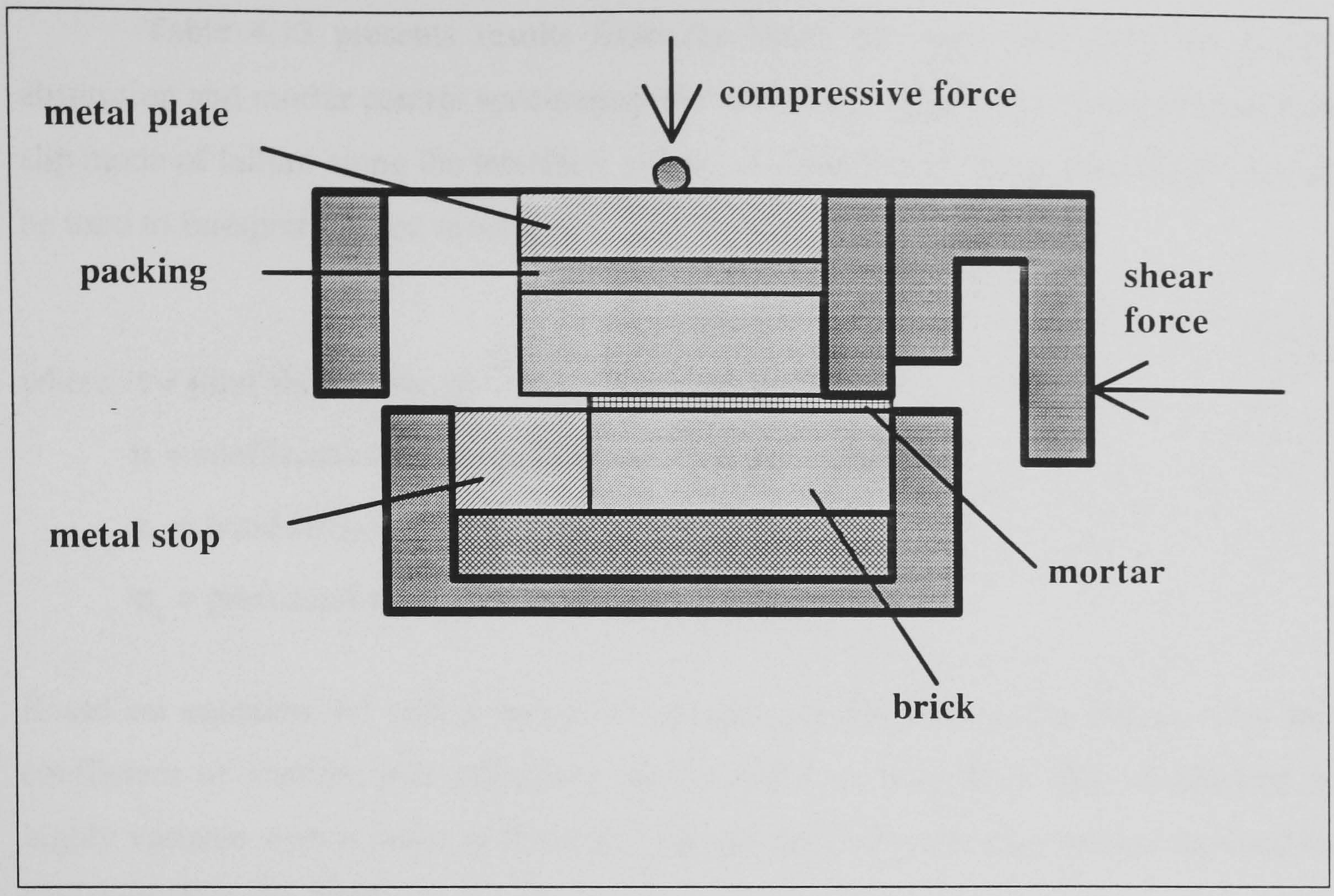

Figure 4.30 Shear box test set-up

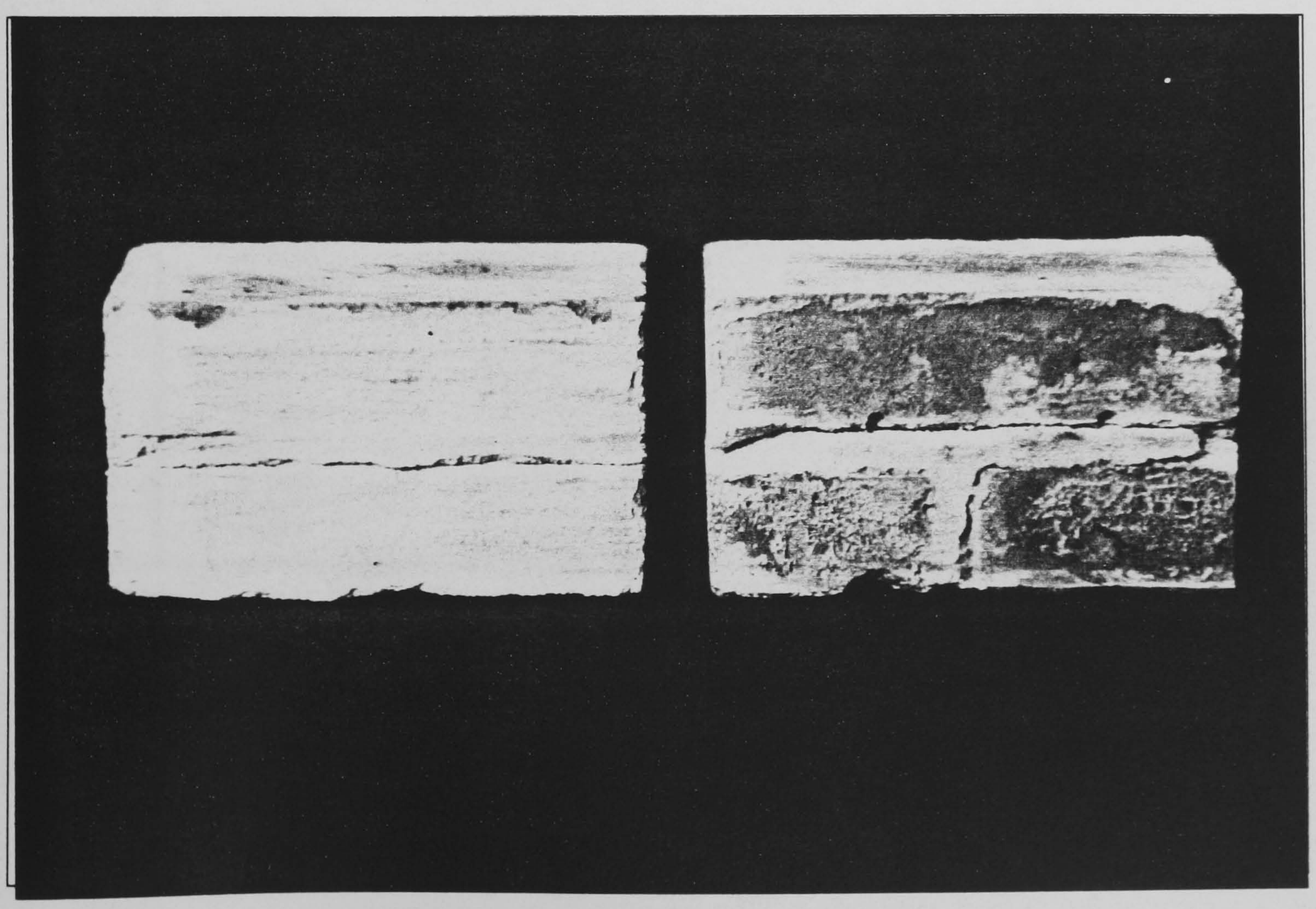

Photo 4.22 Mortar joint shear slip failure mode

Table 4.13 presents results from the shear box tests (including results for absorption and mortar control specimens). For low levels of precompression and a shear slip mode of failure along the interface, a Coulomb-Mohr type of equation [Ref. 78] can be used to interpret the test results:

$$\tau = \tau_0 + \mu\sigma_n \qquad (4.1)$$

where τ = joint shear strength

μ = coefficient of friction between brick and mortar

τ_0 = bond strength for $\sigma_n = 0$

σ_n = precompression normal to the bed joints

Based on equation 4.1 and a regression analysis of the test results (figure 4.31) the coefficient of friction was calculated and included in table 4.13. This coefficient is highly variable with a range of 0.3 to 1.1 (model and full scale clay bricks) reported in literature [Ref. 90, 104].

Couplet group	Mortar cube compressive strength	Mortar cylinder tensile strength	I.R. Absorption	Average shear bond strength	Coefficient of friction
	MPa	MPa	kg/m²/min	MPa	-
T-I	0.85	0.071	0.28	0.308	0.517
T-II	0.92	0.079	0.297	0.36	0.638
M	1.123	0.092	0.308	0.361	0.914
D	2.288	0.189	0.262	0.41	0.74
H	2.171	0.187	0.227	0.43	0.9
R	3.286	0.29	0.456	0.429	0.803
B	3.248	0.318	0.17	0.904	1.302
O	3.93	0.34	0.225	0.787	1.202

► The average shear bond strength is taken as the mean of the high and low values for different levels of precompression.
► I.R. Absorption results based on tests conducted during casting of the couplets.
► Coefficient of friction was obtained from the regression analysis on the test results

Table 4.13 Shear bond test results

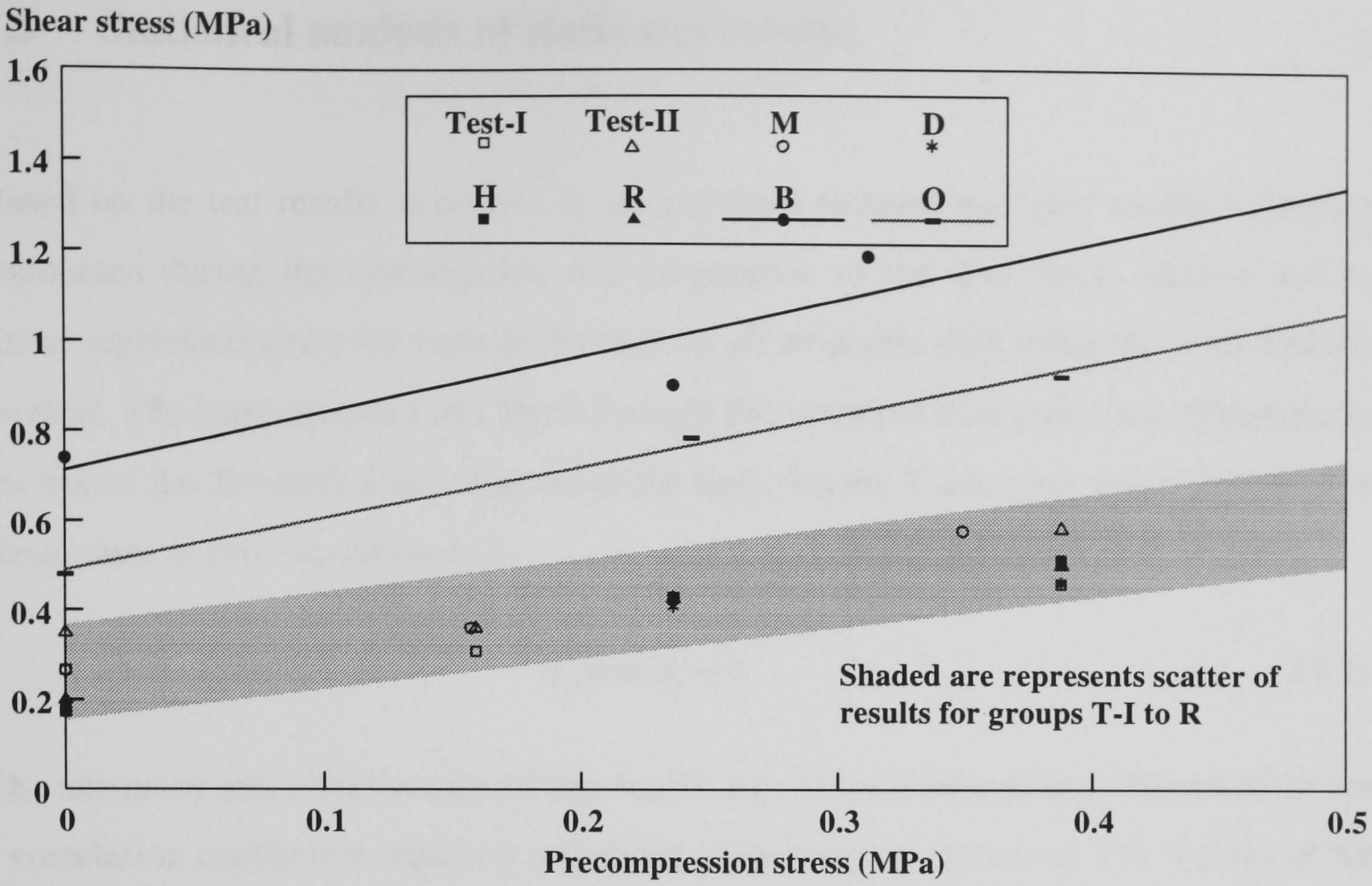

Figure 4.31 Regression analysis on bond test results

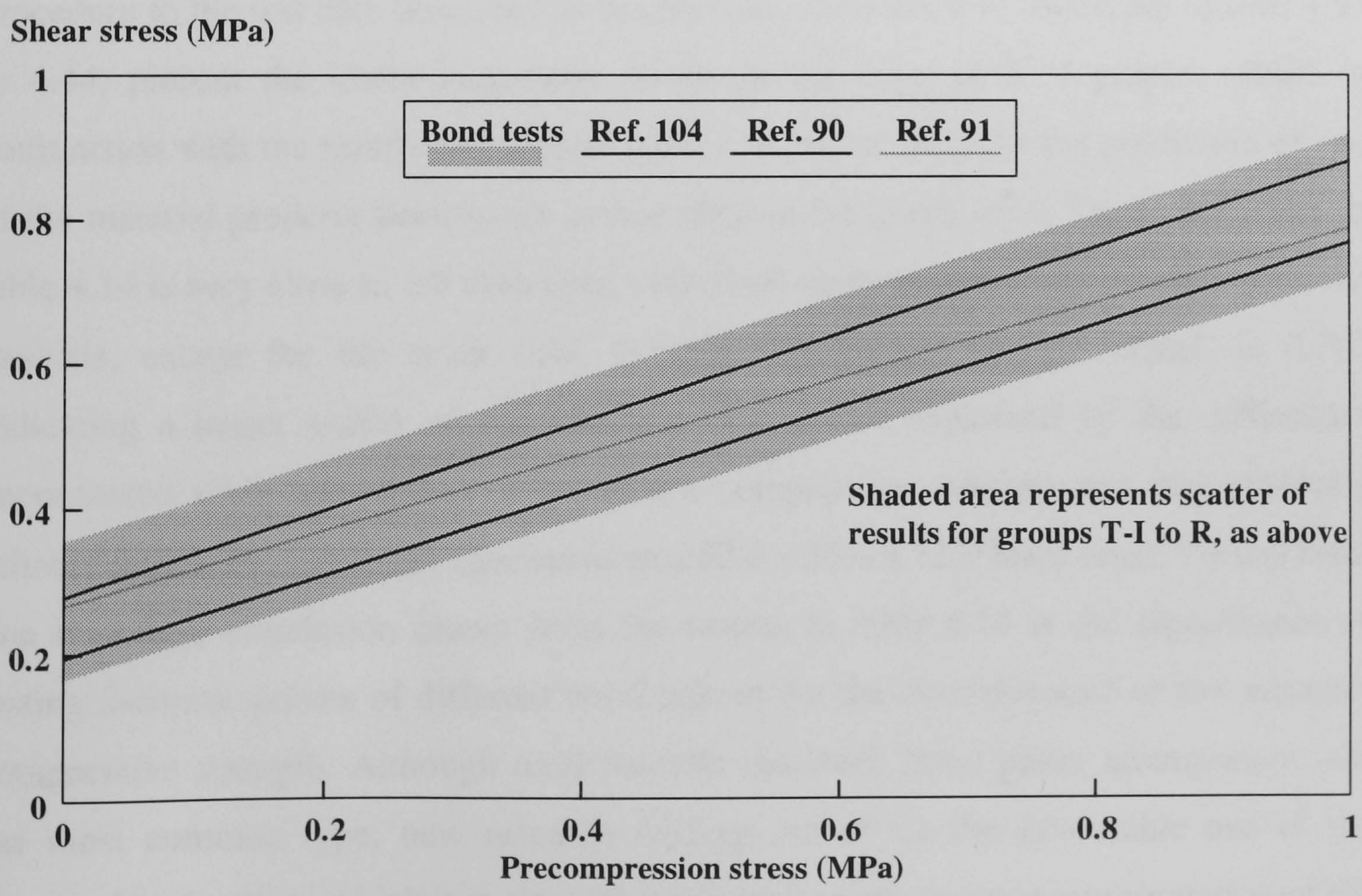

Figure 4.32 Comparison of bond results for groups T-I to R with Ref. 90, 91, 104

4.5 Statistical analysis of static test results.

Based on the test results described in the previous sections and also results from tests conducted during the investigation and preparation of the trial mixes (section 4.2.1), linear regression analyses were performed on all available data using the *least-squares method.* The least-squares lines fitted through the scattered data points are described by the use of the X-coefficient (slope-m of the line) and the Y-intercept value (b) which in these cases is zero (equation 4.2).

$$Y_i = mX_i + b \tag{4.2}$$

The adequacy and effectiveness of any linear regression relationship is described by the r correlation coefficient which is a positive value ranging from 0 to 1.0. Values of the r-coefficient ranging from 0.8 to 1.0 indicate reliability for the regression relationship (equation 4.2) in the prediction of the dependent variable [Ref. 102].

Table 4.14 presents the results from the application of the above statistical procedure to the test data described in the previous sections. The following figures 4.33 to 4.44, present the linear regression results in the form of X-Y graphs, which in conjunction with the results included in table 4.14 can be used for the prediction of one of the material property parameters as described in the graph axes. The r coefficient in table 4.14 is very close to 1.0 indicating very good agreement with the linear regression analysis, except for the brick cube to unit compressive strength which is 0.785 indicating a larger scatter of the data and this can be explained by the difficulties encountered while attempting to perform a compressive strength test and obtaining reliable results on such small specimens as a 50.8 x 25.4 x 12.7 brick units. Furthermore one important conclusion drawn from the results in table 4.14 is the significance of testing 5-course prisms of different bond pattern for the determination of the masonry compressive strength. Although until recently the stack bond prism arrangement was the most common type, new research findings report on the favourable use of the running bond pattern which it is claimed, provides a more accurate representation of the masonry compressive strength assuming the specimen under test is used for the determination of the compressive strength of a complete masonry system built with the

same bond pattern. In addition it has been reported that running bond prisms give lower values for compressive strength in the order of 3% to 10%, although in this study the difference was found to be almost insignificant (table 4.14). Finally the masonry modulus of elasticity in relation to the compressive strength obtained from 5-course prisms, and the shear modulus in relation to the masonry modulus of elasticity are related with the linear equations 4.3 and 4.4 that include the regression coefficients taken from table 4.14:

$$\mathbf{E_{M(sec.)} = 861\, f'_M} \tag{4.3}$$

$$\mathbf{G_{M(sec.)} = 0.25\, E_{M(sec.)}} \tag{4.4}$$

where $E_{M(sec.)}$ is the modulus of elasticity (secant at 45%),

$G_{M(sec.)}$ is the shear modulus (secant at 45%) and

f'_M is the compressive (5-course prism) strength of masonry.

Based on Ref. 104 values of 600 to 1000 have been reported for the coefficient in equation 4.3 whereas Ref. 78 reports a more close spaced range of 500 to 600 and Ref. 105 proposes a value of 500 for solid clay stack bond masonry (North American brick with frog) based on statistical analysis of an extensive database including over 2500 prism tests but excluding results from Europe and the rest of the world. The value shown in equation 4.3 lies on the upper level of the range reported so far and includes scale effects that might have influenced the results although appropriate steps were taken to minimise these as described in previous sections.

Equation 4.4 relates the shear and compressive modulus of elasticity with a coefficient of 0.25, which is based on results using the in-plane diagonal tensile test set-up described in section 4.4.3. There are hardly any published results for the shear modulus of masonry and the ones that do exist [Ref. 16] are not comparable since this test set-up is sensitive to the type and mechanical properties of the brick and mortar materials as well as the type and size of the specimen. In most cases the shear modulus

is approximated as 0.4 times the modulus of elasticity, but this is based on the assumption that masonry is an isotropic material and its Poisson's ratio is 0.2.

X-variable	Y-variable	Test Variable	X-coefficient (slope m)	Std. error of X-coefficient	r
Brick cube compressive strength	Brick unit compressive strength	-	**1.36959**	0.0729	0.785
Brick cube compressive strength	Brick cylinder tensile splitting strength	-	**0.08544**	0.0035	0.817
Brick cube compressive strength	Brick modulus of elasticity	-	**925.8495**	42.4968	0.92
Brick unit compressive strength	Brick modulus of elasticity	-	**643.4539**	17.6845	0.971
Mortar cube compressive strength	Mortar cylinder tensile splitting strength	-	**0.09782**	0.0033	0.932
Mortar cube compressive strength	Mortar modulus of elasticity	-	**1368.783**	74.556	0.902
Mortar cube compressive strength	Masonry compressive strength	Same brick specimens	**1.6812**	0.0948	0.886
Masonry compressive strength	Masonry modulus of elasticity	Same brick, same mortar specimens	**860.9059**	39.1037	0.928
Masonry (stack-bond) compressive strength	Masonry (running-bond) compressive strength	Same brick, same mortar specimens	**0.9306**	0.0138	0.992
Masonry compressive strength	Masonry shear (diagonal tensile) strength	Same brick, same mortar specimens	**0.0819**	0.0046	0.934
Masonry modulus of elasticity	Masonry shear modulus (modulus of rigidity)	Same brick, same mortar specimens	**0.2496**	0.0128	0.938

Table 4.14 Linear regression analysis results for figures 4.33 to 4.43

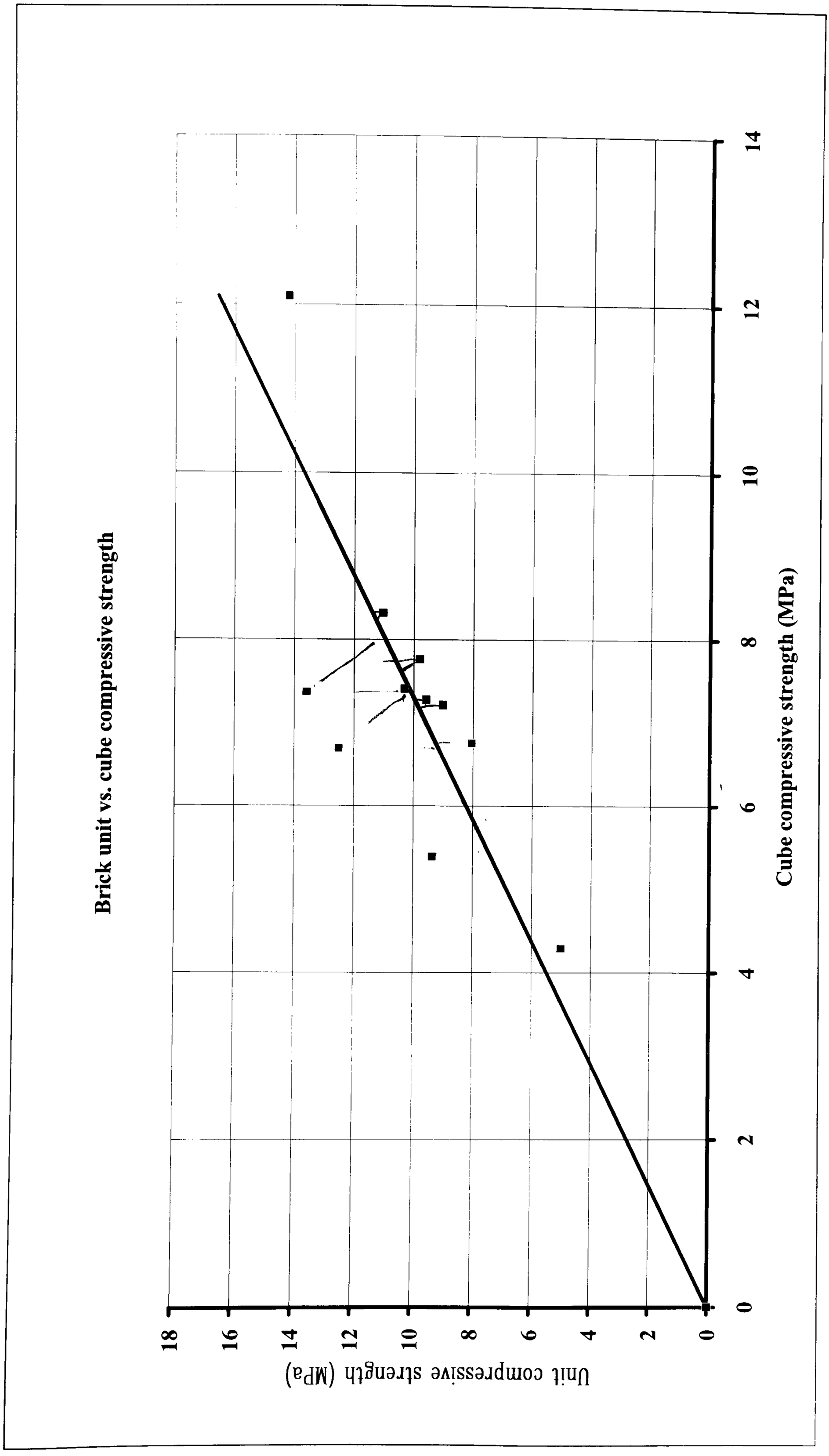

Figure 4.33 Brick compressive strength test data

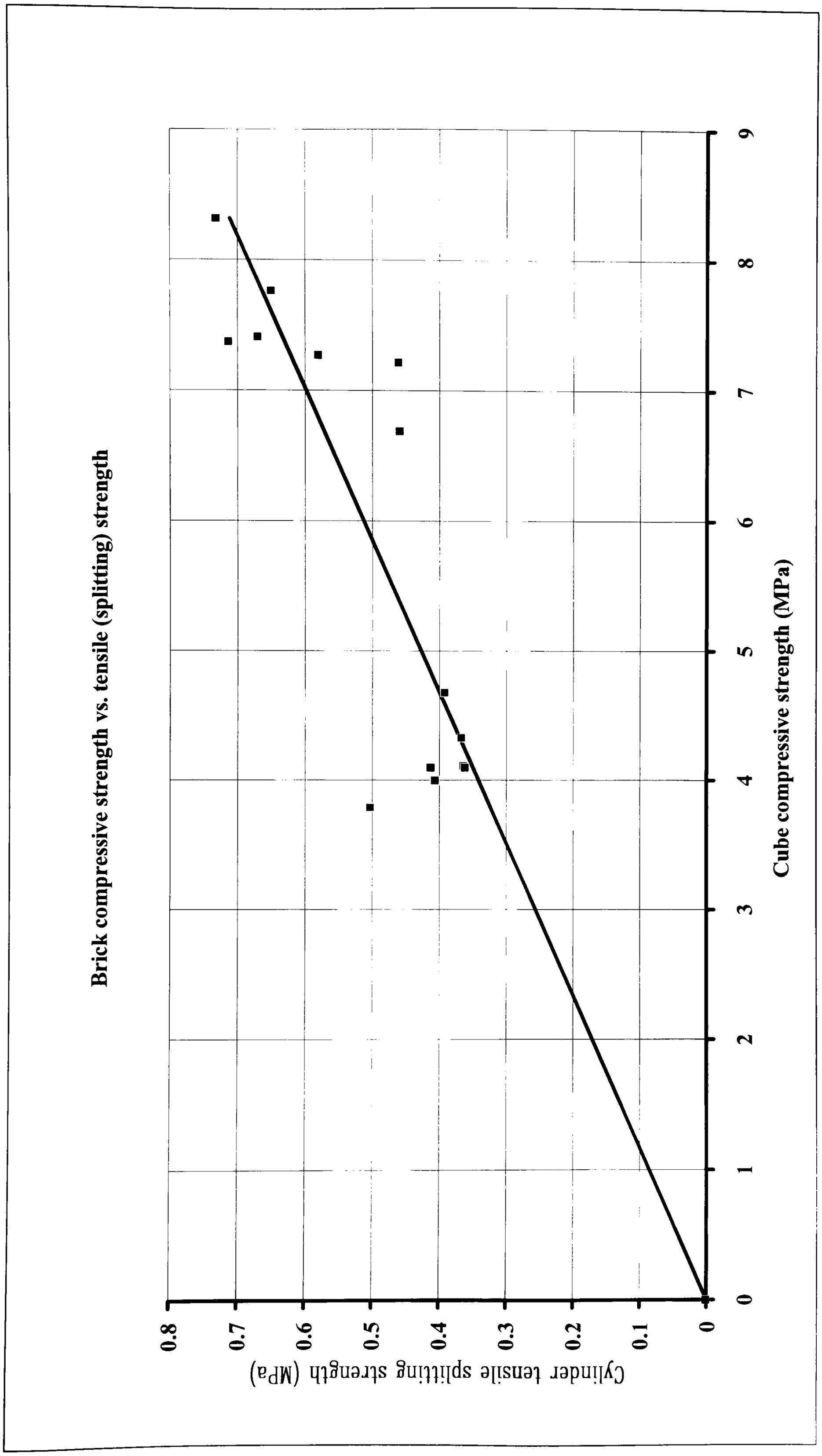

Figure 4.34 Brick compressive-tensile splitting strength test data

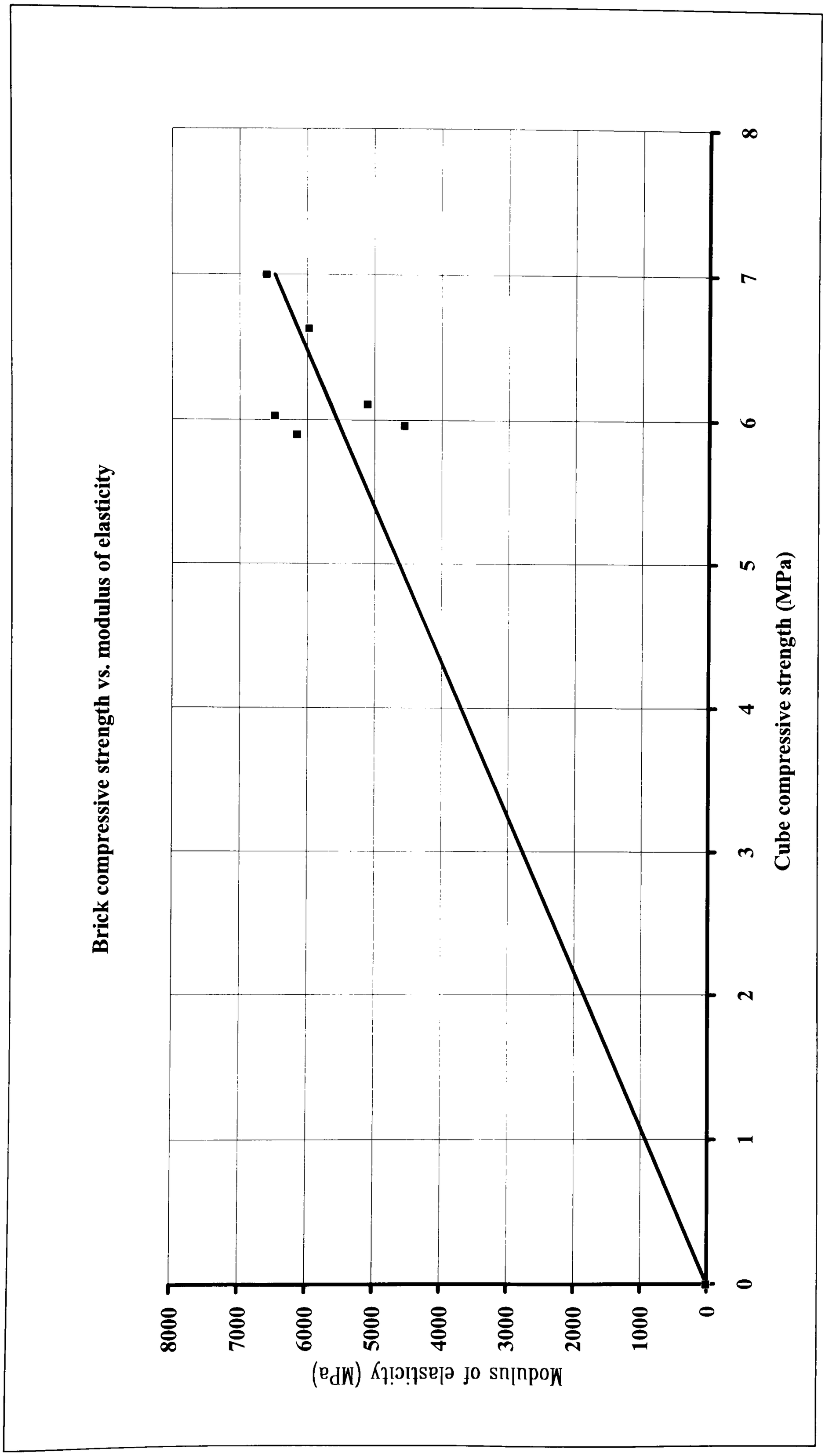

Figure 4.35 Brick compressive strength-modulus of elasticity test data

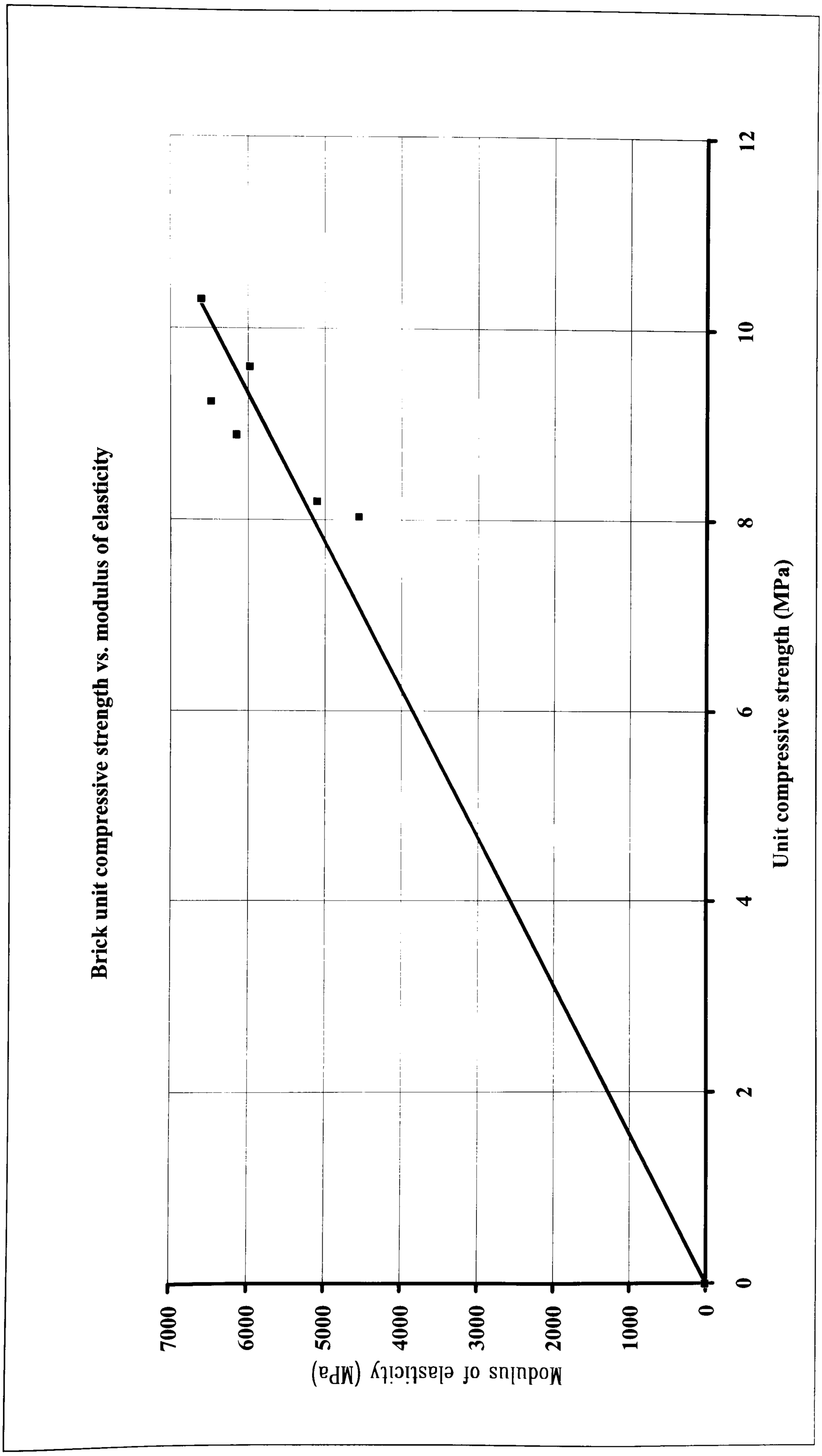

Figure 4.36 Brick unit compressive strength-modulus of elasticity test data

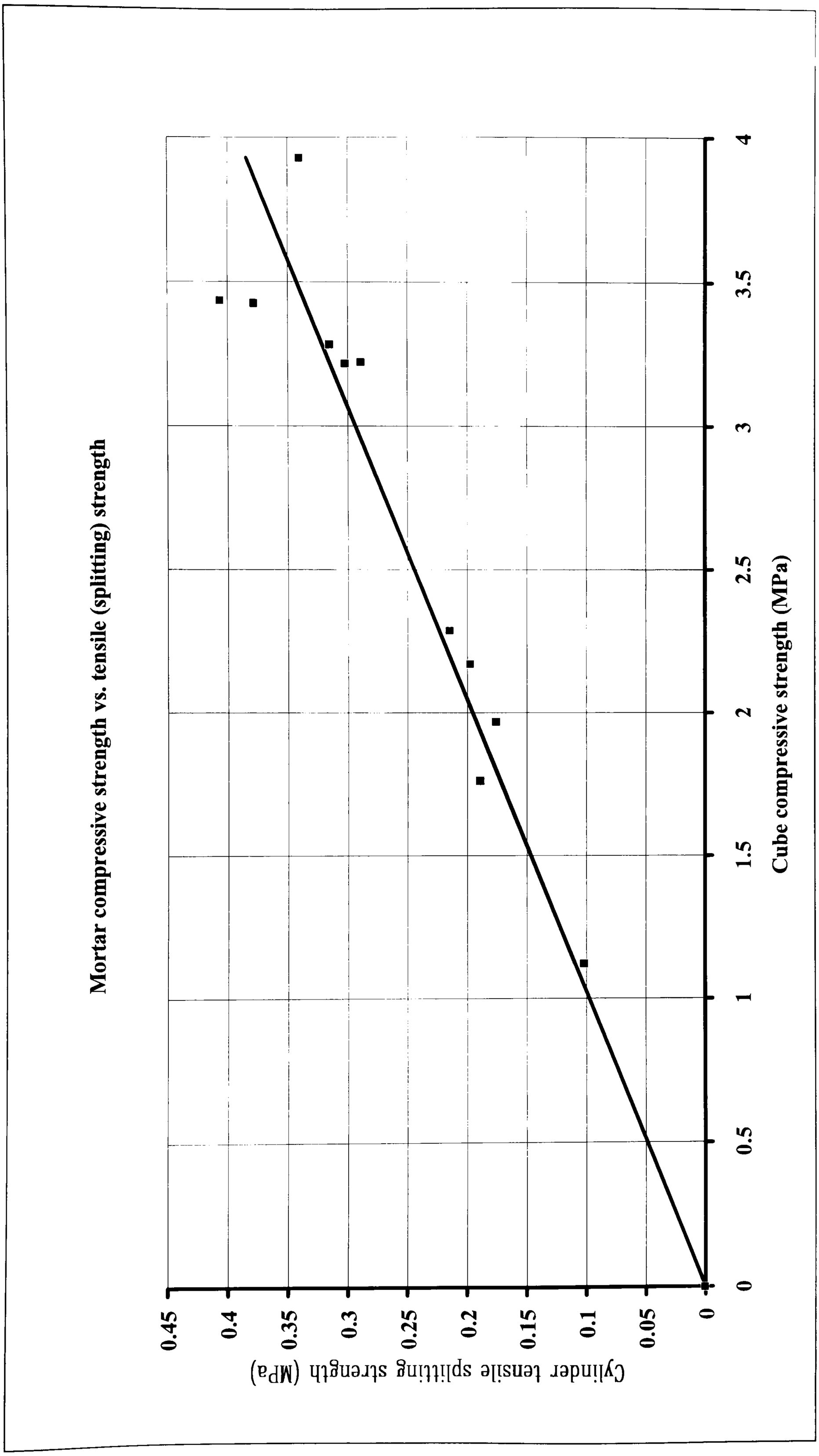

Figure 4.37 Mortar compressive-tensile splitting strength test data

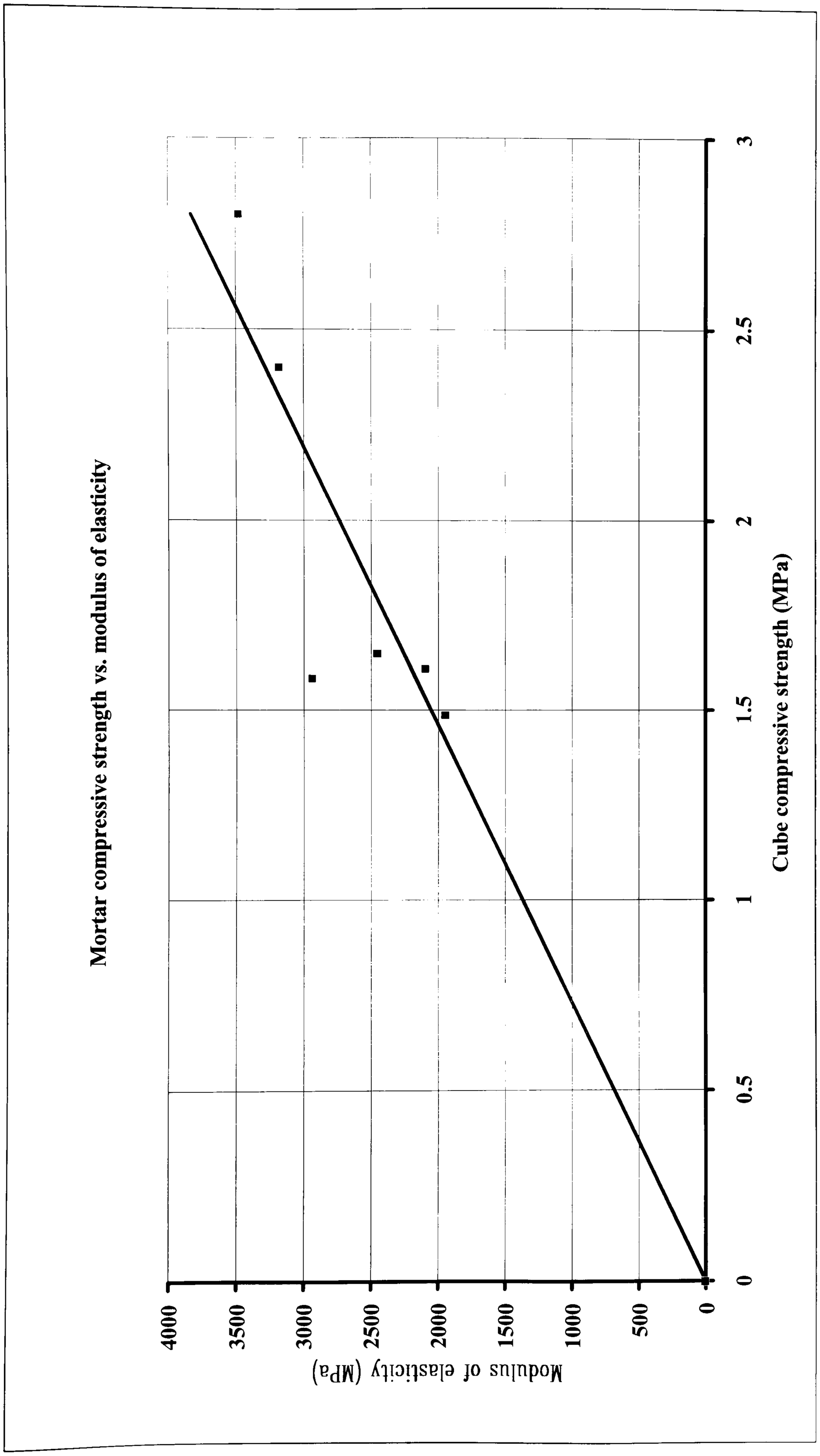

Figure 4.38 Mortar compressive strength-modulus of elasticity test data

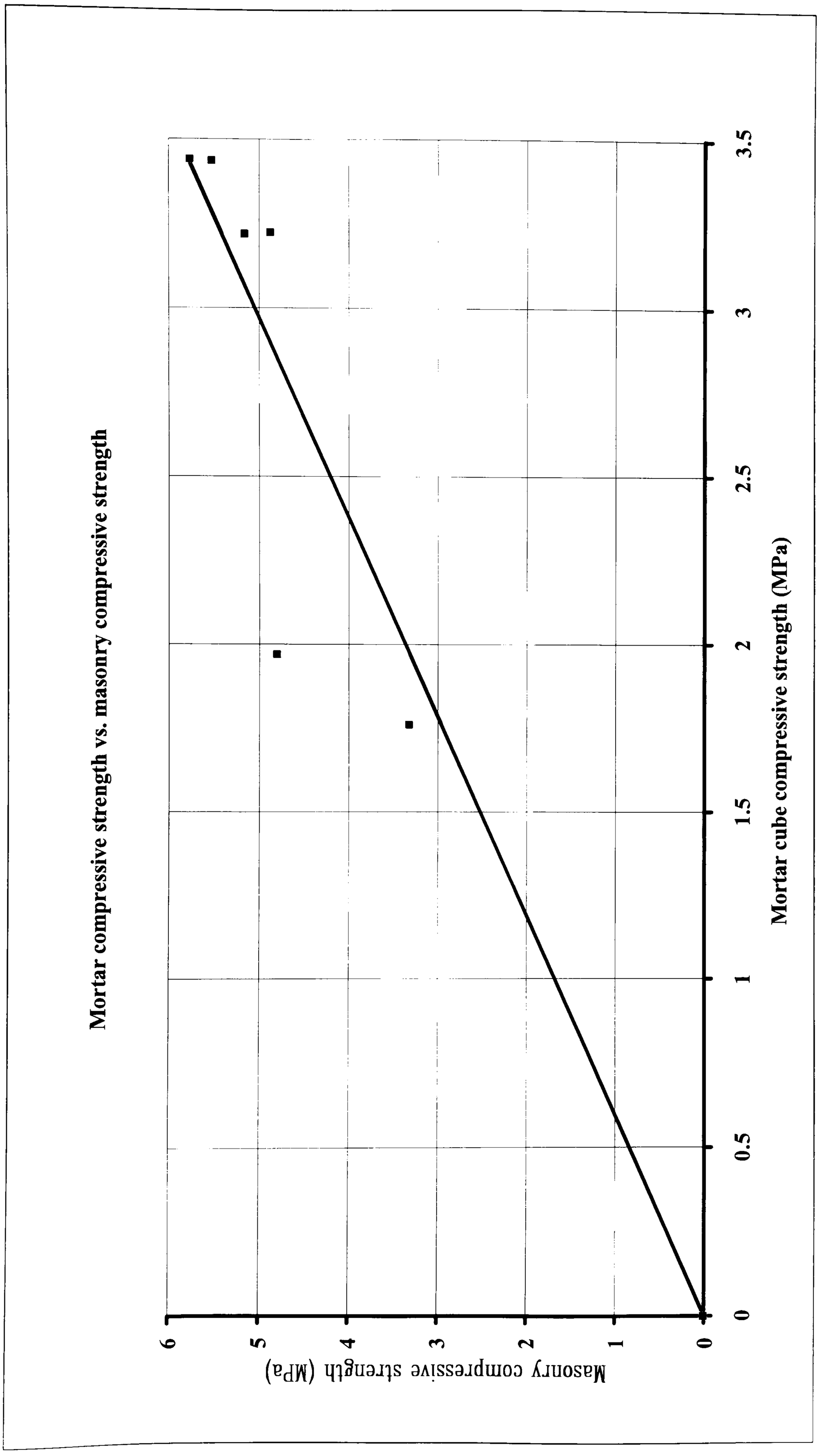

Figure 4.39 Mortar compressive strength-masonry compressive strength test data

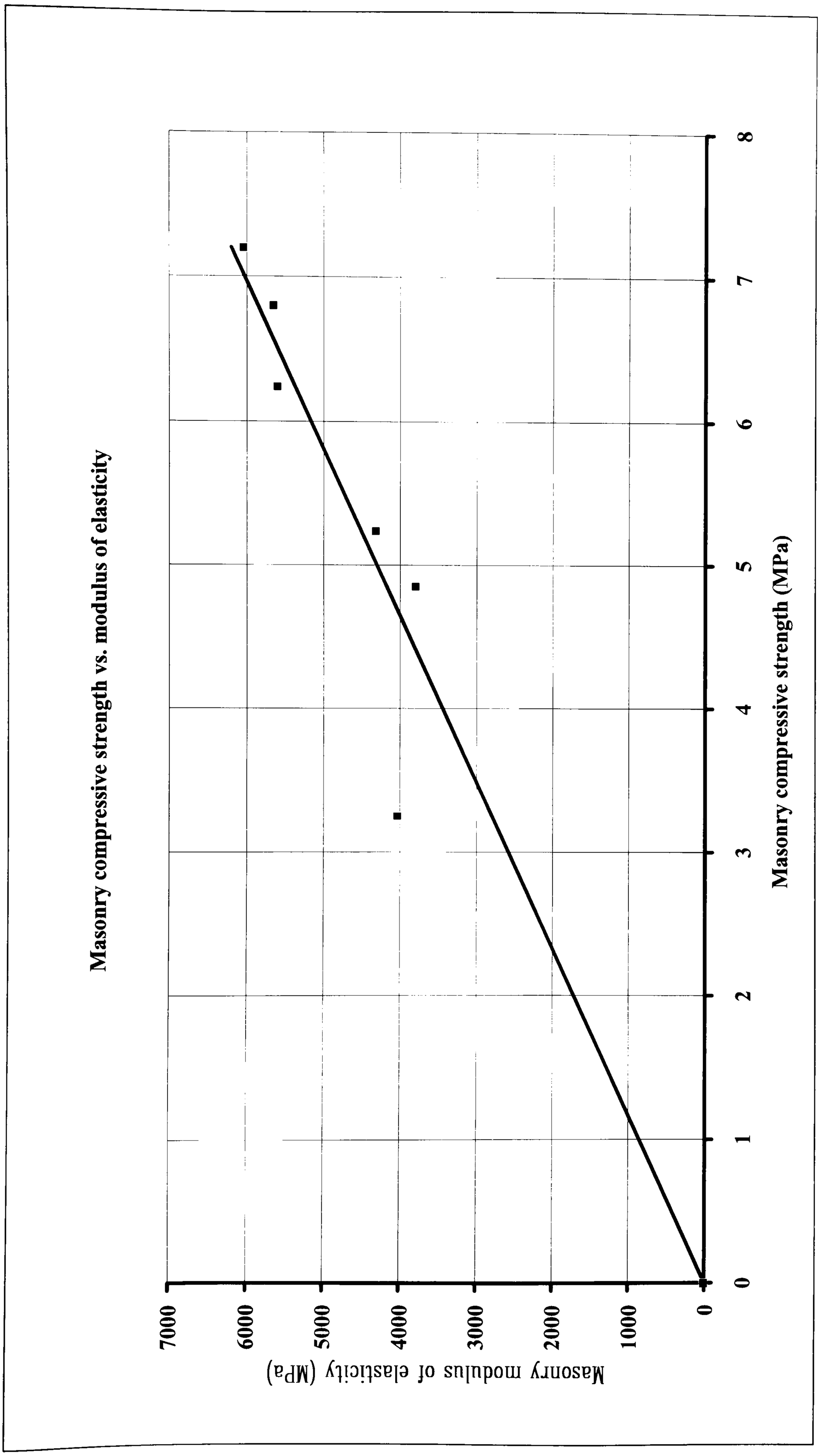

Figure 4.40 Masonry compressive strength-modulus of elasticity test data

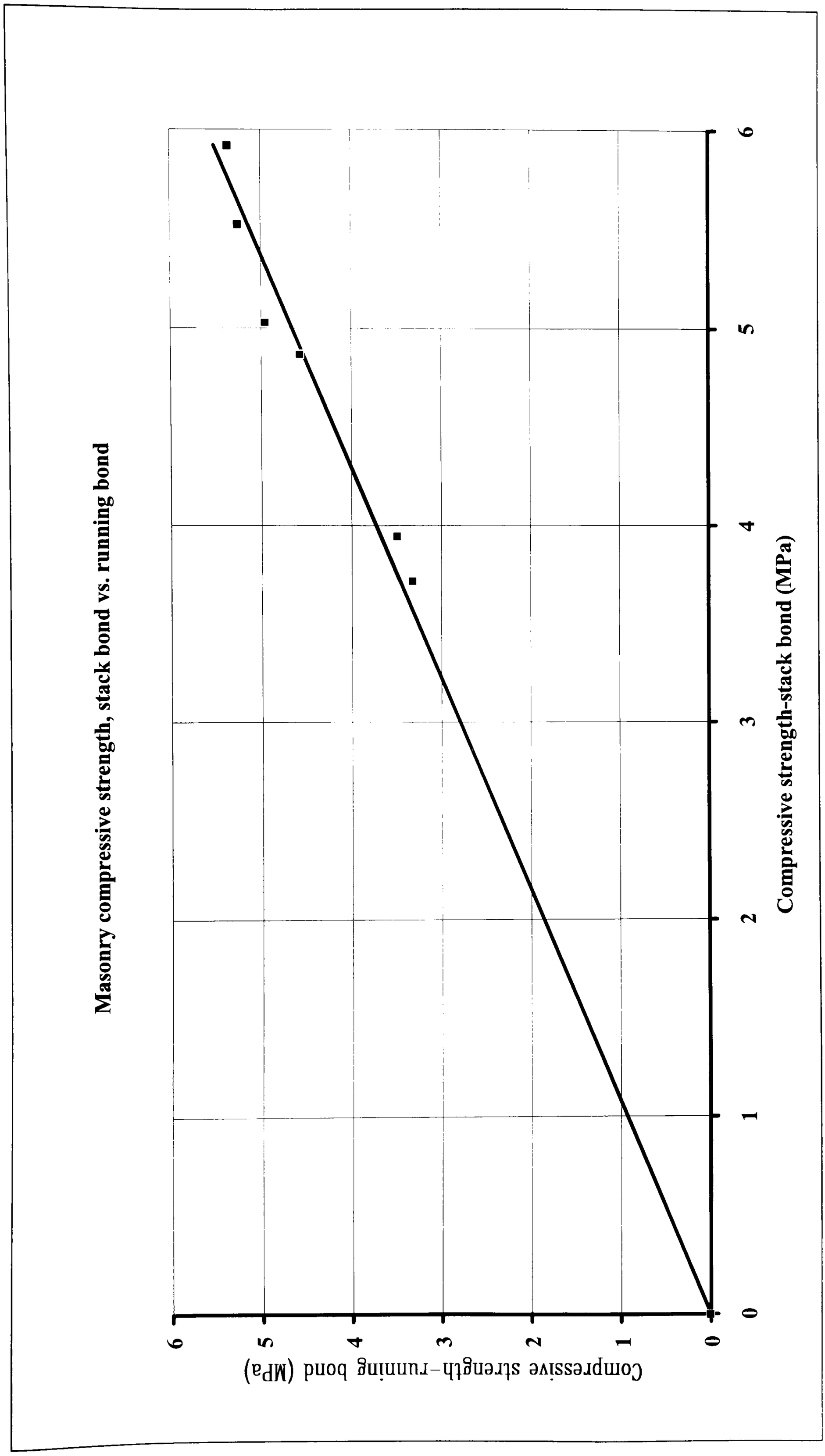

Figure 4.41 Masonry running-stack bond prisms compressive strength test data

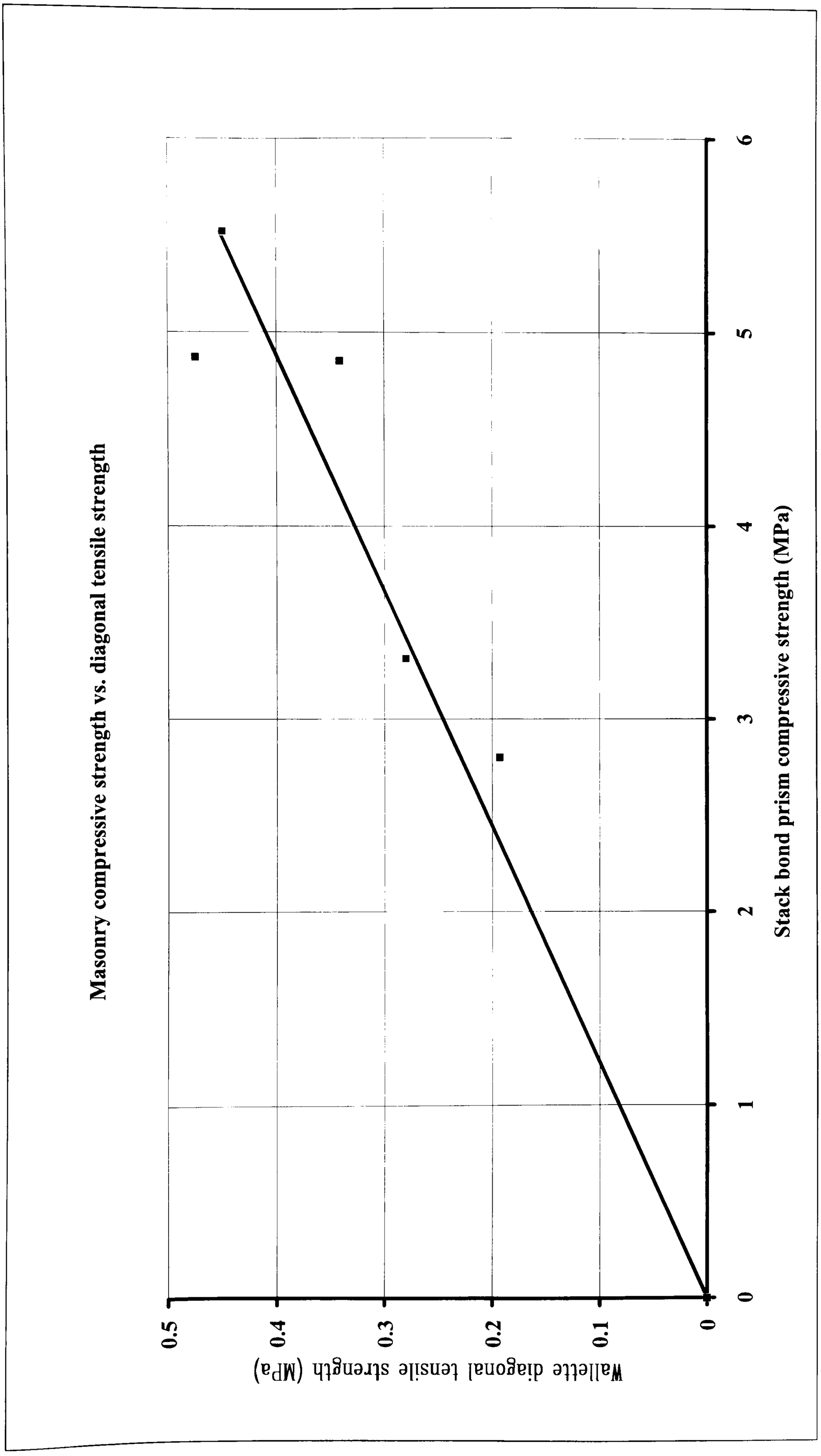

Figure 4.42 Masonry compressive-diagonal tensile (shear) strength test data

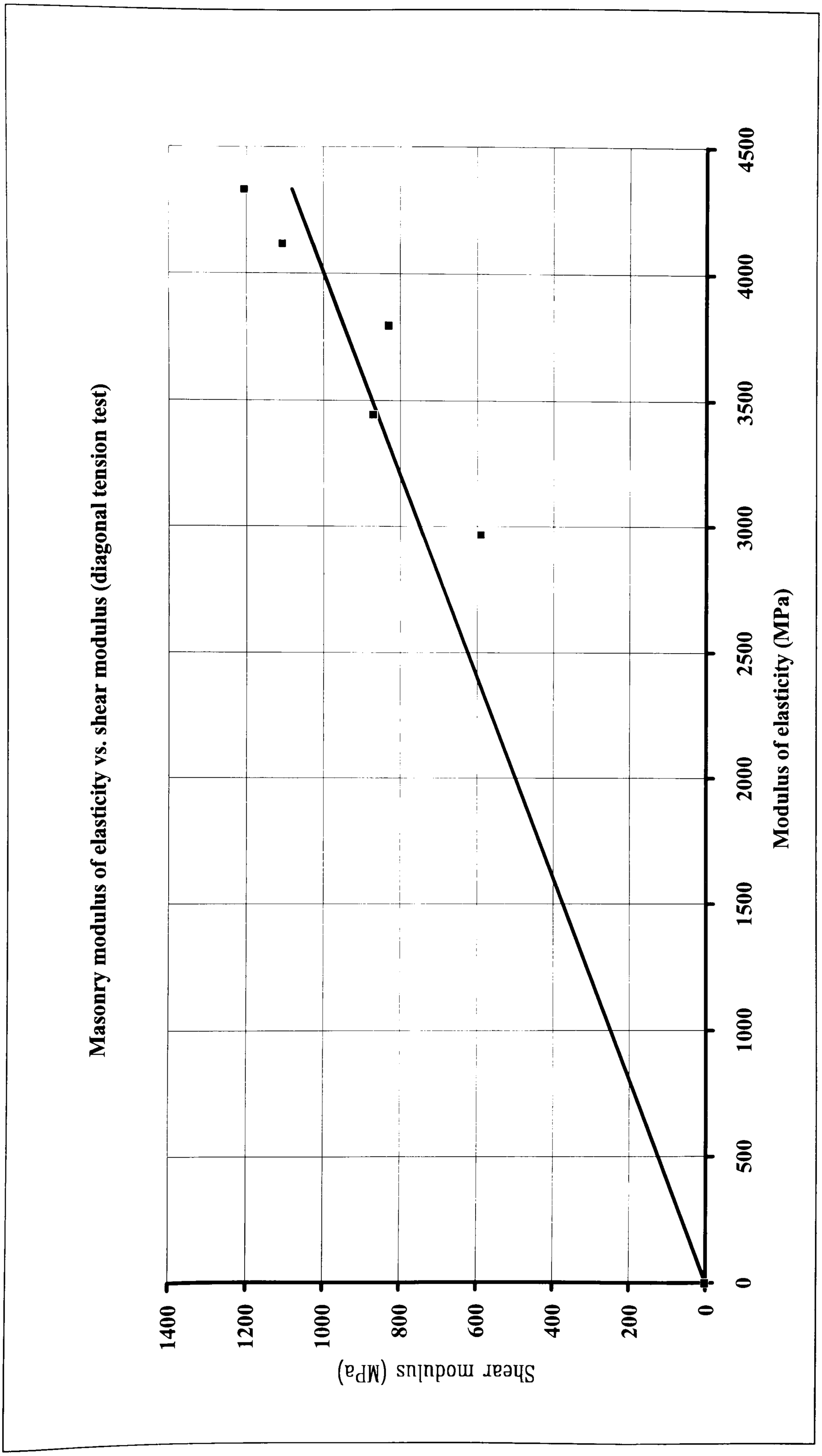

Figure 4.43 Masonry modulus of elasticity-shear modulus (modulus of rigidity) test data

4.6 Conclusions.

The first and most important objective of this experimental investigation was to design, develop and produce small scale masonry components that could be used for the subsequent construction and testing of 1:4 scale shear walls under dynamic loading. During the planning process it was discovered through an extensive literature review that there is a consistent lack of knowledge with regards to the fundamental behaviour of masonry and its mechanical properties. As a result a comprehensive program of static tests was devised and executed with the aim of establishing the strength, stiffness and overall performance of the model components. The results proved not only useful for the purposes of the present experimental work but also provided data for any subsequent continuation and expansion of the research objectives dealt with in this thesis. In association to the laboratory tests described in this chapter an analytical investigation was also conducted and is described in detail in chapter 6. The main conclusions arising from the static tests performed during this first stage are summarised in the following paragraphs.

A trial and error procedure was used with the aim of producing two different brick units with regards to strength and unit weight. Based on the similarity conditions set out in chapter 2, a brick unit had to be developed with a 1:4 reduction in strength and stiffness but a 4:1 increase in unit weight (material density). Such an attempt has been previously dismissed as not feasible since a reduction in strength conventionally implies a reduction in weight and as a result artificial mass simulation laws have been developed and universally used for the study of model structures and structural assemblies subjected to cyclic or general dynamic excitations. Since no direction comparison with full scale structures was available two bricks were produced with low strength and stiffness properties, with the second one having a 3:1 increase in density and unit weight by the addition of fine lead shot to the mix composition. The remaining properties of the model bricks such as the absorption characteristics were also examined in detail and an excellent similarity was achieved with commercially produced full scale clay bricks.

One of the advantages of casting bricks in the laboratory using purpose-built moulds, is the opportunity to also cast control specimens (e.g. cylinders) that would be used for the determination of the compressive and tensile strength of the masonry components thus overcoming the difficulties associated with the testing of actual units due to their shape. For example one of the most reliable methods often used in research for the determination of the brick tensile strength, involves drilling cylindrical cores from the body of the units or alternatively, subjecting the unit to a tensile splitting failure by loading the top and bottom sides with point compressive loads along its width. Results from such tests are often poorly correlated mainly due to the variability of the basic material properties along the length or width of the units usually attributed to the manufacturing process involved [Ref. 90].

With the constituent materials fully described through their mechanical properties (e.g. compressive-tensile strength, modulus of elasticity), model assemblage testing followed, involving a number of units and mortar joints in the form of couplets, prisms and wallettes in order to obtain the mechanical properties of masonry through experimental procedures that have been previously used and reported in technical literature [Ref. 1, 90, 107 and relevant Standards]. The first test involved measuring the overall water absorption capacity of the model units as well as the initial rate of suction which determines the quality and strength of the bond between bricks and mortar at the joints. The very fine gradation sand used in the composition mixes of both bricks and mortar was initially dictated by the similarity conditions with regards to grain (aggregate) size, but was later discovered that it was a positive influence on the absorption characteristics of the model bricks by creating tiny pores on their surface and improving both bond and friction between the two materials. During the next stage masonry prisms of various aspect ratios and bond patterns were investigated for the determination of the compressive strength, elastic modulus and stress strain characteristics. Steps were taken to minimise scale effects by introducing reduced scale platens and Teflon packing in the experimental set-up together with modified instrumentation devices (LVDTs) to measure the deformation of the specimens up to failure. Cracking patterns were consistent to similar ones observed by other researchers both in full and reduced scale prisms (compare photos 4.13, 4.14 with photo 4.23).

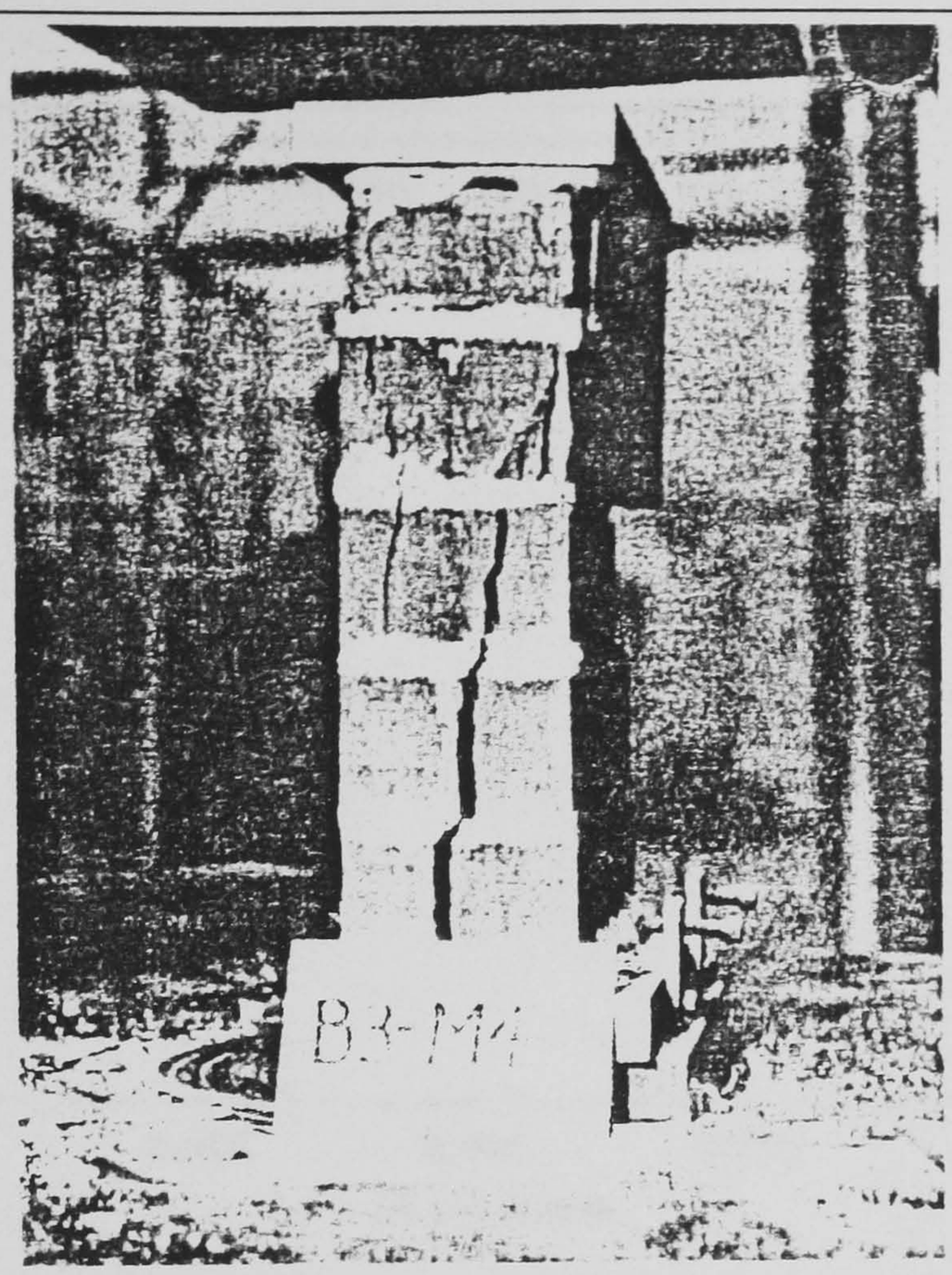

Photo 4.23 Cracking pattern of full scale 5-course prism [Ref. 68]

Diagonal in-plane tensile tests were carried out on different sizes of model wallettes following ASTM and RILEM recommendations, in order to obtain the masonry shear (tensile spitting) strength and modulus of rigidity. The smallest size of specimen that could still produce reliable results is proposed together with details of the complete experimental set-up and procedures. Special attention was paid to the scaling of the size of the loading corners (shoes) prescribed by the two codes, where both sets were designed, manufactured and evaluated. Figures 4.44 and 4.45 include results from this investigation together with similar data of model specimens available in literature [Ref. 1 and 53]. Due to lack of experimental data in literature, the comparisons are made with model square wallettes constructed from stronger units and mortar and are therefore restricted to the overall shape of the shear stress-strain curves. This is demonstrated in greater detail in figure 4.45, where the same curves are plotted in non-dimensional form by dividing the shear stress and shear strain data with their respective peak values (also noted in figure 4.44).

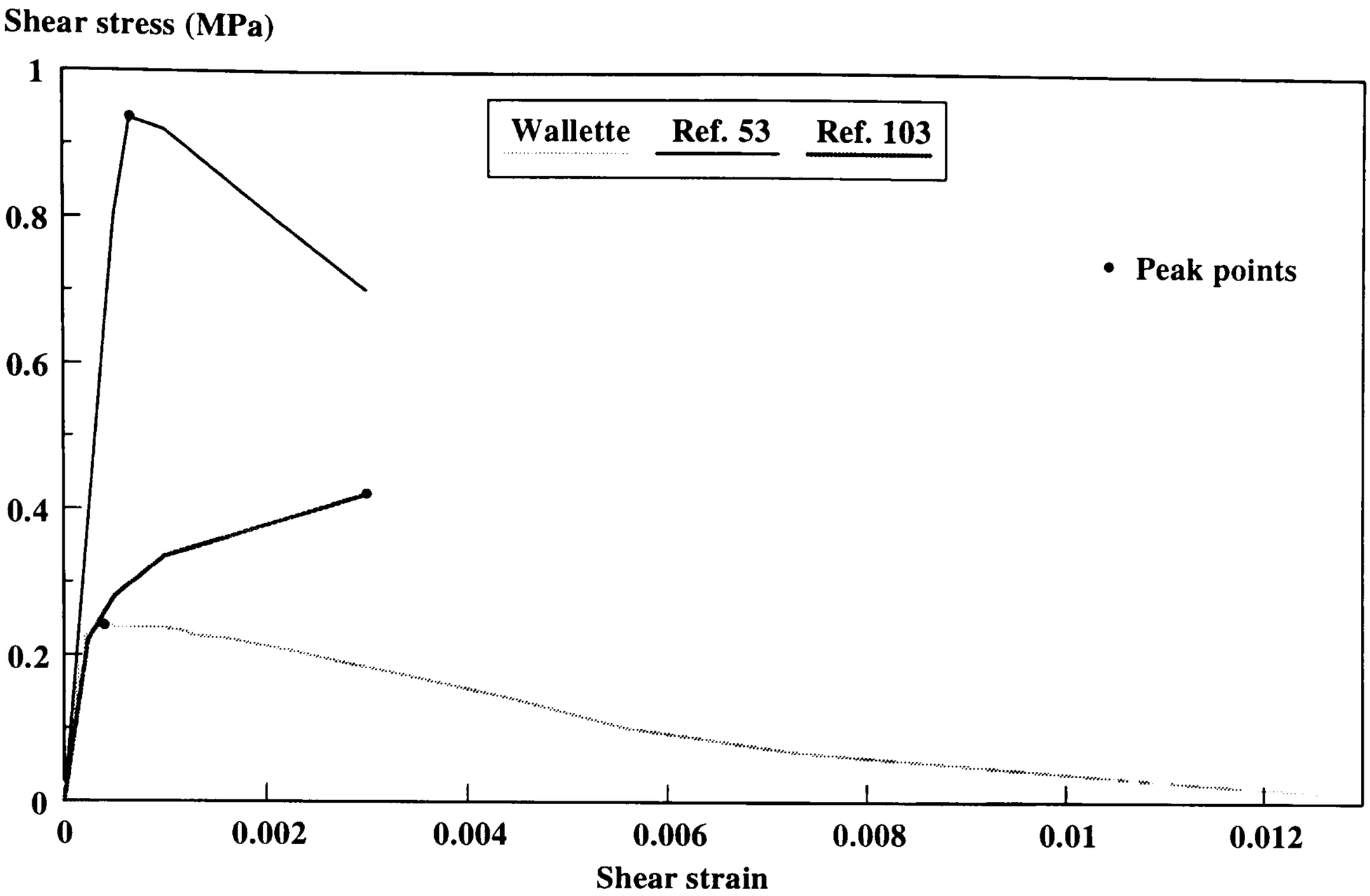

Figure 4.44 Shear stress-strain curves (different strength specimens)

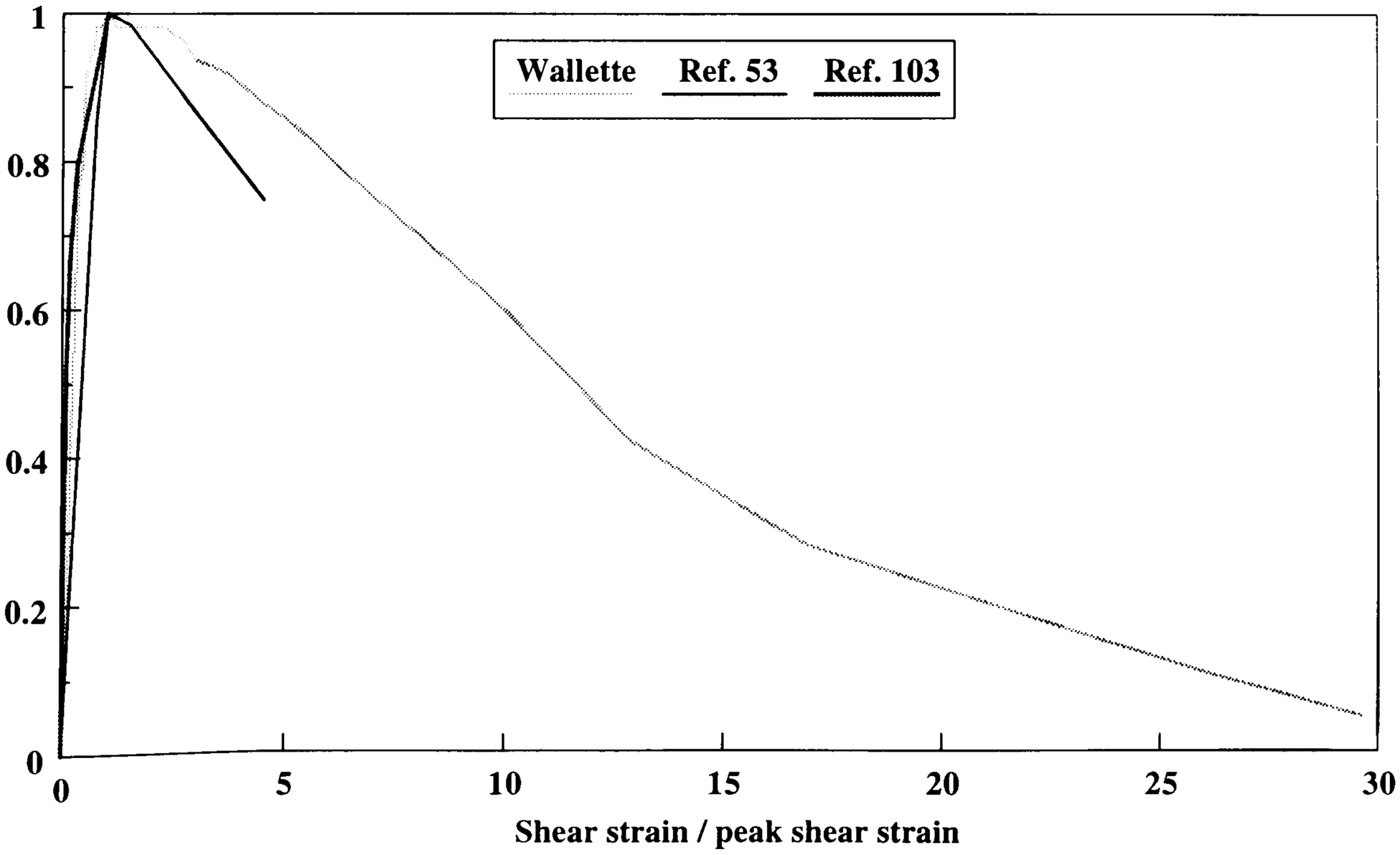

Figure 4.45 Dimensionless shear stress - strain curves for comparison

The final test that was carried out to obtain the shear bond strength at the brick-mortar interface by using a fairly simple experimental set-up. The shear box arrangement is usually employed in the experimental testing of soil samples but was adapted to accommodate model brick couplets. The intended mode of failure was successfully reproduced and the results provided a fairly accurate description for the bond strength (shear bond and friction). Literature suggests that there is no clear relationship between bond strength and absorption or mortar strength. Results from the bond tests confirmed this and also indicated, that higher mortar strength and/or low I.R.S., will result in higher interface bond strength.

Finally a statistical analysis based on the least-squares method was carried out for the test results to identify any trends in the correlation of the mechanical properties and to compare these with data available in technical literature. In almost all the cases the regression r-coefficients lie in the upper confidence limits, indicating that predictions for the value of one of the variables analysed would be acceptable if the other variable is experimentally measured. The brick and mortar tensile strengths can be determined if the compressive strength is known since the regression coefficients (8.5% and 9.8% for brick and mortar respectively) agree remarkably well with published results from similar tests [Ref. 78, 90]. Masonry modulus of elasticity is correlated to the masonry compressive strength and although it is slightly higher than values reported in recent literature it still falls within acceptable limits. In addition, accounting for scale effects which will inevitably increase the strength properties of any model material, it follows similar conclusions [Ref. 105] that the value of 1000 to 1200 (equation 4.3) used in many codes (e.g. ACI/ASCE/TMS-1992 Building Code Requirements for Masonry Structures, suggested value of 1000) is an overestimation of the elastic modulus of brick masonry. The same applies to the shear modulus where it is usually taken as 0.4 of the modulus of elasticity assuming a Poisson's ratio value of 0.2. Based on diagonal tests on masonry wallettes following ASTM and RILEM guidelines and statistical correlation of the results, a value of 0.25 was found to be more representative which is considerably lower. It should be noted that the Italian Seismic Code [Ref. 108] recommends an even lower value of 0.17 based on test results from similar larger scale specimens. The shear modulus value, also indicated anisotropy in the composite material, in relation to the experimentally measured Poisson's ratio values.

Chapter 5

Shaking table tests on model masonry panels

5.1 Introduction.

The second phase of this experimental research program concentrated on the manufacture of a small size shaking table, for the subsequent dynamic testing of 1:4 scale brick masonry infill shear walls. The walls are modelled on low-aspect full-scale unreinforced masonry panels that are incorporated as infill components to moment-resisting frames in the form of interior and exterior partitions. There are cases when these are accounted for in the design process and contribute to the overall resistance of a structure subjected to horizontal loads, or are just built with no detailed provisions for connection or separation from the main structural elements (beams, columns) often resulting in unfavourable contribution to the structure's dynamic behaviour. A short description of the role that infill panels play in earthquake resistant design is given below to introduce the methodology adopted in this experimental study and the modelling procedures considered in the choice for the model dimensions and boundary conditions.

The first case considers panels that are built tightly to the surrounding elements and in particular reinforced concrete frames where elastic shortening, creep and shrinkage of the concrete sections as well as moisture expansion of the clay brick masonry can result in axial loads to be transferred to the infill [Ref. 78], which combined with lateral forces, create a biaxial state of stress in the masonry panels. This action is coupled with the frame-infill interaction due to the separate deformation characteristics of the two components (frames deflecting in flexural mode while infills attempt to deform in shear mode).

If the infill is separated from the frame by the provision of movement joints or gaps, the only design requirement is usually restricted to the panel stability against out-of-plane collapse. Nevertheless secondary parameters such as the self-weight of the walls in the full height of the building which will lower the fundamental natural period, as well as any structural configuration irregularities with regards to the placement of the walls for convenience or architectural reasons in non-symmetrical patterns (shift of centre of rigidity), may alter the structural response due to applied seismic forces and place a higher strength demand on structural elements that are not designed with such considerations in mind.

Finally for bearing-wall structural systems where masonry shear panels are designed to carry both lateral and vertical loads, provision of adequate reinforcement is dictated by seismic codes and in most cases these types of buildings are prohibited in all areas of high seismic activity [Ref. 108].

The geometric dimensions of a panel subjected to lateral loads have been shown to influence the behaviour and failure mode as well as the cracking and ultimate strength [Ref. 109]. As the length increases in relation to the height of the panel the mode of failure changes from a flexural/shear sliding (along the mortar joints) mode to a diagonal tensile/shear mode. These parameters in turn are highly influenced by the axial load acting on the infill which depending on its magnitude, tends to increase the shear strength and brick-mortar interface bond strength resulting in higher ultimate strength. Furthermore, the boundary conditions and fixity of the panels affect the behaviour in relation to the bounding frame members and the contact (beam/column to wall) interface bond present, since the resulting interaction between the structural components caused by lateral loading dictates the cracking pattern, ultimate strength and final mode of failure for the complete system (chapter 3). The above considerations become more profound in the case of reduced scale models, since it is not always possible to reproduce exactly all the parameters necessary for the case of *complete* similarity without sacrificing some others along the way.

5.2 Choice of modelling parameters.

Since the modelling scale is the first and most important parameter to be considered during the planning stages of an experimental study, the selection is left to the investigator depending on the available economic and technical resources, complexity and degree of difficulty and level of effort involved. Smaller does not necessarily mean cost effective, but to an extent aspects of the experimental set-up such as materials (less volume), machinery (less power), instrumentation and data acquisition can reduce the overall cost of planning and executing a series of experiments. One of the most important parameters for consideration is time, which relates closely to cost and repeatability of a model experiment (figure 5.1). For example the complexity involved in the construction of small scale models is related to the time available for the completion of the study and in turn to the materials and components chosen as the most suitable for representing the true behaviour of a similar full scale structure, based on cost margins and available technical resources. In turn the number of experiments that are necessary to produce results that can be statistically correlated is directly related to the time available, since smaller scale models have a faster turnover with respect to casting and curing (as in this case where more than one wall could be prepared at the same time and tested in consecutive days).

The planning stage of the experimental investigation involved the selection of suitable scale for the model masonry walls and the boundary conditions that should be imposed in order to simulate as accurately as possible full scale elements. The choice of 1:4 scale for the models related in part to the available laboratory floor space for setting up the shaking table and the machinery to operate it. The walls were designed as rectangular single-leaf panels of 753 mm length, 445 mm height and width of 25.6 mm. This represents a low aspect ratio panel ($h/l = 0.6$) which based on available literature results would be expected to be dominated mainly by shear action effects when subjected to lateral cyclic forces (section 5.3). Mortar joints were scaled down to 2.5 mm throughout using techniques described in section 5.6.

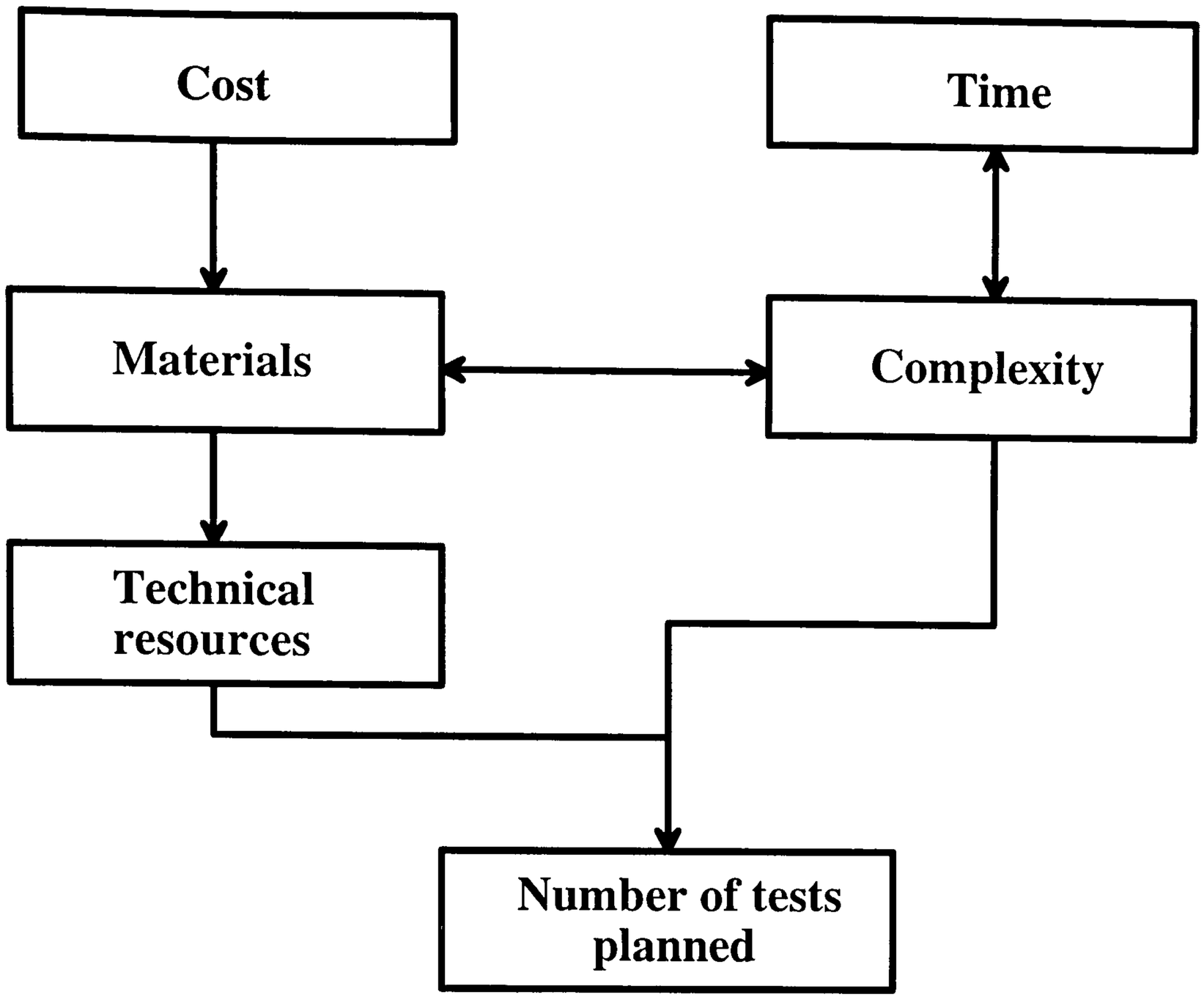

Figure 5.1 Diagram of the parameters involved in the planning of experimental small scale model investigations

A steel frame was designed and manufactured consisting of top and bottom rectangular steel beams and side columns made out of spring-steel sections (section 5.4). No attempt was made to accurately model the surrounding frame except for the section dimensions of the members, since frame-panel interaction was not considered as a primary parameter for investigation in this study. Self-weight of the walls was 18 kg (brick type I-ordinary) and 44 kg (brick type II-heavy). Based on the method of artificial mass simulation (section 2.4.2), additional inertia mass in the form of six lead bars of 180 kg total weight was securely attached to the top beam (self-weight 20 kg). This partly accounted for the relaxation of the density similitude requirement resulting from the 1:4 scale factor. Accelerations in excess of 1.0g (m/sec^2) were dictated by similarity conditions (*simple* model) within an operating frequency range of 0 to 40 Hz. These are related to the available maximum displacement of the shake table platform and the weight of the combined system. Sinusoidal excitations resembling a ramp input function were applied to the models with a rise time of about a second followed by 4 seconds of the specified ground motion input. Table acceleration

varied between 0.02g and 1.8g depending on the strength of each of the walls tested. Correspondingly the experimentally measured displacements of the models would be expected to be about 4 times less than displacements experienced by a similar full scale masonry wall when subjected to the same loading history.

5.3 Failure modes of shear walls and infill panels subjected to cyclic in-plane excitations.

Although shear walls and infill masonry panels exhibit similar failure modes when subjected to both laboratory generated and actual earthquake loading histories, there are some distinct differences associated with the bounding frame which influences, and in turn is influenced by the behaviour of the infill masonry wall. Infill walls mainly form part of the internal or external partitioning arrangement. Occasionally they are designed to perform as a lateral load resisting element and thus contribute to the overall resistance and energy dissipation capacity of the structural system [Ref. 103, 109]. For cases where no concrete or steel frames are in place to confine an unreinforced masonry shear wall, stability and resistance of the system is dominated by the axial forces acting down on the walls (e.g. dead load). In such cases there are usually three modes of failure that can occur (figure 5.2), depending on the magnitude of the axial and horizontal forces and the mechanical properties of the masonry wall.

The first case (mode-I) results from high axial loads which tend to cause vertical splitting cracks in the panel similar to failures observed for small masonry assemblages like 5-course prisms. For moderate magnitudes of applied lateral load, joint failure might occur parallel and at an angle to the line of action of the horizontal load which will tend to spread the damage in irregular patterns. The second case (mode-II) represents a diagonal tensile cracking mode of failure which is a result of combined action by axial and lateral loads and depends on the tensile strength of the brick units and mortar joints. This is by far the most common and undesirable mode of failure for typical shear walls and infill panels alike.

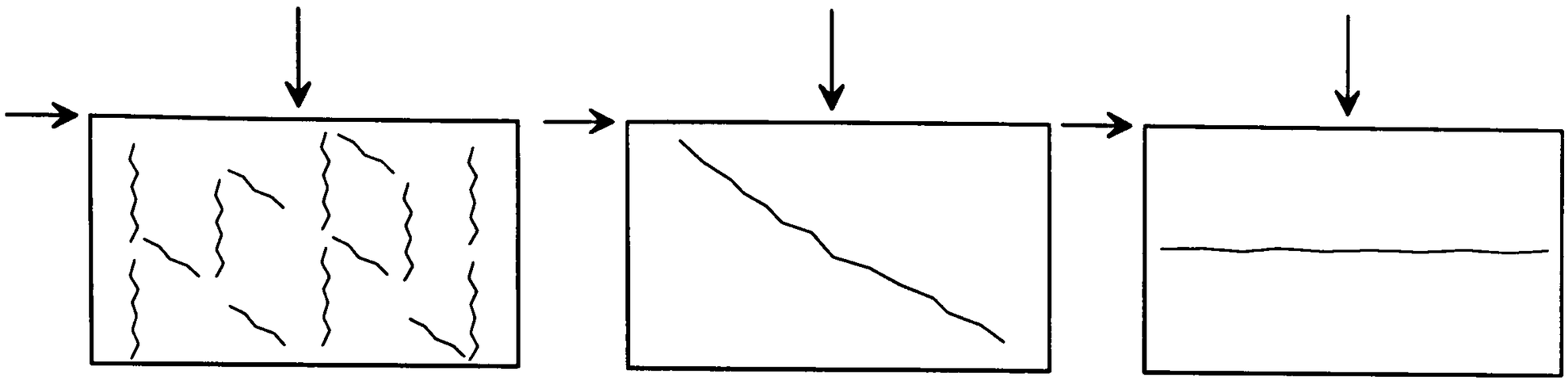

Figure 5.2 Masonry shear wall failure modes

The third failure mode would mostly occur in secondary walls of a bearing-load structural system, which are not directly influenced by axial forces resulting in a joint failure mode with sliding along the joints and the brick-mortar interface usually originating at or close to the middle part of the wall. It should be noted that these modes of failure are mostly encountered in unreinforced masonry where the resistance of the wall to the applied forces is dependent entirely on the properties of the constituent materials.

In the case of infill masonry walls where a surrounding concrete or steel frame transfers the lateral load via the beam or diaphragm connection, similar failure modes are observed, except for mode-I since the axial load is primarily carried by the frame members. An additional mode of failure which is characteristic for very strong panels and relatively weak frames, can occur in infilled frames. This mode of failure involves crushing of the masonry at the loaded corners as a result of the formation of the compression strut resulting from differential deformations between panel and frame (section 3.3.2 - figure 3.10). For strong panels where diagonal tensile cracking might be limited or confined to the centre of the panel, the compression strut transmits the lateral forces to the infill through the opposite loaded corners at the beam-column joints. This is not considered as a failure condition for the infill, but might contribute to the formation of flexural plastic hinges in the columns near the loaded corners.

Destructive failure modes of infill panels have been observed extensively in recent and past earthquakes. On July 15 1995 an earthquake of magnitude M = 6.1 occurred near the city of Aigio (epicentre 15 km to the northeast) in southern Greece, an area of moderate seismic activity. There were 26 fatalities, with 11 of these in a three storey reinforced concrete hotel building which was heavily damaged and is shown in photo 5.1. Although briefly reported in the media and in several publications (SECED Newsletter, Vol. 9, No. 2 and the Bulletin of the European Association for Earthquake Engineering, Vol. 14, No. 1), it has not been post-examined in detail or properly documented in any report. Following the earthquake the author visited the area where the hotel was located and most of the damage was concentrated. Photo 5.2 shows another section of the Eliki hotel which did not collapse, but was heavily damaged with many masonry walls failing in a combined sliding shear mode. Photos 5.3 and 5.4 were taken from another 2 storey reinforced concrete building which was adjacent to the only other structure (a 6 storey block of flats) that also partially collapsed. Photo 5.3 shows a typical cross-diagonal tensile mode of failure of an unreinforced masonry wall with visible separation at the contact with the column faces. Photo 5.4 shows another diagonal cracking pattern which is not as symmetric about the centre of the panel like the one shown in photo 5.3. This would probably be a result of the variability of the constituent material properties commonly found in masonry structural systems. Another possibility for this cracking irregularity could be that the horizontal wide crack at the upper left corner (separation and joint sliding) coupled with the vertical crack at the bottom right corner, which judging by the their width must have occurred at the beginning of the seismic loading cycle, shifted the cross-diagonal cracking pattern towards the right side of the panel and away from the centre. The opposite diagonal crack is visibly narrower and in addition another horizontal crack at the beam-panel interface can be seen at the upper right corner which would have resulted in loss of stability and inevitable collapse if the earthquake had a longer duration. Non-symmetrical cracking patterns were also recorded in the model masonry walls described in section 5.8.

Photo 5.1 Collapsed section of the Eliki hotel in Aigio, Greece

Photo 5.2 Sliding-shear failure of masonry infill panels in the Eliki hotel

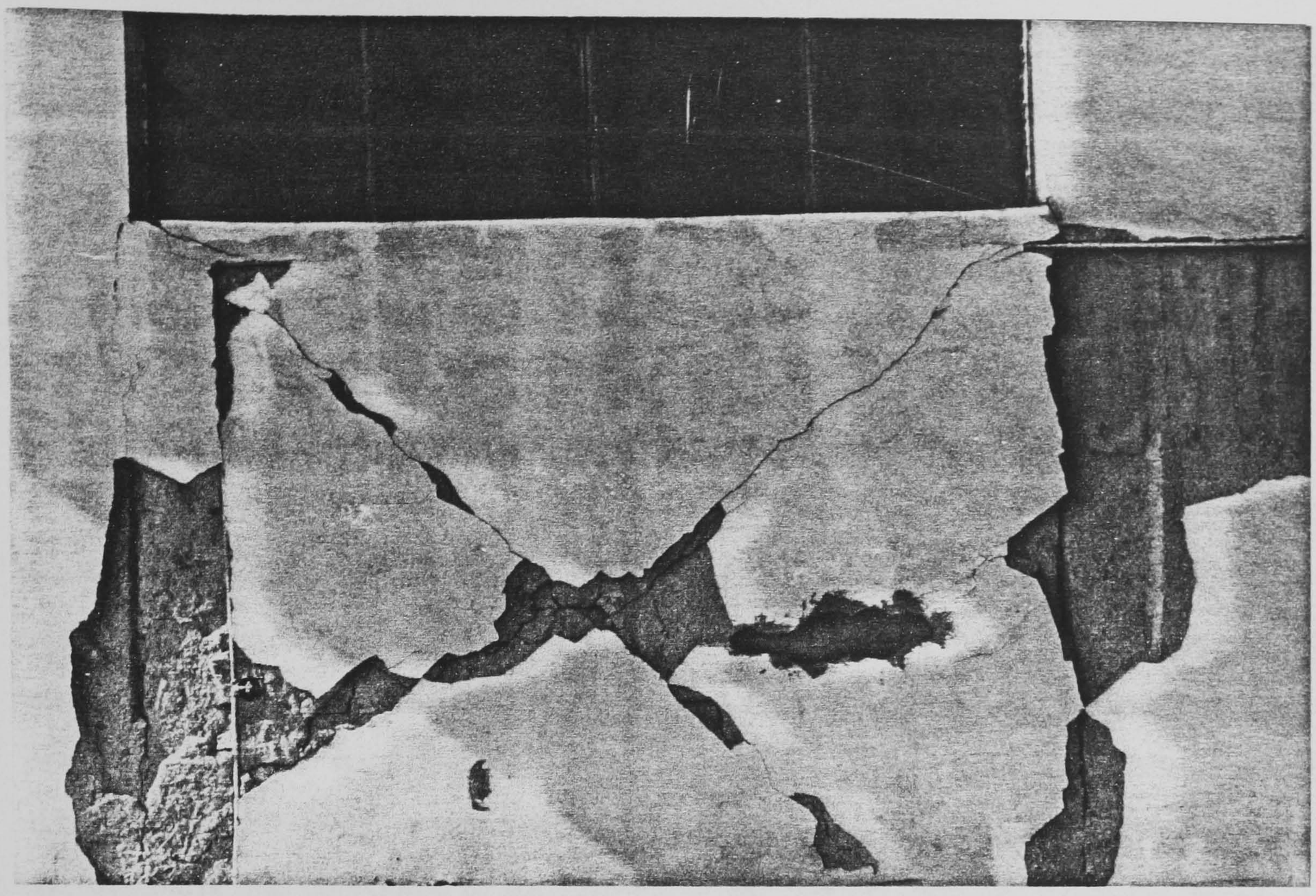

Photo 5.3 Cross-diagonal tensile failure of unreinforced masonry infill wall

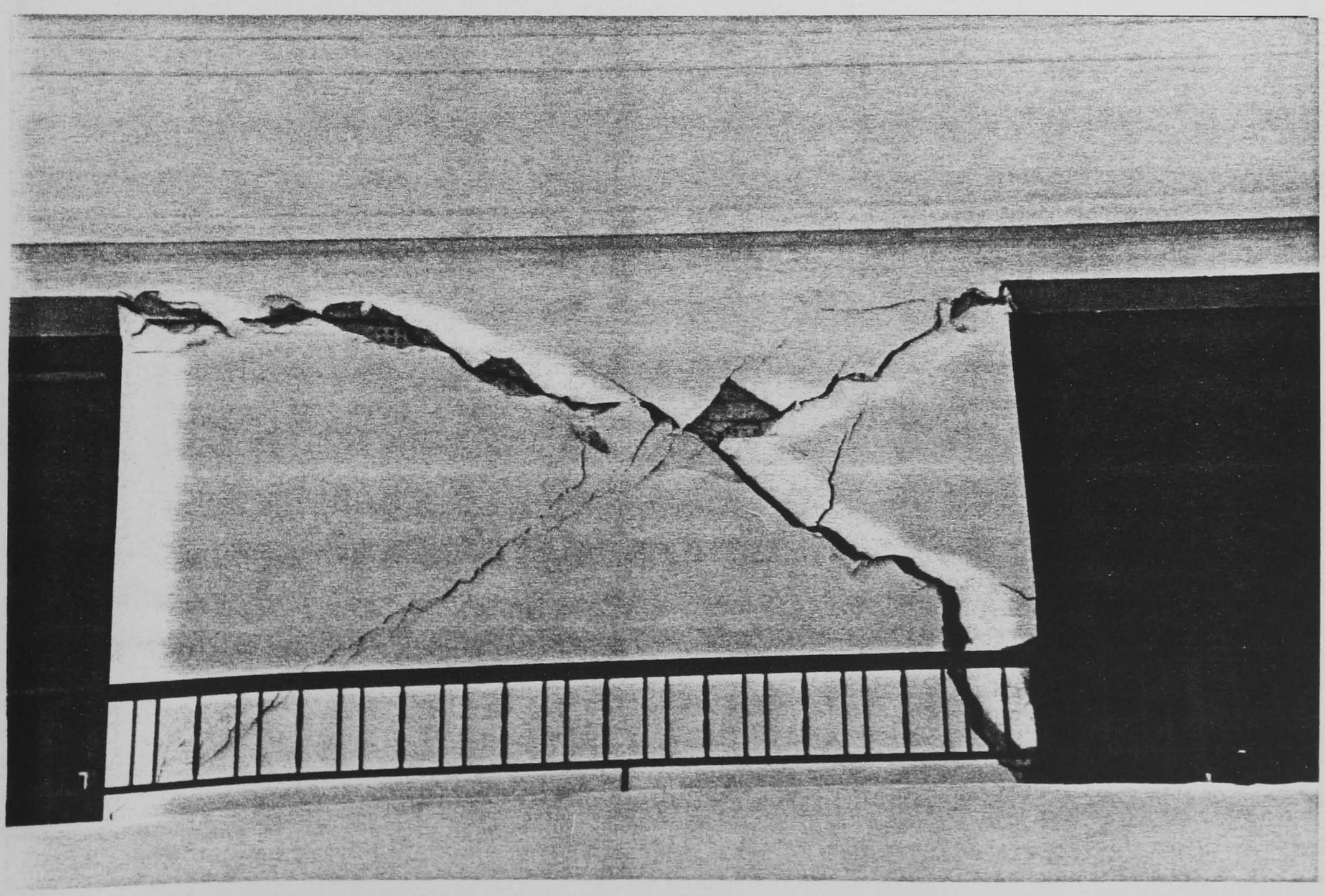

Photo 5.4 Cross-diagonal tensile non-symmetrical failure of masonry infill wall

5.4 Description of the shaking table facility.

The shaking table used for the dynamic tests was manufactured at the departmental workshop based on a design that allowed manual selection of the frequency and amplitude characteristics of the platform motion. The lower part is bolted at several locations to the concrete floor using high tensile strength rawbolts, projecting several centimetres into the concrete floor whereas the platform was formed of a grid of steel channel sections welded onto a (1.2 m x 1.3 m) table. Four roller supports allow the platform to move freely relative to the base coupled with a central steel bar which is anchored to the floor at three equally spaced points along the direction of motion as shown in figure 5.3. An electrical motor is used to drive the platform through a transfer frame which was specifically designed to control the amplitude of the applied displacement. Figures 5.4a and 5.4b show sections of the frame together with details of various parts that contribute to the transfer of the motion from the electrical motor to the shake table platform.

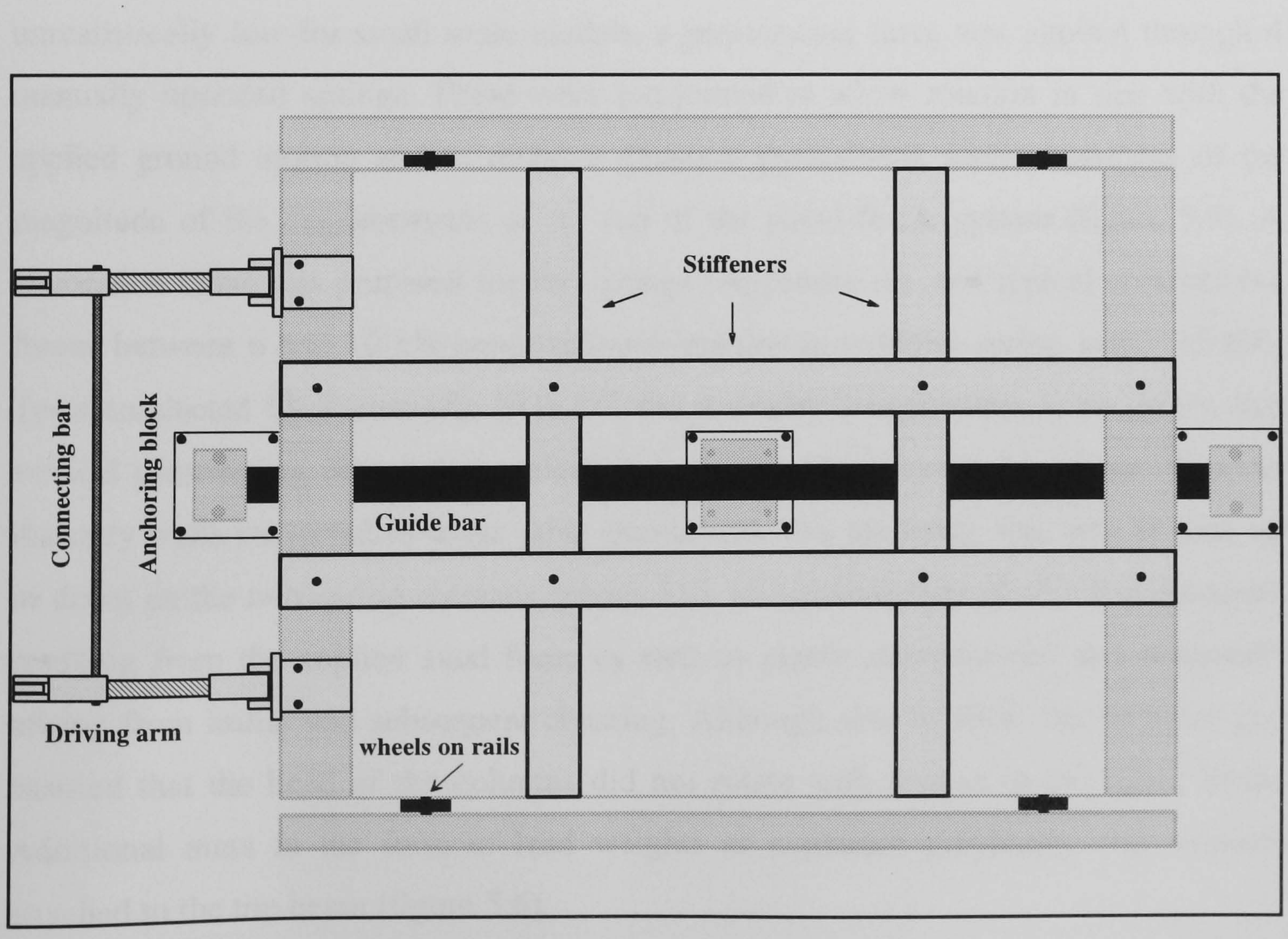

Figure 5.3 Plan of the shaking table

In the centre of the transfer frame a mechanism consisting of a set of rectangular bars suspended on pivot joints from the top of the frame, swing in line with the direction of motion. The lower end of these bars transfer the action to the shake table platform (figure 5.4b). The perforations in the steel sections shown in figures 5.4a-b were introduced in order to reduce the weight of the steel sections without reducing their strength, as their inertia would impose excessive strain on the motor. A secondary arrangement is set between the two perforated steel sections and carries the fixed pivot point which can be manually adjusted to alter the table amplitude of motion (figure 5.4b). A purpose-built steel frame was fixed to the top of the shake table platform at several locations along the centre line. This frame consisted of two rectangular sections to act as the top and bottom beams. Each had a machined central seating area 3 mm in depth which accommodated the mortar bedding for the infill walls (photo 5.5). The columns at each end of the beams, were made out of spring steel sections so as to remain elastic regardless of the deformations imposed on the frame members by the applied ground motion. In order to provide the vertical confinement which would inhibit flexural failure to increase the working stresses in the walls, which are always unrealistically low for small scale models, a prestressing force was applied through 4 manually operated springs. These were pin-jointed to allow rotation in line with the applied ground motion and to retain a constant prestressing force regardless of the magnitude of the displacements at the top of the panel-frame system (figure 5.5). A calibration chart was prepared for the springs (Appendix A), and typical compressive forces between 6 and 10 kN were imposed (maximum working spring load - 15 kN). Tests conducted by Tomazevic [Ref. 27] for a similar arrangement, have shown that vertical prestressing does not significantly influence the dynamic behaviour of model masonry walls subjected to shake table excitations. The top beam was able to slide up or down on the two spring columns (photo 5.6), to accommodate elastic displacements resulting from the applied axial force as well as plastic deformations and settlement arising from initial and subsequent cracking. Although able to slide, the restraint also ensured that the head of the columns did not rotate with respect to the upper beam. Additional mass in the form of lead weights as explained previously was securely attached to the top beam (figure 5.6).

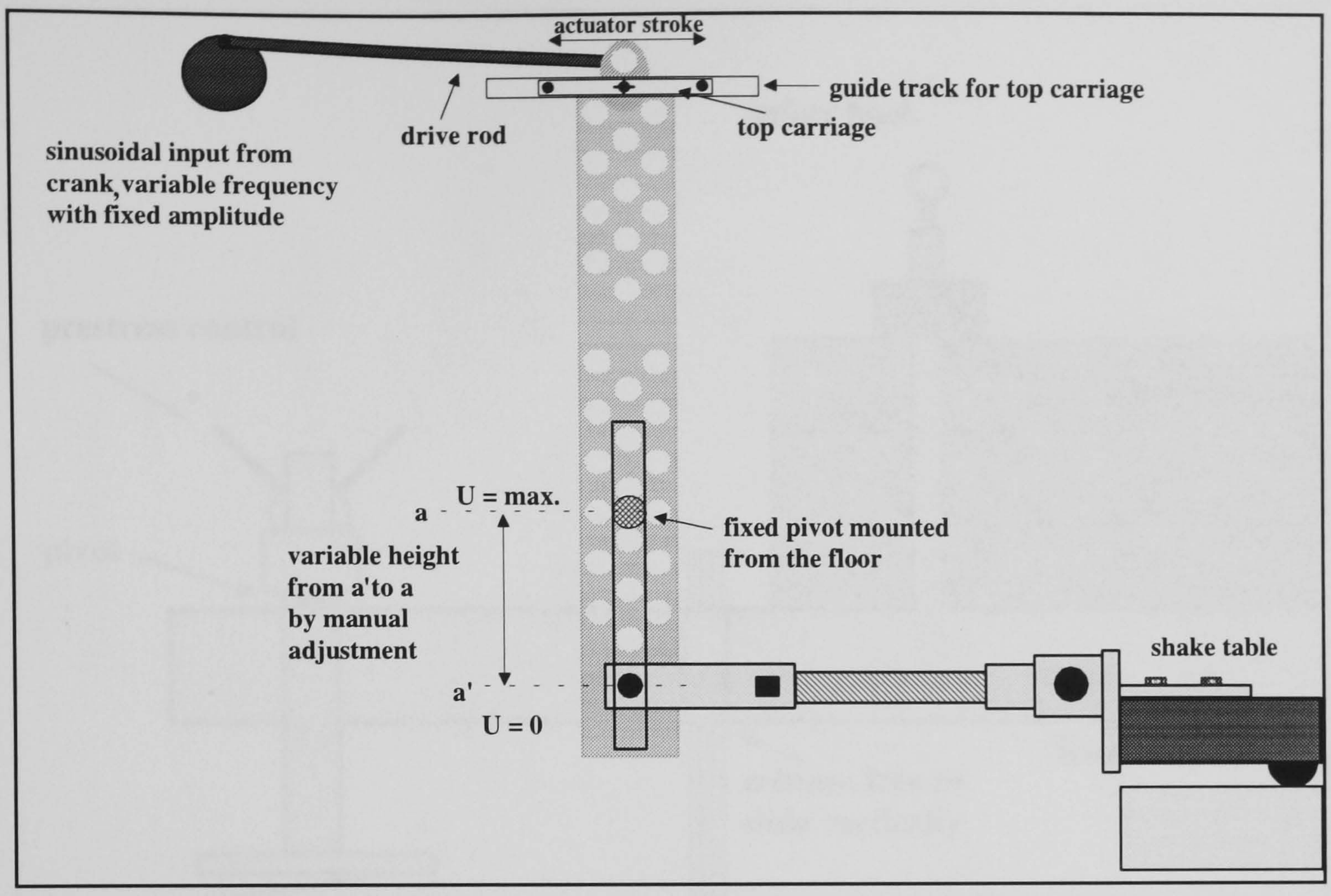

Figure 5.4a Transfer frame (inside) elevation - driving and motion mechanisms

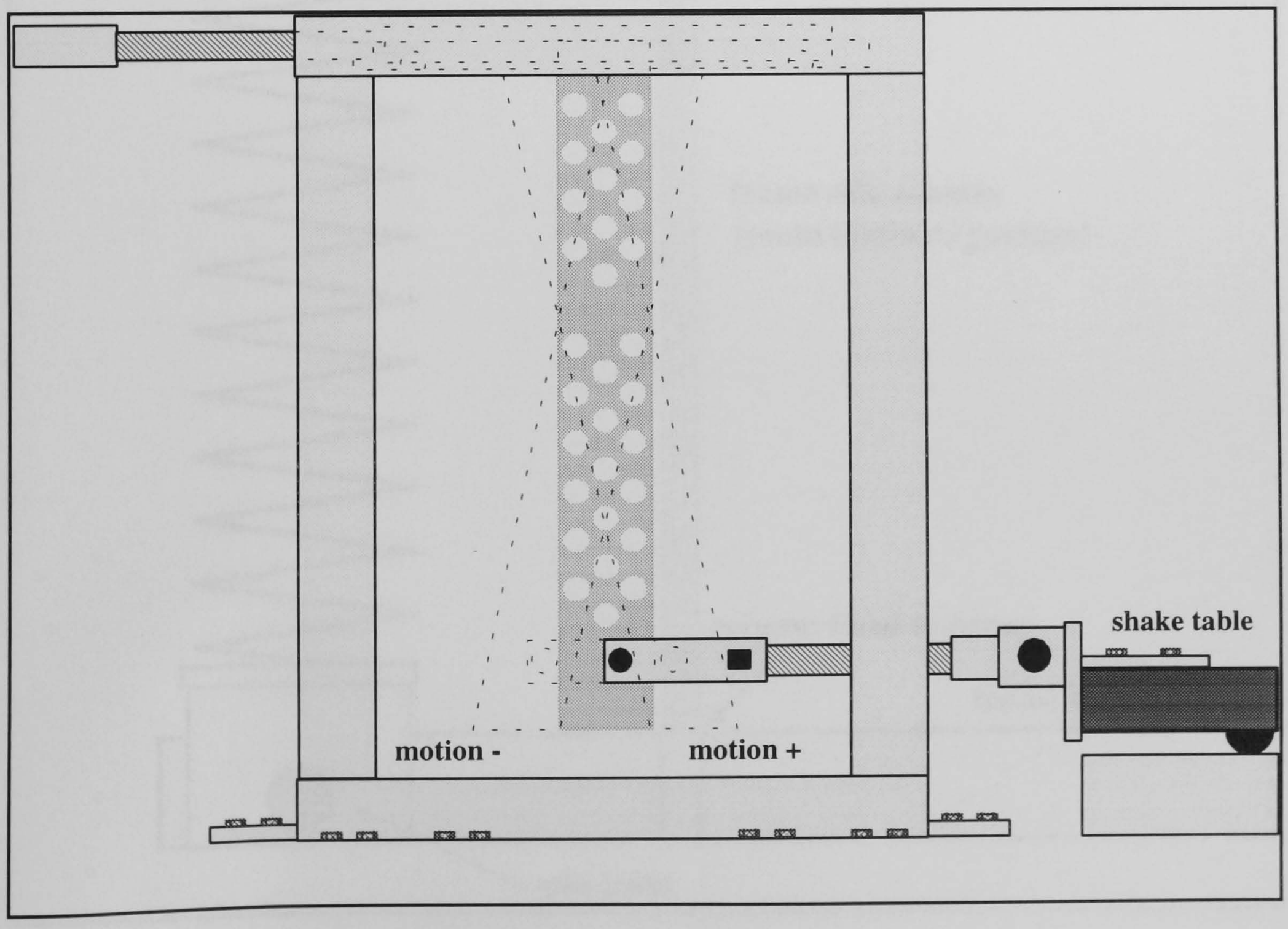

Figure 5.4b Elevation - transfer frame

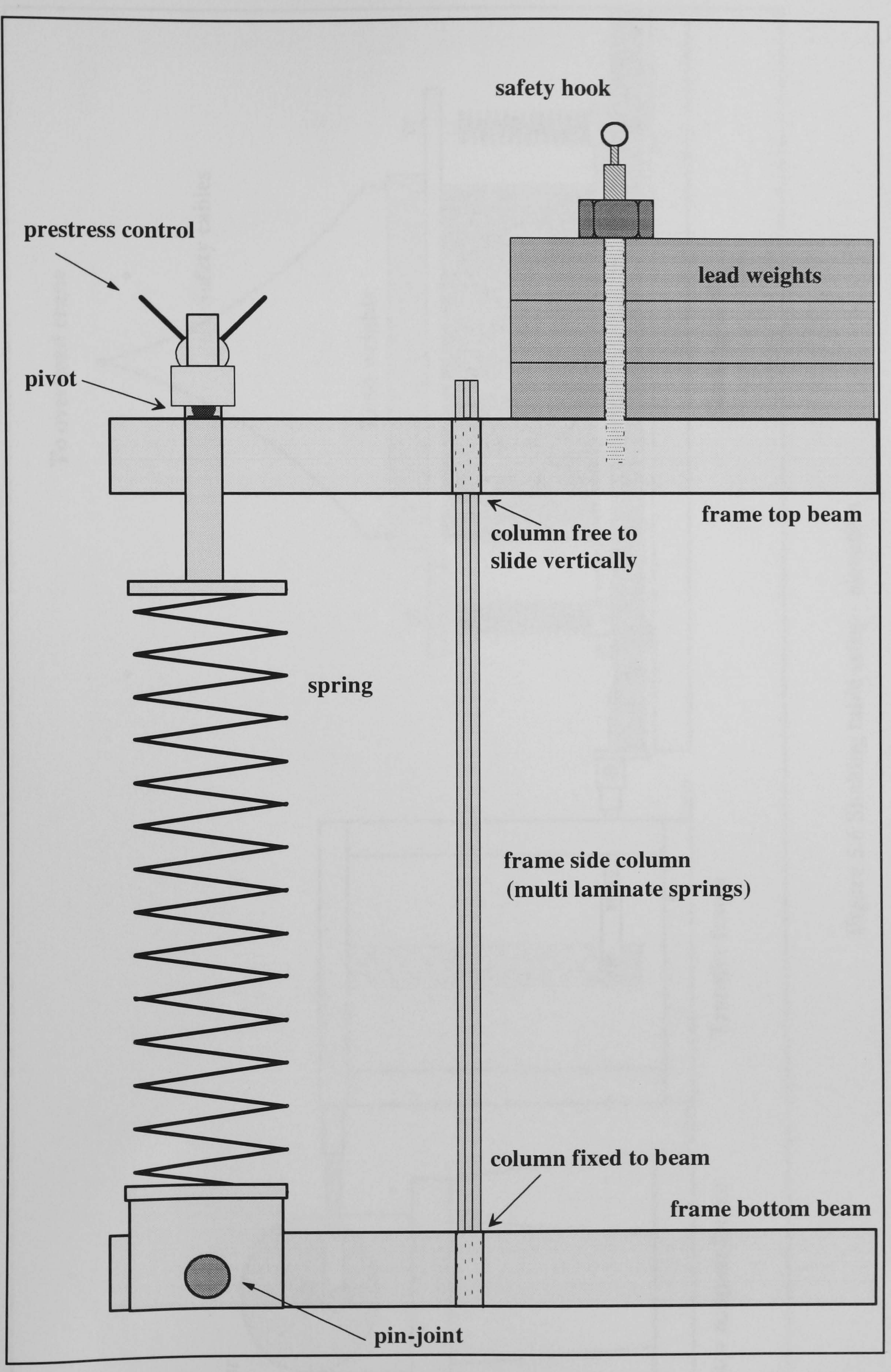

Figure 5.5 Model frame and prestressing spring details

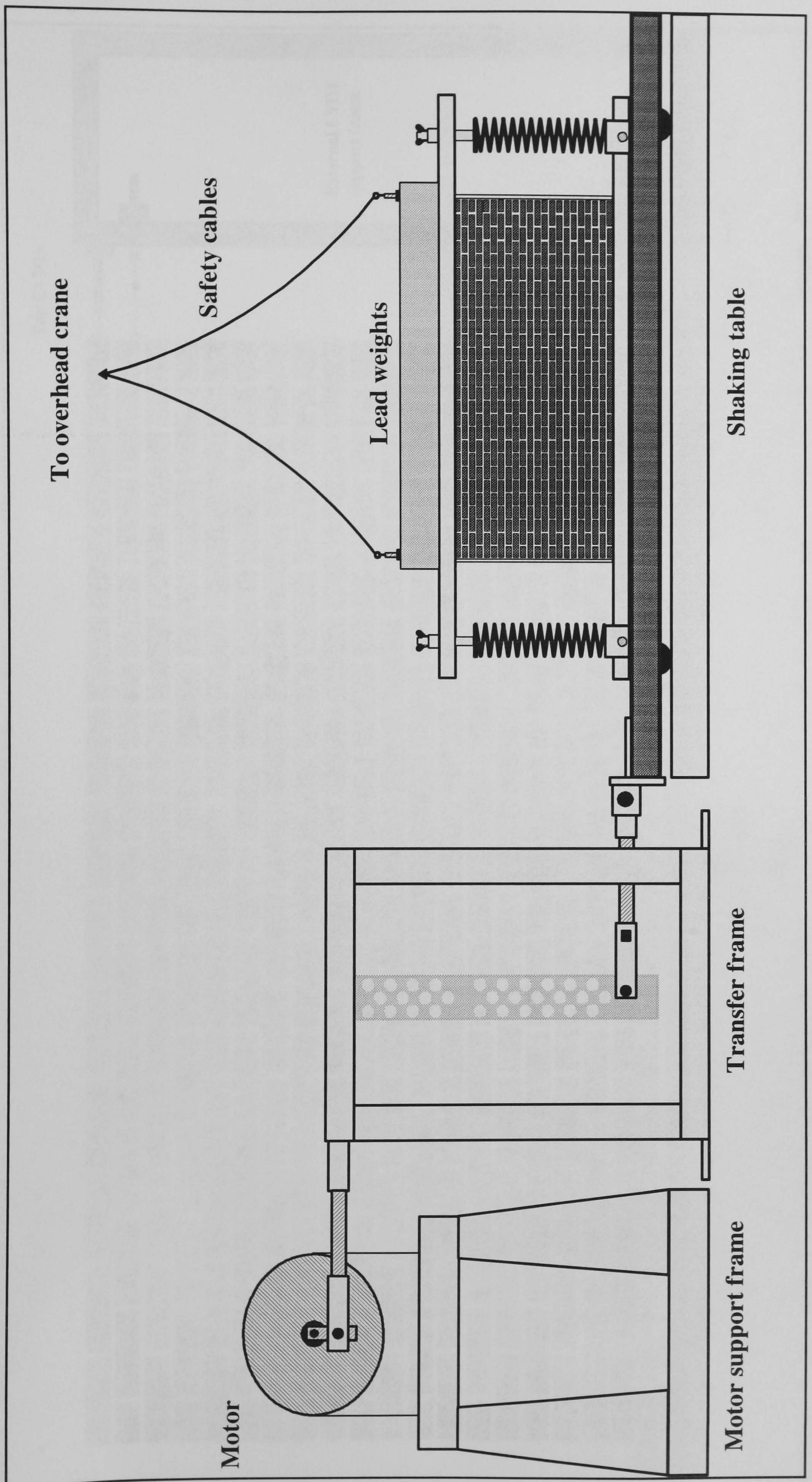

Figure 5.6 Shaking table setup - elevation

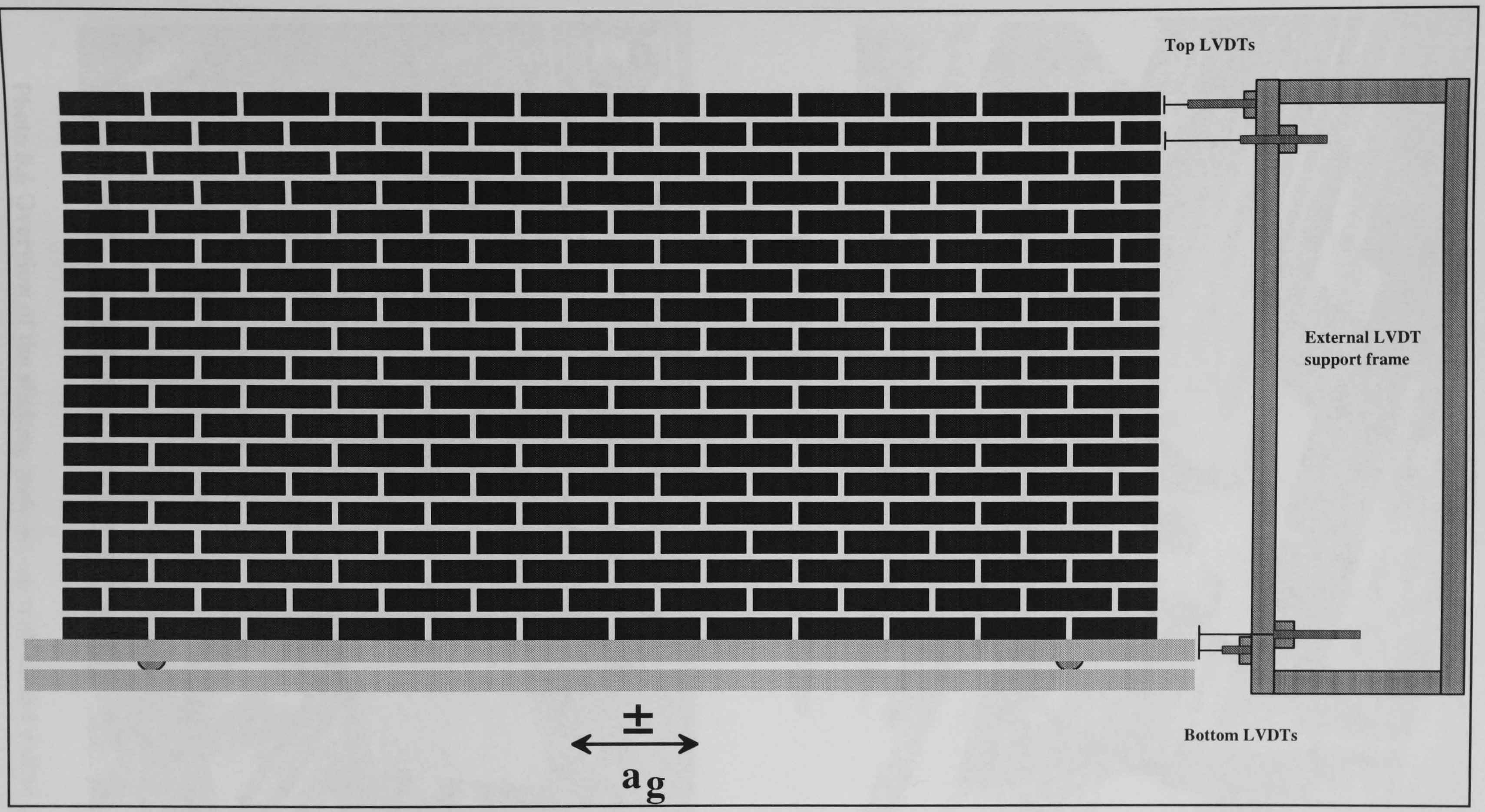

Figure 5.7 Instrumentation setup

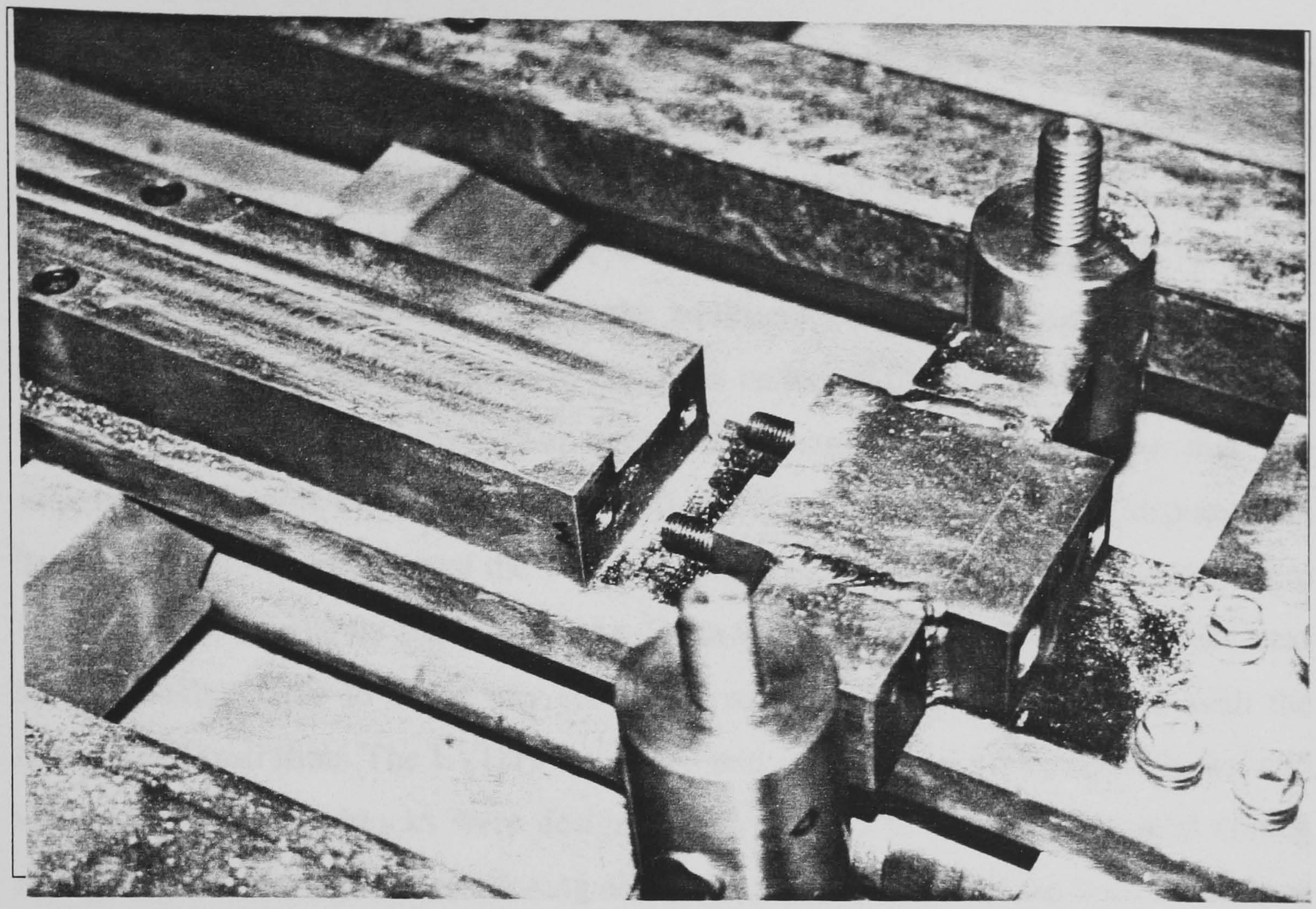

Photo 5.5 Close-up detail of the bottom beam

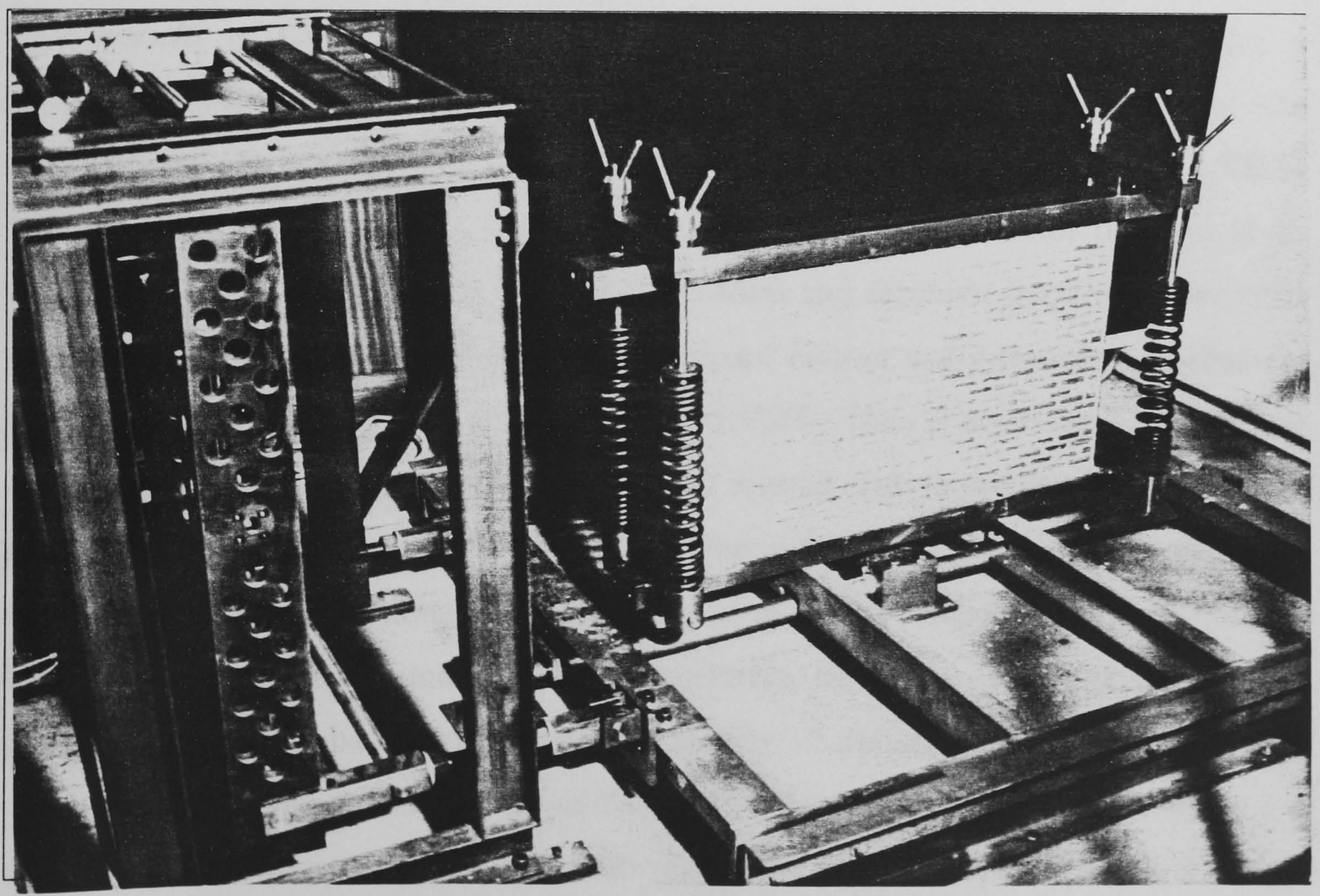

Photo 5.6 Overview of the shaking table set-up with model wall in place

For safety reasons the lead weights were loosely suspended from an overhead crane so that should brittle collapse occur and the panel disintegrate, which is characteristic of shear dominated failures in masonry walls, these would not drop onto the equipment and destroy it. It should be noted that photo 5.6 was taken during preliminary testing of the table set-up and does not include the additional channel steel sections that were incorporated as stiffening elements to the shake table platform and shown in figure 5.3. Finally the experimental test set-up included an external reference frame that was designed to support the instrumentation (figure 5.7). Since the relative displacement between the top and bottom of the wall was one of the dynamic response parameters to be measured, a separate frame was manufactured and securely bolted on the wall next to the shaking table to avoid any secondary response that would interfere with the transducer's operation. The LVDTs were mounted on the frame using steel blocks with extension arms. The blocks were designed with vertical as well as horizontal sliding mechanisms to allow exact positioning and alignment to the side of the wall. Procedures regarding instrumentation and data acquisition are covered in more detail in section 5.5.

In order to test the reliability of the electrical motor and the shaking table set-up with regards to the reproduction of the intended sinusoidally-varying motions, a calibration procedure was performed which involved measuring the frequency and amplitude of the applied motion together with displacement readings from LVDTs attached to the table platform. It was discovered that when the motor operates at its minimum frequency (5 Hz) and amplitude, *backlash* and *resonant frequency* associated phenomena interfered with the platform horizontal motion and introduced mechanical noise to the waveform signals acquired by the LVDTs; (this is not related to electrical noise which was also present in the system and is dealt with in section 5.5). For motor operating frequencies above 8 Hz this effect diminished rapidly considering the large number of bolted connections in the assembly of the motor support and of the transfer frame, together with the unavoidable play between the shake table platform rolling mechanisms and the base, very good reproduction of the intended sinusoidal ground motion was obtained over the range of 8 Hz to 15 Hz. This is illustrated in figures 5.8 and 5.9, which show comparative waveforms of one complete cycle for two different motor operating frequencies (5 Hz and 9 Hz), with mathematically derived sine-curves for corresponding frequencies and amplitudes of motion.

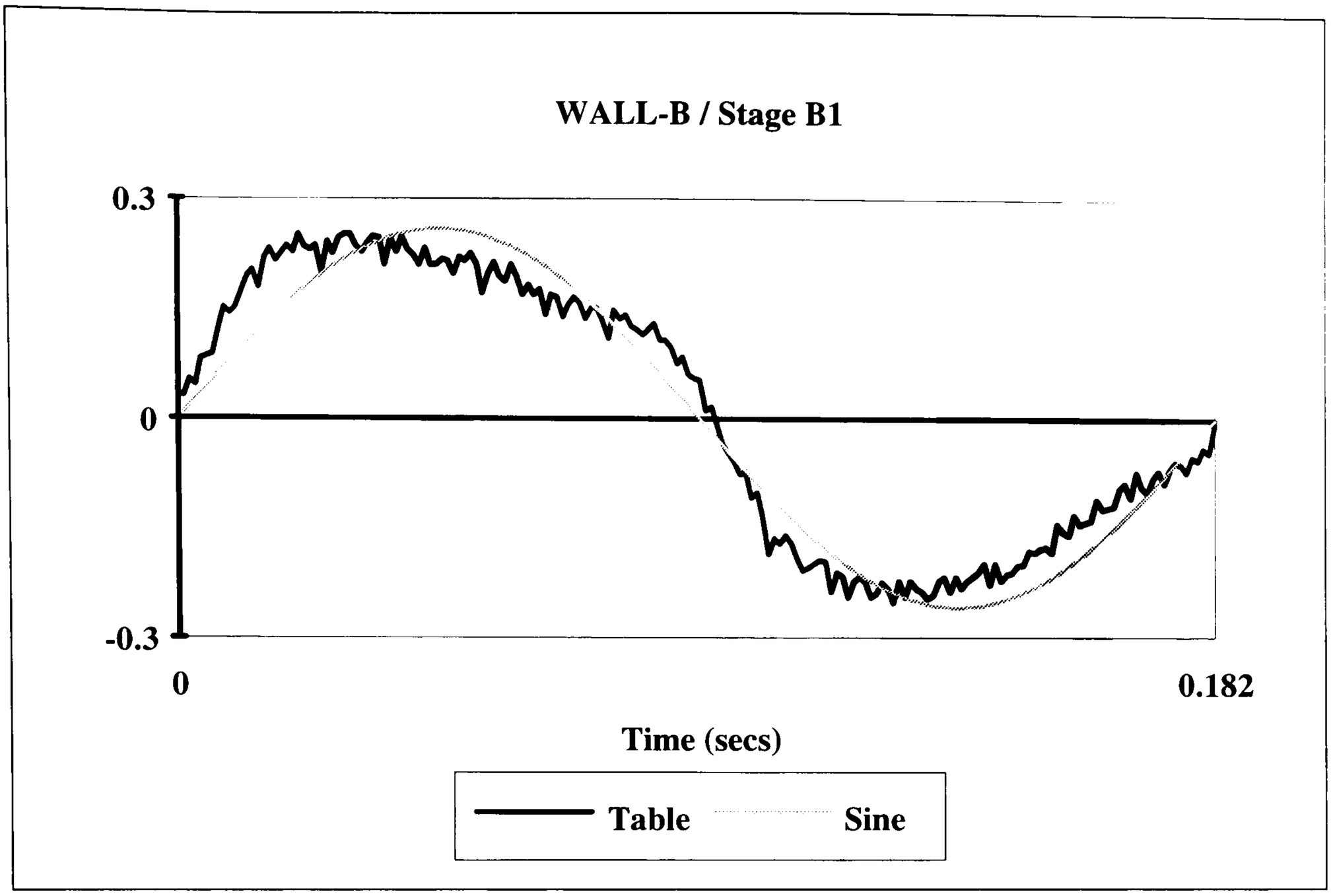

Figure 5.8 Table motion at 5 Hz compared with 5 Hz sine wave (same amplitude)

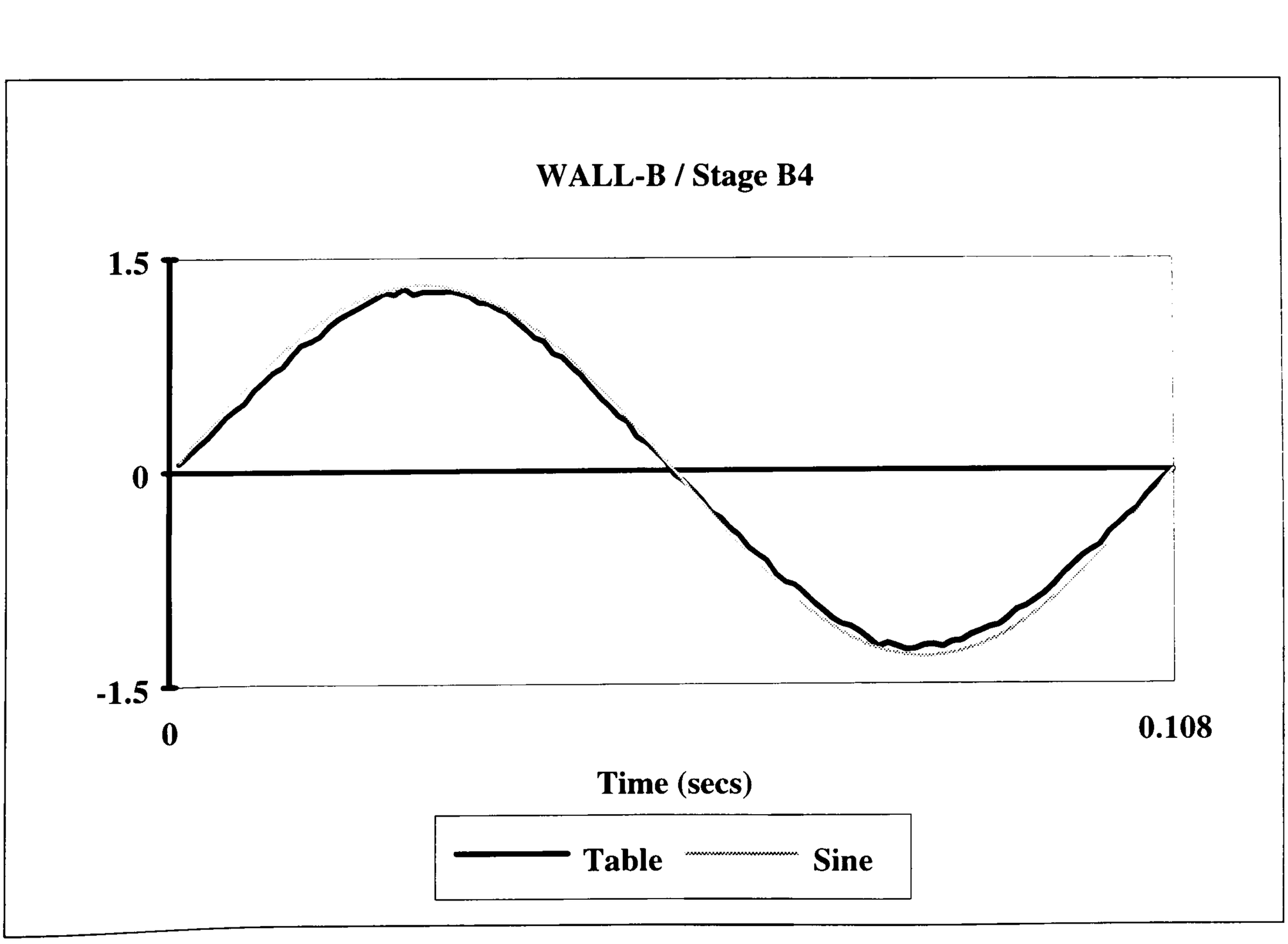

Figure 5.9 Table motion at 9 Hz compared with 9 Hz sine wave (same amplitude)

5.5 Instrumentation and data acquisition.

Due to lack of funding the dedicated instrumentation was limited, in particular no suitable acceleration transducers were available for the dynamic testing stage of this investigation. The author's alternative was to use his high quality LVDTs and process the data to obtain acceleration values. Displacement transducers should possess a linear working range which is as close as possible to the displacement to be measured. Preliminary calculations (section 5.7), suggested that the top of the wall might exceed 5 mm horizontal displacement at the highest ground motion displacement envisaged for collapse of the walls. Such displacements required LVDTs with a working range of ± 10 mm but these have limited resolution in the below ± 5 mm range. Since for a major component of the tests the walls would only be subjected to displacements in the order of 1/10 of a millimetre, it was necessary to use two types of transducers. The smaller range LVDTs would be dedicated to picking-up signals up to a maximum of ± 5 mm. For larger magnitudes, the second type (± 10 mm) would be in place to record the deformation.

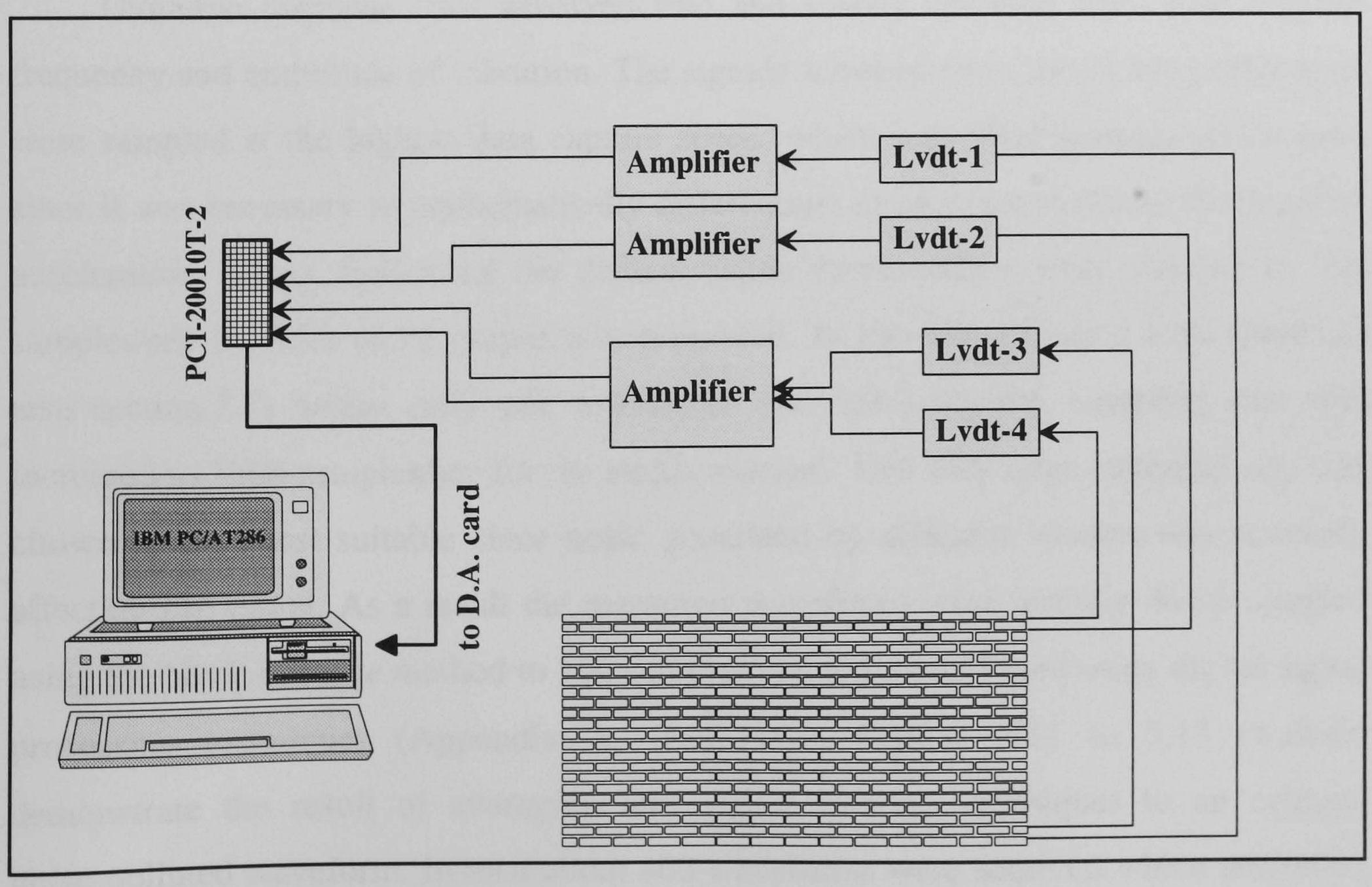

Figure 5.10 Data acquisition set-up for shaking table test

As a result 4 LVDTs were mounted on the external frame described in section 5.4, two located at the shake table platform level and two at the top end of the wall. The output was fed to amplifiers and in turn to the termination panel for transfer to the data acquisition board (figure 5.10). The LVDTs were connected to 2.8 mm diameter rods which in turn were inserted into a hole drilled in one of the upper corner bricks and glued with epoxy resin and an arrangement of nuts and washers that were attached to both faces of the wall for added security. The type of fixing that was used in the first wall only is shown in photo 5.7. A different set-up which involved a similar secure fixing for the attachment rod but a different connection to the LVDT, is shown in photo 5.8 and was used in all subsequent tests, since it was discovered that the initial set-up caused damage to the transducer when the wall experienced rigid body rotations due to shaking table malfunction. Furthermore if a wall was to collapse by a brittle mode of failure, the transducer would have to be released by the action of its own spring to avoid damage. The second set-up incorporated a Teflon protective sleeve and a round flat head made from the same lightweight material so that it could vertically slide in relation to the rod if necessary.

Dynamic response tests involved free and forced vibration tests with varying frequency and amplitude of vibration. The signals acquired from the shaking table tests were sampled at the highest data capture speed, which was 1000 samples/sec/channel since it was necessary to mathematically differentiate these twice to obtain the required acceleration values. Following the differentiation process these were reduced to 500 samples/sec in order to be graphically presented. In the free vibration tests (hammer tests-section 5.7) where only one transducer was involved, the sampling rate was increased to 3000 samples/sec for the single channel. This very large sampling rate was chosen as the most suitable since noise generated by different sources was seriously affecting the signal. As a result the measured waveforms were initially down-sampled using the *block-average* method to 500 samples/sec and then filtered using digital signal processing techniques (Appendix A, [Ref. 110]). Figures 5.11 to 5.13 (wall-O) demonstrate the result of averaging and digital filtering techniques to an original noise-polluted waveform. In total about 400 waveforms were acquired which amounted to more than 10 megabytes of unconverted data.

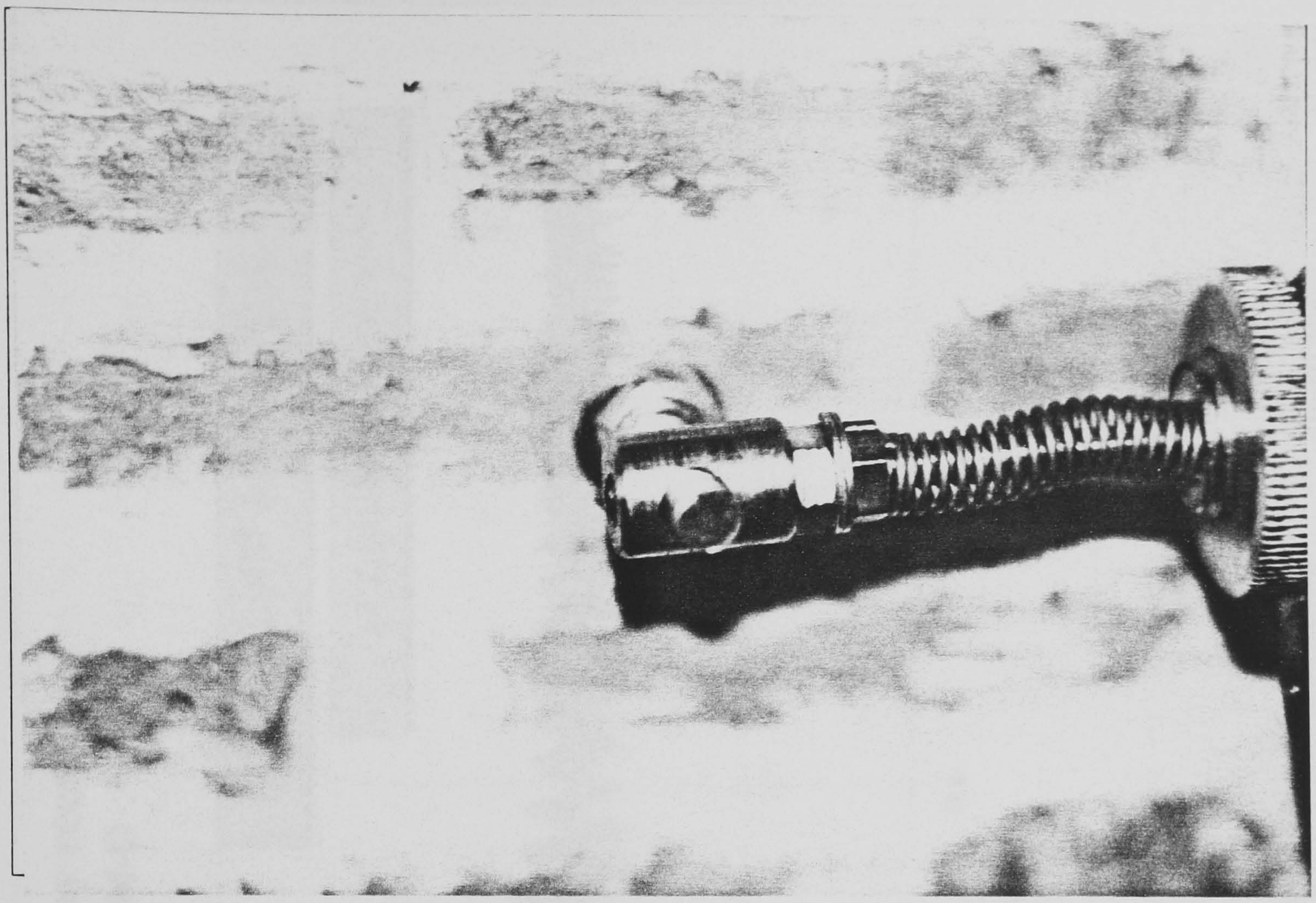

Photo 5.7 Close-up detail of LVDT set-up

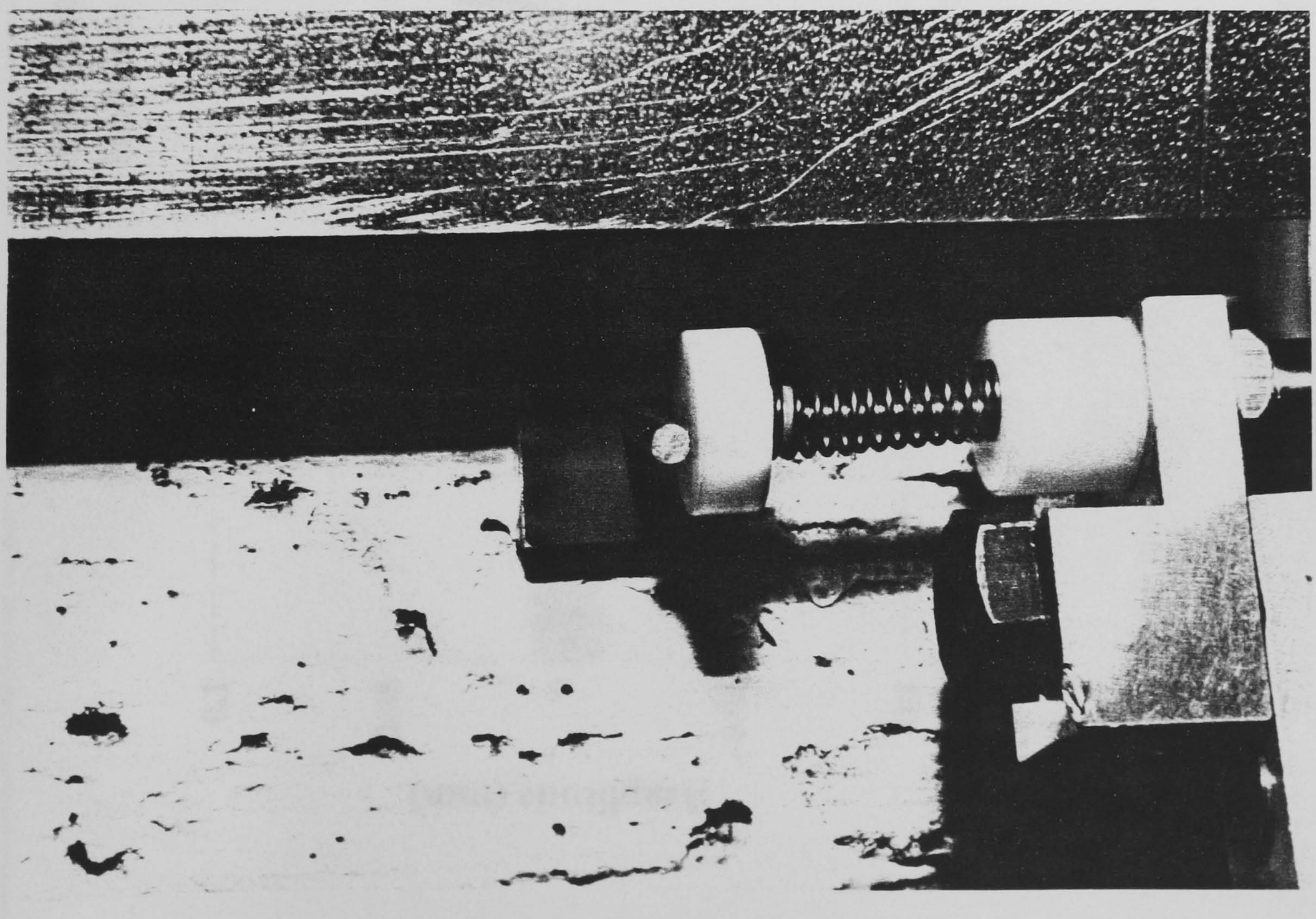

Photo 5.8 Close-up of alternative LVDT set-up with Teflon fixings

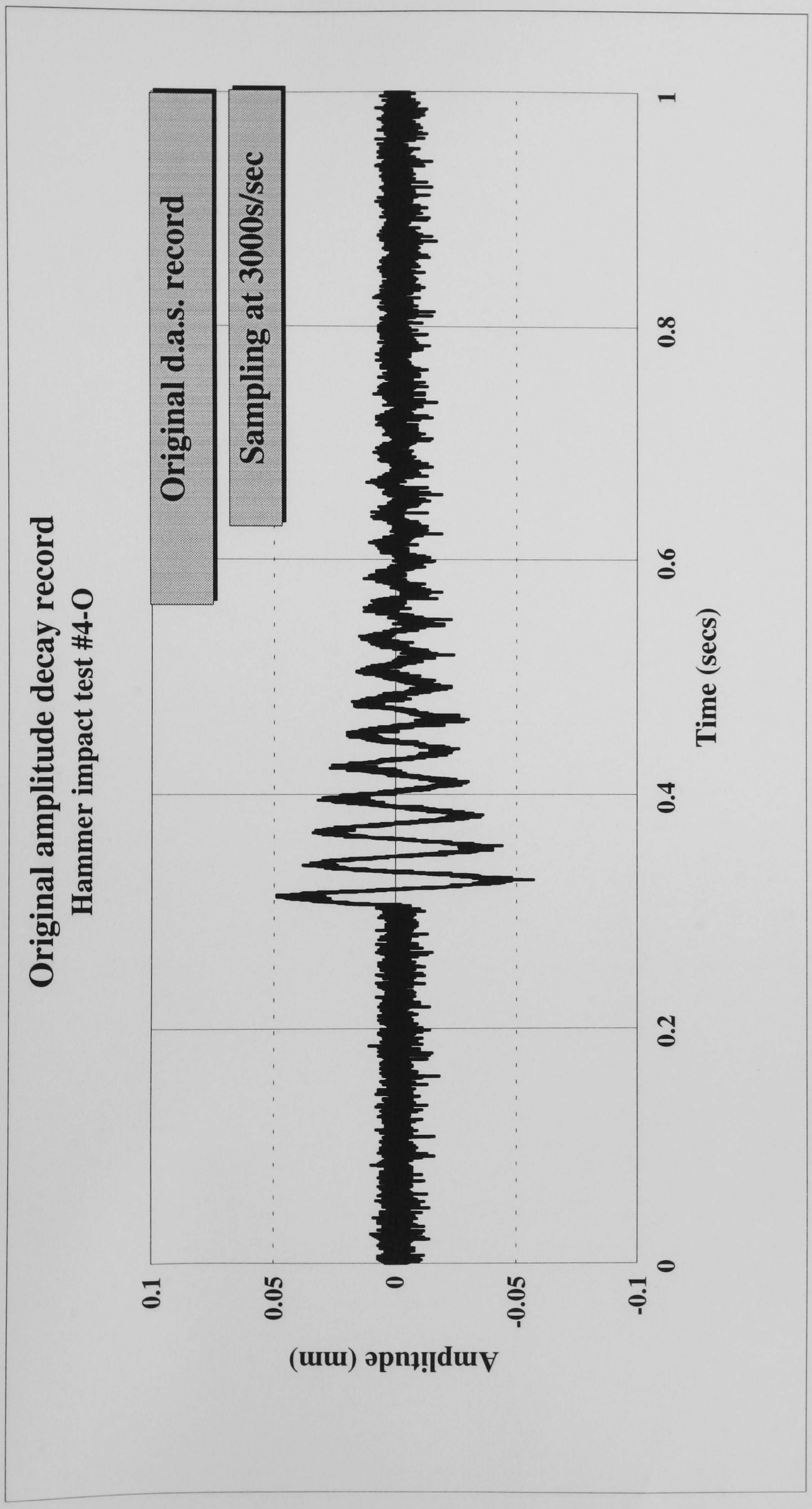

Figure 5.11 Noise polluted free vibration amplitude decay record

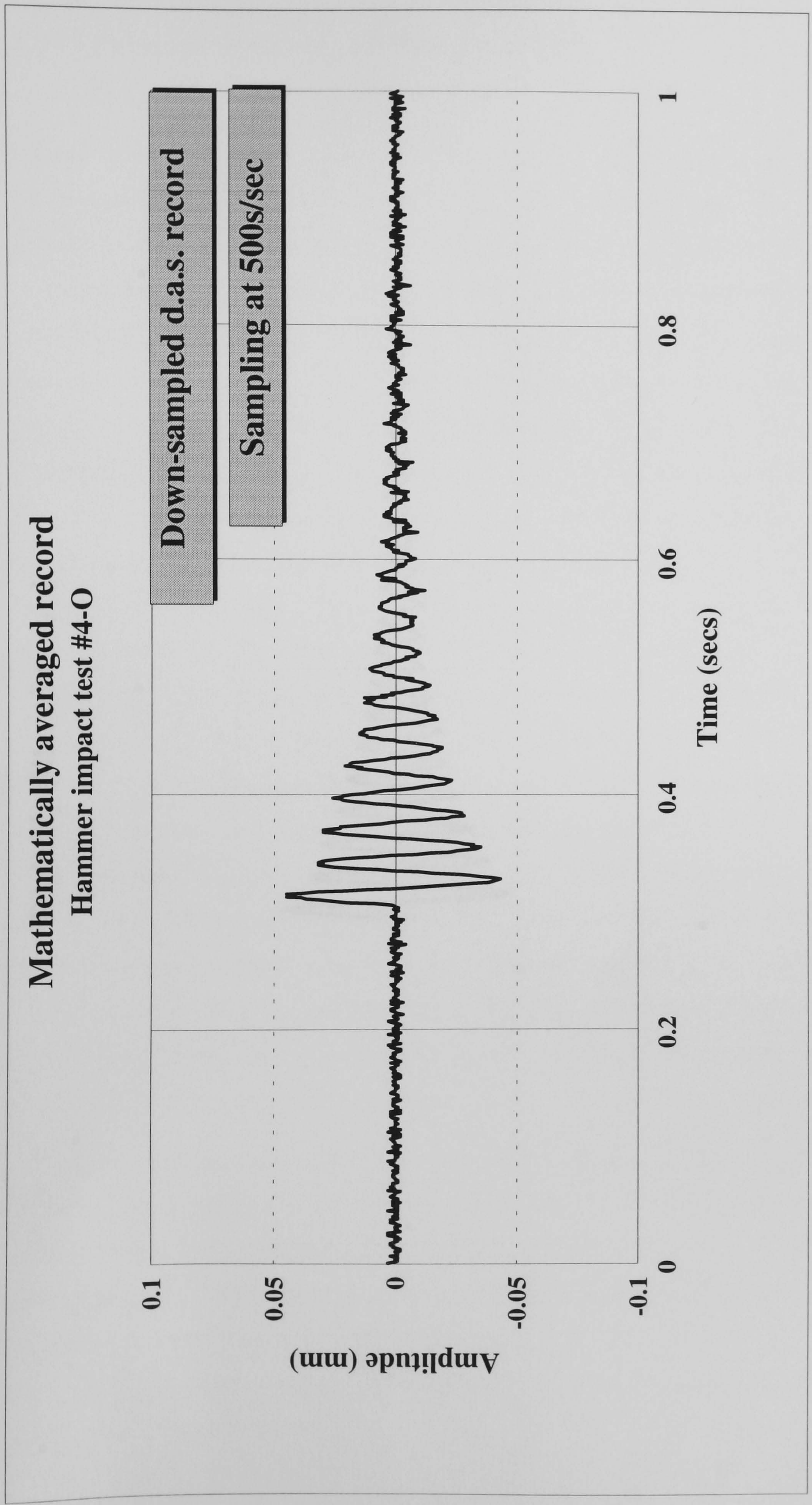

Figure 5.12 Smoothed record (1:6 block average)

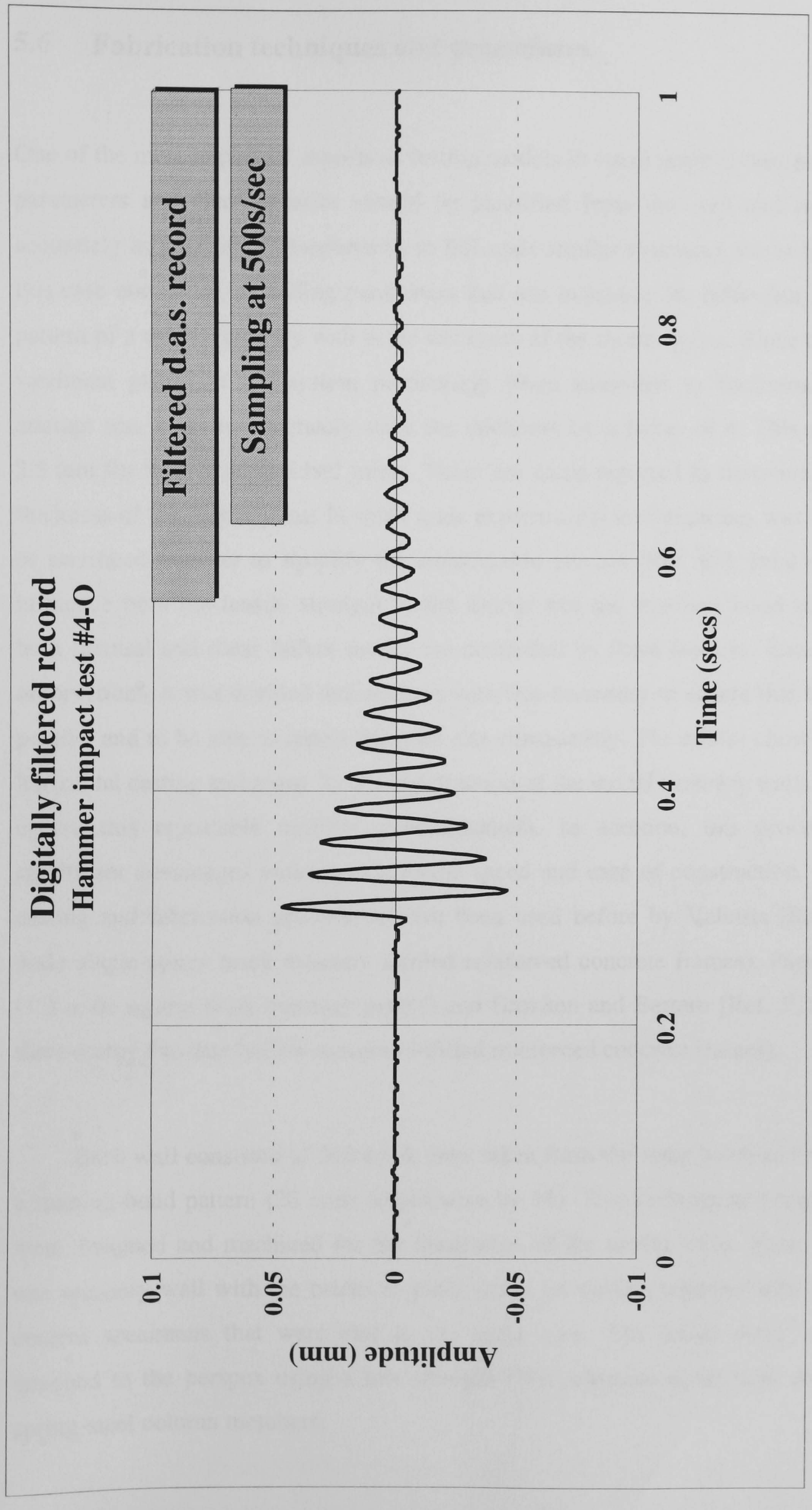

Figure 5.13 Digitally filtered record

5.6 Fabrication techniques and procedures.

One of the most important aspects of testing models in small scale is that the important parameters and characteristics should be identified from the start and modelled as accurately as possible if comparisons to full scale similar structures are to be made. In this case one of the modelling parameters that can influence the behaviour and failure pattern of a model masonry wall is the thickness of the mortar joints. Since these act as weakness planes in the system particularly when subjected to horizontal loads an attempt was made to accurately scale the thickness by a factor of 4. This amounts to 2.5 mm for both head and bed joints. There are cases reported in literature where the thickness of the mortar joints in small scale experimental investigations was overlooked or sacrificed in order to simplify the construction process [Ref. 62]. Joint dimensions influence both the tensile strength of the mortar and the interface bond strength and both flexural and shear failure modes are controlled by these features. Based on these observations, it was decided that extreme care was necessary to ensure that bricks were parallel and to be able to repeat the joint size consistently. The author chose to adopt a horizontal casting technique for the construction of the model masonry walls in order to ensure this repeatable uniform joint thickness. In addition, this procedure gave significant advantages with regards to the speed and ease of construction. Horizontal casting and fabrication procedures have been used before by Valiasis [Ref. 35] (1:3 scale single-storey brick masonry infilled reinforced concrete frames), Page [Ref. 58] (1:2 scale square brick masonry panels) and Brokken and Bertero [Ref. 57] (1:3 scale three-storey two-bay hollow masonry infilled reinforced concrete frames).

Each wall consisted of 392 brick units taken from the same batch and arranged in a running-bond pattern (28 units length-wise by 14). Two rectangular perspex casings were designed and machined for the fabrication of the model walls. Photo 5.9 shows one masonry wall with the bricks in place ready for casting together with samples of control specimens that were cast at the same time. The bricks were individually attached to the perspex using a low strength PVA adhesive along with the two side spring-steel column members.

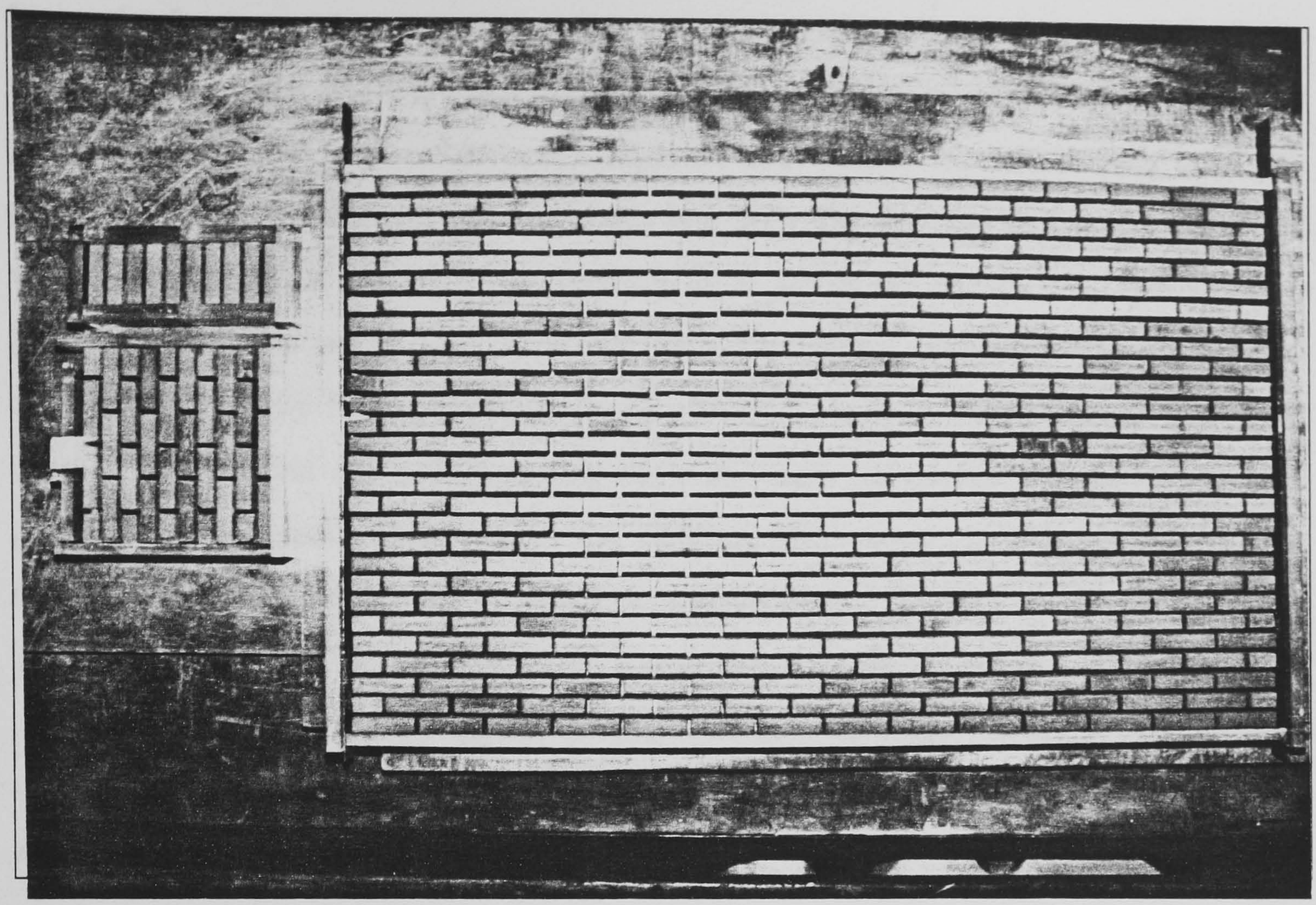

Photo 5.9 Brick wall and control specimens glued on Perspex casing

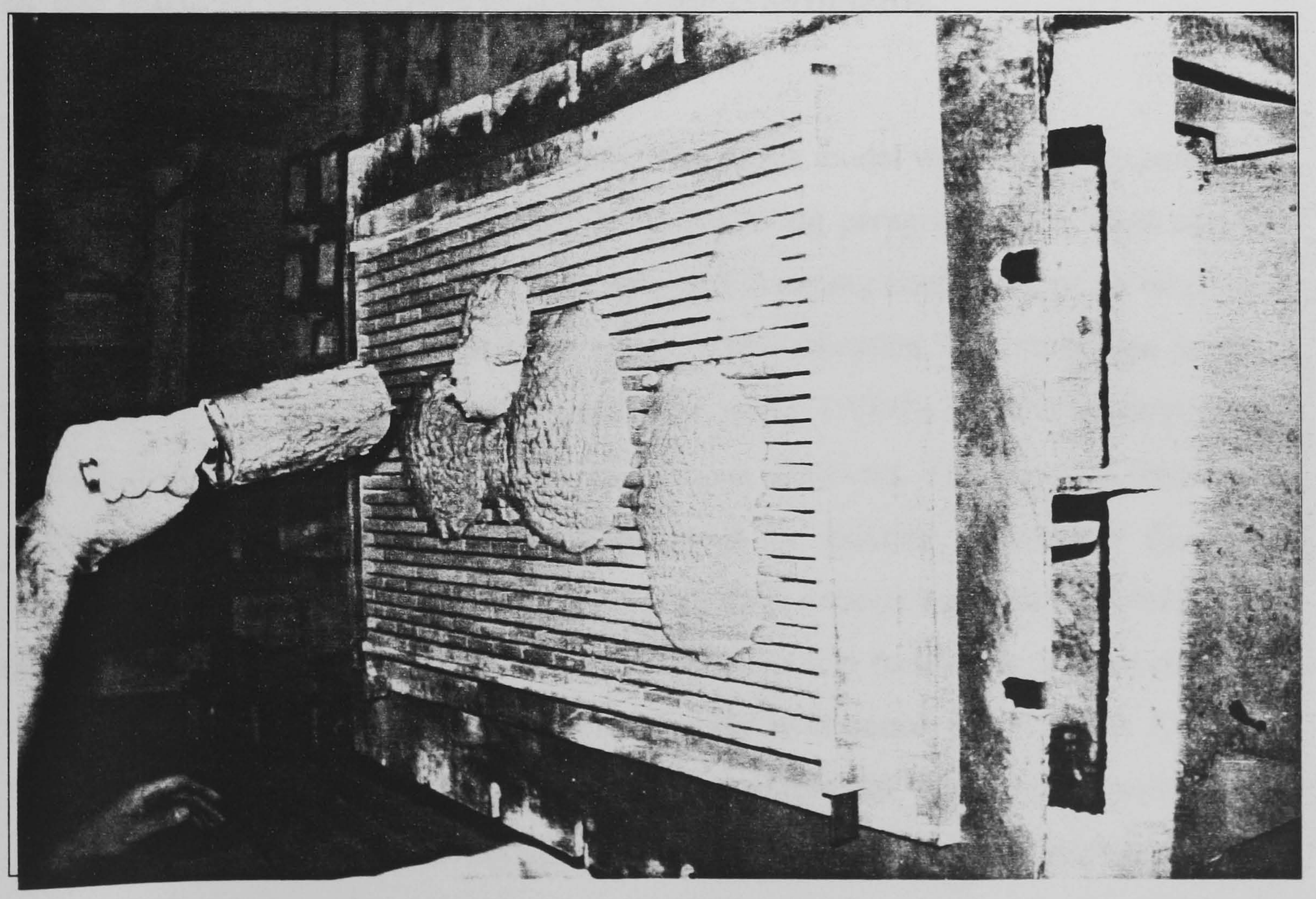

Photo 5.10 Mortar joint casting on vibrating table

Since the base was transparent, a grid was drawn on a sheet of paper and placed underneath, in order to ensure that the gaps left between the units for casting the mortar joints, were as close as possible to the target 2.5 mm width. Once a complete wall was prepared it was left undisturbed for about one hour for the glue to harden. Later the whole assembly was placed on a vibrating table where the mortar was cast into the joints as shown in photo 5.10. Together with the control specimens the walls were covered with tightly fitted polythene sheets and left to cure in a temperature controlled room at 20^0 C. One day before testing the walls were uncovered, separated from the perspex backing and positioned on the shaking table using rapid-hardening cement mortar with approximately the same strength as the mortar used for casting the masonry joints. At the same time, the lead mass was attached to the top beam together with the prestressing force that was applied through the four springs. Finally a thin layer of white emulsion was applied to the face of the walls to ease the identification, marking and recording of the cracking patterns.

5.7 Theoretical and experimental procedures for the determination of the natural frequencies and damping coefficients.

For the determination of the dynamic properties of the model walls simple experimental methods were used and are described in the following paragraphs. The most accurate method of determining the natural frequency and damping coefficient of an intact wall is by using the frequency-response to small forced vibration. The technique involves measurement of the displacement amplitude using LVDTs or accelerometers and relating it to the driving frequency of the applied vibrations. The resonant frequencies and the damping coefficients can be obtained by exciting a structure through a frequency range extending both below and above the expected natural frequencies. The damping coefficients can be determined by the half-power bandwidth method observing the attenuation changes shown by the experimentally obtained data over the frequency range. In general all the methods currently available for the determination of the dynamic properties of a structural system have limitations and some degree of error is inherent. The choice of a particular experimental procedure is usually dictated by the

available technical resources. In this study the resonant frequency for the models was obtained by striking the end of the top steel beam with a plastic hammer and recording the resulting decaying displacement amplitude of the panel at the opposite end. Readings collected by the data acquisition system were down-sampled and digitally filtered (section 5.5). The filtered data was imported in a spreadsheet, where by using special macro-language routines the natural frequency values were calculated for each case. Similarly equivalent viscous damping ratios were obtained by using the logarithmic decrement method for the first 3 consecutive cycles of the free vibration decay curves.

Natural frequencies were calculated before each test using equations 5.2 to 5.4 [Ref. 78]. For a cantilever wall modelled as a solid cantilever beam and subjected to a horizontal load V acting at the top, the deflection due to bending deformations (first term in eq. 5.1) and shear deformations (second term) is:

$$\Delta_c = \frac{Vh^3}{3EI} + \frac{aVh}{GA} \tag{5.1}$$

where h is the clear height of the wall (445 mm)

E is the modulus of elasticity

$I = L^3t/12$, is the second moment of area for an equivalent cross section

G is the shear modulus (taken as 0.25 E, section 4.5)

$A = Lt$, is the cross-sectional area in the horizontal plane

t is the wall thickness (25.6 mm)

L is the wall length (753 mm)

a is the shape coefficient equal to 1.2 for rectangular sections.

For a wall fixed at both ends equation 5.1 becomes:

$$\Delta_f = \frac{Vh^3}{\mathbf{12}EI} + \frac{aVh}{GA} = \frac{V}{Et}\left[\frac{h^3}{L^3} + 4.8\frac{h}{L}\right] \tag{5.2}$$

(Equations 5.1 and 5.2 demonstrate the contribution of the aspect ratio, h^3/L^3 for the first term and h/L for the second, to the total deflection of the wall).

The initial lateral stiffness (K) for an uncracked panel can then be calculated using the following equation:

$$K = \frac{V}{\Delta} \quad \text{(N/m)} \tag{5.3}$$

The stiffness of the spring steel columns should be added to the value obtained from equation 5.3, but since it is only 0.0006 of the stiffness of the masonry walls it can be omitted from the calculations. The fundamental natural frequency is then obtained from equation 5.4:

$$f = \frac{\sqrt{\frac{K}{M}}}{2\pi} \quad \text{(Hz)} \tag{5.4}$$

where M is the effective lumped mass taken as $M = M_{top} + 0.3\ M_{wall}$

M_{top} = 200 kg

M_{wall} = 18 kg or 44 kg depending on the brick type.

In addition analytical calculations based on the finite element method were performed using procedures described further in chapter 6. Bricks and mortar joints were modelled using two-dimensional, 8-noded, isotropic elements with individually prescribed material properties, while the bounding frame was modelled using 2-noded beam elements. Consistent mass matrices were prescribed in the analyses which were expected to provide an upper bound solution for the natural frequencies. For comparison purposes lower bound results were anticipated from the calculations described above with the effective mass lumped at the top of the wall.

5.8 Shaking table test results.

In total eight model walls were fabricated but only six of these were tested since handling operations involved in the transfer of the specimens from the curing room to the shaking table resulted in unacceptable damage to two. The six walls that were

successfully tested included four specimens with deliberately varied strength of the constituent materials. The fifth wall was built with the second brick with substantially increased mass (44 kg instead of 18 kg). The final test was carried out on a wall similar to the first four but was externally reinforced with wire mesh. The mesh was fixed and tied to both faces of the wall using through ties, consisting of studding (3 mm), nuts and washers. The first two walls were tested 28 days after casting using mortar of a 1:2:9 cement:lime:sand mortar consistency. The remaining four walls used a 1:2:6 cement:lime:sand mix as it was clear that improved workability was required during fabrication. To maintain similitude in the strength requirements these walls were therefore tested between 7 and 14 days after casting, when the mortar had approximately the same compressive and tensile strength as the 1:2:9 mix. Tests commenced by first subjecting each wall to free vibration excitations followed by sinusoidally-varying ground motions produced by the shaking table. Each test sequence involved an initial series of small amplitude motions to detect the onset and location of cracks as these appeared. Since crack development and propagation were essential for the description of the hysteretic behaviour and energy dissipation characteristics of the model infill shear walls, these were photographically recorded using an SLR camera operated in high speed mode (5 frames/second). For the last three tests video recording equipment was also employed in an attempt to film and record the final collapse sequence.

In section 5.8 each of the shaking table tests for the six model infill shear walls is presented in order of test date. For each wall, natural frequency and equivalent viscous damping coefficients are included together with the measured free vibration amplitude decay waveforms. Visual records of the cracking patterns were selected from a large number of still photographs taken during and after each testing stage and clearly indicate the position, sequence and propagation of cracking. Finally complete dynamic displacement histories and hysteresis curves (*loops*) showing the relative displacement at the top of a wall in relation to the applied ground motions (cyclic lateral load acting at the top beam) are also presented. Before each test is described individually, the results for the six model walls are summarised for reference purposes in table 5.1. These include the static test results from the control specimens using procedures described in chapter 4 and the dynamic properties measured during free vibration tests.

Measured properties	Wall-O	Wall-B	Wall-D	Wall-H	Wall-R	Wall-M
Brick compressive strength[1]	10.1	8.42	7.21	11.21	4.92	6.49
Brick tensile strength[2]	0.986	0.75	0.713	0.67	0.39	0.459
Mortar compressive str.	3.93	3.248	2.288	2.171	3.286	1.123
Mortar tensile strength	0.34	0.318	0.189	0.187	0.28	0.092
Masonry compressive str.[3]	5.28	5.61	5.13	7.12	3.91	4.01
Masonry shear strength[4]	0.516	0.482	0.425	0.647	0.28	0.328
Interface bond strength	0.787	0.904	0.41	0.43	0.429	0.361
I.R. suction[5] **(kg/m²/min)**	0.225	0.17	0.252	0.297	0.456	0.308
Mortar flow[6]	248 %	245 %	258 %	250 %	255 %	258 %
Prestressing spring force[7]	10 kN	12 kN	9 kN	8 kN	8 kN	7 kN
Wall self-weight	18 kg	18 kg	18 kg	44 kg	18 kg	18 kg
Ground accel. at first crack	0.923g	0.786g	0.879g	1.03g	0.884g	1.372g
Max. acceleration	1.15g	1.09g	1.61g	1.409g	1.56g	>2.5g
Ground accel. at failure[8]	0.963g	-	1.593g	1.293g	1.589g	1.976g
Max. base shear force[9]	2.35kN	2.22kN	3.28kN	3.05kN	3.18kN	>5kN
Natural frequency (initial)	41.7Hz	44.5Hz	39.1Hz	42.5Hz	38.5Hz	40.5Hz
Damping[10] **(initial)**	4.9%	6.4%	4.4%	4.1%	4.8%	3%
Natural frequency at failure	31.33Hz	31.25Hz	18.5Hz	19.9Hz	19.03Hz	14.3Hz
Damping at failure	8.5%	11.6%	9.7%	5.6%	11.2%	12.5%

(All strength values expressed in **MPa**)

(Tests on control specimens conducted same or next day after shake table tests)

[1] Based on 50 mm cubes.

[2] Based on 102 x 35 mm cylinders.

[3] Based on 50.8 x 73.5 x 25.6 mm 5-course stack-bond prisms.

[4] In-plane diagonal tensile strength for 93 x 93 x 25.6 mm wallettes.

[5] BS 3921:1985, Appendix H.

[6] BS 4551:1980, Section 3 and Appendix A.

[7] Spring force (not including 2 kN from self-weight of the added inertia mass).

[8] Failure is defined at the stage where extensive damage was observed in the walls.

[9] Base shear is the product of the added mass times the ground acceleration.

[10] Equivalent viscous damping factors (%) obtained from free vibration decay records.

Table 5.1 Summary of shake table tests (including constituent material properties)

In the following sections a number of terms are introduced to simplify the classification of the large quantity of data acquired during the shaking table tests. A ***stage*** represents a testing cycle where one of the controlling parameters (frequency or amplitude) of the applied sinusoidal motions was kept constant while the other was varied. A stage consists of a series of ***runs***, each one representing a 5 second shake table motion (ramp functions of 1 second rise time). Therefore for each testing stage with constant frequency/amplitude of vibration a number of runs was performed, each one for a different amplitude/frequency respectively. Each stage was assigned an alphanumeric label to identify the wall and corresponding stage and run number (e.g. table 5.2). In the dynamic response figures (displacement vs. time), **b** and **w** represent the bottom and top (mounted on the wall), LVDTs respectively. For reasons of clarity only the first 0.6 seconds of each displacement waveform are presented, with all runs in any one stage combined together to demonstrate the influence of the applied ground motion on the dynamic response (displacement amplitude) of the model walls. ***Relative displacement*** is obtained by the difference between the top and bottom LVDT readings, and represents the displacement of the wall at the beam level relative to the base. The active mass is multiplied by the ground acceleration to obtain the horizontal ***load*** values. This is plotted against relative displacement to obtain the hysteretic behaviour of the system as progressive cracking developed. The photographs show the cracking patterns with the order in which these appeared shown by consecutive numbers. The pattern numbers are also included in the tabulated summary for each test sequence, to indicate the stage and run and imposed ground acceleration relative to the corresponding crack situation.

Although the target was to keep the driving frequency constant for each stage and amplify the ground acceleration by increasing the table platform amplitude, this was not always possible due to mechanical problems associated with the motor and driving mechanisms. However, a wide range of different frequency and acceleration cycles were applied, to both the elastic and post-cracking phases for each wall, to assess the dynamic behaviour and energy absorption characteristics in relation to the different parameters as presented in table 5.1.

5.8.1 First test : wall-O.

Wall-O was the first test to be carried out on the newly assembled shaking table. It provided information on the basic operational capabilities and the limitations of the system for planning subsequent tests. A large number of runs were performed with very small changes to the frequency and amplitude of vibration. Initially the driving frequency was kept constant while the acceleration was increased. Following the appearance of the first crack, the driving frequency was varied together with the ground acceleration, although this was not always possible as explained in the previous section. In the following pages the developing dynamic behaviour has been laid out in detail in the order shown below.

- ► Free vibration amplitude decay records - hammer tests (figures 5.14 to 5.19).
- ► Displacement records (5.20 to 5.30).
- ► Sample hysteresis curves (5.31, 5.32).
- ► Photographs of the cracking patterns (photo 5.11 to 5.14).
- ► Summary of dynamic response (figure 5.33).

The test procedure for wall-O is summarised in table 5.3, while results for the first natural frequency using the methods described previously are shown below in table 5.2.

Theoretical	**Finite element**	**Hammer test**
61.2 Hz	73.4 Hz	41.67 Hz

Table 5.2 Natural frequency results (initial value) for wall-O

Stage/Run	**Table accel.**	**Driving freq.**	**Damage**	**Natural freq.**	**Damping ratio**	**Rel. displ.**	**Comments**
	g	**Hz**	**Crack #**	**Hz**	**%**	**mm**	
O1/R1	0.04	5.4	-	41.67	4.9	0.034	Constant driv. frequency
O1/R2	0.077	5.4	-	-	-	0.035	
O1/R3	0.137	5.4	-	-	-	0.044	

(Table continued)

O1/R4	0.088	6.1	-	-	-	0.056	Constant driv. frequency
O1/R5	0.145	6.1	-	-	-	0.062	
O1/R6	0.246	6.1	-	-	-	0.11	
O1/R7	0.167	7	-	-	-	0.055	Constant driv. frequency
O1/R8	0.236	7	-	-	-	0.07	
O1/R9	0.385	7	-	-	-	0.151	
O2/R1	0.209	6.8	-	-	-	0.06	Constant driv. frequency
O2/R2	0.83	7.2	-	-	-	0.744	**Tensile cracking near the centre of the panel**
O2/R3	1.141	6.9	**1**	40.45	5.4	1.1	
O3/R1	0.579	5.5	-	-	-	0.215	Varied driv. frequency
O3/R2	1.051	6.9	**2**	-	-	0.929	**Further tensile cracking**
O3/R3	0.401	6.7	-	-	-	0.214	**Column separation**
O3/R4	0.923	7.8	**3**	40	5.7	0.736	
O4/R1	0.424	6.1	-	-	-	0.431	Varied driv. frequency
O4/R2	0.691	6.8	-	-	-	0.616	
O4/R3	0.958	7.6	**4**	35.72	5.4	0.686	**Stepwise diagonal tensile cracking**
O4/R4	0.175	9	-	-	-	0.2	
O5/R1	0.943	6.8	-	-	-	0.4	Varied driv. frequency
O5/R2	0.846	9	-	-	-	0.728	**Further cracking along the main diagonals**
O5/R3	1.084	7.5	**5**	35.7	5.9	0.491	
O6/R1	0.246	6.4	-	-	-	0.255	LVDT failure in O6/R2
O7/R1	0.301	5.6	-	-	-	0.151	Varied driv. frequency
O7/R2	0.161	6.2	-	-	-	0.101	
O7/R3	0.32	6.6	-	-	-	0.244	
O7/R4	0.455	6.8	-	-	-	0.421	
O8/R1	0.65	5.6	-	-	-	0.704	Varied driv. frequency
O8/R2	0.273	6.5	-	-	-	0.204	
O8/R3	0.506	6.8	-	-	-	0.501	
O8/R4	0.661	7.3	-	-	-	0.715	
O9/R1	0.837	7	-	-	-	0.546	Constant driv. frequency
O9/R2	0.732	6.9	-	-	-	0.799	**Extension of crack 5 towards the corners**
O9/R3	0.936	7.1	**6**	31.33	8.5	0.367	

(Crack numbers correspond to the cracking as noted in the photographs)

Table 5.3 Wall-O testing sequence

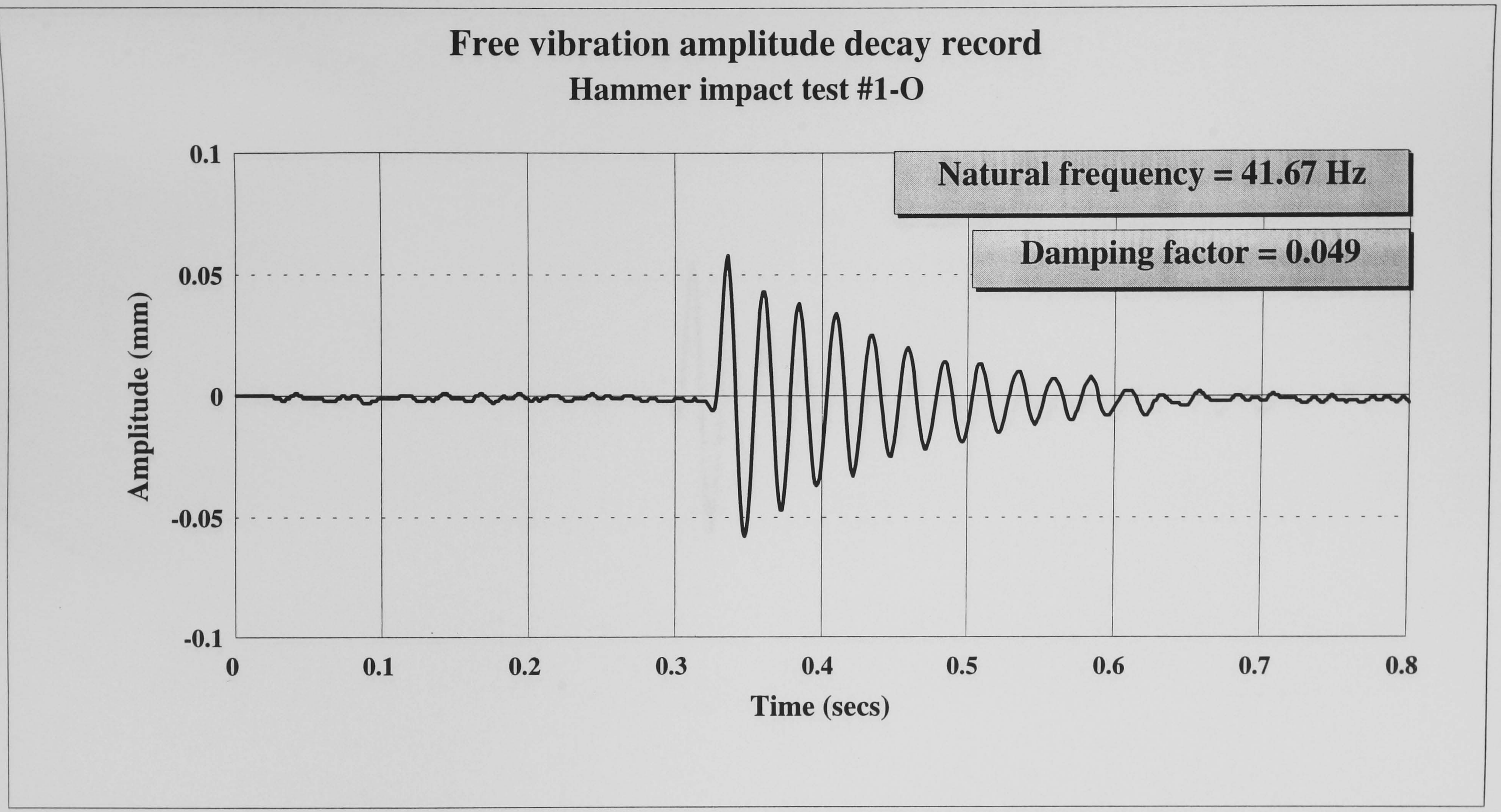

Figure 5.14 Initial free vibration amplitude decay

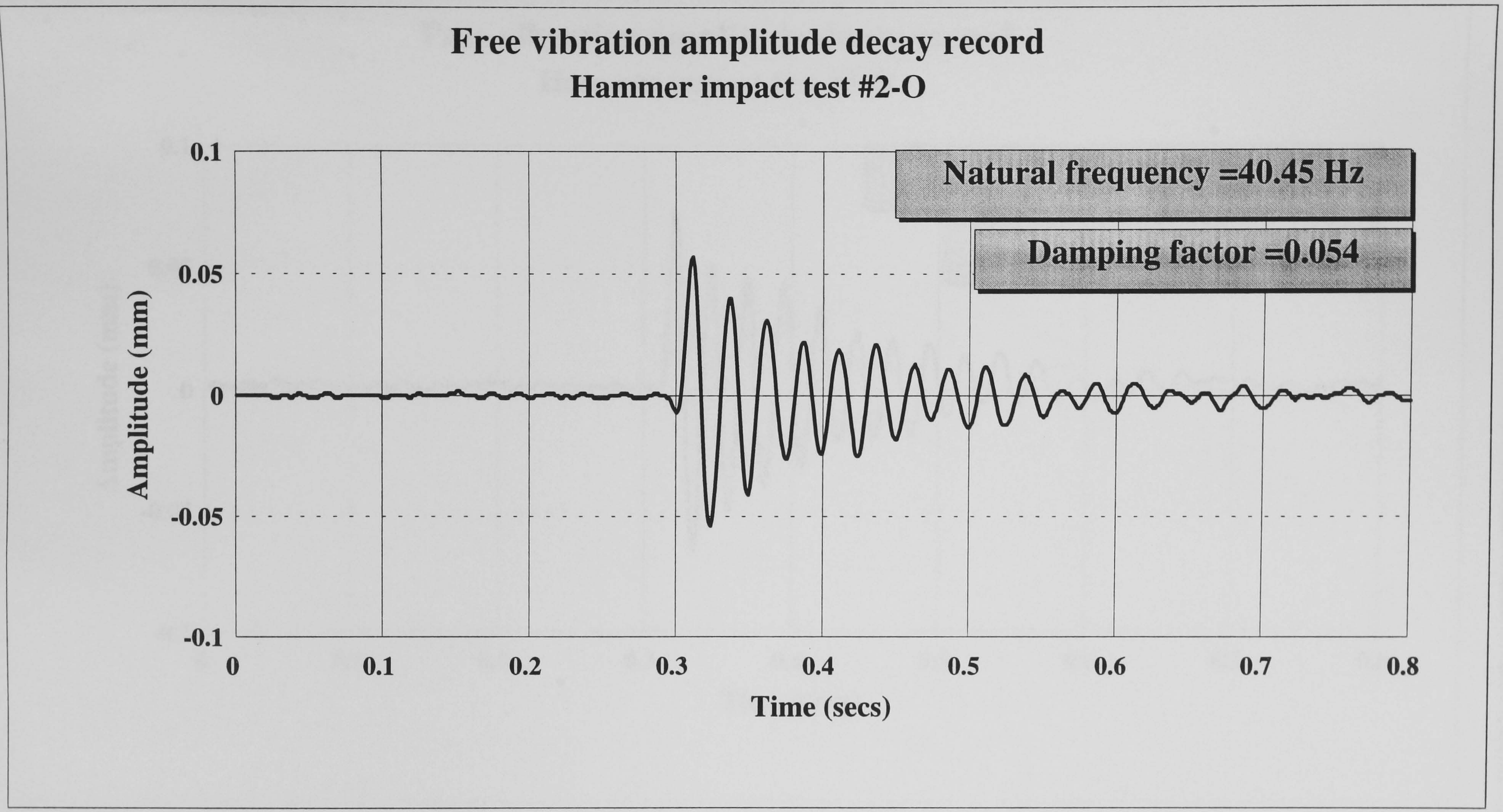

Figure 5.15 Free vibration amplitude decay after crack 1

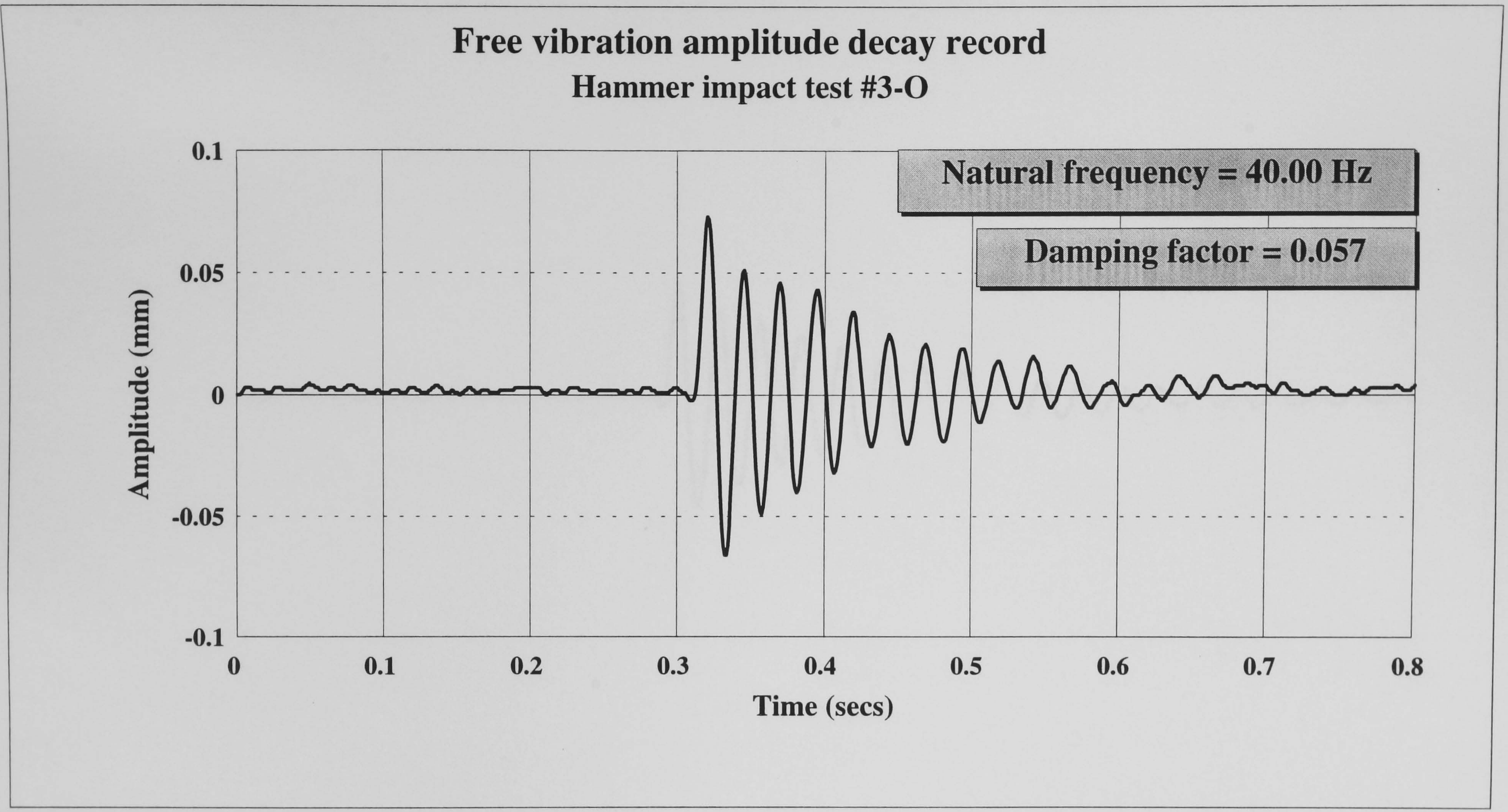

Figure 5.16 Free vibration amplitude decay after crack 2

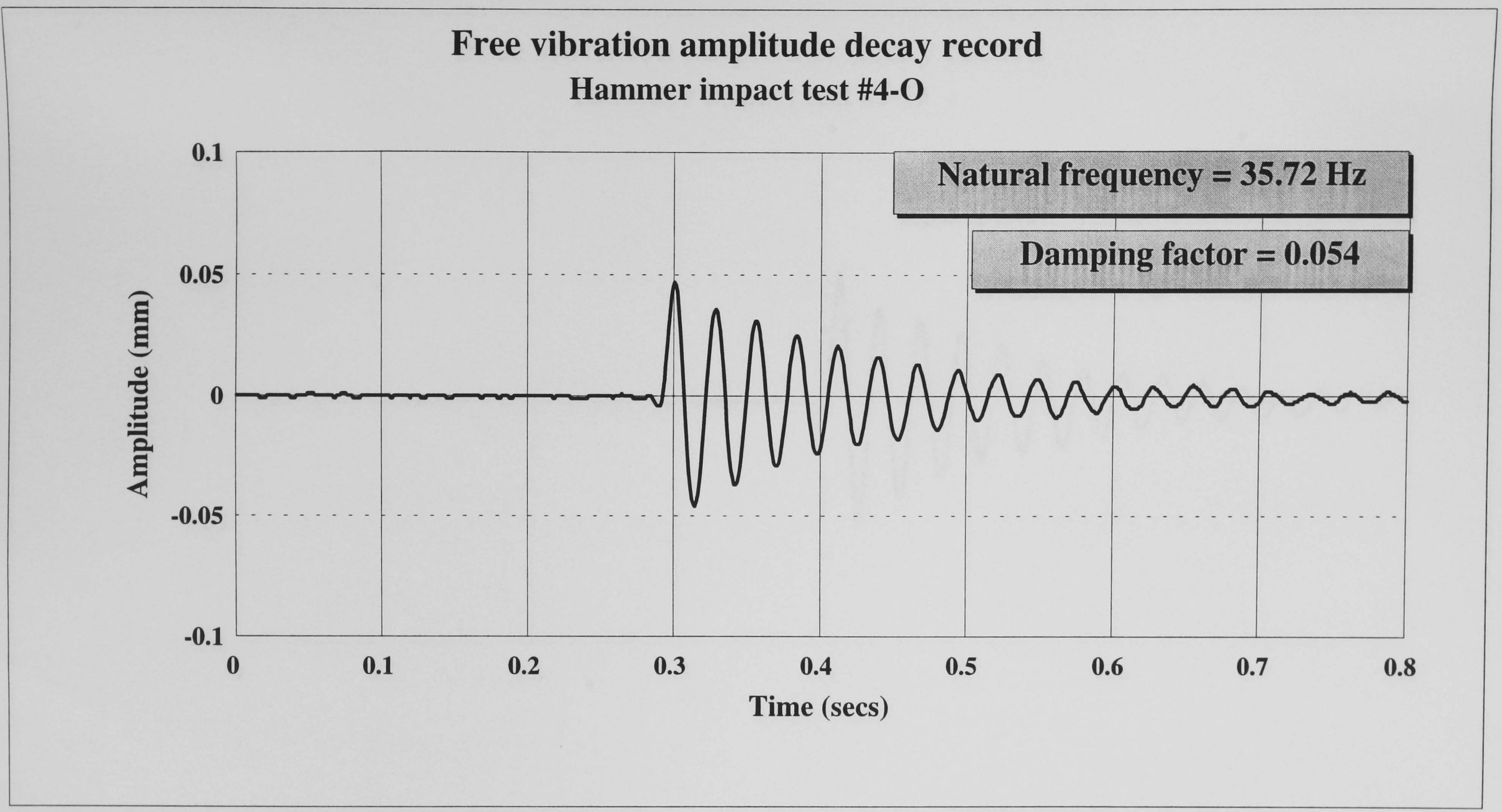

Figure 5.17 Free vibration amplitude decay after crack 3

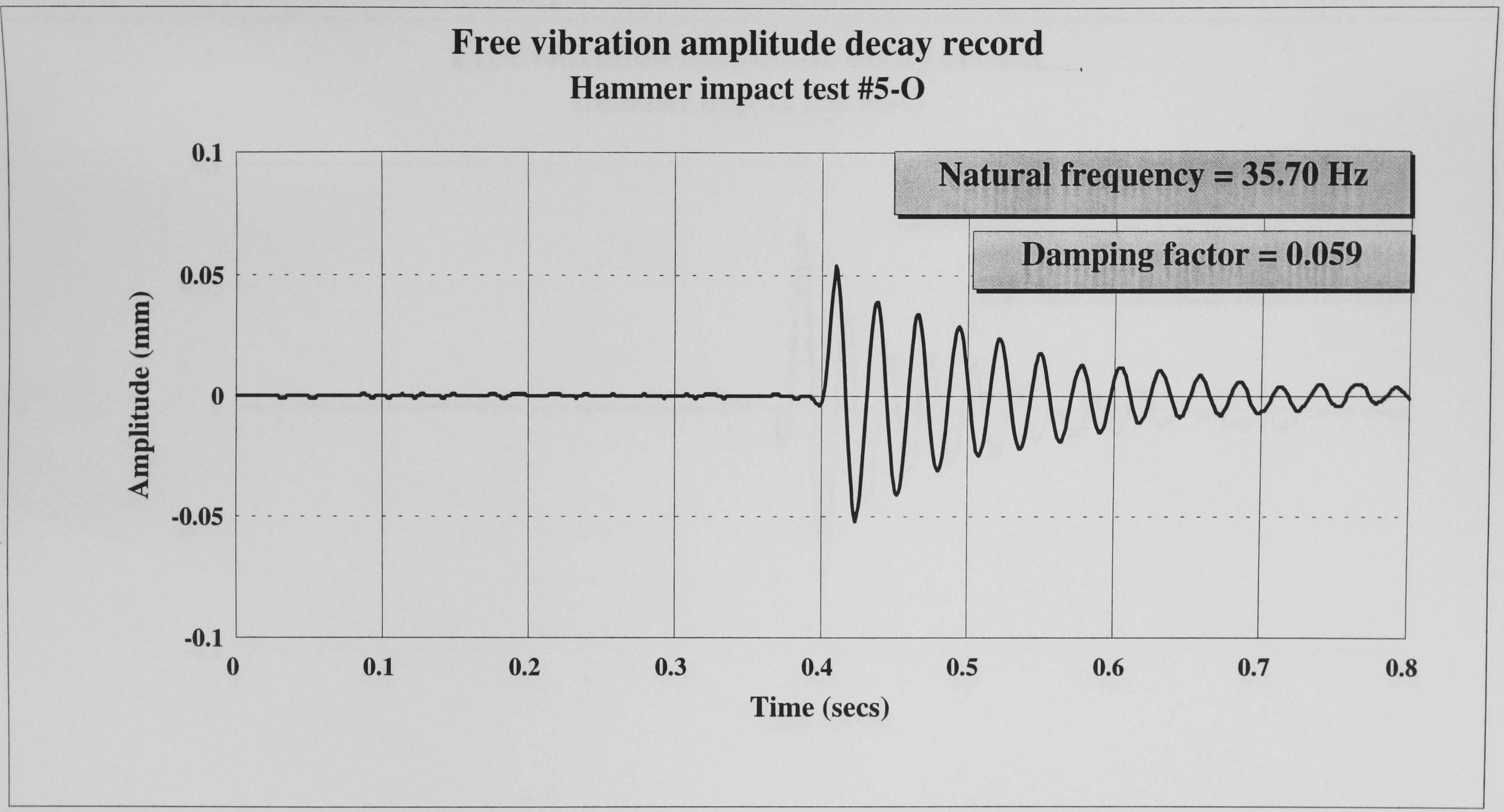

Figure 5.18 Free vibration amplitude decay after crack 4

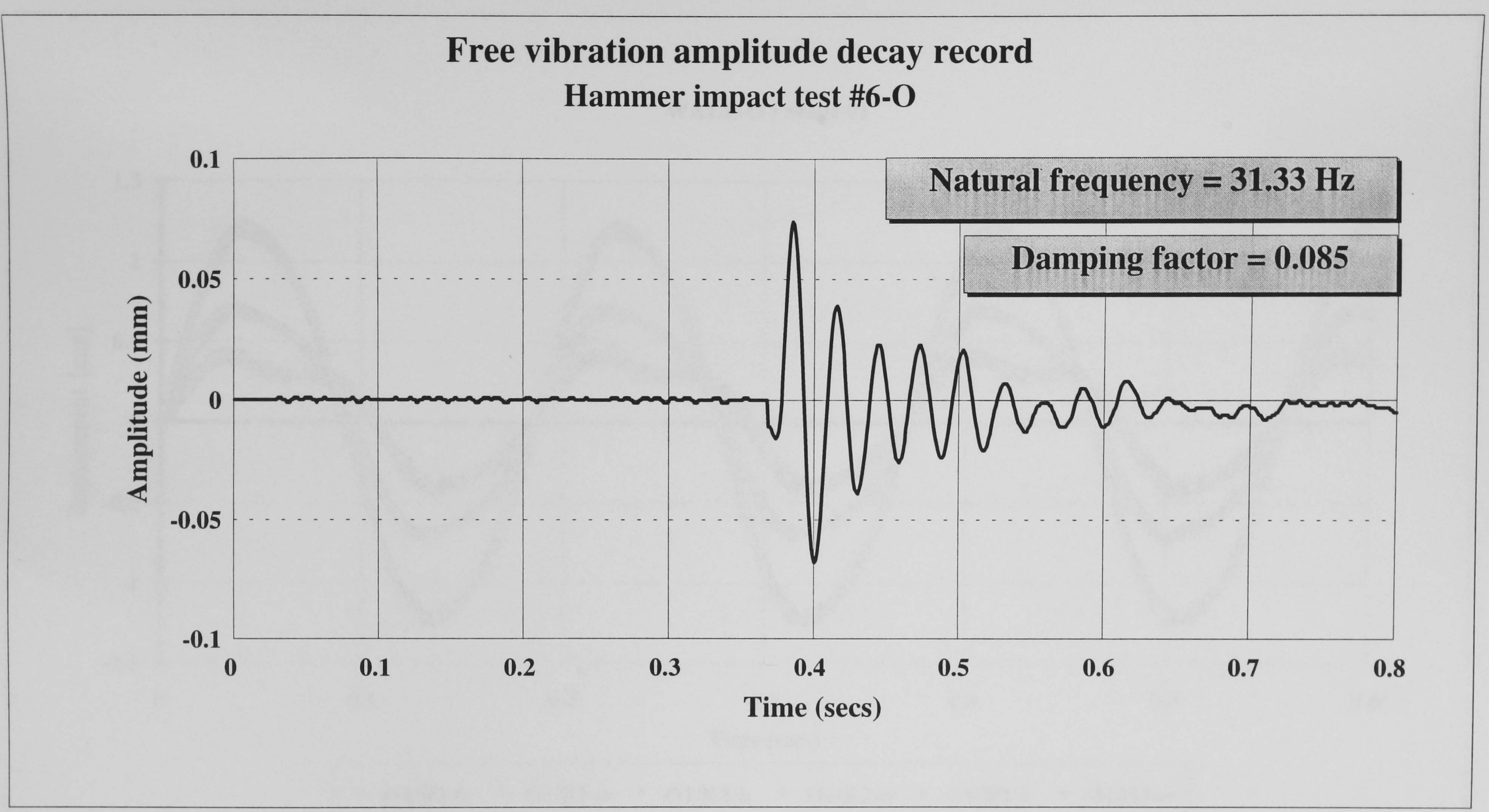

Figure 5.19 Free vibration amplitude decay after crack 5

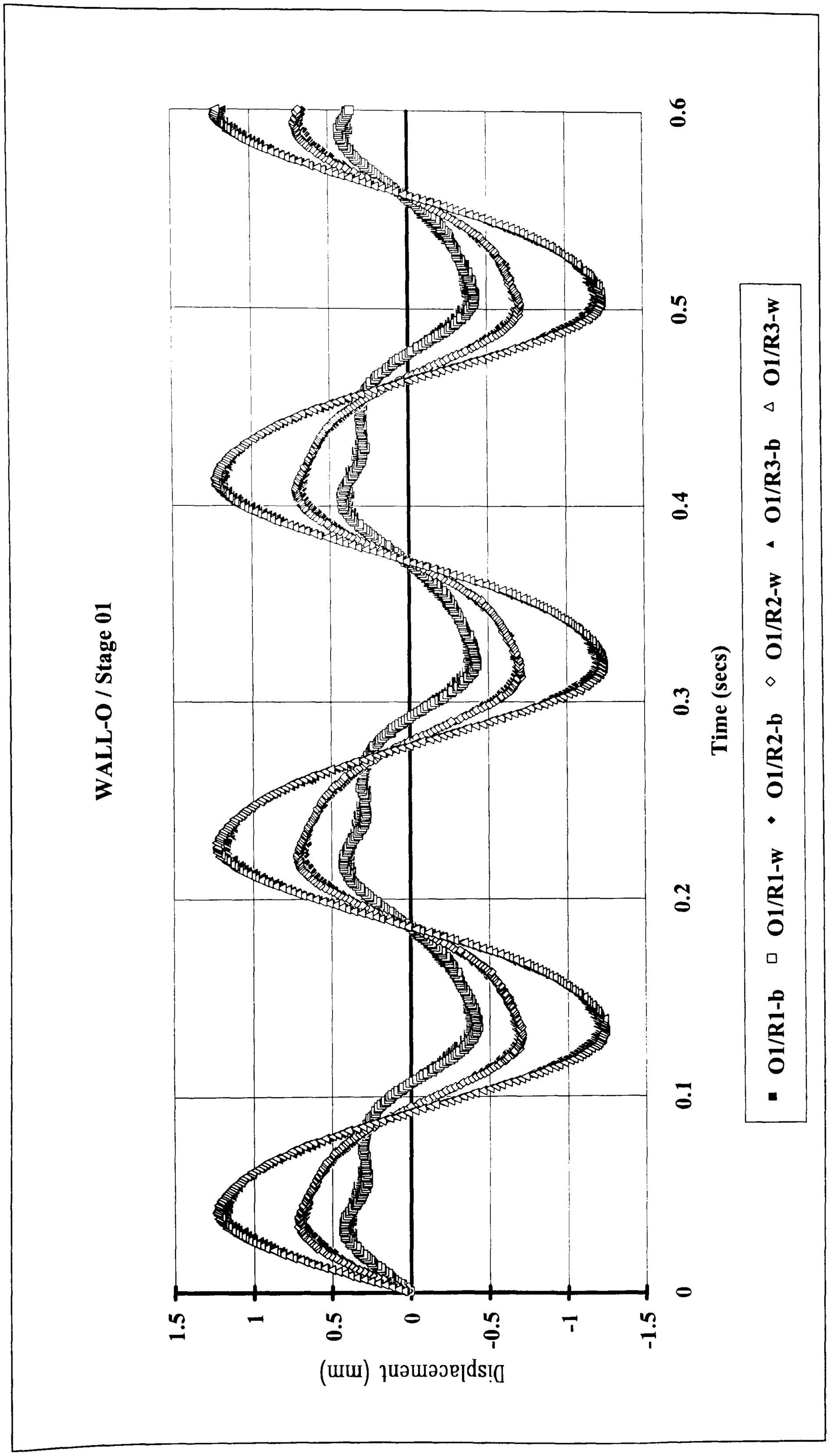

Figure 5.20 Wall-O / Stage O1a

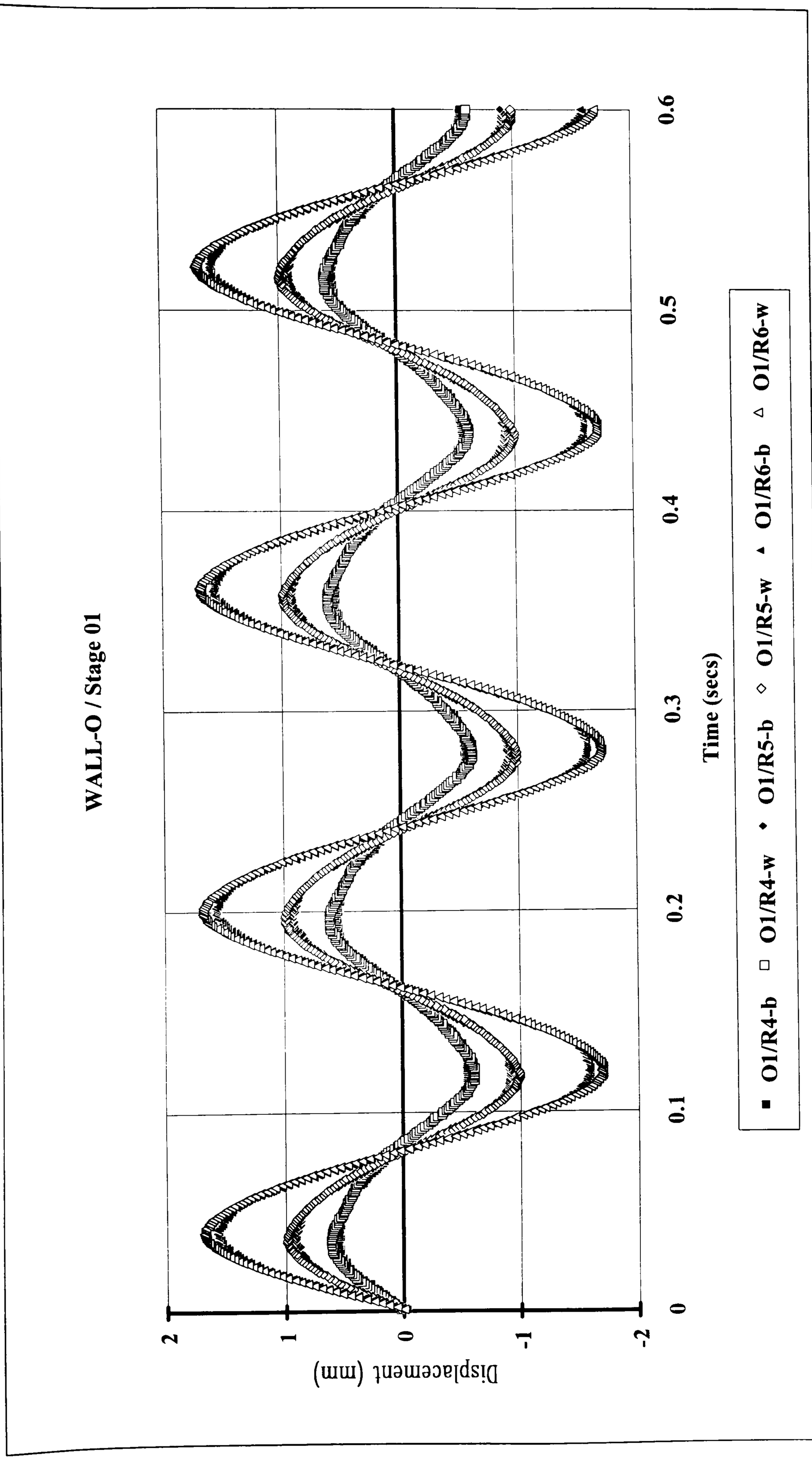

Figure 5.21 Wall-O / Stage O1b

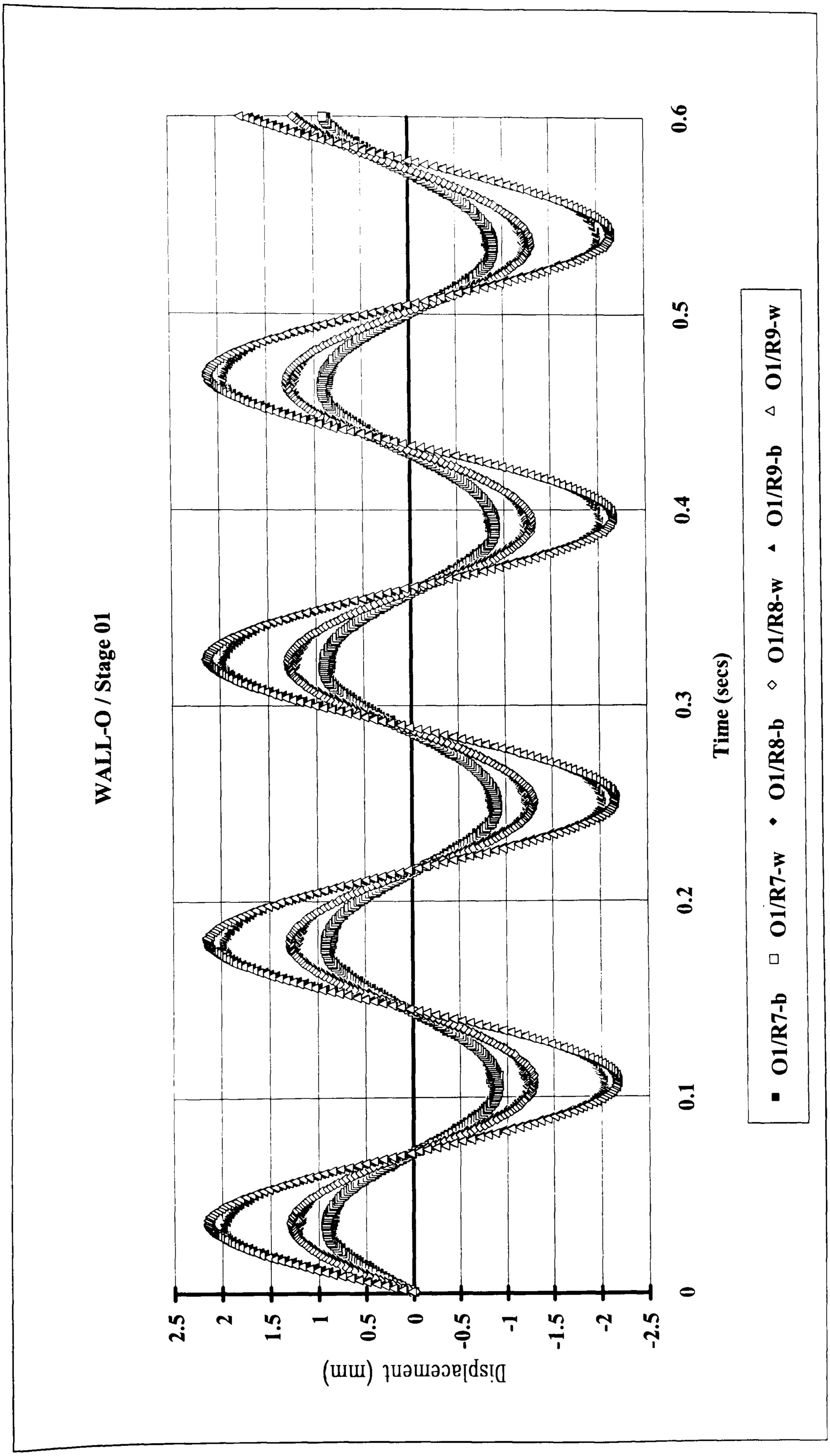

Figure 5.22 Wall-O / Stage O1c

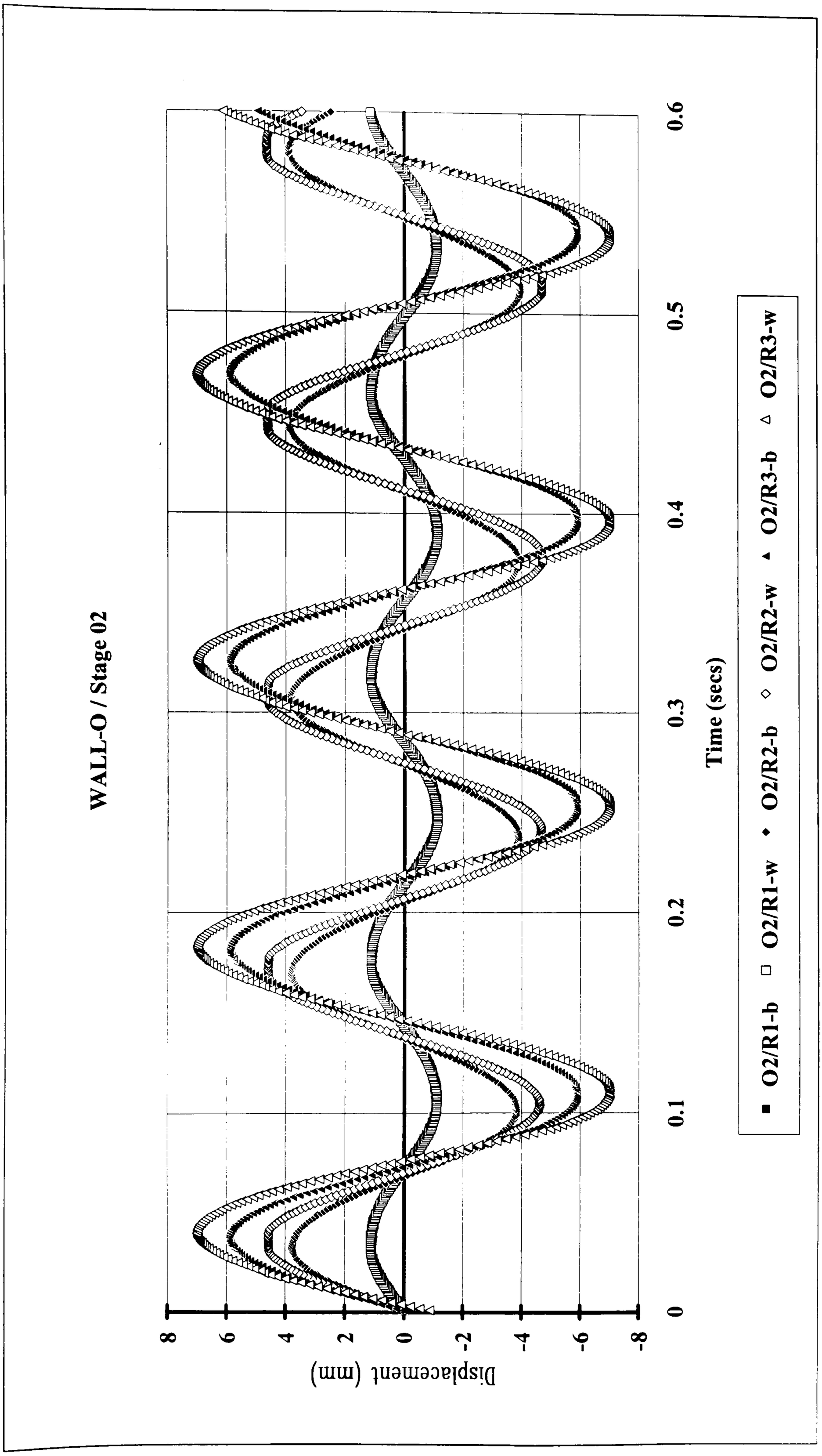

Figure 5.23 Wall-O / Stage O2

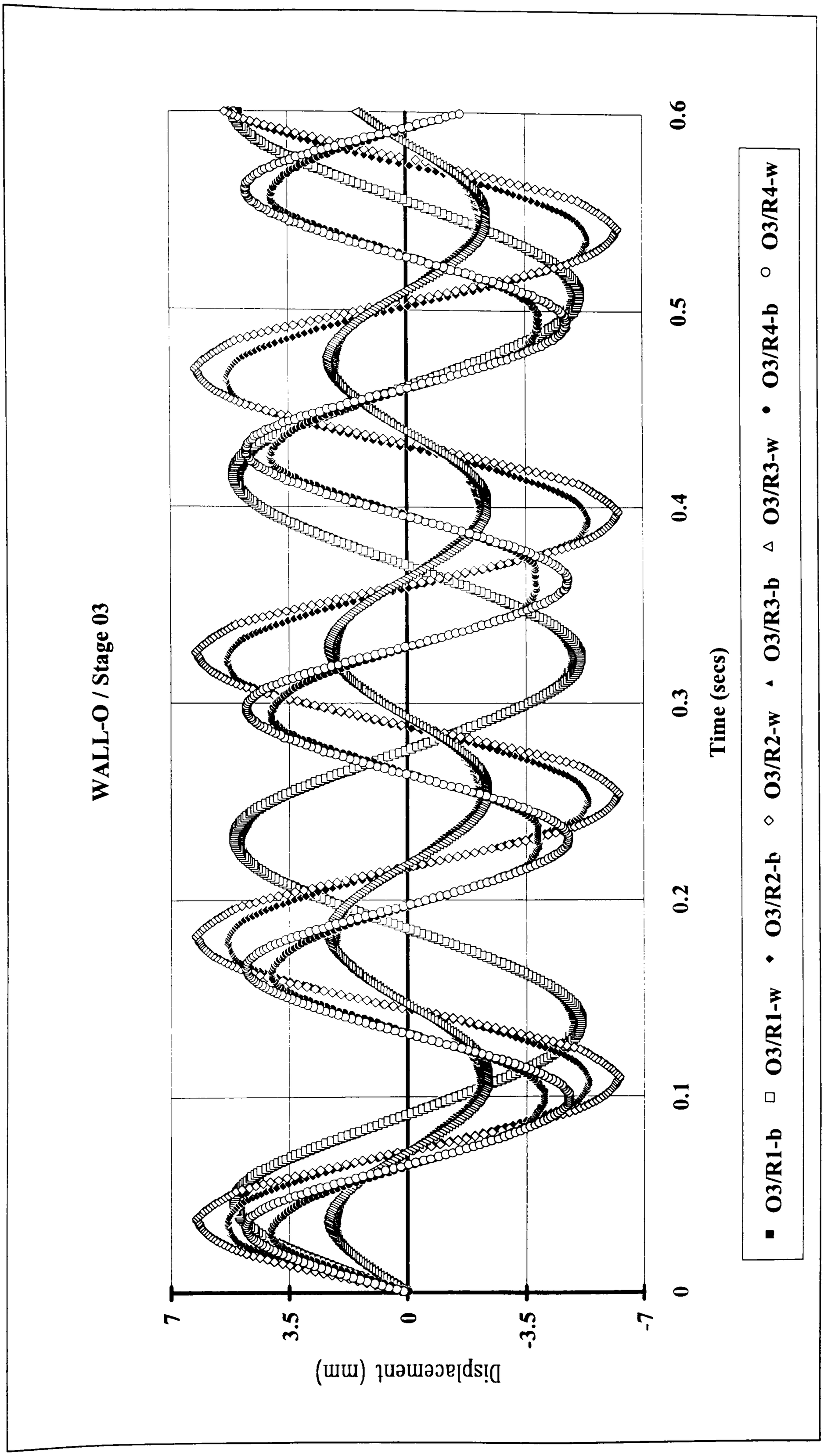

Figure 5.24 Wall-O / Stage O3

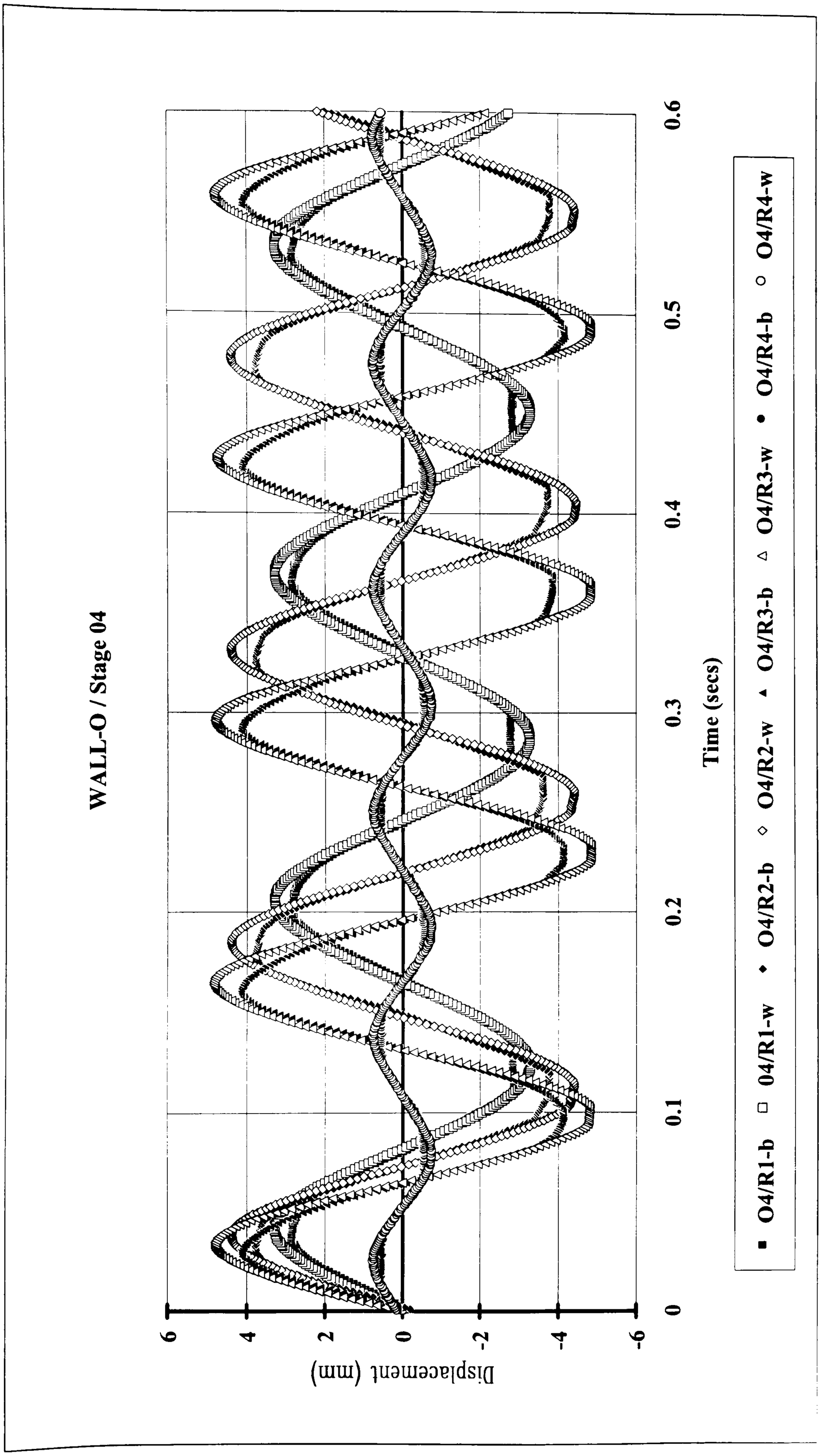

Figure 5.25 Wall-O / Stage O4

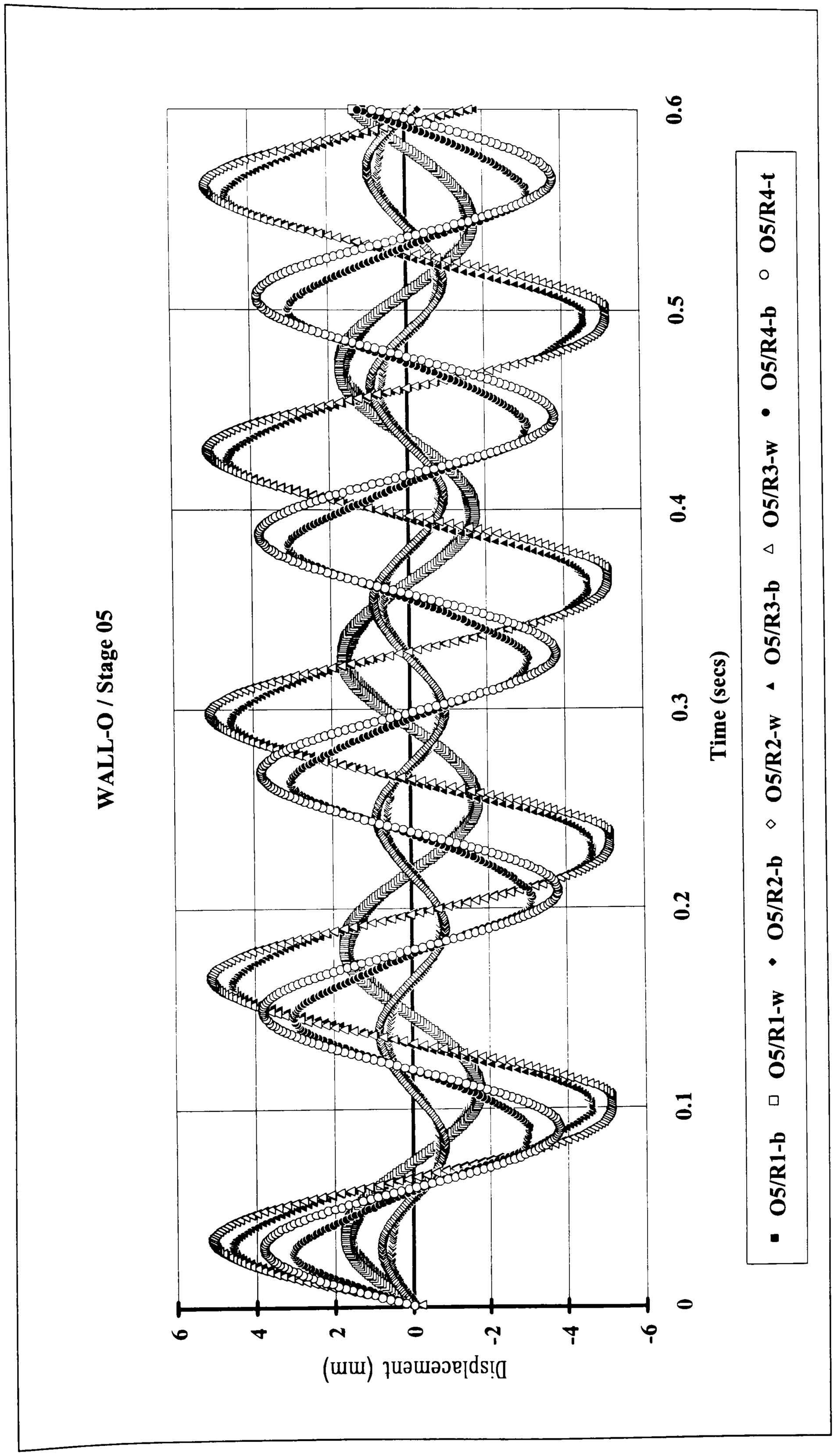

Figure 5.26 Wall-O / Stage O5

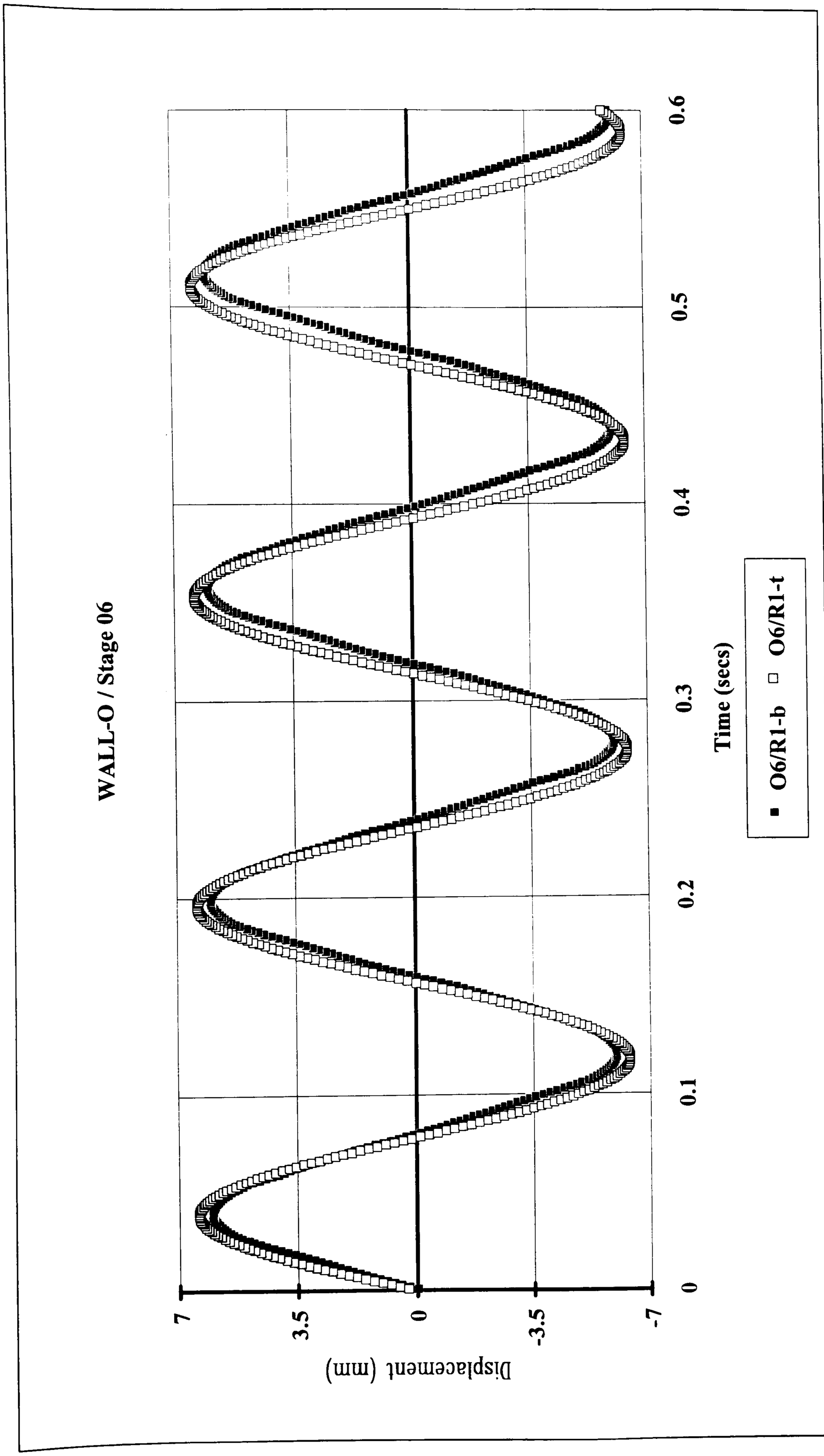

Figure 5.27 Wall-O / Stage O6

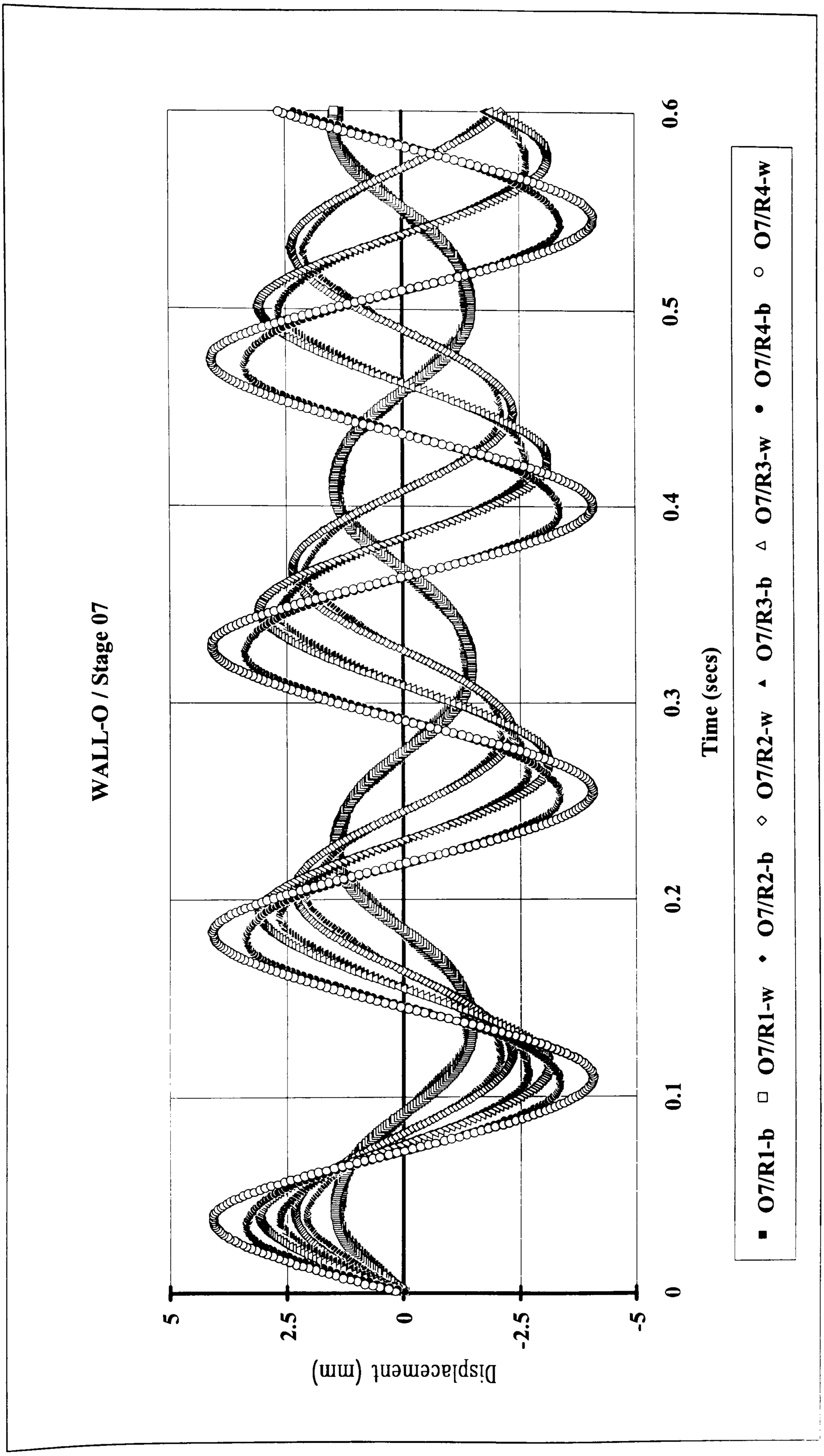

Figure 5.28 Wall-O / Stage O7

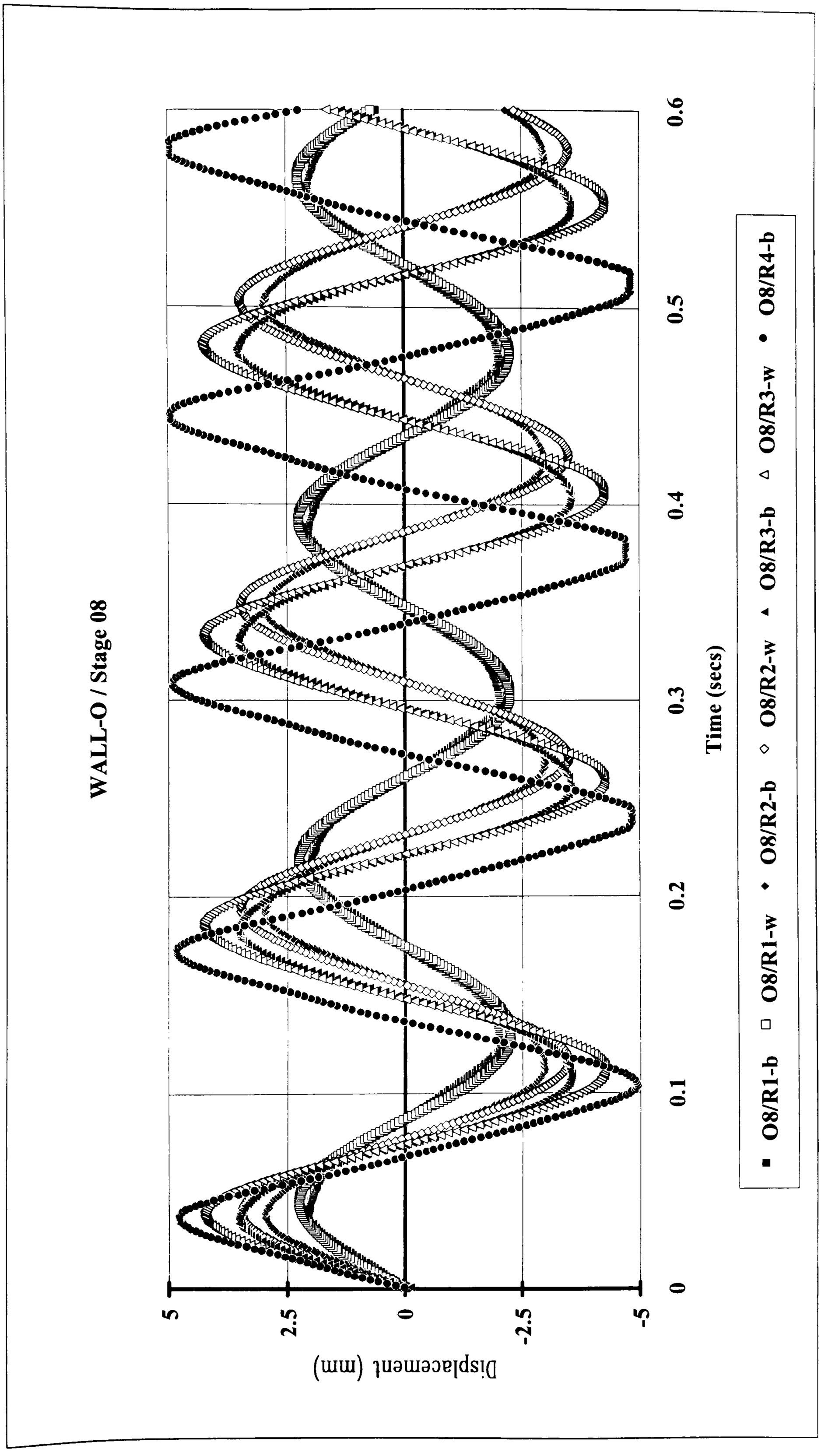
WALL-O / Stage 08
Displacement (mm)
5
2.5
0
-2.5
-5
0
0.1
0.2
0.3
0.4
0.5
0.6
Time (secs)
O8/R1-b
O8/R1-w
O8/R2-b
O8/R2-w
O8/R3-b
O8/R3-w
O8/R4-b
O8/R4-w
Wall-O / Stage O8

Figure 5.29 W

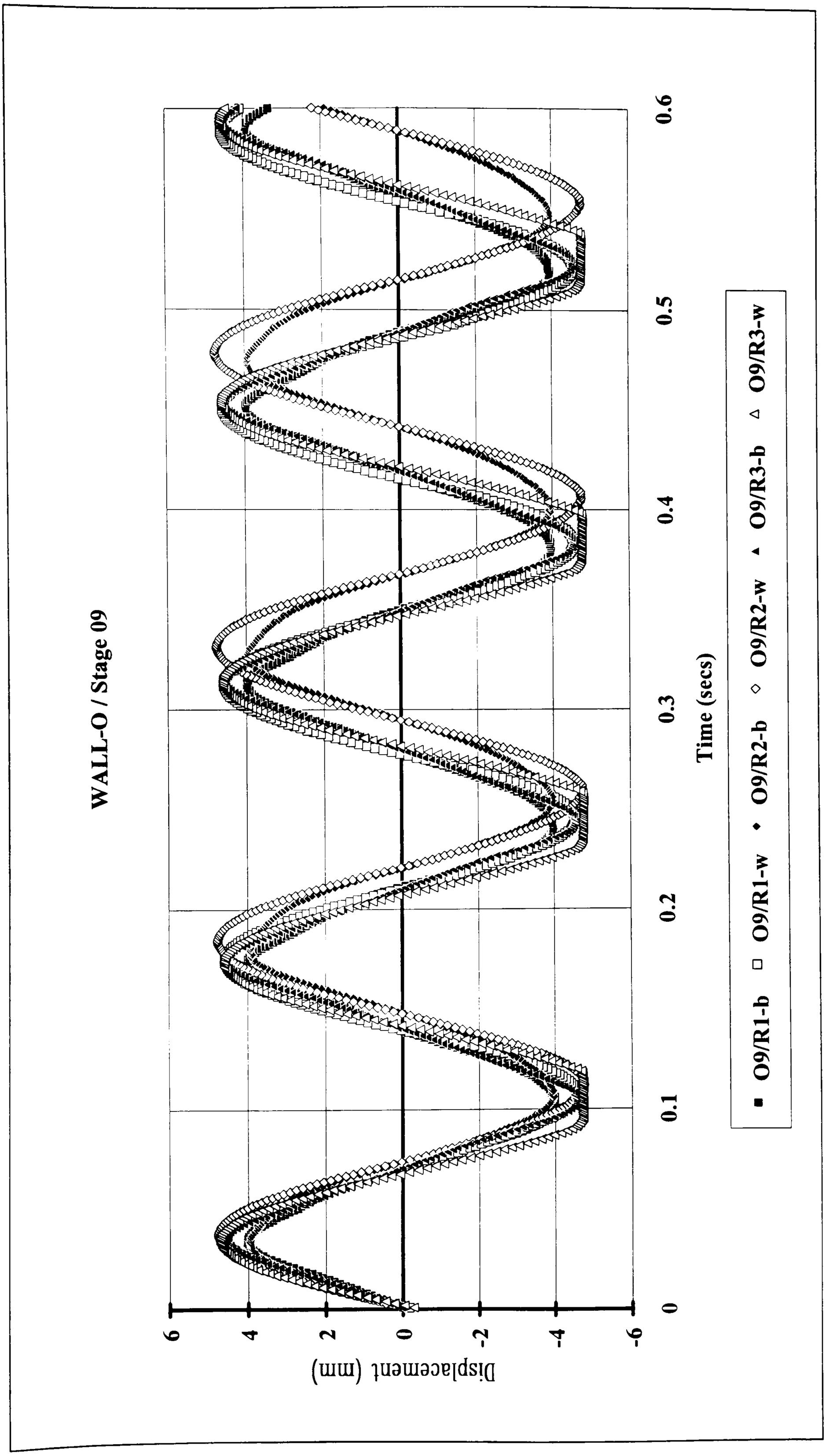

Figure 5.30 Wall-O / Stage O9

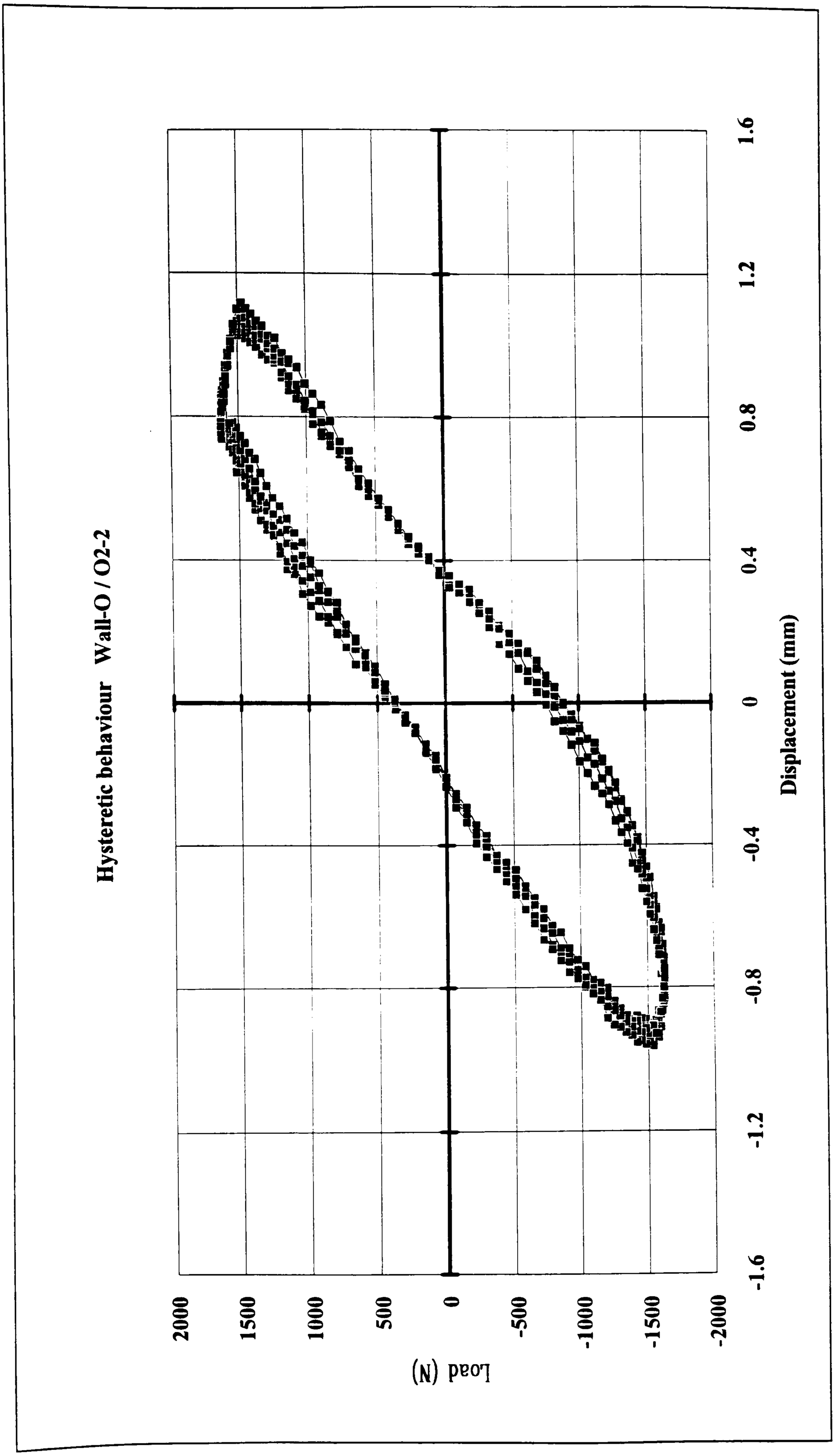

Figure 5.31 Wall-O / Hysteretic Behaviour - Stage O2

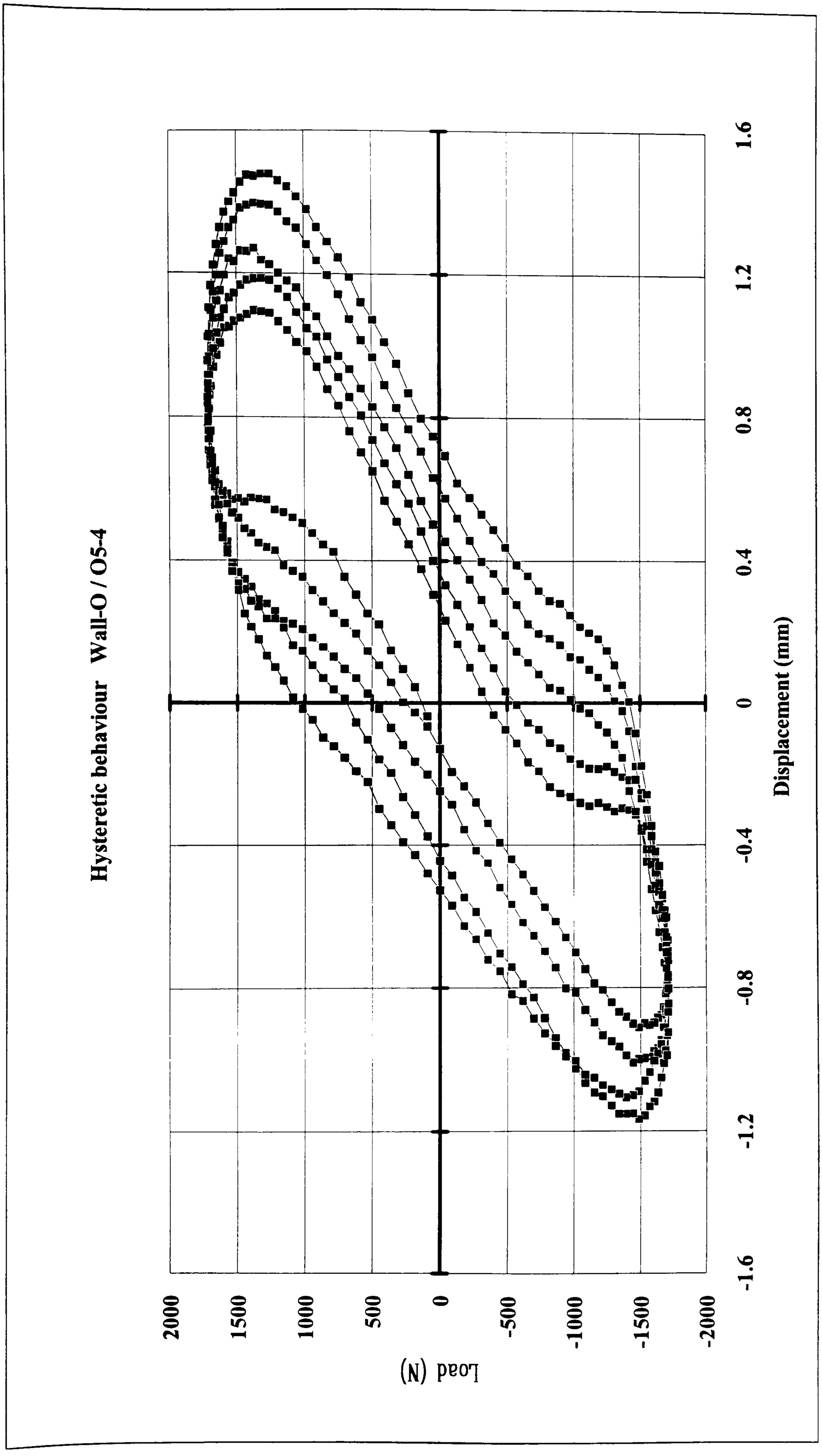

Figure 5.32 Wall-O / Hysteretic Behaviour - Stage O5

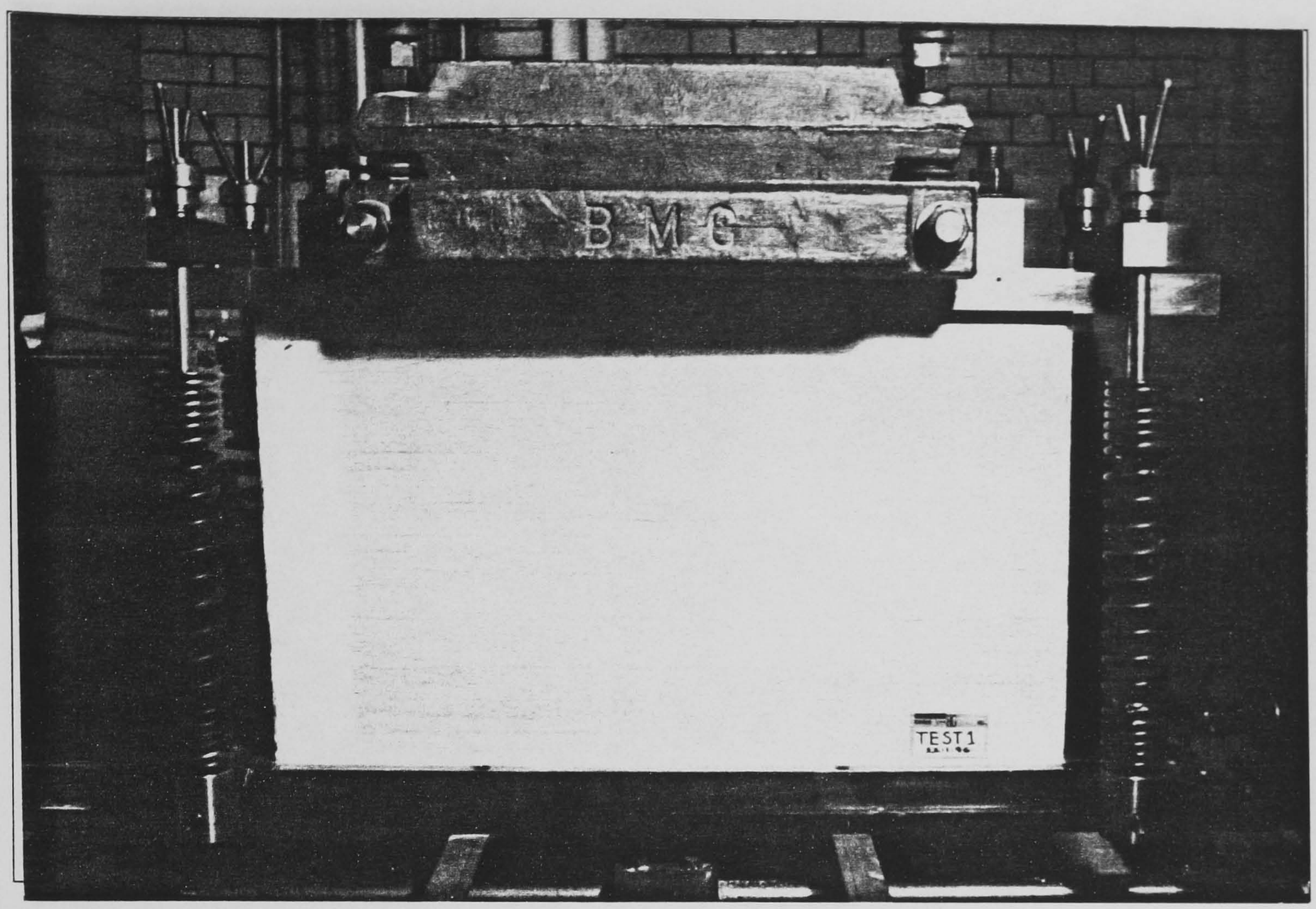

Photo 5.11 Wall-O ready for testing

Photo 5.12 Column-panel separation and brick crushing (wall-O)

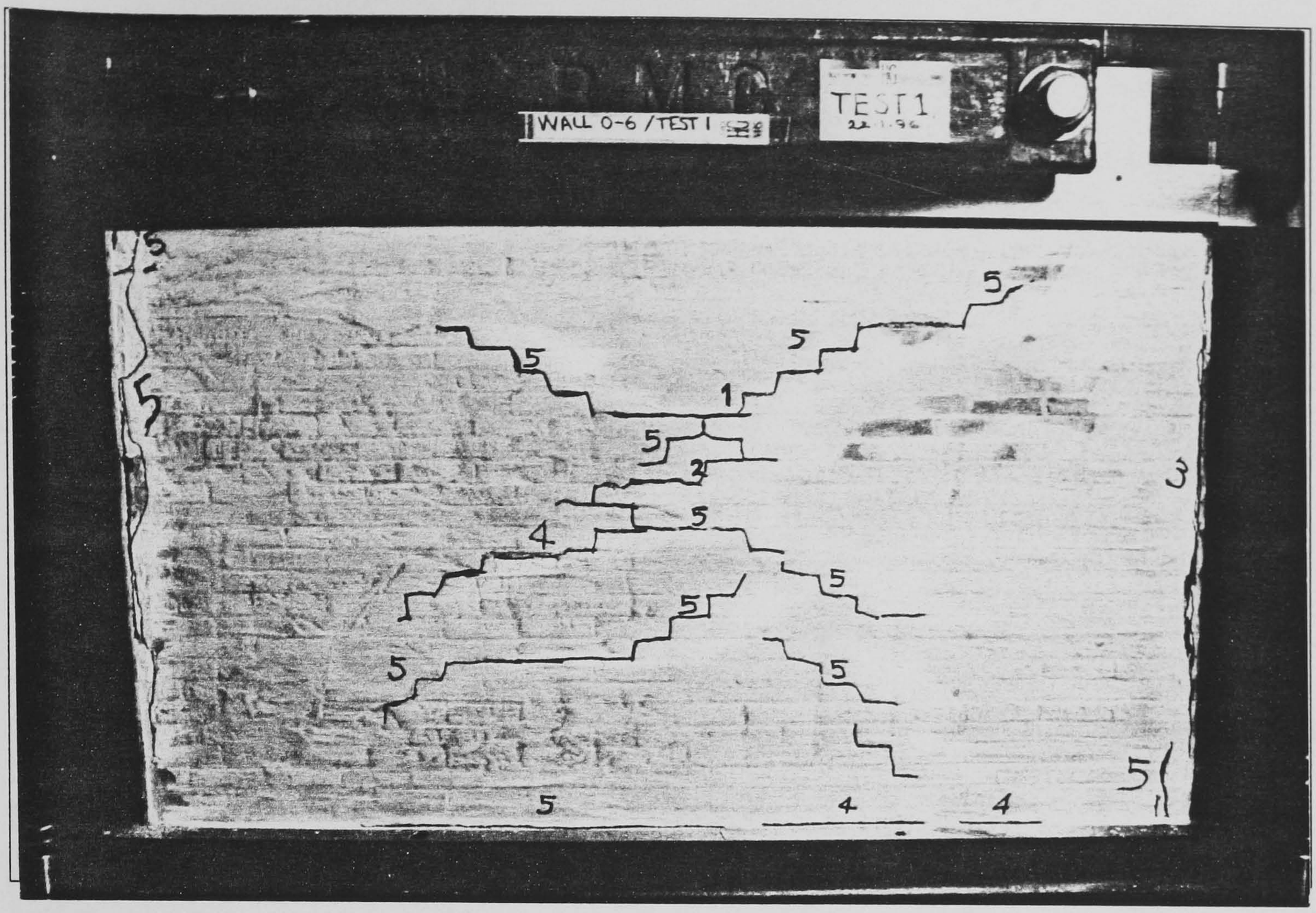

Photo 5.13 Cracking at 1.08g ground acceleration (wall-O)

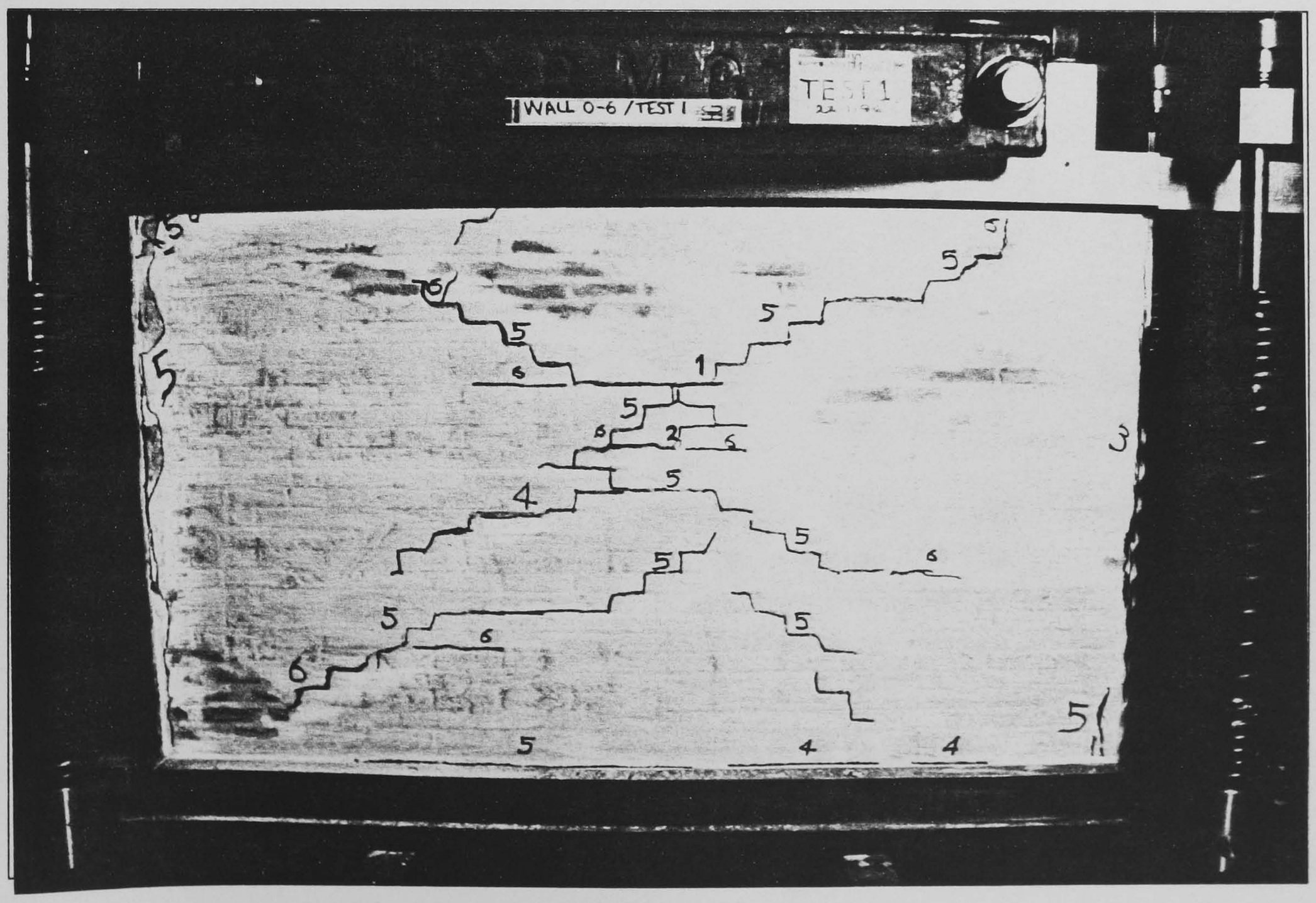

Photo 5.14 Wall-O final cracking pattern

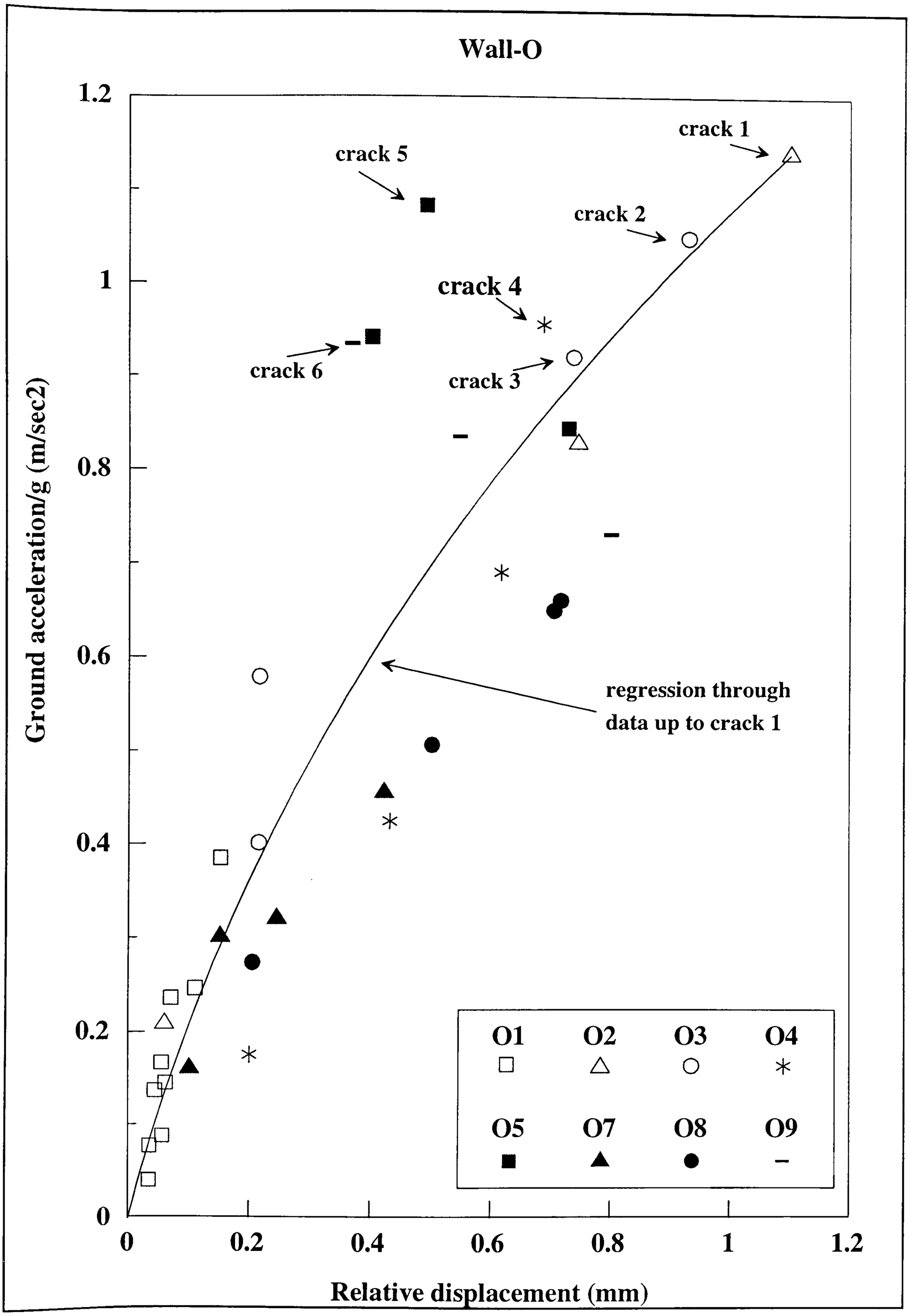

Figure 5.33 Summary of dynamic response for wall-O

5.8.1.1 Observations for wall-O.

The first two panels (wall-O and wall-B) were tested 30 days after casting and were in every aspect substantially stronger with respect to the rest. Wall-O was subjected to accelerations reaching 0.83g with no apparent cracking. Crack 1 (photo 5.13) occurred at 1.14g just above mid-height at the centre of the panel. Crack 2 occurred 3 bricks below and similarly to the first crack, extended two brick lengths horizontally and continued in a stepwise pattern for about three brick widths downwards. Separation at the column interfaces occurred at an acceleration of 0.92g which the author found surprisingly high, considering the low bond that would have developed between the panel and the flat rectangular steel column members even for high strength mortar. It seems more likely that debonding must have occurred earlier but separation was not recorded. With increased intensity of the applied ground motion the debonding extended to the full height of the panel-column interface accompanied by limited local crushing of the bricks (photo 5.12). Repeated cycles, of lower intensity, gave rise to cracks 4 and 5 which connected with the previous ones (crack 1 and 2), extending the damage towards the corners. Photo 5.14 shows the final cracking pattern, which was confined mostly to the middle section where the highest stress concentrations are expected. Due to malfunction of the motor after stage O9 no further testing was carried out. Energy dissipation for the panel can be seen in the hysteresis loops (figures 5.31 and 5.32), where a stabilisation in the upper part of the curves is evident (figure 5.32) related to the damping mechanisms (friction and cracking) that counteract stiffness degradation. Although the cracks described before extended in length and connected to form a symmetrical pattern, the length of the horizontal cracks at the base remained unchanged due to the action of the axial force which increased friction and bond strength and provided confinement with respect to the applied ground motion. With this wall exhibiting a typical cross-shaped *diagonal tensile cracking* failure with no further substantial stiffness degradation, this would appear to contradict the opinion that this type of failure is generally brittle with no ductile post-cracking hysteretic behaviour. This argument is dealt with in section 5.9, where it is substantiated by similar findings and conclusions from a number of researchers during recently performed experimental investigations.

5.8.2 Second test : wall-B.

Wall-B was subjected to a smaller amount of stages and runs than wall-O. These two panels had similar mechanical properties (apart from the brick-mortar interface shear bond strength). It was intended to apply similar excitations with respect to the driving frequency and ground acceleration, although this was not always possible. However stages B1 (O1/R1-2-3) and B5 (O4) are comparable to this respect and as explained later in this chapter, similarities between the two walls were observed in the dynamic characteristics, response and behaviour. In the following pages the developing dynamic behaviour has been laid out in detail, in the order shown below.

- Free vibration amplitude decay records - hammer tests (figures 5.34 to 5.37).
- Displacement records (5.38 to 5.45).
- Sample hysteresis curves (5.46, 5.48).
- Photographs of the cracking patterns (photo 5.15 to 5.20).
- Summary of dynamic response (figure 5.49).

The test procedure for wall-B is summarised in table 5.5, while results for the first natural frequency using the methods described previously are shown in table 5.4.

Theoretical	**Finite element**	**Hammer test**
64.8 Hz	75 Hz	44.48 Hz

Table 5.4 Natural frequency results (initial value) for wall-B

Stage/Run	Table accel.	Driving freq.	Damage	Natural freq.	Damping ratio	Rel. displ.	Comments
	g	Hz	Crack #	Hz	%	mm	
B1/R1	0.021	5.4	-	44.48	6.4	0.056	Constant driv. frequency
B1/R2	0.072	5.4	-	-	-	0.07	
B1/R3	0.119	5.4	-	-	-	0.083	
B2/R1	0.219	6.8	-	-	-	0.03	Constant driv. frequency
B2/R2	0.294	6.8	-	-	-	0.072	**Column separation**
B2/R3	0.48	6.8	**1**	40.83	7.8	0.236	
B3/R1	0.583	8.5	-	-	-	0.397	Constant driv. frequency
B3/R2	0.74	8.5	**2**	-	-	0.808	**Corner cracking**
B3/R3	0.581	8.7	-	-	-	0.837	
B4/R1	0.192	9.7	-	-	-	0.182	Varied driv. frequency
B4/R2	0.451	9.2	-	-	-	0.343	
B4/R3	0.86	8.6	-	-	-	0.735	
B5/R1	0.179	7.6	-	-	-	0.162	Varied driv. frequency
B5/R2	0.779	8.3	-	-	-	0.755	
B5/R3	0.46	10	-	-	-	0.463	
B5/R4	0.989	7.8	-	-	-	0.822	**Localised horizontal joint cracking**
B5/R5	1.12	7.4	**3**	31.5	10.6	0.508	
B6/R1	0.786	9.6	-	-	-	0.498	Varied driv. frequency
B6/R2	0.67	10.2	-	-	-	0.424	
B7/R1	1.05	8.1	-	-	-	0.404	LVDT failure in B7/R2
B8/R1	0.94	11.8	-	-	-	0.419	Varied driv. frequency
B8/R2	1.09	8.2	-	-	-	1.071	
B8/R3	0.798	10.6	-	-	-	0.37	
B9/R1	0.98	-	**4**	31.25	11.6	-	Axial compressive force removed **Corner crushing Flexural (joint sliding) failure near the base**

(Crack numbers correspond to the cracking as noted in the photographs)

(The top LVDTs were removed in the last stage-B9 following failure of the top corner)

Table 5.5 Wall-B testing sequence

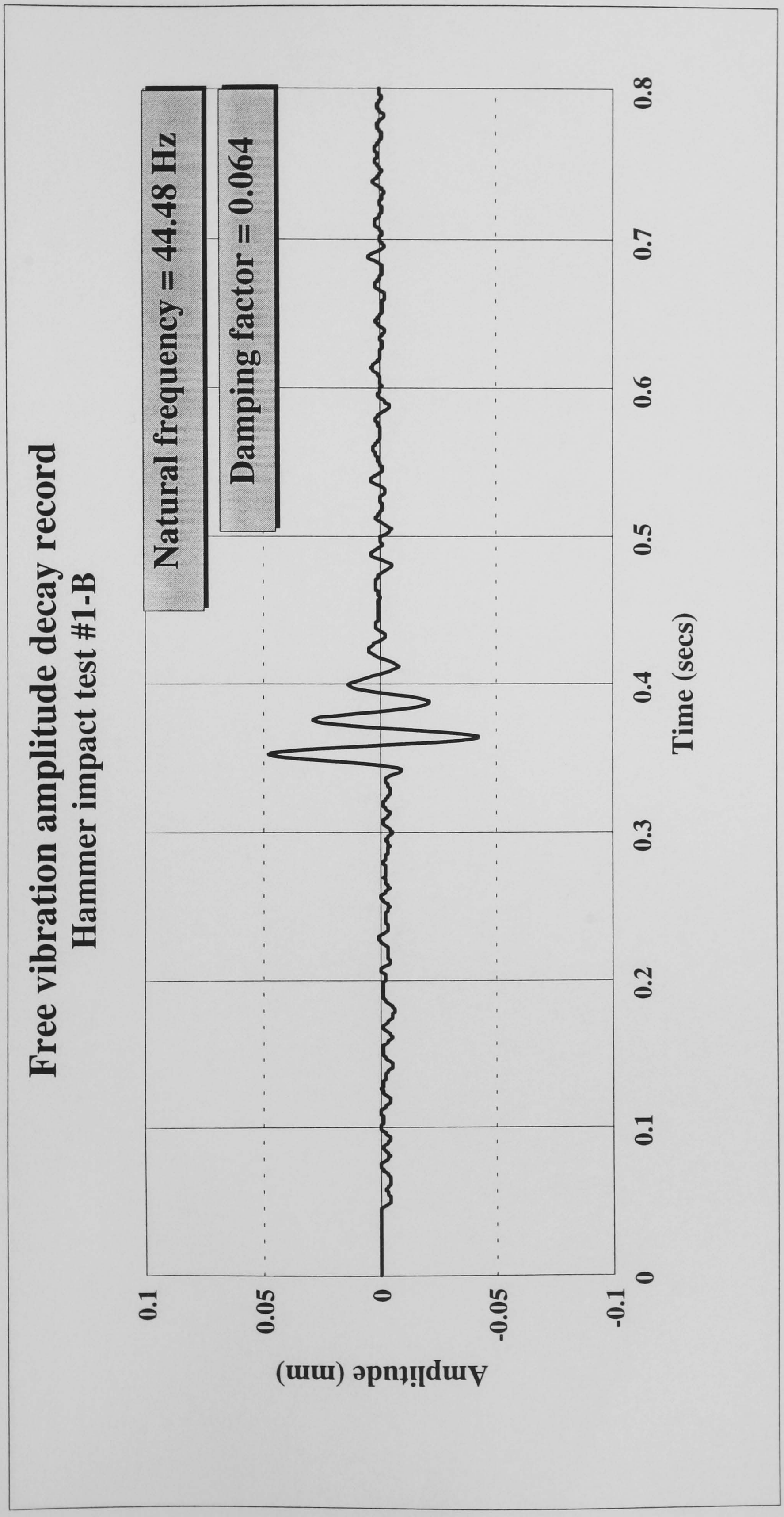

Figure 5.34 Initial free vibration amplitude decay

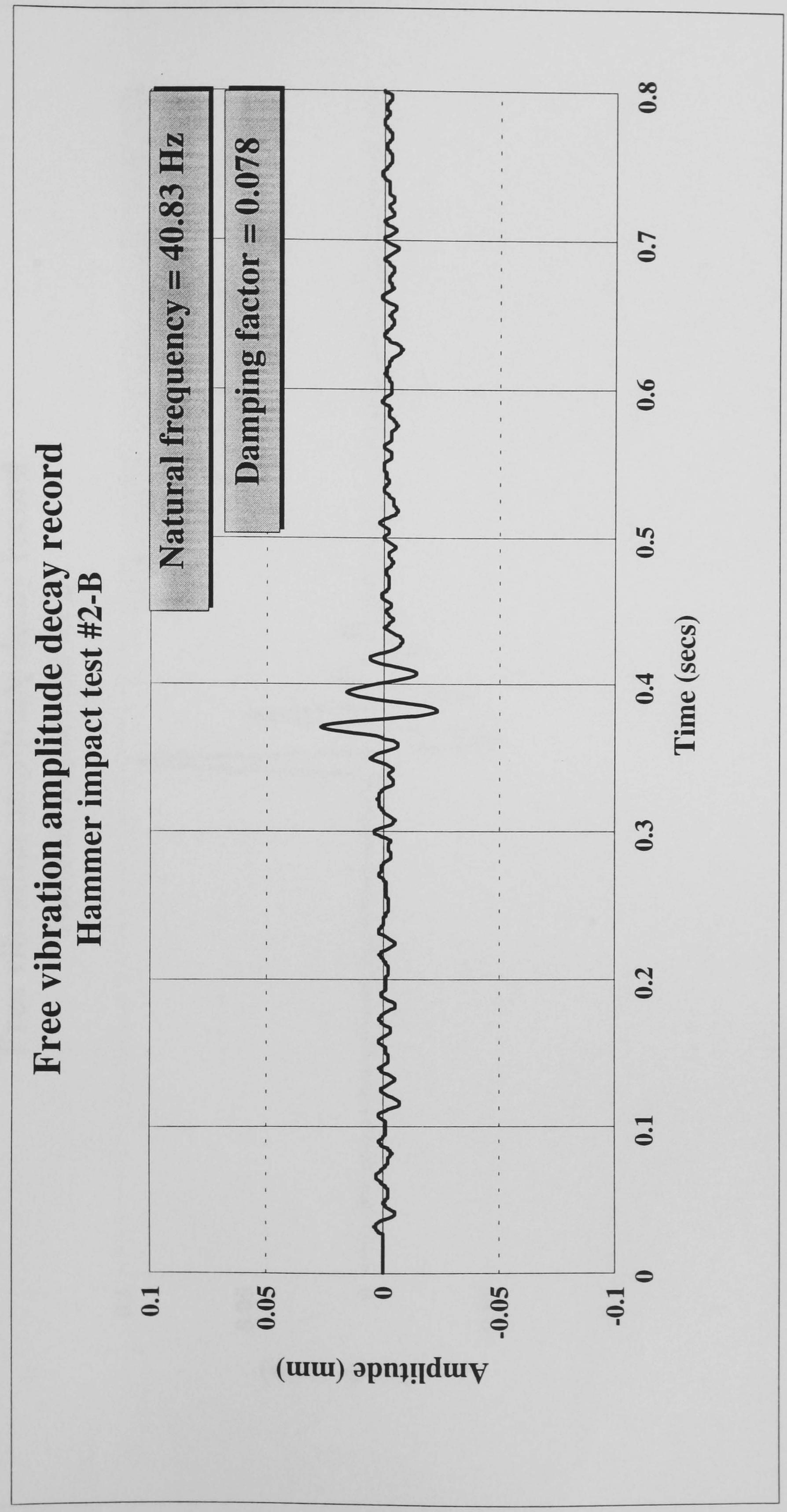

Figure 5.35 Free vibration amplitude decay after crack 1

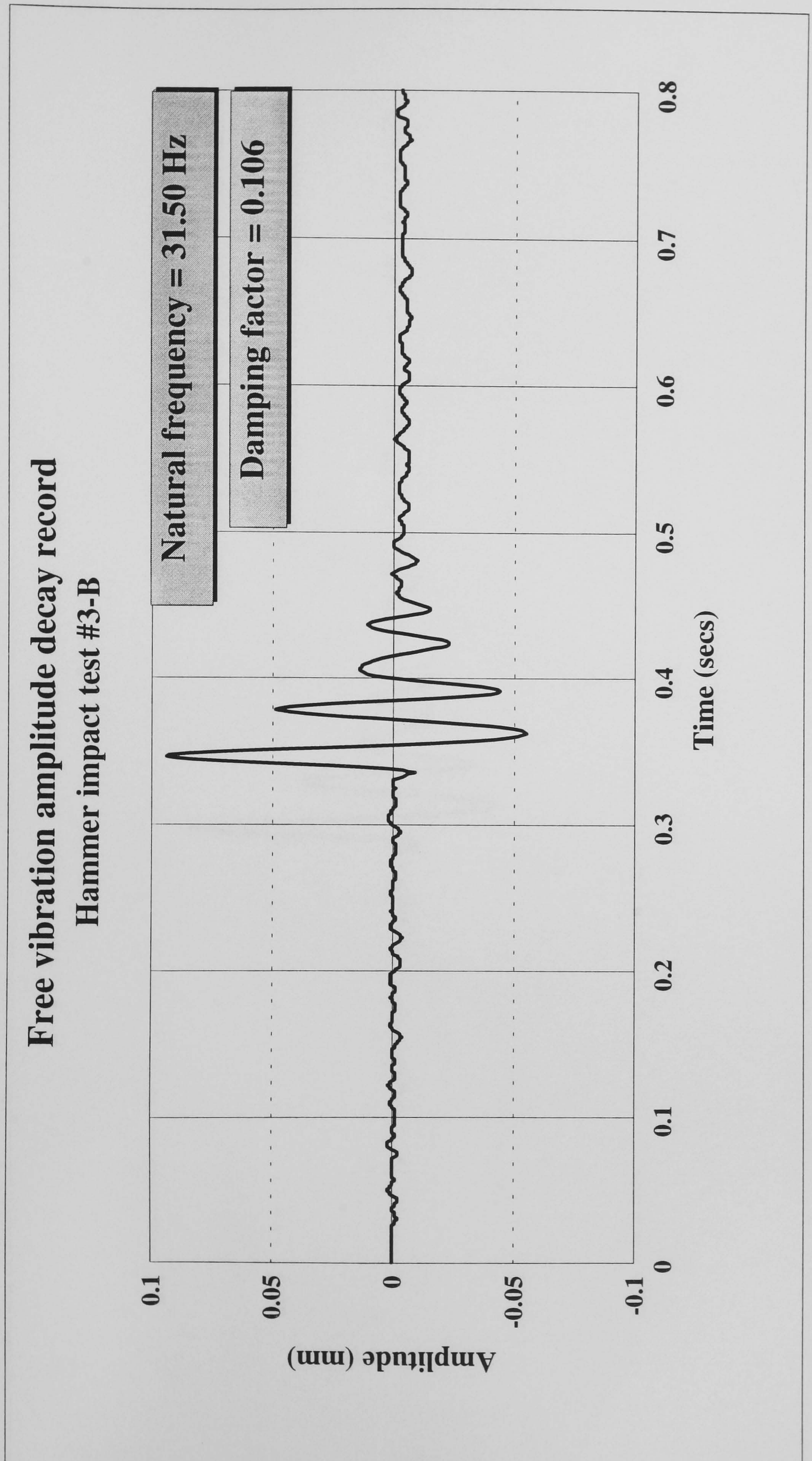

Figure 5.36 Free vibration amplitude decay after crack 2

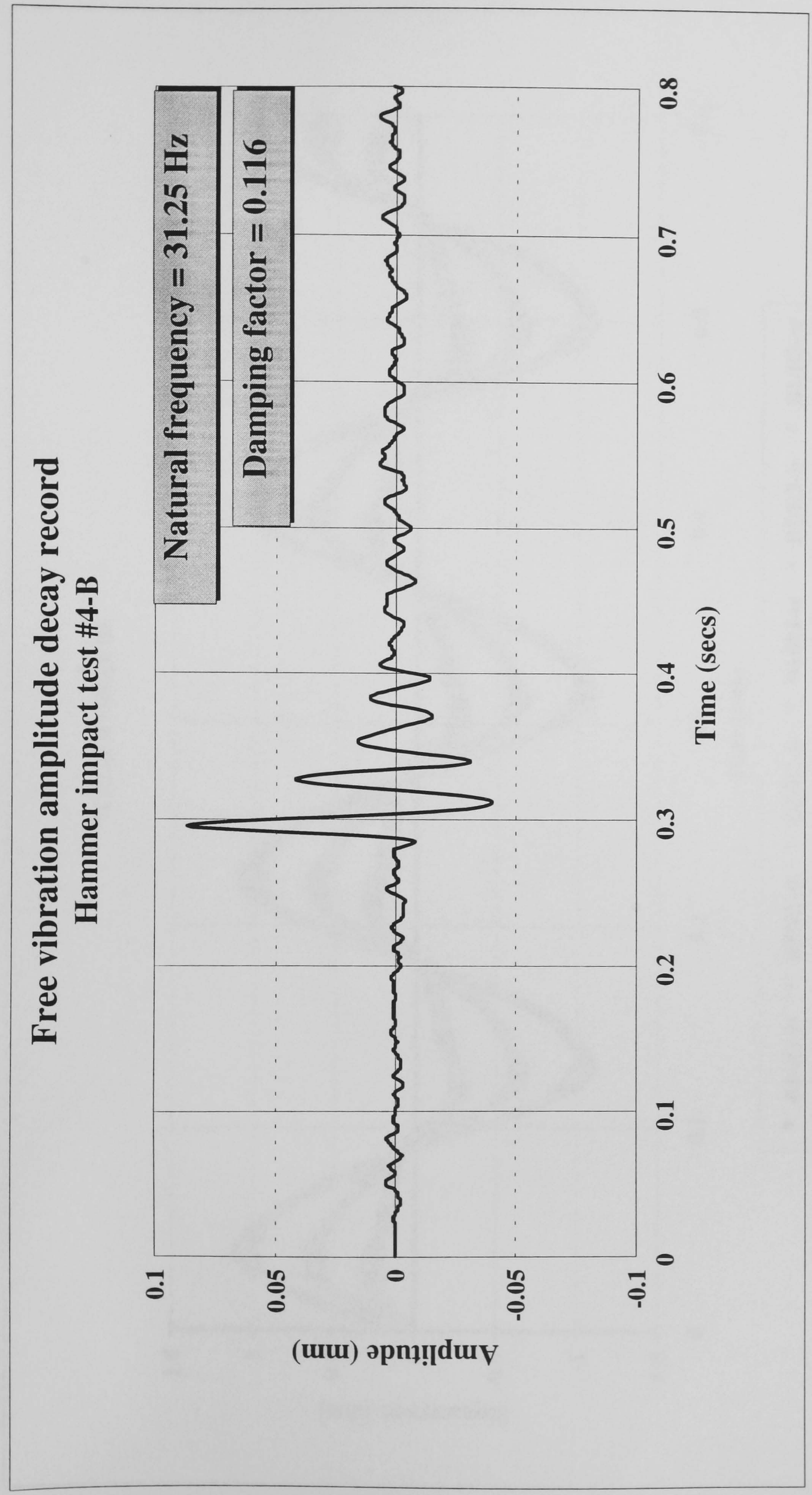

Figure 5.37 Free vibration amplitude decay after crack 3

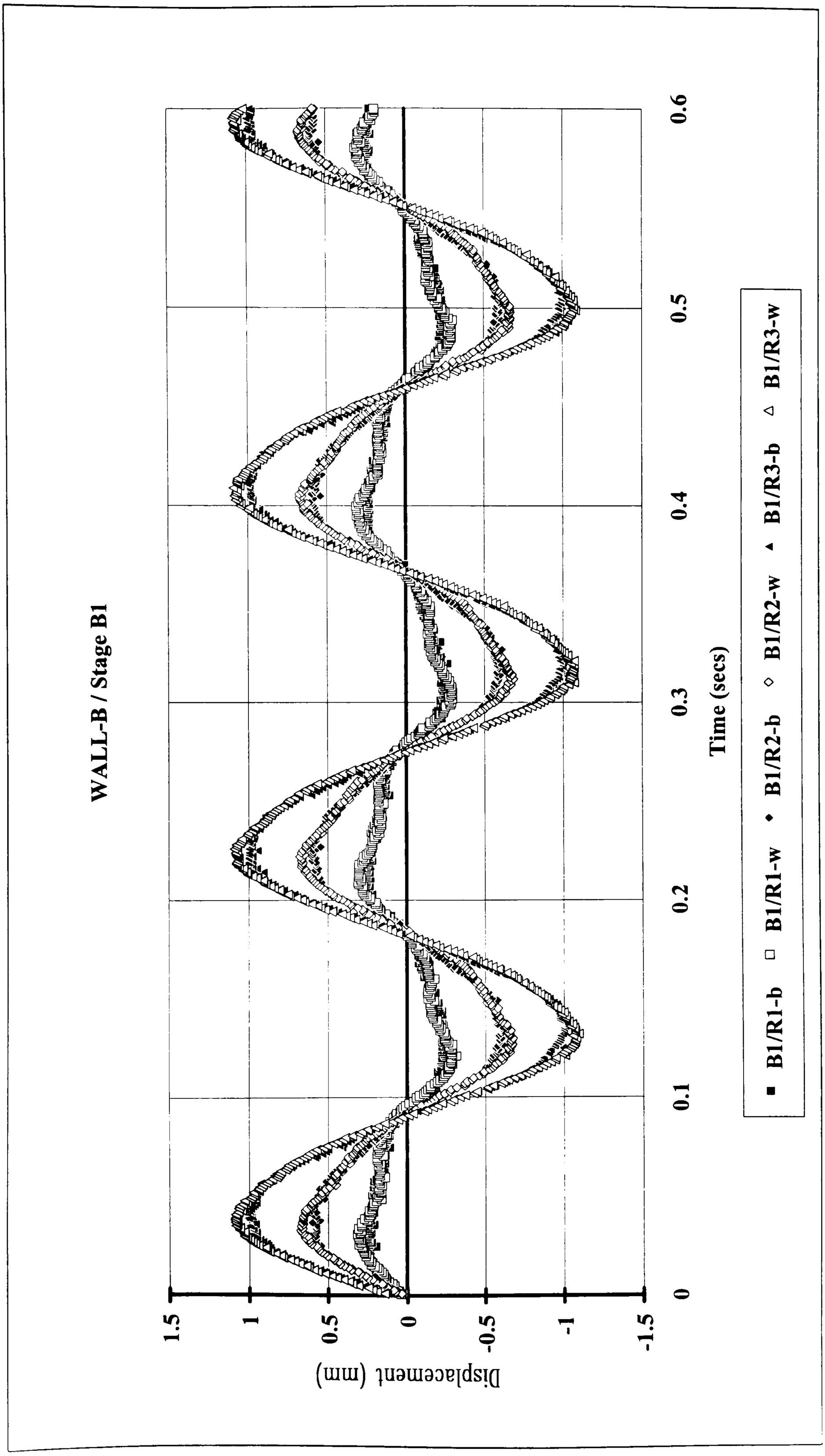

Figure 5.38 Wall-B / Stage B1

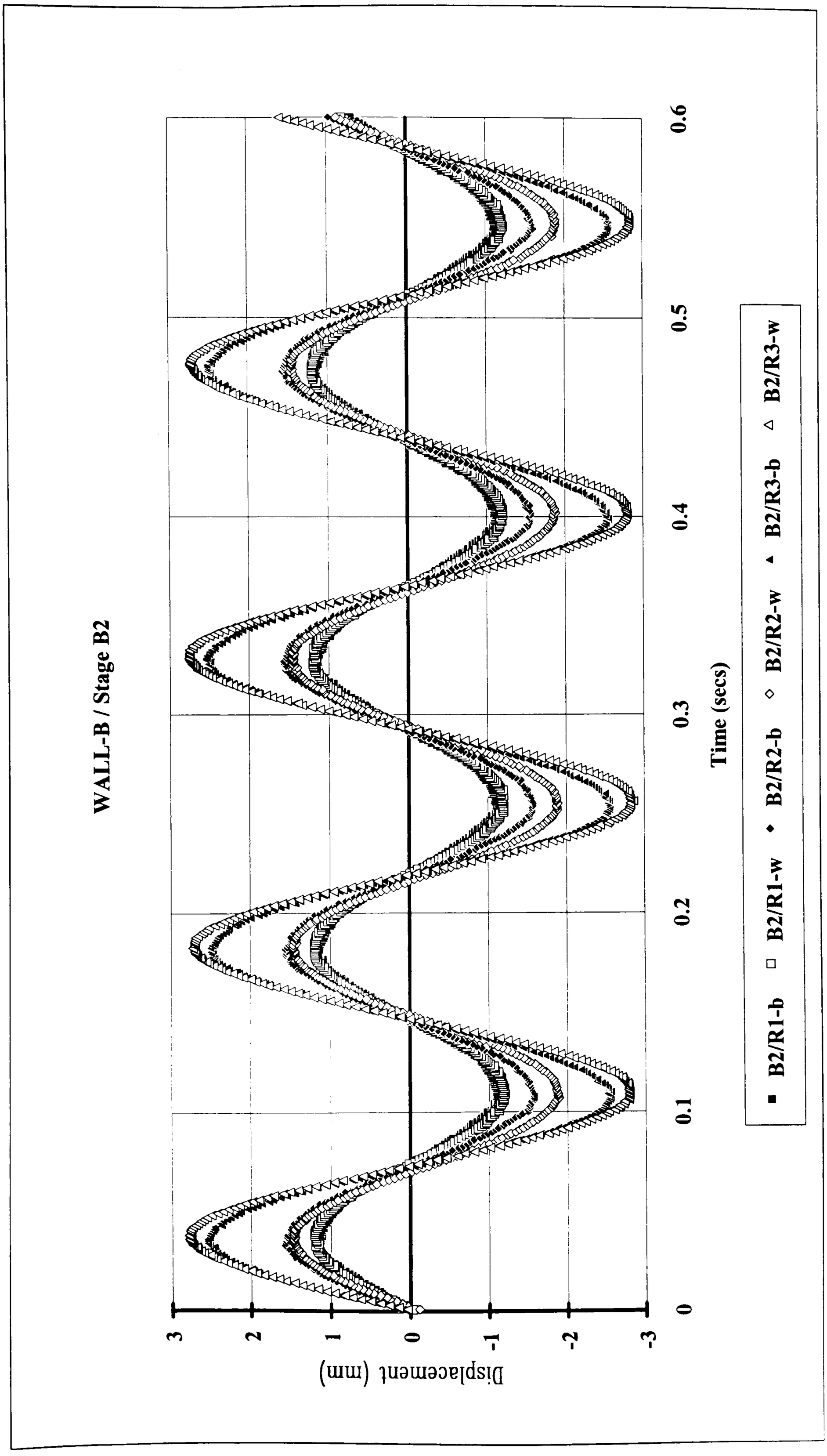

Figure 5.39 Wall-B / Stage B2

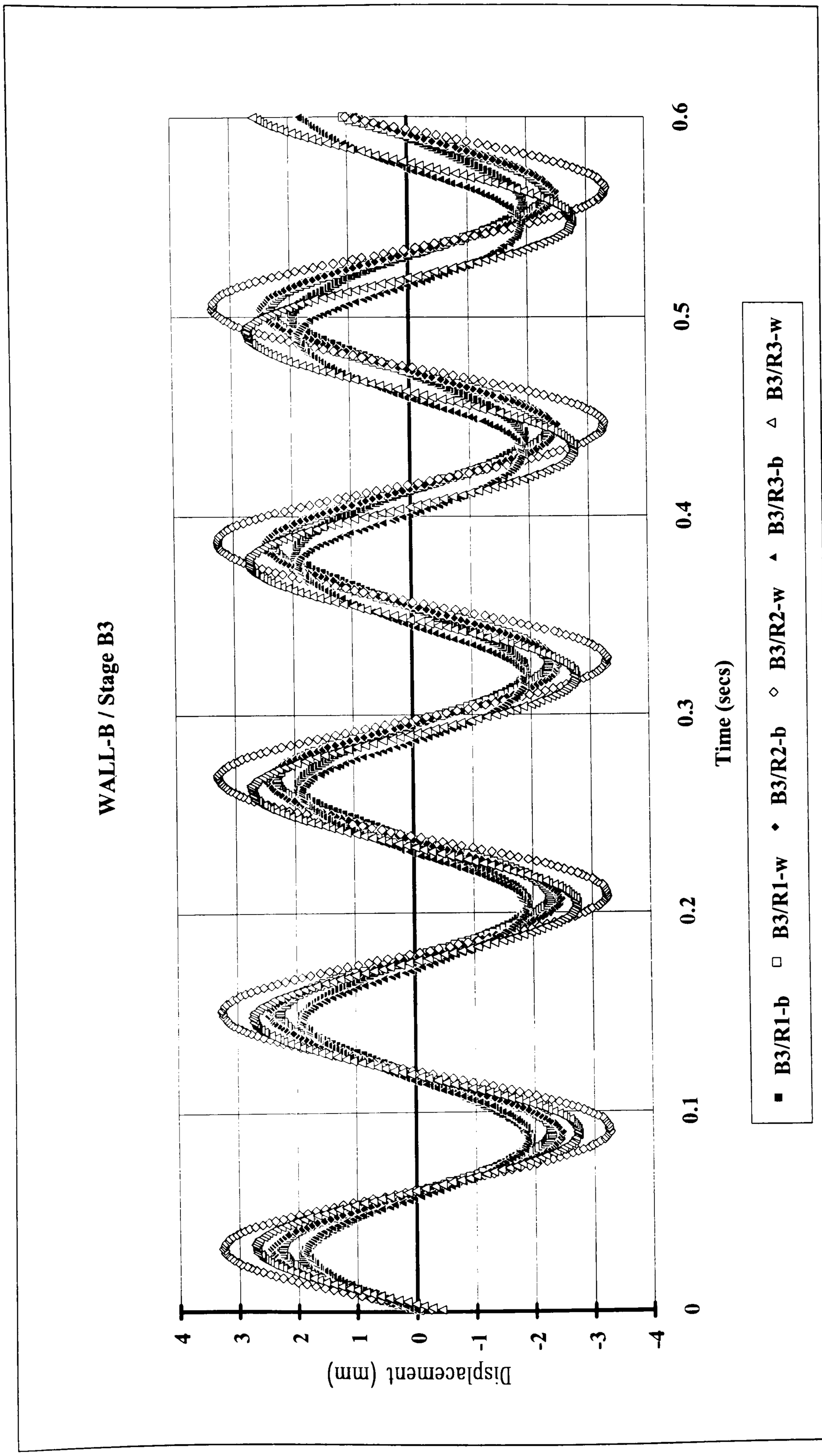

Figure 5.40 Wall-B / Stage B3

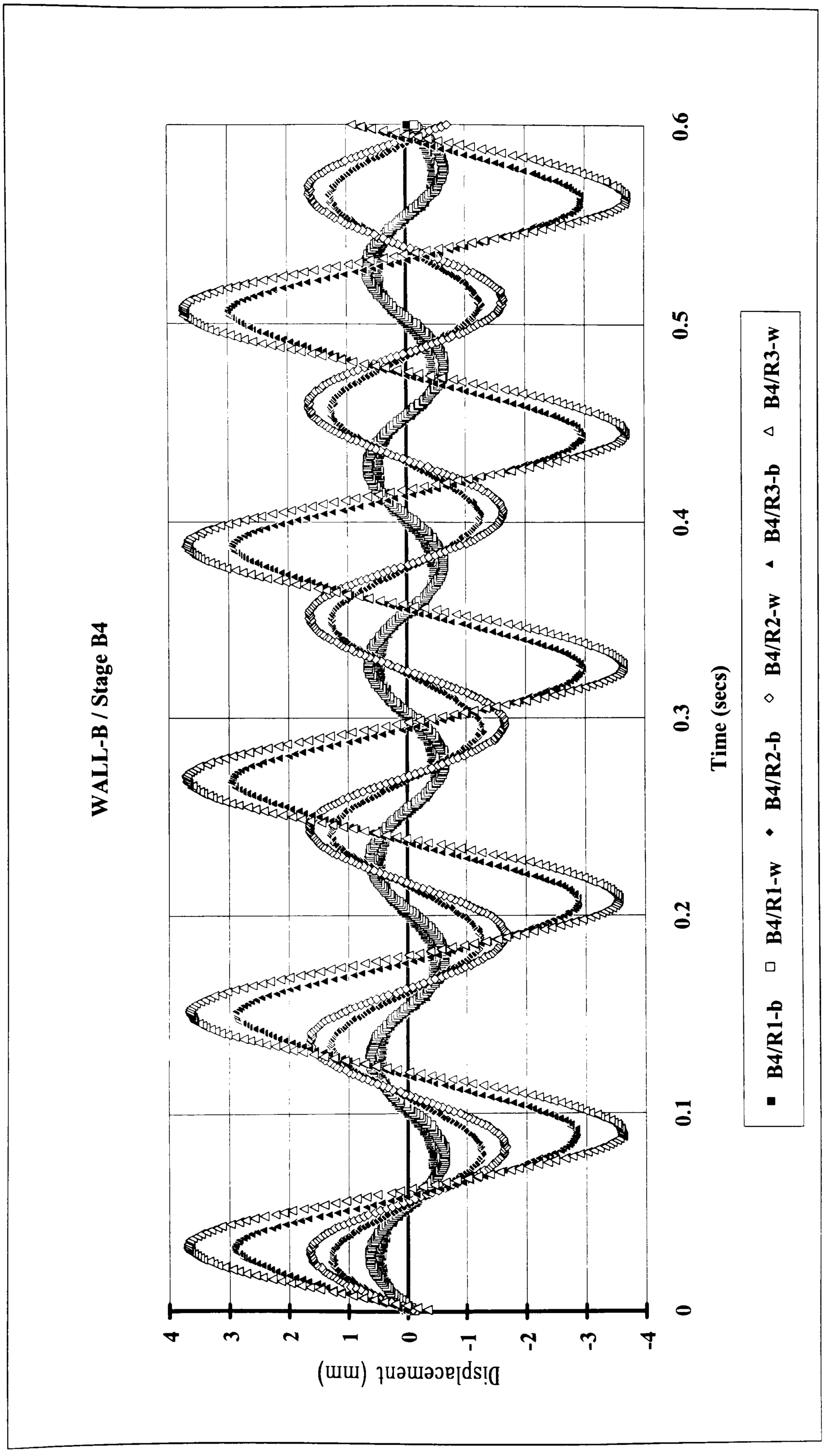

Figure 5.41 Wall-B / Stage B4

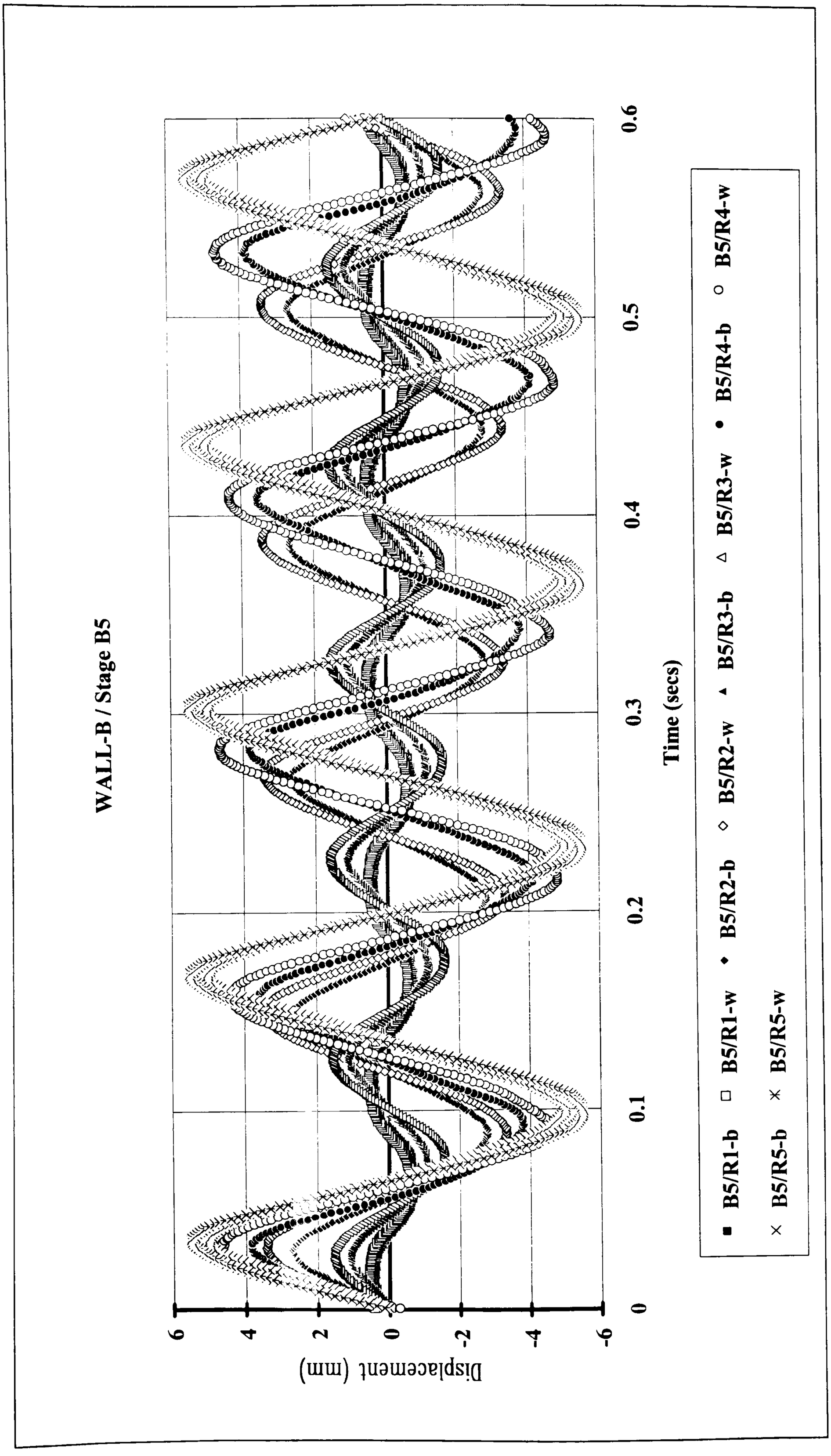

Figure 5.42 Wall-B / Stage B5

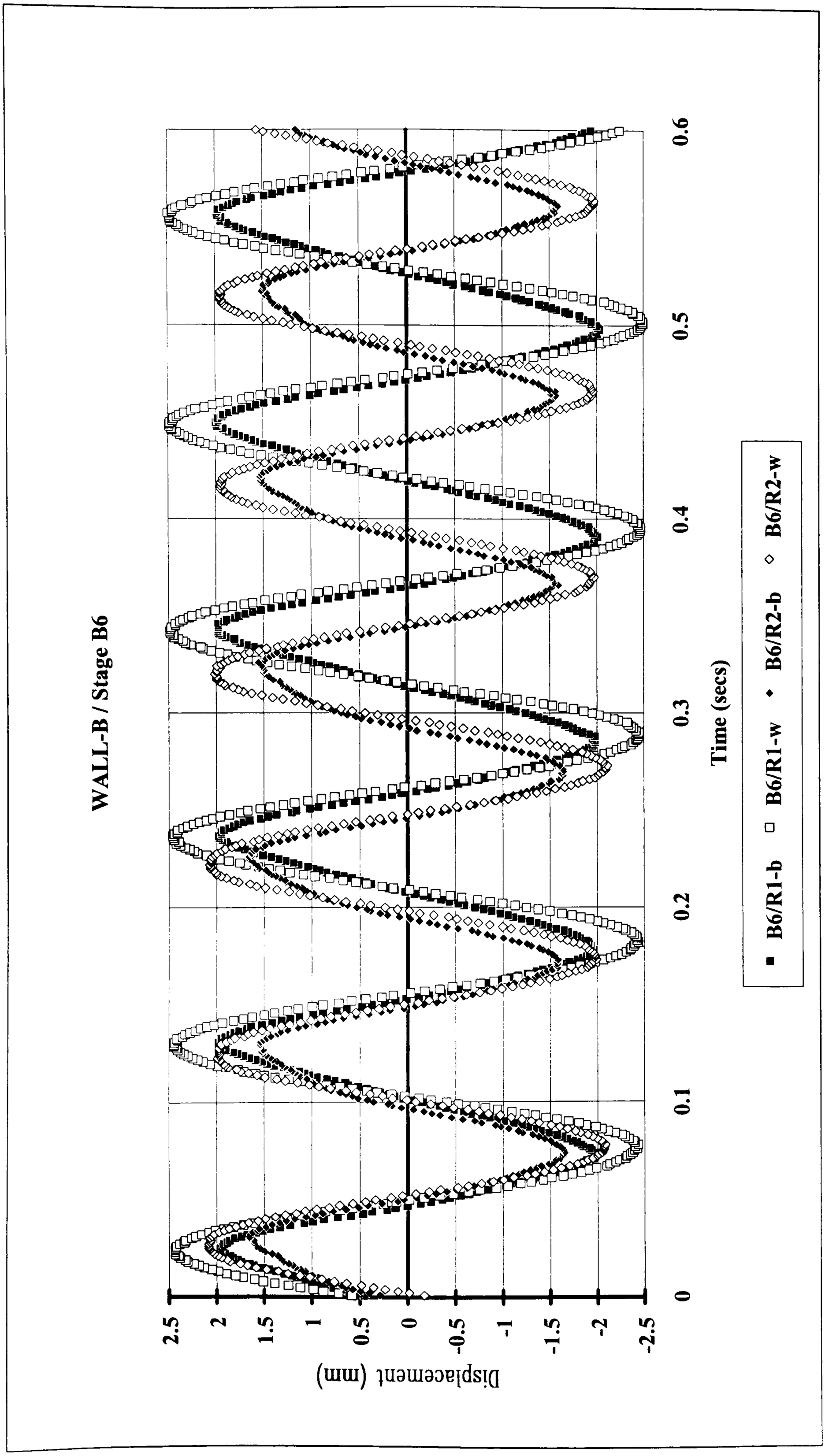

Figure 5.43 Wall-B / Stage B6

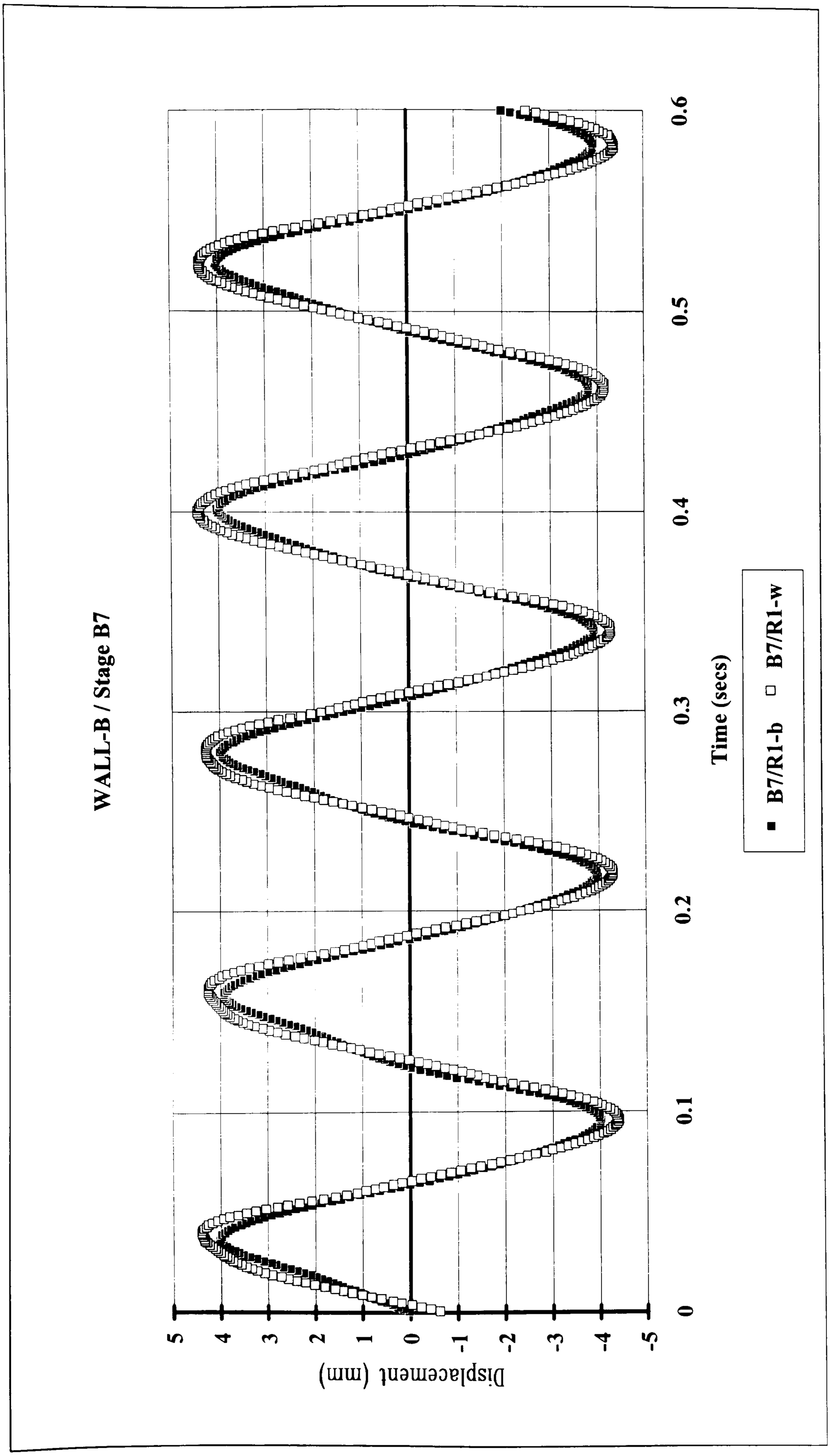

Figure 5.44 Wall-B / Stage B7

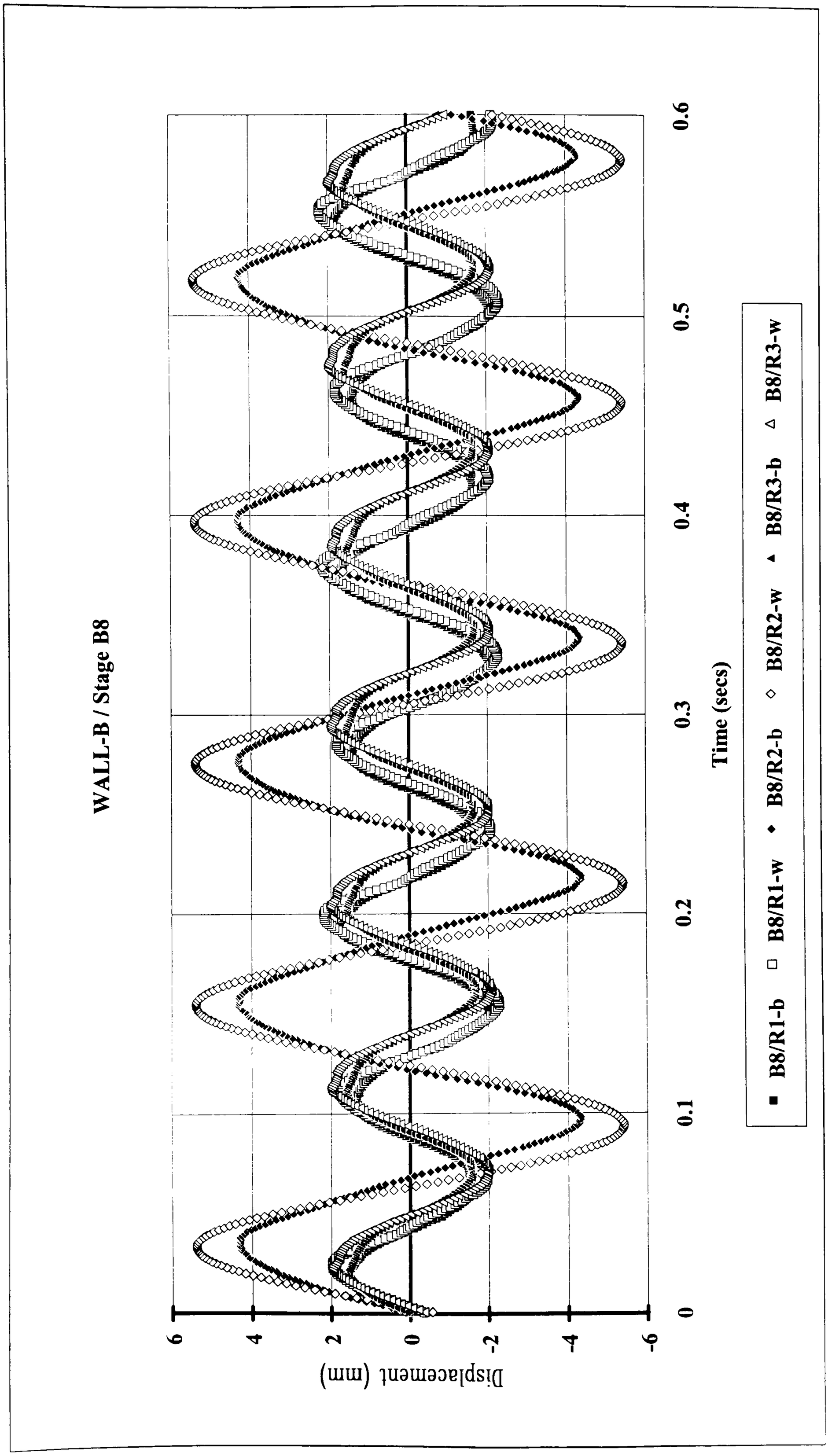

Figure 5.45 Wall-B / Stage B8

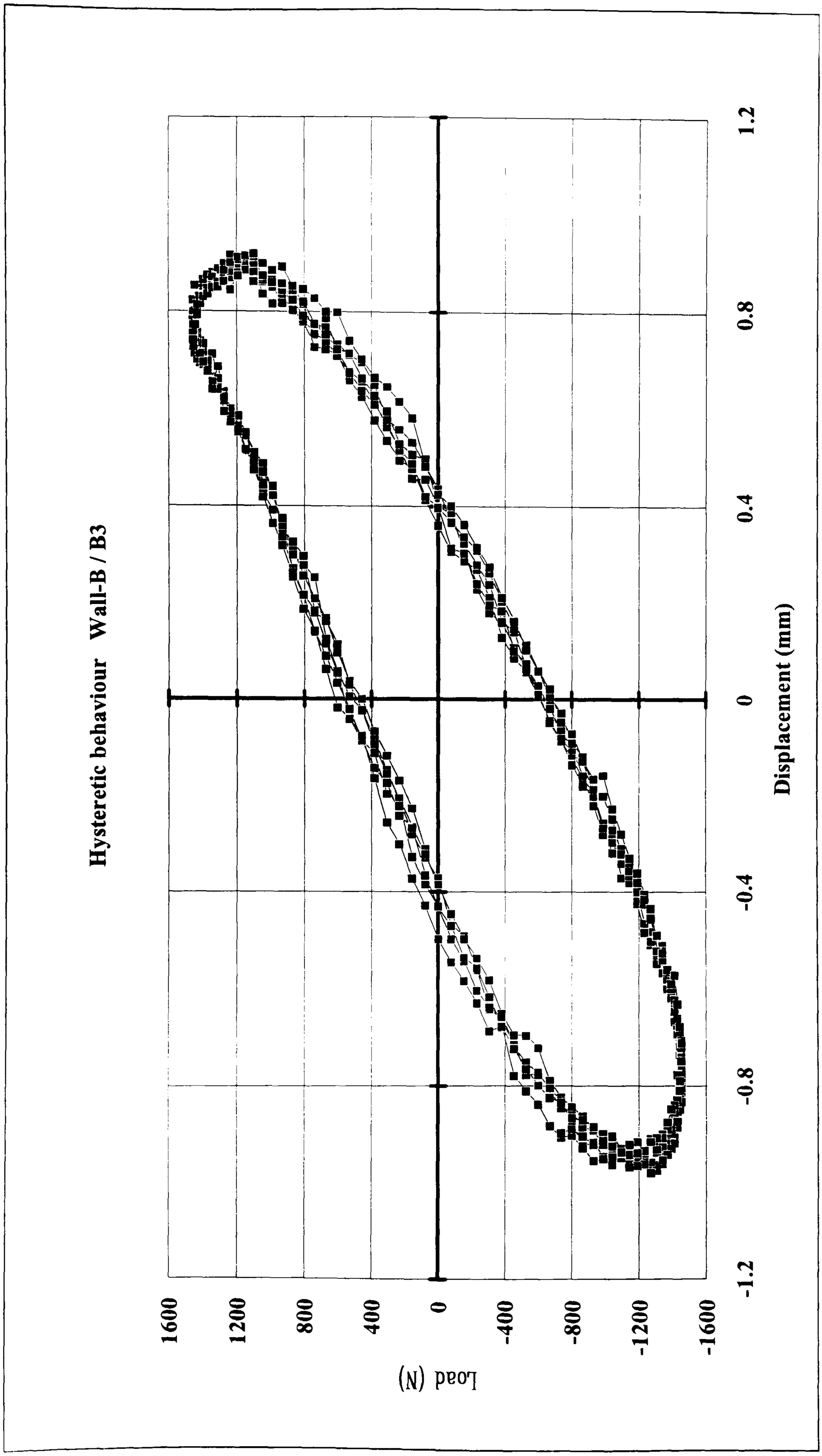

Figure 5.46 Wall-B / Hysteretic behaviour - Stage B3

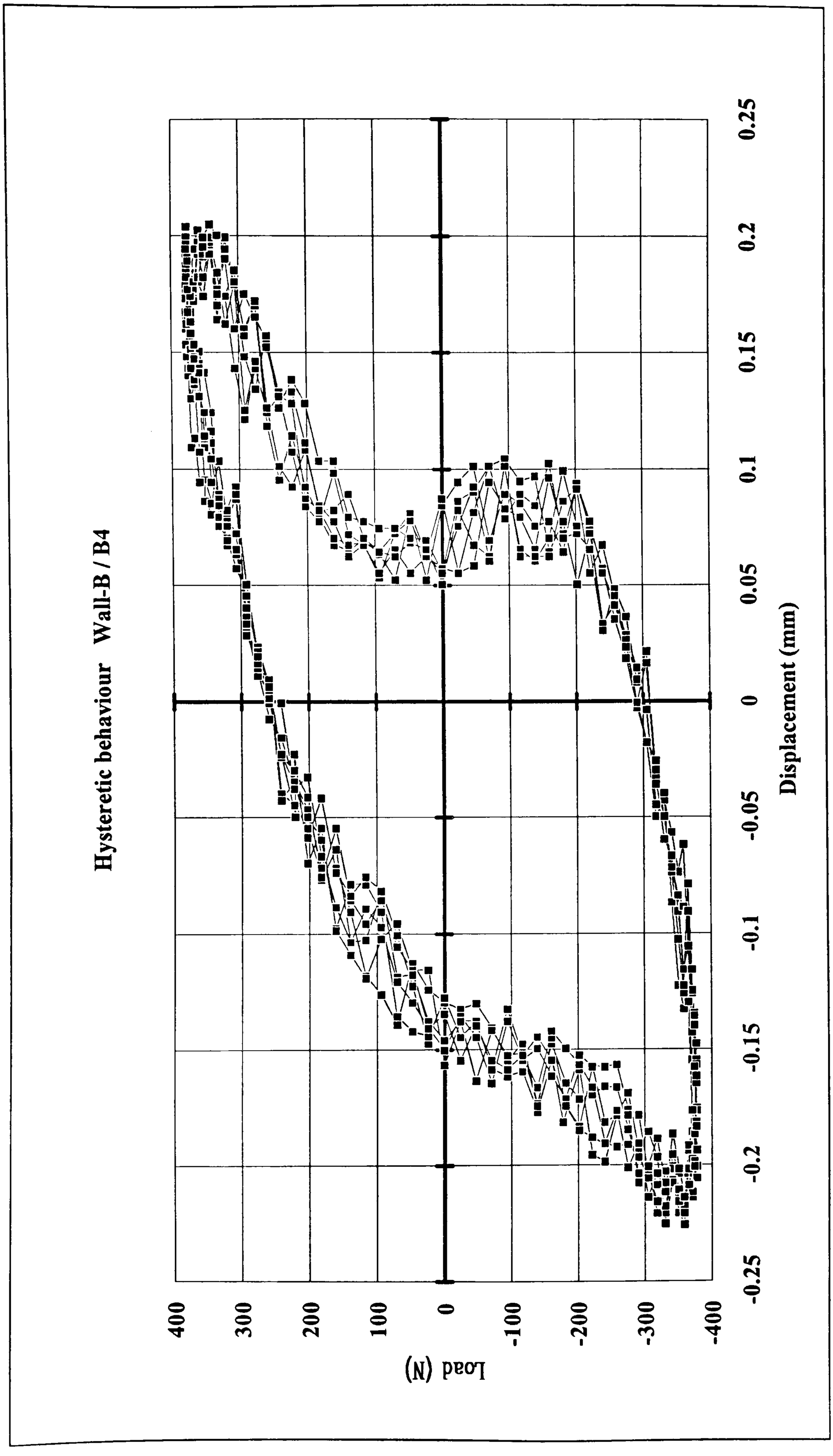

Figure 5.47 Wall-B / Hysteretic behaviour - Stage B4

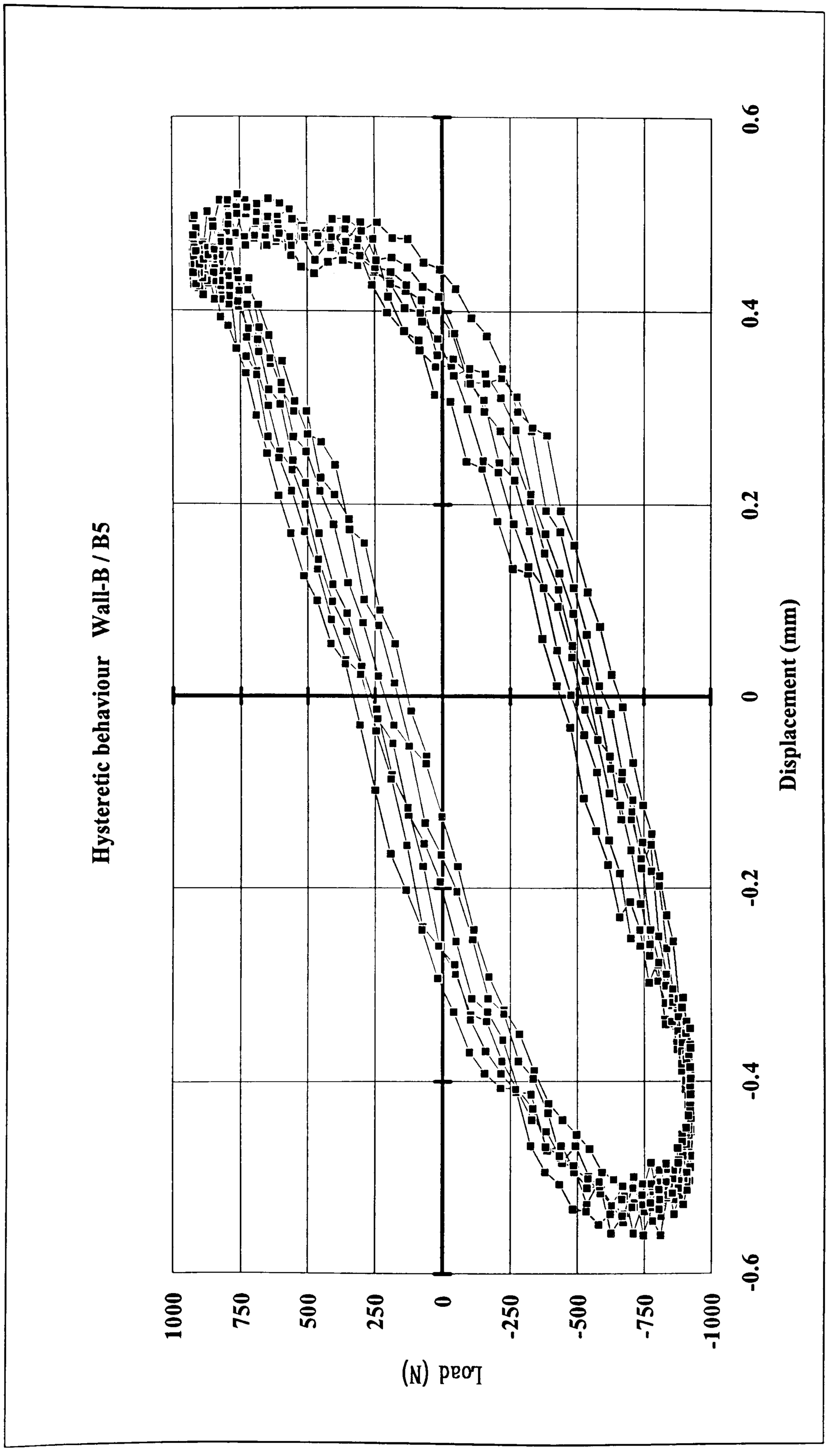

Figure 5.48 Wall-B / Hysteretic behaviour - Stage B5

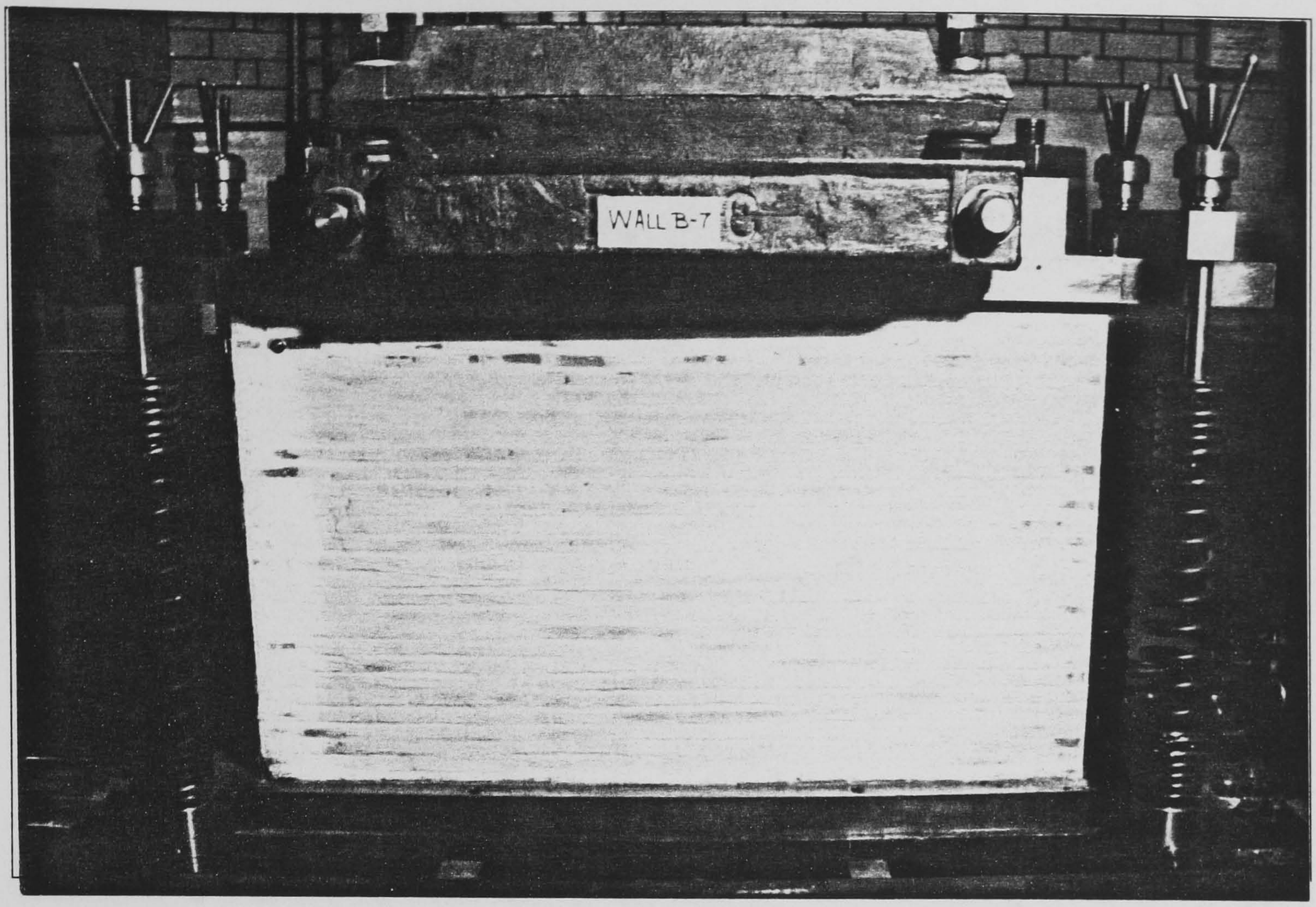

Photo 5.15 Wall-B ready for testing

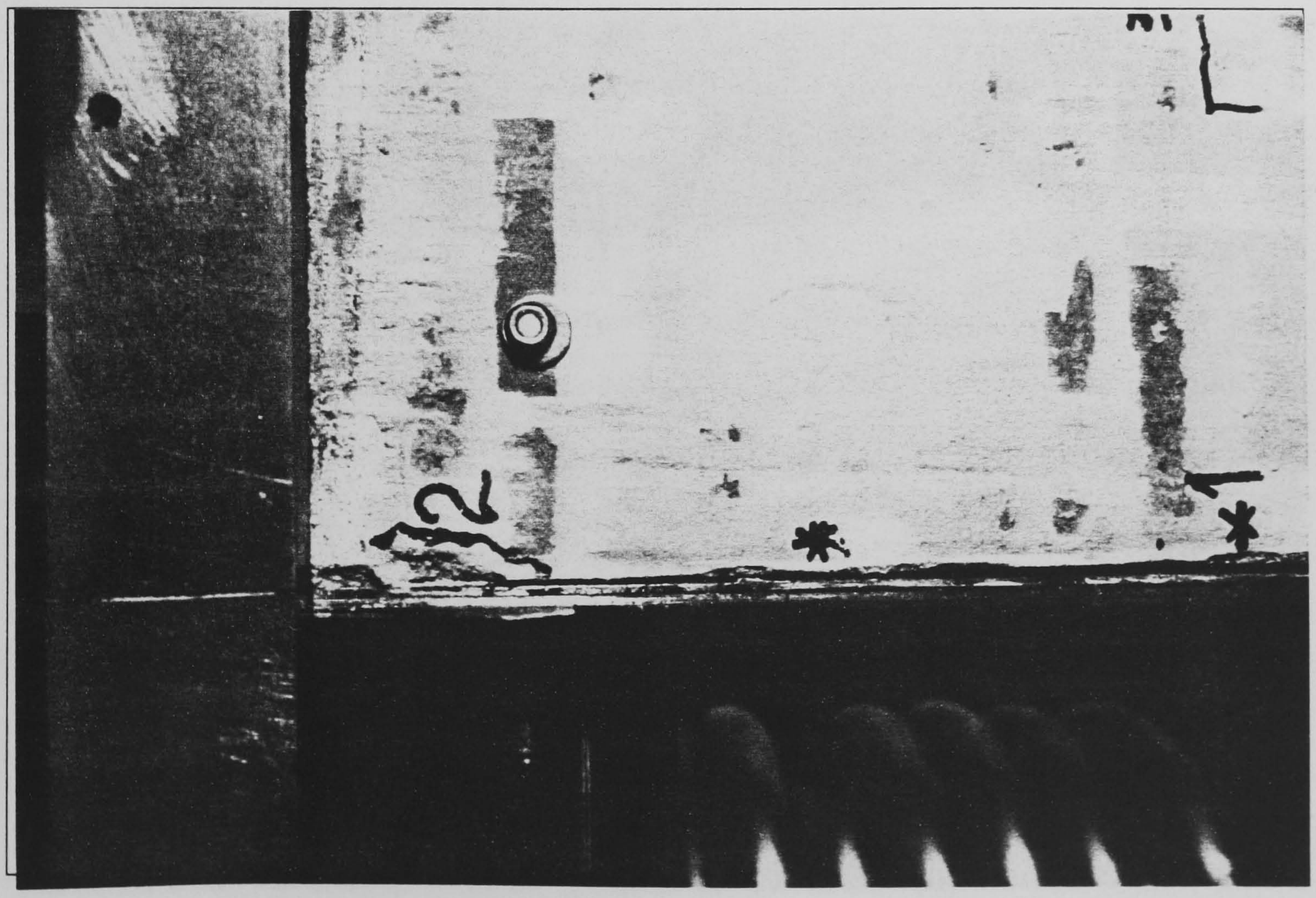

Photo 5.16 Column-panel separation (wall-B)

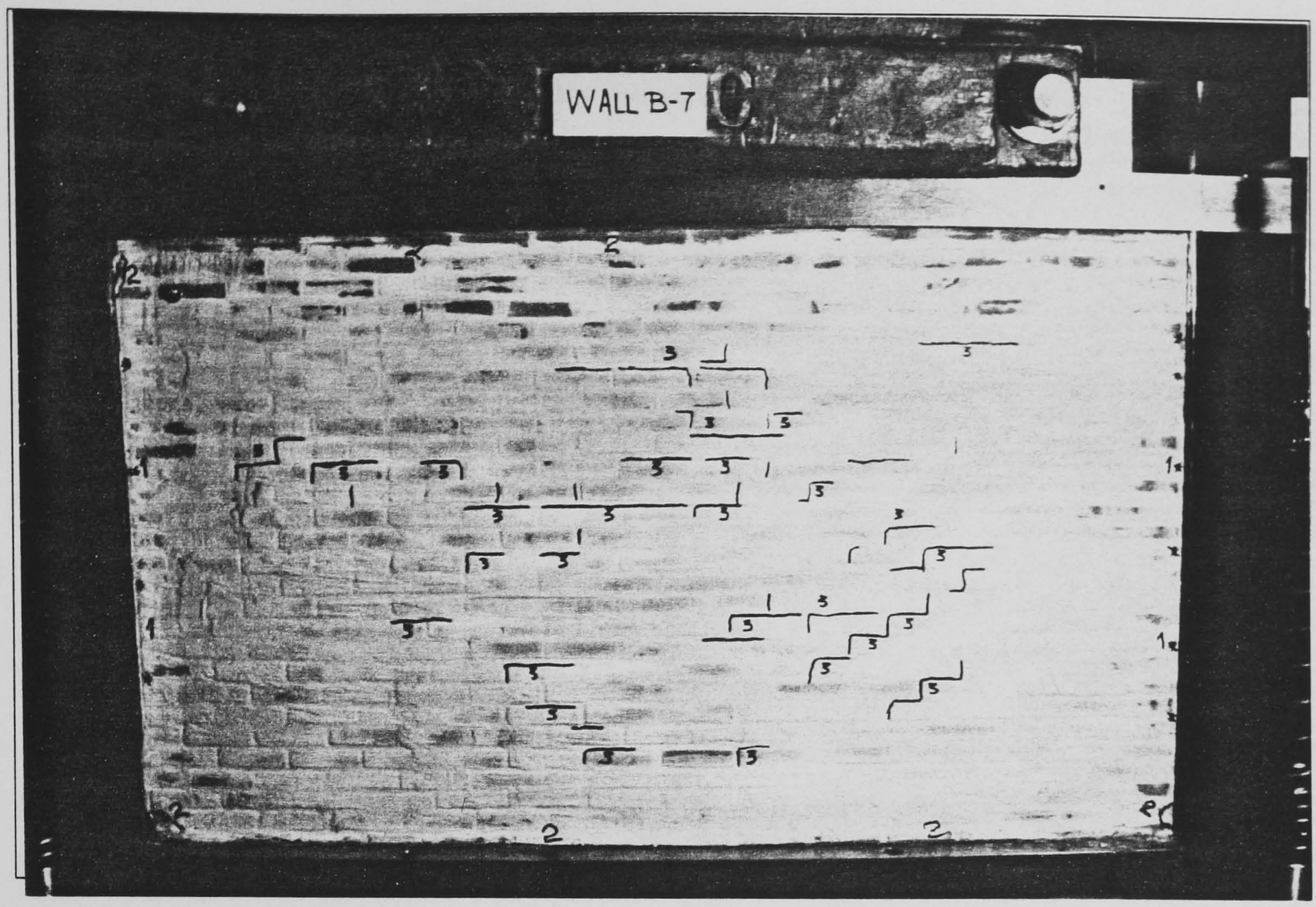

Photo 5.17 Cracking at 0.48g ground acceleration (wall-B)

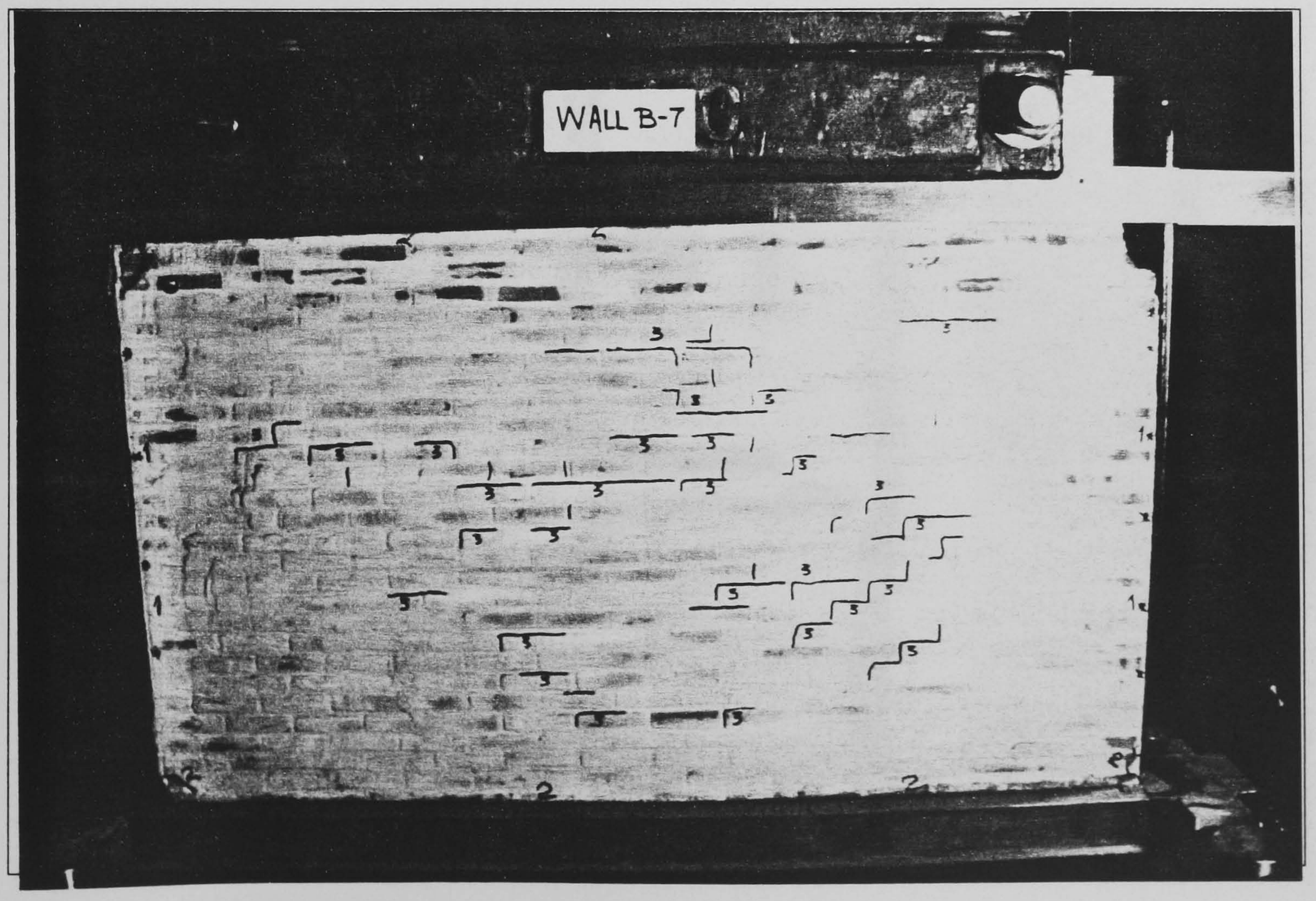

Photo 5.18 Corner crushing failure mode (wall-B)

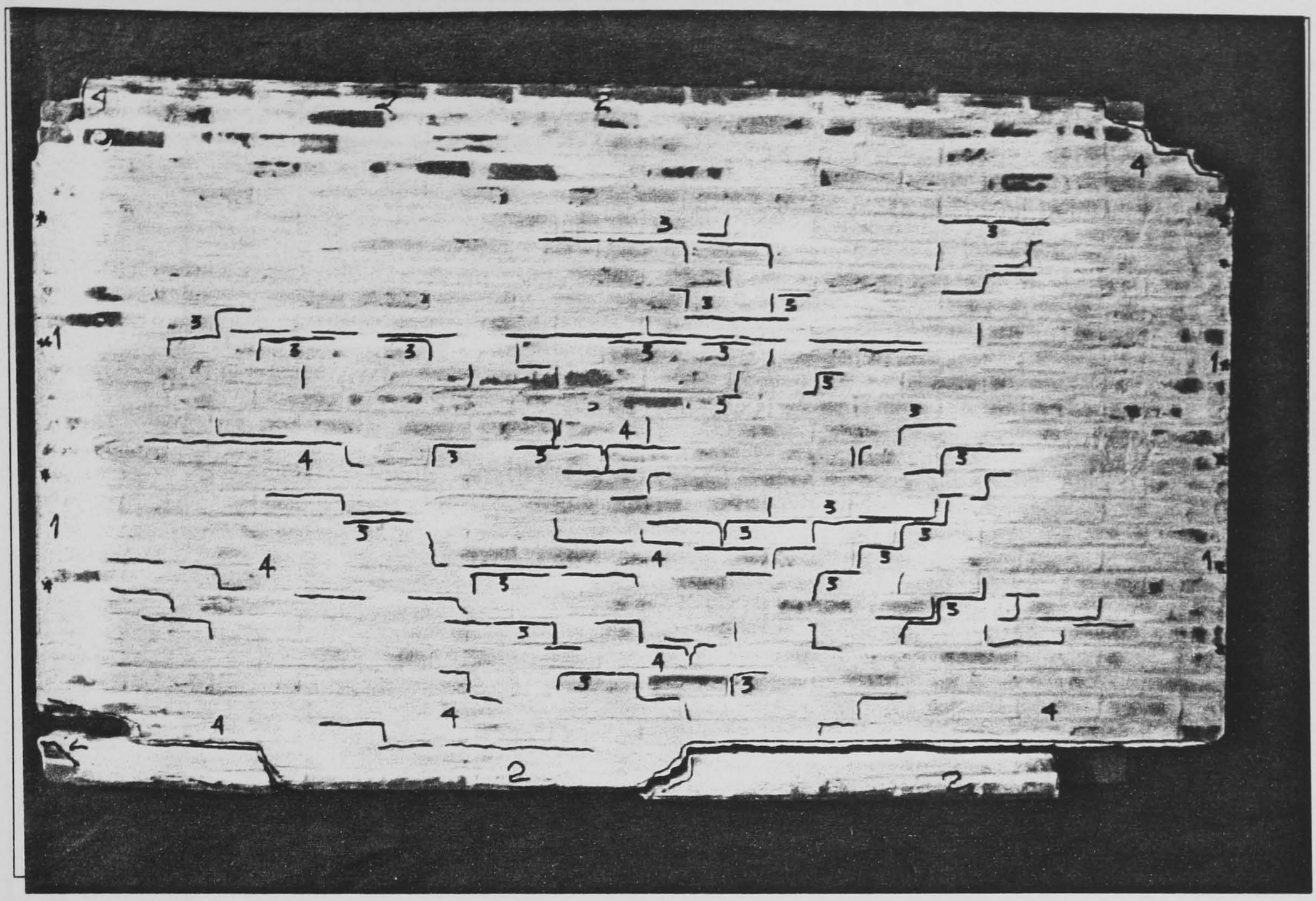

Photo 5.19 Flexural failure after removal of axial force (wall-B)

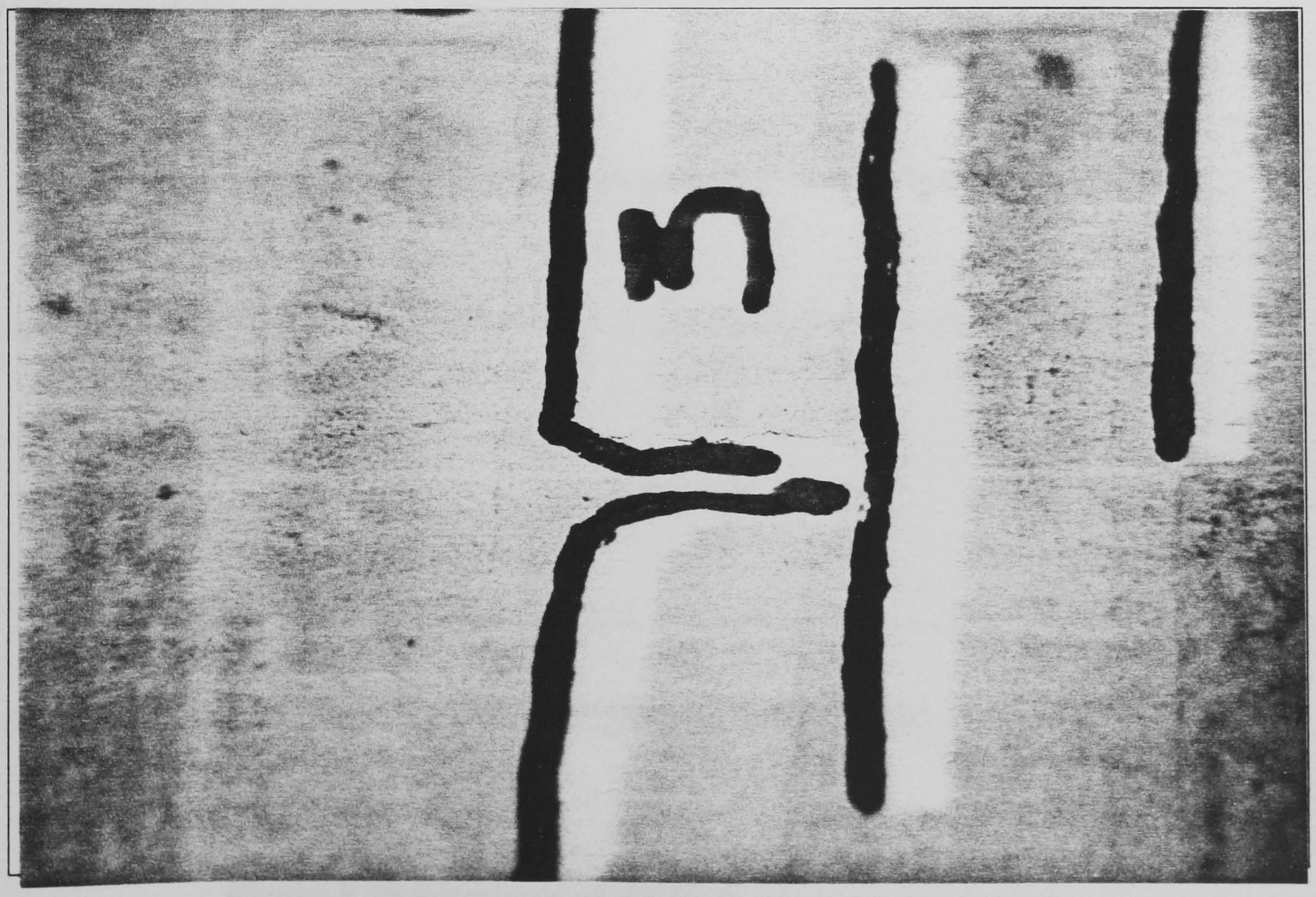

Photo 5.20 Brick-mortar interface microcracking (wall-B)

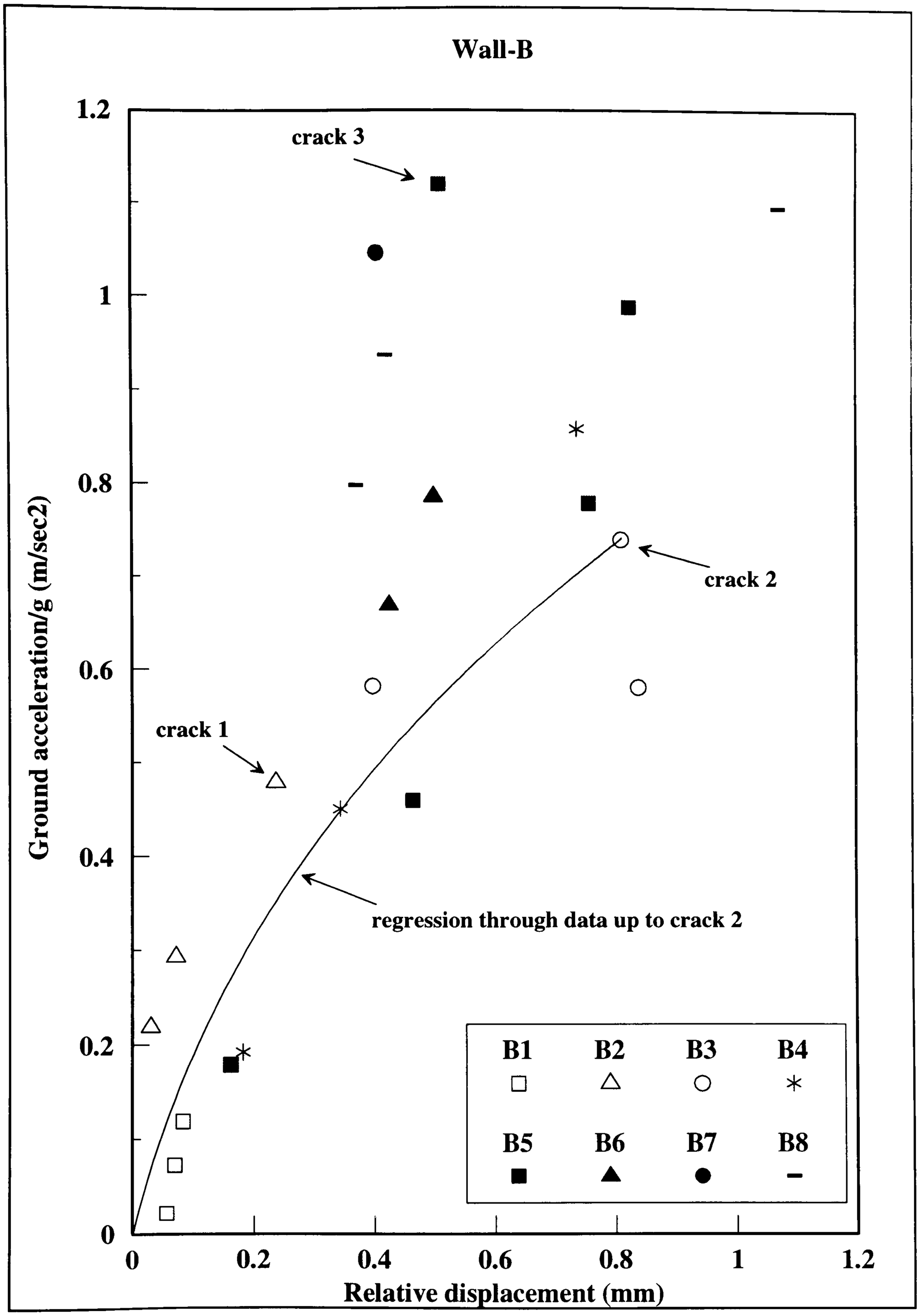

Figure 5.49 Summary of dynamic response for wall-B

5.8.2.1 Observations for wall-B.

The second panel which was also tested at 30 days after casting, was similar to the first one with respect to the compressive and shear strength of the model masonry. The first crack appeared after several low amplitude cycles at the column to panel interface with a ground acceleration of 0.48g (photo 5.16). With increased intensity corner crushing occurred (crack 2), indicating the formation of the compression strut mechanism. Small cracks with no symmetrical pattern were observed in the panel at an acceleration of 1.12g. (photo 5.17). These localised failures are more likely to be a result of the variability in the masonry mechanical properties, mortar gaps resulting from unfilled or unconsolidated joints and shrinkage micro-cracking (photo 5.20). With repeated cycles of the same and higher intensity, typical *compression strut failure* occurred with the two upper corners crushing and falling off the panel (photo 5.18). Since it is this mechanism which is responsible for transferring the applied horizontal load to the masonry panel, no further substantial cracking would have resulted with increased amplitudes of vibration. As a result the axial prestressing force was removed and one more cycle of 0.98g acceleration was applied (B9/R1), which resulted in flexural cracking at the base of the panel with horizontal sliding along the mortar joints (photo 5.19).

The experimentally obtained bond strength for wall-B (couplet shear box test), at the brick-mortar interface was 38% more than wall-O and about double the value measured for the 4 panels. The equivalent viscous damping coefficient reached 11.6% after the appearance of crack 4 (flexural cracking), together with a reduction in the natural frequency value similar to the one observed for wall-O. The *corner crushing* failure mode, is typical for strong masonry panels subjected to cyclic ground loading [Ref. 78]. It eventually separates the infill wall from the bounding frame at and around the corner interface resulting in loss of load transfer. This failure mode rarely occurs for infill panels which are weaker than the surrounding steel or concrete frame, and their contribution to the dynamic and hysteretic behaviour of the system is difficult to assess and quantify.

5.8.3 Third test : wall-D.

Wall-D was primarily subjected to constant driving frequency and increasing ground acceleration excitations. Since this panel was weaker than walls O and B, it was anticipated that cracking would initiate at a lower intensity. Subsequently, it was decided that for the first three stages, only minor increase in the applied ground motion (acceleration) should be applied. Furthermore, measured values for the initial natural frequency, suggested the presence of possible shrinkage micro-cracking in wall-D as in the other five panels, possibly resulting from uneven or inadequate curing as explained earlier in this chapter. This could accelerate the initiation of cracking and in particular diagonal tensile stepwise cracking through the mortar joints or the interface. In the following pages the developing dynamic behaviour has been laid out in detail, in the order shown below.

- ► Free vibration amplitude decay records - hammer tests (figures 5.50 to 5.54).
- ► Displacement records (5.55 to 5.60).
- ► Sample hysteresis curves (5.61 to 5.64).
- ► Photographs of the cracking patterns (photo 5.21 to 5.36).
- ► Summary of dynamic response (figure 5.65).

The test procedure for wall-D is summarised in table 5.7, while results for the first natural frequency using the methods described previously are shown in table 5.6.

Theoretical	**Finite element**	**Hammer test**
58.9 Hz	69.2 Hz	39.06 Hz

Table 5.6 Natural frequency results (initial value) for wall-D

Stage/Run	Table accel.	Driving freq.	Damage	Natural freq.	Damping ratio	Rel. displ.	Comments
	g	Hz	Crack #	Hz	%	mm	
D1/R1	0.073	6.2	-	39.06	4.4	0.019	Constant driv. frequency
D1/R2	0.134	6.2	-	-	-	0.082	
D1/R3	0.24	6.2	-	-	-	0.166	
D2/R1	0.394	7.7	-	-	-	0.2	Constant driv. frequency
D2/R2	0.514	7.7	**1**	-	-	0.595	**Column separation Minor horizontal cracking near the base**
D2/R3	0.879	7.7	**2**	-	-	0.854	
D3/R1	0.268	9.4	-	-	-	0.357	Constant driv. frequency
D3/R2	0.321	9.4	-	-	-	0.471	
D3/R3	0.406	9.4	-	-	-	0.726	
D4/R1	0.6	-	**3 / 4**	24.6	5.2	-	Top LVDT failure-no data **Stepwise diagonal tensile cracking**
D5/R1	0.7	-	**5**	20.95	7.5	-	Top LVDT failure-no data **Extension of crack 5 towards the corner**
D6/R1	0.82	9.8	**6**	20.83	7.9	0.877	**First diagonal crack complete, formation of second diagonal crack**
D7/R1	1.608	7.9	**7**	18.51	9.7	1.21	**Second diagonal crack extended to the corners, corner cracking, widening of first diagonal crack**
D8/R1	1.563	7.9	-	-	-	1.599	**Collapse**

(Crack numbers correspond to the cracking as noted in the photographs)

(Although shaking table displacement was measured during stages D4 and D5, the top LVDTs failed and no results were available).

Table 5.7 Wall-D testing sequence

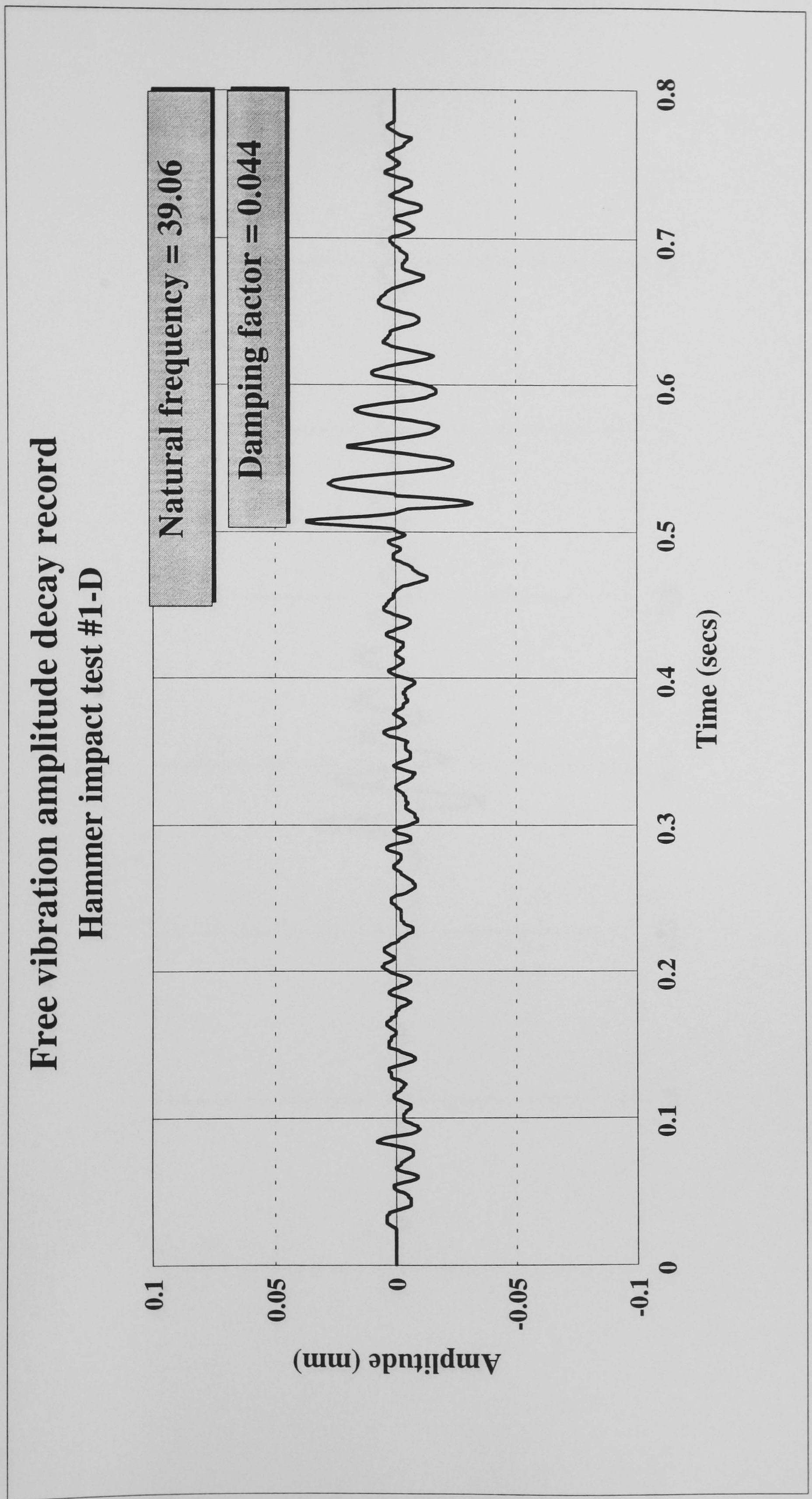

Figure 5.50 Initial free vibration amplitude decay

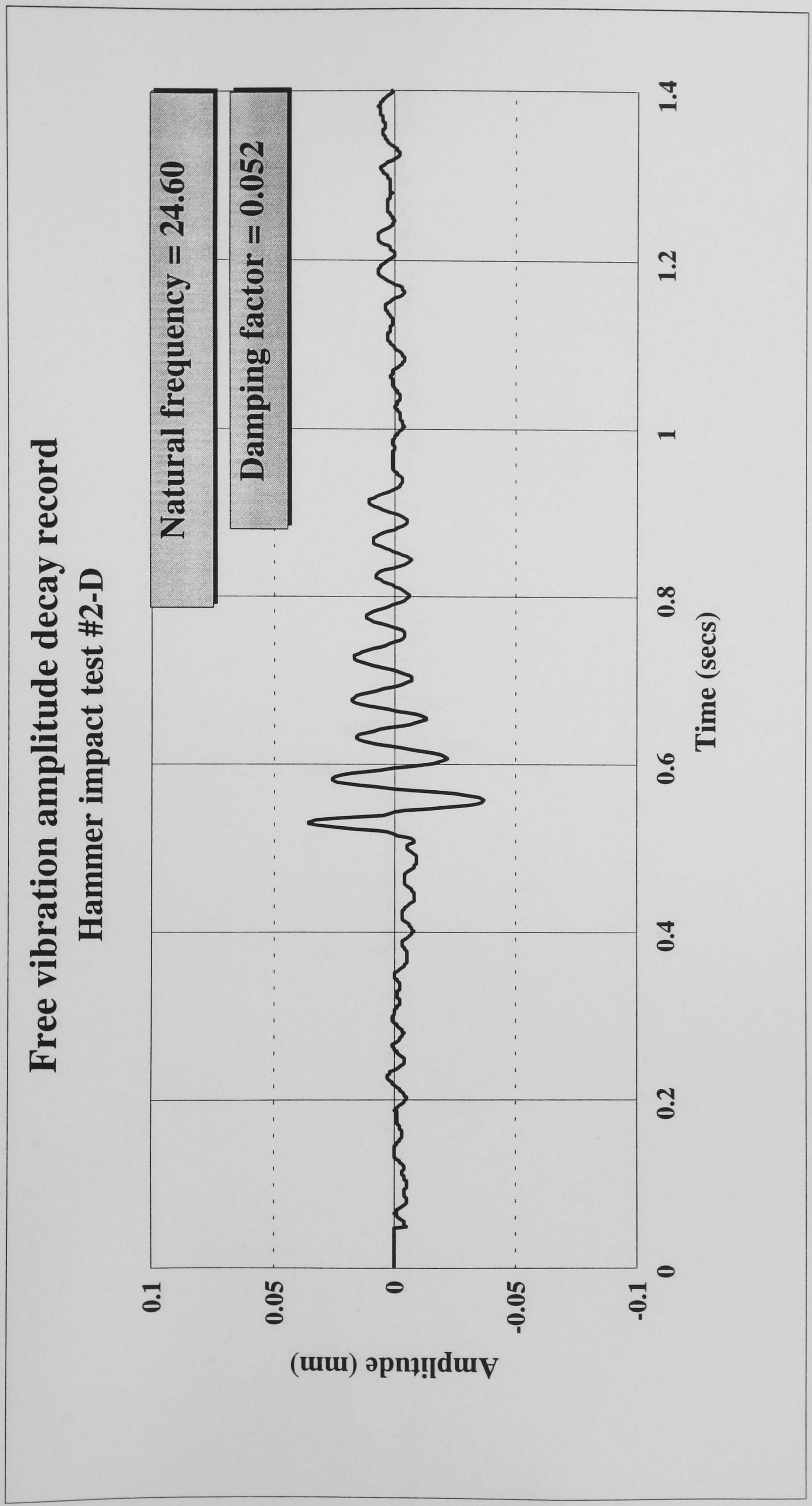

Figure 5.51 Free vibration amplitude decay after crack 4

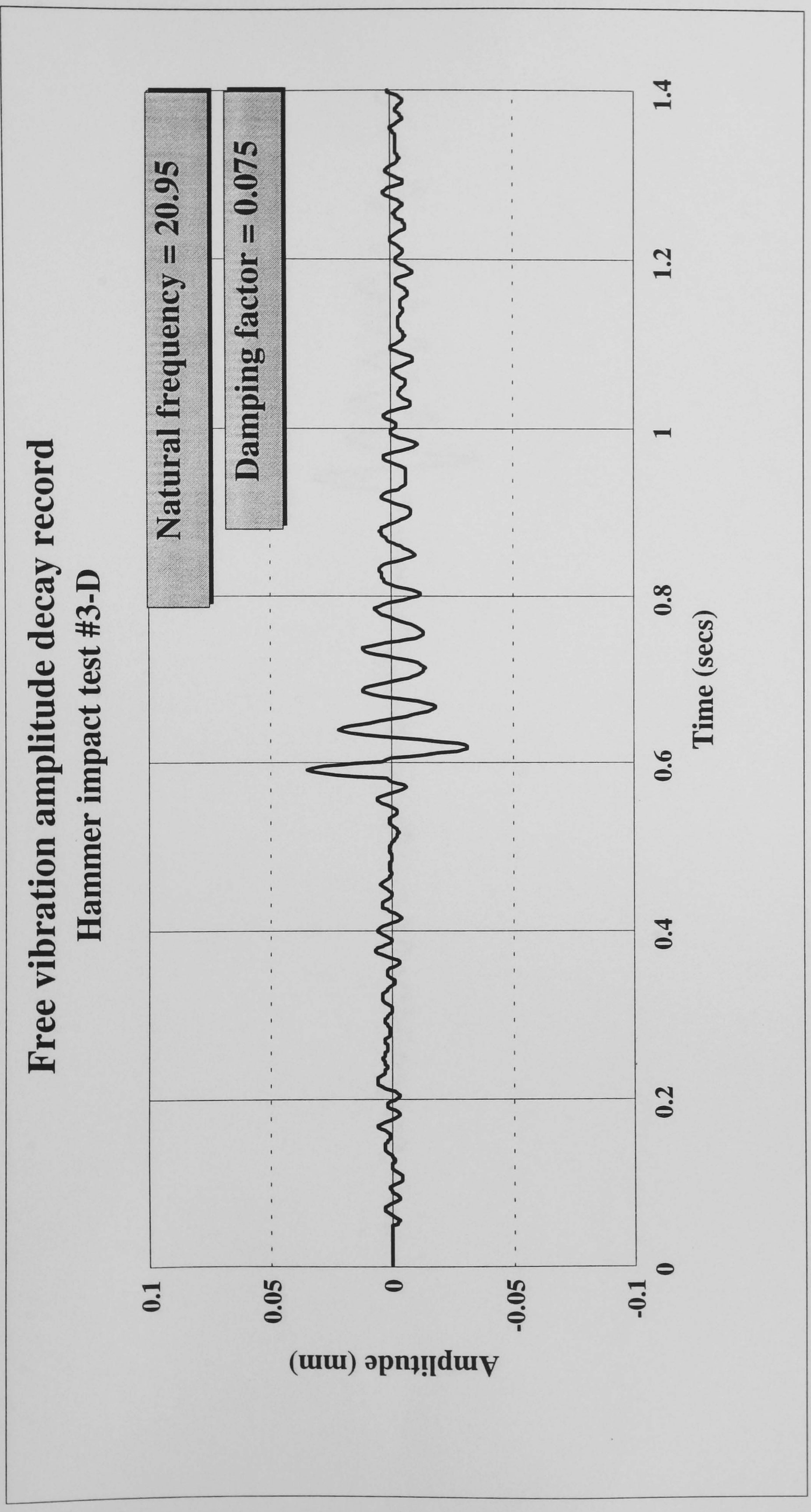

Figure 5.52 Free vibration amplitude decay after crack 5

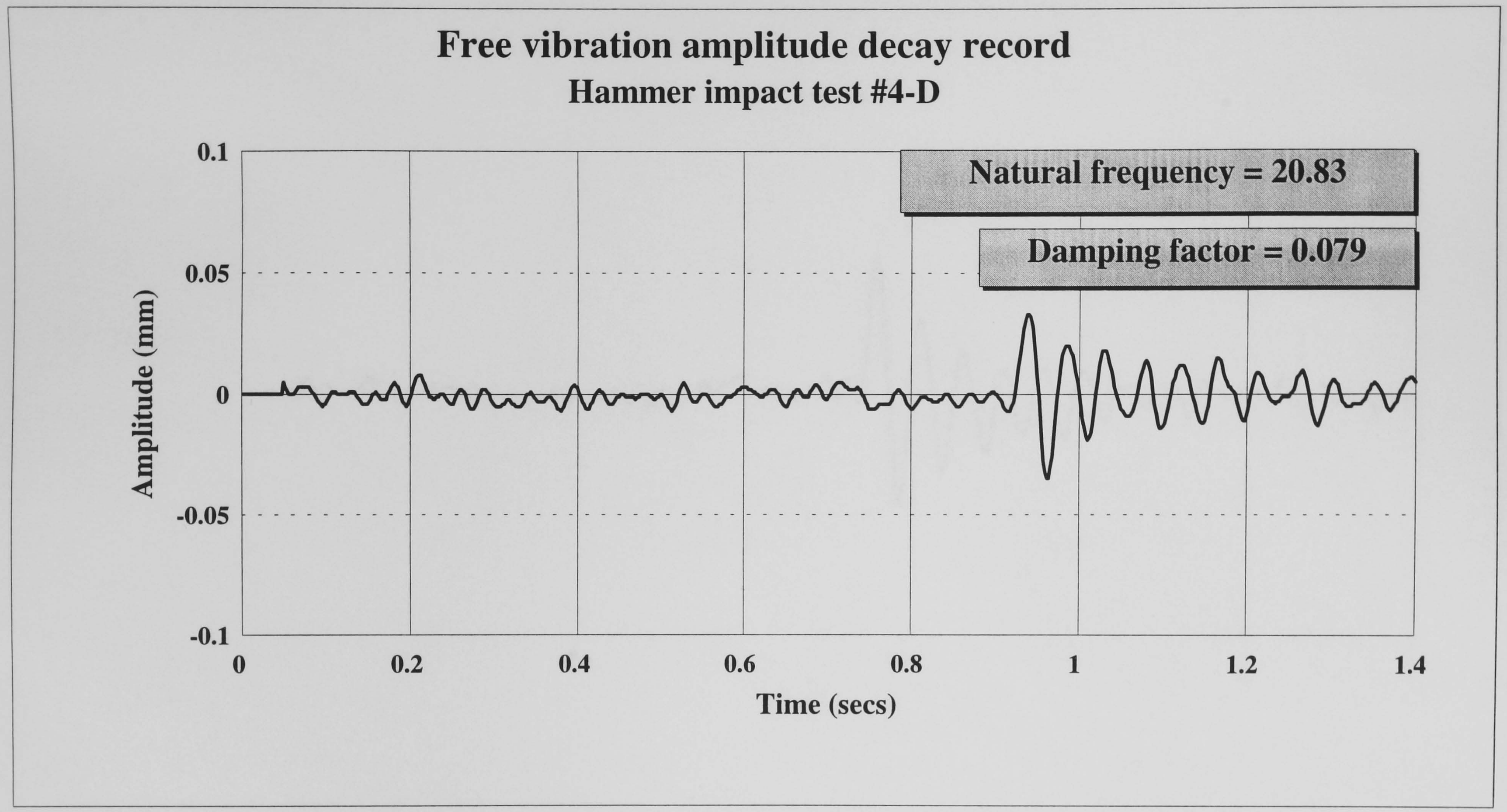

Figure 5.53 Free vibration amplitude decay after crack 6

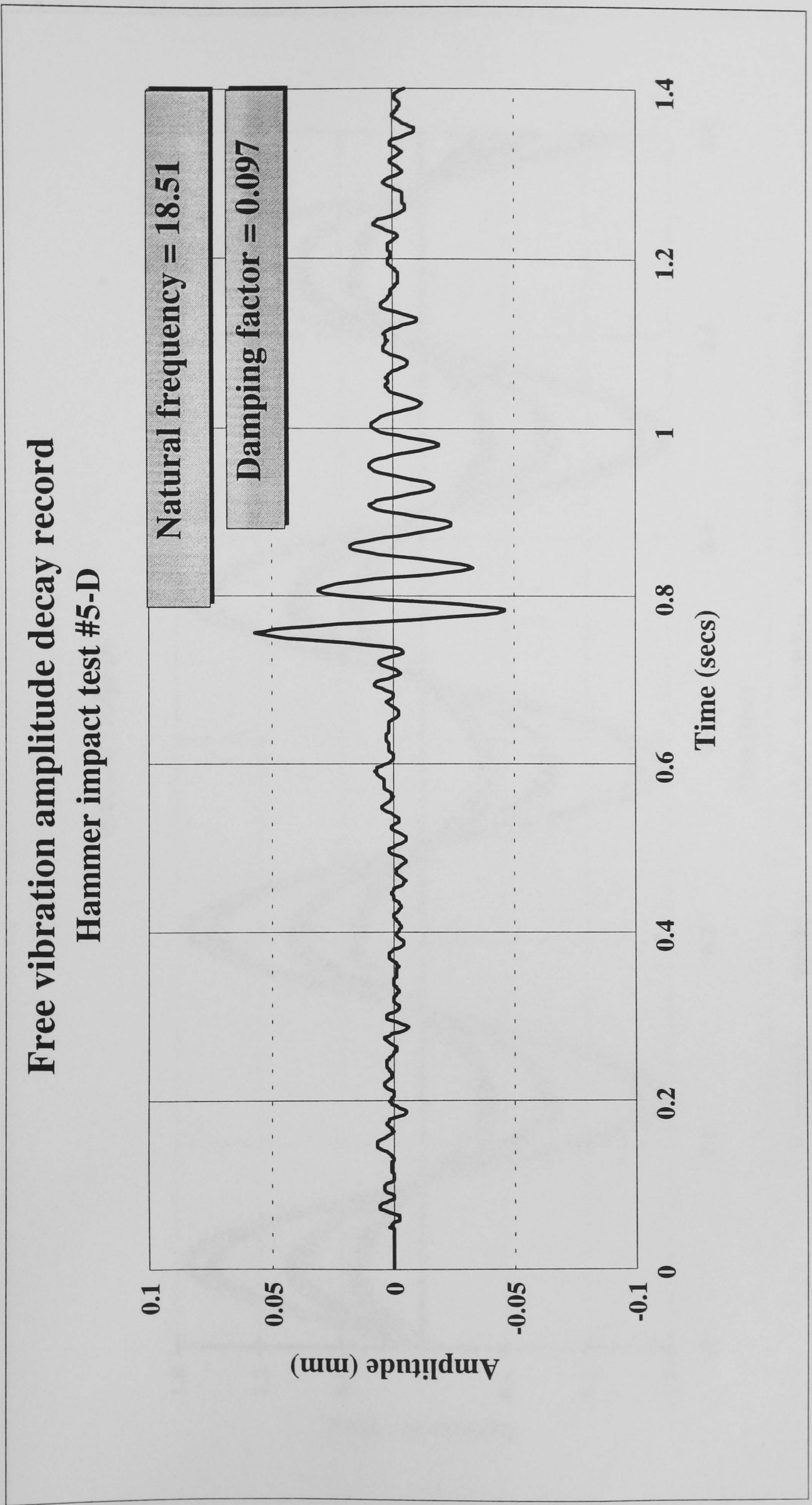

Figure 5.54 Free vibration amplitude decay after crack 7

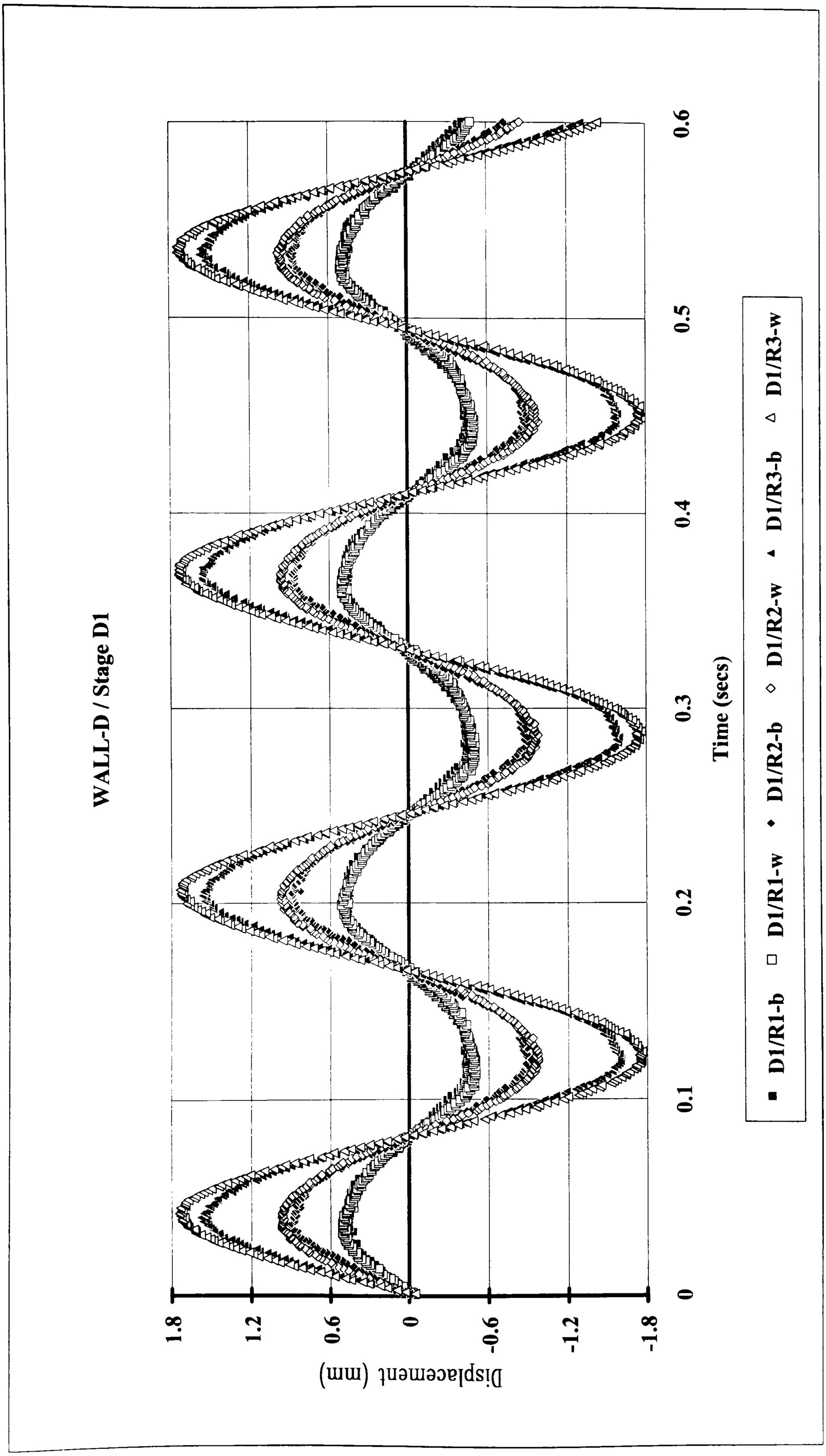

Figure 5.55 Wall-D / Stage D1

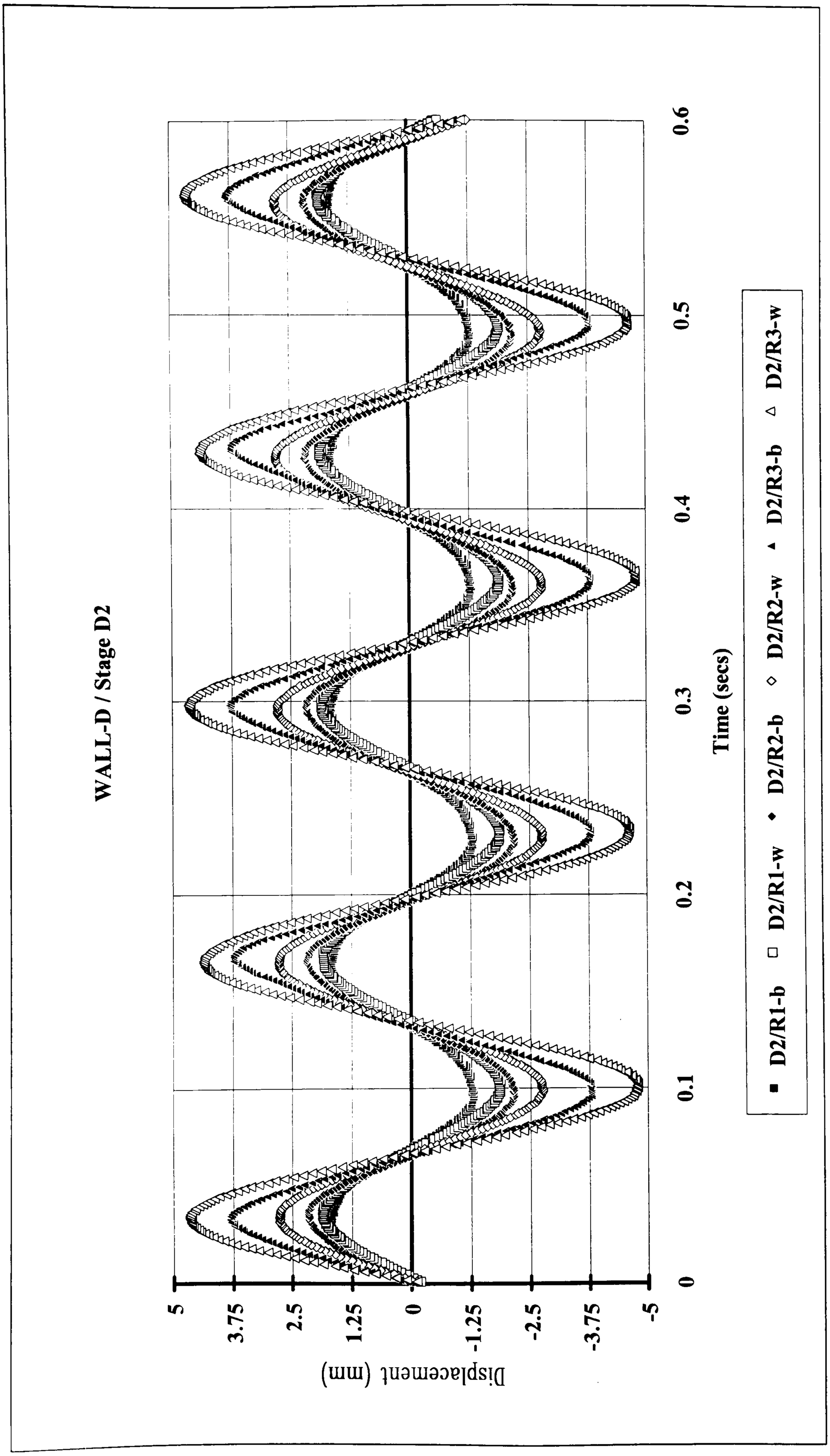

Figure 5.56 Wall-D / Stage D2

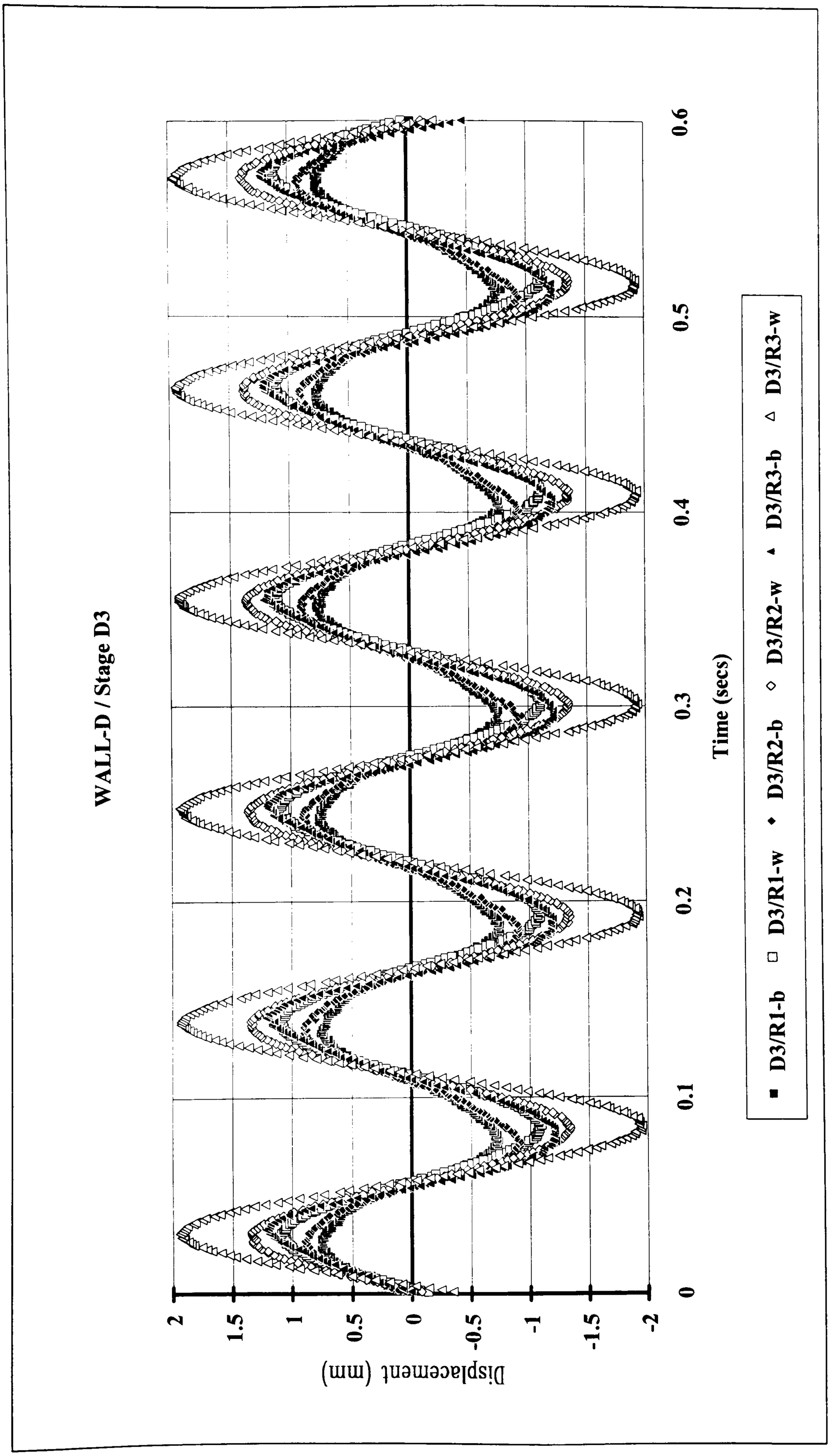

Figure 5.57 Wall-D / Stage D3

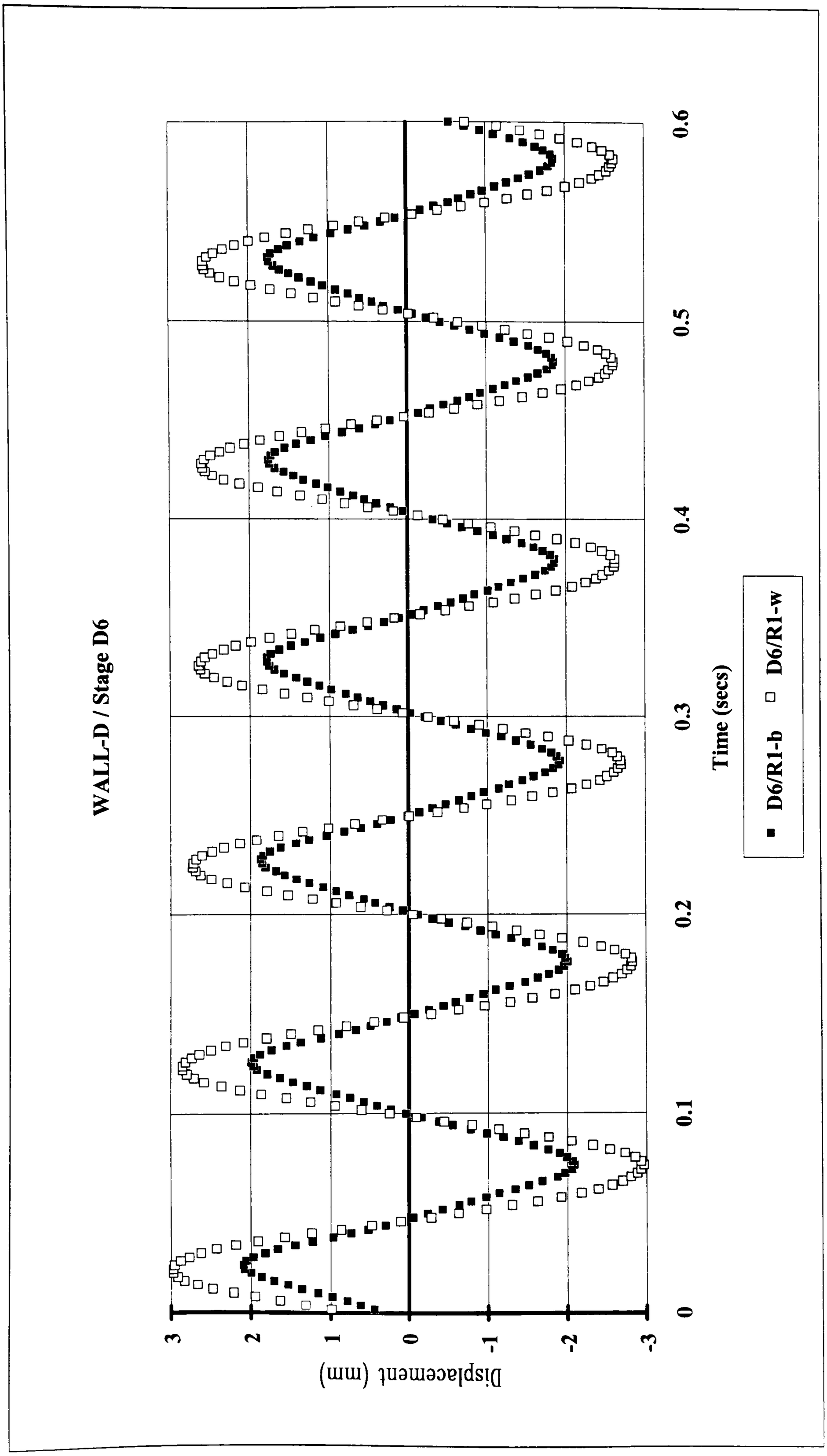

Figure 5.58 Wall-D / Stage D6

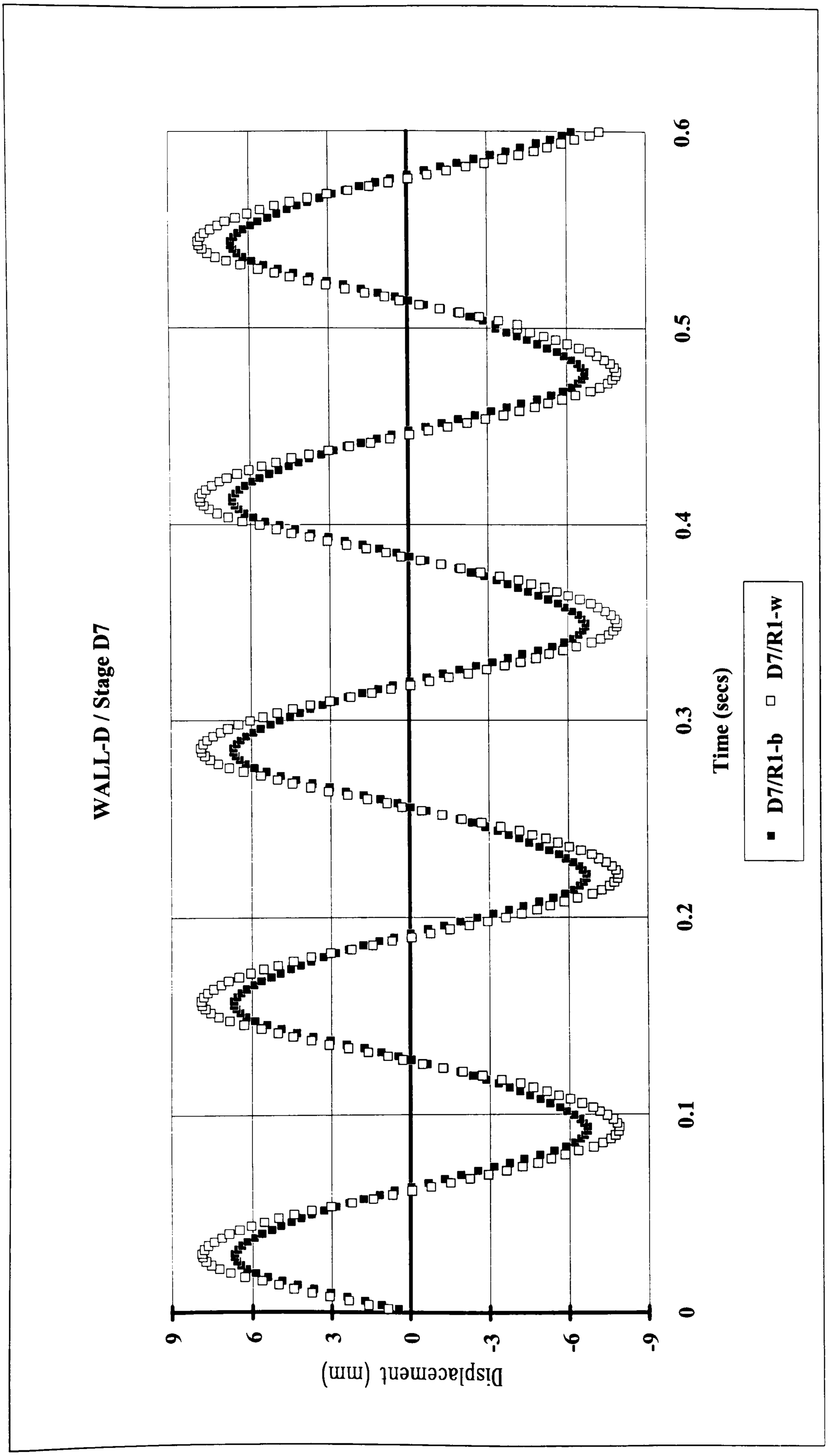

Figure 5.59 Wall-D / Stage D7

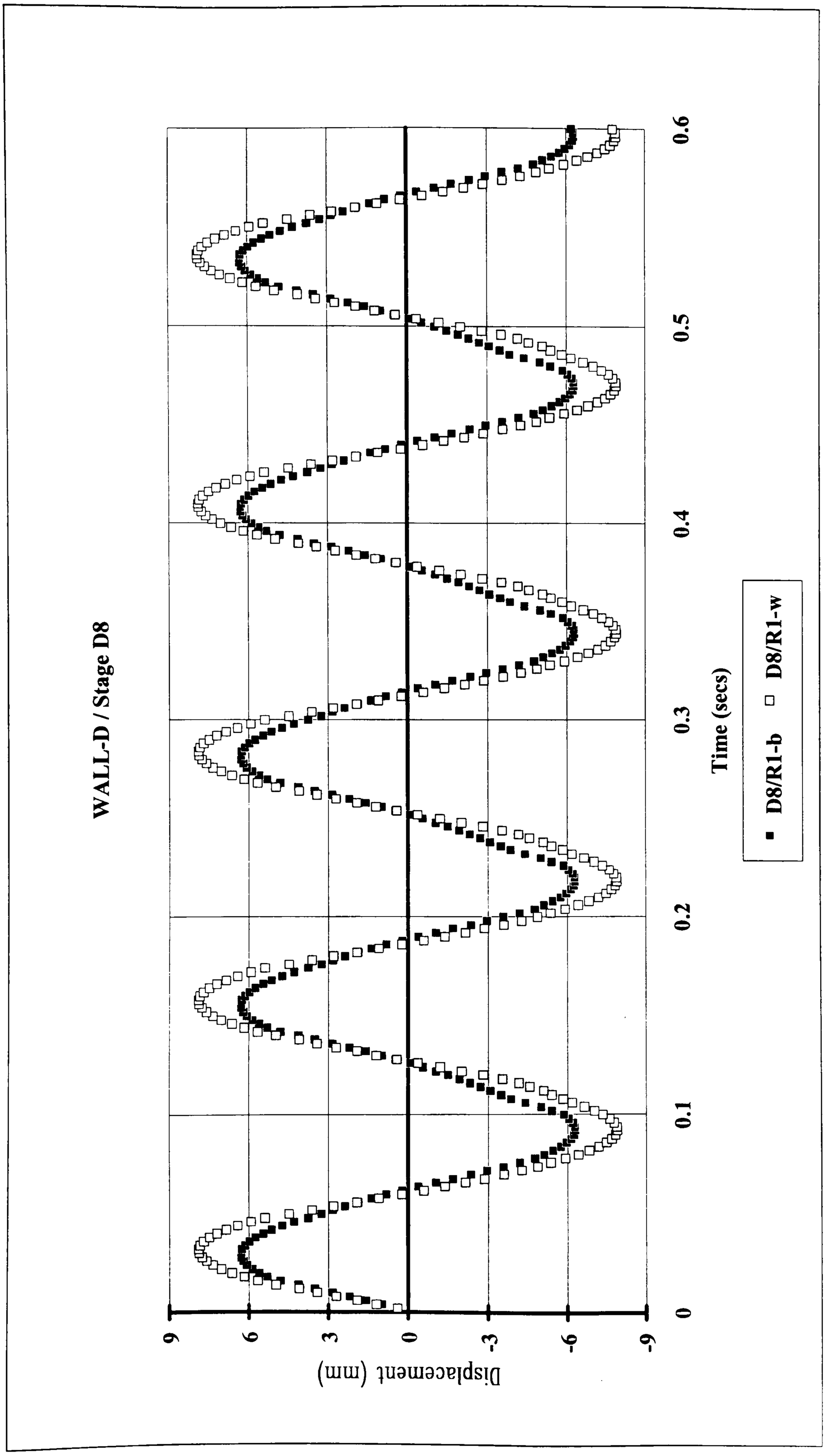

Figure 5.60 Wall-D / Stage D8

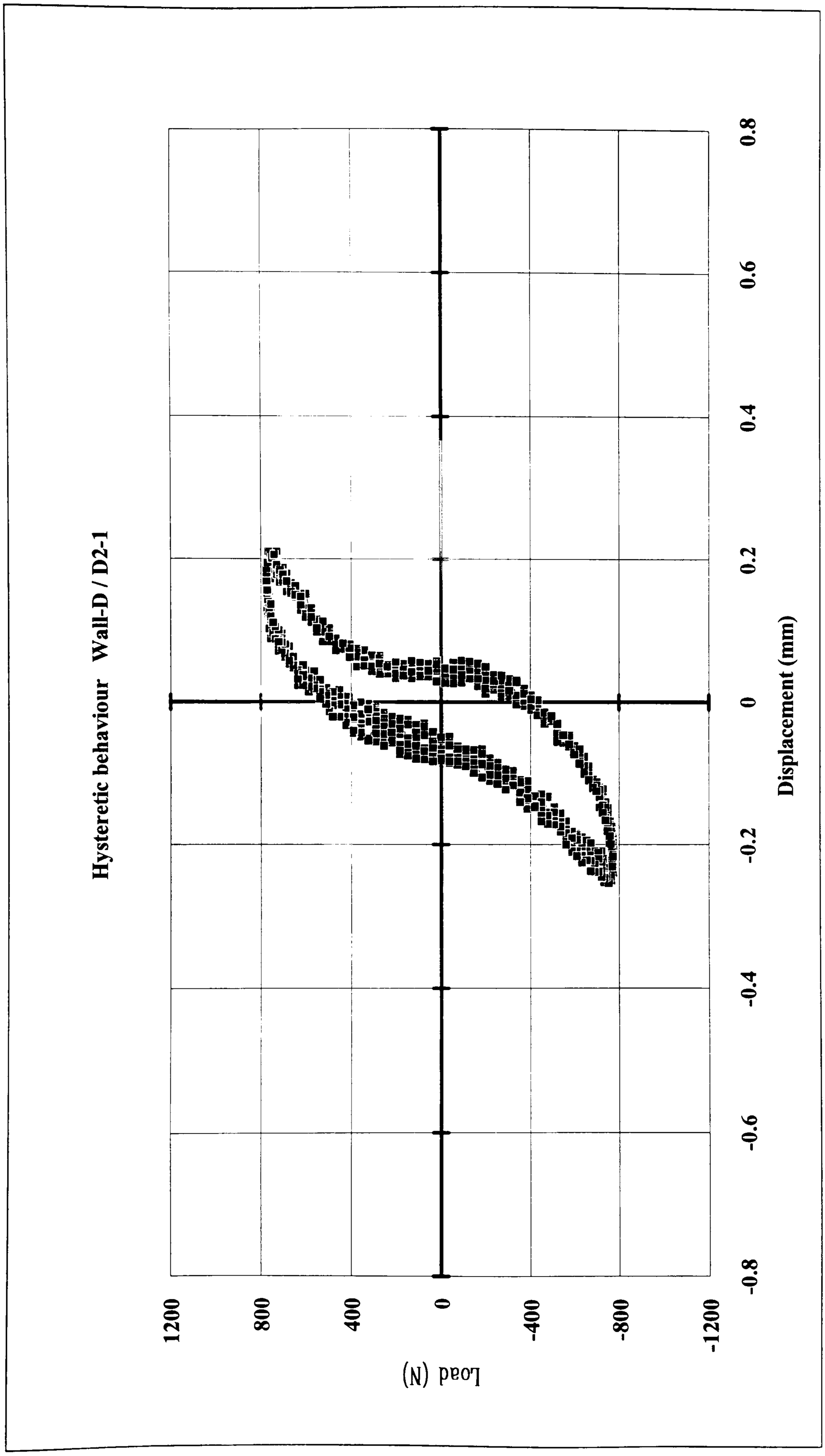

Figure 5.61 Wall-D / Hysteretic Behaviour - Stage D2/R1

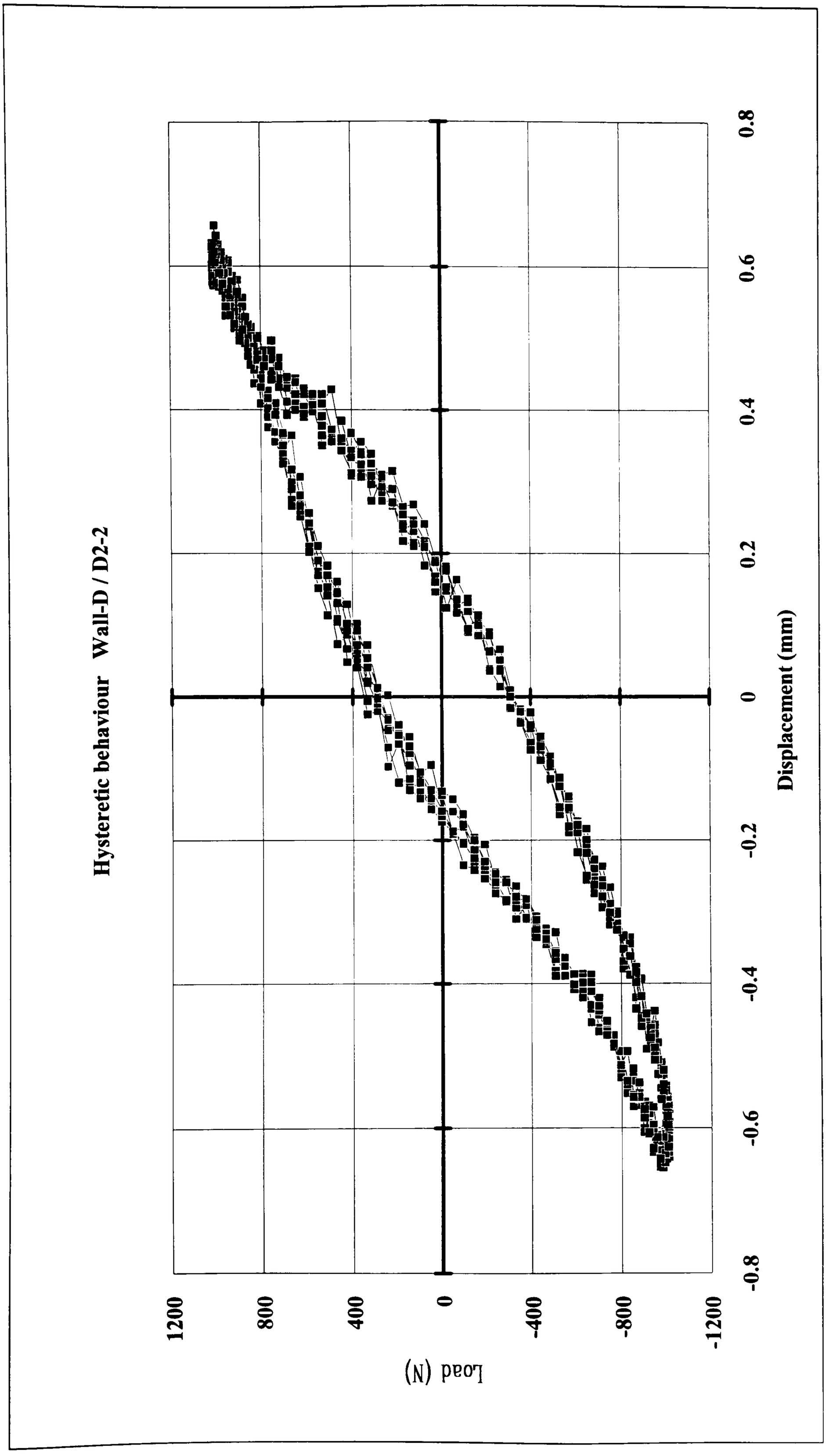

Figure 5.62 Wall-D / Hysteretic Behaviour - Stage D2/R2

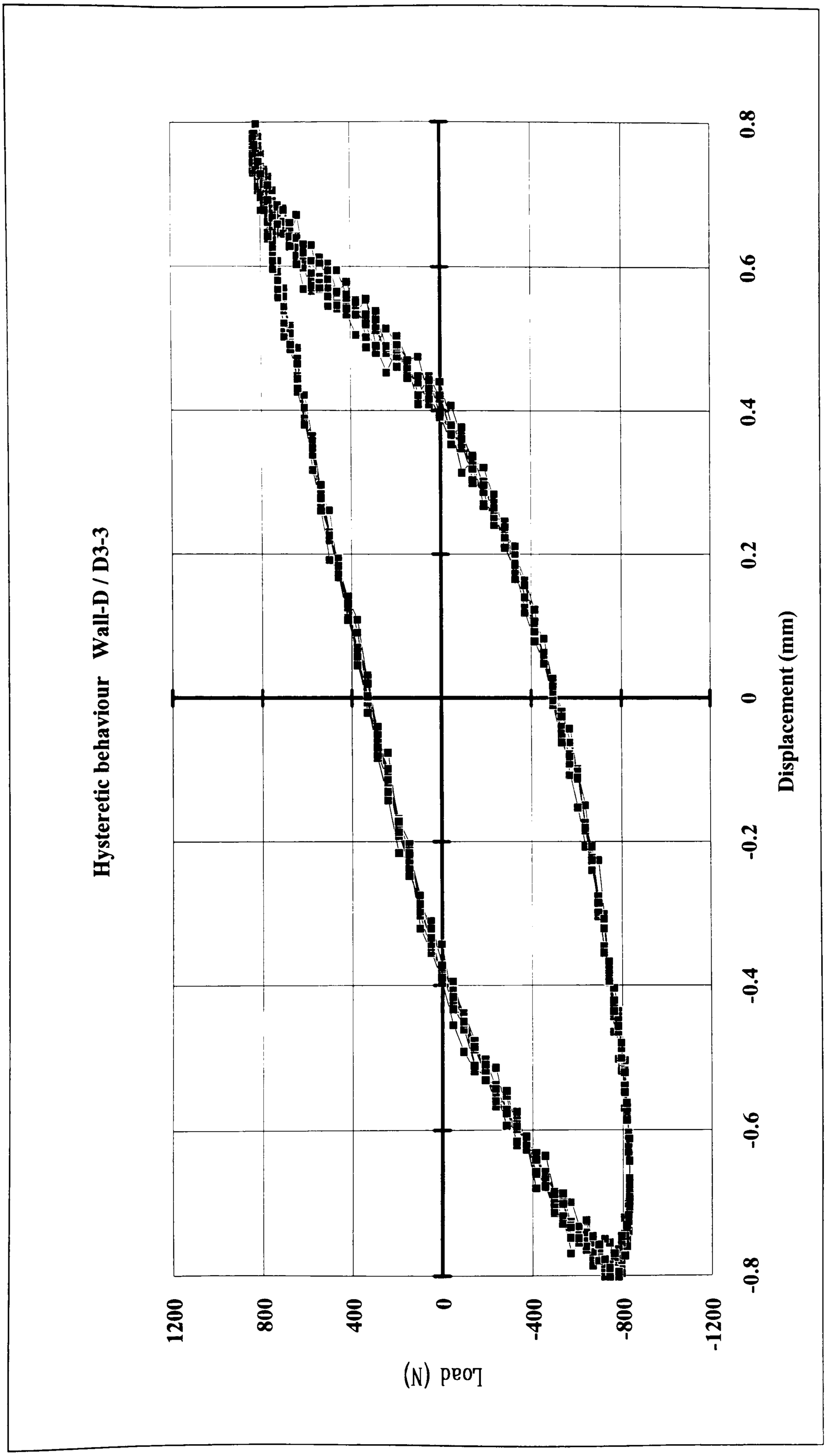

Figure 5.64 Wall-D / Hysteretic Behaviour - Stage D3/R3

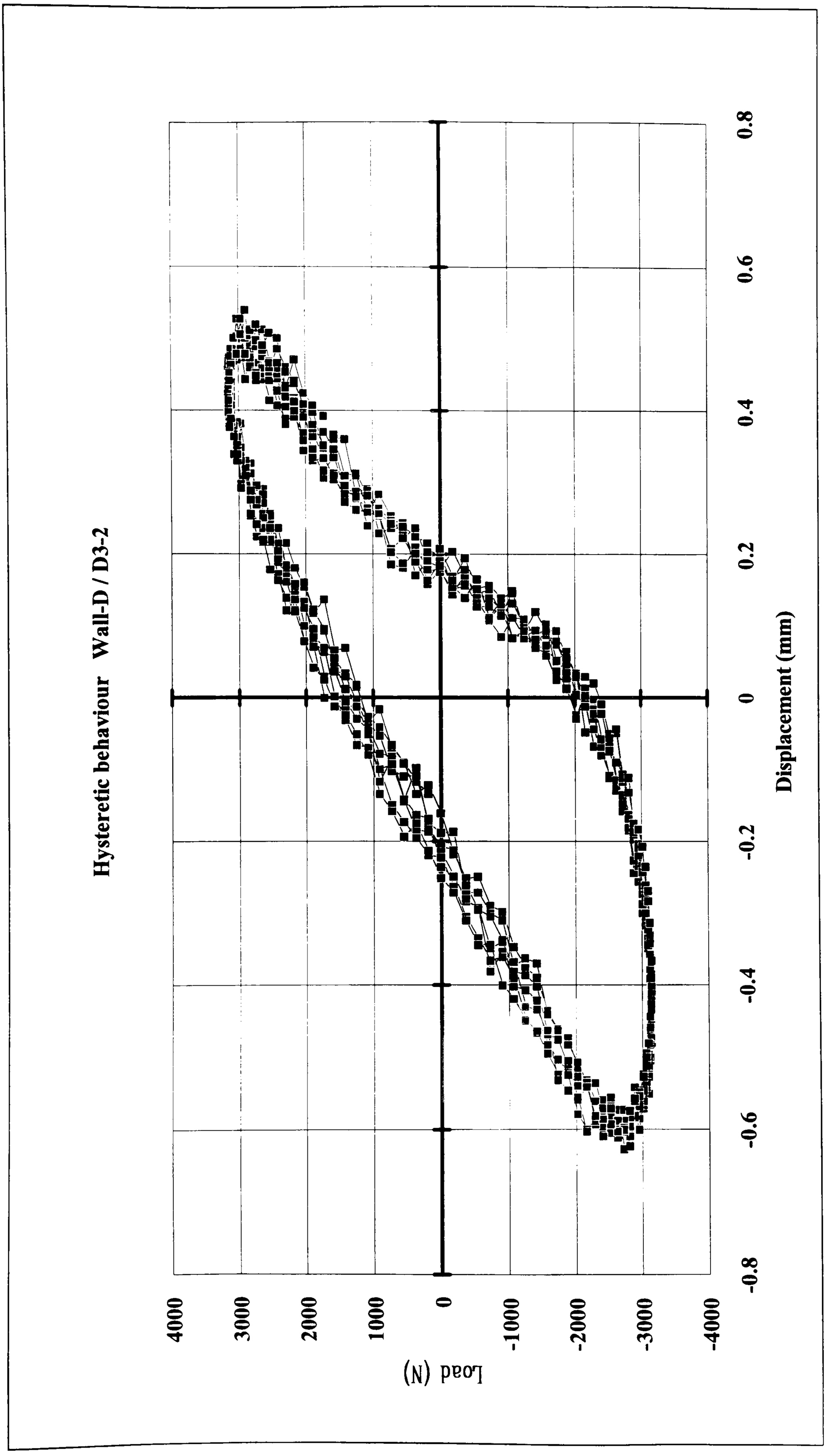

Figure 5.63 Wall-D / Hysteretic behaviour - Stage D3/R2

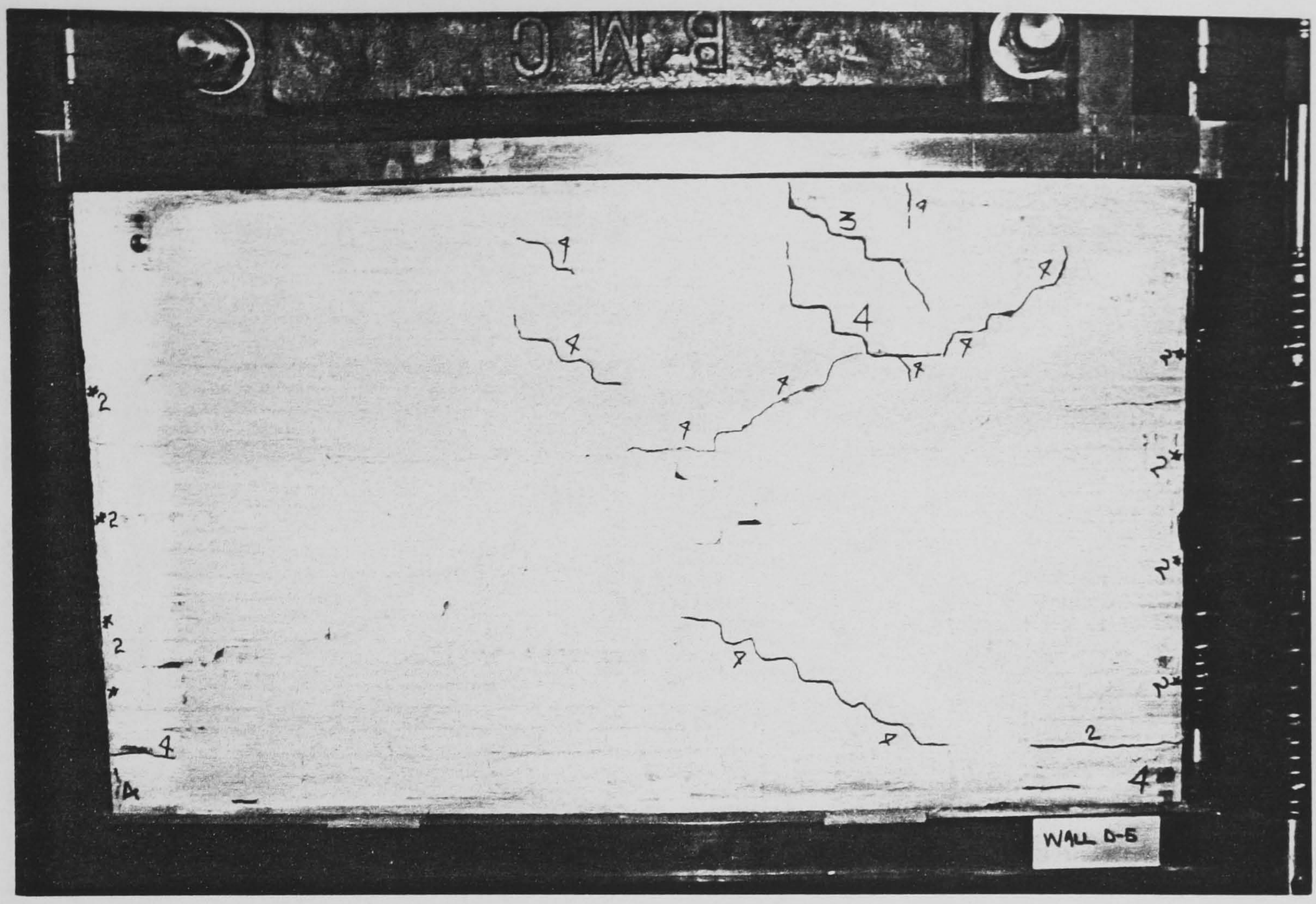

Photo 5.21 Wall-D initial cracking pattern

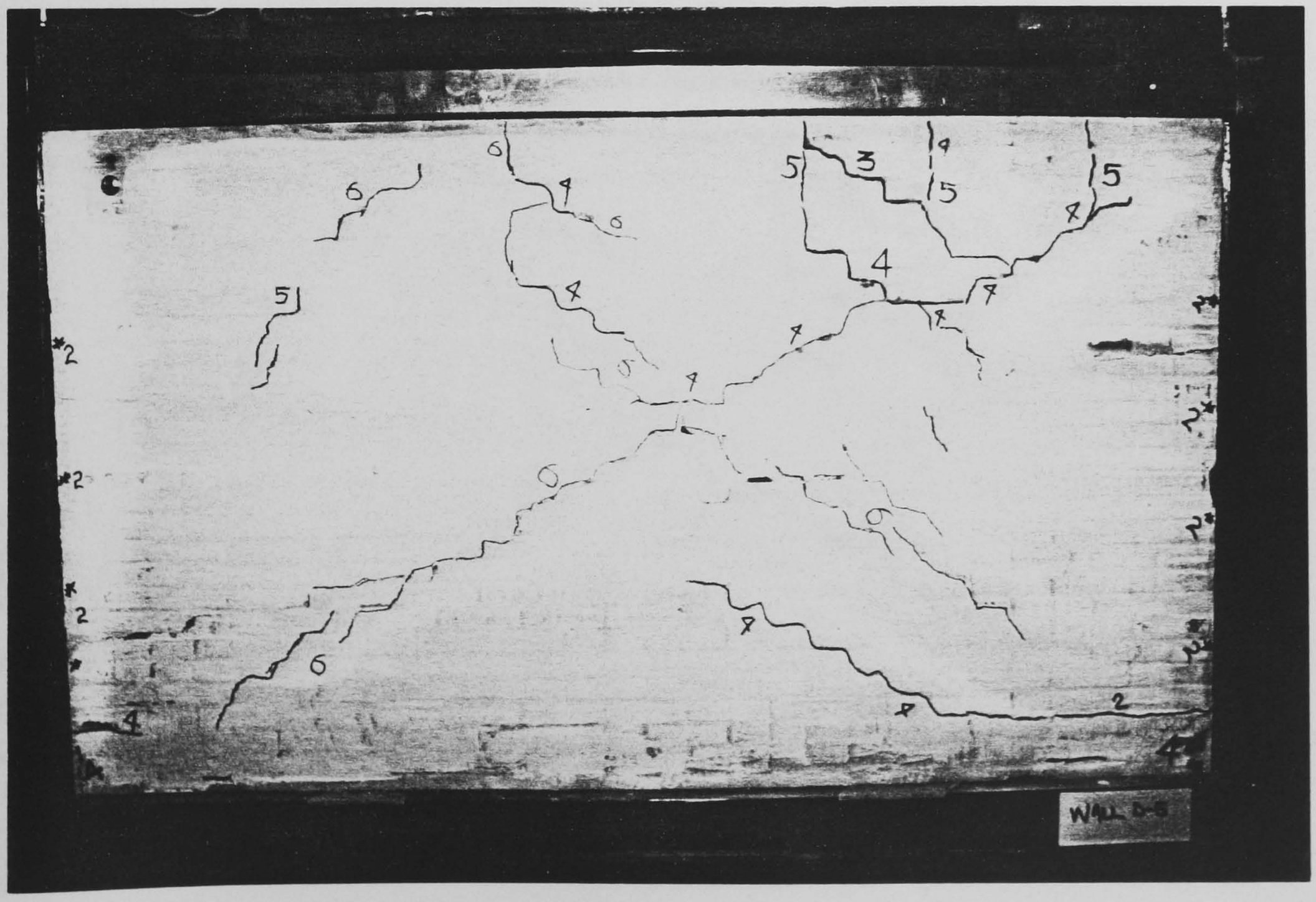

Photo 5.22 Formation of diagonal shear crack (wall-D)

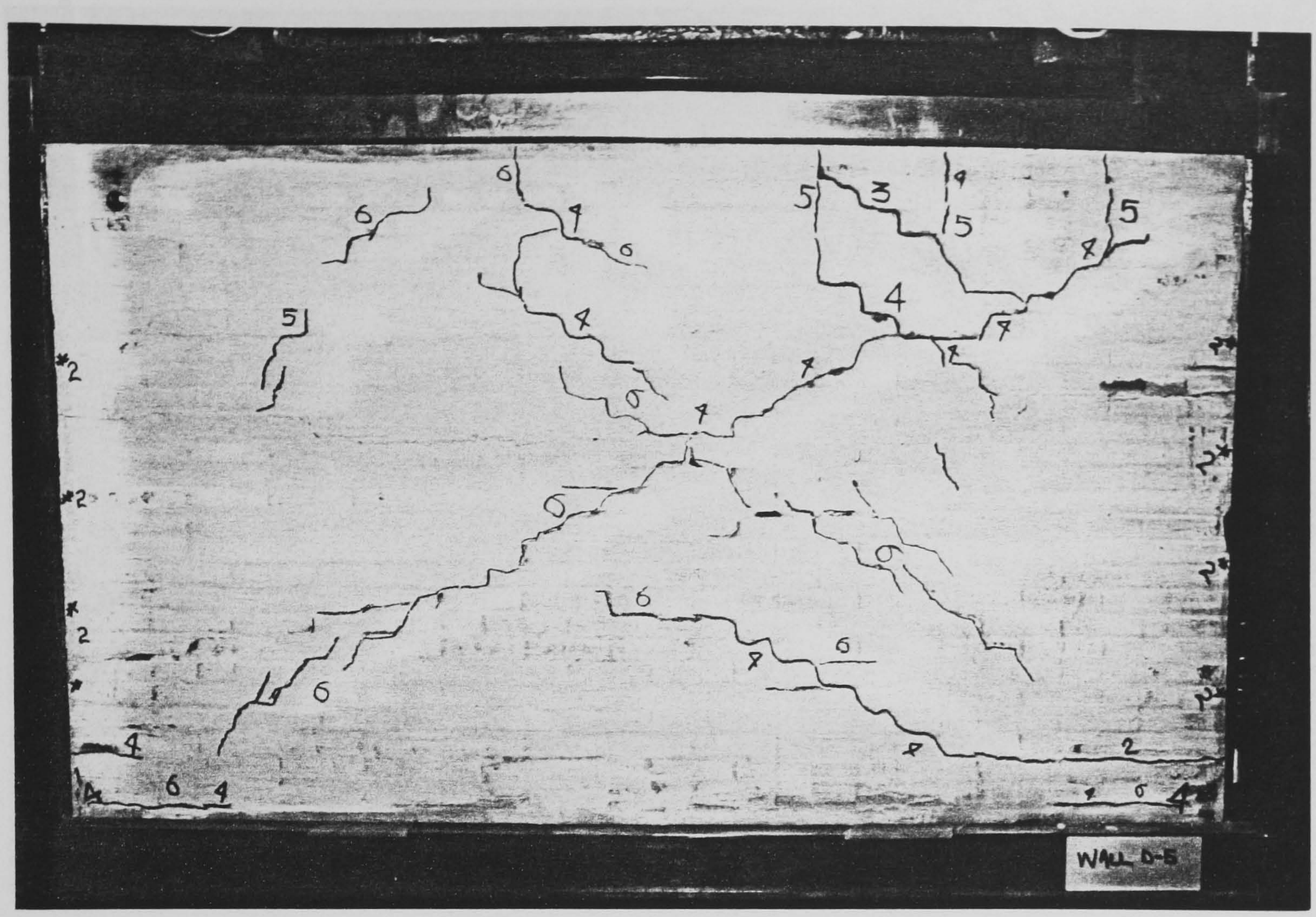

Photo 5.23 Diagonal and limited flexural cracking at the base (wall-D)

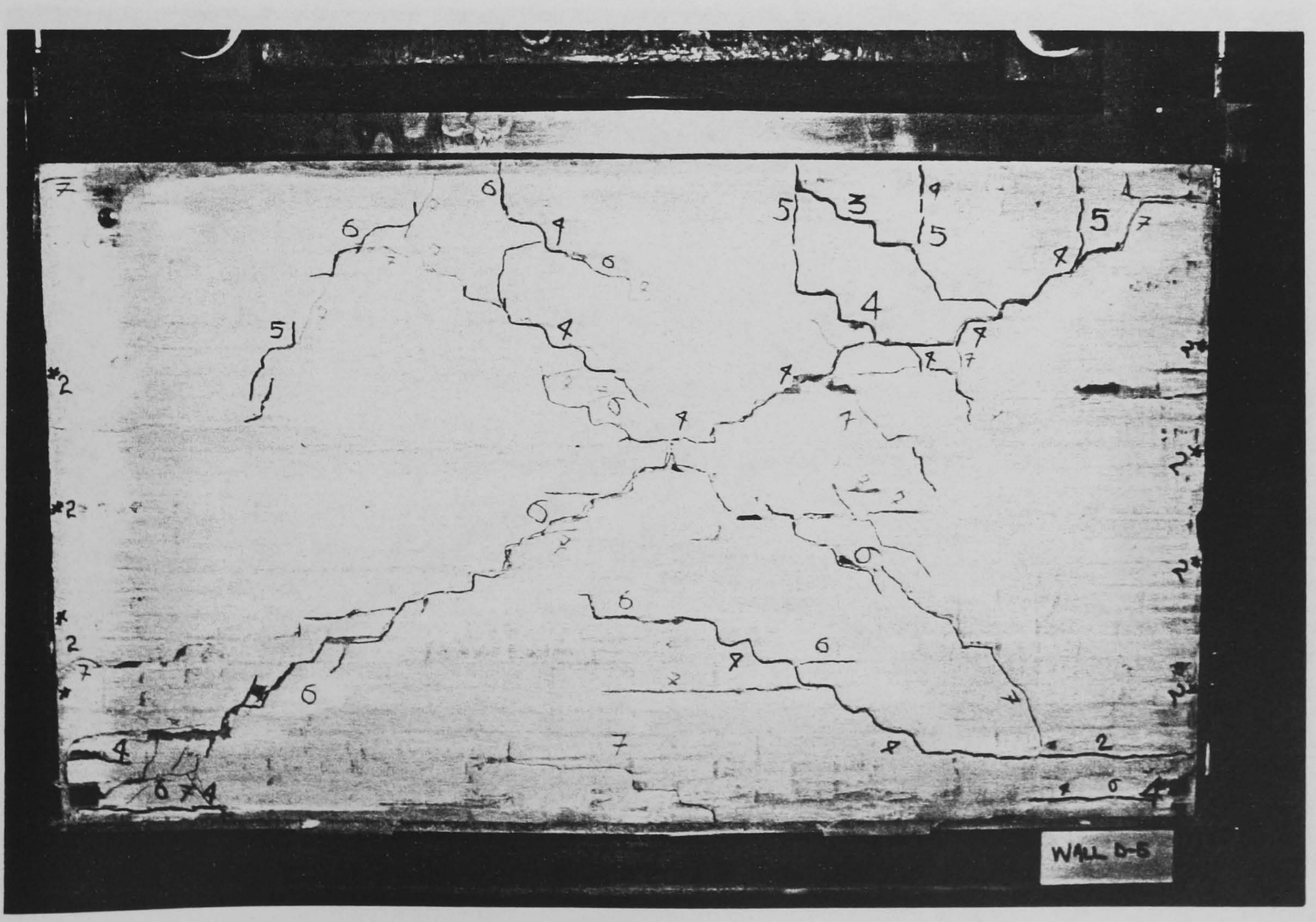

Photo 5.24 Crack 7 and formation of second diagonal crack (wall-D)

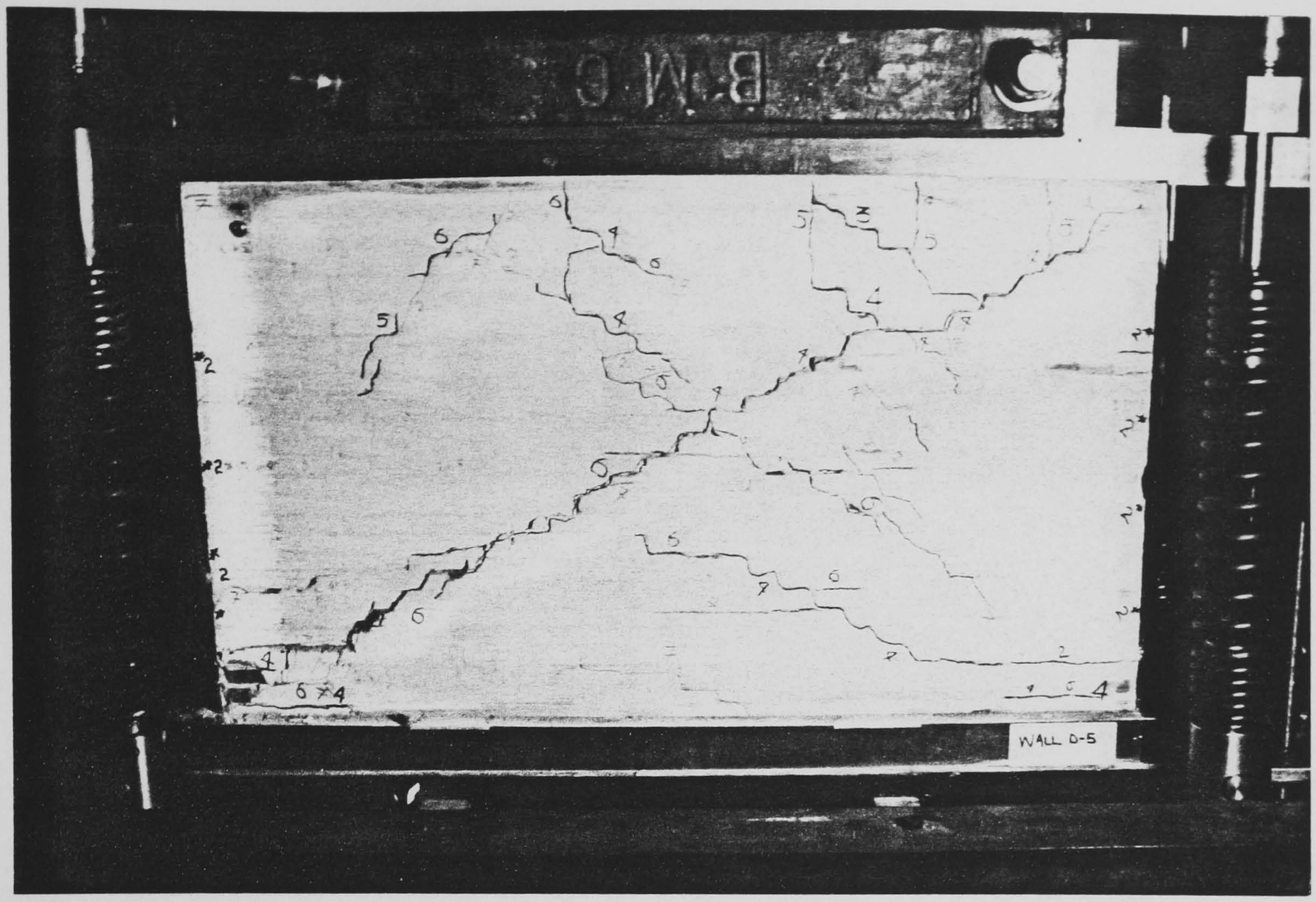

Photo 5.25 Collapse sequence-frame 1 (wall-D)

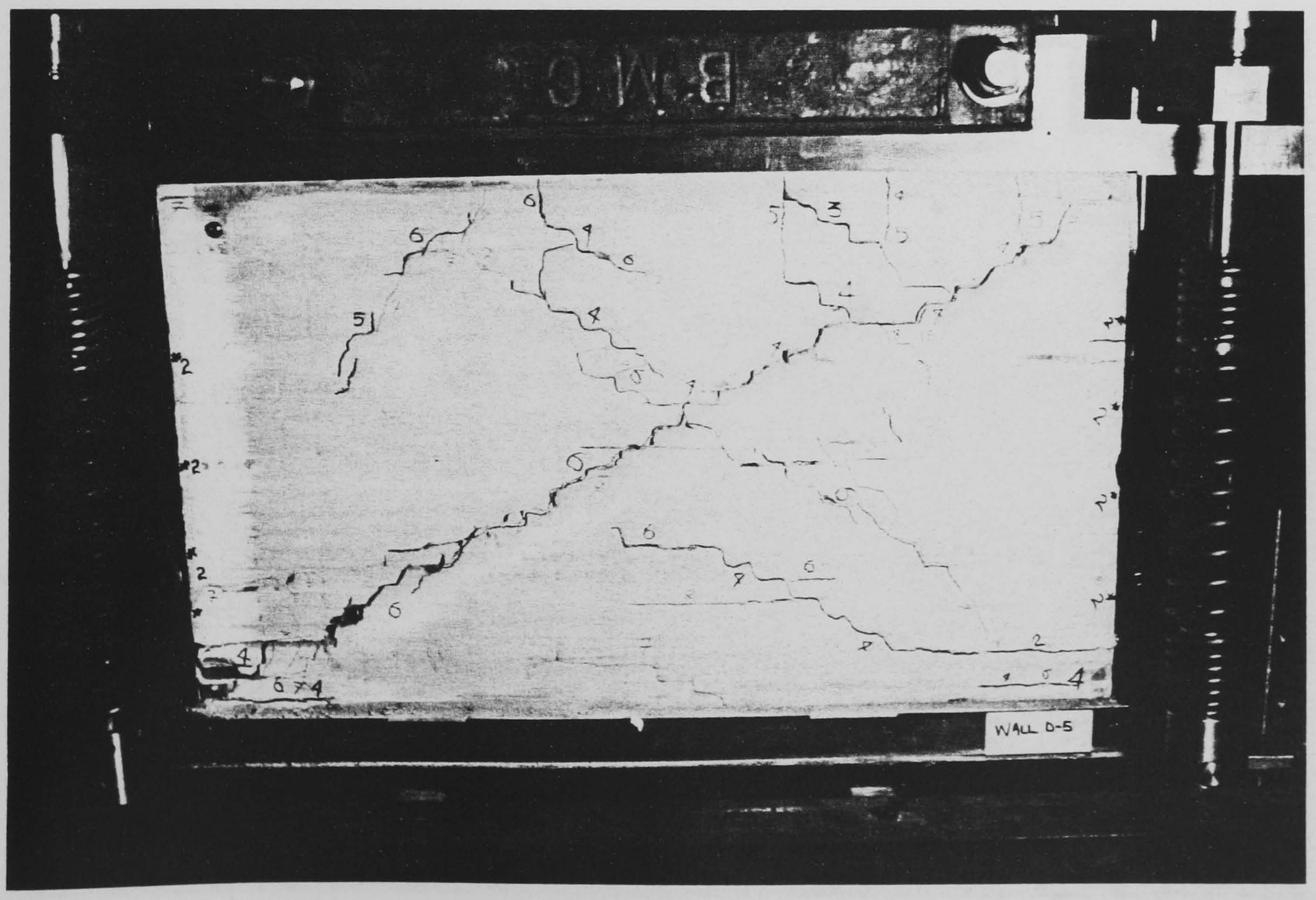

Photo 5.26 Collapse sequence-frame 2 (wall-D)

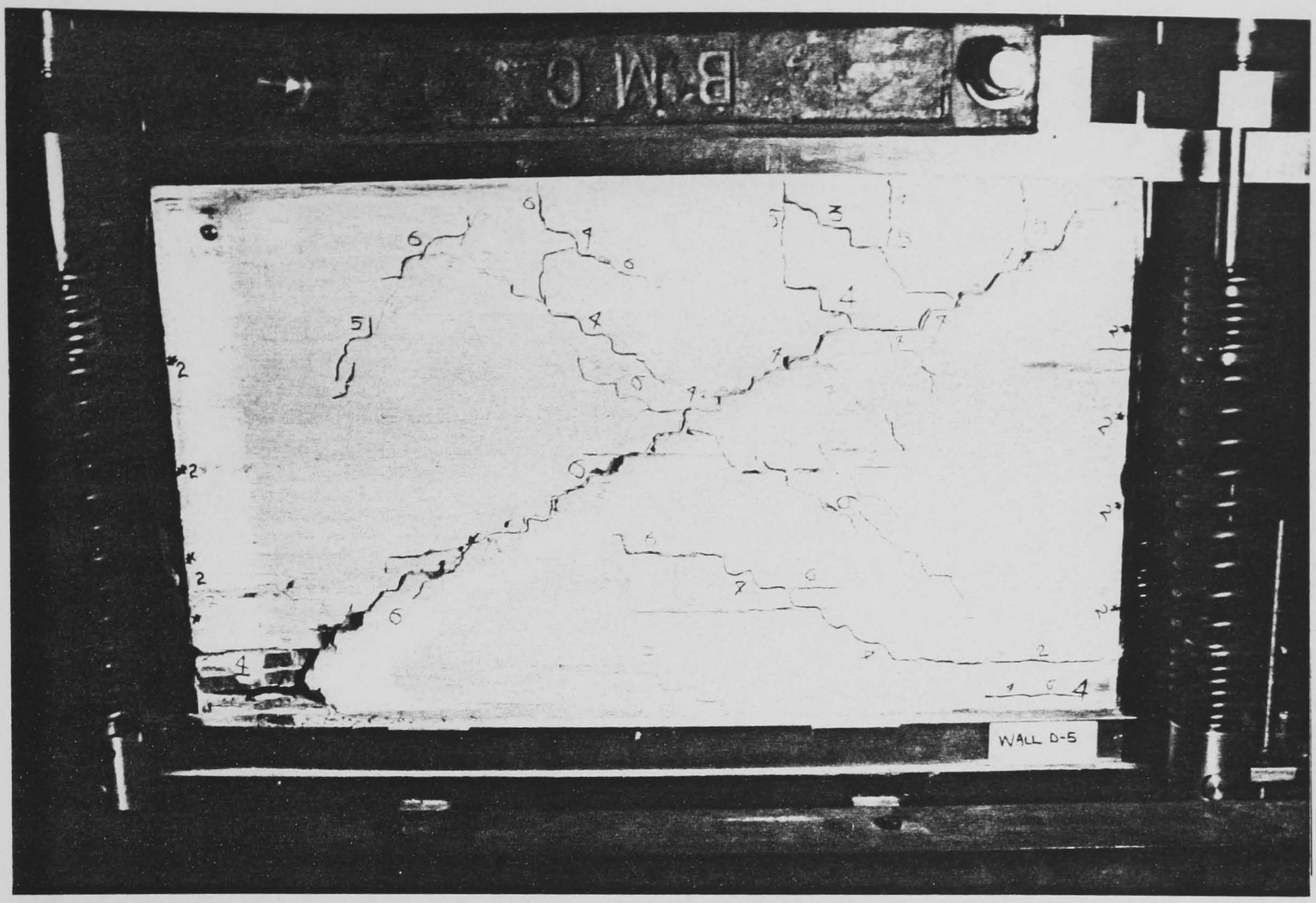

Photo 5.27 Collapse sequence-frame 3 (wall-D)

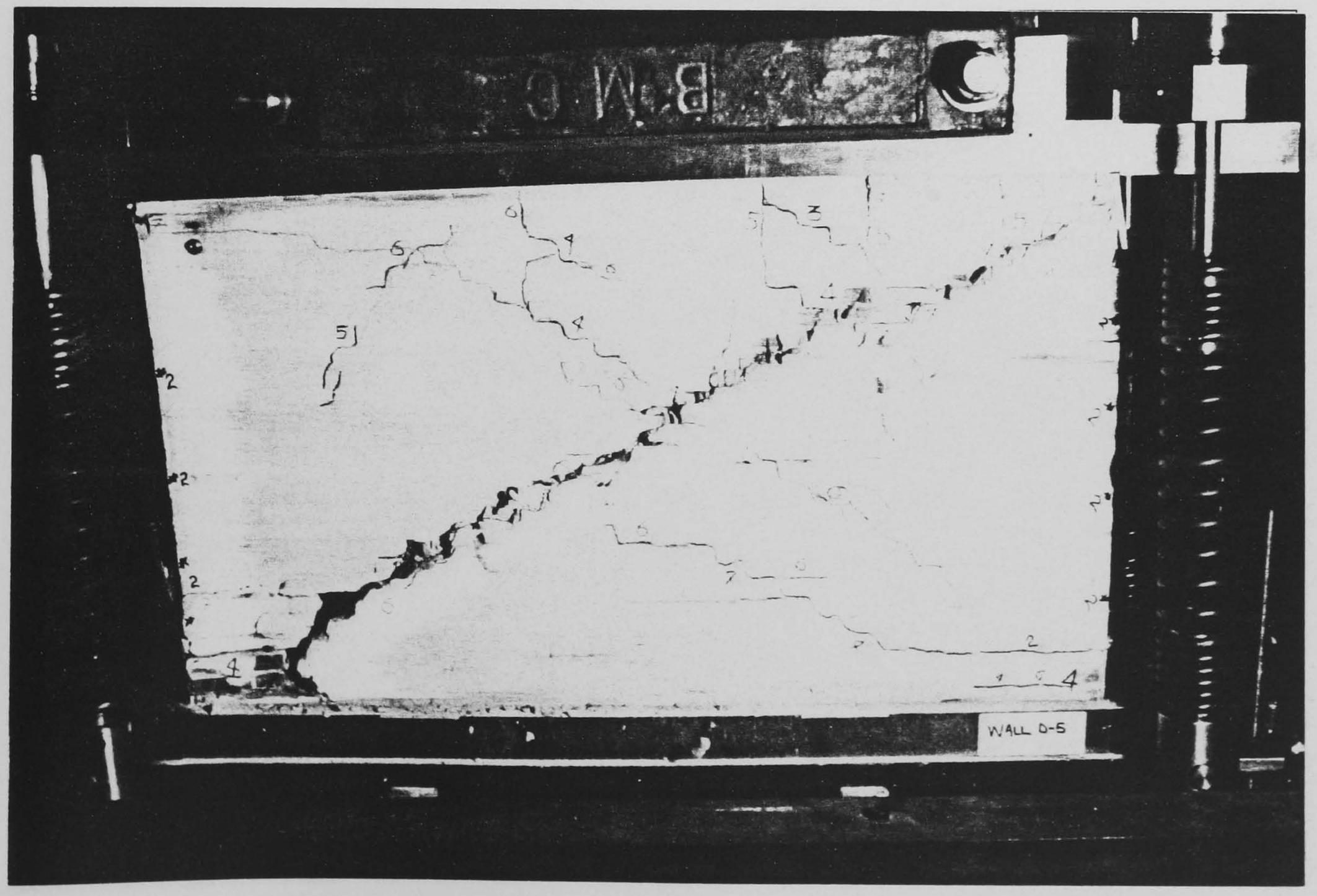

Photo 5.28 Collapse sequence-frame 4 (wall-D)

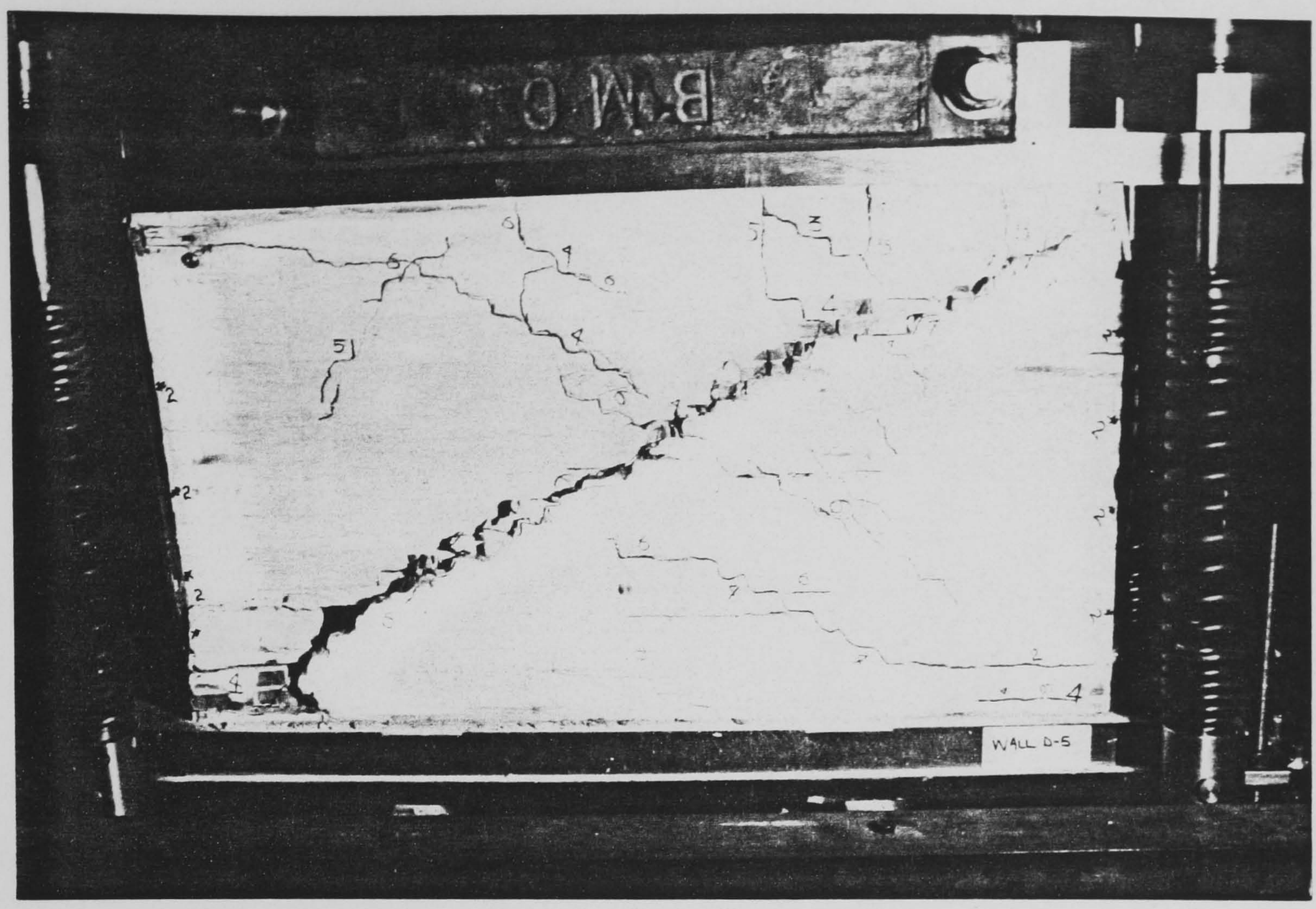

Photo 5.29 Collapse sequence-frame 5 (wall-D)

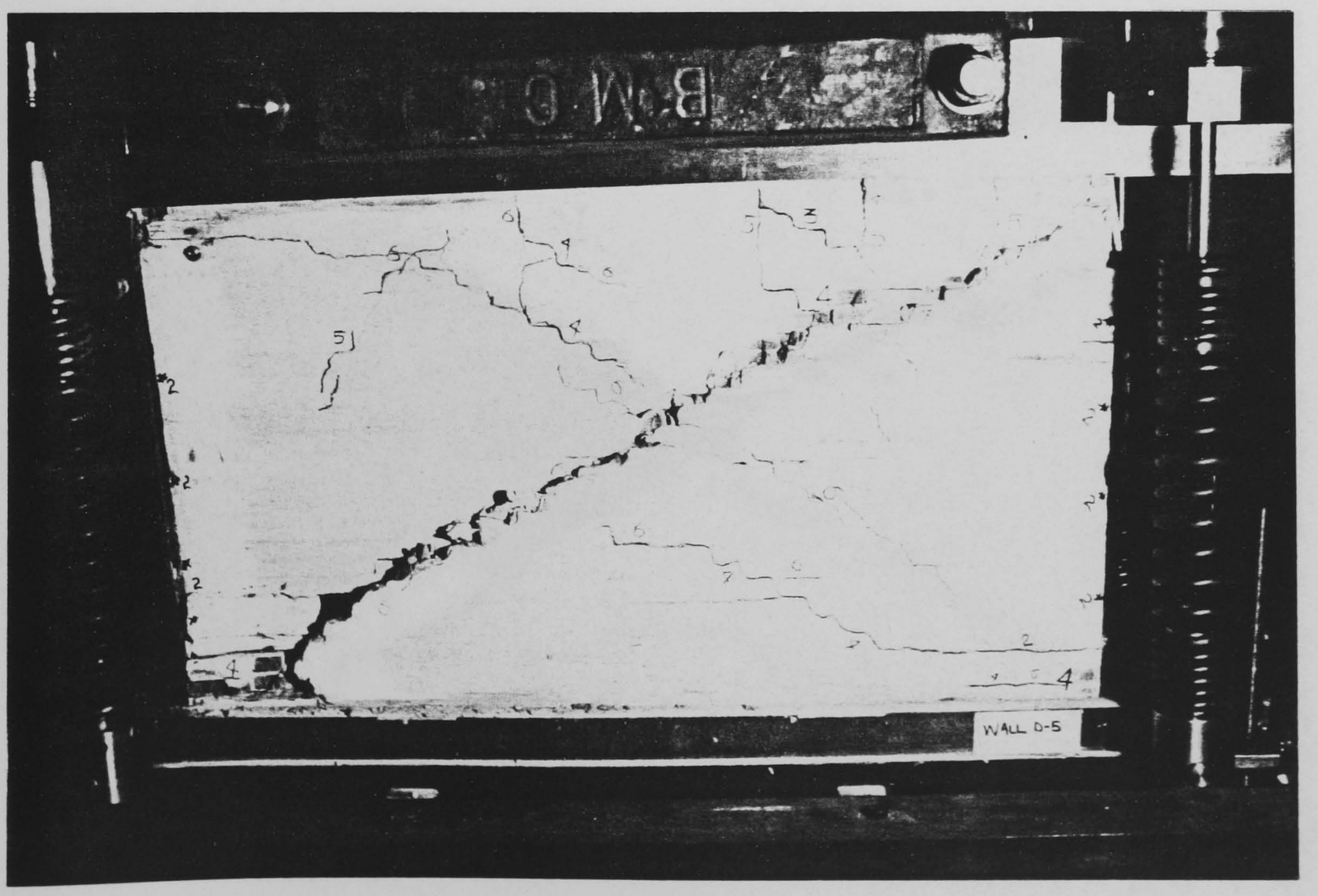

Photo 5.30 Collapse sequence-frame 6 (wall-D)

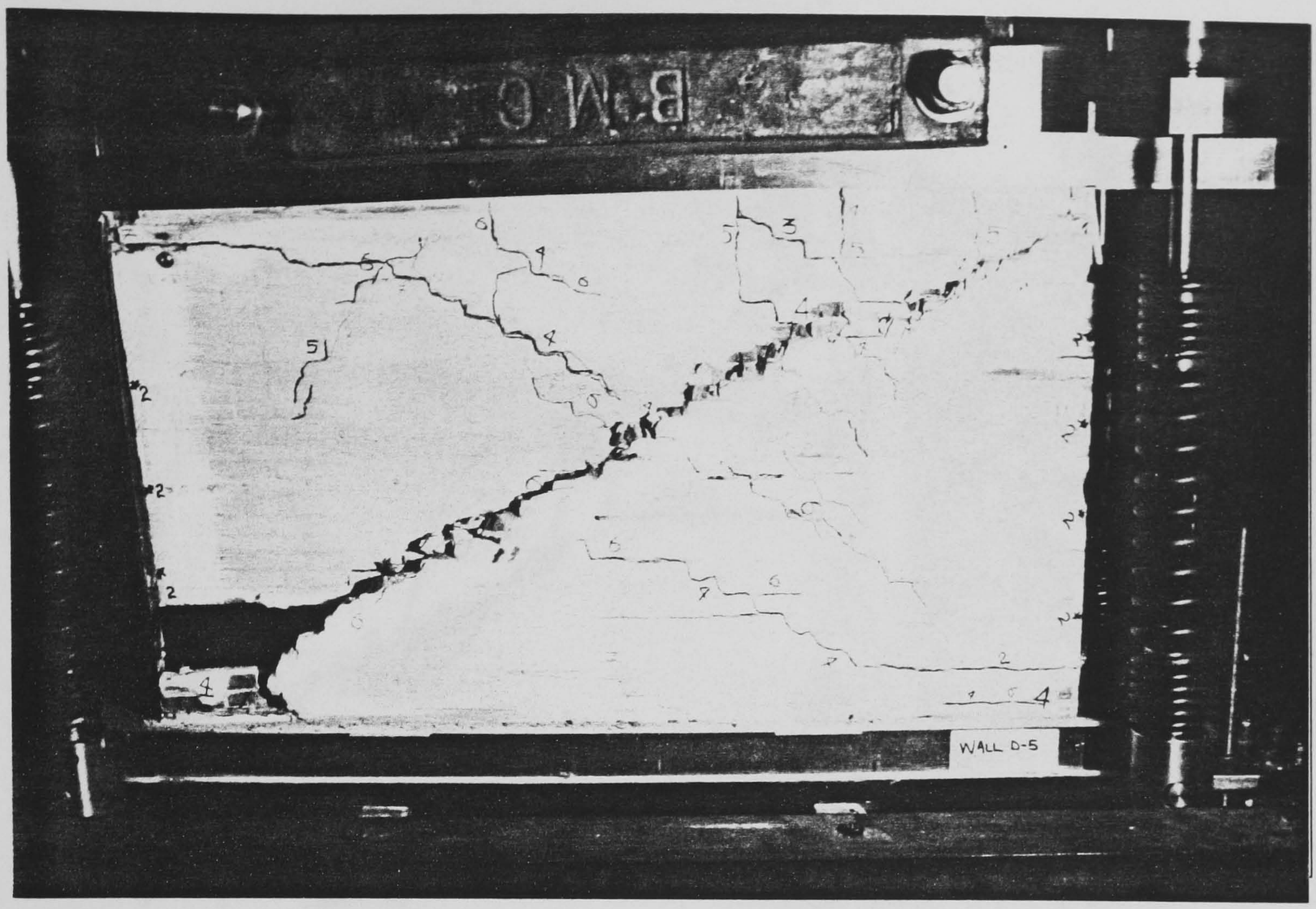

Photo 5.31 Collapse sequence-frame 7 (wall-D)

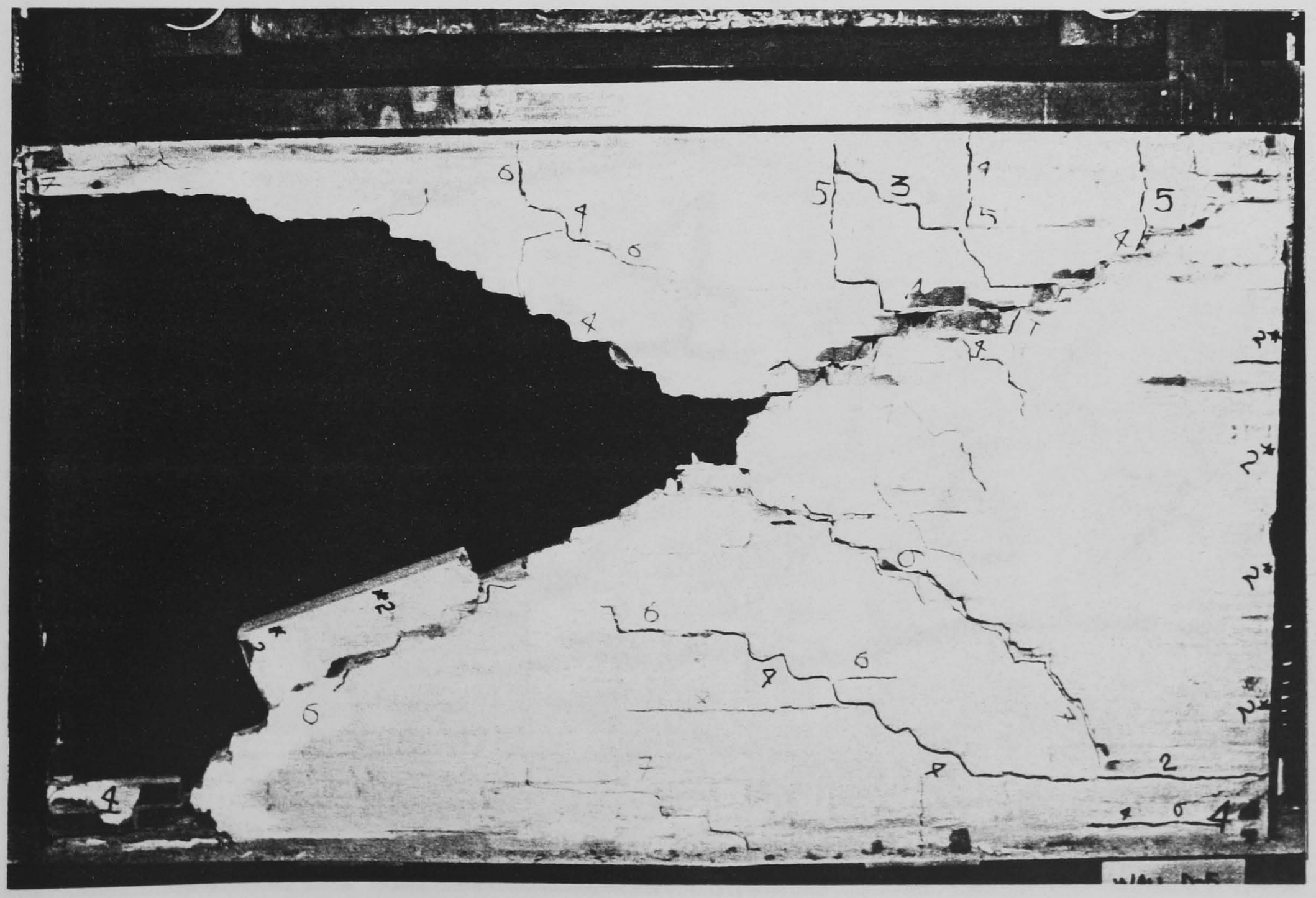

Photo 5.32 Cross shaped final diagonal failure and collapse (wall-D)

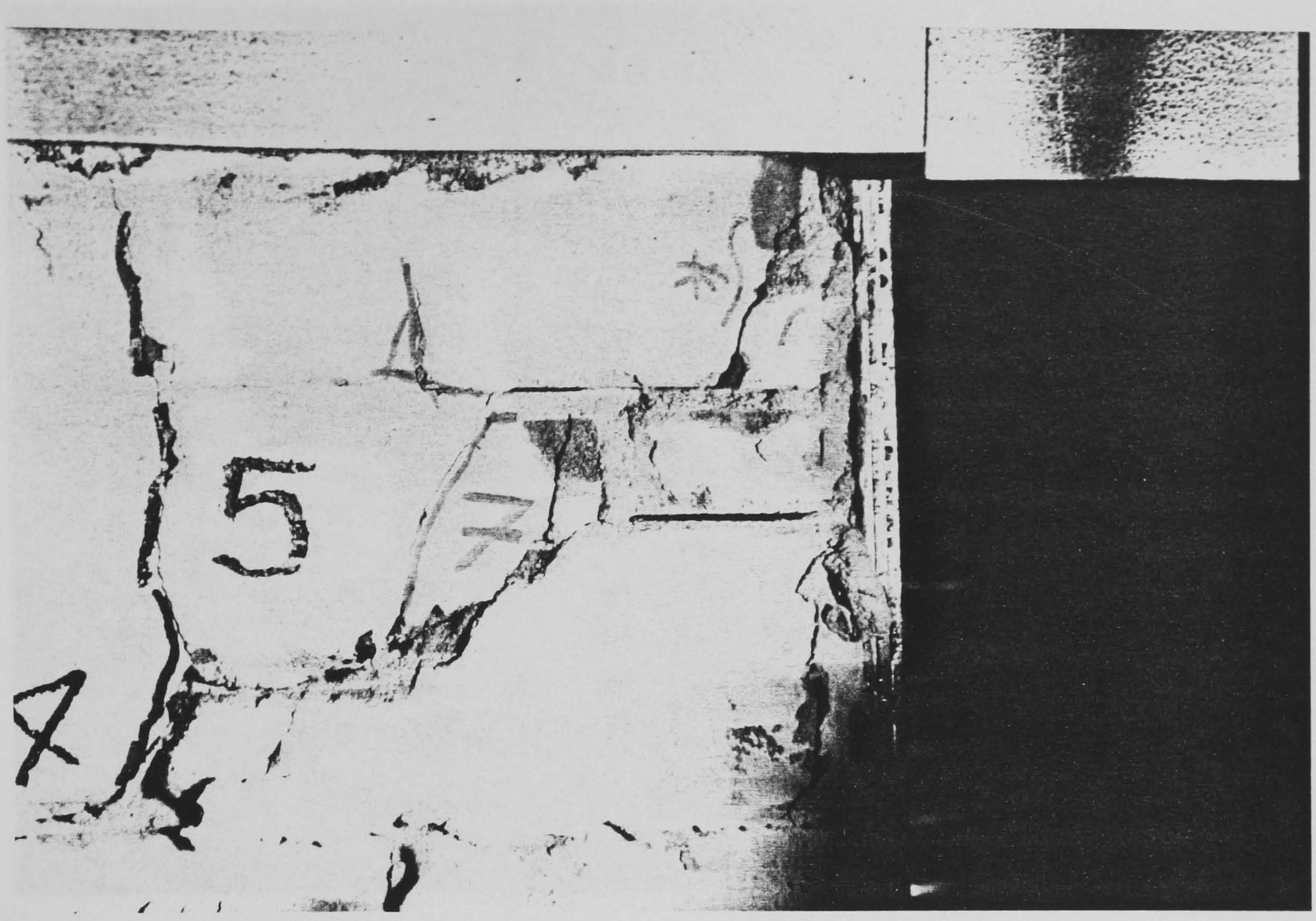

Photo 5.33 Upper left corner crushing (wall-D)

Photo 5.34 Opposite (lower left) corner crushing (wall-D)

Photo 5.35 Centre of symmetry of diagonal cracking pattern (wall-D)

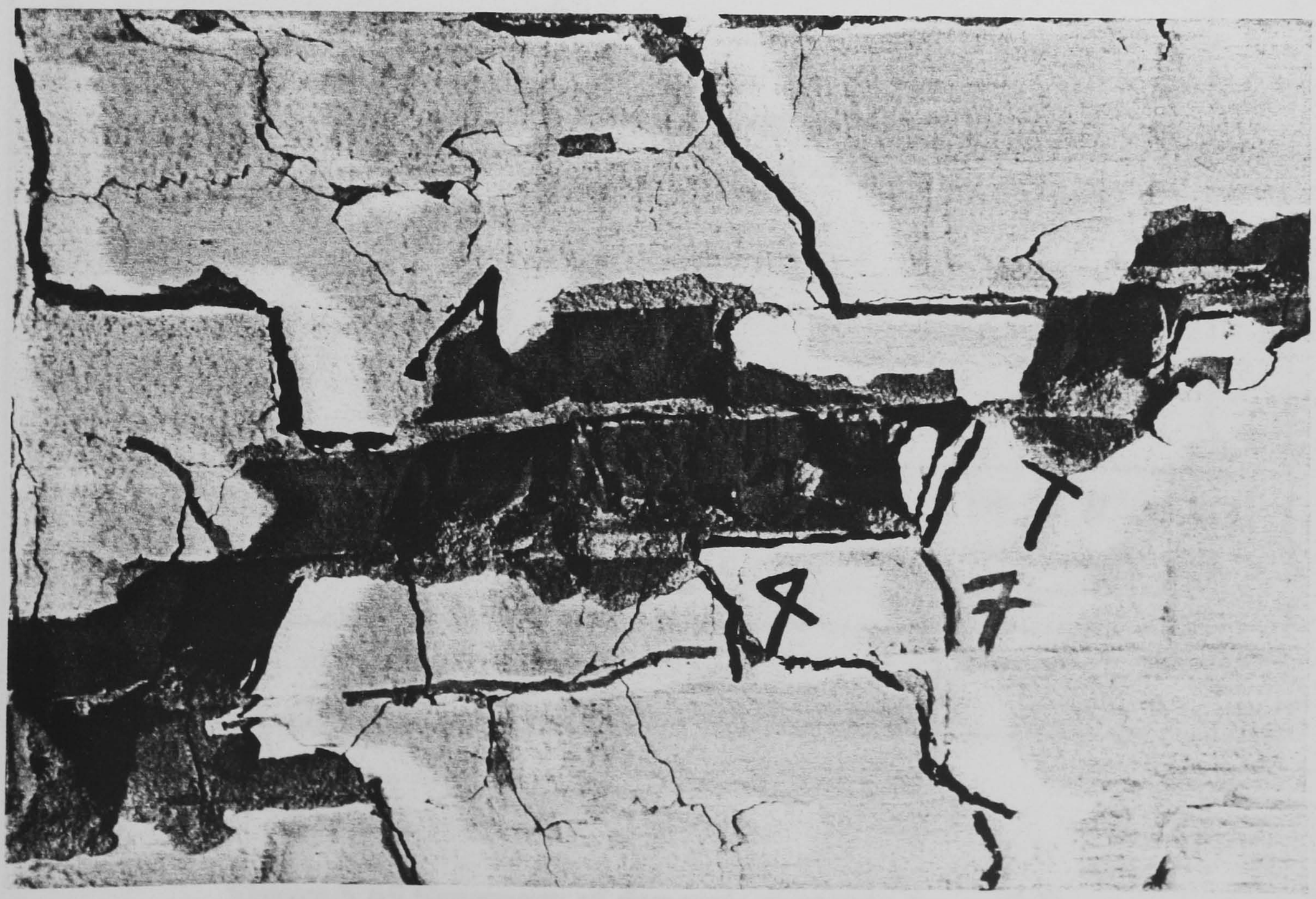

Photo 5.36 Close-up details of diagonal shear cracking (wall-D)

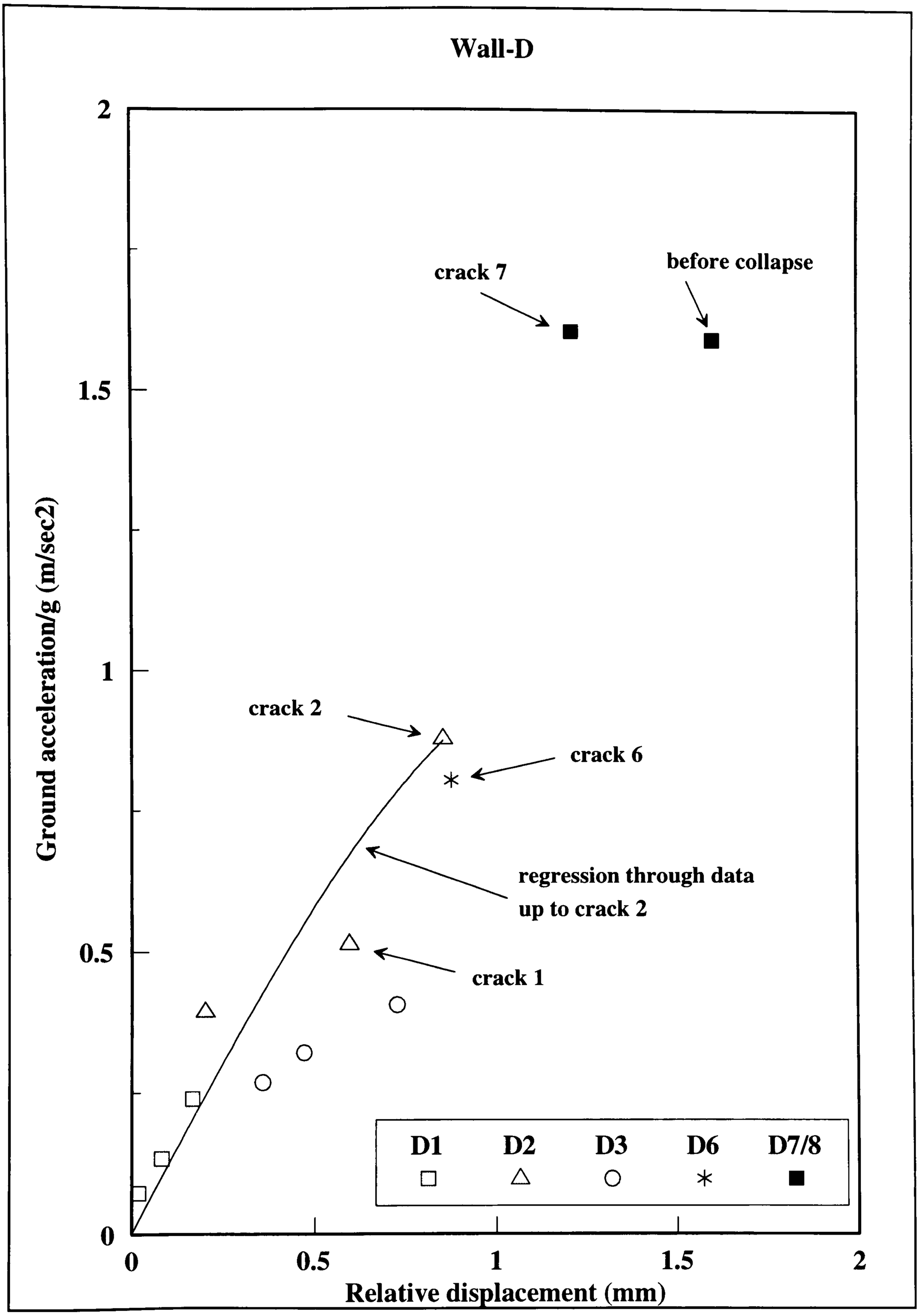

Figure 5.65 Summary of dynamic response for wall-D

5.8.3.1 Observations for wall-D.

Wall-D was built with bricks having approximately the same strength as the two previous ones. It was tested at 14 days after casting which resulted in a lower strength mortar. By adjusting the absorption properties of the bricks, which involved wetting the units in parts and conducting the I.R.S. test until the desired value was obtained, comparatively lower interface bond strength was measured from shear box tests on couplet assemblages. Localised cracking at the column interfaces occurred at an acceleration of 0.5g and extended to the full height during the following stage at an acceleration of 0.84g. Cracks 3, 4 and 5 occurred at a slightly lower acceleration of 0.64g and 0.7g respectively (photo 5.21). Although crack 3 appeared near the top of the panel and extended downwards, crack 4 originated at the centre and extended towards the upper right corner. Crack 6 occurred at an acceleration of 0.82g and by joining with crack 4 it extended to the opposite lower left corner (photos 5.22 and 5.23). Further cracks were also recorded above the middle section of the panel as well as from the centre extending towards the lower right corner. A typical cross-shaped pattern can be observed as crack 7 (recorded at an acceleration of 1.6g) is extending towards the upper left corner, whereas the other diagonal crack has connected the two opposite loaded corners. At this point the panel had separated into two sections which slid along the cracking interface with load reversals of the applied cyclic motions (photo 5.24). The wall's natural frequency after the appearance of crack 7 was measured at 18.51 Hz (initial, 39.1 Hz) with a corresponding increase in the damping coefficient of 9.7% (initial, 4.4%). The final stage involved a loading cycle that was aimed at causing the collapse of the panel with an applied acceleration of 1.56g. This sequence lasted about 4 seconds and was photographically recorded at high speed in 36 frames. A representative selection is shown in photos 5.25 to 5.32 which show the main diagonal crack opening and the wall collapsing due to loss of stability related partly to crushing of the masonry at the lower left corner, and partly to the formation of a new crack which can be seen as it develops in photos 5.28 to 5.31 and completes the formation of the cross-diagonal pattern. Photos 5.33 to 5.36 show close-up details of the damaged panel just before the final stage, and in particular photo 5.35 shows the origin and intersection point of the two main diagonal cracks.

5.8.4 Fourth test : wall-H.

Wall-H was also subjected to a combination of increasing frequency-acceleration ground excitations. The first three stages follow the same pattern with respect to the intensity of the applied ground motion. After the appearance of the first crack, only a slight increase in the ground acceleration resulted in further damage. The last stage with a lower intensity of the applied ground motion, caused the collapse of the wall in a brittle explosive mode. In the following pages the developing dynamic behaviour has been laid out in detail, in the order shown below.

- ► Free vibration amplitude decay records - hammer tests (figures 5.66 to 5.68).
- ► Displacement records (5.69 to 5.74).
- ► Sample hysteresis curves (5.75 to 5.77).
- ► Photographs of the cracking patterns (photo 5.37 to 5.44).
- ► Summary of dynamic response (figure 5.78).

The test procedure for wall-H is summarised in table 5.9, while results for the first natural frequency using the methods described previously are shown in table 5.8.

Theoretical	Finite element	Hammer test
66.1 Hz	77.4 Hz	42.48 Hz

Table 5.8 Natural frequency results (initial value) for wall-H

Stage/Run	Table accel.	Driving freq.	Damage	Natural freq.	Damping ratio	Rel. displ.	Comments
	g	Hz	Crack #	Hz	%	mm	
H1/R1	0.135	5.4	-	42.47	4.1	0.091	Increasing driv. frequency
H1/R2	0.237	6.1	-	-	-	0.17	
H1/R3	0.417	6.8	-	-	-	0.359	
H2/R1	0.206	5.4	-	-	-	0.193	Increasing driv. frequency
H2/R2	0.316	6.1	-	-	-	0.23	
H2/R3	0.529	6.8	-	-	-	0.532	
H3/R1	0.305	5.4	-	-	-	0.24	Increasing driv. frequency
H3/R2	0.451	6.1	-	-	-	0.029	
H3/R3	0.696	6.8	-	-	-	0.719	
H4/R1	1.03	6.8	-	-	-	1.2	Increasing driv. frequency **Stepwise diagonal and horizontal shear sliding cracking**
H4/R2	1.262	7.4	**1**	23.2	4.4	1.599	**Minor corner cracking**
H5/R1	1.405	7.7	**2**	19.95	5.5	1.799	**Formation of first diagonal crack Corner crushing**
H6/R1	1.294	6.8	**-**	-	-	2.2	**Collapse**

(Crack numbers correspond to the cracking as noted in the photographs

Table 5.9 Wall-H testing sequence

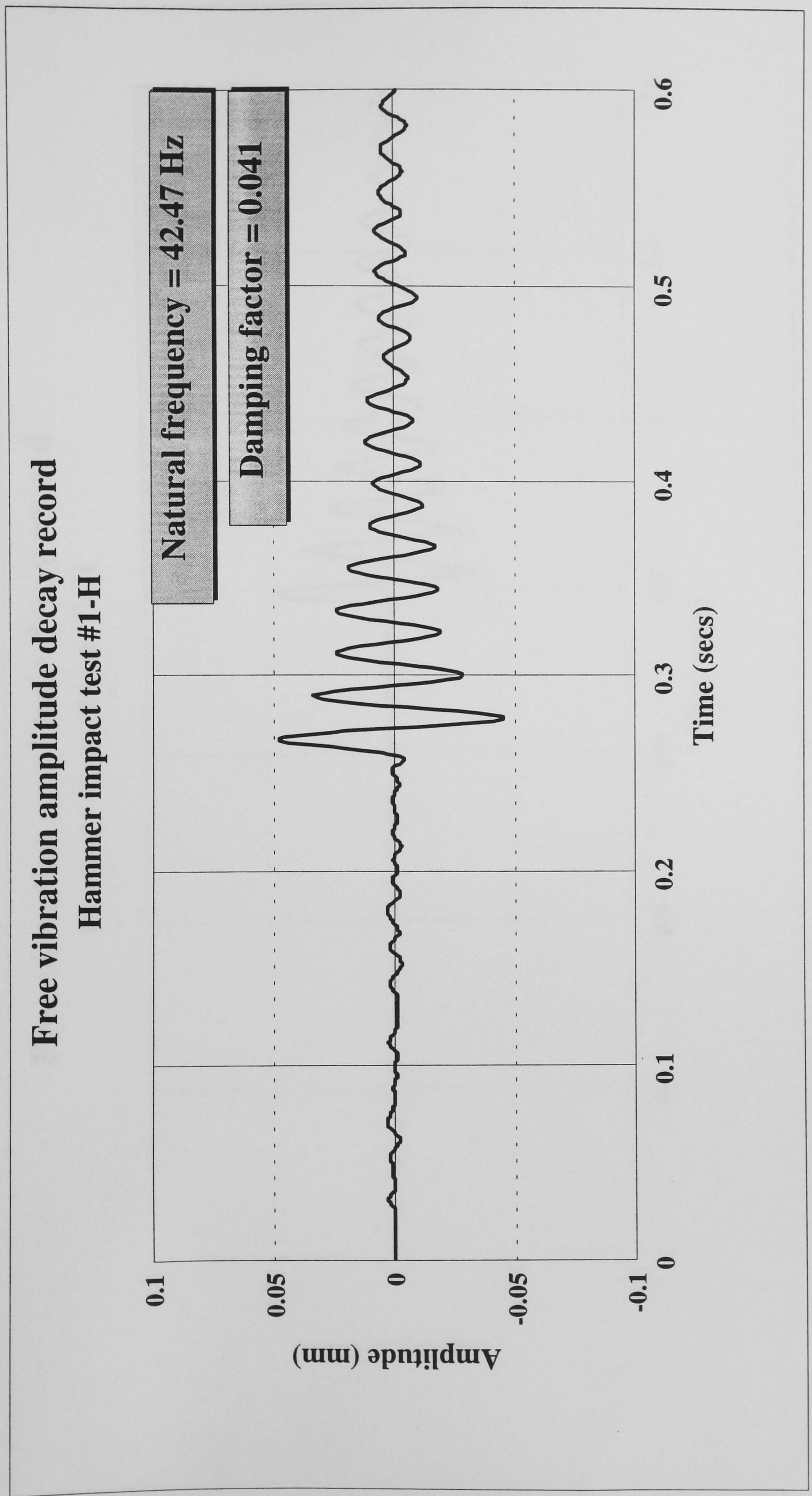

Figure 5.66 Initial free vibration amplitude decay

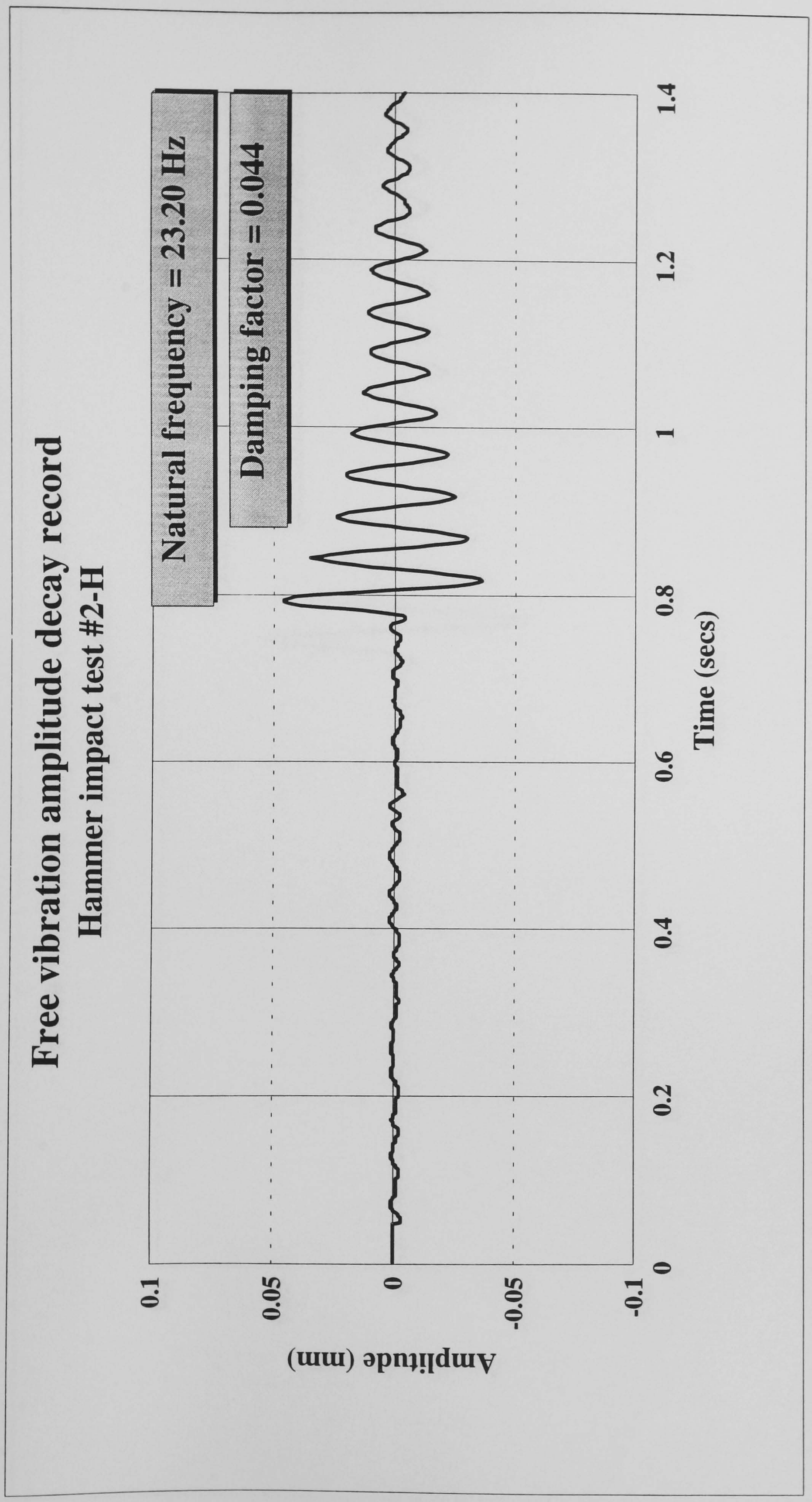

Figure 5.67 Free vibration amplitude decay after crack 1

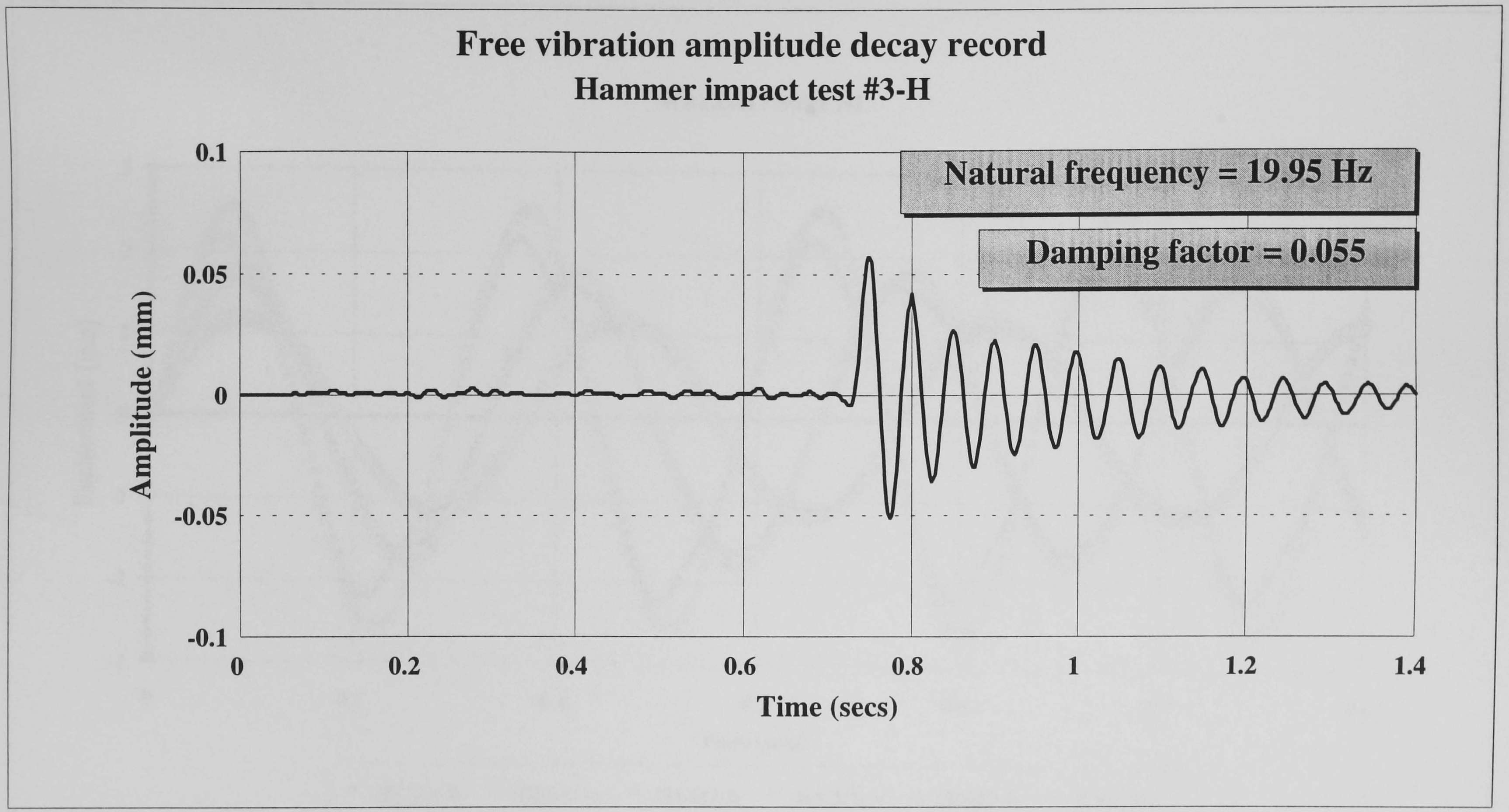

Figure 5.68 Free vibration amplitude decay after crack 2

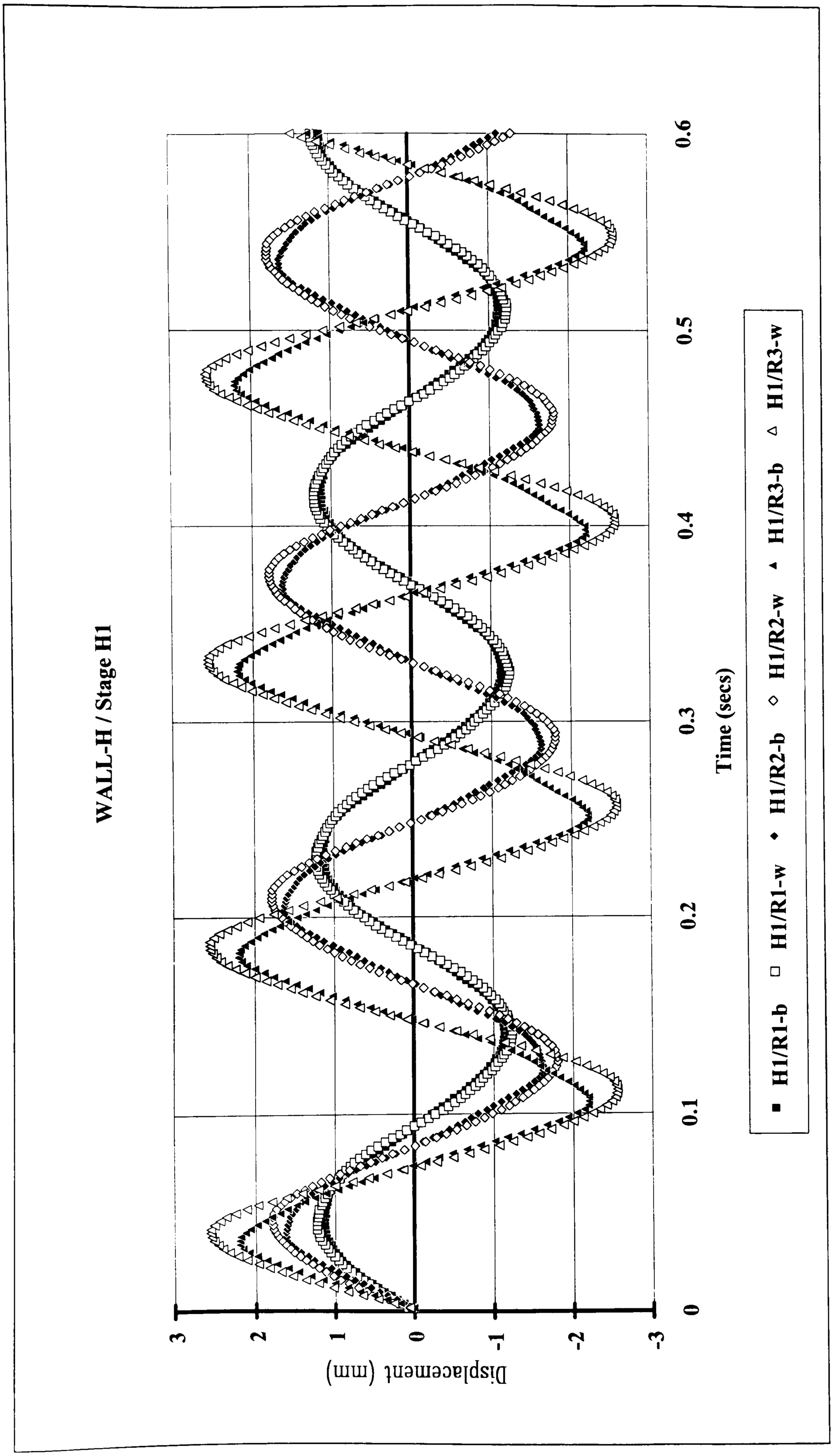

Figure 5.69 Wall-H / Stage H1

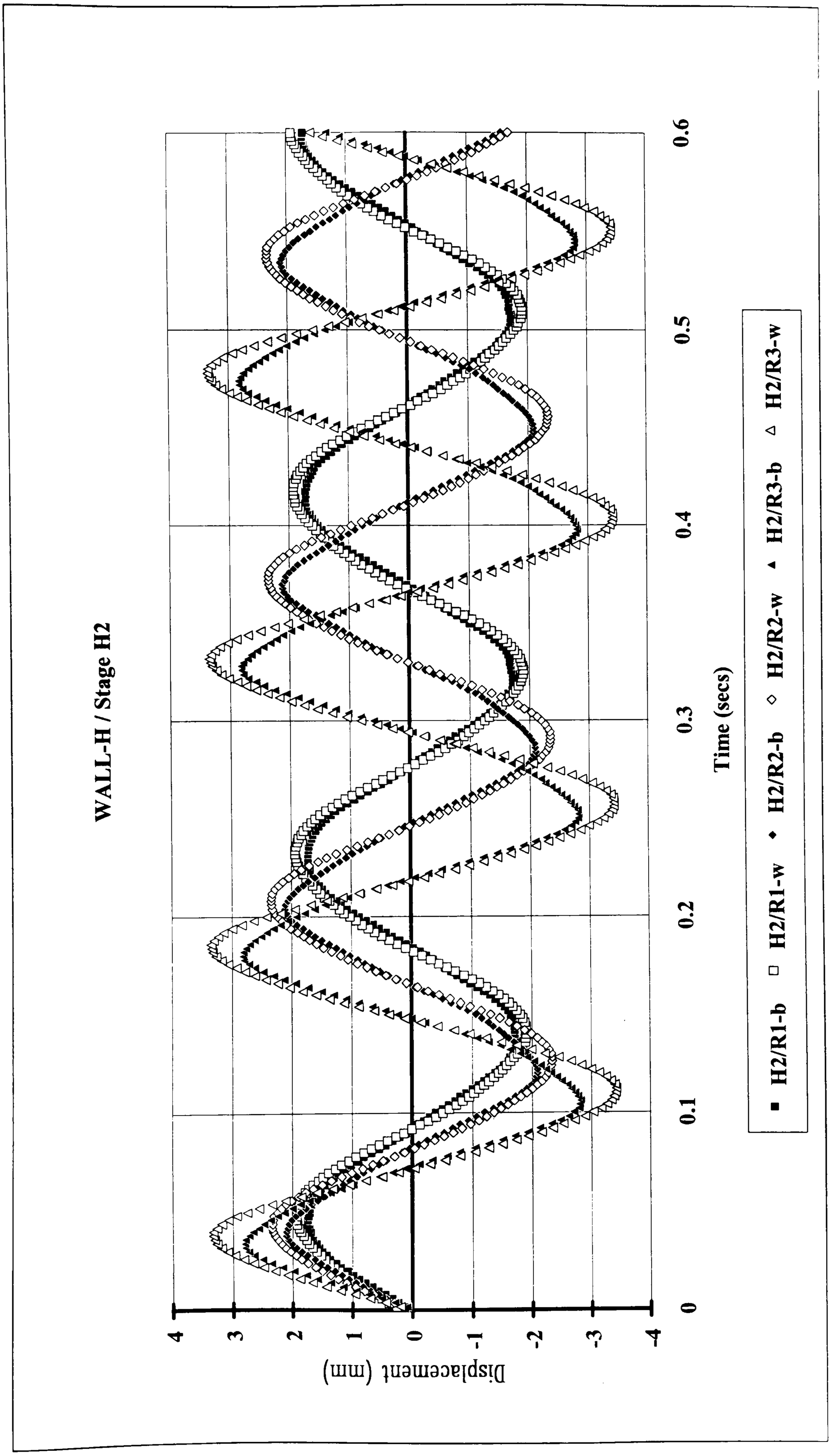

Figure 5.70 Wall-H / Stage H2

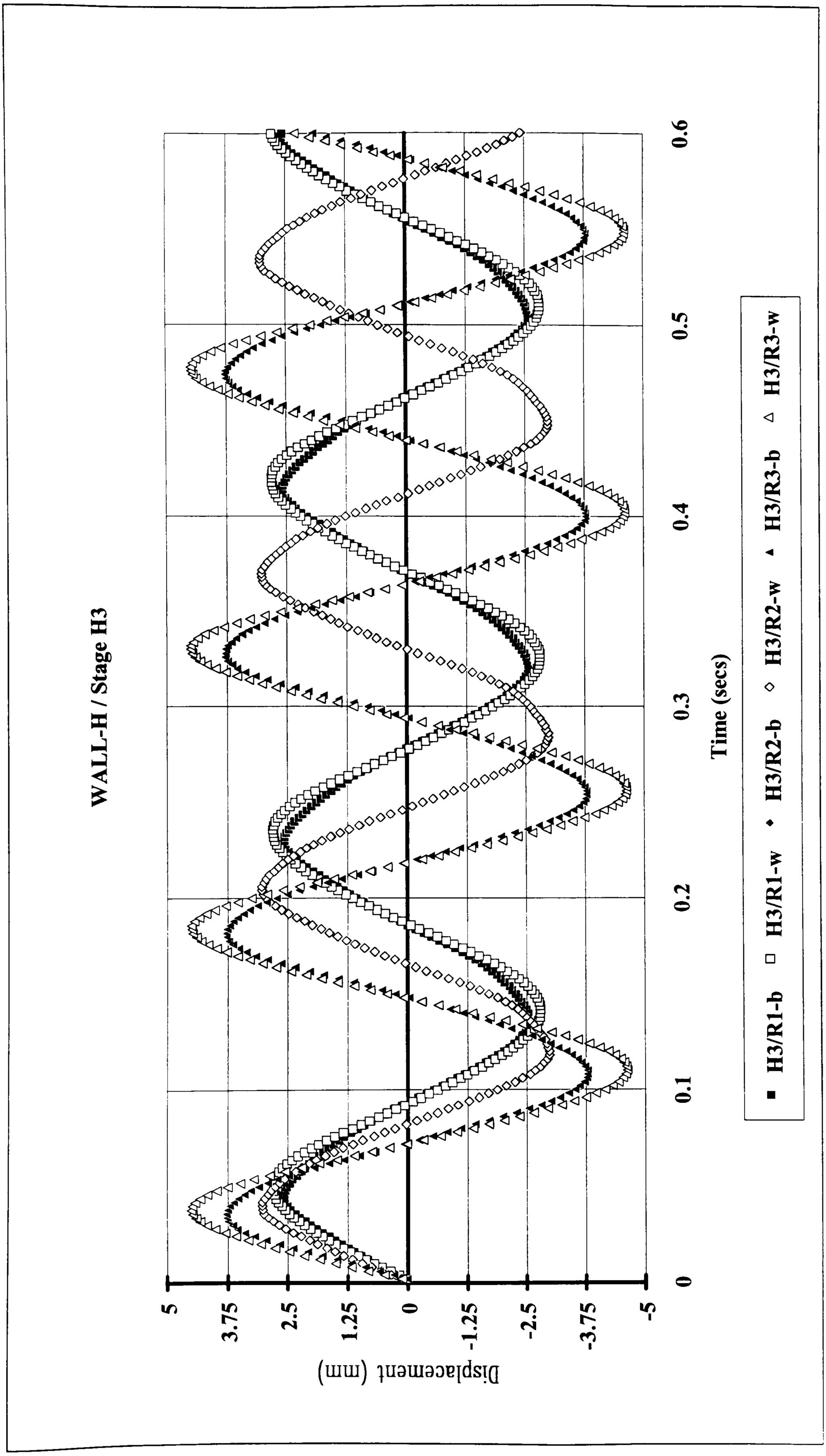

Figure 5.71 Wall-H / Stage H3

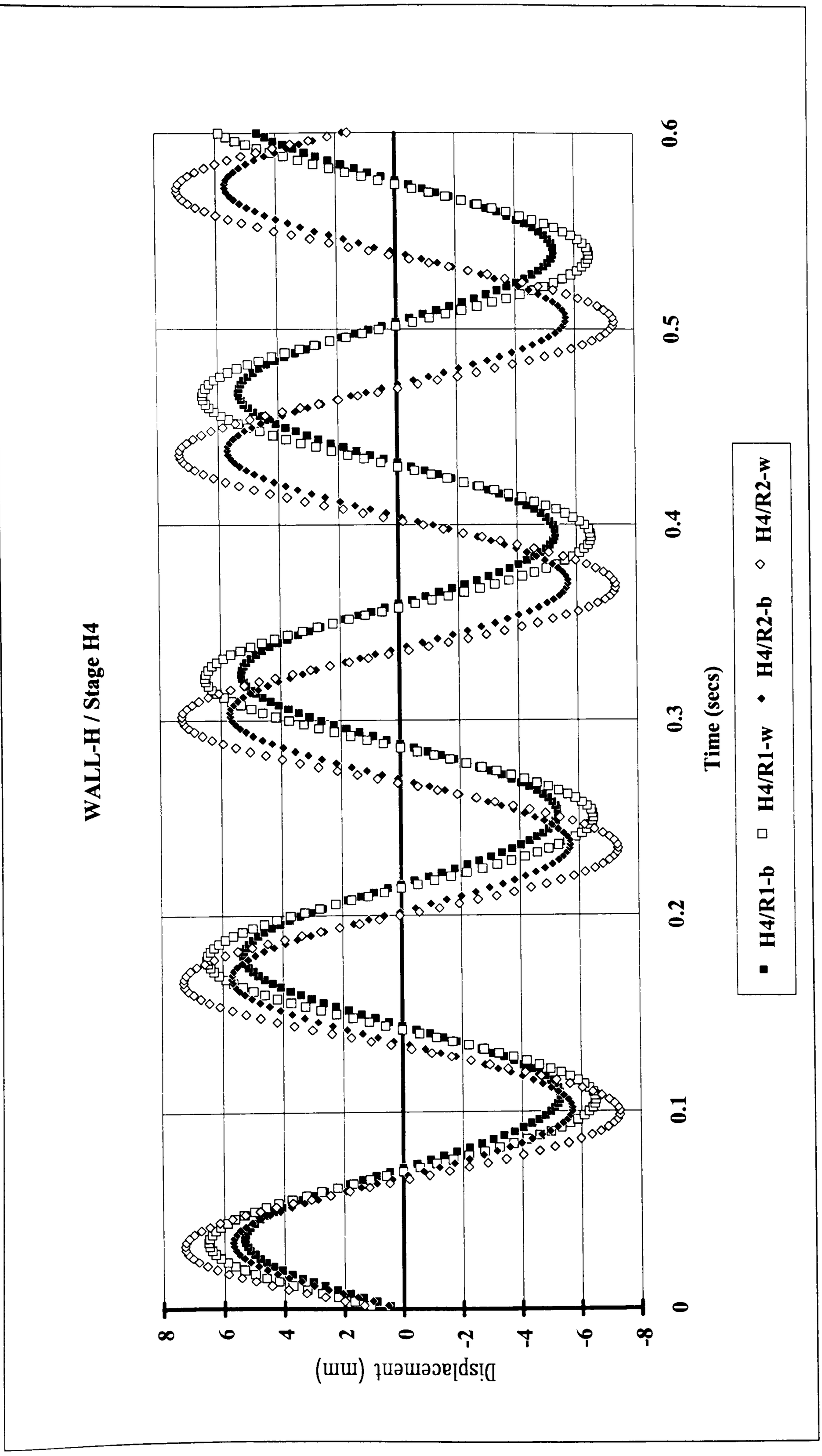

Figure 5.72 Wall-H / Stage H4

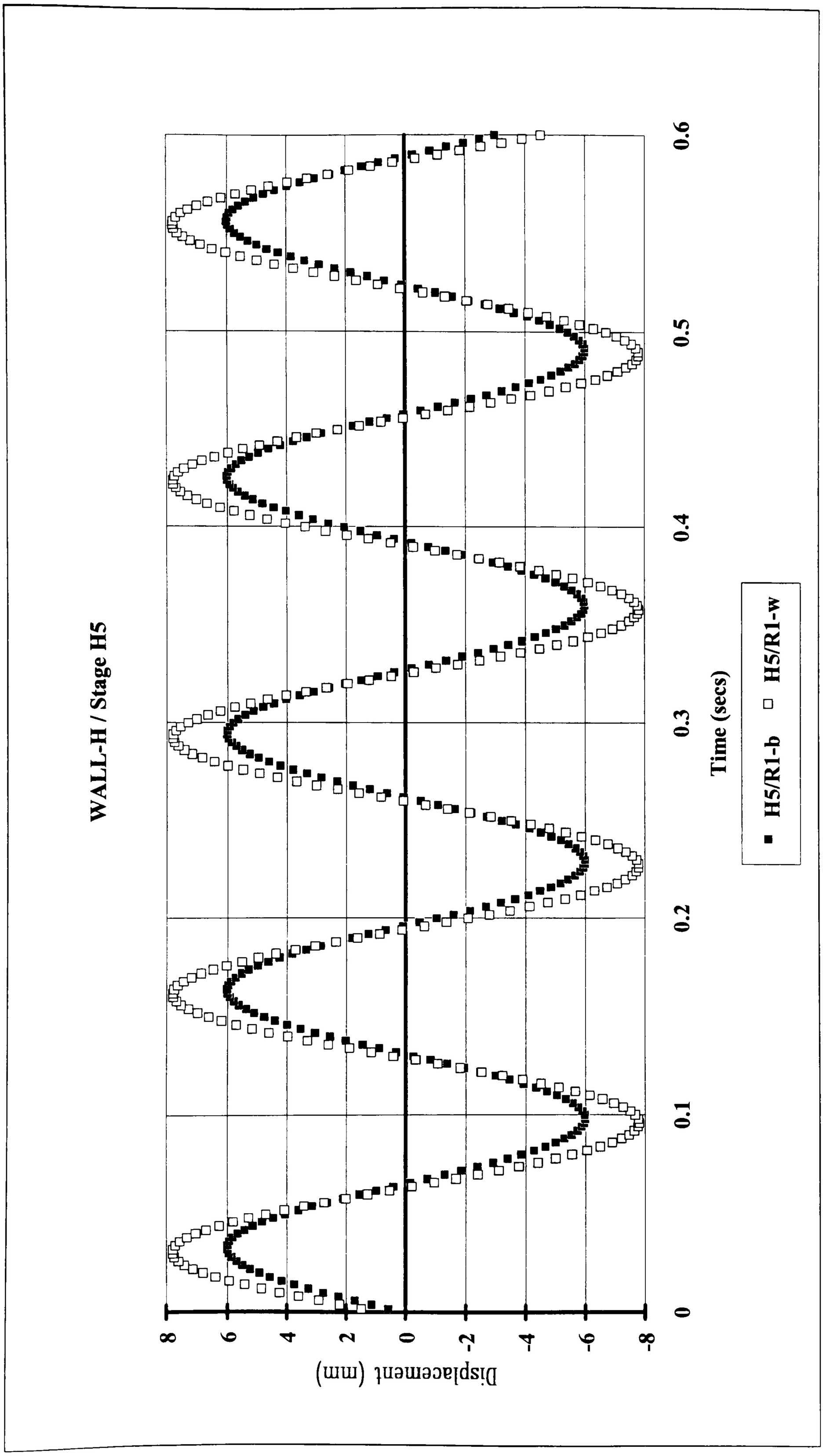

Figure 5.73 Wall-H / Stage H5

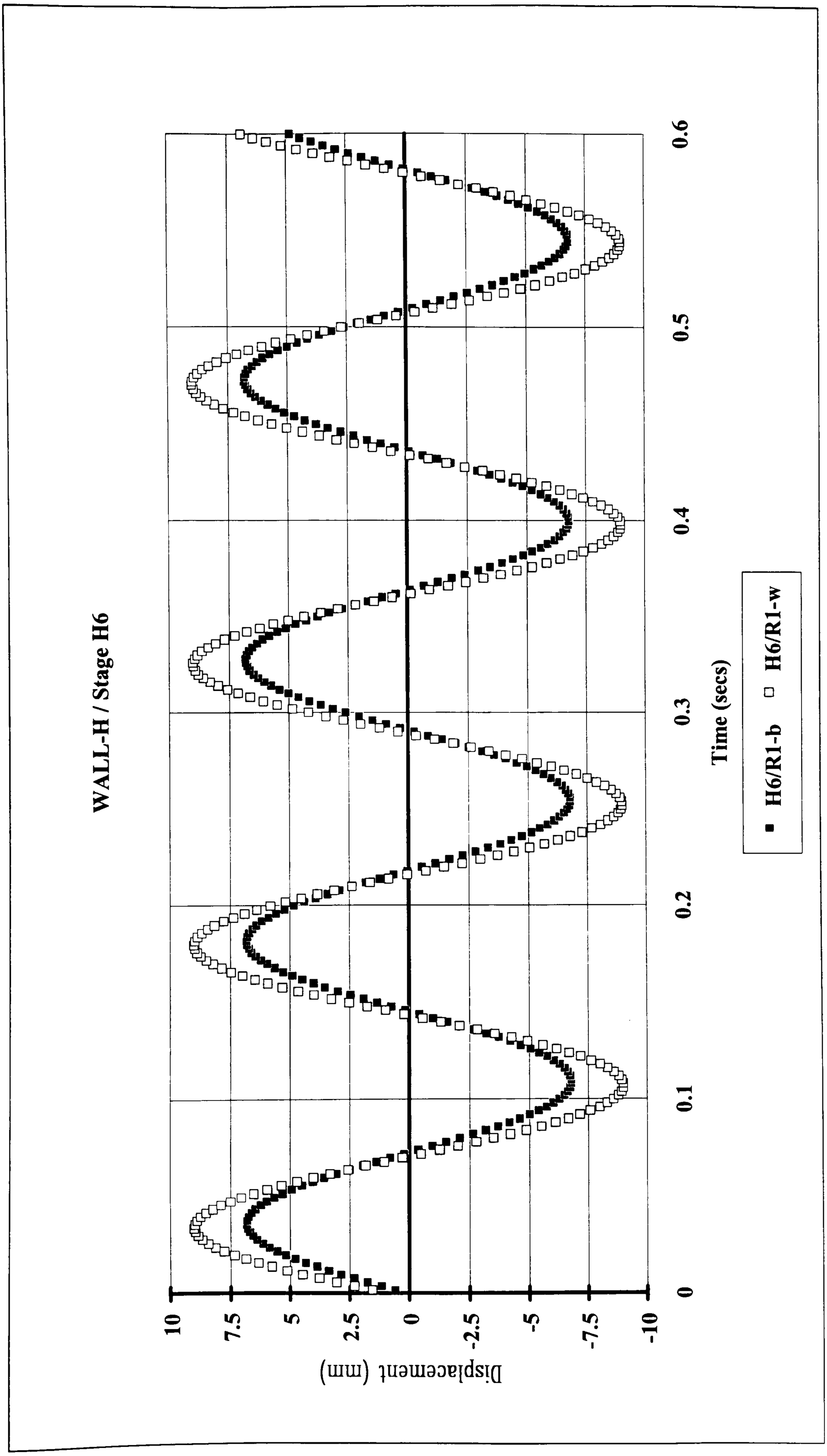

Figure 5.74 Wall-H / Stage H6

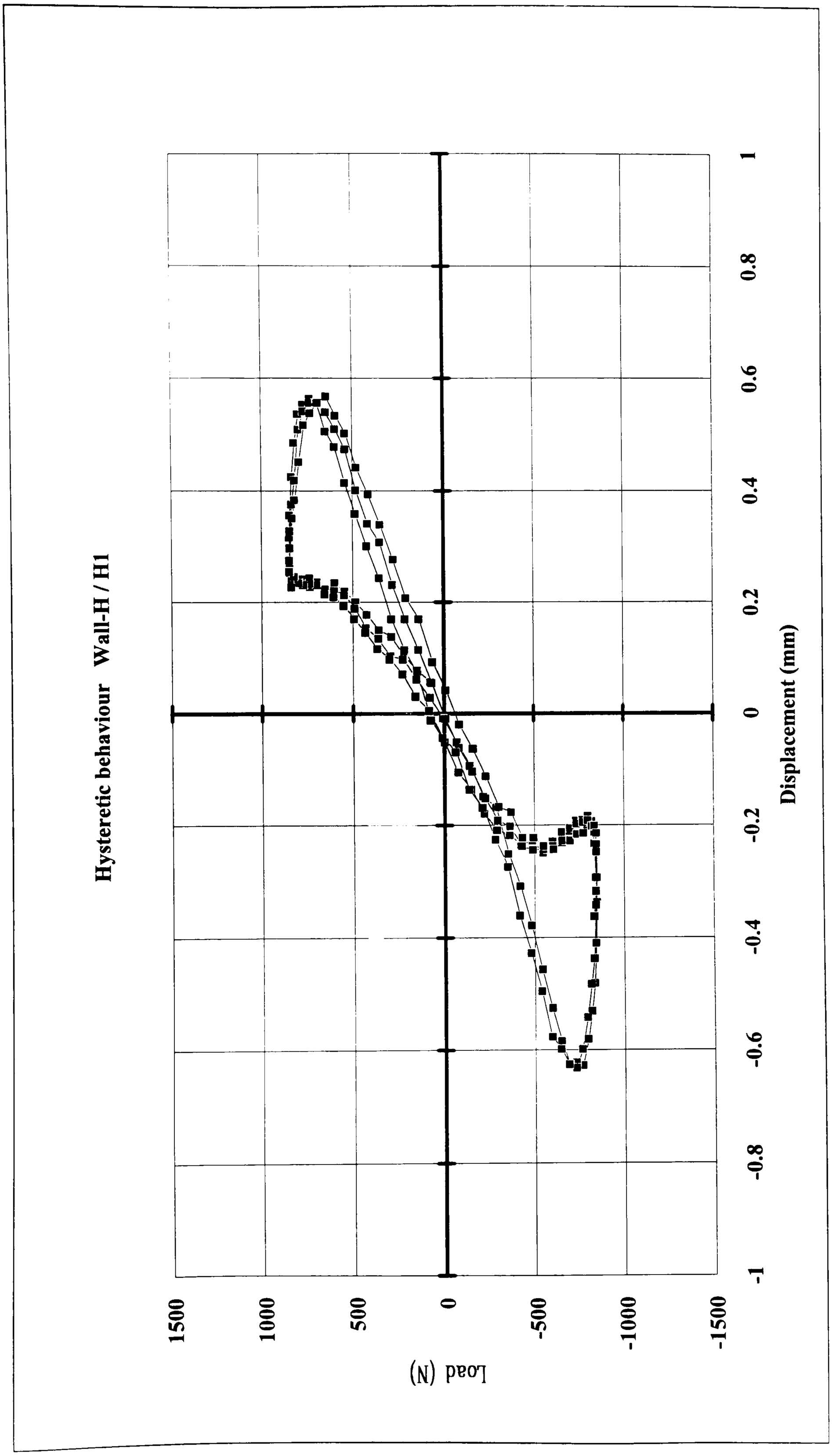

Figure 5.75 Wall-H / H1 Hysteretic Behaviour - Stage H1

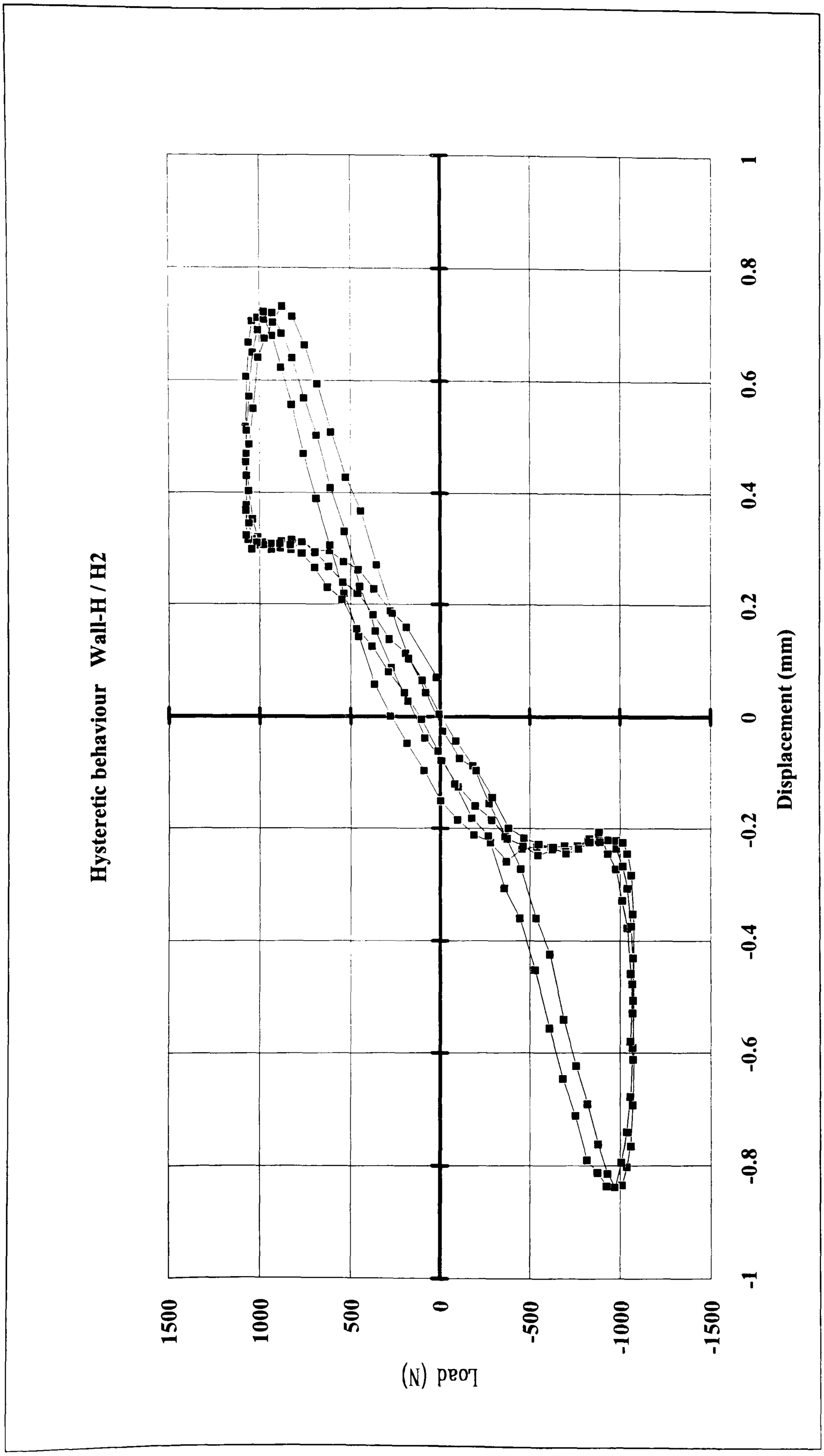

Figure 5.76 Wall-H / Hysteretic Behaviour - Stage H2

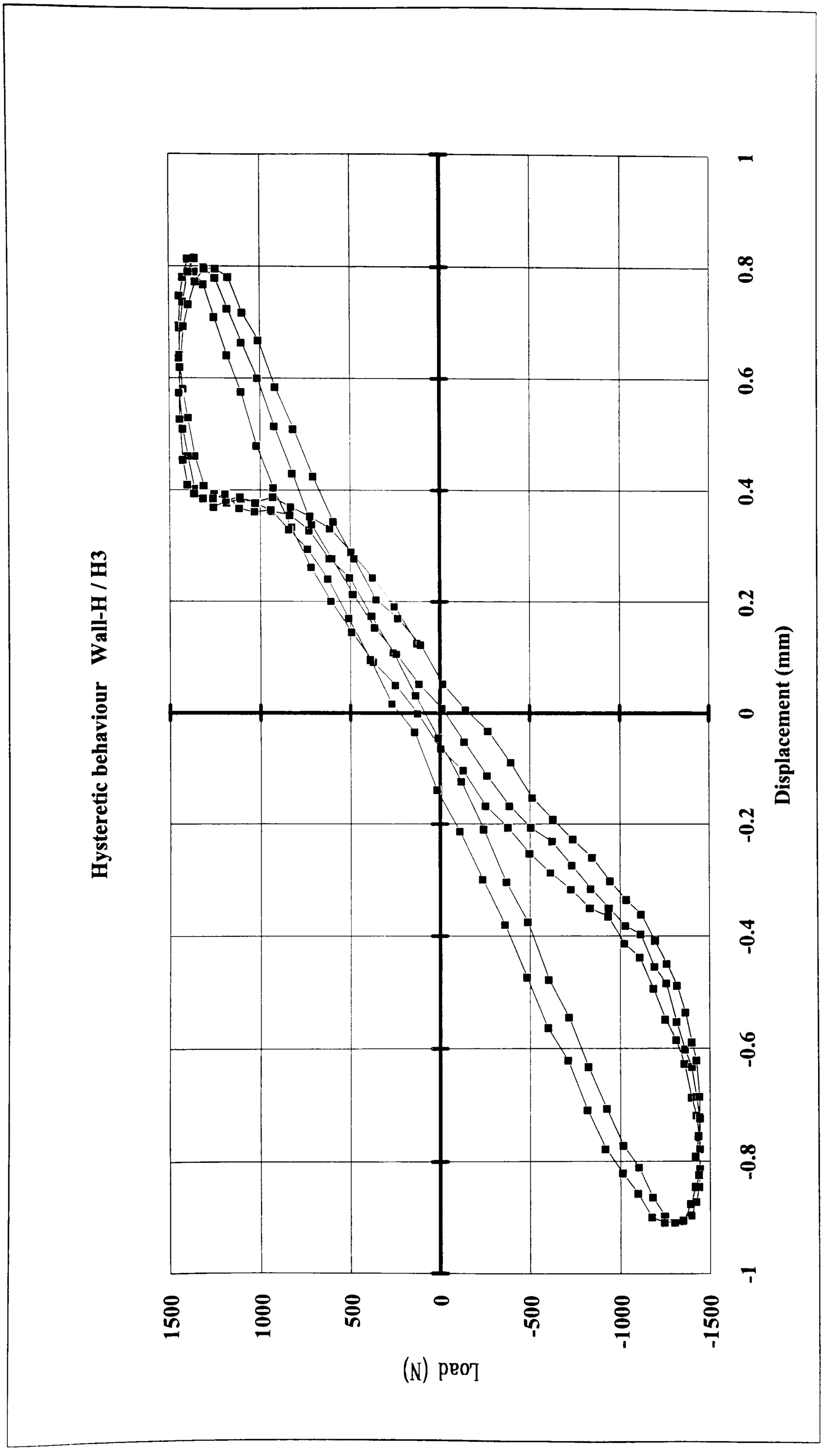

Figure 5.77 Wall-H / Hysteretic Behaviour - Stage H3

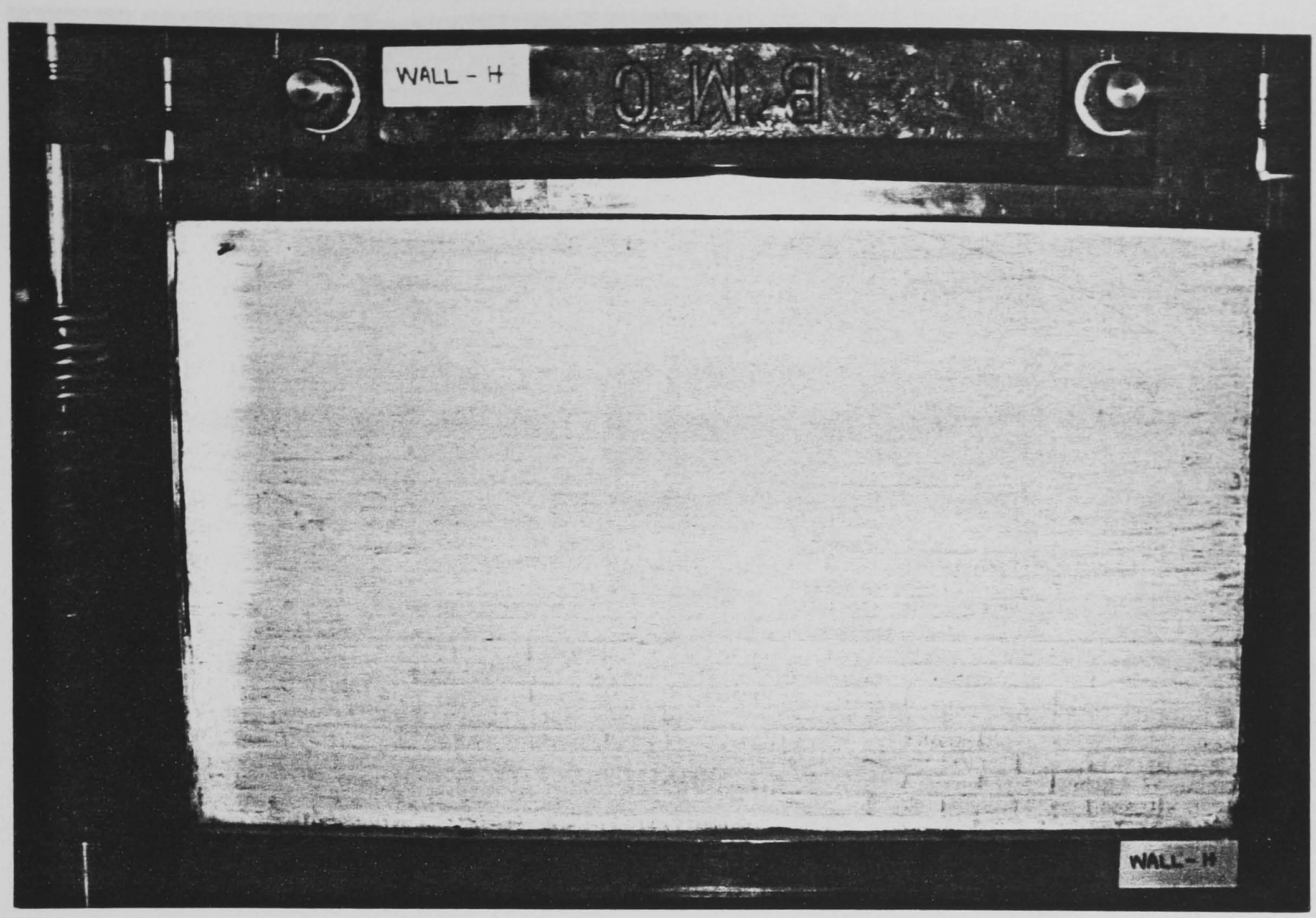

Photo 5.37 Wall-H ready for testing

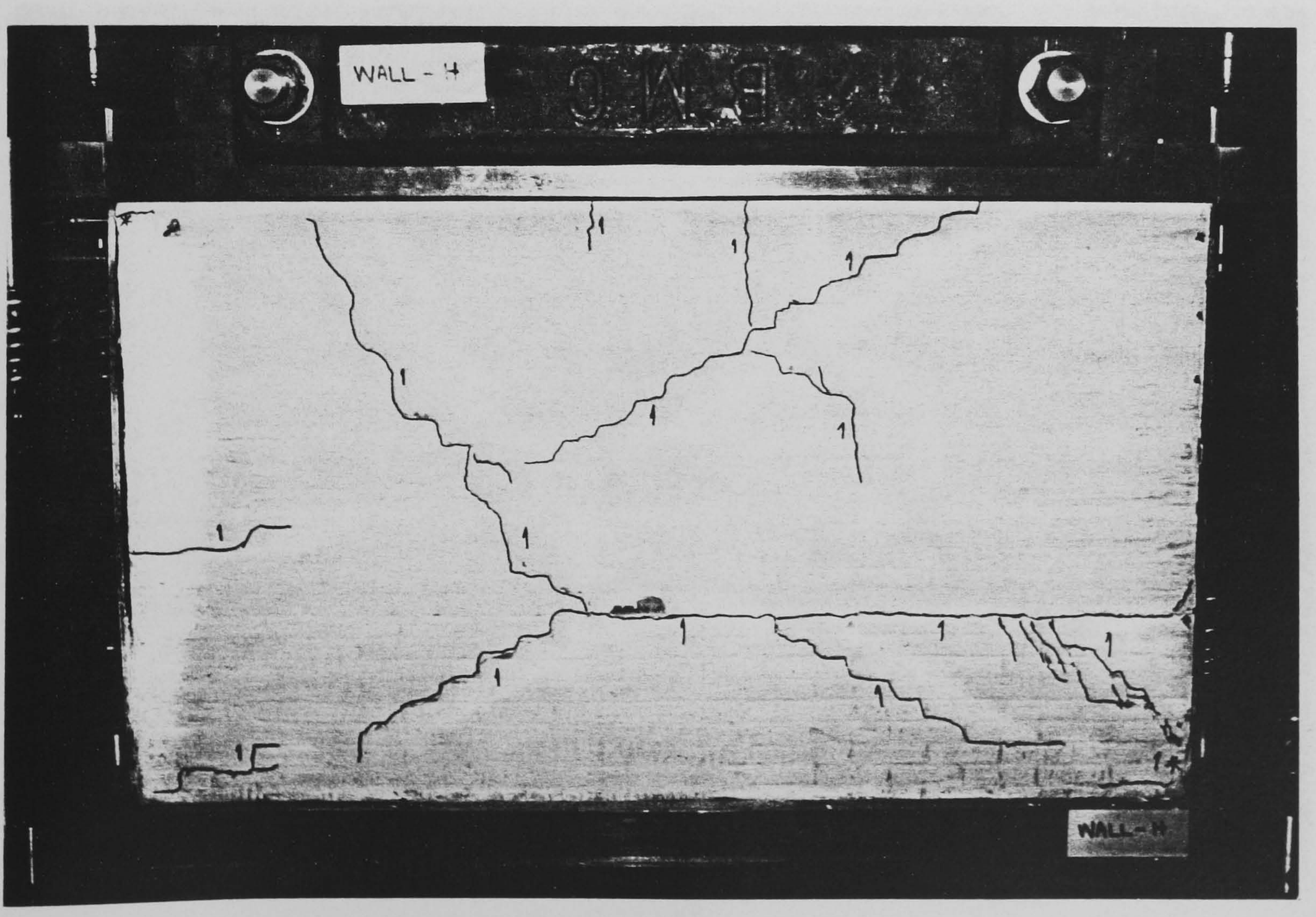

Photo 5.38 Crack 1 (wall-H)

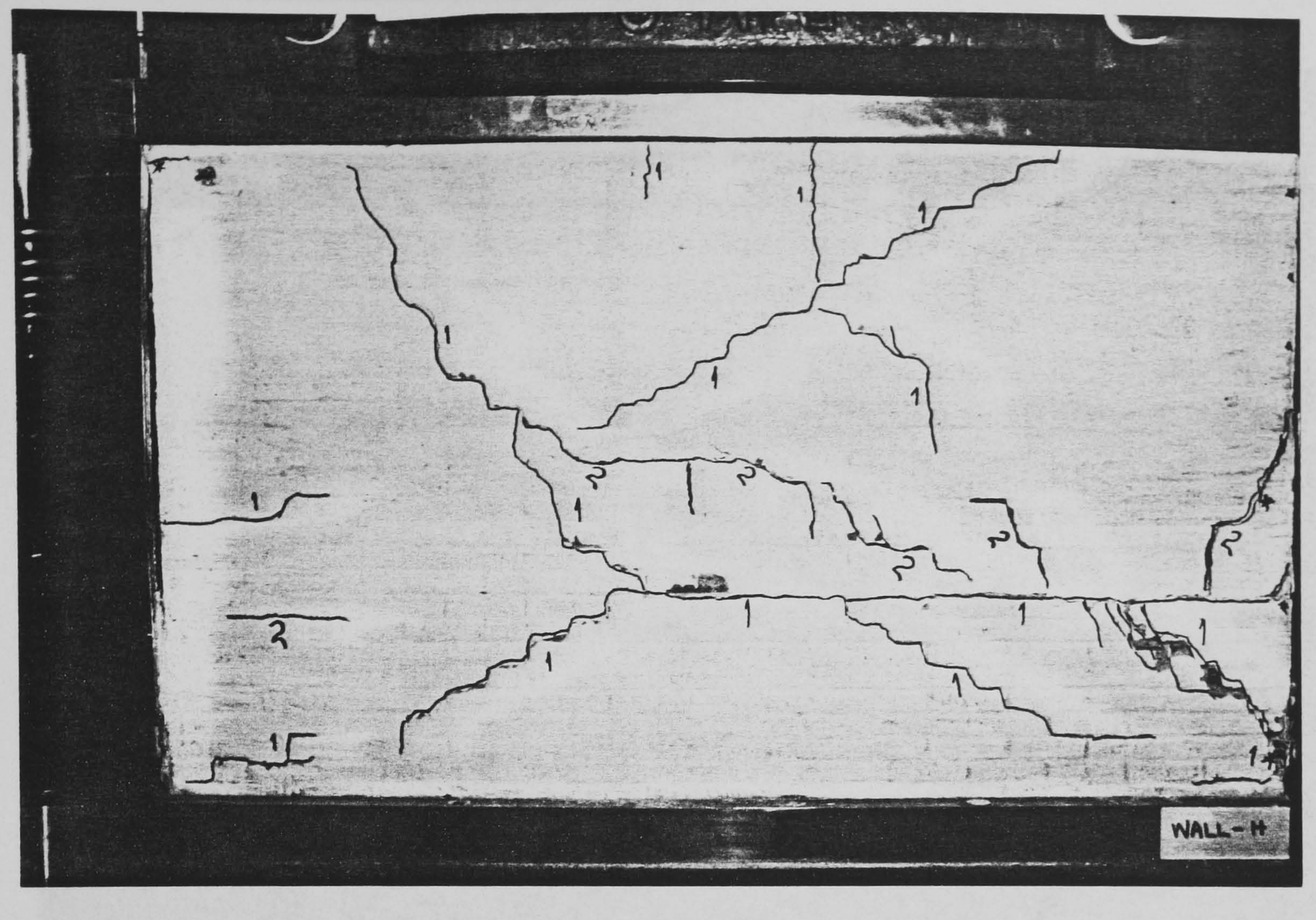

Photo 5.39 Crack 2 and lower corner crushing (wall-H)

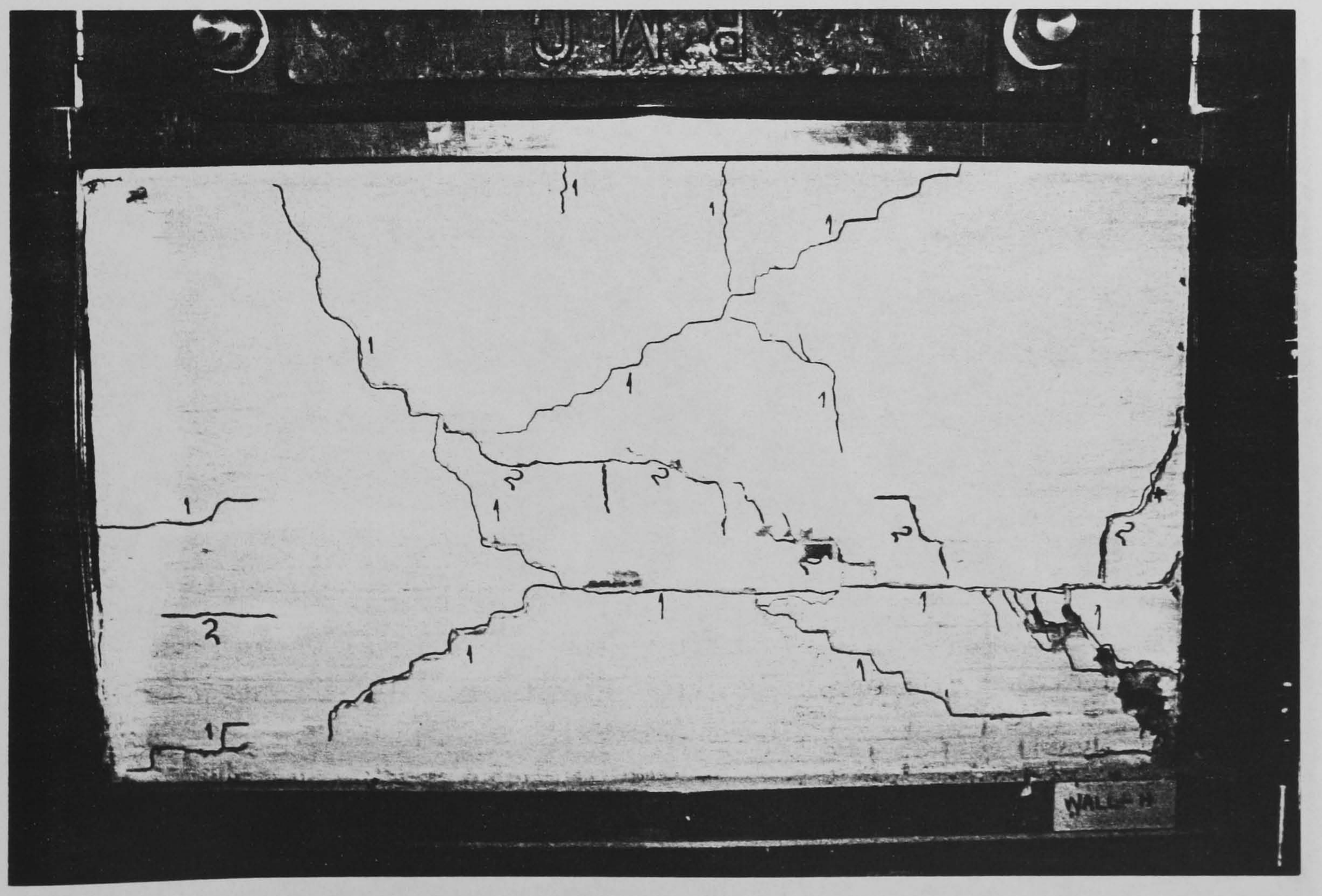

Photo 5.40 Collapse sequence-frame 1 (wall-H)

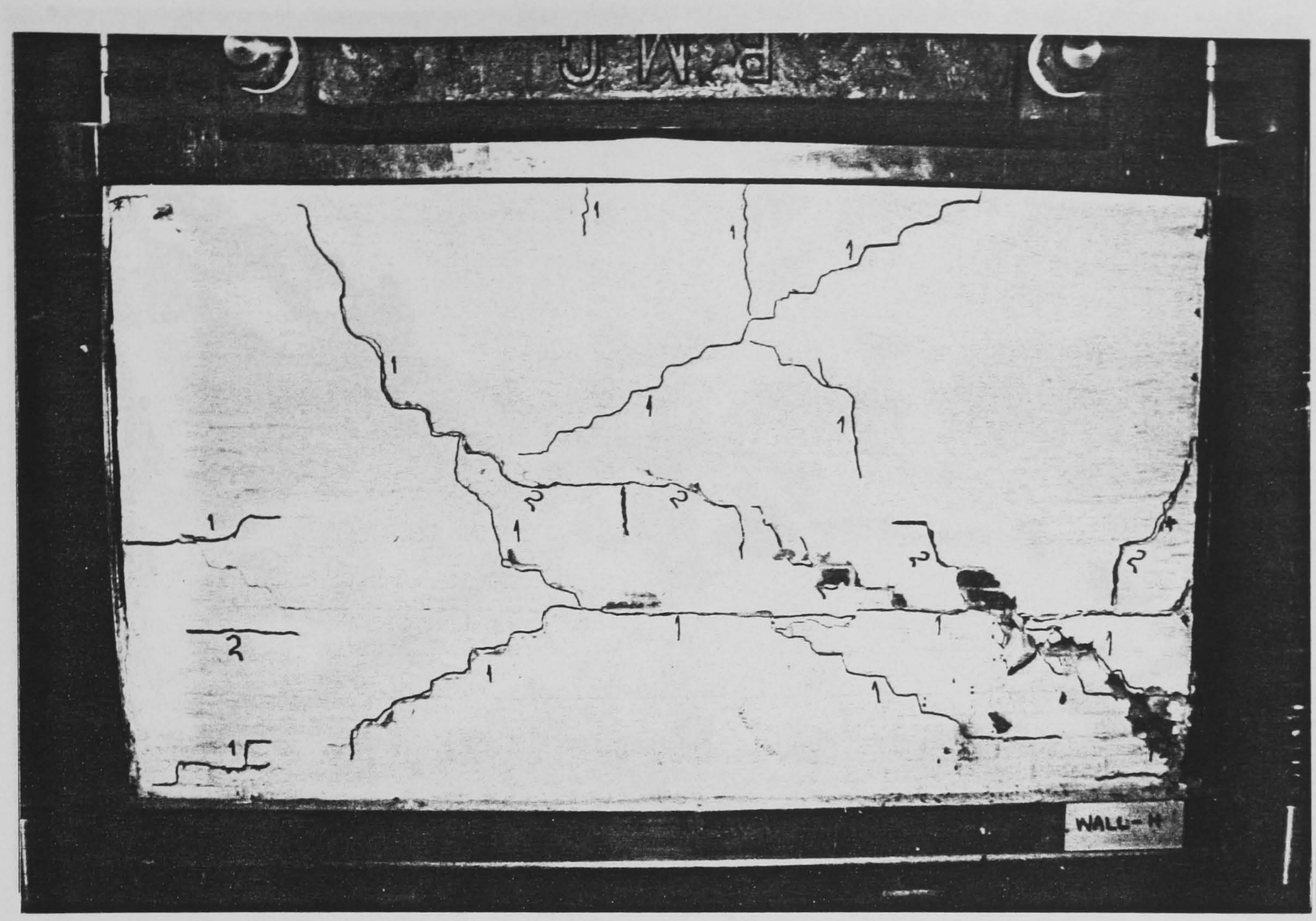

Photo 5.41 Collapse sequence-frame 2 (wall-H)

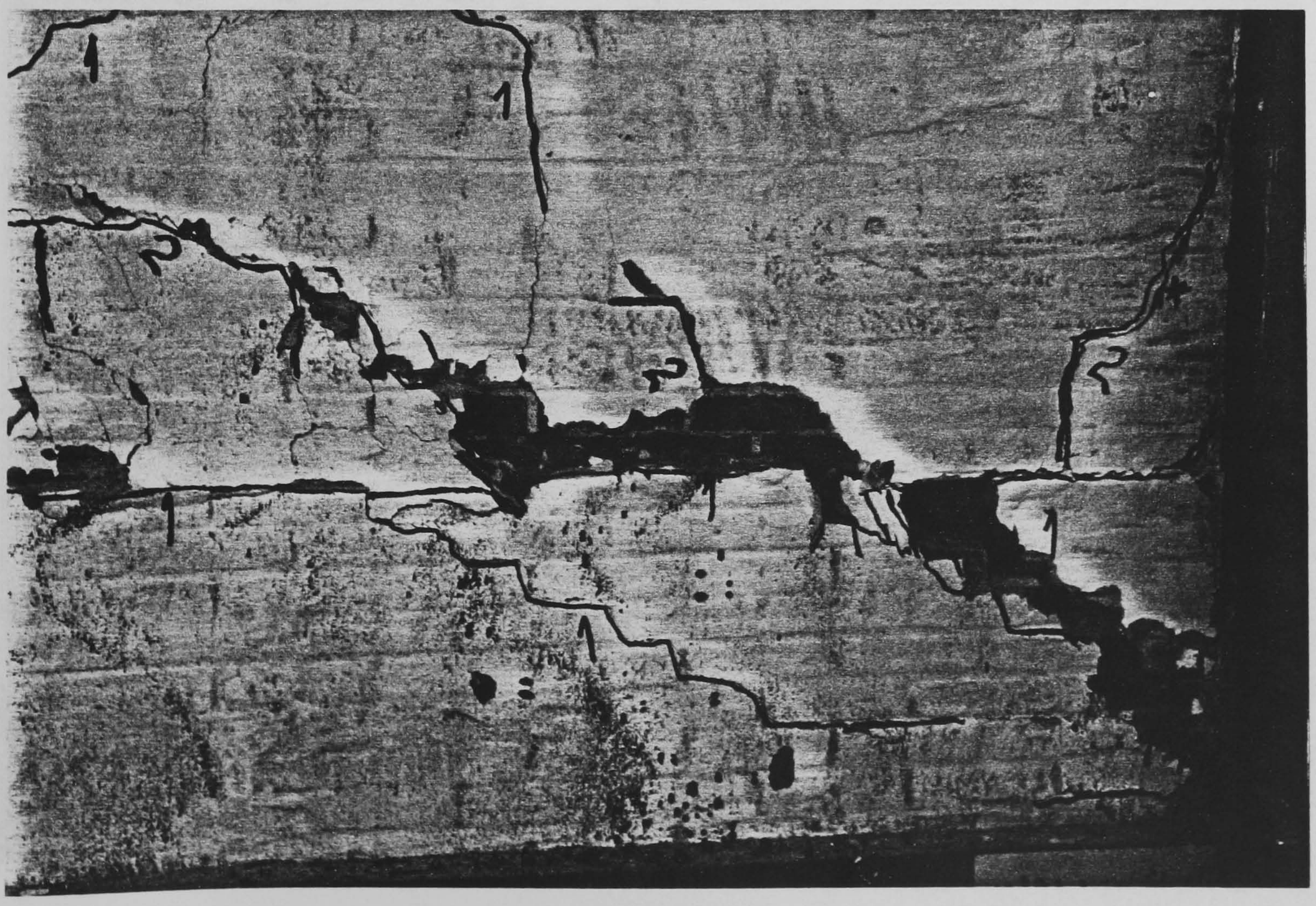

Photo 5.42 Close-up detail during collapse sequence-frame 3 (wall-H)

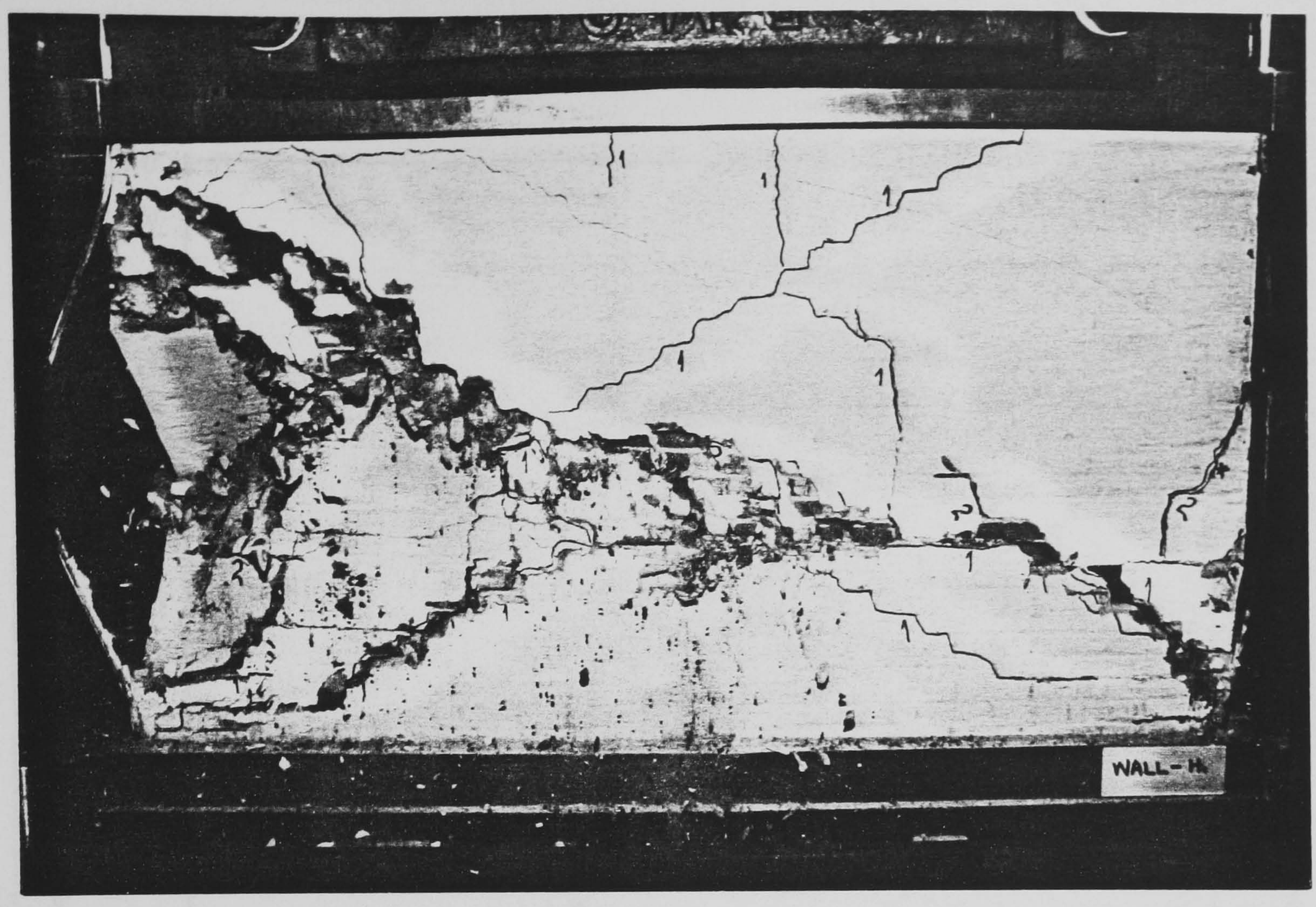

Photo 5.43 Collapsing of wall-H sequence-frame 4

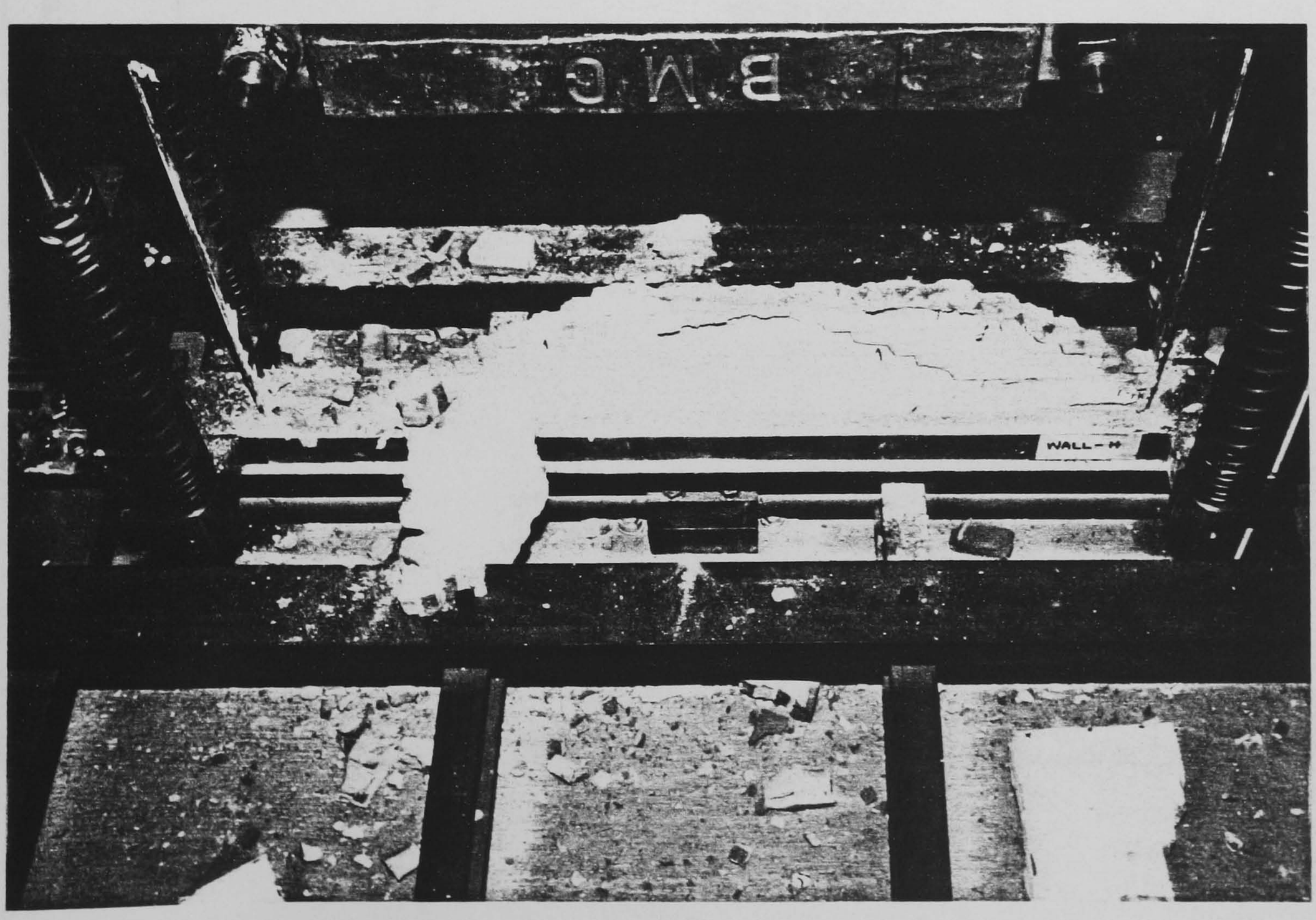

Photo 5.44 Final sequence-frame 5 (wall-H)

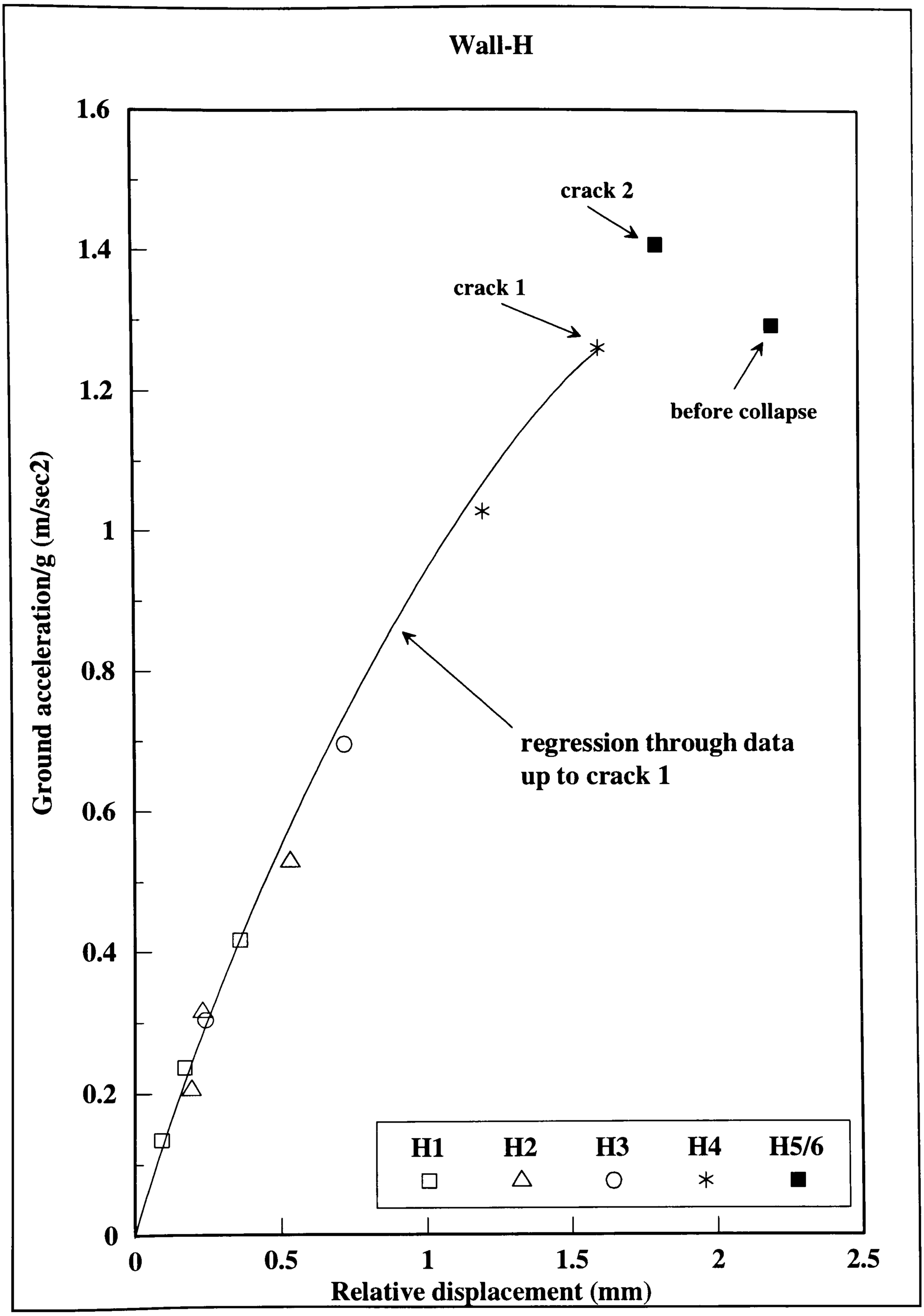

Figure 5.78 Summary of dynamic response for wall-H

5.8.4.1 Observations for wall-H.

This panel was built with the second type of brick units which incorporated lead shot in the casting mix. As a result the weight of the wall increased by about 150% in comparison with the other panels. This increase in the panel self-weight was not high enough to contribute to any major changes in the fundamental natural frequency. Since no similar test is reported in literature, where extra mass was incorporated into the material itself as well as lumped at the top, results from this test cannot be compared or correlated. After several cycles of increased intensity of the applied ground motion, crack 1 appeared at an acceleration of 1.26g. A horizontal flexural crack was first observed spanning half the panel length, followed by several stepwise diagonal cracks (photo 5.38). Crack 2 appeared at the centre of the panel at an acceleration of 1.4g, and subsequently extended to connect parts of the first crack from the lower right to the top left corner, whereas the horizontal crack did not extend in length, possibly due to the effect of the prestressing axial force. Crushing of the two opposite corners of the main diagonal also occurred at this stage (photo 5.39). With the shaking table vibrating at 1.29g acceleration, the panel degraded rapidly and collapsed in a brittle mode. Photos 5.40 to 5.44 present the collapsing sequence which was photographically recorded at high speed and show the appearance of many new cracks as these occurred during a cycle which lasted less than 4 seconds. Final collapse (photo 5.43 and 5.44), is attributed to the extent of the cracking especially around the diagonal and the loss of stability which caused the left part of the panel to buckle due to the imposed weight and axial prestressing. A hammer impact test just after crack 2 appeared, measured a substantial decrease in the natural frequency (19.95 Hz) but only a small change in the equivalent viscous damping coefficient (5.5%). Compared with wall-D which had similar mechanical properties, this panel failed in a brittle mode and at a lower acceleration. One of the key differences observed between the two failure modes, was the extensive horizontal crack observed in wall-H, which coupled with the diagonal shear crack, caused the upper part of the panel to slide relatively to the bottom, with ground acceleration reversals, which as shown in photo 5.42 resulted in local crushing of the masonry at the lower end.

5.8.5 Fifth test : wall-R.

Wall-R was subjected to a similar pattern of increasing motor driving frequency and ground acceleration in the first five stages. The bricks for this wall were intentionally produced with a low compressive and tensile strength. Combined with a relatively strong mortar, it was anticipated that failure would involve tensile cracking and splitting of the units rather than mortar at the joints. After each crack occurred in the wall, the intensity of the applied ground motion was reduced to observe the post-cracking response. In the following pages the developing dynamic behaviour has been laid out in detail, in the order shown below.

- ► Free vibration amplitude decay records - hammer tests (figures 5.79 to 5.81).
- ► Displacement records (5.82 to 5.89).
- ► Sample hysteresis curves (5.90 to 5.91).
- ► Photographs of the cracking patterns (photo 5.45 to 5.56).
- ► Summary of dynamic response (figure 5.92).

The test procedure for wall-R is summarised in table 5.11, while results for the first natural frequency using the methods described previously are shown in table 5.10.

Theoretical	**Finite element**	**Hammer test**
54.7 Hz	67.1 Hz	38.46 Hz

Table 5.10 Natural frequency results (initial value) for wall-R

Stage/Run	Table accel.	Driving freq.	Damage	Natural freq.	Damping ratio	Rel. displ.	Comments
	g	Hz	Crack #	Hz	%	mm	
R1/R1	0.252	5.6	-	38.46	4.8	0.195	Increasing driv. frequency
R1/R2	0.383	6.3	-	-	-	0.302	
R1/R3	0.616	7.1	-	-	-	0.619	
R2/R1	0.322	5.6	-	-	-	0.265	Increasing driv. frequency
R2/R2	0.348	6.3	-	-	-	0.515	
R2/R3	0.727	7.1	-	-	-	0.737	
R3/R1	0.428	5.6	-	-	-	0.437	Increasing driv. frequency
R3/R2	0.624	6.3	-	-	-	0.678	
R3/R3	0.912	7.1	-	-	-	0.914	
R4/R1	0.502	6.2	-	-	-	0.503	LVDT failure in R4/R2
R5/R1	0.841	7.1	**1**	-	-	0.618	**First crack with irregular pattern (localised compressive vertical splitting associated with flaws in the units)**
R6/R1	0.884	6.9	**2**	-	-	0.8	**Stepwise symmetrical diagonal tensile cracking**
R6/R2	0.625	6.1	-	-	-	0.541	
R7/R1	1.534	7.5	**3**	-	-	1.11	**Corner cracking Extension of crack 2 towards the corners**
R7/R2	0.588	6.4	-	-	-	0.995	
R8/R1	1.559	7.5	**4**	21.74	7.7	1.25	**Further diagonal stepwise tensile cracking Corner crushing**
R8/R2	0.646	6.2	**5**	19.03	11.2	0.923	
R9	1.2	-	-	-	-	-	**Collapse**

(Crack numbers correspond to the cracking as noted in the photographs)

(Instrumentation was removed from the wall in stage R9, following crushing of the upper corner where the LVDTs were located).

Table 5.11 Wall-R testing sequence

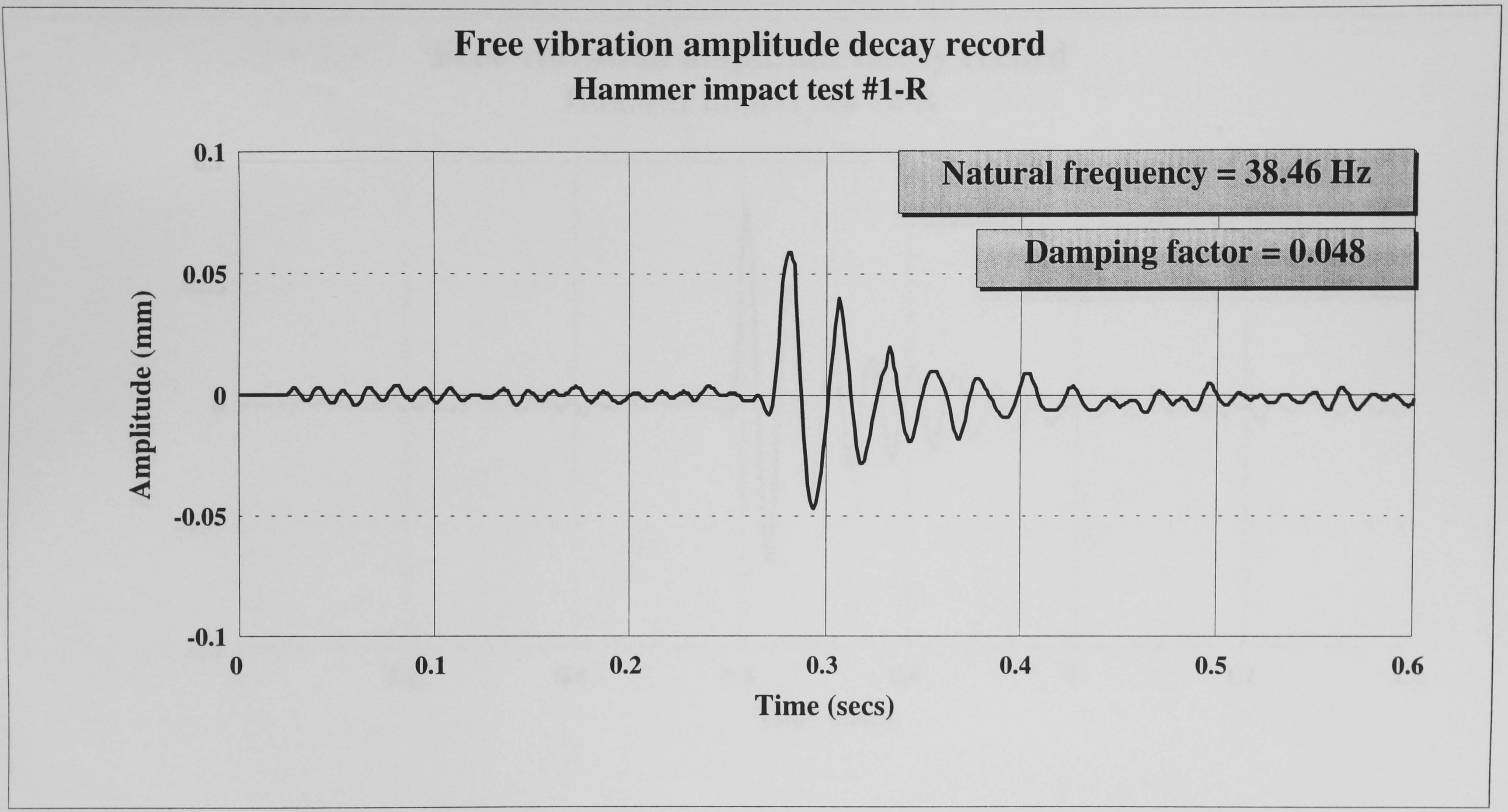

Figure 5.79 Initial free vibration amplitude decay

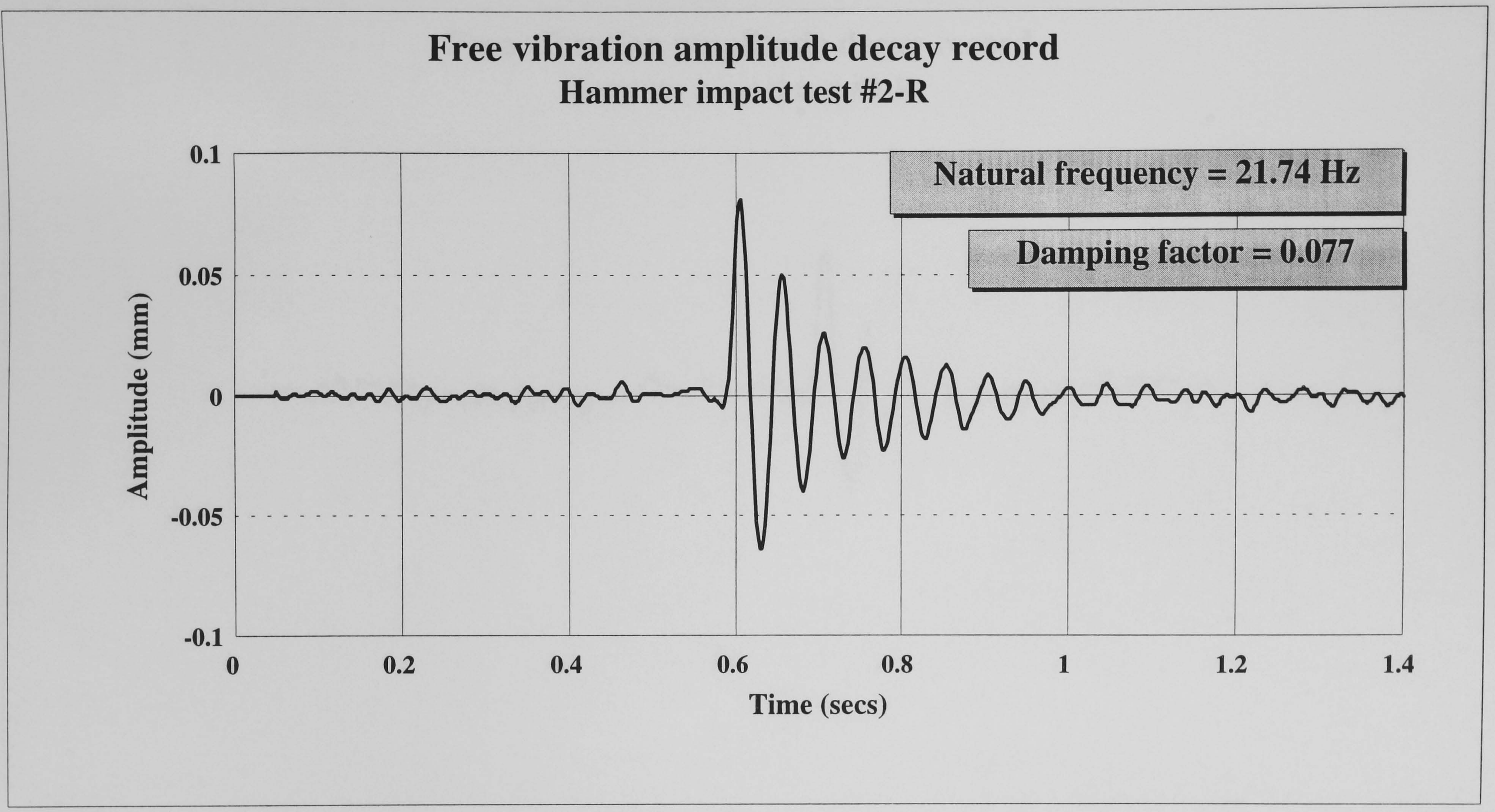

Figure 5.80 Free vibration amplitude decay after crack 4

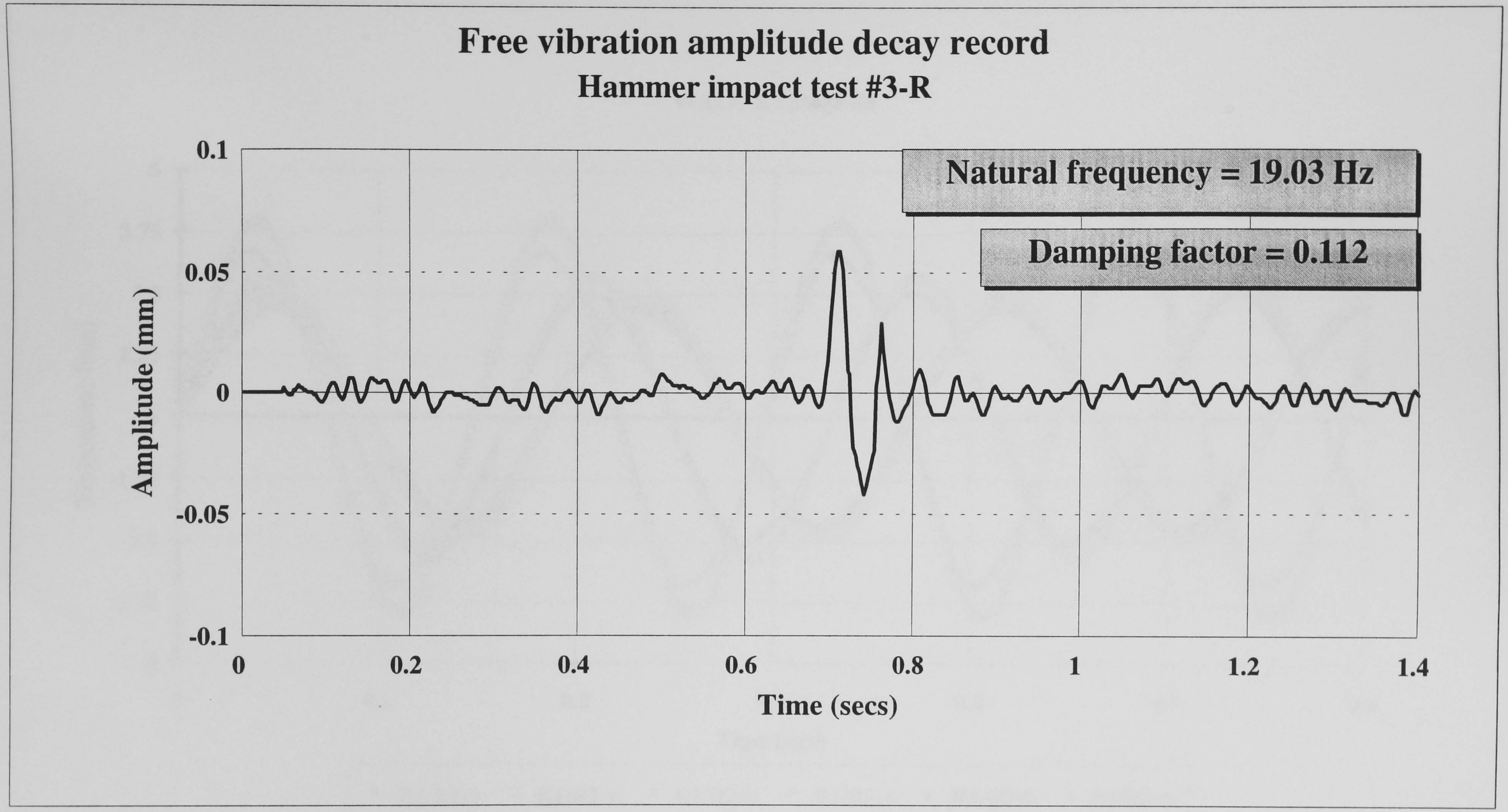

Figure 5.81 Free vibration amplitude decay after crack 5

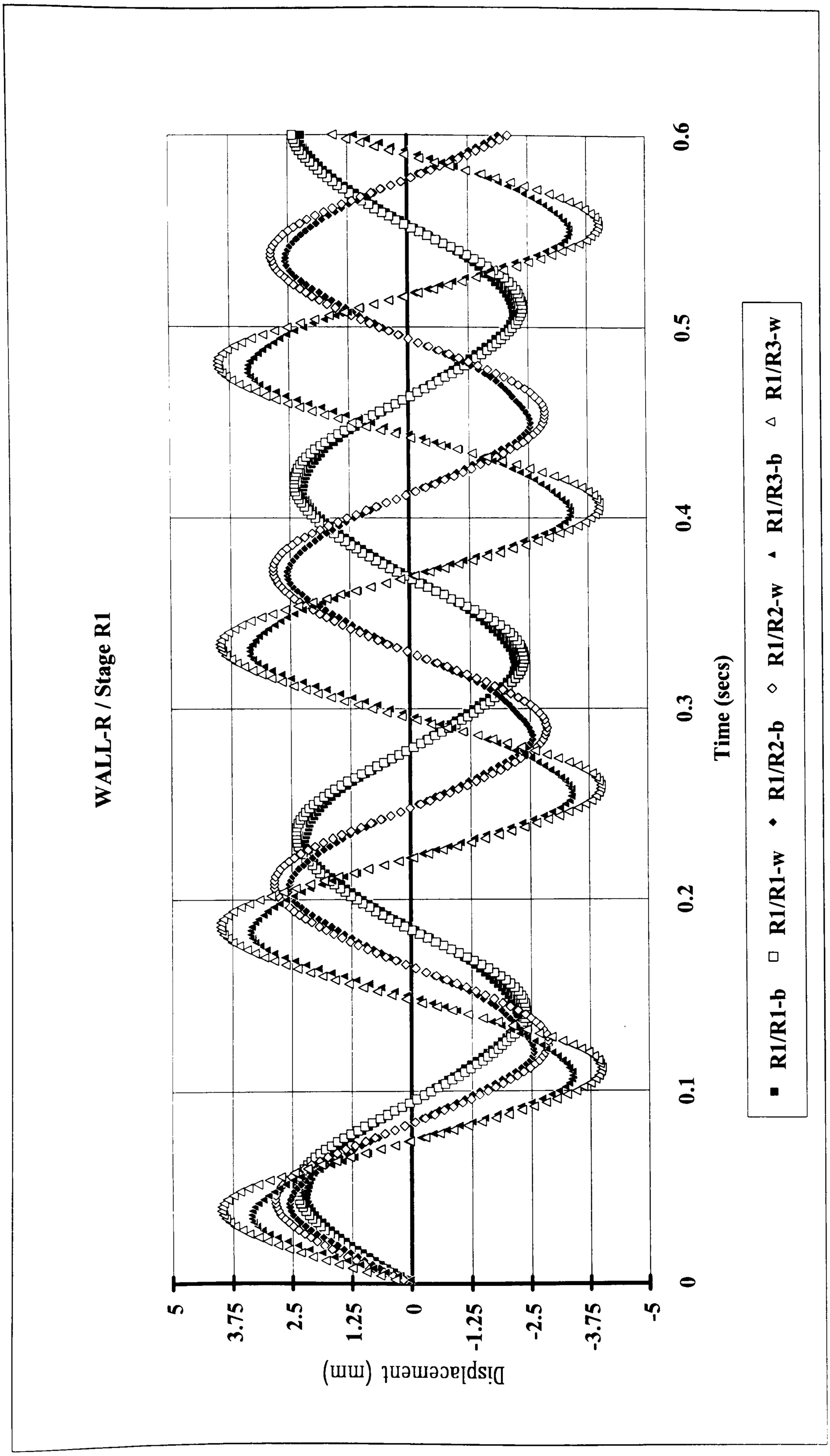

Figure 5.82 Wall-R / Stage R1

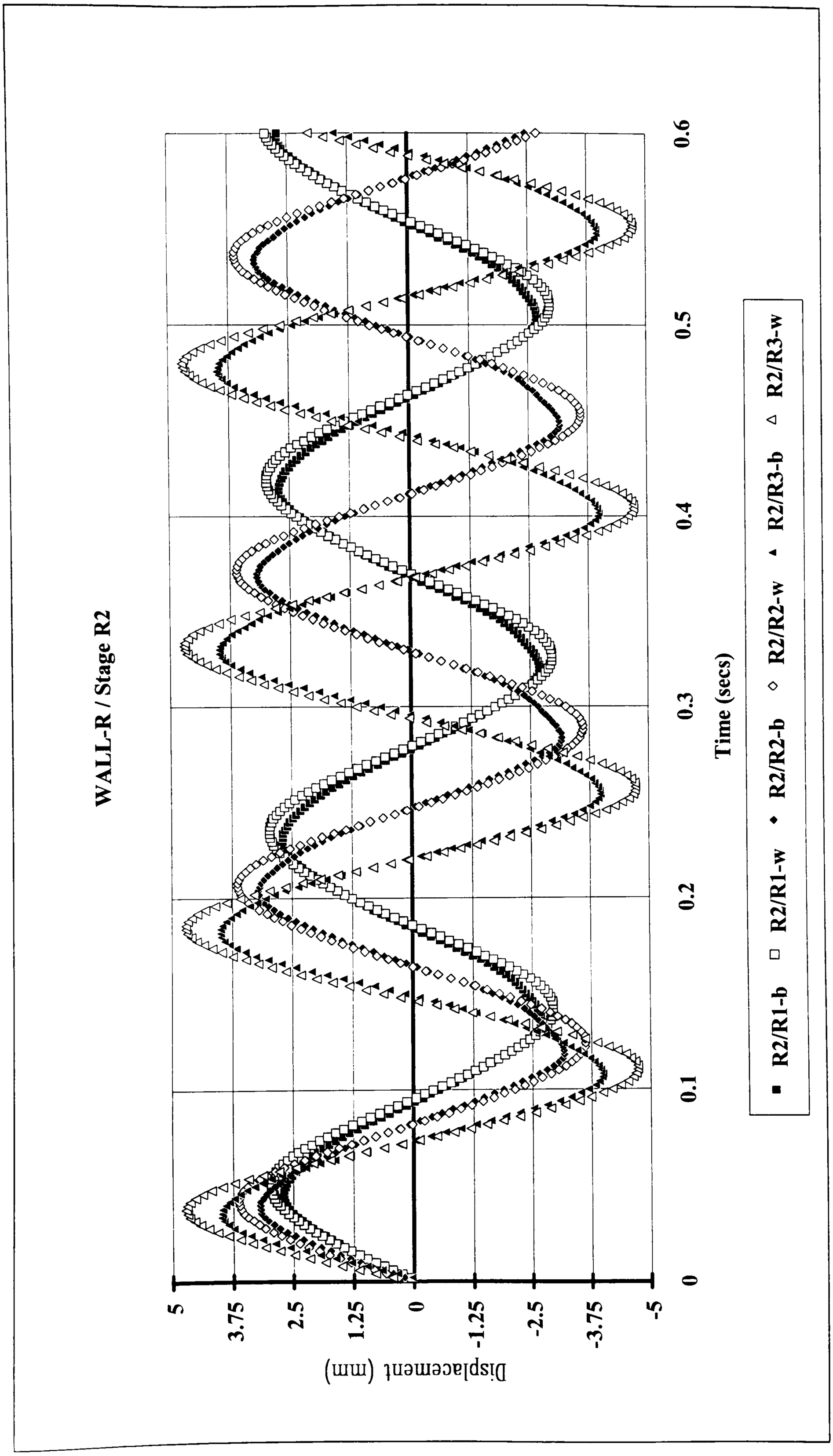

Figure 5.83 Wall-R / Stage R2

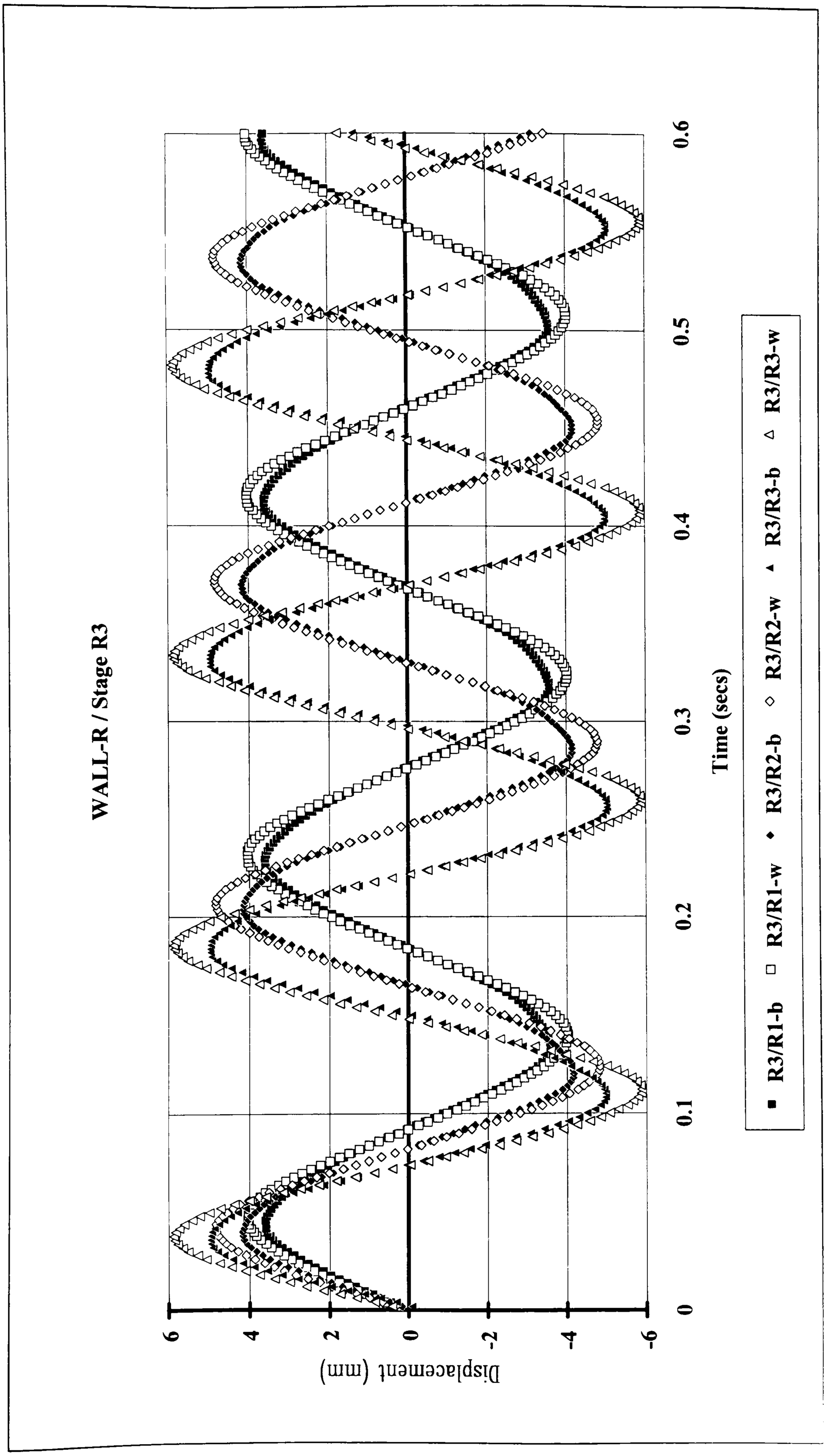

Figure 5.84 Wall-R / Stage R3

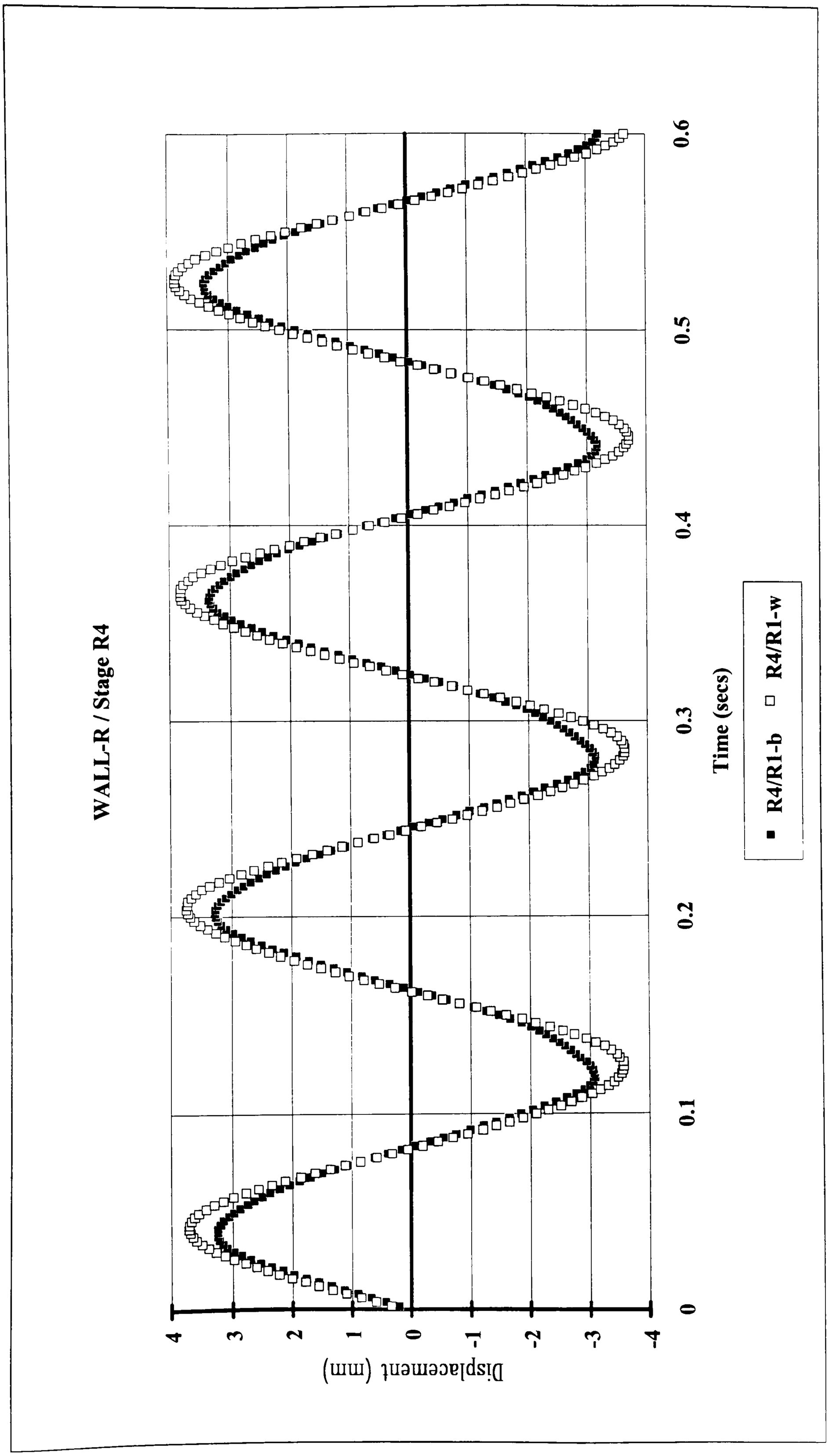

Figure 5.85 Wall-R / Stage R4

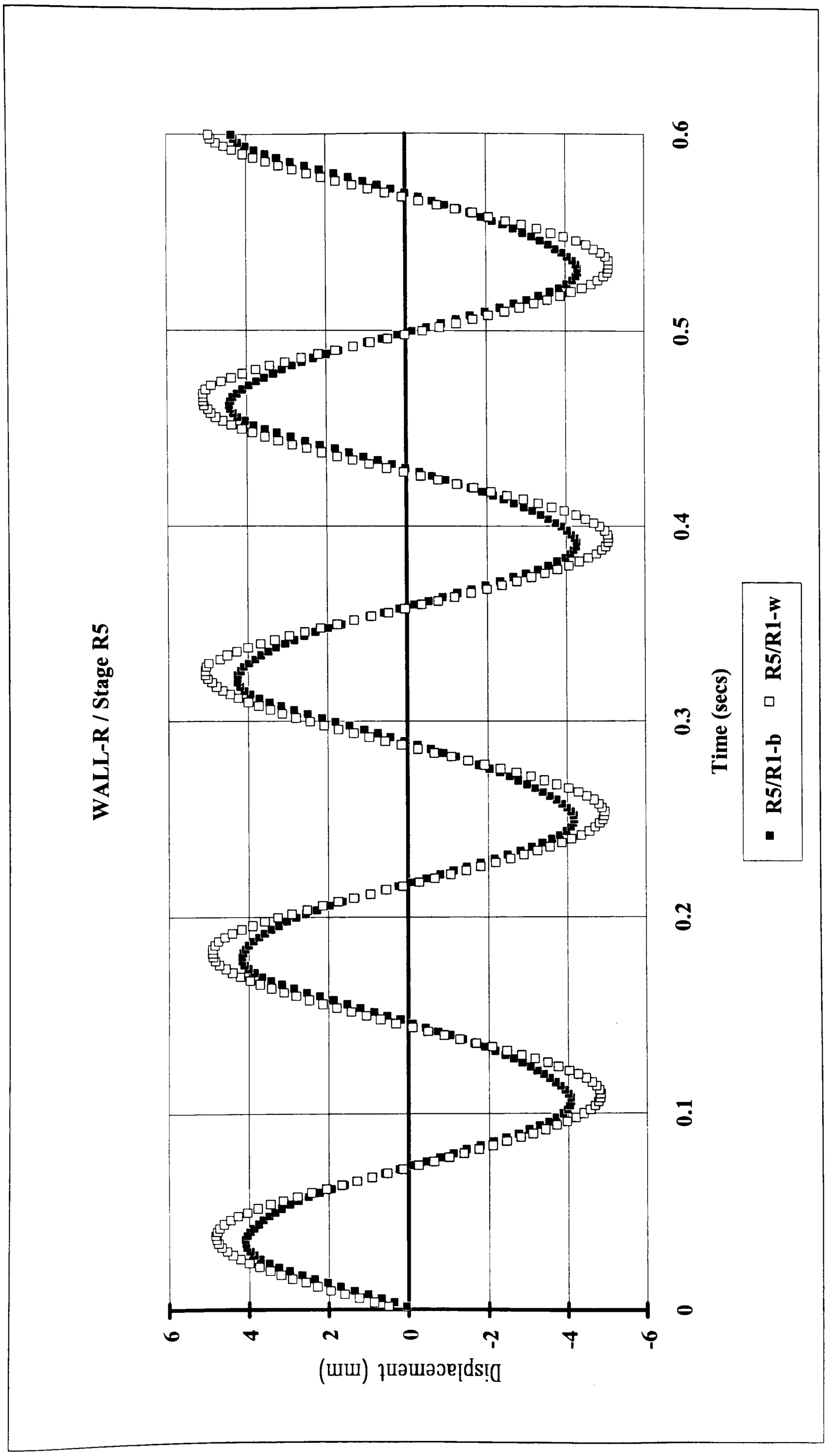

Figure 5.86 Wall-R / Stage R5

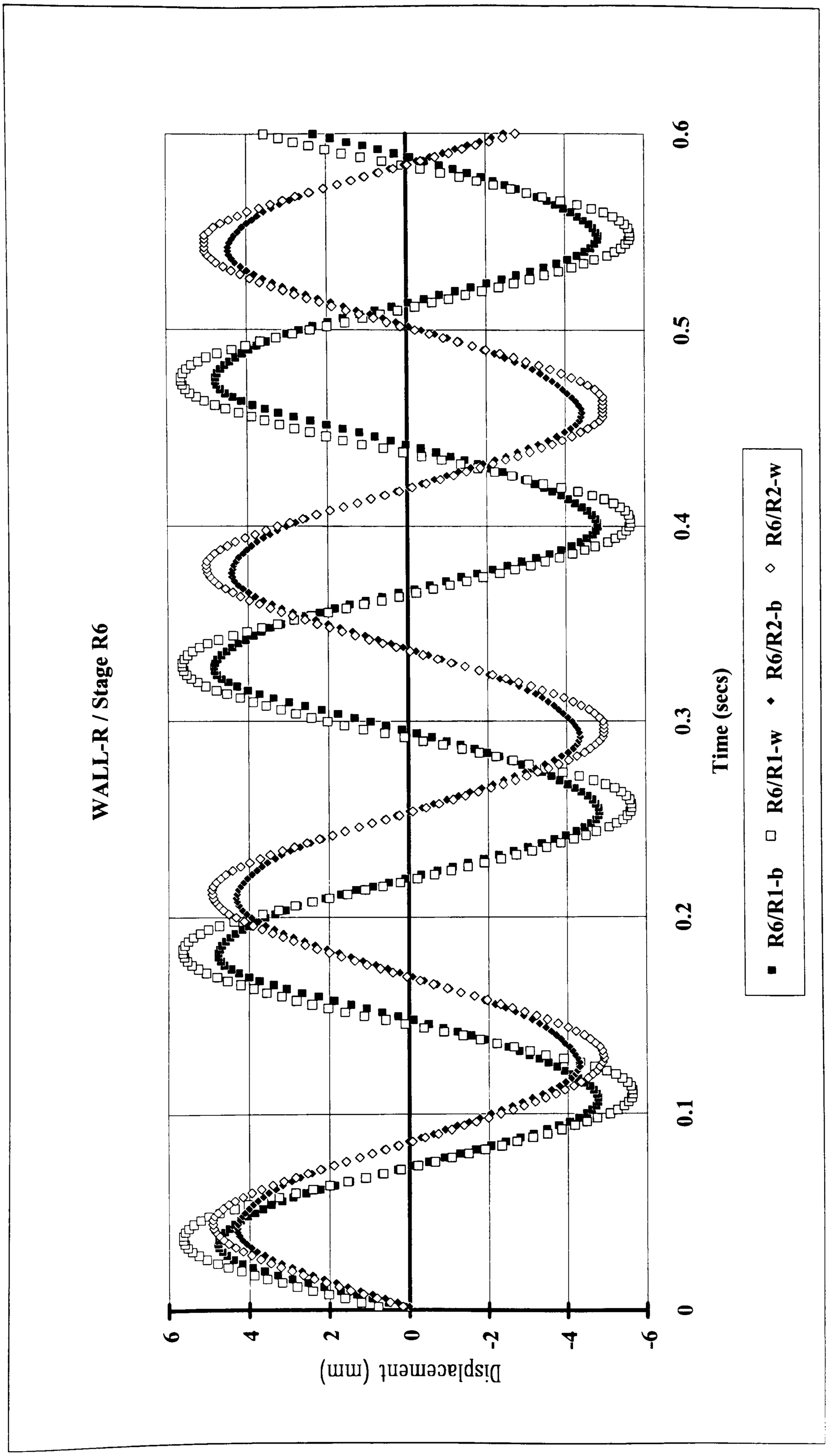

Figure 5.87 Wall-R / Stage R6

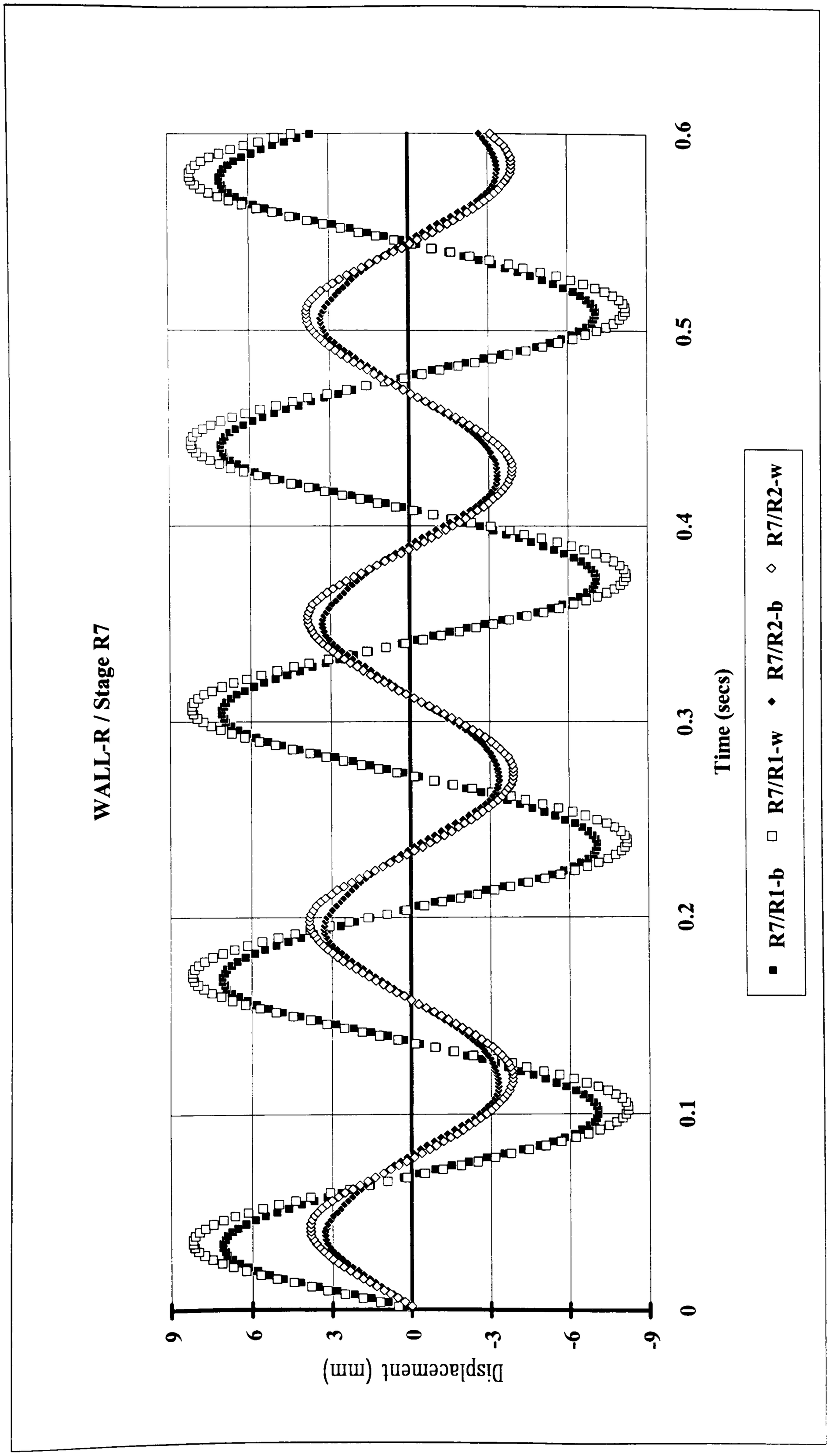

Figure 5.88 Wall-R / Stage R7

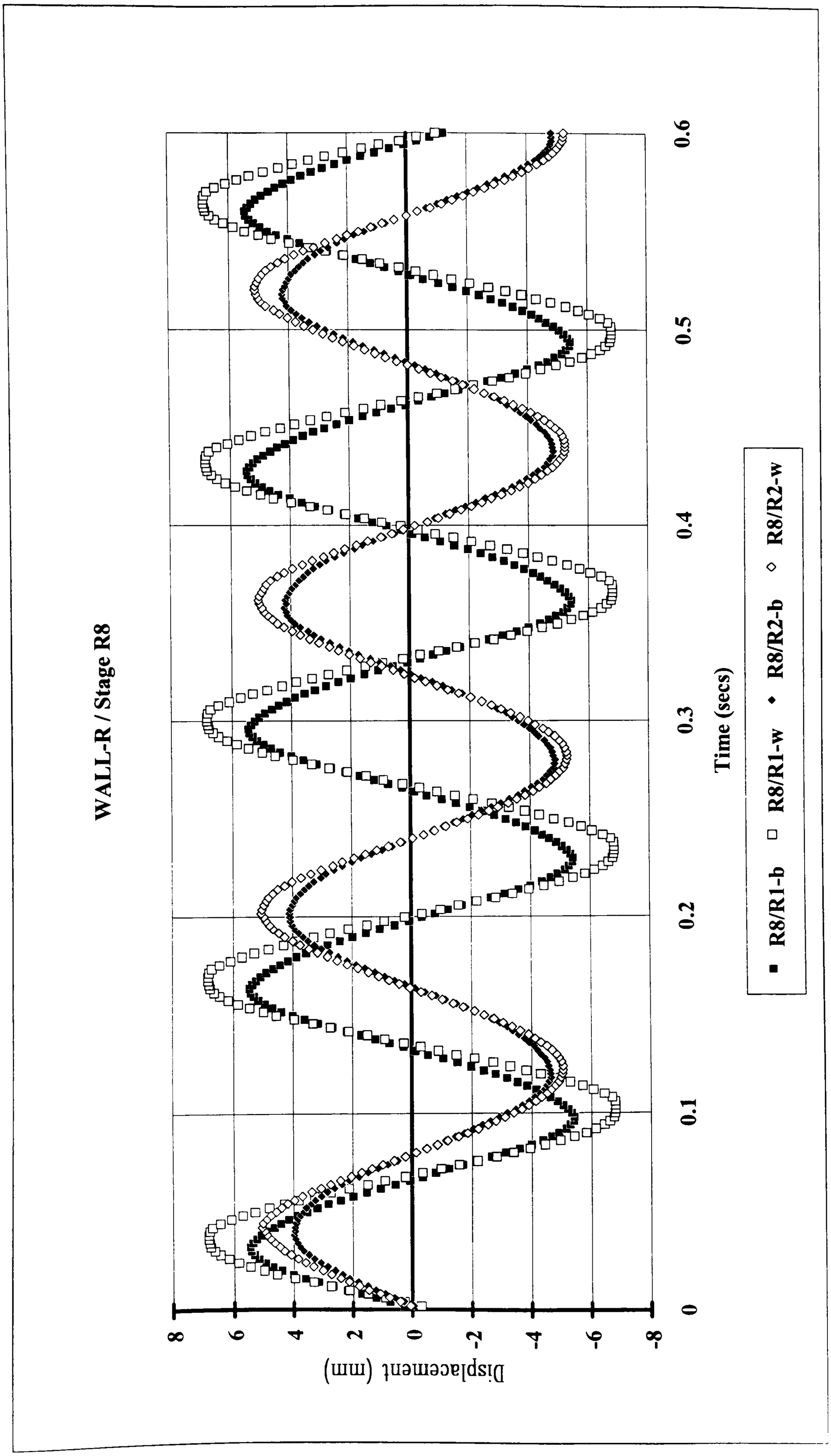

Figure 5.89 Wall-R / Stage R8

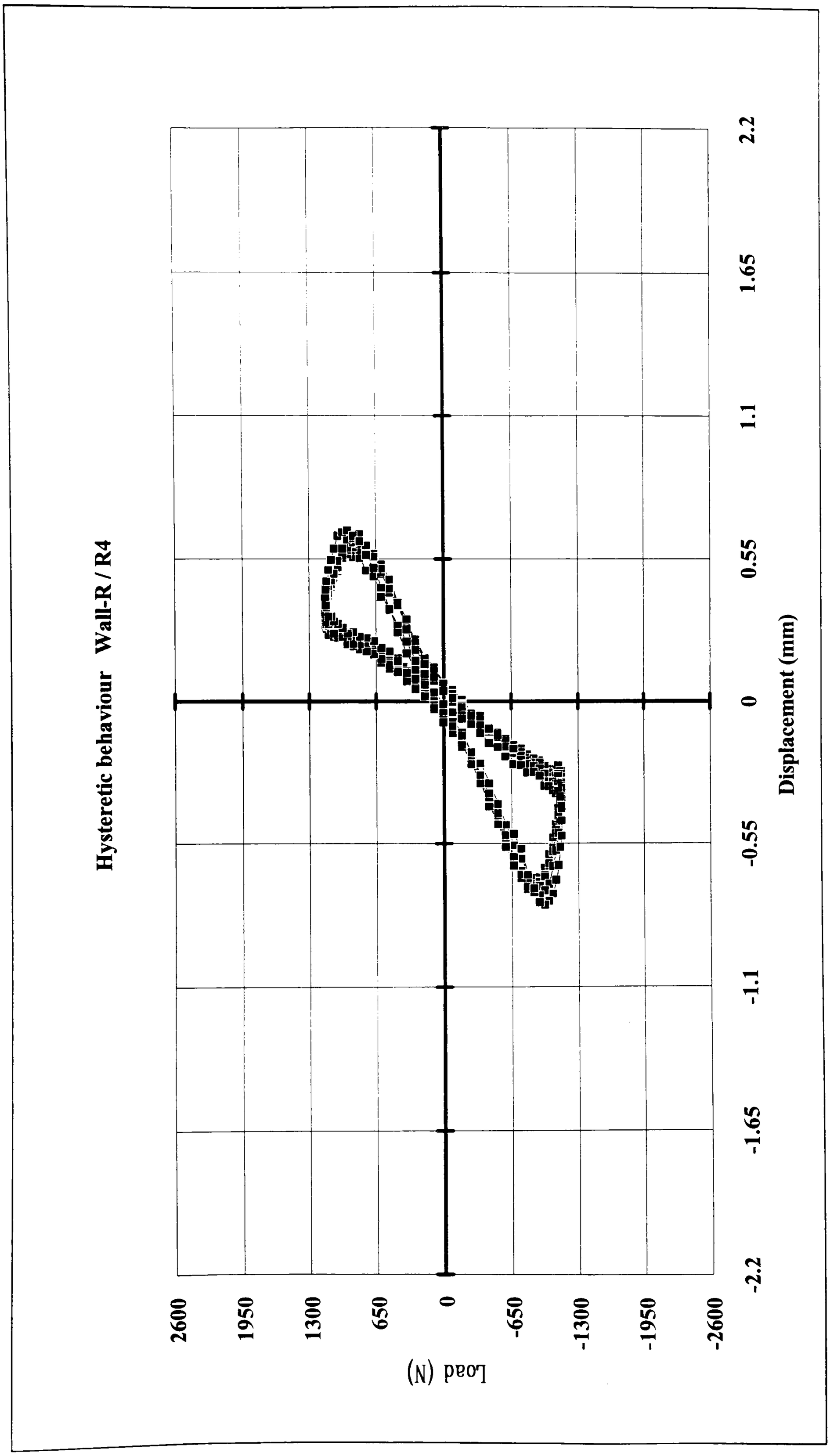

Figure 5.90 Wall-R / Hysteretic Behaviour - Stage R4

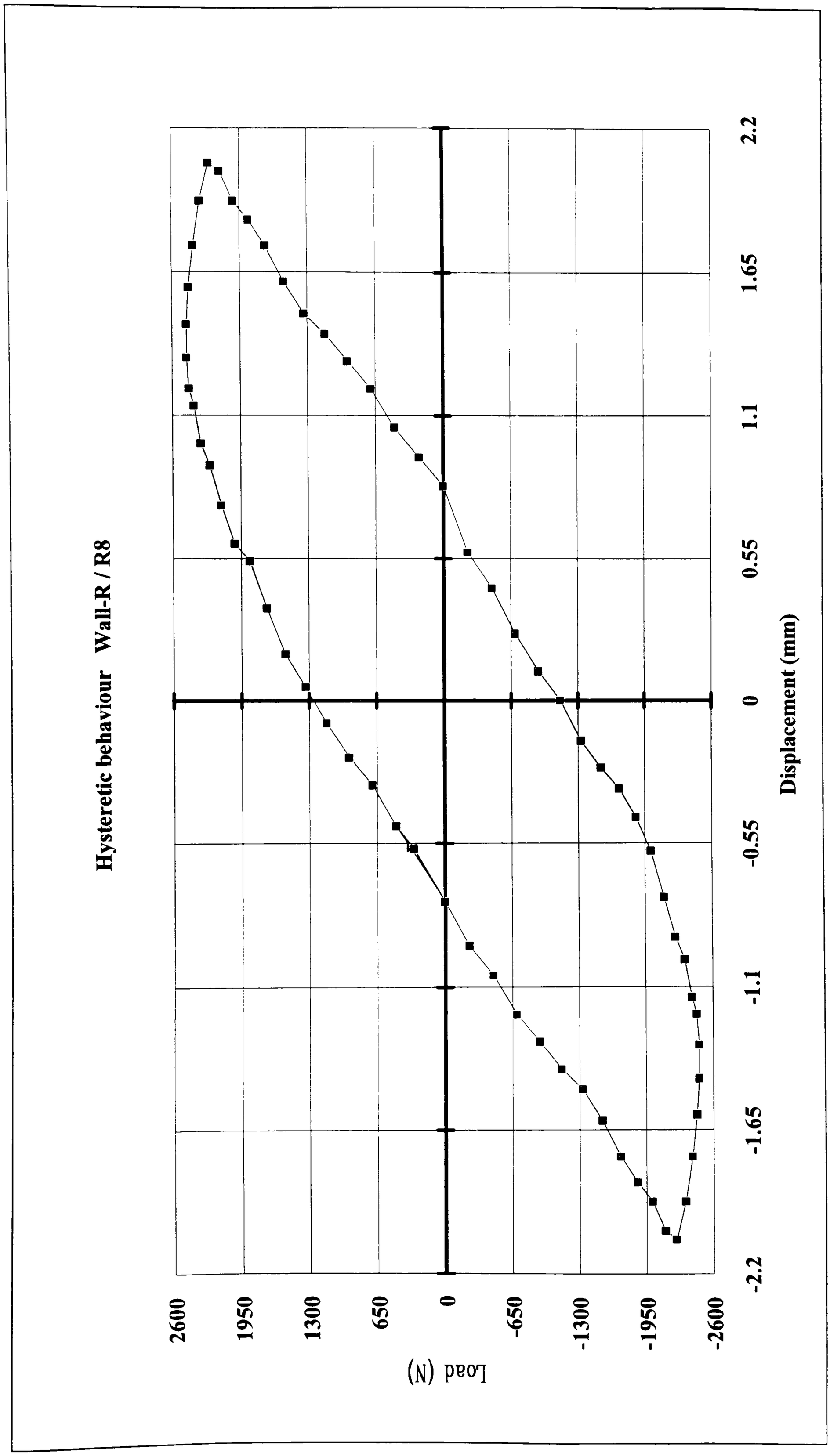

Figure 5.91 Wall-R / Hysteretic Behaviour - Stage R8

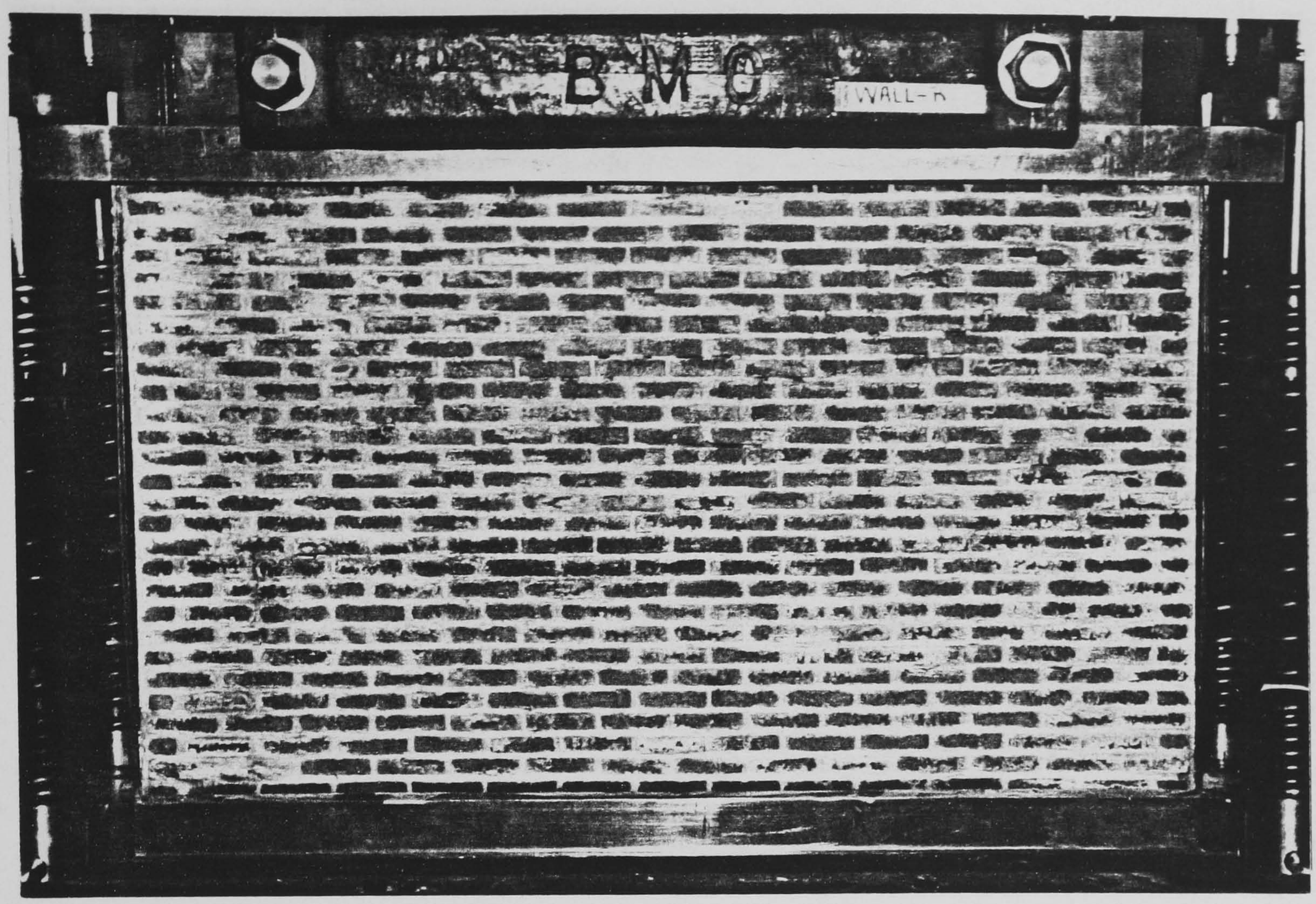

Photo 5.45 Wall-R ready for testing

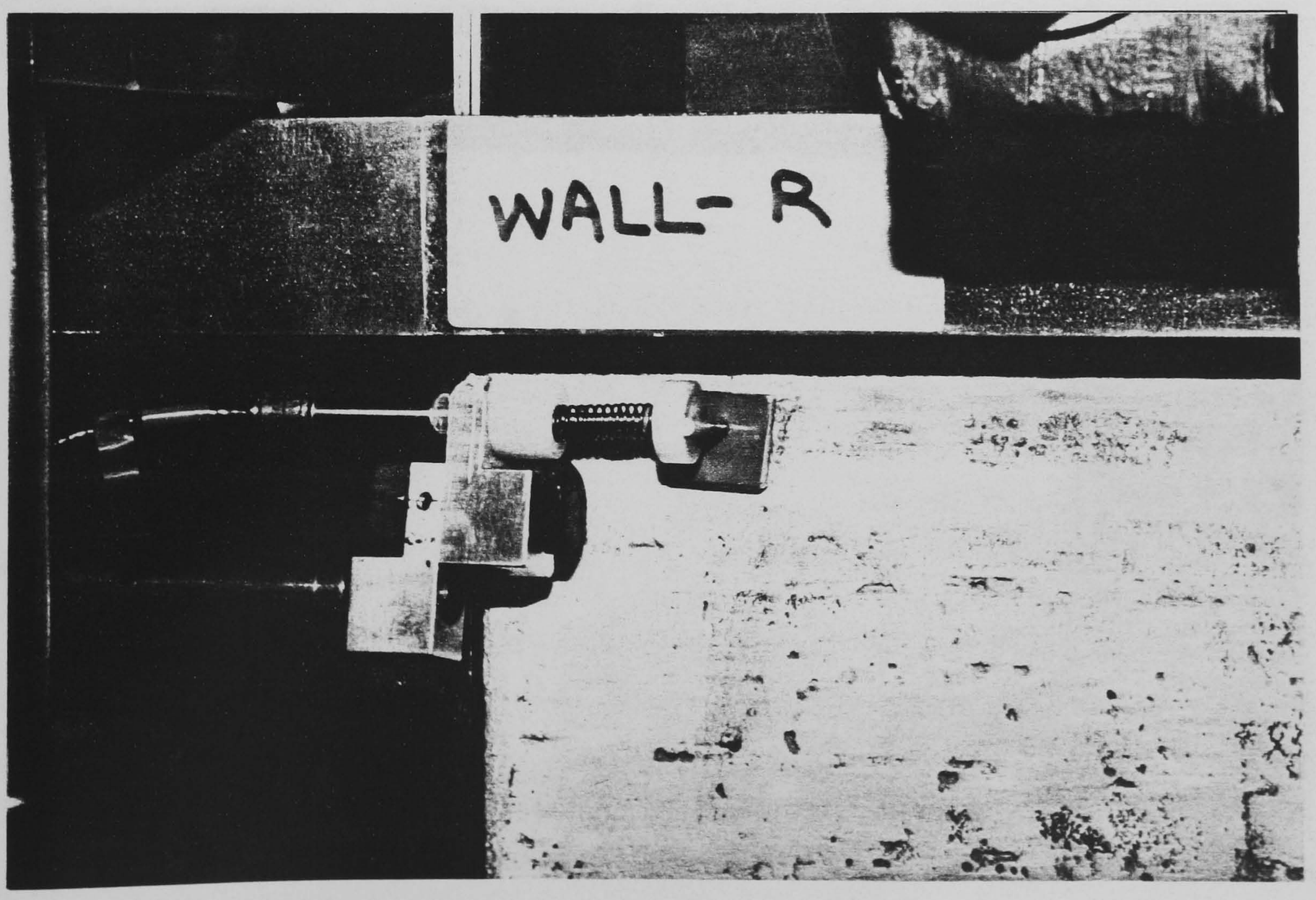

Photo 5.46 Instrumentation detail (wall-R)

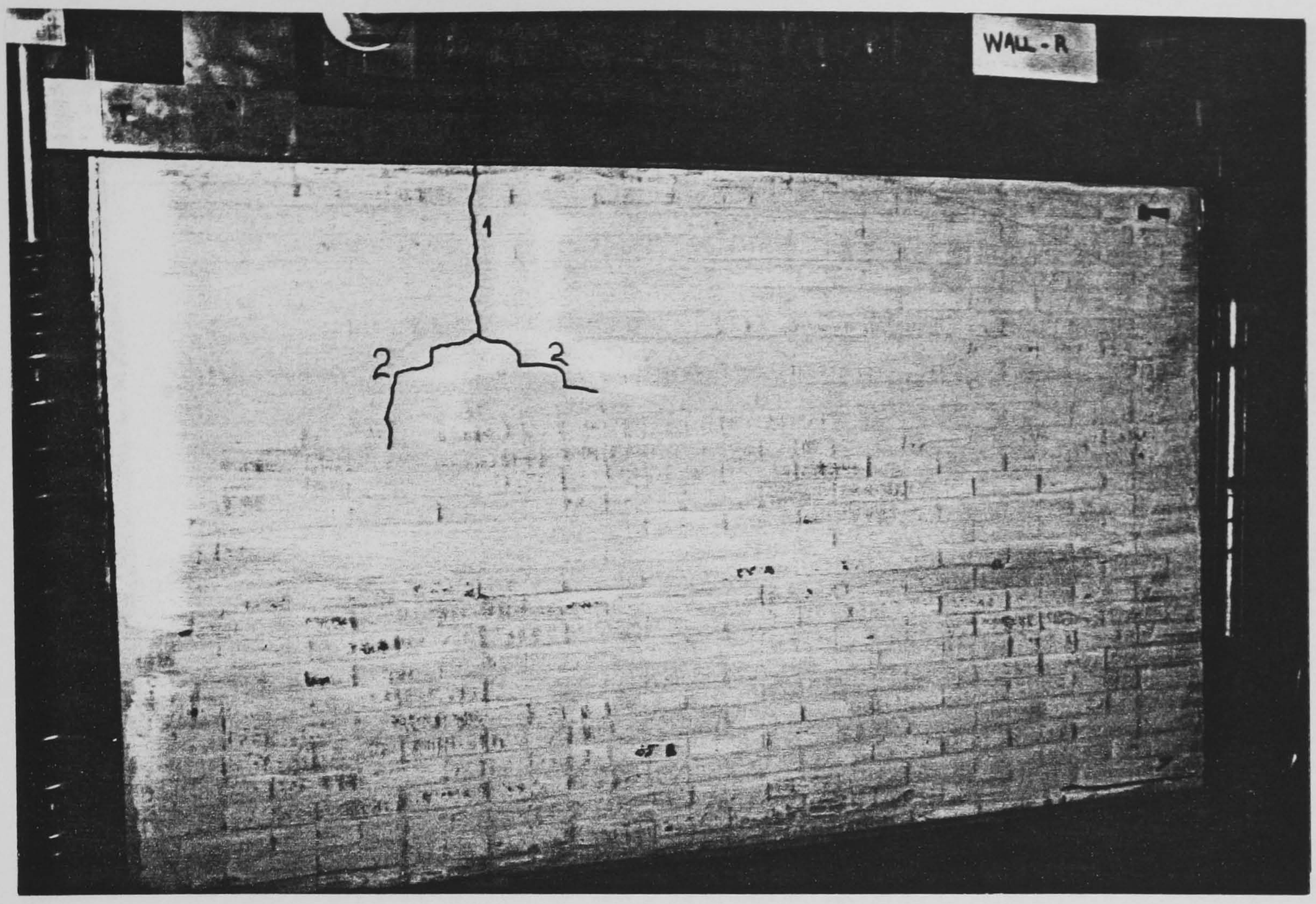

Photo 5.47 Crack 1 (wall-R)

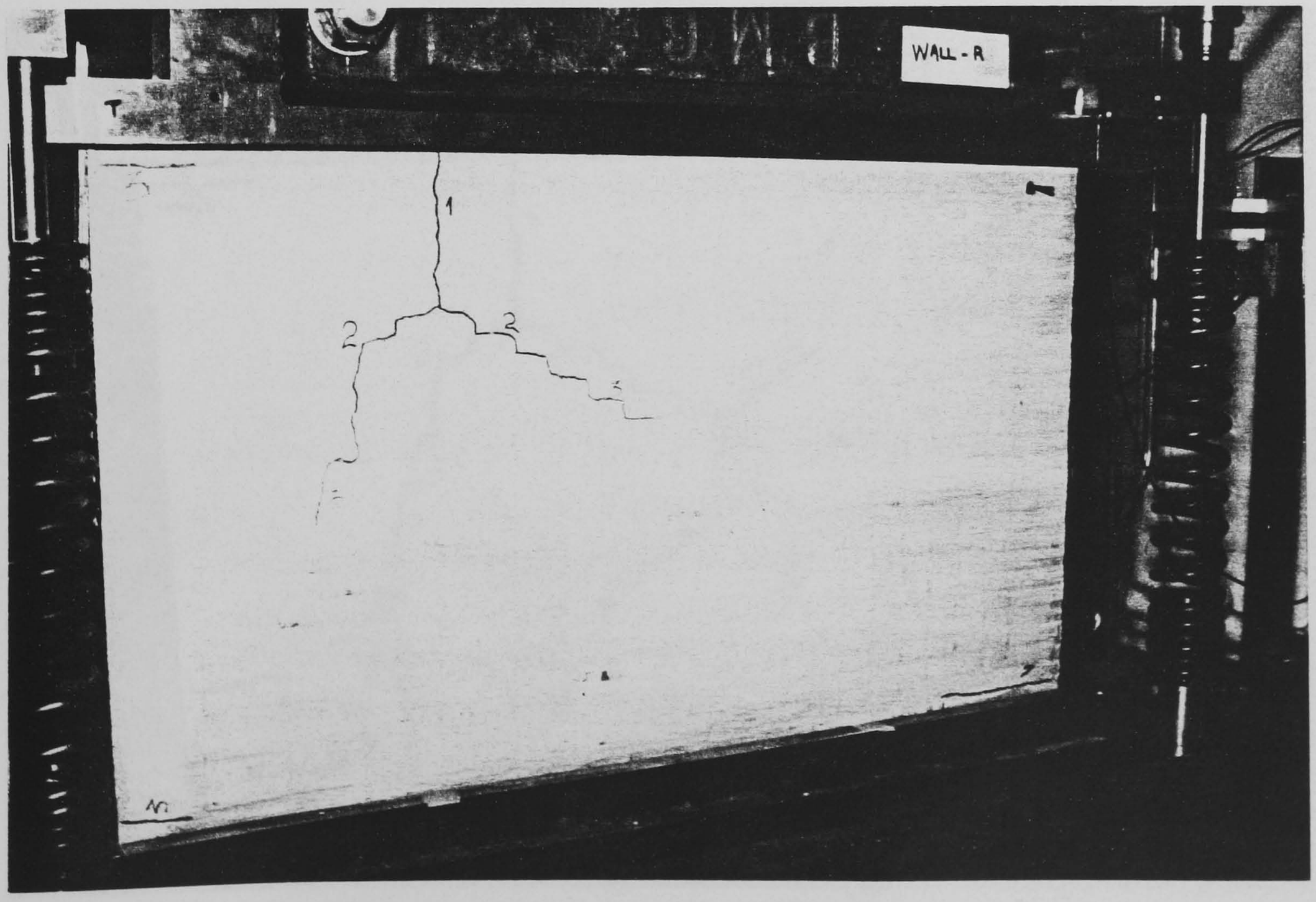

Photo 5.48 Crack 2 and 3 (wall-R)

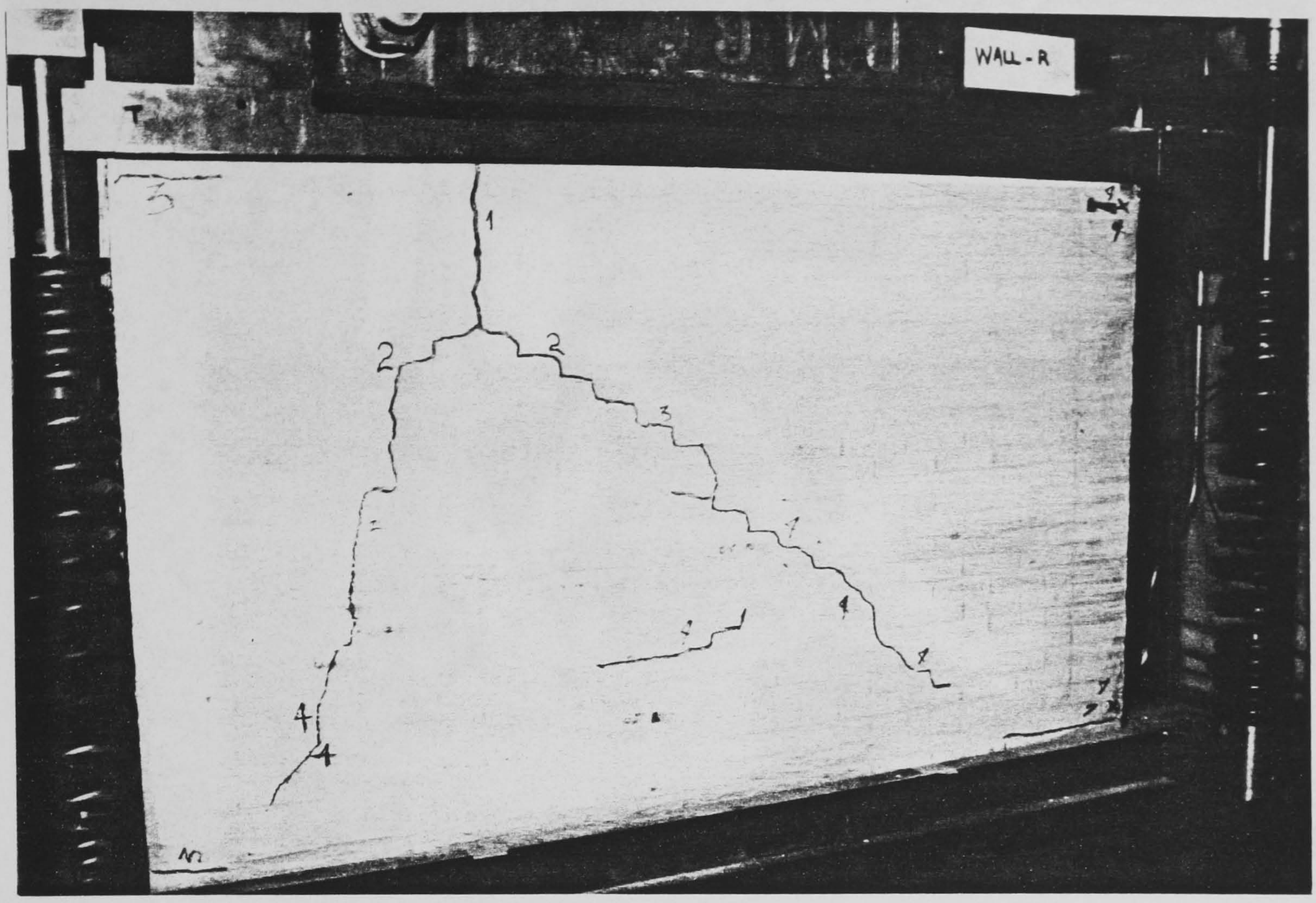

Photo 5.49 Crack 4 (wall-R)

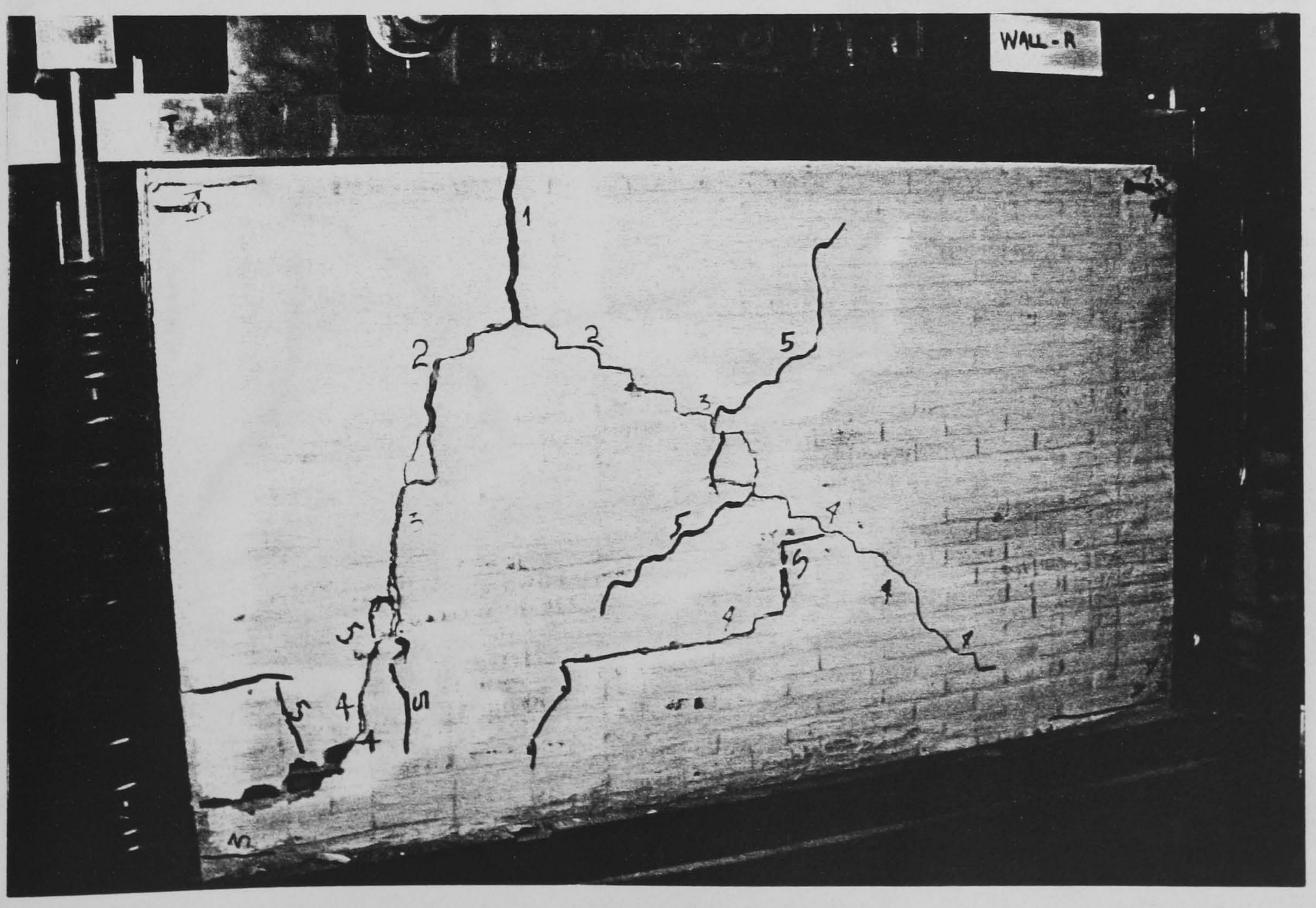

Photo 5.50 Crack 5, widening of crack 1 and corner crushing (wall-R)

Photo 5.51 Close-up detail of upper left corner crushing (wall-R)

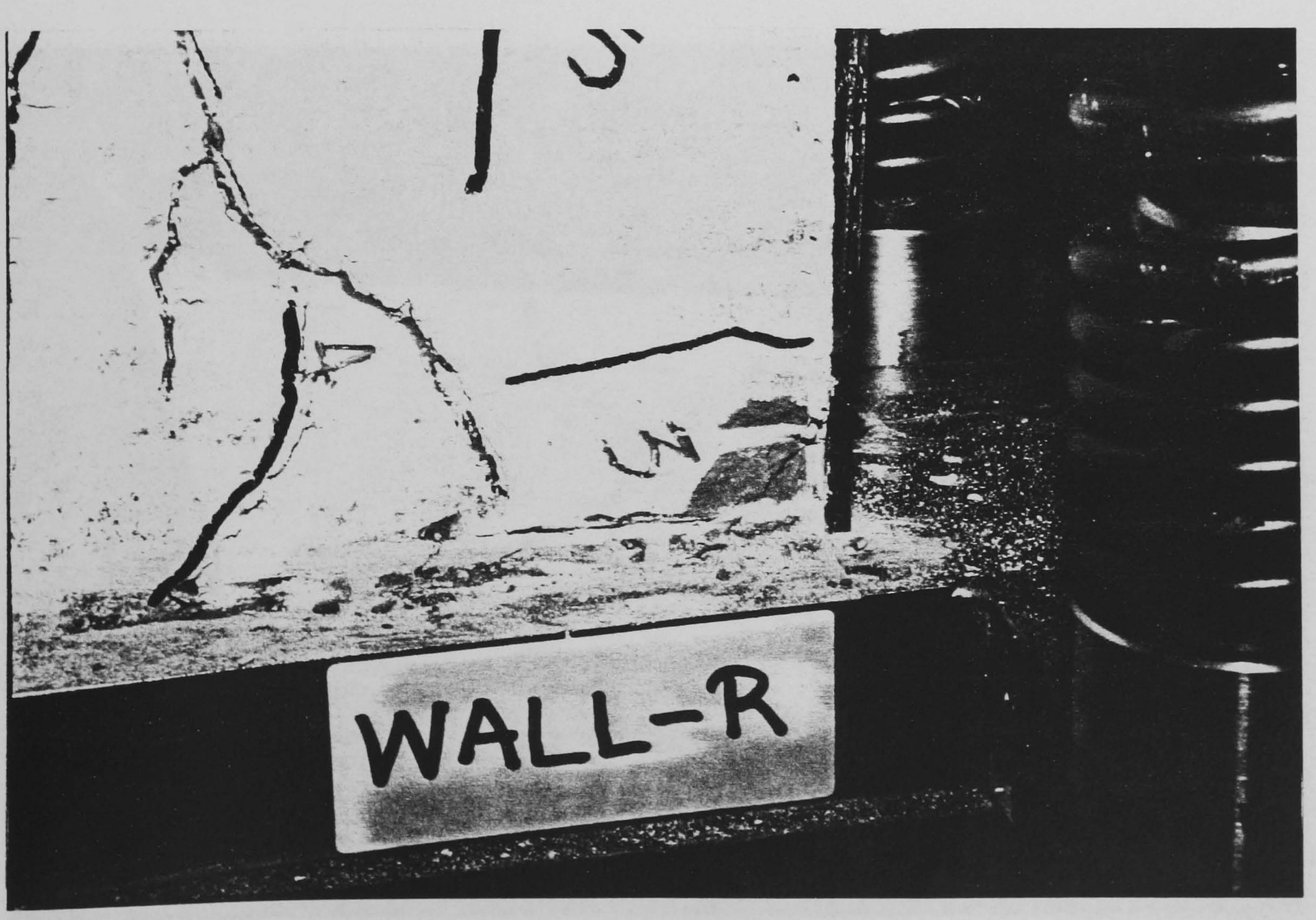

Photo 5.52 Close-up detail of opposite (lower right) corner crushing (wall-R)

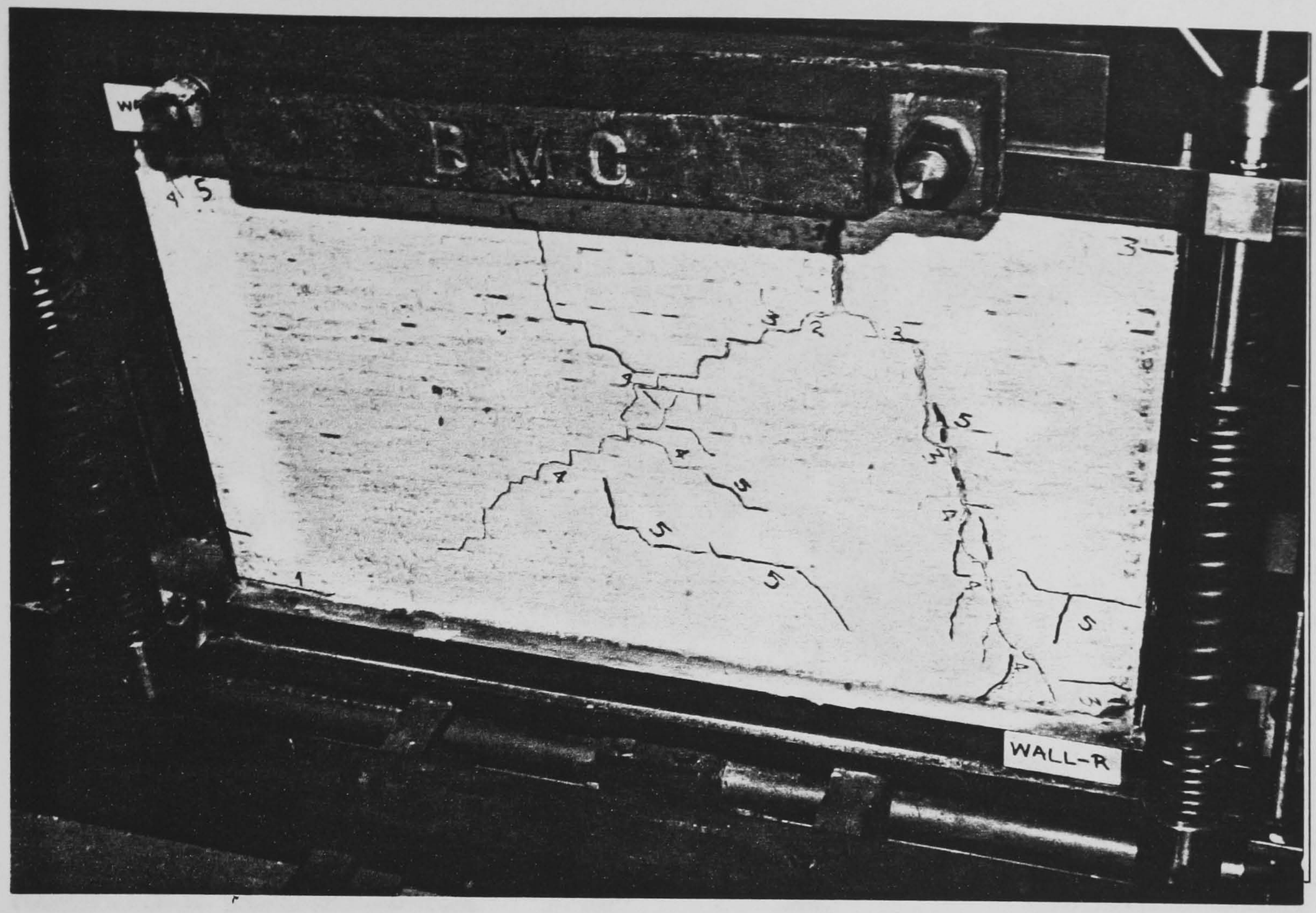

Photo 5.53 Collapse sequence-frame 1 (wall-R)

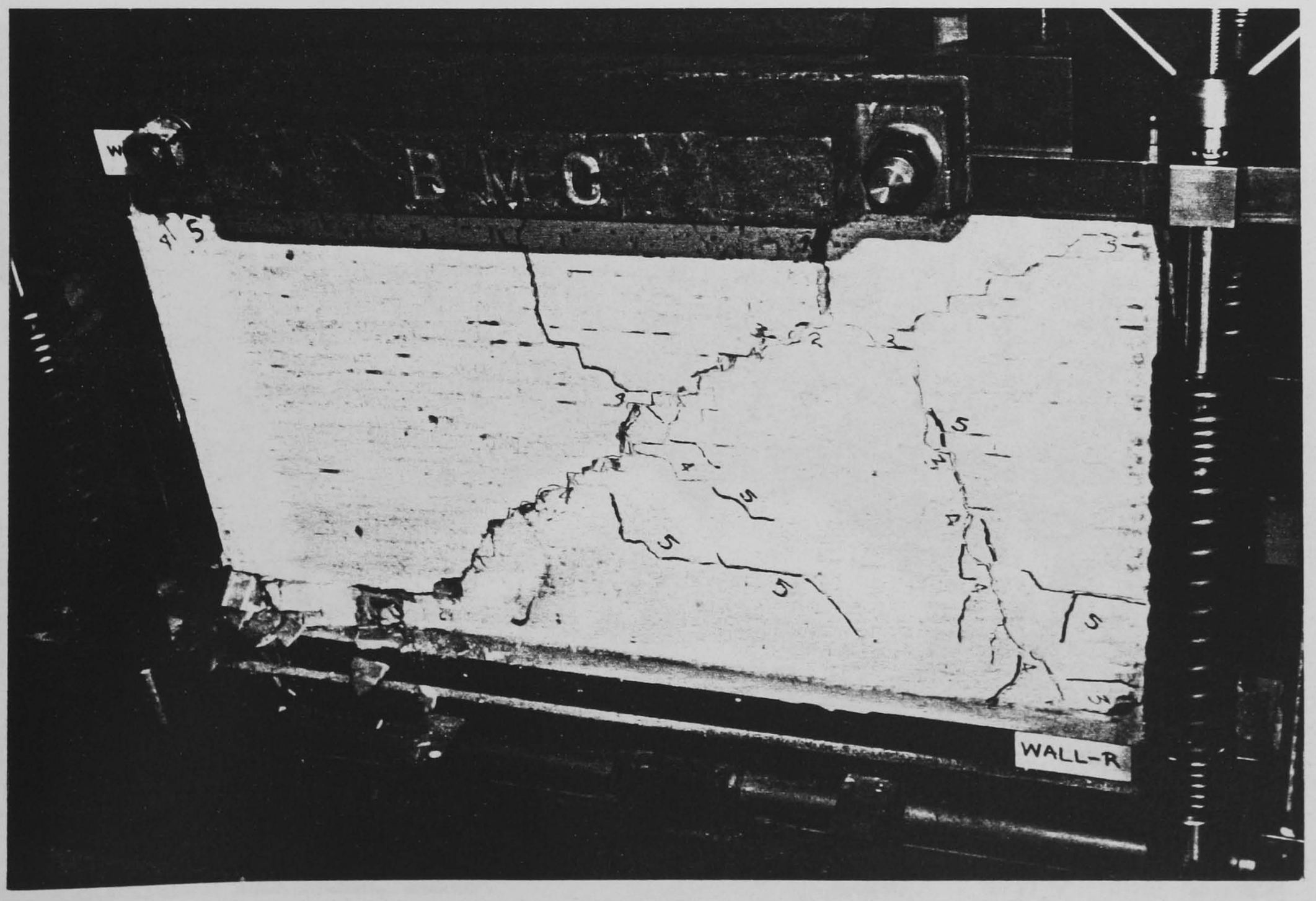

Photo 5.54 Collapse sequence-frame 2 (wall-R)

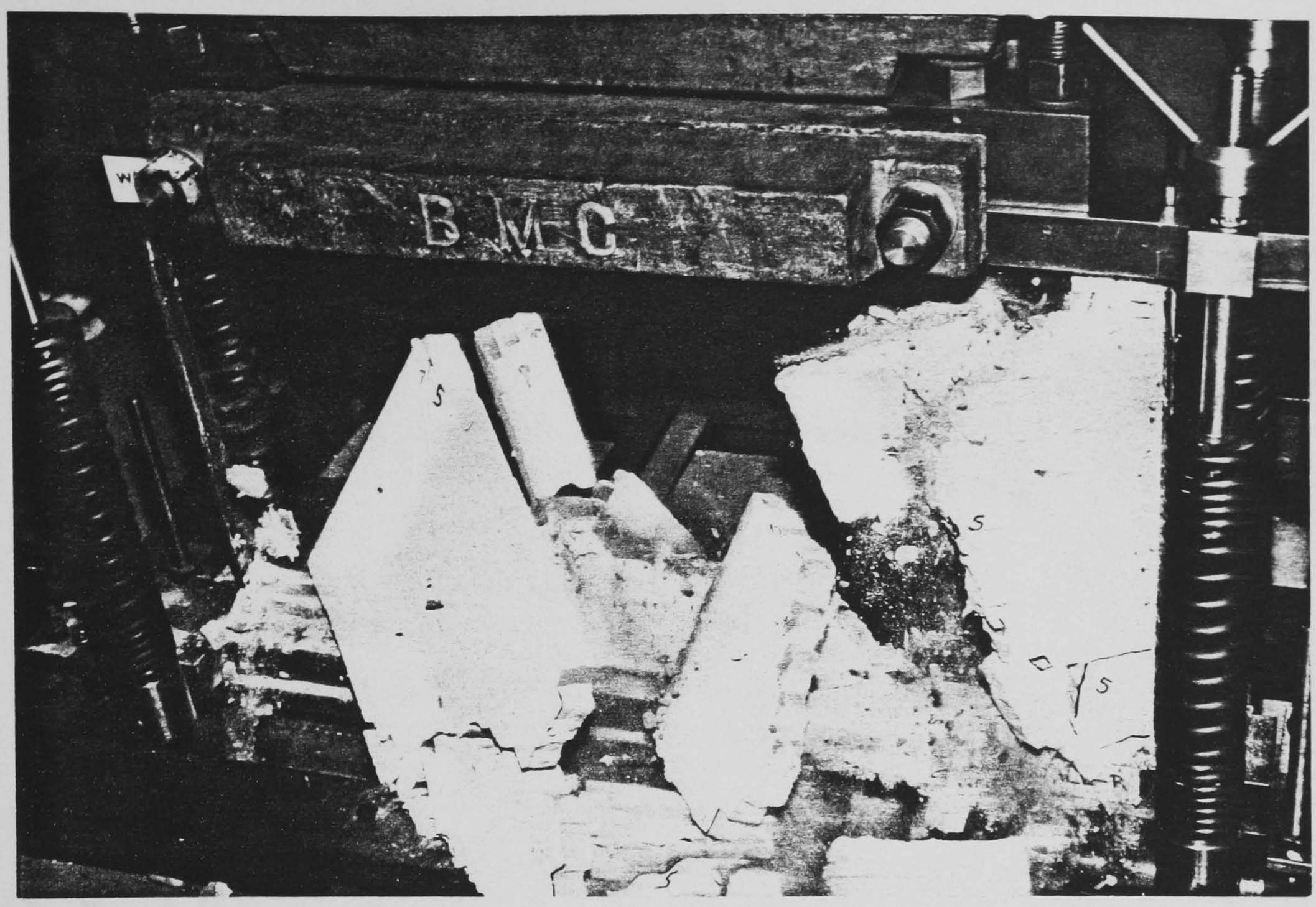

Photo 5.55 Collapse sequence and destruction-frame 3 (wall-R)

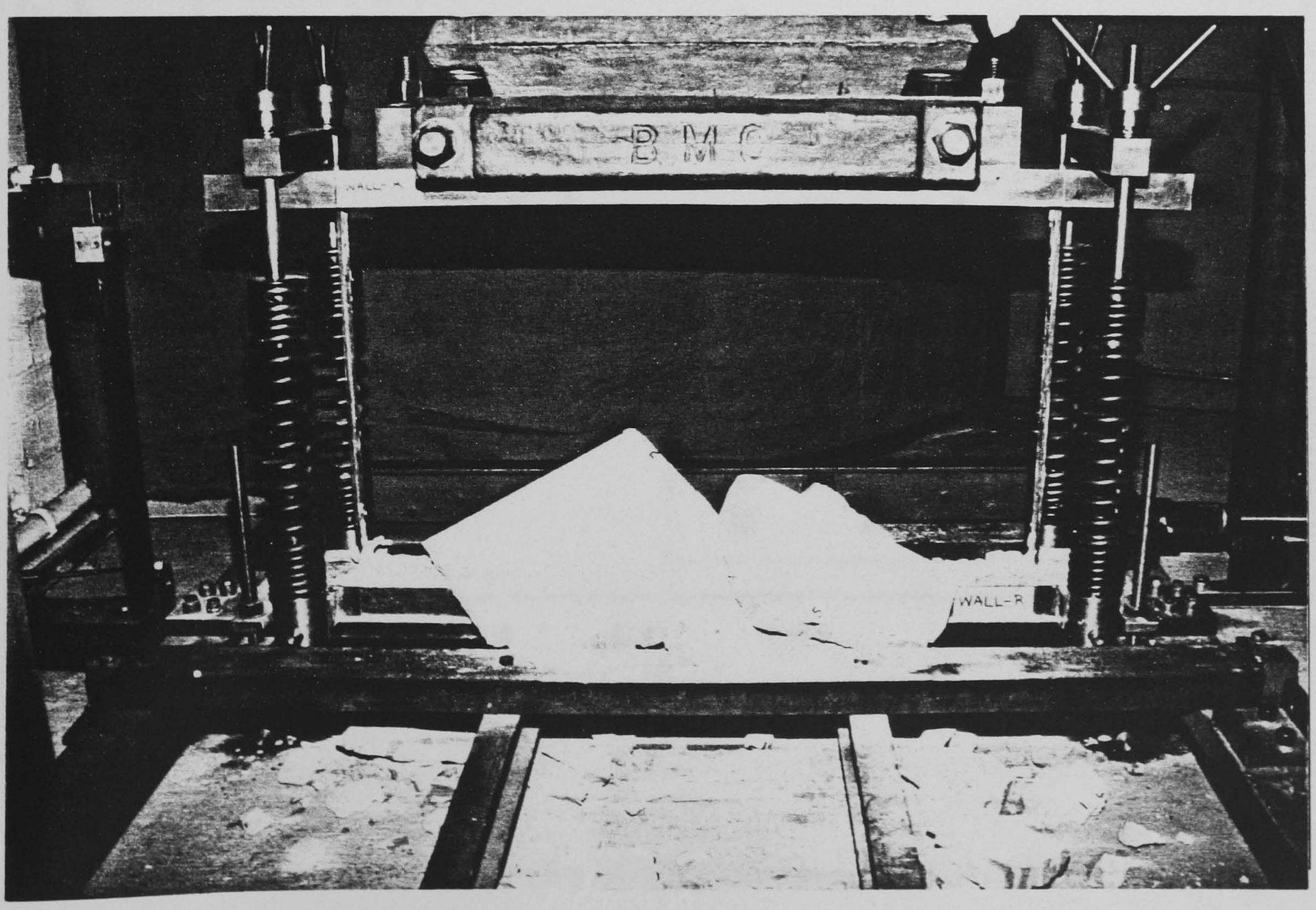

Photo 5.56 Final sequence-frame 4 (wall-R)

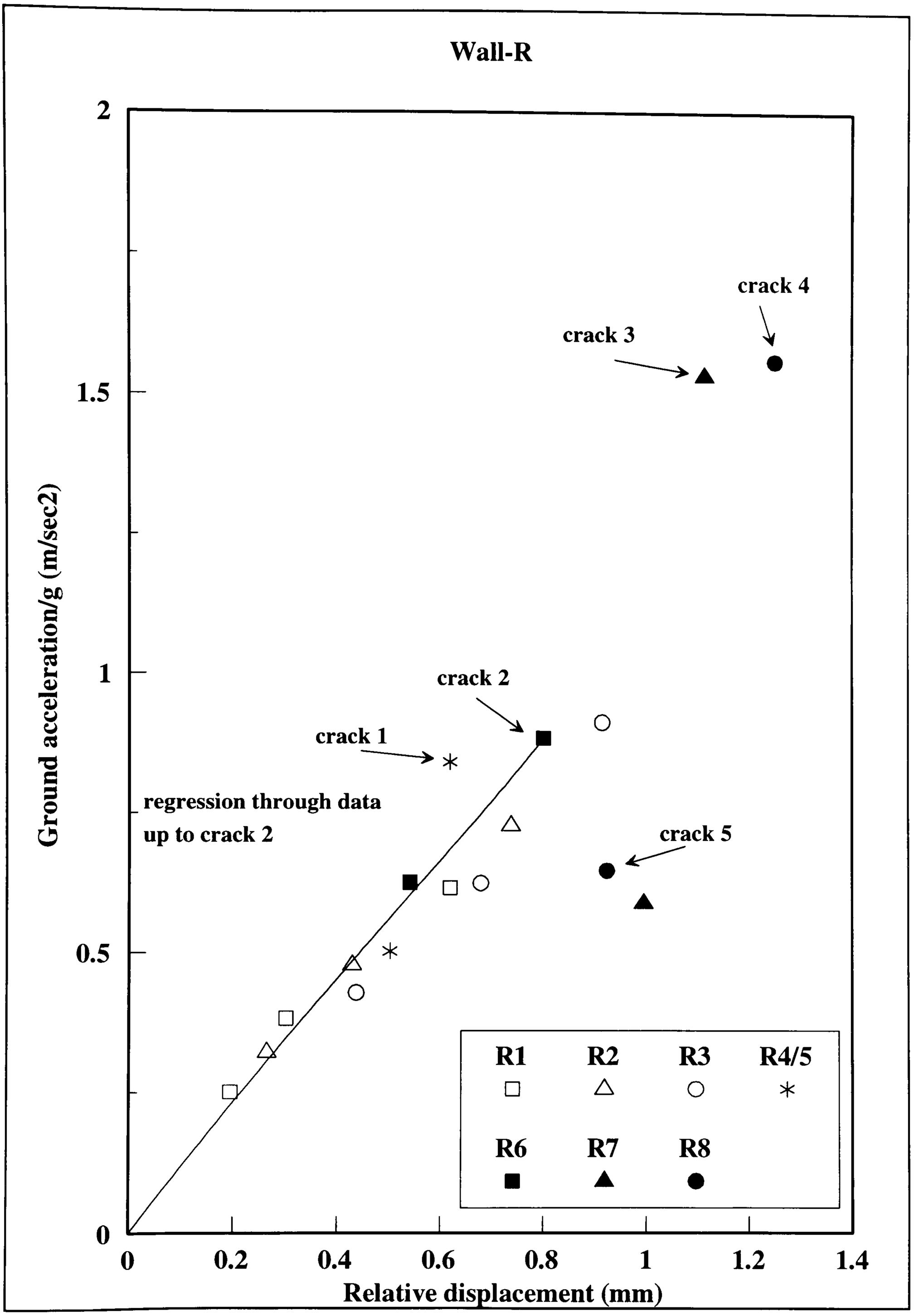

Figure 5.92 Summary of dynamic response for wall-R

5.8.5.1 Observations for wall-R.

This panel was relatively weak with respect to the brick and mortar compressive and tensile strength. Although wall-R was prestressed to only 15% of the masonry compressive strength, crack 1 which appeared at an acceleration of 0.84g originated at the top of the panel and extended downwards for about 80 mm (photo 5.47). As mentioned before, this would probably be a result of flaws or general defects in the brick units. A small horizontal crack also appeared along the mortar joint near the bottom of the panel and close to the right corner. During the next stage crack 2 appeared under a slight increase in the applied ground acceleration (0.88g). This pattern resulted in the shift of the centre of symmetry for the loaded diagonals and can be seen in photos 5.48 and 5.49, where cracks 3 and 4 occurring at accelerations of 1.53g and 1.56g respectively, extended towards the bottom corners resembling the typical cross-diagonal cracking pattern observed in the previous tests. During the next stage and at a lower acceleration of 0.65g crack 5 appeared, whereas crack 1 opened-up width-wise to about 3 mm. Corner crushing was also observed and is shown in photos 5.51 and 5.52. After this stage the panel had effectively divided into two sections that were sliding with respect to each other along the main diagonal crack. Finally with the top LVDTs removed and the shaking table set for a ground motion of 1.2g acceleration, the wall was subjected to a loading sequence (4 seconds), that ultimately caused collapse with an explosive failure mode. Photos 5.53 to 5.56 present this collapsing sequence frame by frame, where the main diagonal crack extended towards the loaded corners and finally connected to a horizontal flexural crack (photo 5.53 lower left corner), which ultimately resulted in the collapse of the panel. The final failure mode shown in photo 5.54, was a result of the applied axial forces due to the prestressing mechanisms and the additional lead weight which forced the upper left part of the panel to displace downwards crushing the underlying masonry (lower left corner in photo 5.54). A marked reduction in the natural frequency was accompanied by a large increase in the equivalent viscous damping coefficient of about 135%. Figure 5.91 demonstrates the hysteretic behaviour and energy dissipation of the panel during the formation of the fifth crack.

5.8.6 Sixth test : wall-M.

Wall-M was subjected to the same pattern of motor driving frequency and ground acceleration in the first 4 stages. External reinforcement was applied to both sides to in an attempt confine and contain the damage. This was tightly anchored to the wall rather than the surrounding frame. The effects of the reinforcement on the dynamic properties was examined and is presented in the free vibration amplitude decay figures. Following initial cracking, the intensity of the applied ground motion was increased up to the limits of the shaking table, to induce damage on the panel and observe the effects of the external reinforcement-confinement. In the following pages results from the dynamic tests are provided in the order shown below.

- ► Free vibration amplitude decay records (figures 5.93 to 5.99).
- ► Displacement records (5.100 to 5.105).
- ► Sample hysteresis curves (5.106 to 5.109).
- ► Photographs of the cracking patterns (photo 5.57 to 5.74).
- ► Summary of dynamic response (figure 5.110).

The test procedure for wall-M is summarised in table 5.13, while results for the first natural frequency using the methods described previously are shown in table 5.12.

Theoretical	**Finite element**	**Hammer test**
60.6 Hz	72.5 Hz	40.50 Hz

Table 5.12 Natural frequency results (initial value) for wall-M

Stage/Run	Table accel.	Driving freq.	Damage	Natural freq.	Damping ratio	Rel. displ.	Comments
	g	Hz	Crack #	Hz	%	mm	
M1/R1	0.069	5.6	-	40.5	3	0.073	Increasing driv. frequency
M1/R2	0.097	6.3	-	-	-	0.063	
M1/R3	0.131	7.1	-	-	-	0.086	
M2/R1	0.094	5.6	-	-	-	0.059	Increasing driv. frequency
M2/R2	0.145	6.3	-	-	-	0.057	
M2/R3	0.193	7.1	-	-	-	0.061	
M3/R1	0.153	5.6	-	-	-	0.095	Increasing driv. frequency
M3/R2	0.225	6.3	-	-	-	0.125	
M3/R3	0.337	7.2	-	-	-	0.217	
M4/R1	0.286	5.6	-	-	-	0.22	Increasing driv. frequency
M4/R2	0.428	6.3	-	-	-	0.448	
M4/R3	0.712	7.2	-	-	-	0.671	
M5/R1	1.29	8.1	-	-	-	1.267	Constant driv. frequency **Stepwise tensile cracking and corner cracking**
M5/R2	1.372	8.1	**1**	25.1	4.7	1.45	
M6	1.77	8	**2**	23.81	4.9	2.64	**Vertical splitting passing through the units**
M7	1.98	8	**3**	21.74	5.4	-	No LVDT data due to corner crushing **Excessive wall damage Wire mesh tensile failure**
M8	>2.5	>10	-	14.28	12.5	-	**Wall separated into sections due to widening of vertical splitting cracks**

(Crack numbers correspond to the cracking as noted in the photographs)

(The instruments were removed from the wall in stages M7 and M8).

Table 5.13 Wall-M testing sequence

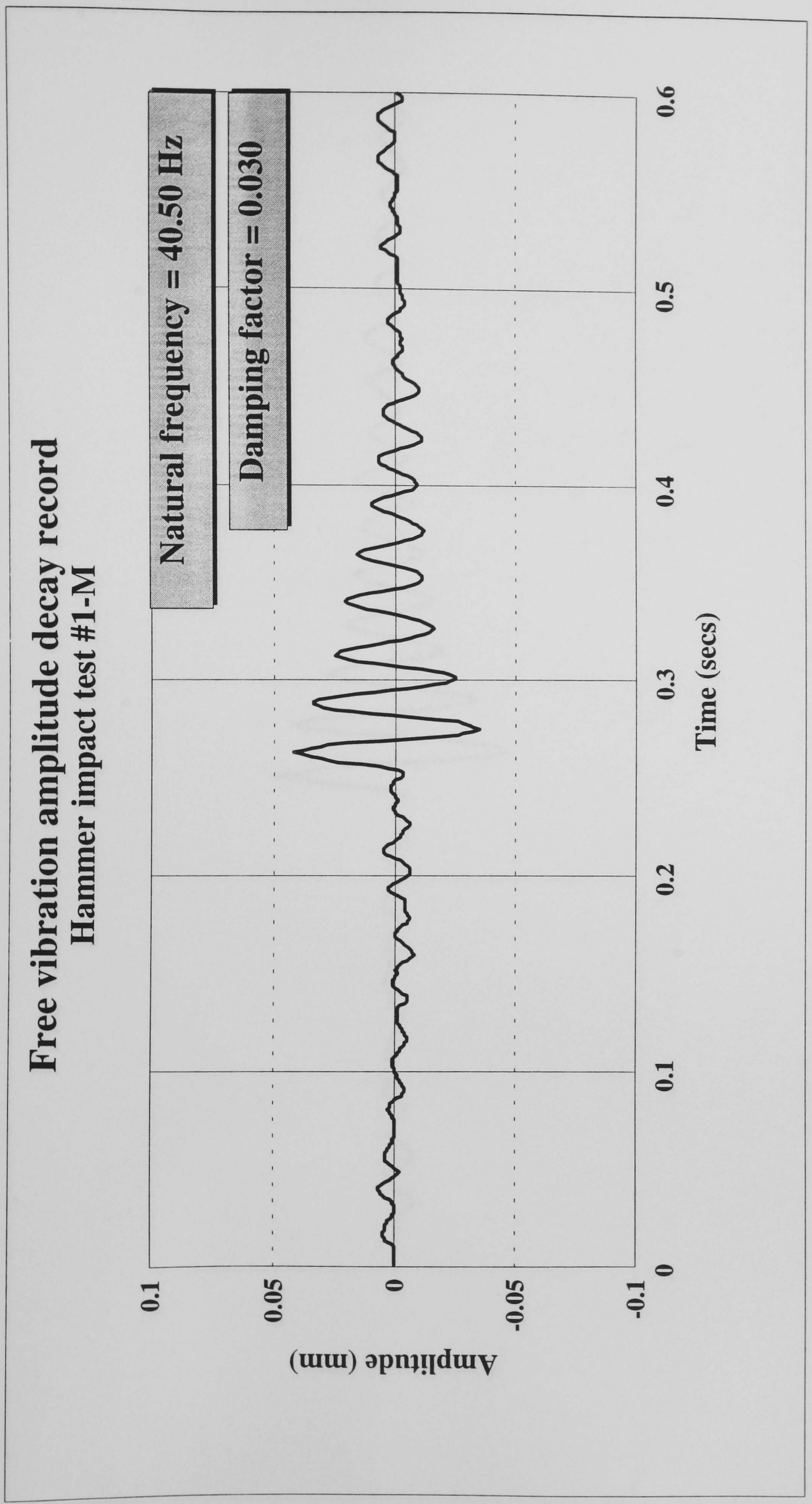

Figure 5.93 Initial free vibration amplitude decay

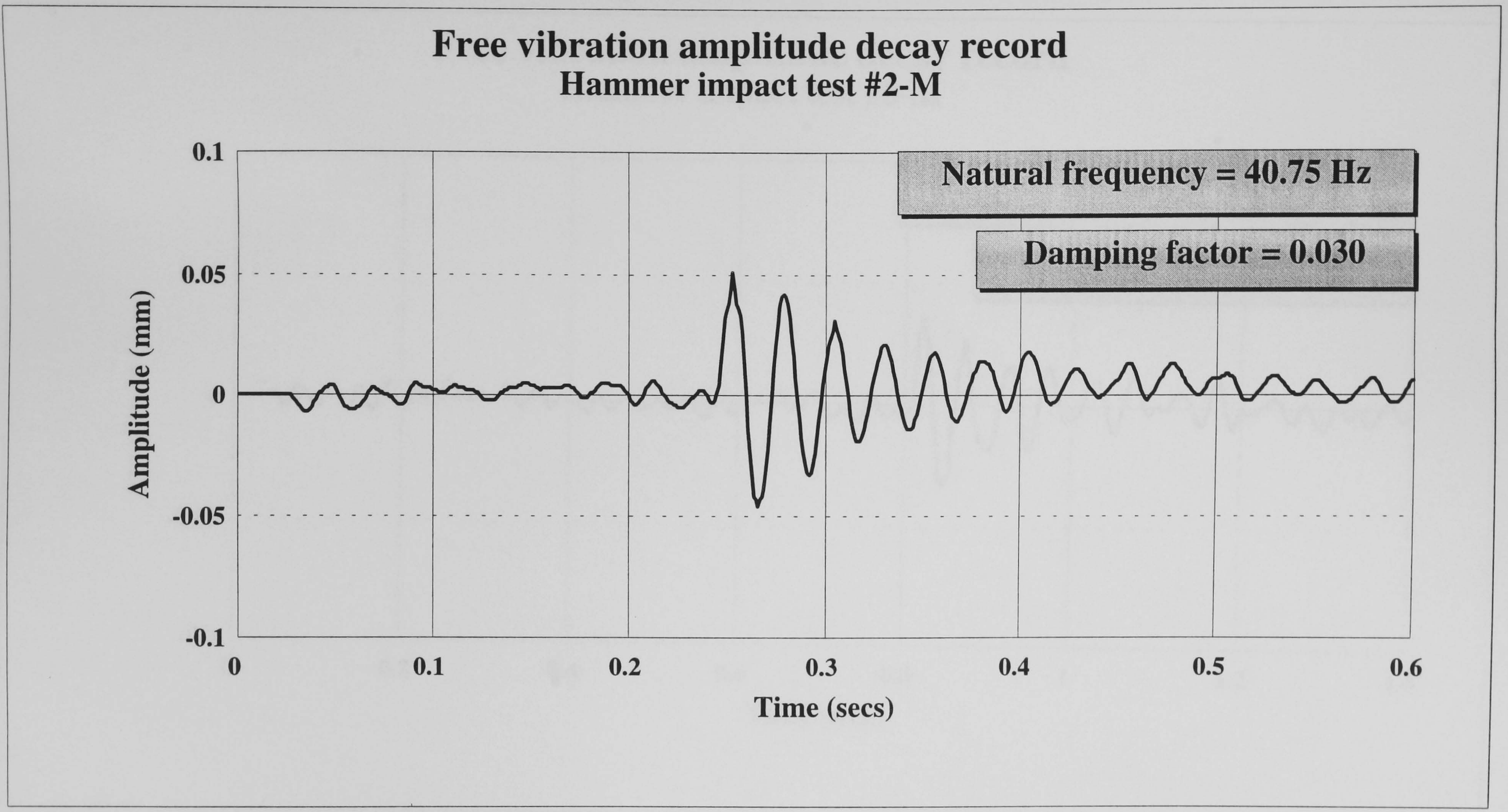

Figure 5.94 Initial free vibration amplitude decay (with wire mesh)

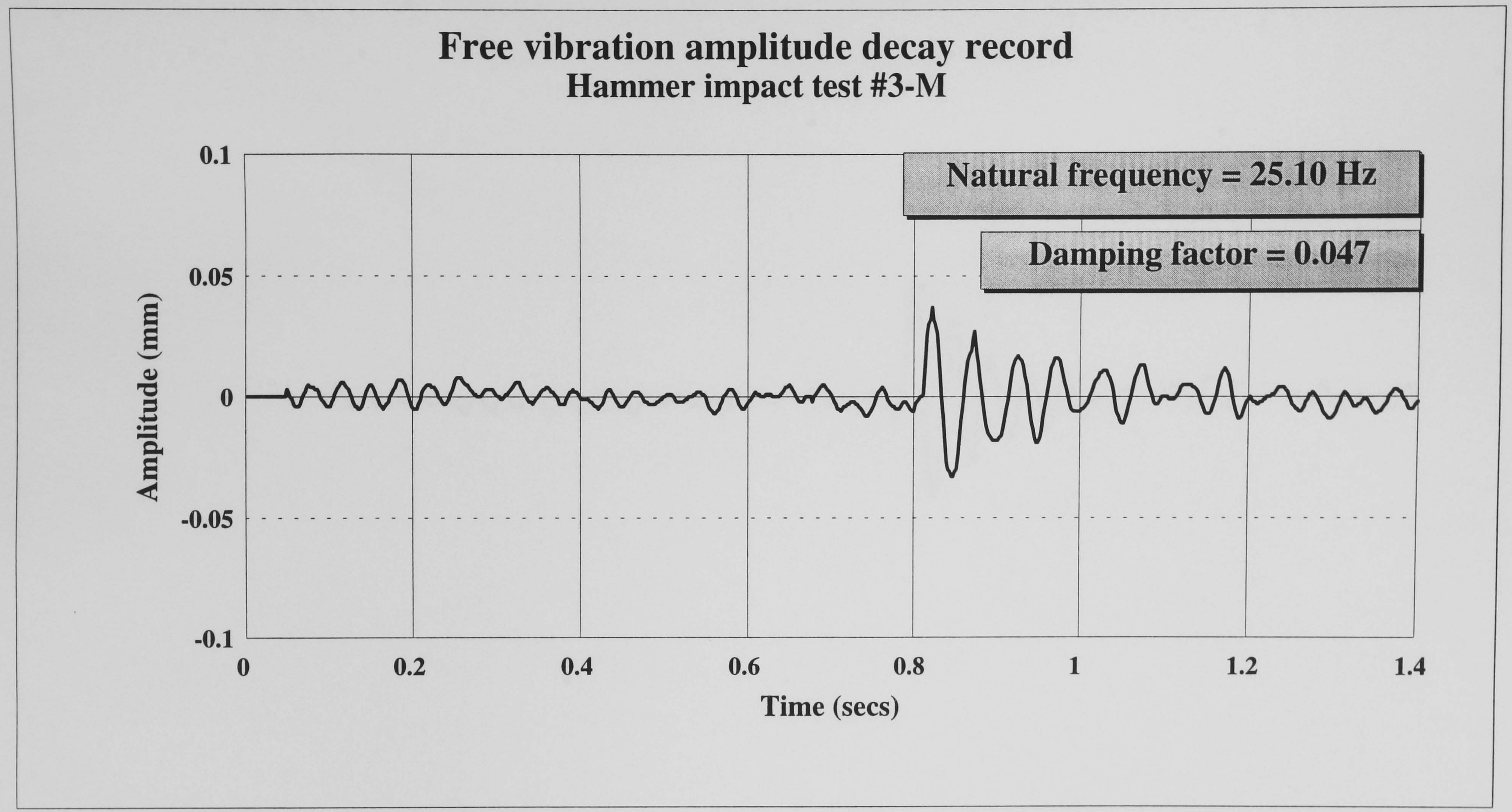

Figure 5.95 Free vibration amplitude decay after crack 1

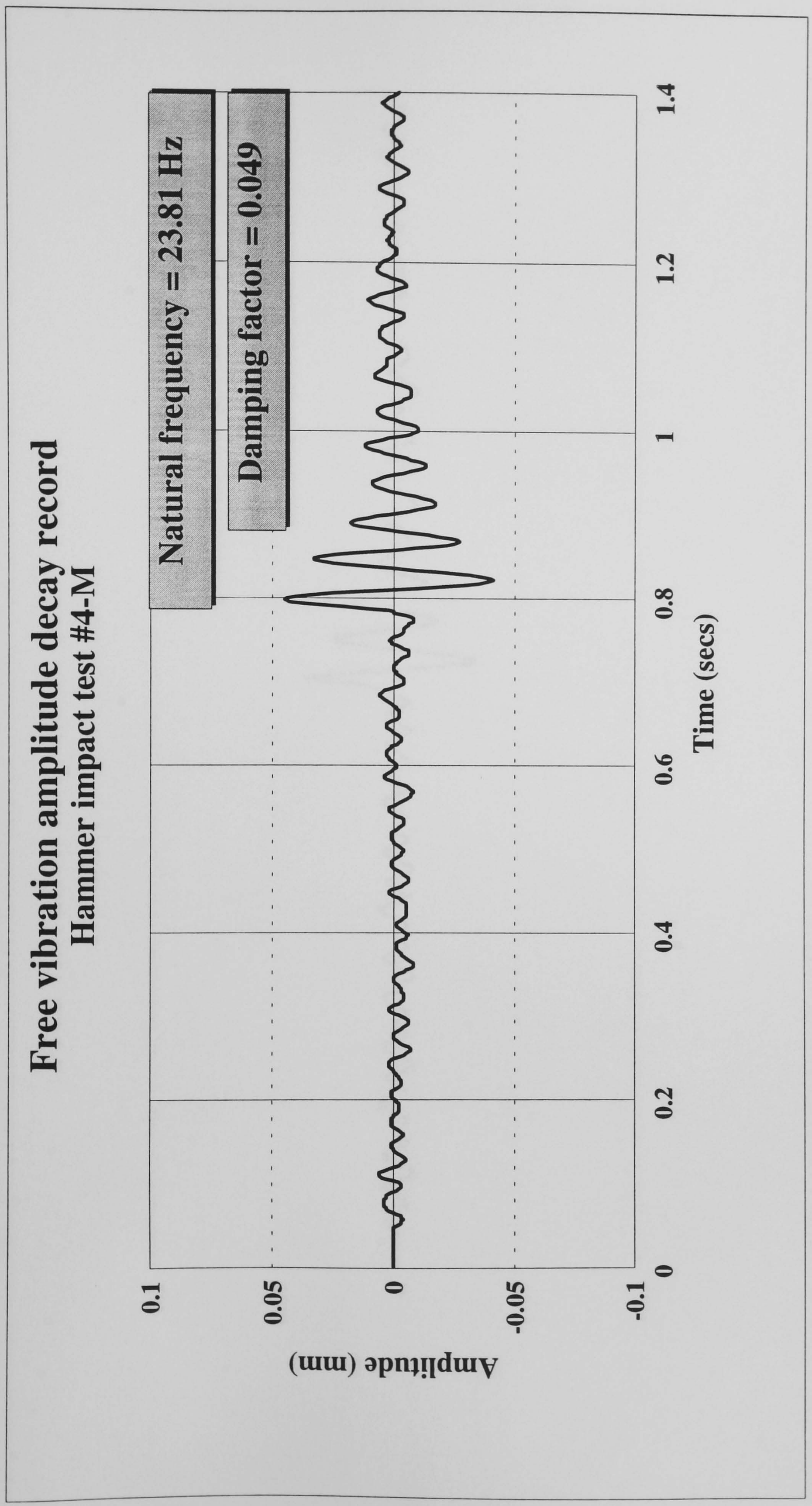

Figure 5.96 Free vibration amplitude decay after crack 2

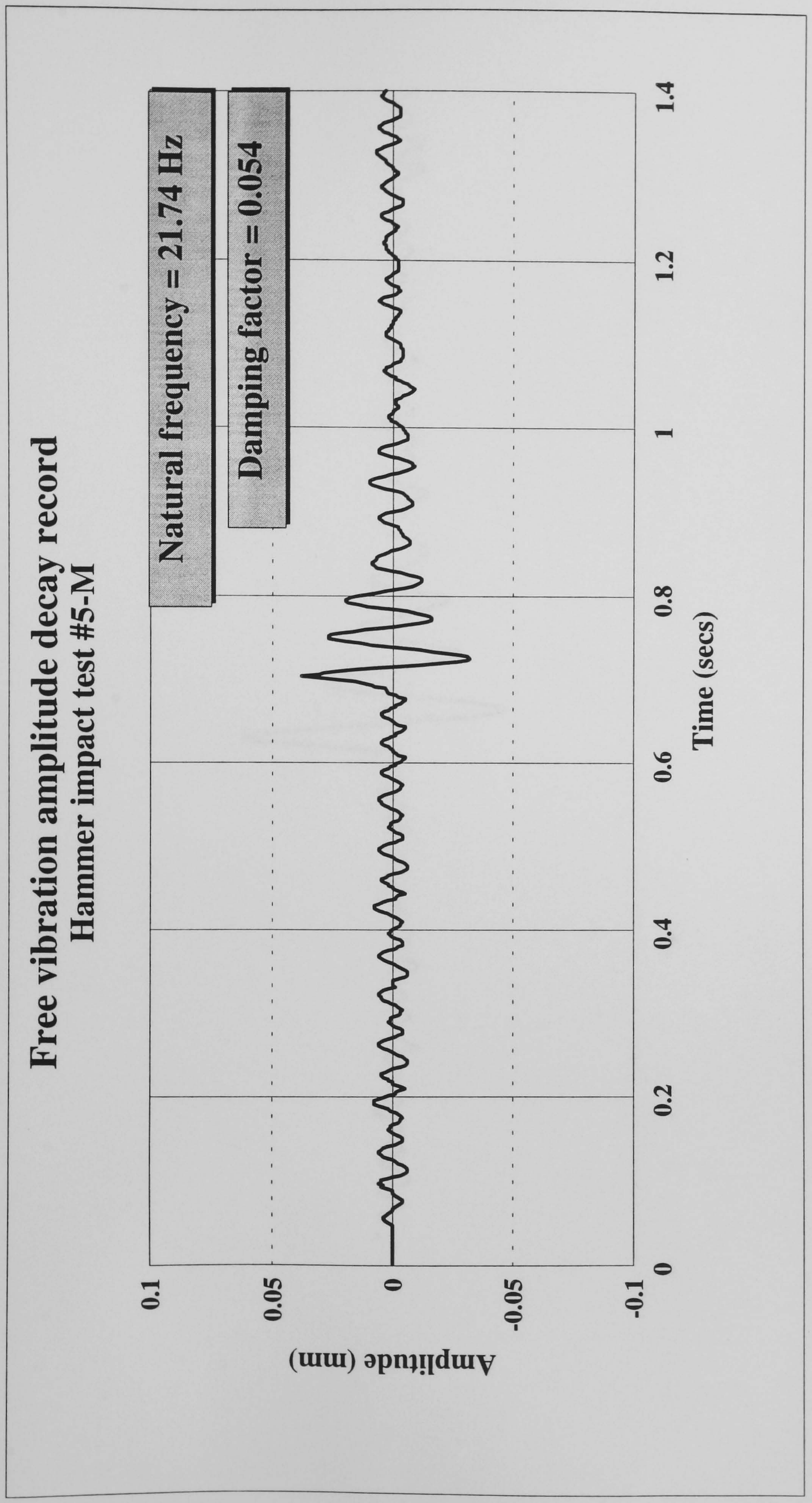

Figure 5.97 Free vibration amplitude decay after crack 3

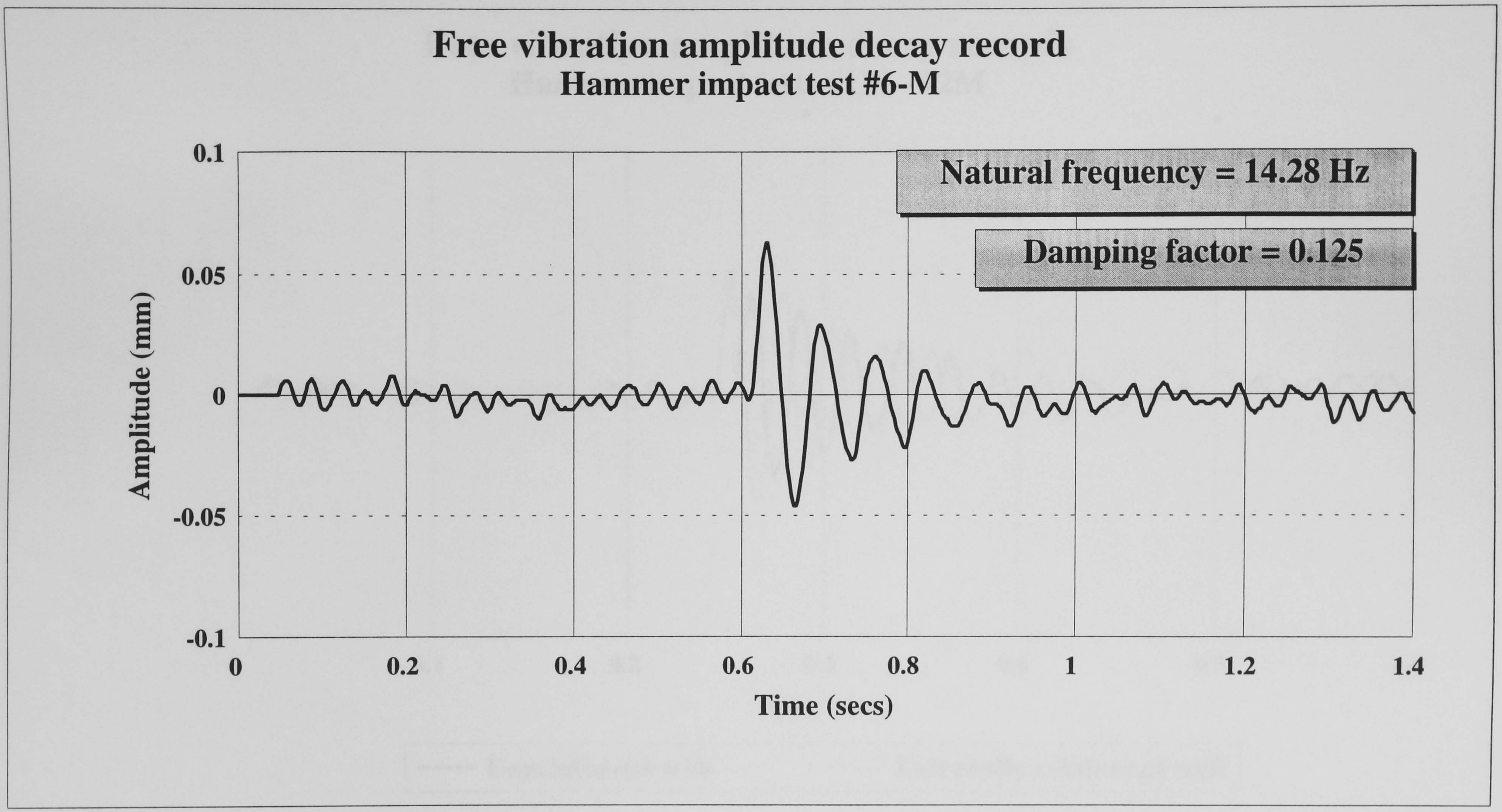

Figure 5.98 Free vibration amplitude decay after last run

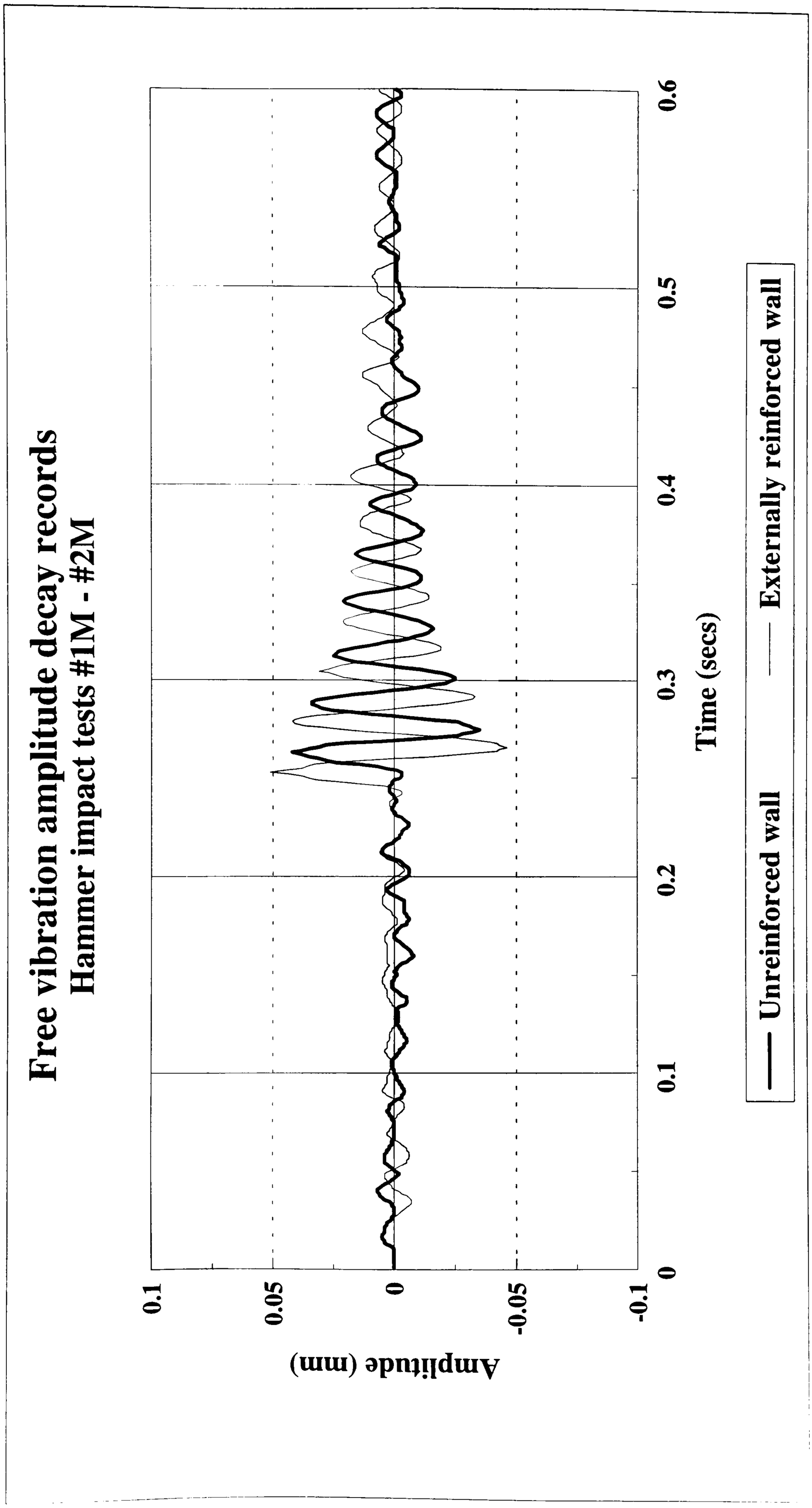

Figure 5.99 Influence of external wire mesh reinforcement on free vibration response

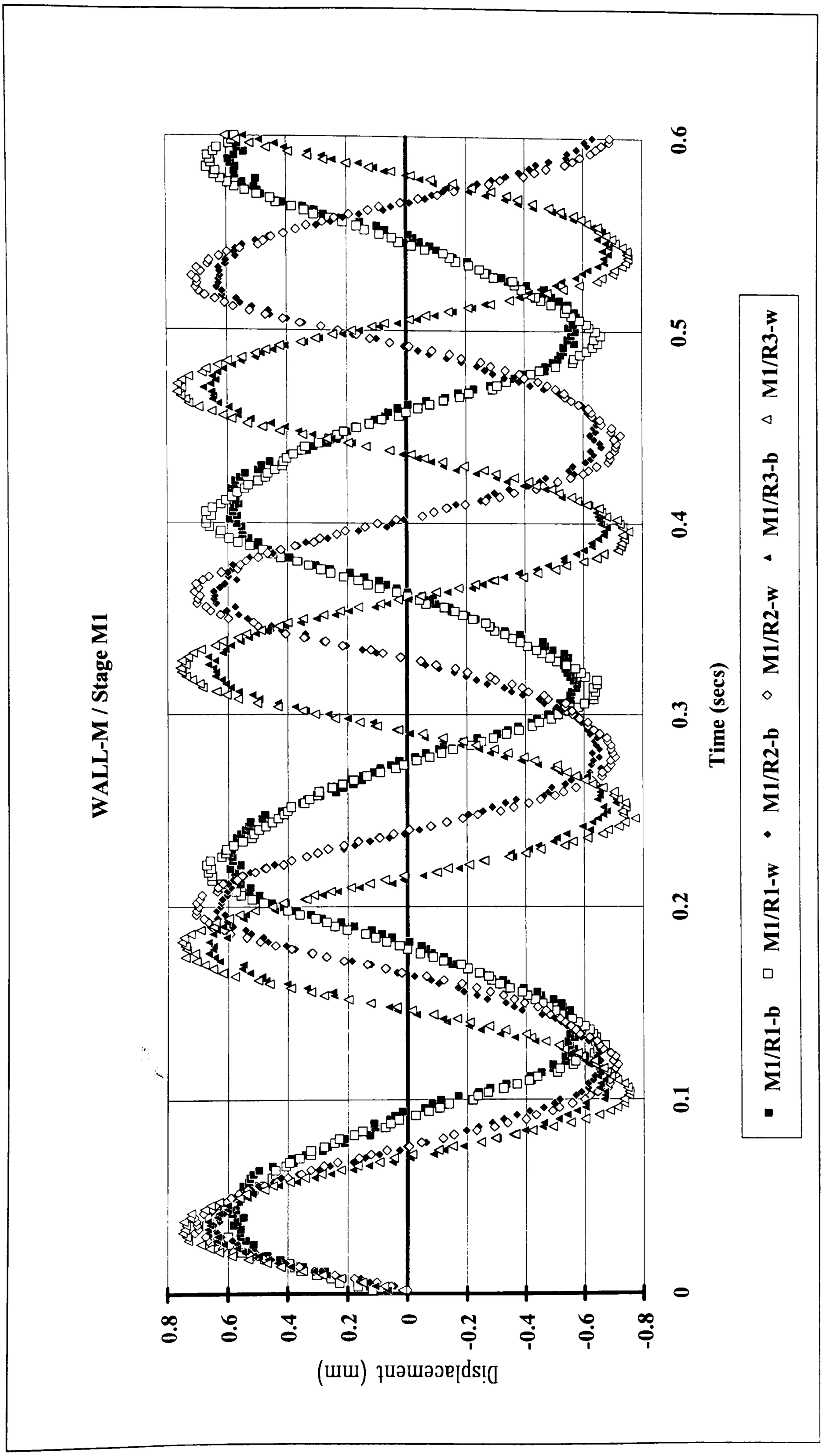

Figure 5.100 Wall-M / Stage M1

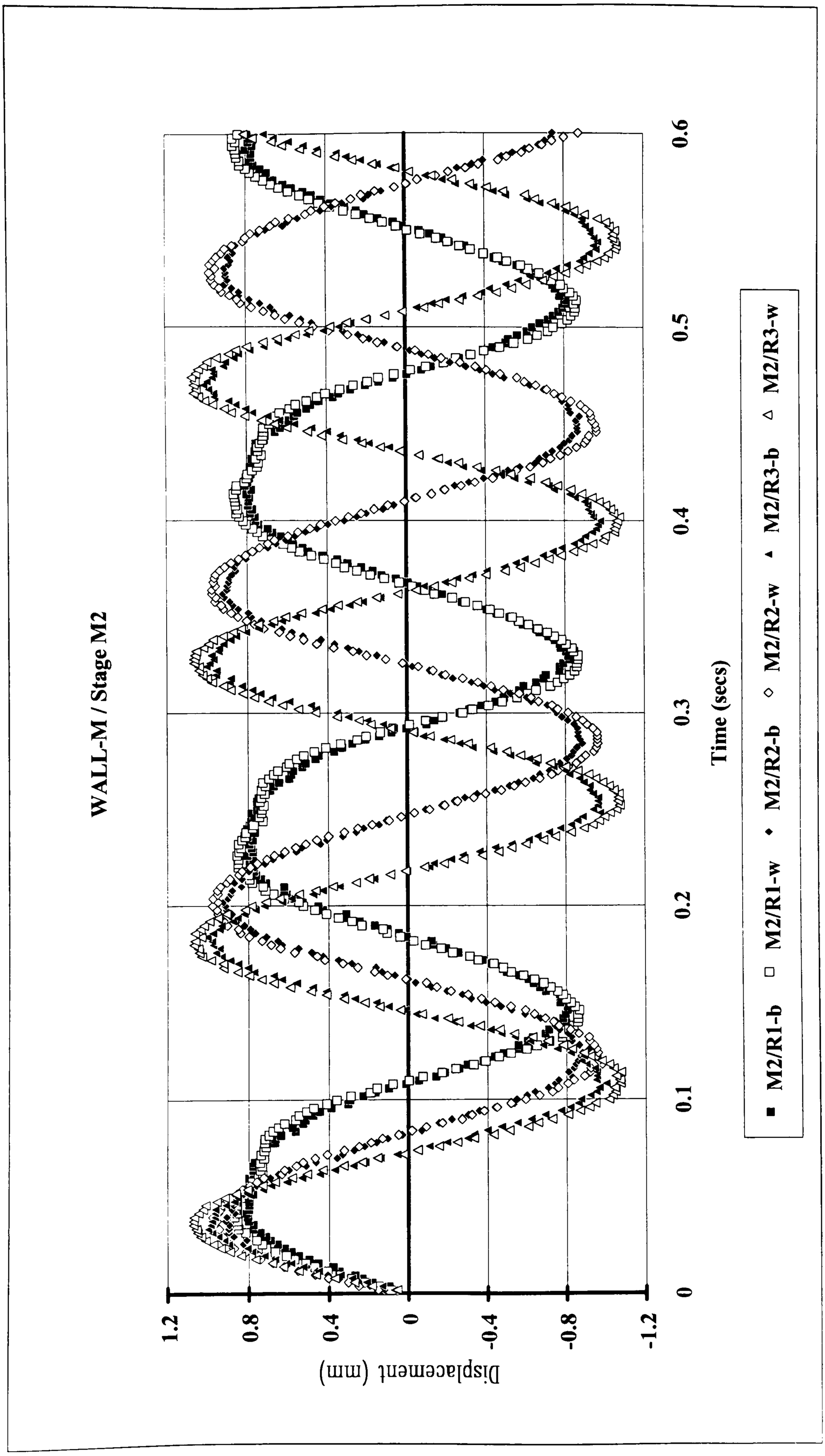

Figure 5.101 Wall-M / Stage M2

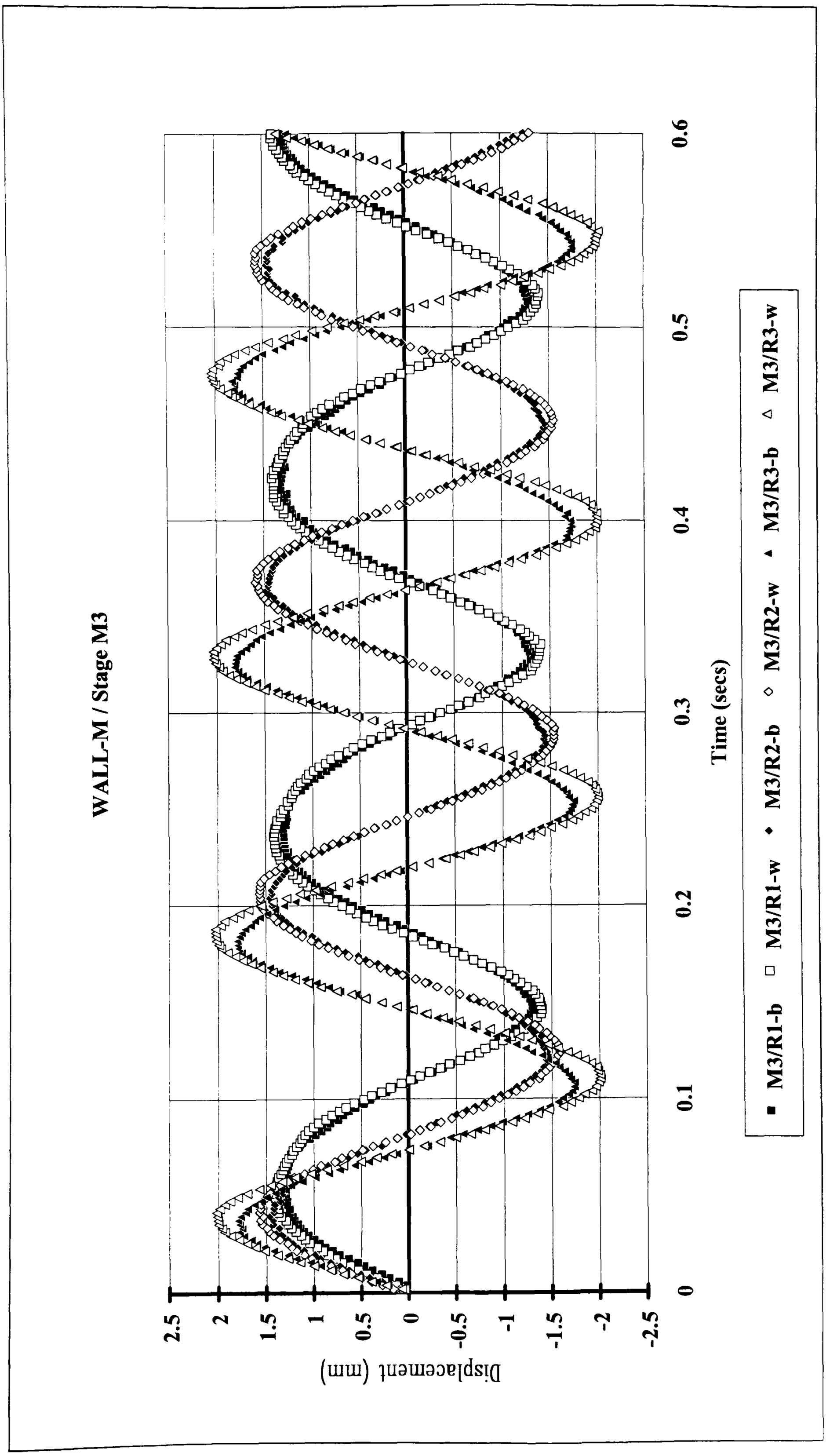

Figure 5.102 Wall-M / Stage M3

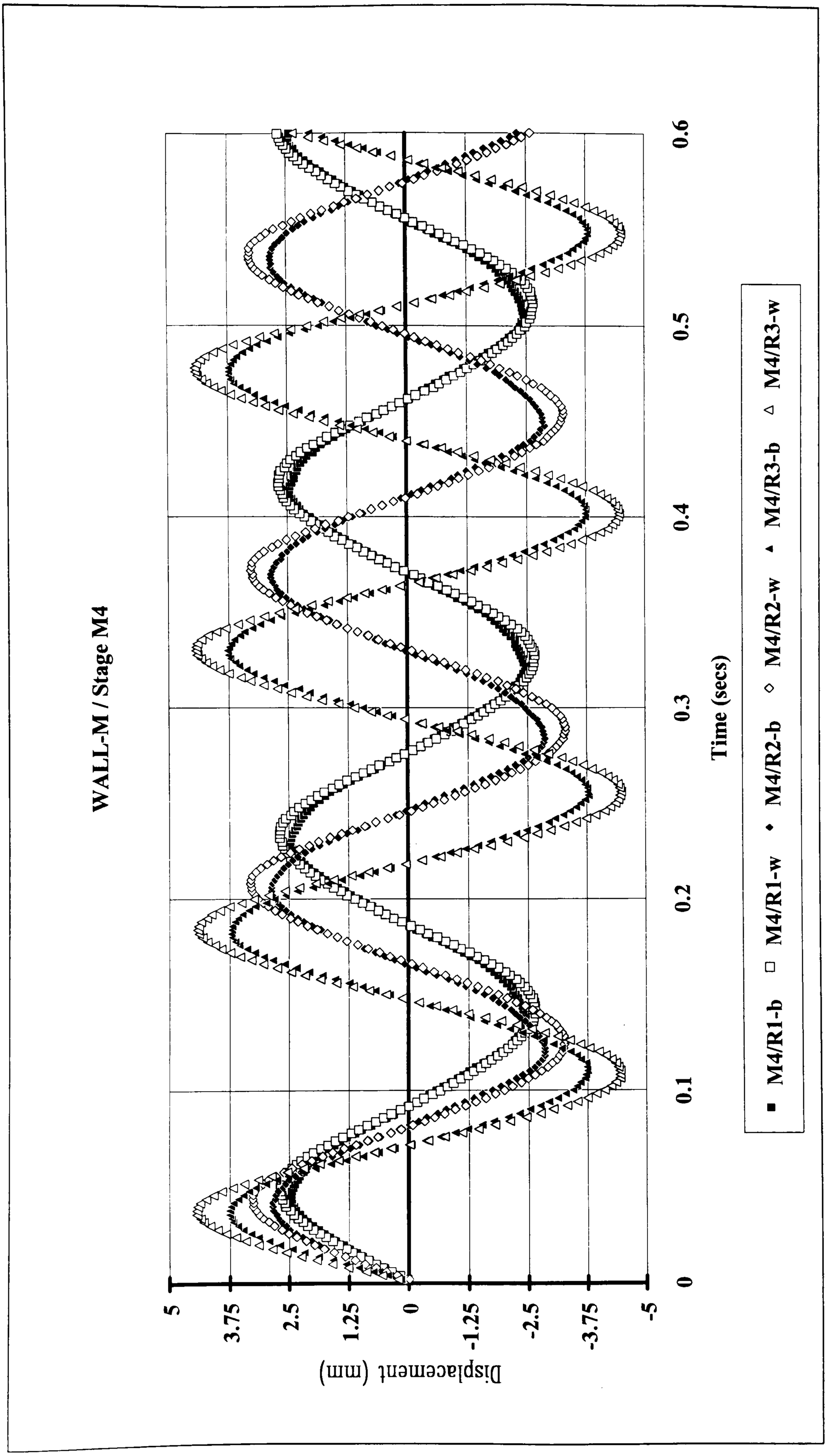

Figure 5.103 Wall-M / Stage M4

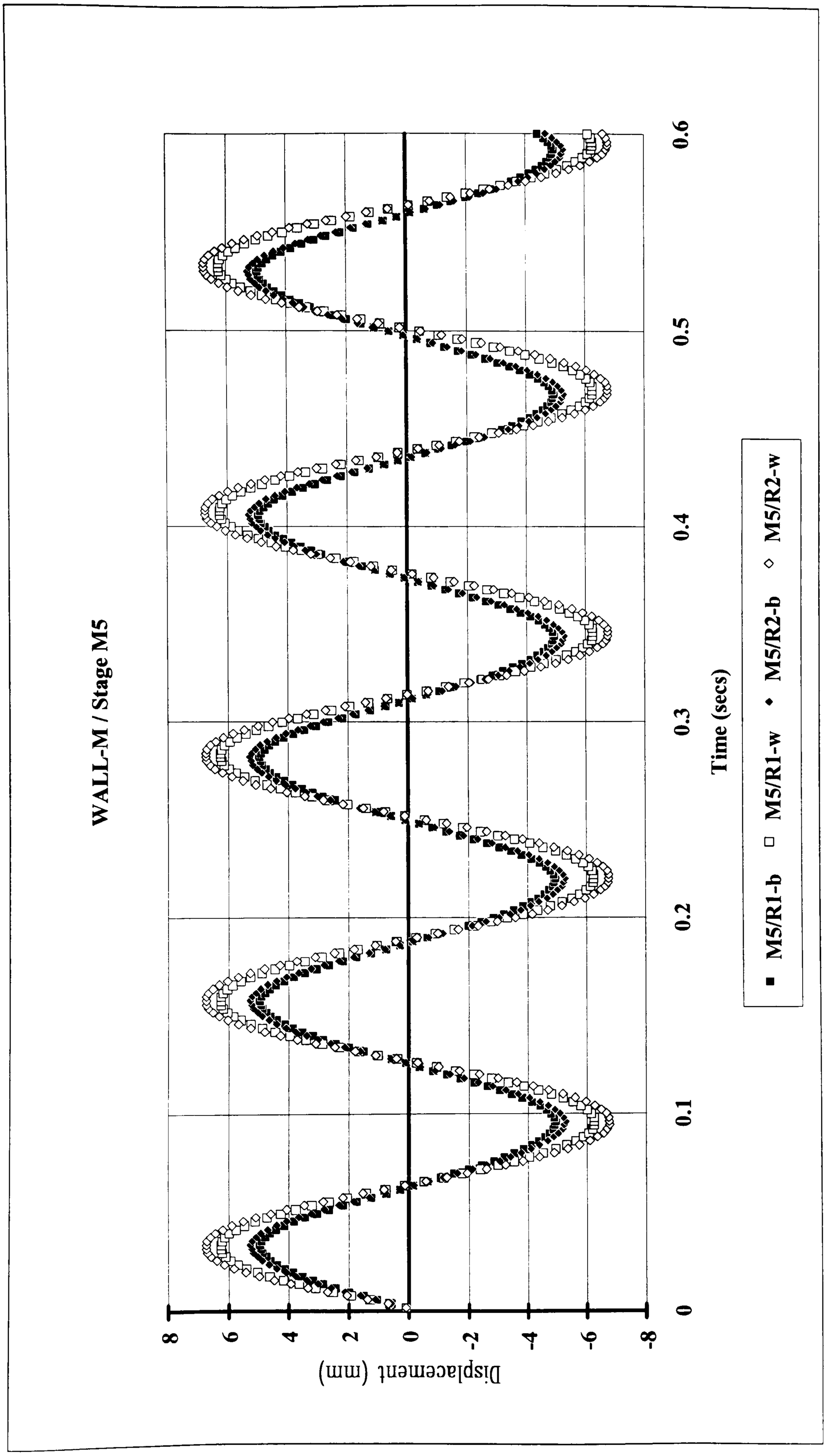

Figure 5.104 Wall-M / Stage M5

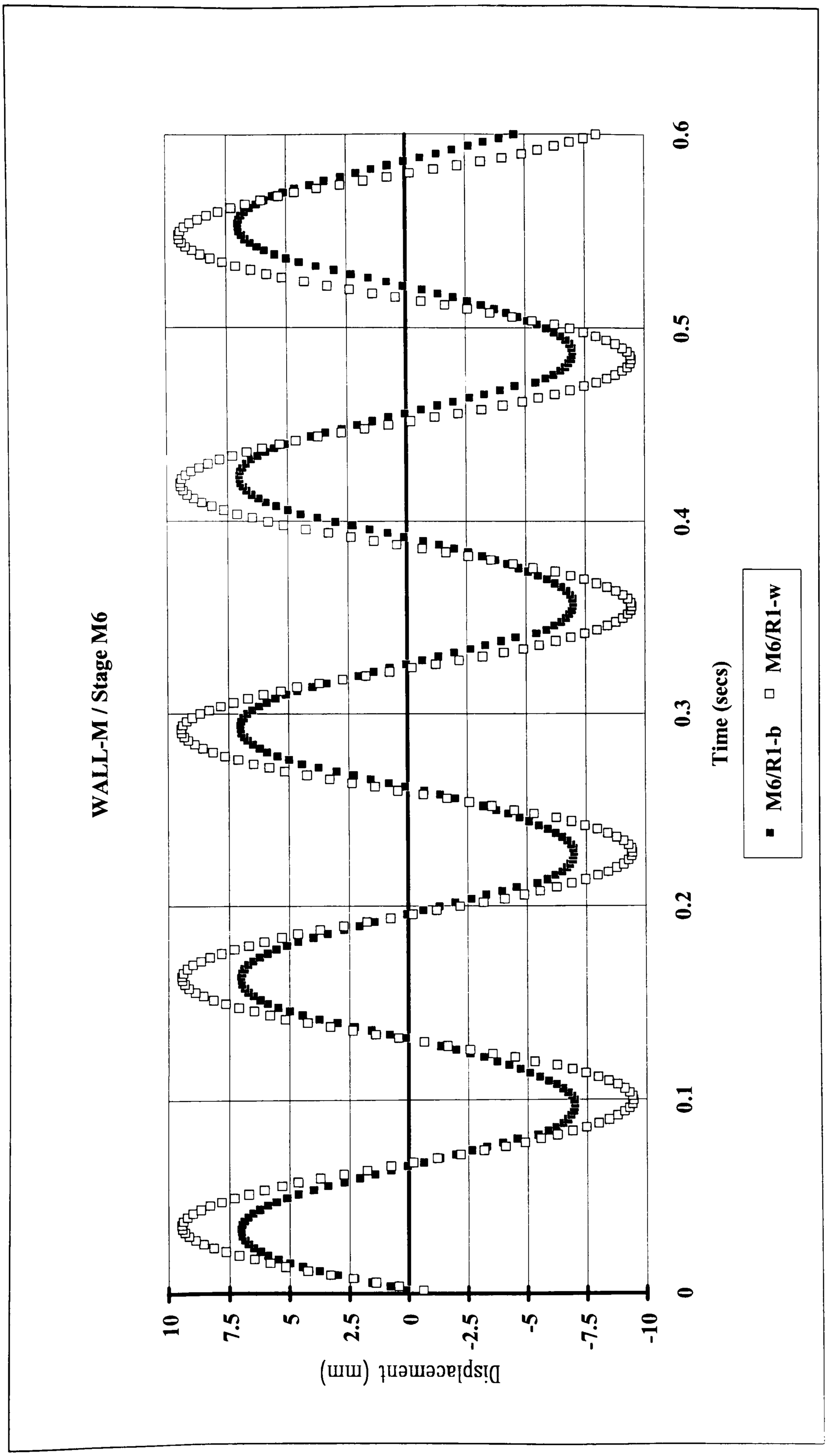

Figure 5.105 Wall-M / Stage M6

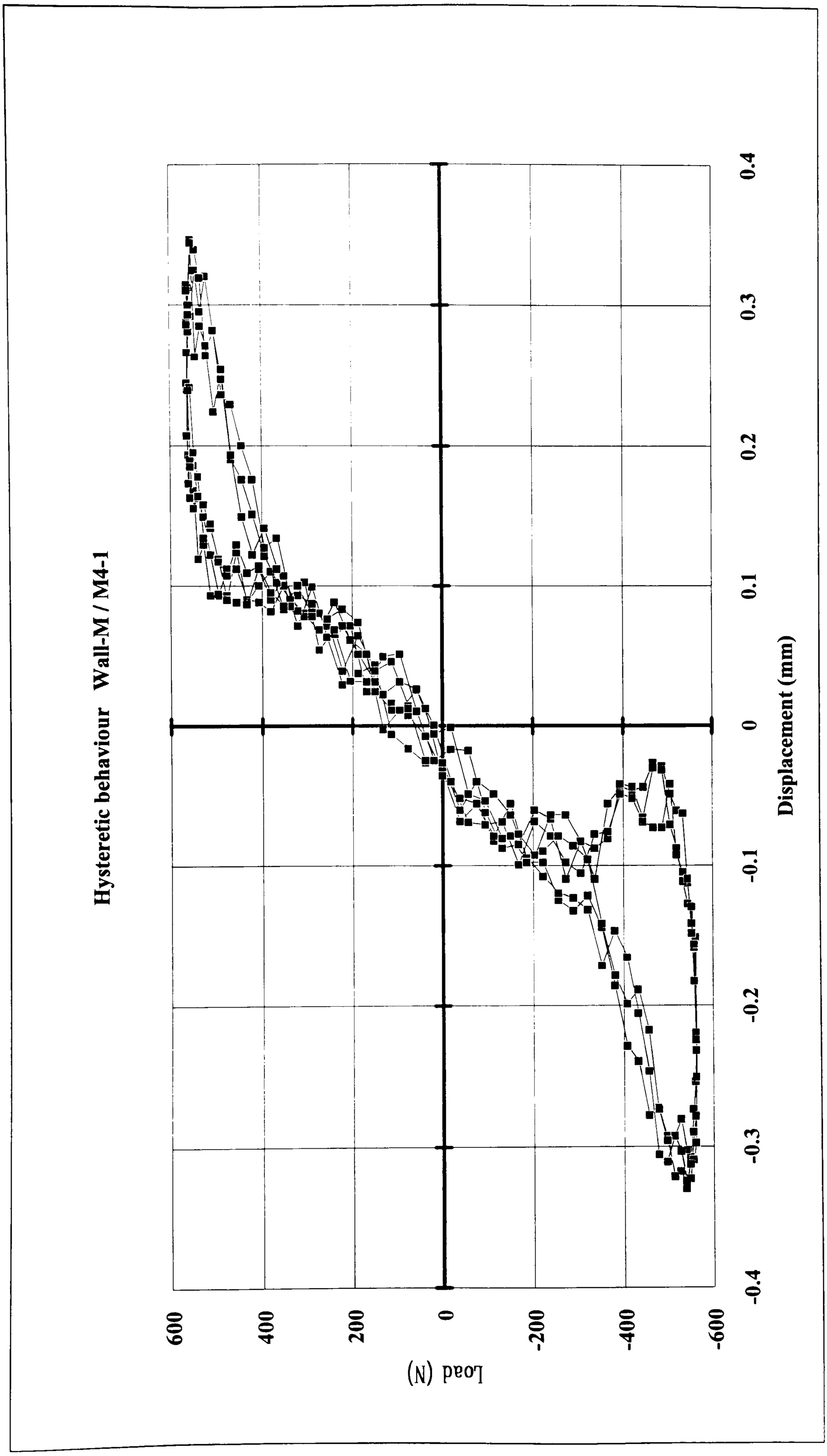

Figure 5.106 Wall-M / Hysteretic behaviour - Stage M4

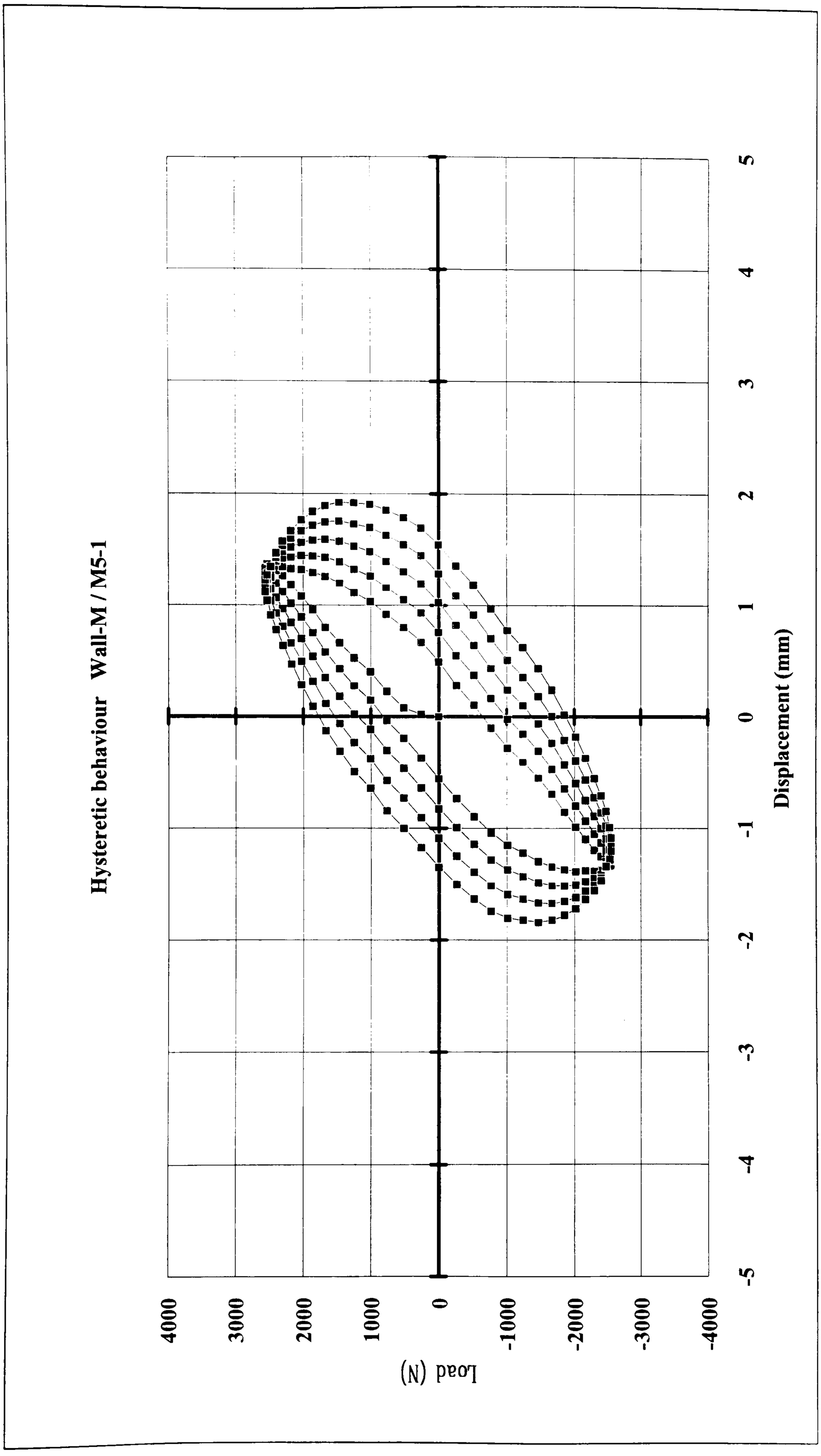

Figure 5.107 Wall-M / Hysteretic Behaviour - Stage M5/R1

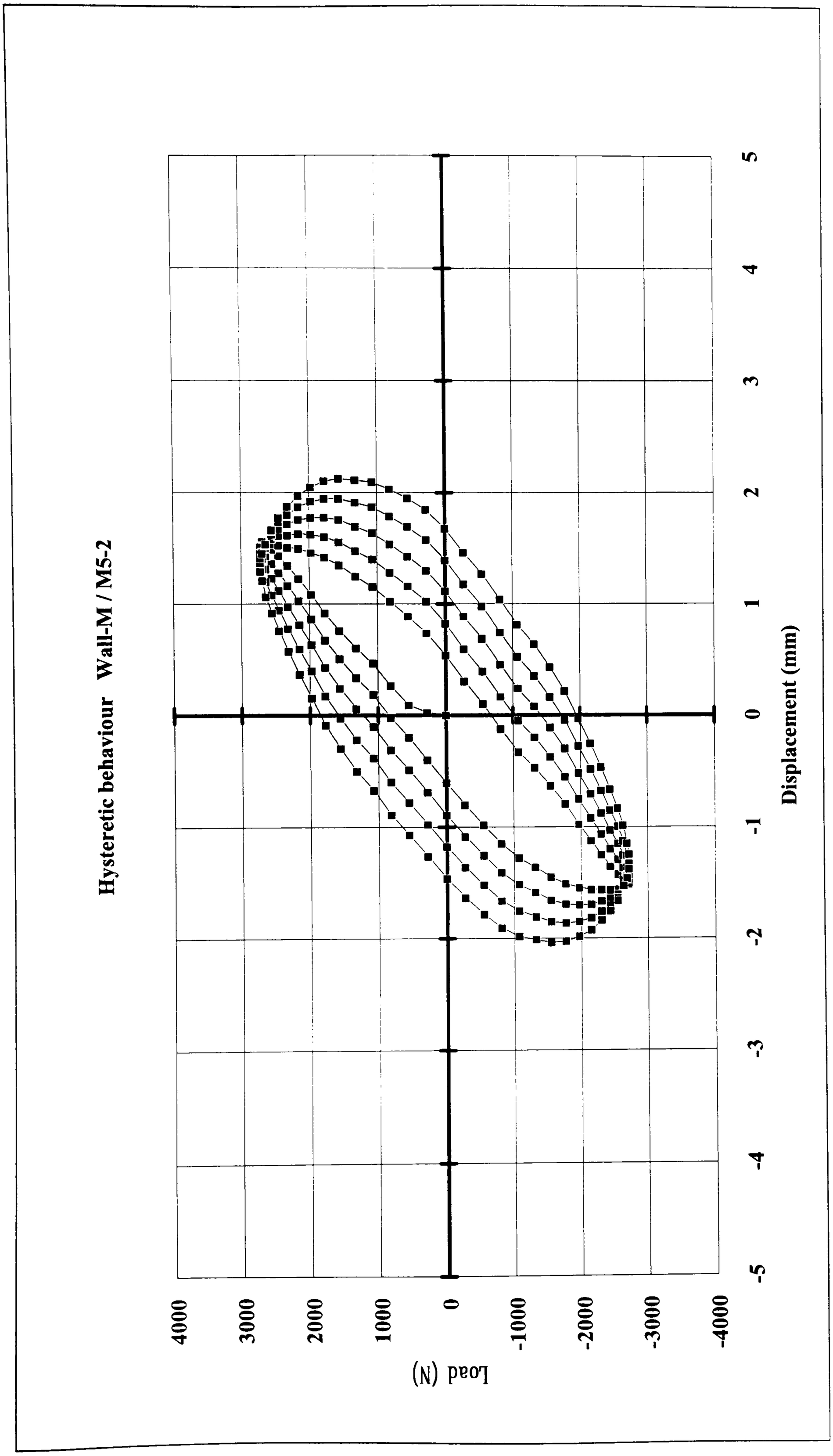

Figure 5.108 Wall-M / Hysteretic Behaviour - Stage M5/R2

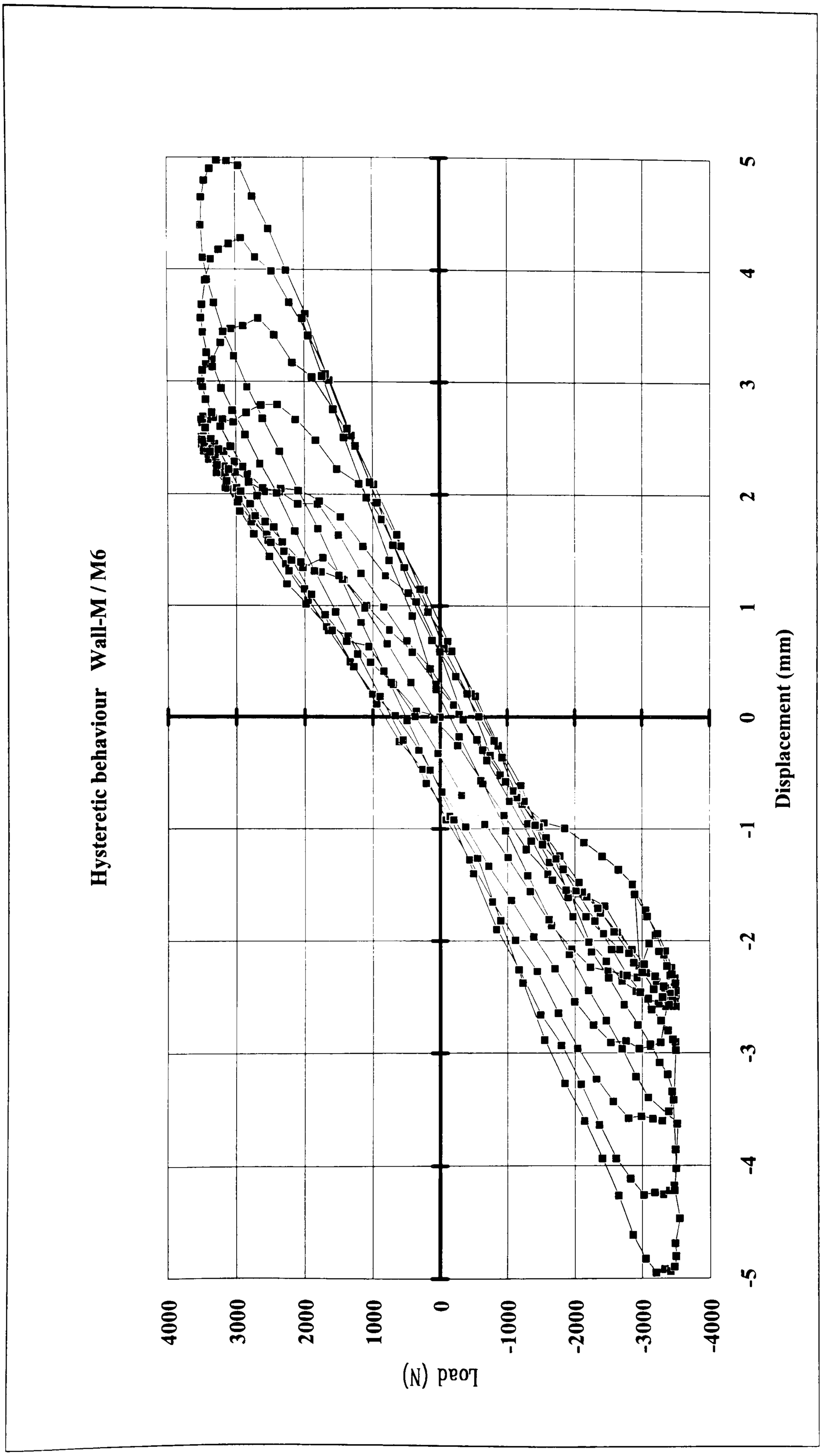

Figure 5.109 Wall-M / Hysteretic Behaviour - Stage M6

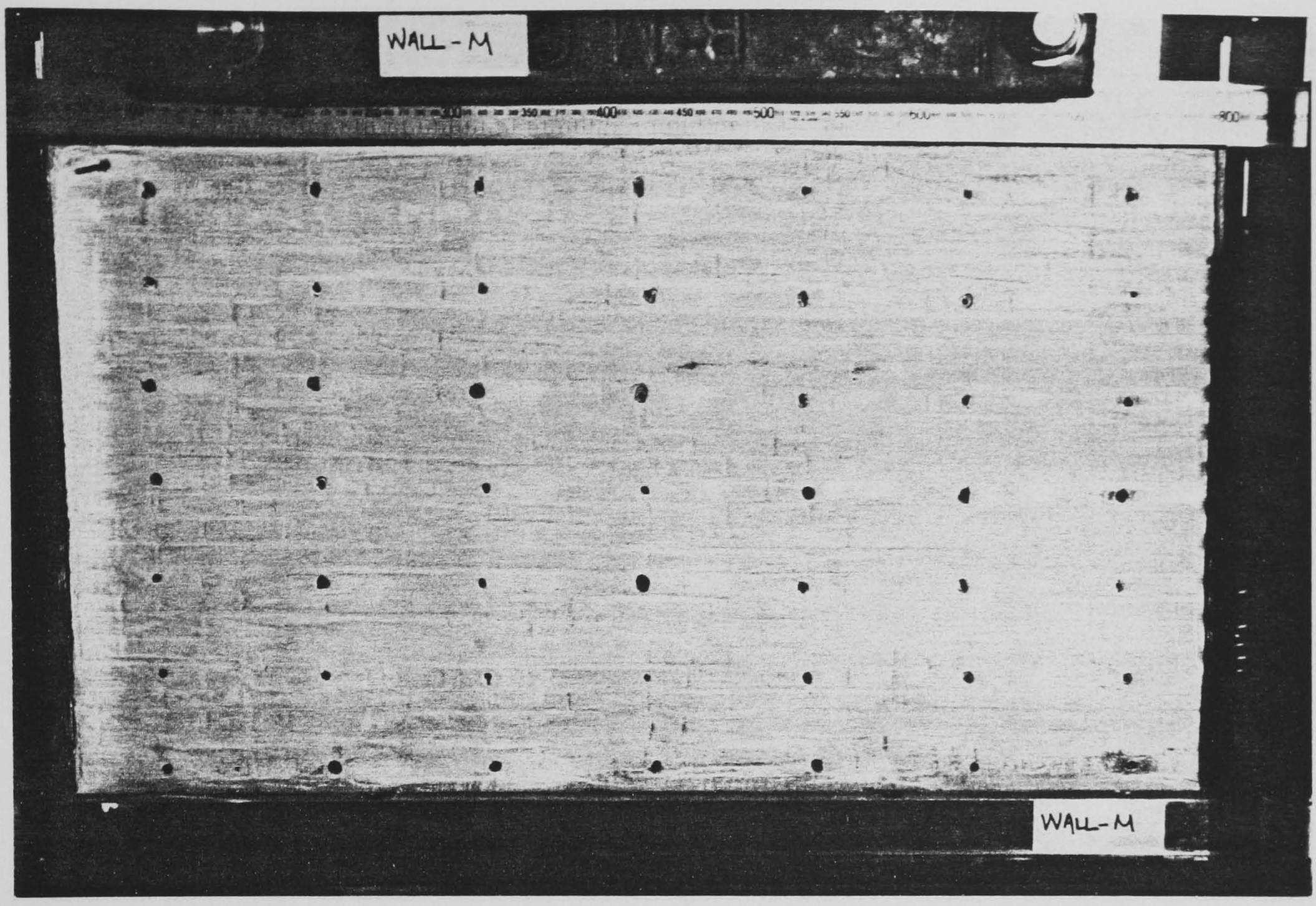

Photo 5.57 Wall-M with drilled holes on the shaking table

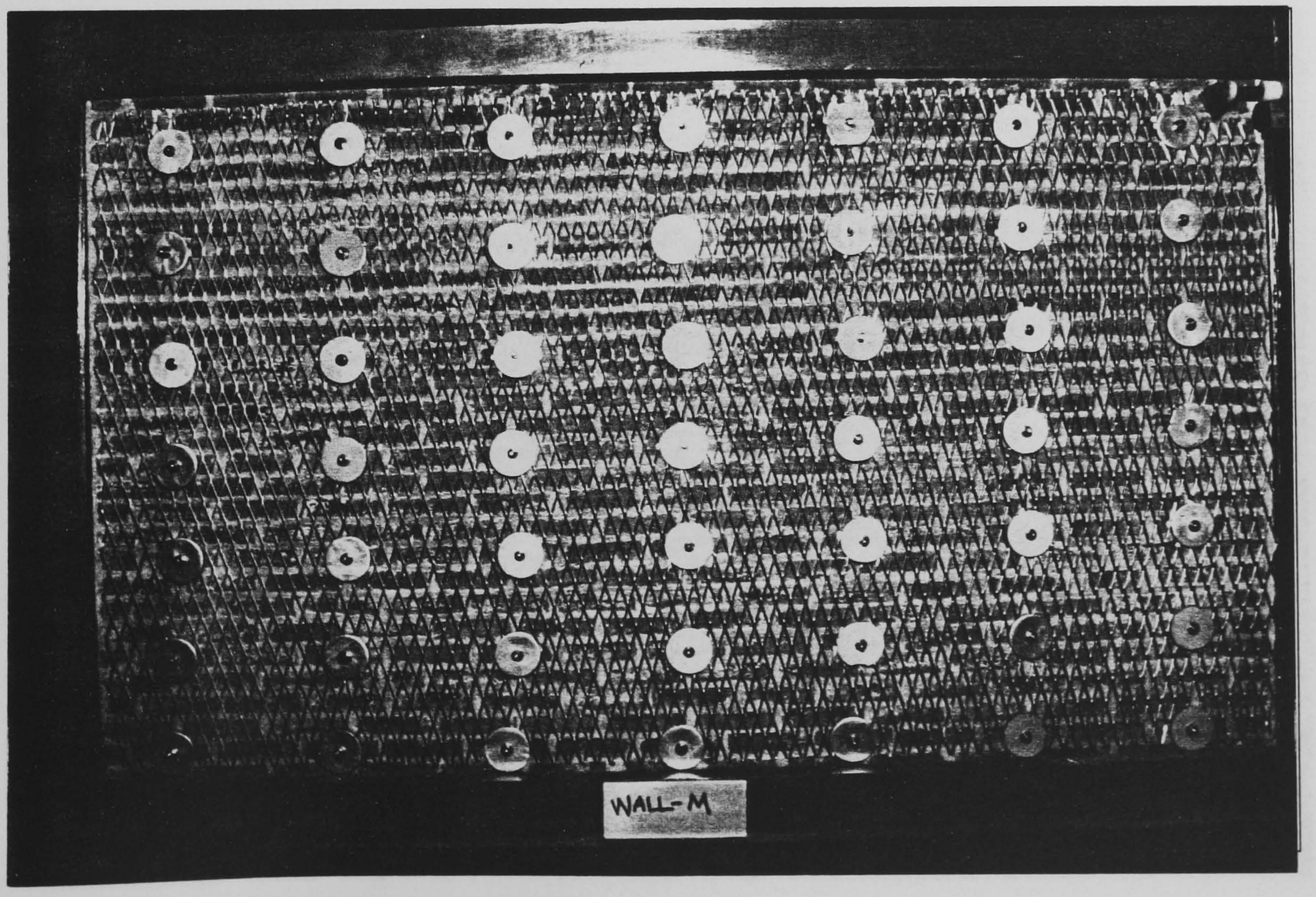

Photo 5.58 Wire mesh reinforcement (wall-M)

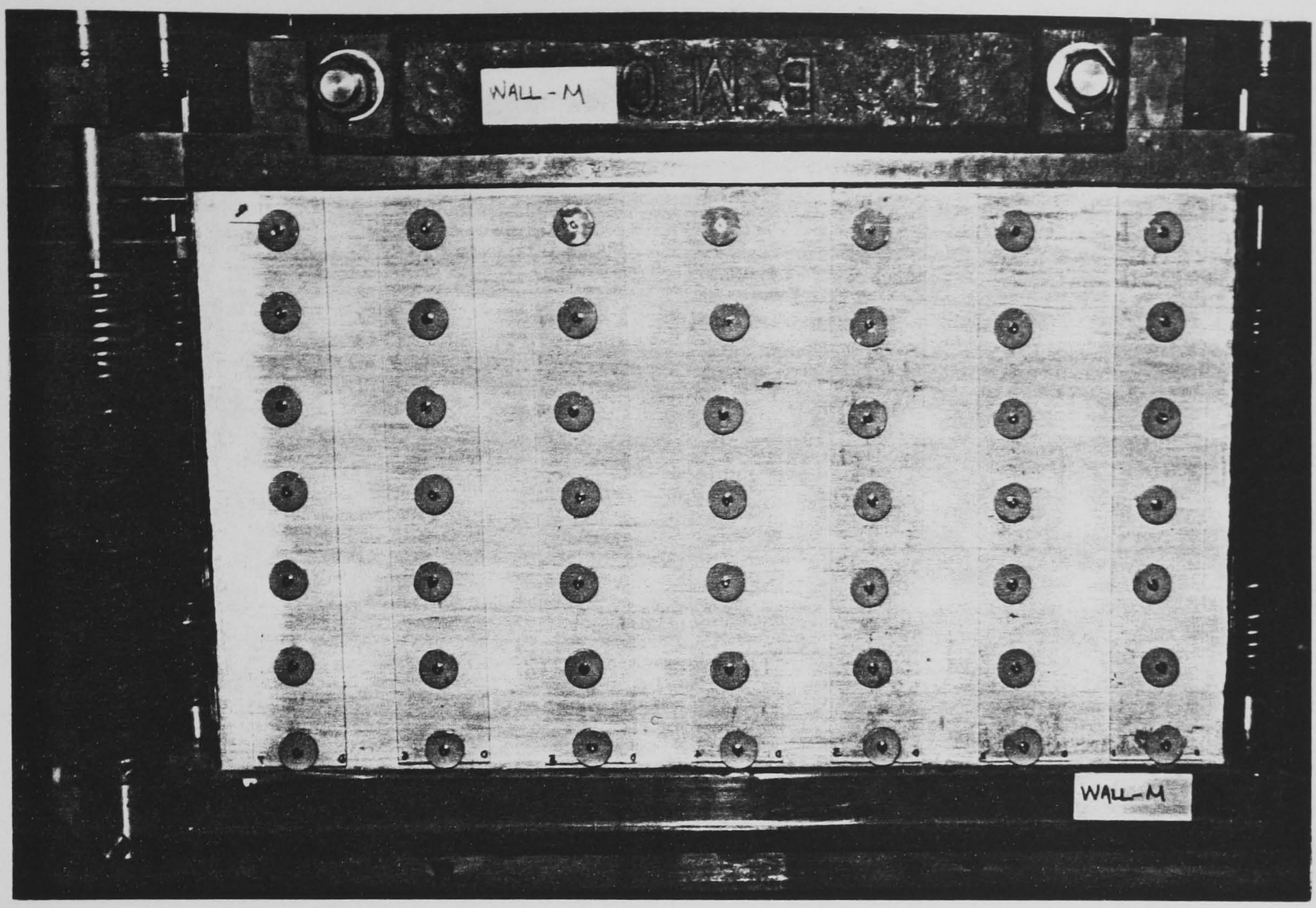

Photo 5.59 Perspex panels on the opposite side (wall-M)

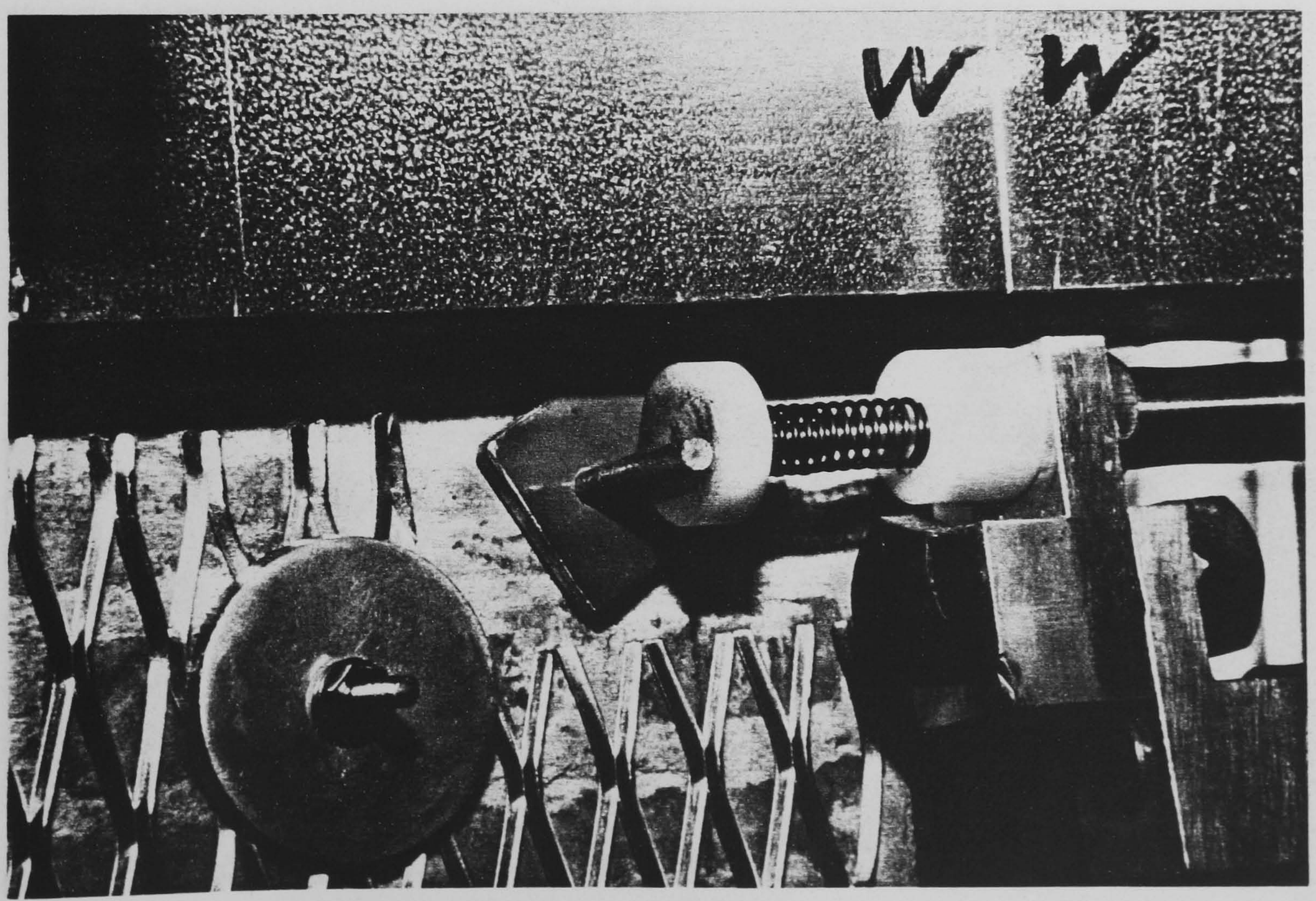

Photo 5.60 Details of instrumentation and mesh anchoring set-up (wall-M)

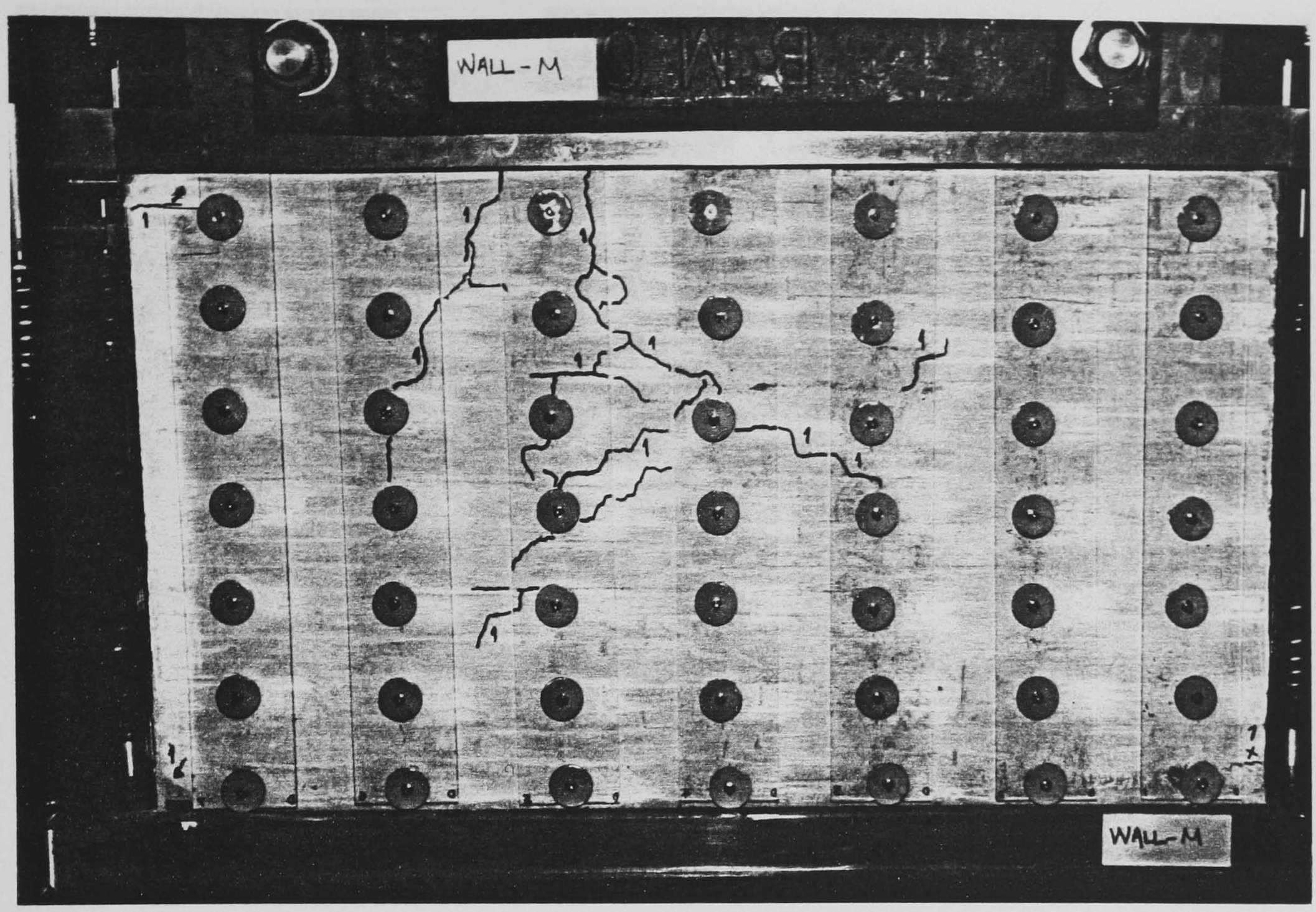

Photo 5.61 Crack 1 (wall-M)

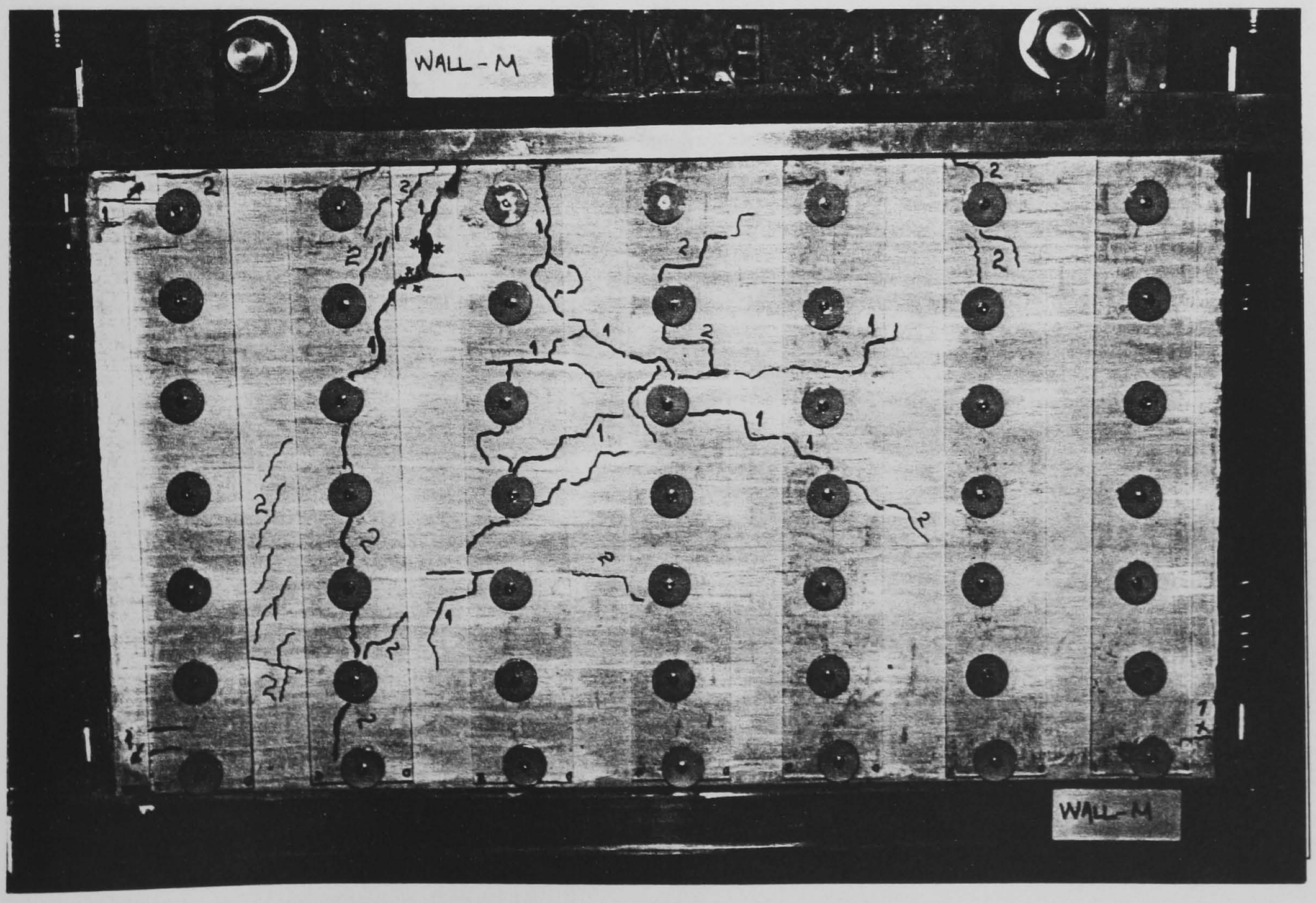

Photo 5.62 Crack 2 (wall-M)

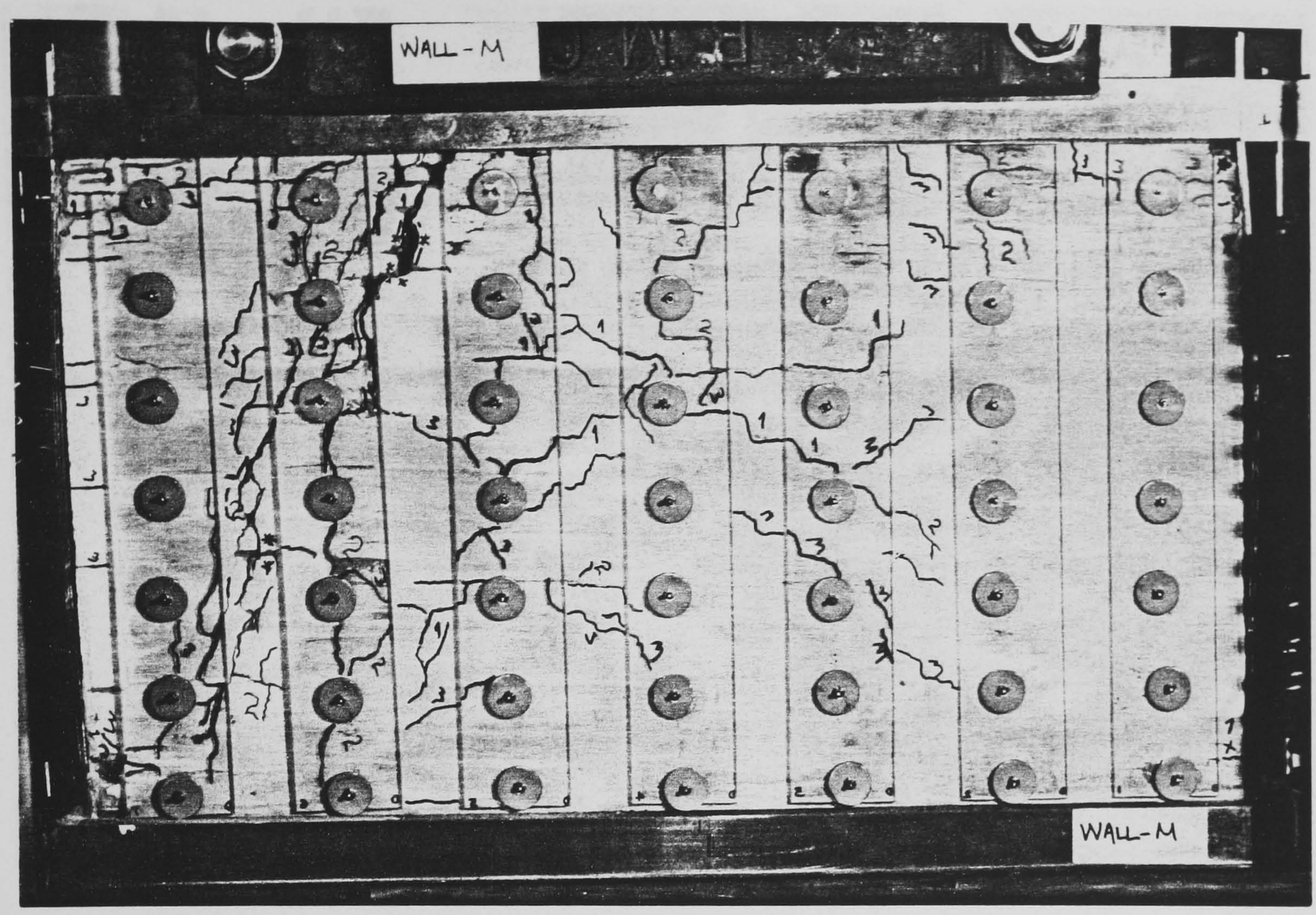

Photo 5.63 Crack 3 including corner crushing (wall-M)

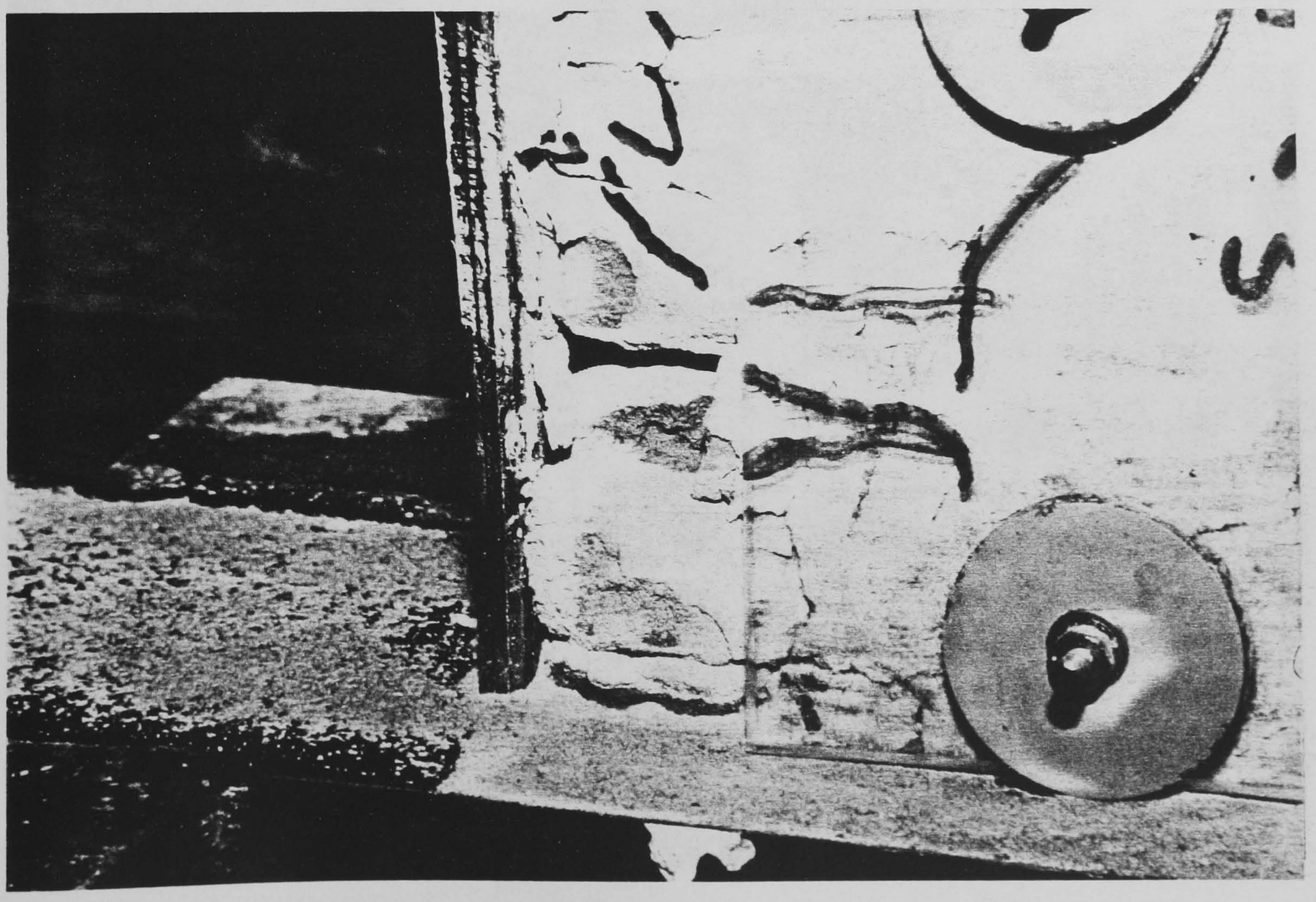

Photo 5.64 Close-up detail of lower left corner crushing (wall-M)

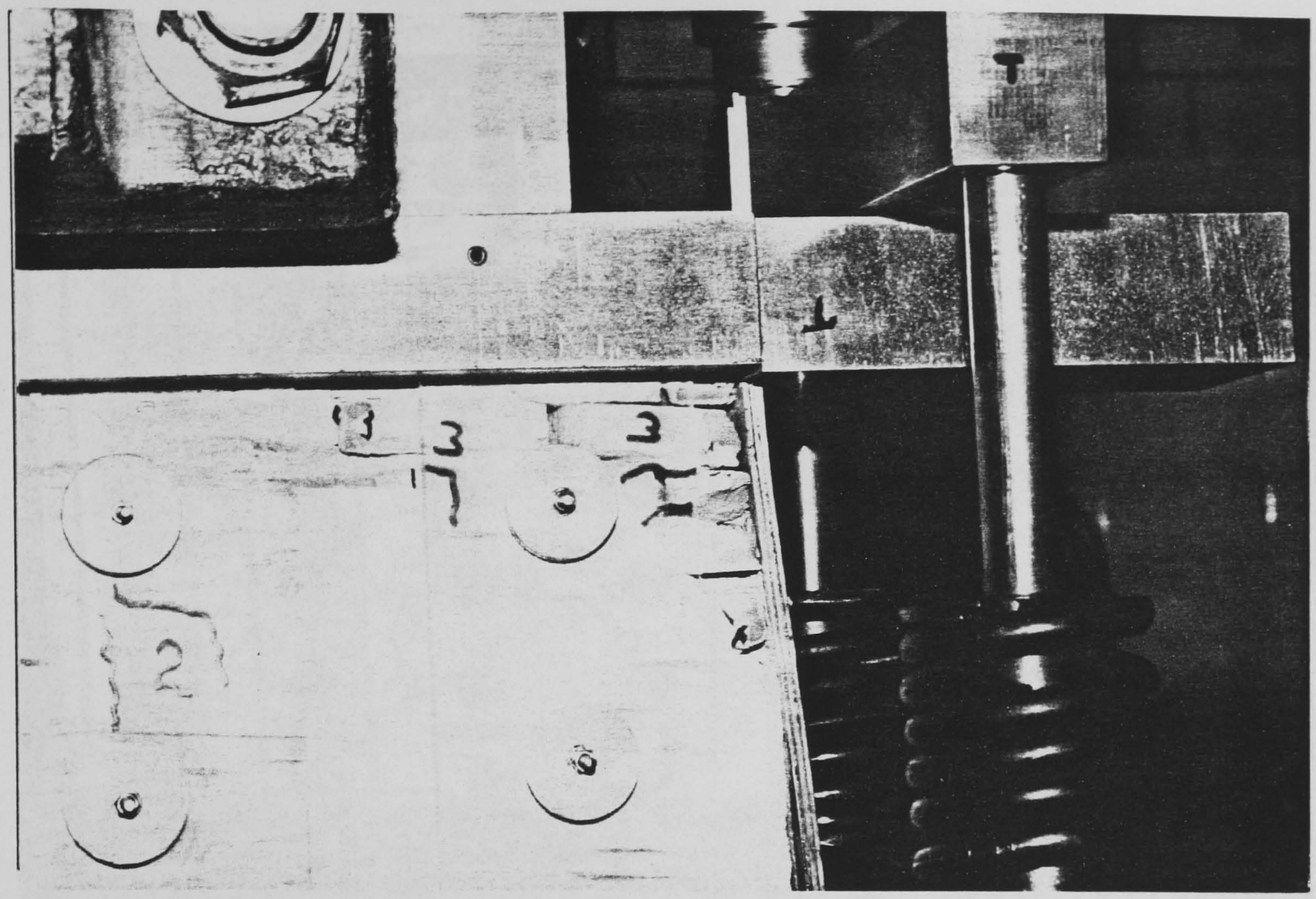

Photo 5.65 Close-up detail of upper right corner crushing (wall-M)

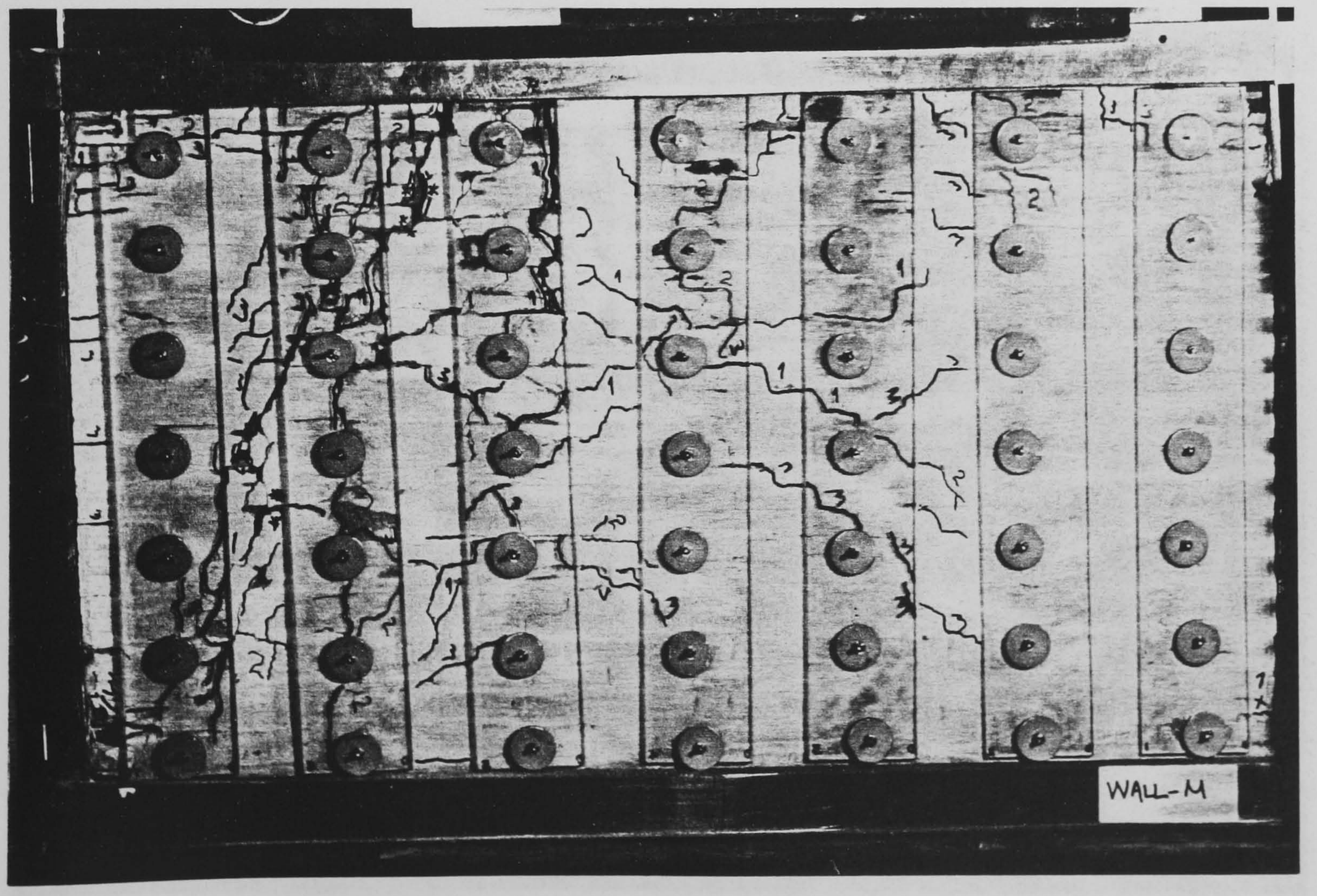

Photo 5.66 Cracking sequence with increasing ground acceleration-1 (wall-M)

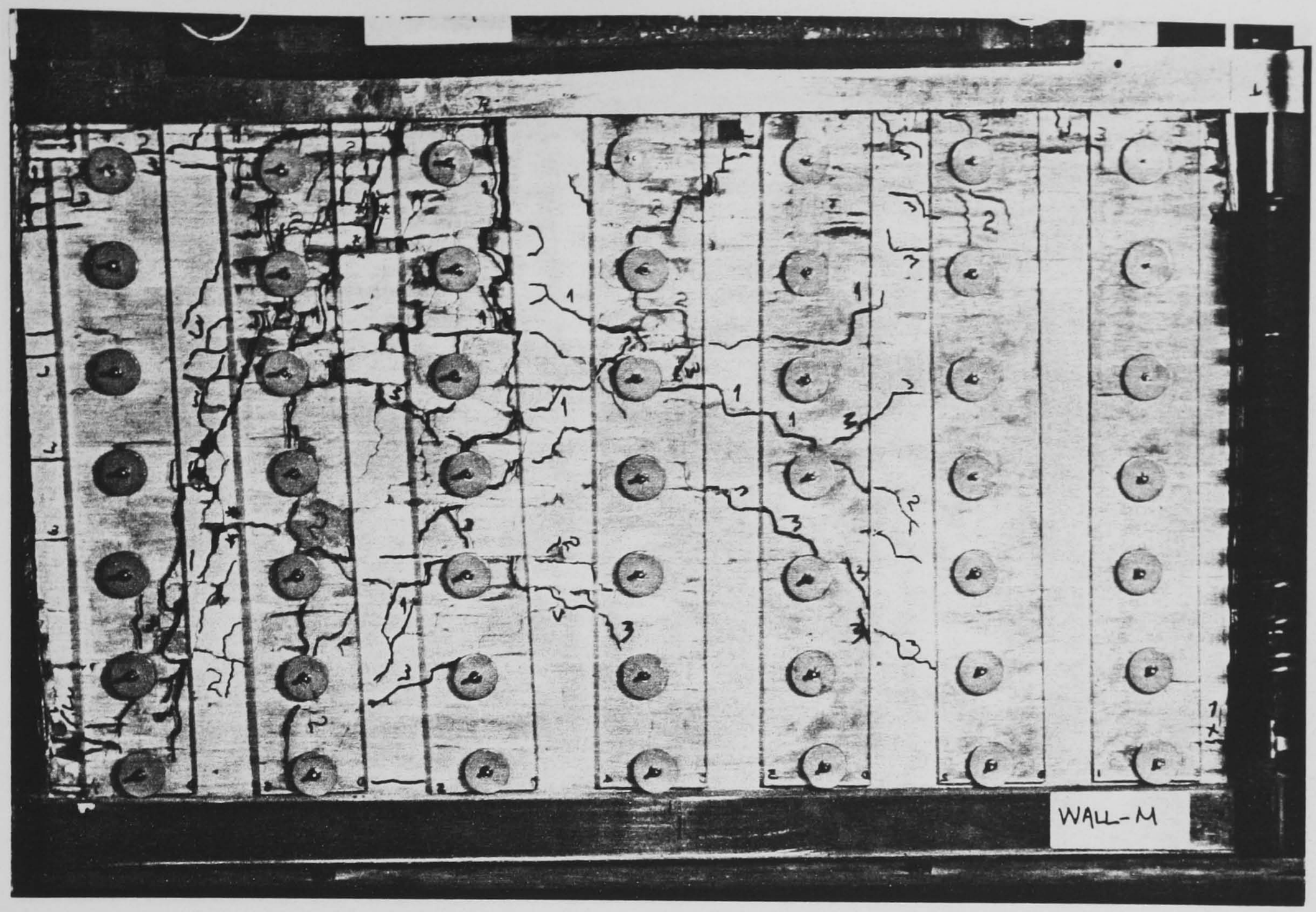

Photo 5.67 Cracking sequence with increasing ground acceleration-2 (wall-M)

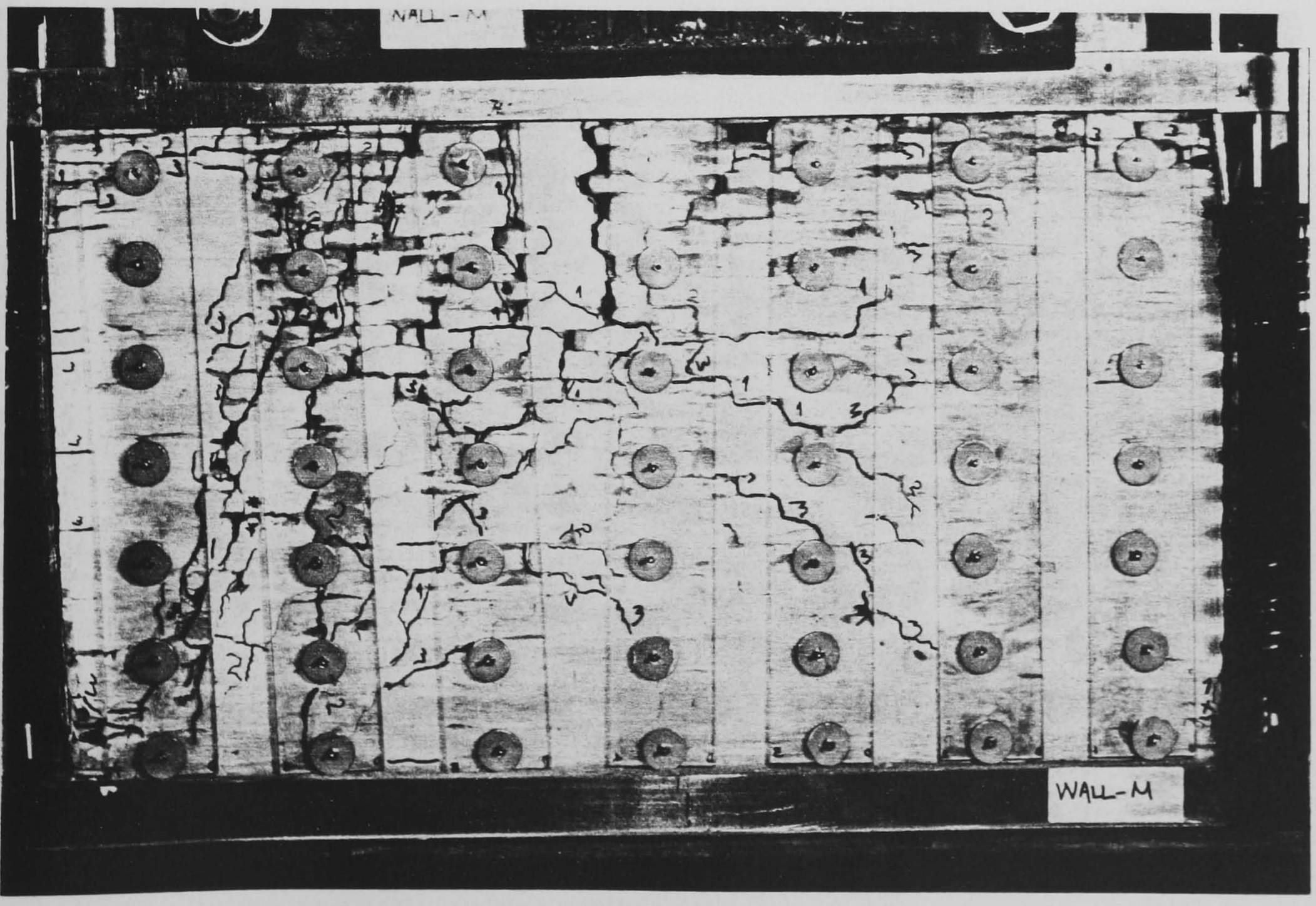

Photo 5.68 Cracking sequence with increasing ground acceleration-3 (wall-M)

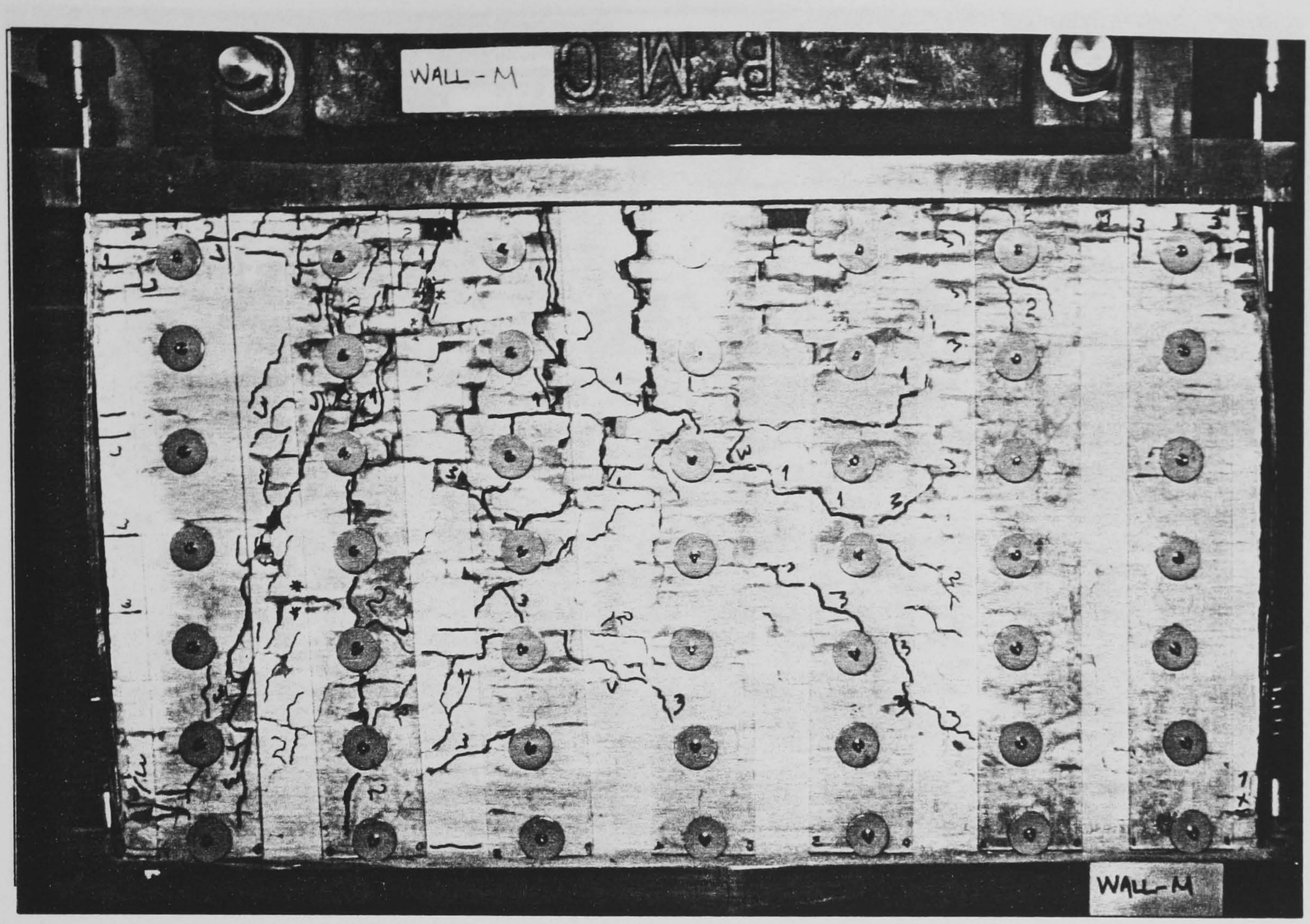

Photo 5.69 Cracking sequence with increasing ground acceleration-4 (wall-M)

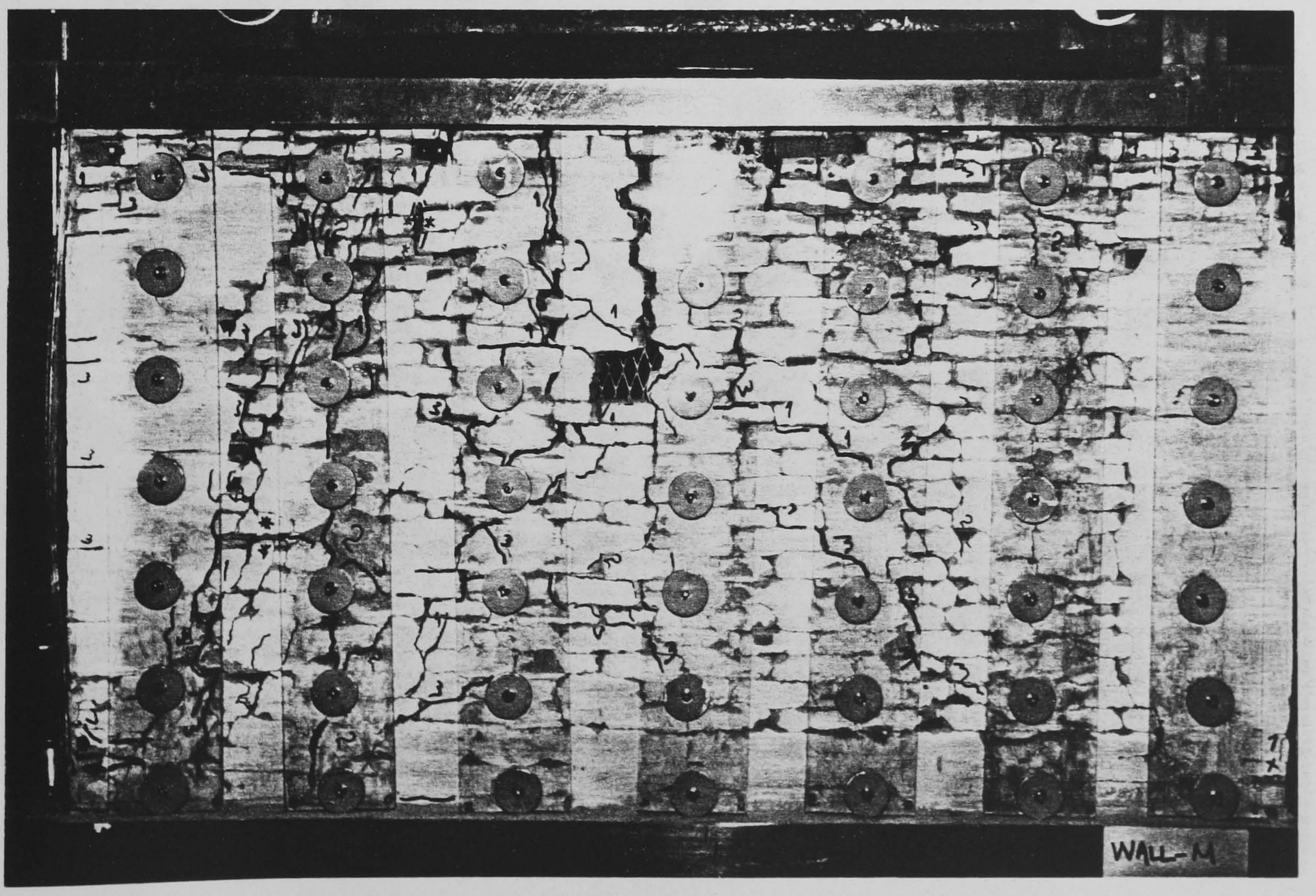

Photo 5.70 Cracking sequence with increasing ground acceleration-5 (wall-M)

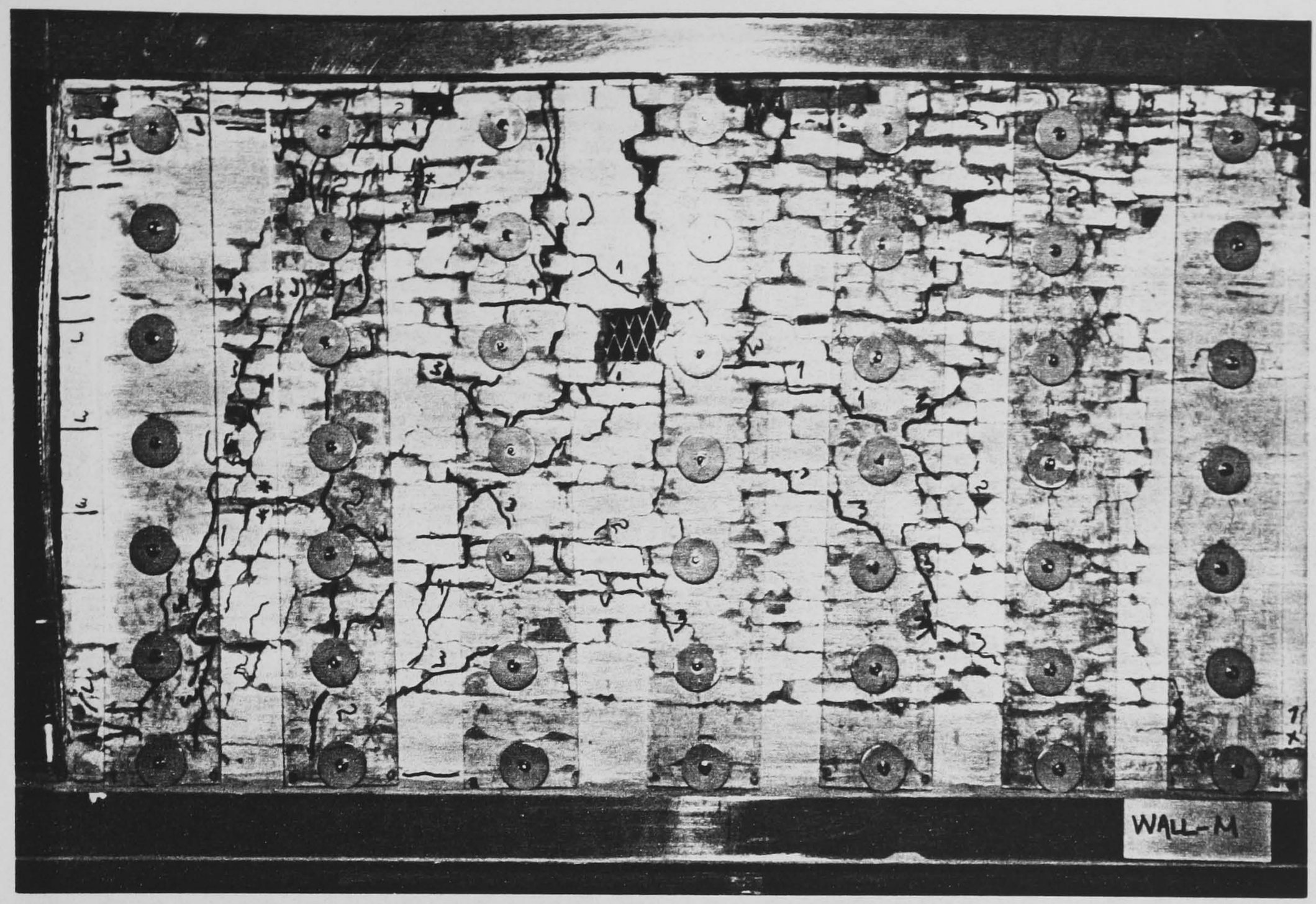

Photo 5.71 Cracking sequence with increasing ground acceleration-6 (wall-M)

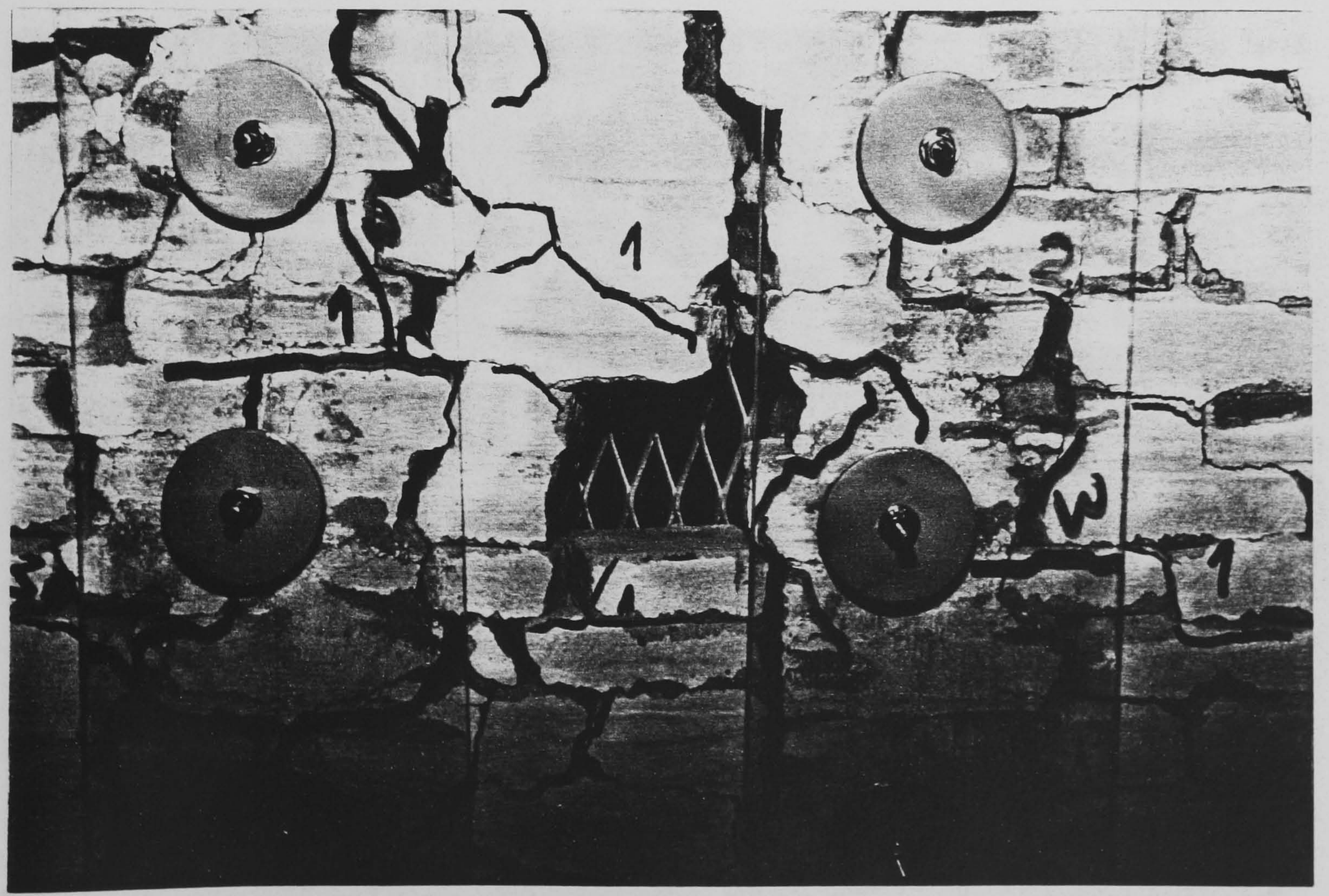

Photo 5.72 Close-up details of the middle section (wall-M)

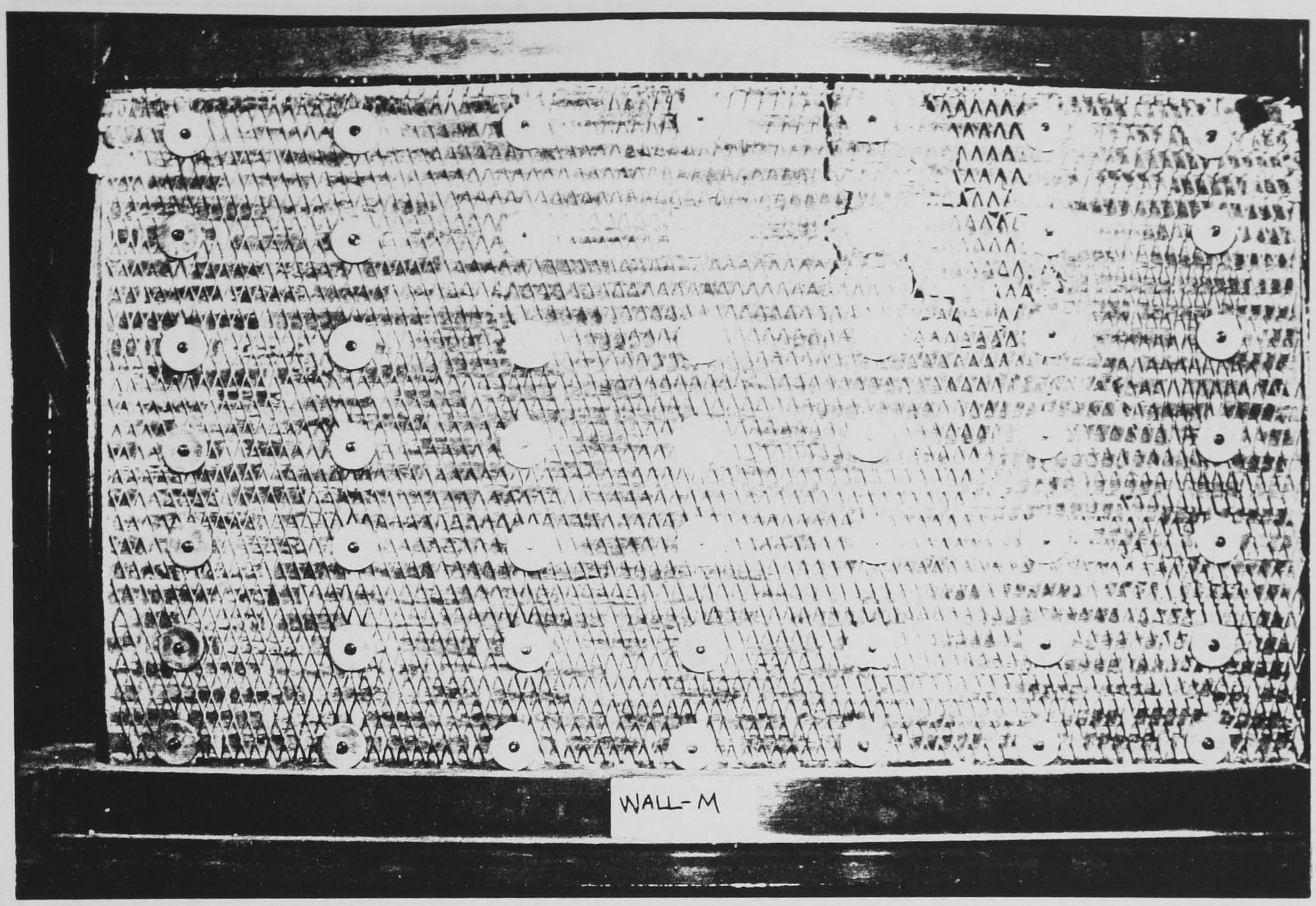

Photo 5.73 Mesh side after appearance of crack 2 (wall-M)

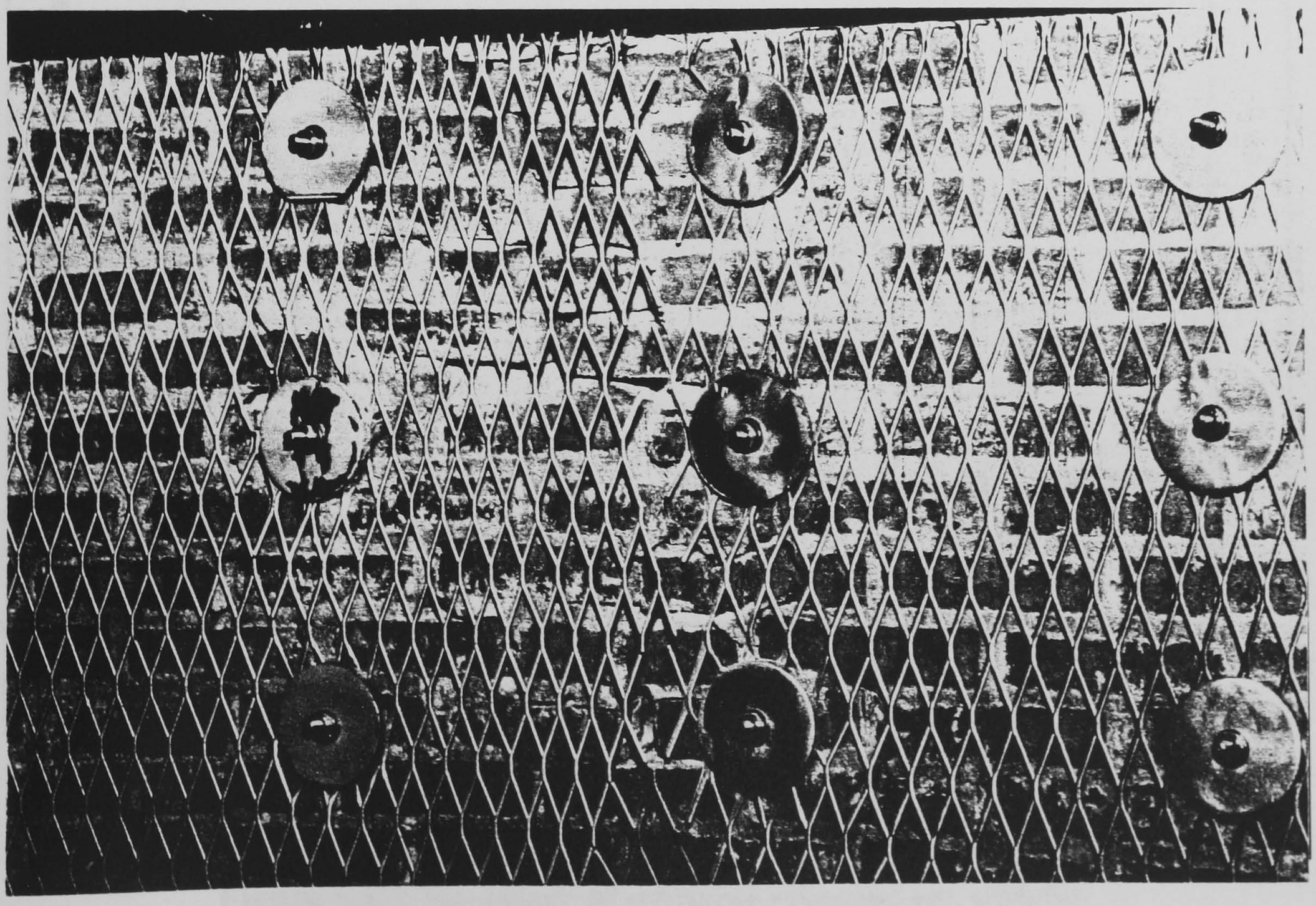

Photo 5.74 Tensile failure of wire mesh reinforcement (wall-M)

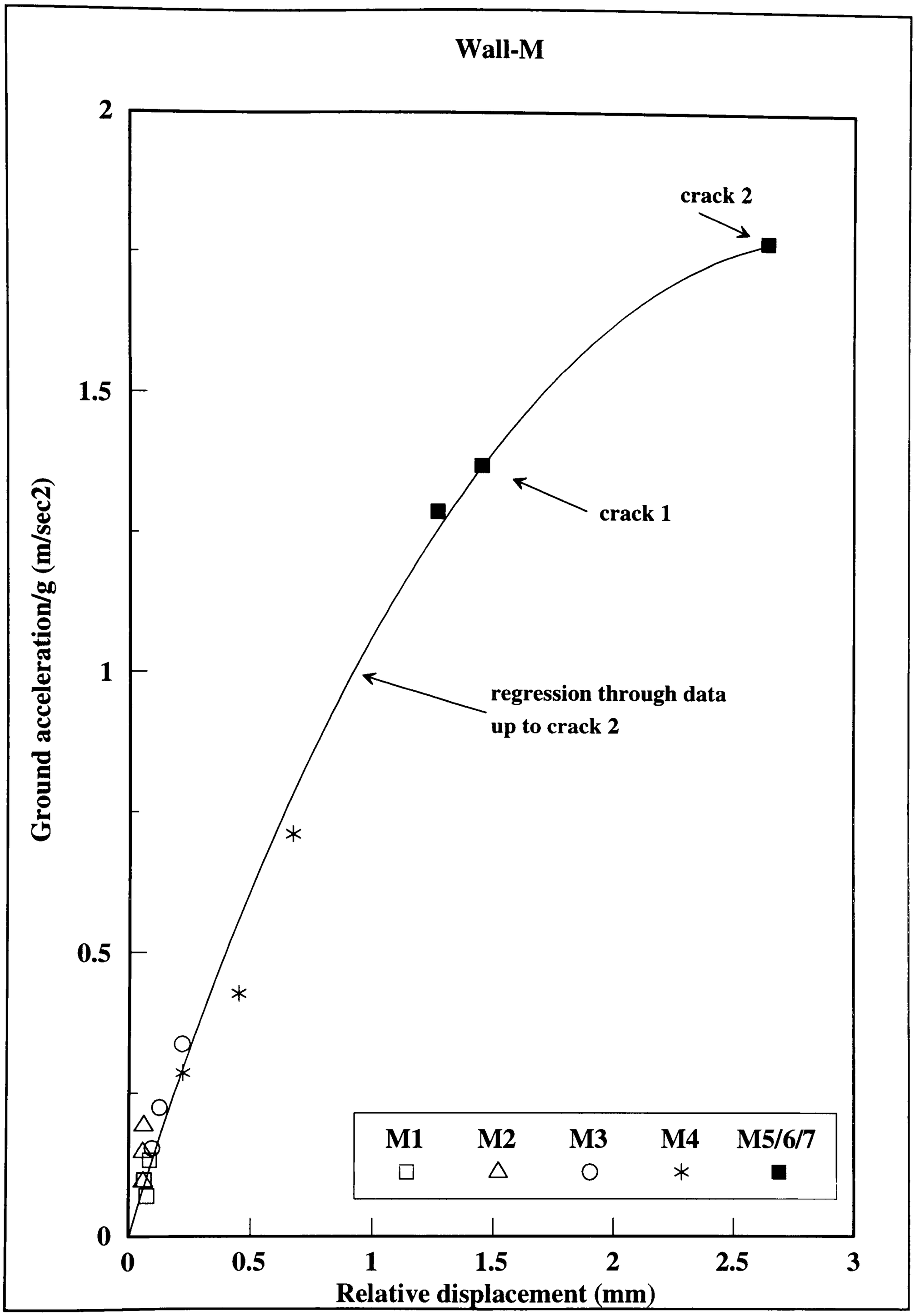

Figure 5.110 Summary of dynamic response for wall-M

5.8.6.1 Observations for wall-M.

Wall-M was tested 7 days after casting with a mortar compressive strength of 1.1 MPa and a tensile strength of 0.09 MPa. The panel was externally reinforced using wire mesh on one side only. In order to study and record the appearance and formation of the cracking patterns, perspex rectangular pieces (420 x 70 x 6 mm thick) where placed on the opposite side and connected to the mesh at 49 points equally spaced on the faces of the panel, with threaded studs (35 mm long with 2 mm diameter), nuts and large diameter machine-cut washers. The bricks were drilled before casting the panels, and after these were moved to the shaking table the mesh was attached and tightly connected to the perspex sections (photos 5.57 to 5.60) This was aimed at imposing some degree of lateral confinement to the panel which improved the dynamic behaviour particularly during the post-cracking stages. Free vibration tests with and without this external reinforcing arrangement revealed no changes in the natural frequency of the panel (figure 5.99).

Several cycles of low intensity amplitude of vibration were imposed and no apparent cracking was observed after inspection of the panel at the end of each stage. At an acceleration of 1.37g crack 1 occurred and spread randomly around the middle-upper section (photo 5.61). During the next stage and at a 1.77g acceleration, crack 2 appeared with no symmetrical pattern and sections of the first crack increased in width as shown in photo 5.62. At an even higher acceleration of 1.98g, crack 3 shown in photo 5.63 appeared, while several of the previous cracks widened. At the end of this stage free vibration tests revealed a 180% decrease in the natural frequency together with a substancial increase for the equivalent viscous damping coefficient (12.5%).

In an attempt to collapse the panel four further cycles of increasing magnitude with respect to the shaking table ground motion were applied up to about 2.5g acceleration with the top LVDTs taken off. The cracking distribution observed during these stages is shown in photos 5.64 to 5.71, where damage was so extensive that most of the bricks separated and tended to 'float' around the mortar joints constrained only by the external wire and perspex reinforcement (photo 5.71). The opposite side of the

panel where the mesh was attached is shown in photos 5.73 and 5.74, where failure of the wire can be seen. Residual stresses resulting from the drilling of the units, combined with a triaxial state of stress due to the applied lateral and axial forces and out-of-plane confinement from the tying mechanisms, localised cracking to the area around the brick units. Several vertical splitting cracks can be observed at the boundaries of the perspex sections although these extended downwards through the mortar head joints rather than the brick units. Had the tensile strength of the bricks being equal to or lower than the mortar's, the wall would have effectively separated into vertical segments with about the same width as the perspex sections. This can be observed in photo 5.72 where part of the masonry fell off the panel and the inside edges of the two perspex sheets coincide with the formation of the vertical splitting cracks. The cracking pattern is mostly concentrated around the mortar joints with a few bricks failing by vertical splitting particularly at the gaps between the perspex sheets.

5.9 Summary of the measured dynamic properties.

The reduction in the natural frequency measured during free vibration tests is illustrated in figure 5.111. The results from all the tests are grouped together to illustrate the behaviour of the panels under increased intensity of the applied sinusoidal ground motion. The shape of the line that connects the points which represent values for the natural frequency show a nonlinear portion which is associated with the stiffness degradation of the panels due to progressive cracking. The plotted lines have a similar shape as the value for the natural frequency is decreasing with perhaps the exemption of the line corresponding to wall-O. The increase in the equivalent viscous damping coefficient is illustrated in figure 5.112 for all the six tests, with values ranging from 3% (initial) to 12.5% (post-cracking). Damping in unreinforced masonry systems results mainly from the combination of the constituent materials internal damping characteristics as well as friction and hysteretic damping due to cracking. Values between 4% and 13% for the in-plane experimentally obtained damping coefficient masonry models, have been reported in literature [Ref. 62, 109, 111, 112].

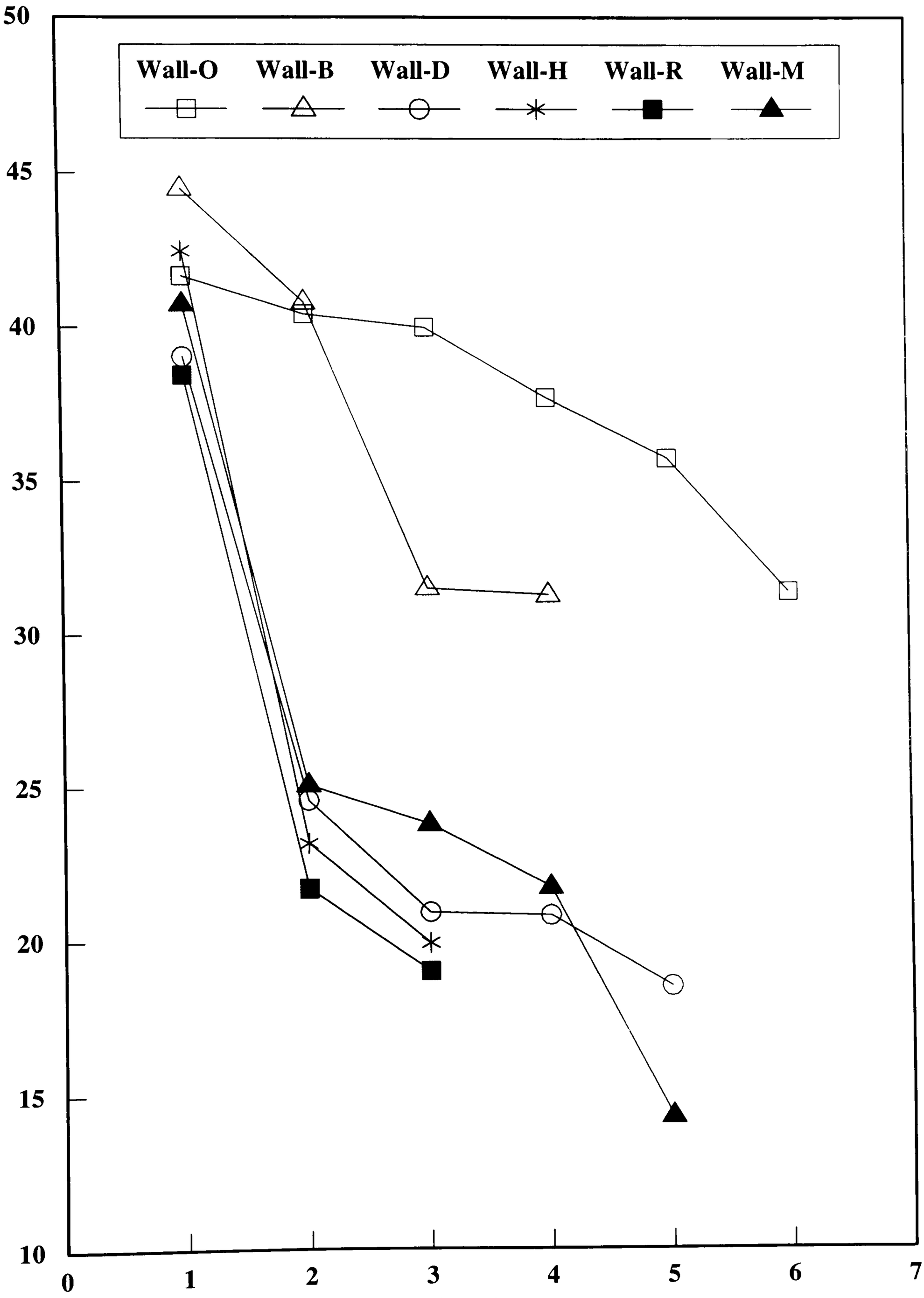

Figure 5.111 Variation of the fundamental natural frequency

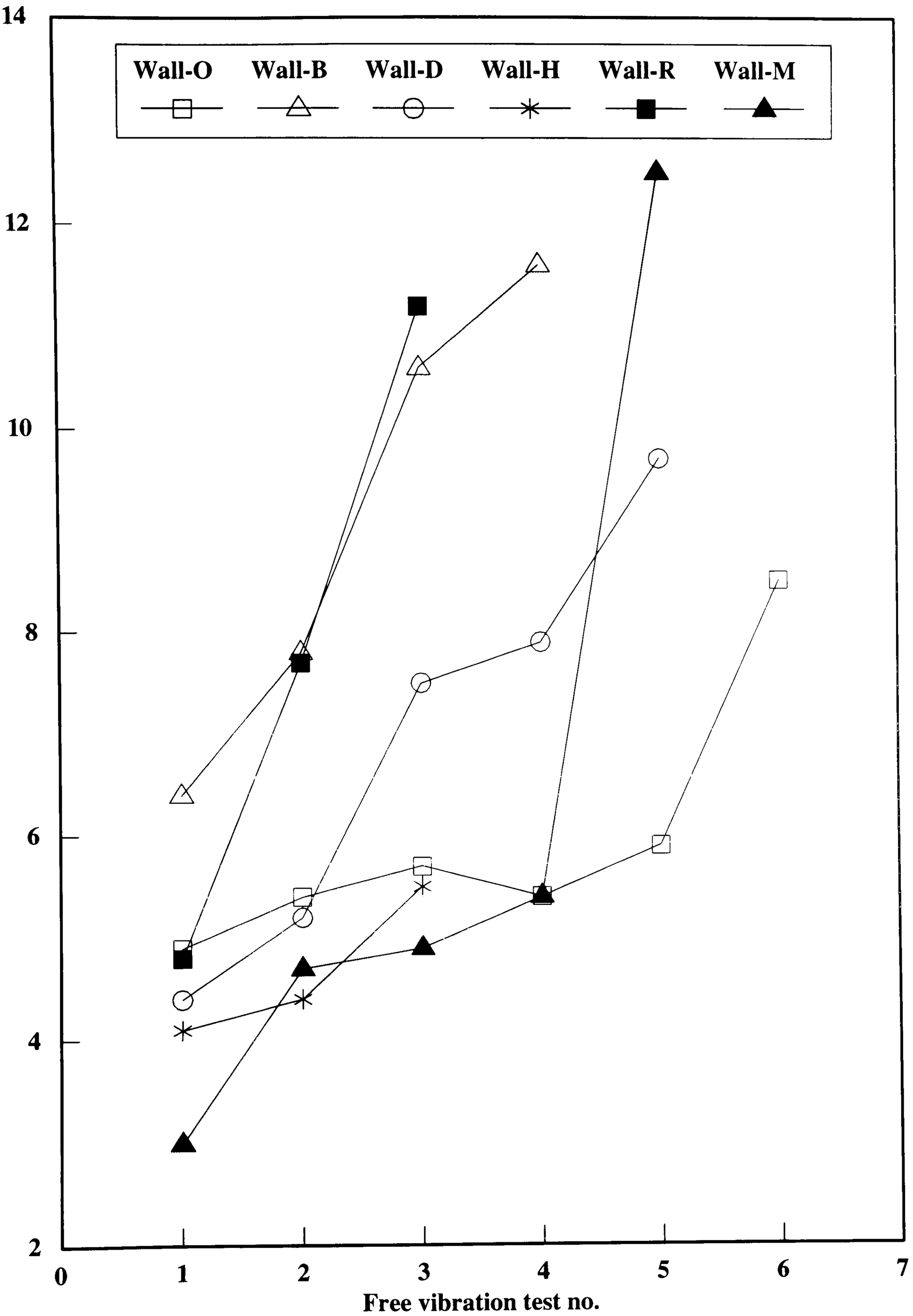

Figure 5.112 Variation of the equivalent viscous damping coefficient

It should be noted that figures 5.111 and 5.112 are plotted with respect to the testing sequence for each test which although meaningless in scientific terms, allows for comparison with similar figures as found in recent technical literature. Figure 5.113 presents results for the measured natural frequency and equivalent viscous damping coefficient, in non-dimensional form. The decrease in the natural frequency together with a corresponding increase in the damping coefficient with progressive damage, show a distinctive trend with respect to the shape of the curves. This can be further emphasised if the data is divided into three regions as shown in figure 5.113.

The upper region corresponds to the first two strong walls (O and B) which although damaged, did not collapse. The middle region (shaded area), groups together data for the three walls (D, R and M) which exhibited ductile behaviour, mainly through shear dominated failures (diagonal tensile cracking). The lower region corresponds to the heavy wall (H), which failed soon after the appearance of the first cracks, in a brittle mode exhibiting limited energy dissipation capacity.

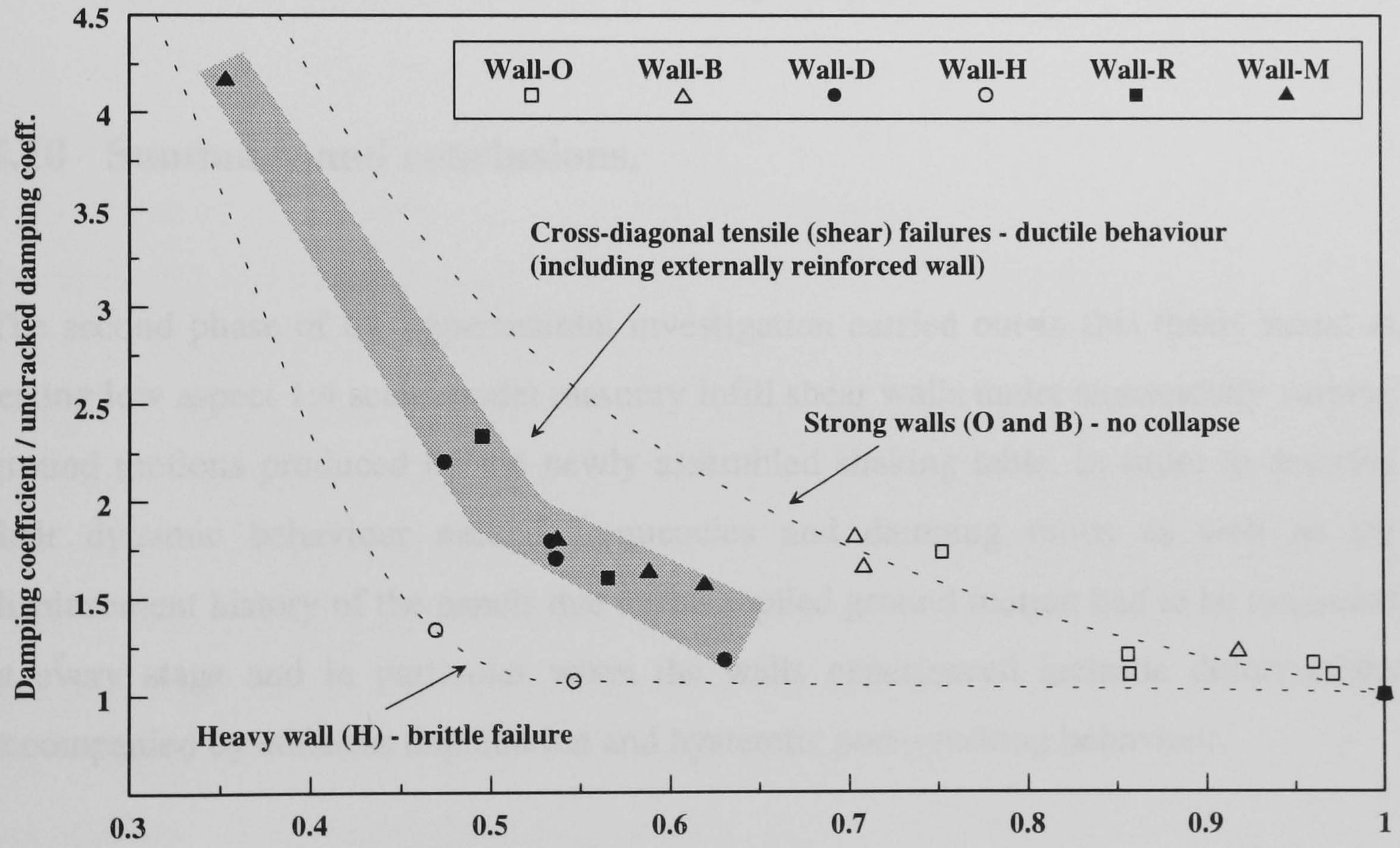

Figure 5.113 Non-dimensional relationship between natural frequency and damping for all tests with progressive damage

Finally table 5.14 provides a summary of the measured natural frequency for all six tests and the corresponding calculated values together with the computed percentage error between them. The theoretical and numerical predictions are based on procedures described earlier.

Test	Hammer tests	Theoretical prediction using equations 5.1 - 5.4	Error	Numerical prediction using F.E. models	Error
	Hz	Hz	%	Hz	%
Wall-O	41.67	61.2	46.87	73.4	76.14
Wall-B	44.48	64.8	45.68	75	68.61
Wall-D	39.06	58.9	50.79	69.2	77.16
Wall-H	42.48	66.1	55.6	77.4	82.2
Wall-R	38.46	54.7	42.22	67.1	74.47
Wall-M	40.5	60.6	49.63	72.5	79.01

Table 5.14 Summary of measured and predicted values for the uncracked fundamental natural frequency for all tests

5.10 Summary and conclusions.

The second phase of the experimental investigation carried out in this thesis aimed at testing low aspect 1:4 scale model masonry infill shear walls under sinusoidally varying ground motions produced by the newly assembled shaking table. In order to describe their dynamic behaviour natural frequencies and damping ratios as well as the displacement history of the panels due to the applied ground motion had to be measured at every stage and in particular when the walls experienced inelastic deformations accompanied by stiffness degradation and hysteretic post-cracking behaviour.

The shaking table facility was designed in such a way to allow frequency and particularly amplitude control to be manually adjusted. Following preliminary trial tests and relying on the experience gained during the static testing phase, the walls were fabricated using a technique that involved casting the mortar joints horizontally on a

perspex base. This ensured that the joints were consistent throughout and their dimensions complied with similarity conditions that dictated a width of 2.5 mm. This important modelling parameter is often overlooked or sacrificed in small scale masonry modelling for reasons of simplicity or difficulties associated with model fabrication (chapter 3).

Due to the lack of dedicated instrumentation all the measurements presented in this chapter were obtained from displacement transducers and subsequently mathematically processed to obtain acceleration values. Since the differentiation procedure by definition tends to accumulate errors with respect to the time parameter, the displacement records were sampled with a period of 0.001 seconds to improve the quality of the results. Electrical noise which was polluting the signals consistently during free vibration tests was dealt with, using digital signal processing techniques.

A steel bounding frame was manufactured with no particular modelling considerations, to be used as part of the experimental set-up. It comprised two rectangular beams with oversized sections in order to attach the additional inertia mass and connect the panel to the shaking table platform. Mortar joints were cast at the beam and column interfaces although composite dynamic behaviour of the panel and frame system was not a primary research objective. As a result the column members were made out of spring steel in order to behave elastically regardless of the magnitude of the applied ground motions. Axial force was imposed in the models to provide confinement and inhibit flexural dominated behaviour as well as to increase the working stresses which are always unrealistically low for models of this scale. The six walls that were tested included one which was built using substantially heavier units resulting in a 2.5 increase in self-weight. The number of tests performed was not adequate to carry out a detailed parametric study and as a result this investigation concentrated on examining the dynamic behaviour of masonry panels subjected to shaking table sinusoidal excitations, when confined by a bounding frame and low to moderate vertical compressive forces. The main conclusions drawn from the six tests are summarised below.

1. Natural frequency

► Measured and computed values for the natural frequency differ markedly for all six tests. The experimentally measured values from the free vibration tests were believed to be influenced by shrinkage cracking which regardless of the method of curing will exist even if it cannot be detected. Reductions in the order of 20% to 40 % in the measured natural frequency of masonry systems compared with analytical predictions, are commonly observed in experimental studies. The hammer impact test is somewhat crude with respect to the point of application and the location of the instrumentation that is picking up the signal. In this case, due to the presence of the flexible column members, the top LVDT was connected to a stud inserted and epoxied in one of the top brick units, whereas the point of impact for the hammer was at the opposite end of the top beam. Equation 5.2 would be expected to provide an upper bound prediction to the lateral stiffness, since it assumes a solid section (shear-beam model) with uniform properties. Finite element methods allow the inclusion of prescribed material properties for the bricks and mortar joints if the panel is discretised as explained in chapter 6 using a two-phase modelling procedure. Since the characteristic mechanical properties of masonry lay between the respective properties of the individual components, it will also overestimate the fundamental natural frequency.

2. Failure modes

► The first two walls (wall-O and wall-B), demonstrated typical masonry infill panel failure modes. While a cross diagonal failure occurred for the first one (wall-O), the second (wall-B), exhibited a corner crushing failure resulting from excessive compressive forces at the loaded diagonal (compressive strut). This implies that for accelerations in excess of 1g the shear and flexure capacity of the wall was not reached. This was partly attributed to the increased interface bond strength between mortar and brick units. Wall-O was subjected to 35 loading cycles and a maximum acceleration of 1.14g. Although a typical cross-shaped diagonal cracking pattern occurred, this did not constitute a failure condition since the compression strut mechanisms continued to transfer lateral load to the panel, well beyond the initial cracking stage. For both tests malfunctioning of the driving mechanisms, did not allow for higher intensities of the applied ground motion, but it is evident that wall-O could have sustained further cycles

of even higher accelerations. The natural frequency was reduced by 32% after the last crack appeared in the panel. The energy dissipation capacity was evidently increasing while damping had risen to 8.5% compared with 4.9% before the test.

► Wall-D was weaker than wall-B with respect to the mortar tensile strength, masonry shear strength as well as interface bond strength. The shaking table had been repaired and modified before this test commenced and as a result higher accelerations were imposed to the panel resulting in failure and collapse. Cross-shaped diagonal cracking was observed which is typical for masonry infill shear walls and is the most commonly recorded failure mode during actual earthquake events. The similarities with photos 5.3 and 5.4 (Aigio earthquake) are very apparent, the centre section in particular where the diagonal cracks originate and spread towards the corners. Since initial cracking, the panel exhibited considerable ductile behaviour mainly through hysteretic damping, for surprisingly high magnitudes of the applied ground acceleration. The panel sustained accelerations in the order of 1.61g which is about double the ground acceleration that caused cracks 5 and 6. This increase in the panel ductility is quite surprising, considering the inherent brittle nature of shear dominated failures and as similarly observed by other researchers, is probably a result of the sliding mechanisms acting along the cracks in the presence of axial forces. Abrams [Ref. 54], performed similar tests on low aspect unreinforced masonry panels subjected to combined cyclic lateral and constant axial forces and measured quite high values for the lateral displacement in comparison with the displacement at peak load. He comments on the beneficial effect that vertical compressive forces have on the ductility and argues "*that unreinforced masonry elements may behave differently than that which is commonly assumed*". Seismic induced shear ductile failures are also summarised by Bruneau [Ref. 111] from a number of experimental investigations reported during the past 10 or so years.

► Wall-H which was built with the heavier bricks, was also subjected to 10 cycles of varied intensity of ground motion without damage. At an acceleration of 1.26g the first crack occurred, which spread almost all over the face of the panel. This was a combined flexural-diagonal shear crack, which caused the panel to collapse after two

loading cycles with 1.4g and 1.3g shaking table acceleration and with a brittle explosive mode.

► Similarly wall-R went through 10 loading cycles before the first cracks appeared at an acceleration of 0.84g and finally collapsed with only one diagonal crack fully developed after imposed accelerations reaching 1.6g. Wall-R was built using the weakest bricks from all the tests, with a tensile strength of only 20% higher than the mortar tensile strength. Considering that mortar in a wall is generally stronger than what is measured in a static test using cubes and cylinders, this explains the irregular cracking pattern recorded in photos 5.48 to 5.54 which involved splitting and tensile failure of the bricks.

► Wall-M was deliberately built using very weak mortar to induce failure at an early stage, in order to investigate the contribution of the external reinforcement on the dynamic behaviour and in particular the adequacy of the confinement it presents to a severely damaged panel. Surprisingly, the panel went through 13 cycles of increased intensity in the applied ground motion, when it eventually cracked at an acceleration of 1.37g. Further cycles approaching 1.98g were applied and although the damage observed was so extensive that individual bricks were literally vibrating, the degree of confinement provided by the external reinforcement prevented out-of-plane collapse. Although much of the damage at the initial stages was attributed to the experimental set-up, the final cracking pattern was a result of the external restraint provided by the wire-mesh and perspex pieces.

► The dynamic response for all six walls is graphically summarised at the end of each section where the cracking is noted as it appeared in each stage. The scatter of data did not allow for a complete statistical analysis to be carried out. However, a regression curve is plotted for the data up to the occurrence of the first crack or in the cases of walls B, D, and R the second crack, (first crack in these walls was observed at the column-panel interface and is therefore excluded). It is interesting to note that for wall-O (figure 5.33), cracks 2 to 6 appeared at a lower relative displacement in comparison with the first crack. This is also evident to a lesser extent in figures 5.49

(wall-B) and 5.65 (wall-D). A possible explanation for this apparent reversal of the response curve (figure 5.33), is the increase in the energy dissipation capacity of the walls through hysteretic damping, which counteracts the effects of the stiffness degradation.

3. Hysteretic behaviour

► Sample hysteresis curves were provided for all six tests to illustrate the energy absorption characteristic of the panels with progressive damage. Walls D, R, and M provide the most impressive hysteretic curves, which clearly show the energy absorption characteristics of the panels between the stages. In wall-D the initial loop (figure 5.61), is wider at the centre and narrower at the two opposite ends. As damage occurs, the two ends begin to widen while the area under the loops is increasing (figures 5.62 to 5.64). In wall-R the first loop (figure 5.90), has a pinched shape at the centre before any damage had at least visually observed. Figure 5.91 which corresponds to the stage R8, clearly indicates the energy absorption capacity of the panel following extensive damage. During this stage, the natural frequency was reduced by 50%, while damping had increased by 134%. Figure 5.106 corresponds to the uncracked wall-M and shows similar pinching at the origin. With increasing damage, it widens in a striking manner (figures 5.107 and 5.108). In most of the hysteresis curves a flat region can be observed at the opposite ends and is attributed to the damping mechanisms for the panels resulting from friction and cracking which tend to counteract the effects of the degrading stiffness.

Chapter 6

Analytical studies using two-phase finite element non-linear models

6.1 Introduction.

Masonry is a non-homogeneous material, consisting of a matrix of brick units and mortar each with different mechanical properties. Joints act as planes of weakness, the mortar having a lower tensile strength, the cracking path is directed by the orientation of the joint layout in relation to the line of action of the external loading. To model such a system requires a numerical method that can incorporate a mesh pattern representative of both constituents, each one having non-linear material properties based on their individual strength and constitutive relationships. A commercially available finite element analysis system primarily used for modelling reinforced concrete which is part of the LUSAS suite of programs was adopted by the author for this study. Development of a purposely-written code would have been prohibitive in terms of time and would have deflected the author from his main experimental program.

6.2 Description of the LUSAS Finite Element Analysis System.

LUSAS is a general purpose finite element package with a very large user base and consists of the analysis module and MYSTRO which is an interactive graphical interface [Ref. 113]. It is furnished with a large selection of element types for two and three-dimensional modelling and it can perform linear, non-linear, static and dynamic analysis depending on the *element* type and *constitutive model* selected. Contact

problems can be treated using linear or non-linear *gap* and *joint* material properties. In addition a set of *interface* and *slideline* models are available that can handle more complicated situations as in the case of the panel-frame contact, with or without friction properties. An option is included that permits the user to assemble purpose-written material models that can be incorporated into the system for greater flexibility. The complete package is available on a 486/33 MHz PC, and the departmental SUN SPARK+ workstation.

6.3 Modelling and discretisation procedures.

A two-dimensional isoparametric plane stress element (QPM8) was adopted for modelling both the brick units and the mortar joints. This is an 8-noded quadrilateral element with a 3*3 integration rule sampled at 9 Gauss points. When used for materially non-linear analyses it might present problems associated with what is known as spurious mechanisms which cause the solution to oscillate around a bifurcation point, a phenomenon which was observed during this investigation while attempting to analyse a wallette under diagonal loading. The nonlinear *strain-softening* model based on 'concrete type' material constitutive behaviour, was chosen as the most suitable for representing both bricks and mortar joints, since its behaviour under biaxial states of stress appear to show the characteristics of masonry if it were assumed that the mortar joints are connected to the brick units at perfectly bonded nodes. For the rest of this chapter this is termed a ***two-phase model*** to represent the masonry system.

In order to trace the response of a non-linear model, an incremental iterative loading procedure is required where displacement increments instead of forces are applied to restrained nodes. The degree of material non-linearity dictates the analysis procedure and usually is very sensitive to the iterative method and convergence criteria selected. For this study a modified Newton-Raphson procedure was adopted with incremental displacement applied at the supports by restraining the nodes in the direction of the applied load. Near a limit point (usually occurring after initial cracking), numerical problems arise which cause the solution to diverge. This can be

partly avoided by the use of *Crisfield's arc-length incrementation* procedure [Ref. 114], which repeatedly halves the current increment to minimise the residual stresses that destabilise the solution and hence convergence is speeded up.

The technique described above, has been adopted for all the models investigated in this study, since it was found that bifurcation points were constantly occurring during the post-cracking analysis phase due to the low strength properties prescribed in order to simulate a brittle material like masonry. When the solution failed to converge a data check was performed to identify numerical or material failure. The smeared crack approach is used by the program to represent the crack planes, occurring when a tensile failure criterion is violated and is accompanied by a reduction in the current Young's modulus to simulate the non-linearity of the stress-strain relationship. The equation adopted by LUSAS for the calculation of the reduced Young's modulus includes terms mainly dependent on the strength of the material in tension, a strain-softening parameter and a shear retention parameter which adjust the modulus of rigidity to accommodate shear transfer resulting from aggregate interlock and friction. These parameters are user defined although the program retains some features for the post-cracking behaviour of the material which are based on experimentally measured values relating to reinforced concrete. The remaining parameters for the complete material description include values for the compressive and tensile strength, modulus of elasticity and Poisson's ratio.

In order to simulate the behaviour of masonry using the above material model, a parametric study was conducted following recommendations from the LUSAS Research and Development staff [Ref. 115], regarding the original formulation of the concrete model and the relation of the strain-softening and shear-retention parameters to the material's plastic behaviour. The anticipated cracking patterns were produced by effectively reducing the brick and mortar tensile strength and finely adjusting the strain softening parameter, by considering that the individual masonry components are brittle under biaxial stress in comparison to concrete, with a short and steep descending branch in the stress-strain curve. This parameter is related to the stress release following cracking of the material and essentially relates the initial cracking strain to the ultimate

tensile strain. As a default LUSAS will accept values between 1 and 100 which demonstrates the uncertainty surrounding its implementation. However for brittle failure, lower values are usually prescribed and in this case these were selected between 5 and 15. The shear retention parameter is used to reduce the value of the post-cracking shear modulus to simulate shear transfer resulting from aggregate interlock, dowel action from the reinforcement and friction. Values less than 0.5 are recommended for shear dominated failures and in the case of the masonry wallettes described later, a range of values between 0.1 and 0.5 were investigated. Recent studies of masonry systems using the finite element method, have successfully implemented the strain softening factor as a means to model and simulate the stress-strain relationship of masonry under biaxial stress [Ref. 94, 95]. Numerical difficulties can arise for very low values of the above described parameters due to the sudden energy release resulting from brittle failures. Since cracking depends on the tensile strength of the modelled material, it is expected that this would be the most important parameter in the modelling process.

Relatively fine meshes were used for modelling the brick and mortar elements and in particular in the wallette and panel cases. Symmetrical modelling could not be adopted due to the presence of the head and bed mortar joints as well as the nature of the boundary conditions, particularly in the case of the square wallette under diagonal in-plane compression.

The first two models (5-course prism, square wallette) were prepared and executed in the SUN workstation (average processor time 2 hours for each non-linear incremental analysis), while the masonry wall model required considerable resources due to the large number of elements. As a result the supercomputer at the University of London Computer Centre (ULCC) was utilised, but due to the limited resources awarded for this study only eigenvalue analyses were performed. The system is based on a CONVEX C3840 with five parallel processors utilising 64-bit architecture, 2Gbytes of main memory and over 30Gbytes of disk storage. Typically 45 minutes of processor time was consumed for each eigenvalue analysis while the stiffness matrix when expanded occupied a peak of 150Mbytes of disk storage.

6.4 Analysis of a 5-course stack bond masonry prism.

The first prism to be modelled, was discretised by using 4 QPM8 elements for each brick and the same type and amount for the mortar joints. Discontinuities in the stress distribution due to the applied load were observed (figure 6.1) between the element boundaries, which is associated with the element distribution in the mesh. The second model consisted of 112 elements with each brick unit represented by 16 and each mortar joint by 8. (figure 6.2). A sample data file prepared for this model is given in Appendix B, section B1. Vertical compressive load was applied at the upper nodes using incremental displacement which as explained before, requires the nodes to be restrained (figure 6.2). The resulting cracking pattern is shown in figure 6.3. Typical vertical splitting cracks can be seen as these originate near the side edges of the prism. Effectively this was considered as a failure state, but the propagation of cracks for higher loads is shown as well in the same figure. The stress distribution parallel and perpendicular to the line of application of the compressive force is shown in figure 6.4, corresponding to the appearance of the first cracks.

Although the experimentally tested masonry prisms crack at the narrow face initially, this could not be simulated here since the non-linear concrete model is only applicable to 2-dimensional elements. The mechanical properties of the units and mortar for prism MP-I (section 4.4.4) were selected as input data for a finite element modelled prism, to compare the results with respect to the cracking compressive strength. The computer model cracked at an applied compressive stress of 5.5 MPa whereas the corresponding value for prism MP-I was measured at 4.85 MPa.

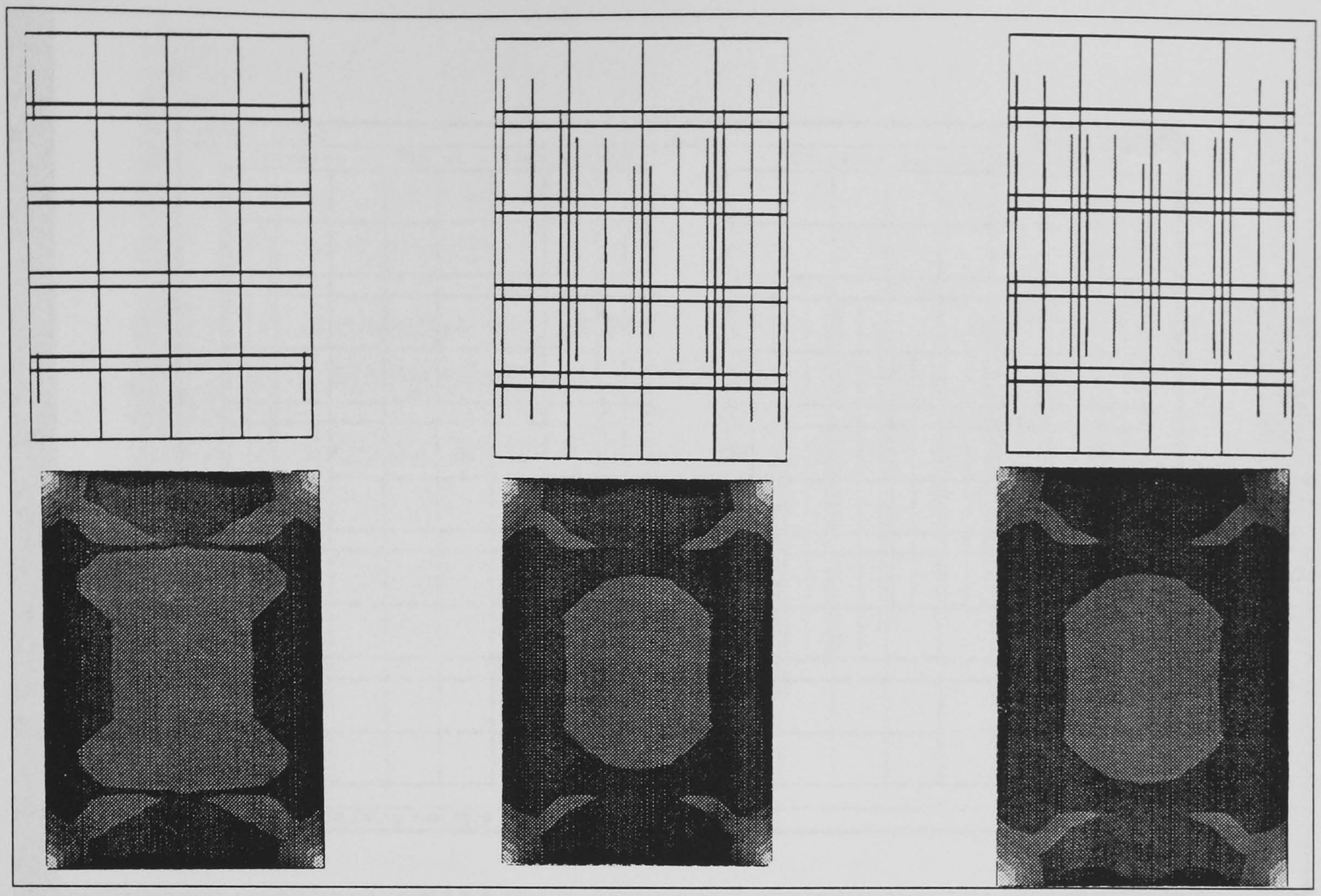

Figure 6.1 F.E. mesh, cracking and *Sy* stress distribution for masonry prism

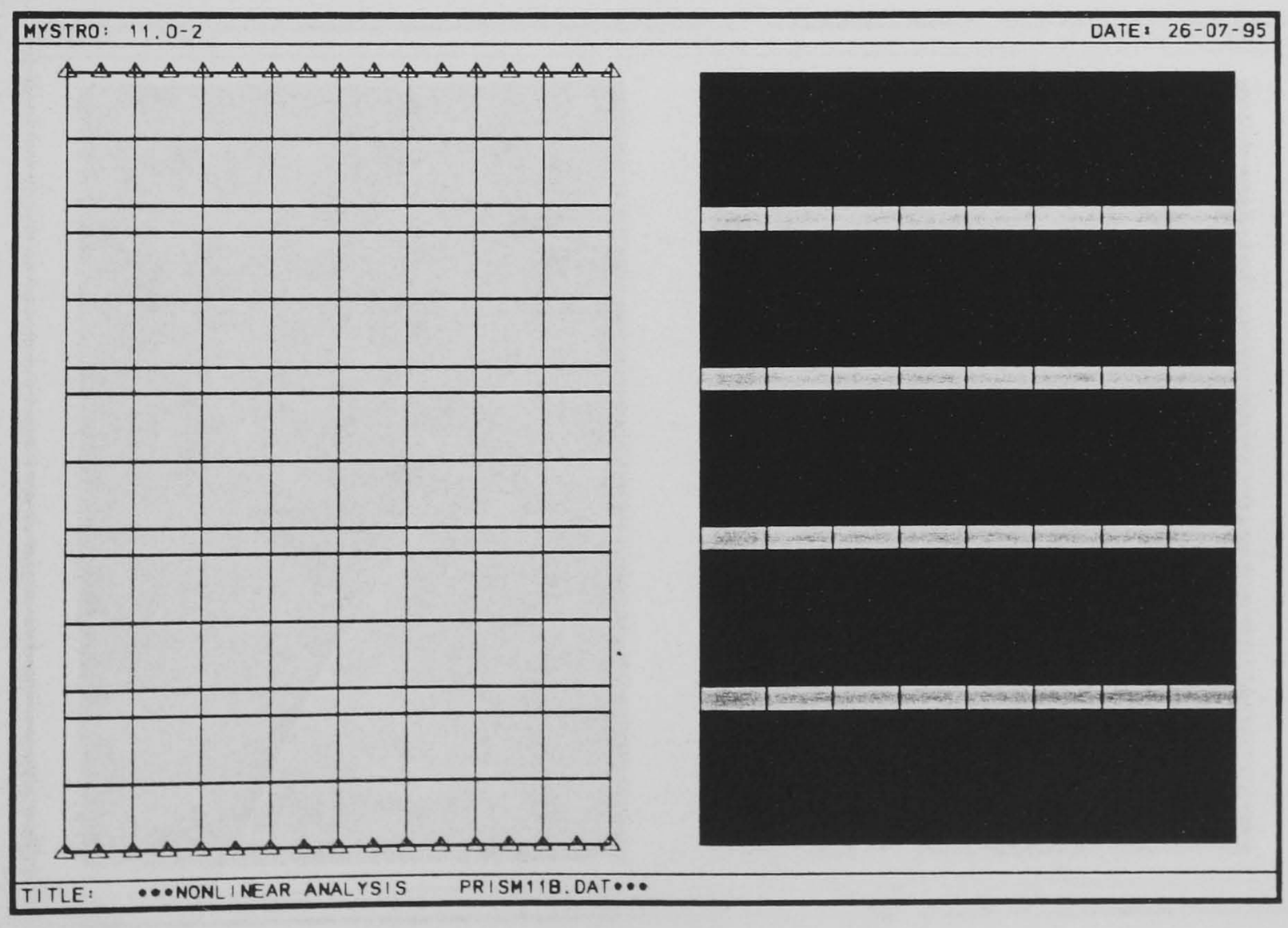

Figure 6.2 F.E. mesh of second masonry prism model (112 elements)

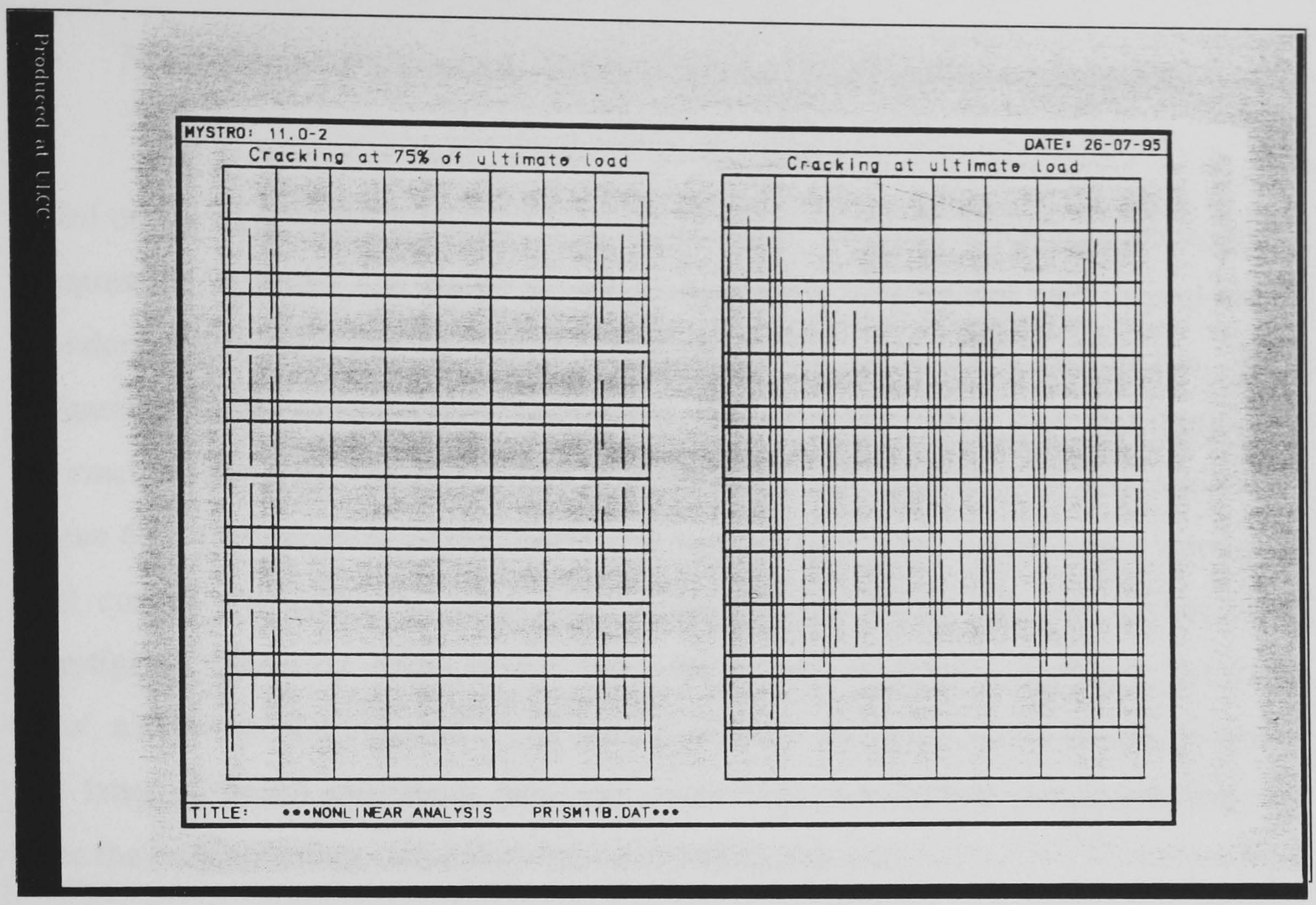

Figure 6.3 Compressive cracking pattern for masonry prism

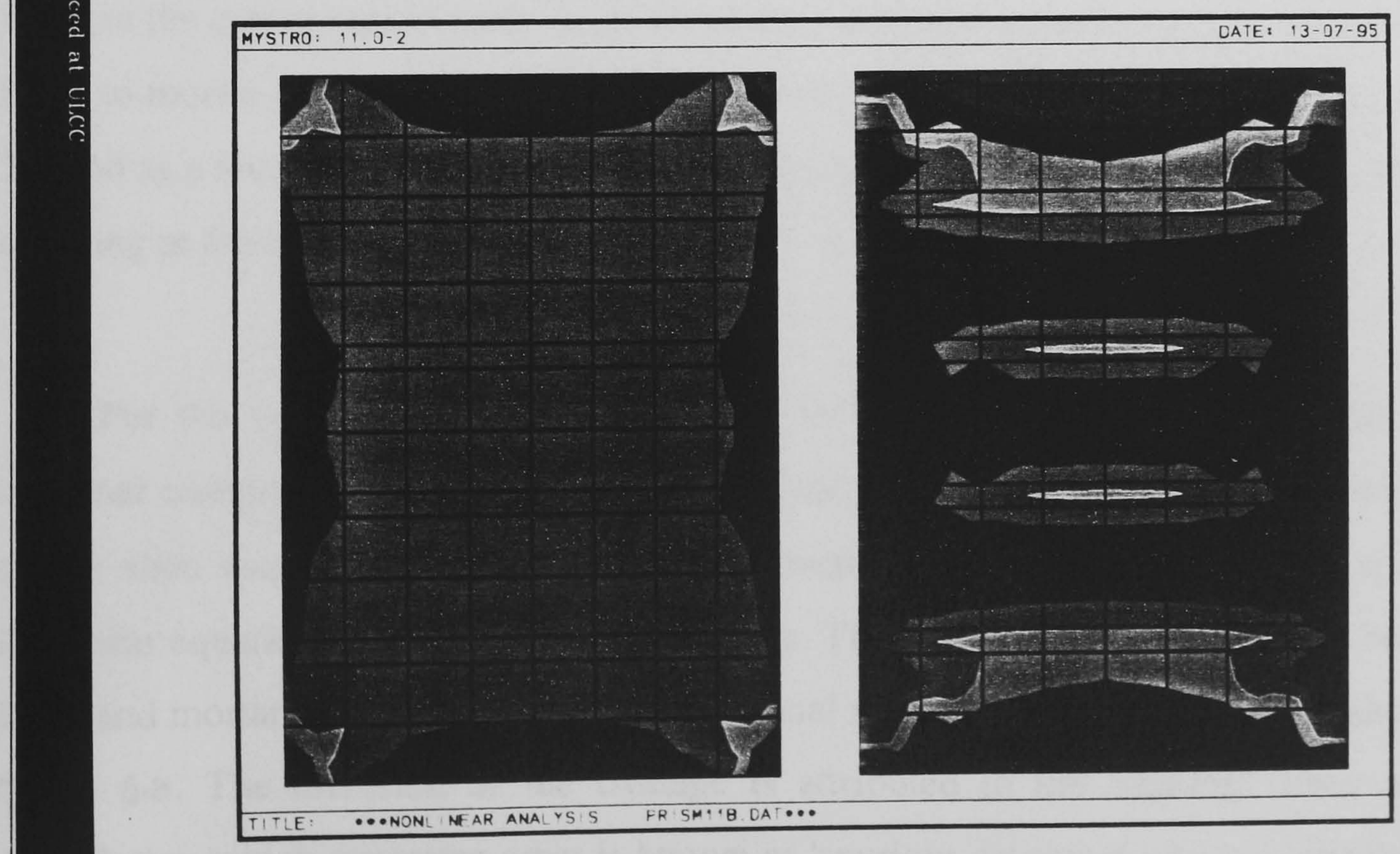

Figure 6.4 Vertical and lateral stress distribution for masonry prism

6.5 Modelling of a square wallette under diagonal compression.

Based on the experimental testing of square masonry wallettes under in-plane diagonal compression, a model was prepared and parametrically investigated with respect to the boundary conditions and the tensile strength of the brick units and mortar. Two different wallettes were analysed to assess the effect of the mortar joint distribution on the cracking patterns. The first model was one and a half units wide by four units high (figure 6.5) The diagonal compressive load was applied at the upper corner through a steel corner. To avoid excessive local stress concentrations, two approaches were investigated. The first involved stiffening the corner elements adjacent to the steel 'shoe', and the second imposed *constraint* equations at the nodes of the corner elements. The latter approach essentially links the nodes with user-defined linear equations, to force the corresponding elements to move as an integral unit.

Figure 6.5 show the cracking pattern where the load was applied at the corner through the steel shoe with no additional considerations. Figure 6.6 show the difference in the cracking pattern on an identical wallette (same properties and material parameters), with the four corner brick elements *constrained*. The cracking concentrates more in the centre region away from the corners which is a more realistic situation. The brick to mortar strength (f_{bc} / f_{mc})and stiffness ratio (E_b / E_m) defined in the data file was 3.3 and as a result cracking along the mortar joints predominates with only limited brick cracking at the centre.

For the next model a 3 unit wide by 10 unit wallette was investigated under diagonal compression (figure 6.7). Based on the findings from the previous study, no corner shoe was modelled and instead the constraint procedure was used by applying the linear equations to the two corner elements. The strength and stiffness ratio between brick and mortar was 2.5 and as a result diagonal splitting cracking resulted as shown in figure 6.8. The diffusion of the damage is attributed to the 'smeared crack model' formulation which generates what is known as 'spurious cracking' which generally does not affect or pollute the solution [Ref. 116] . Since this model is currently undergoing further development its limitations should be taken into account.

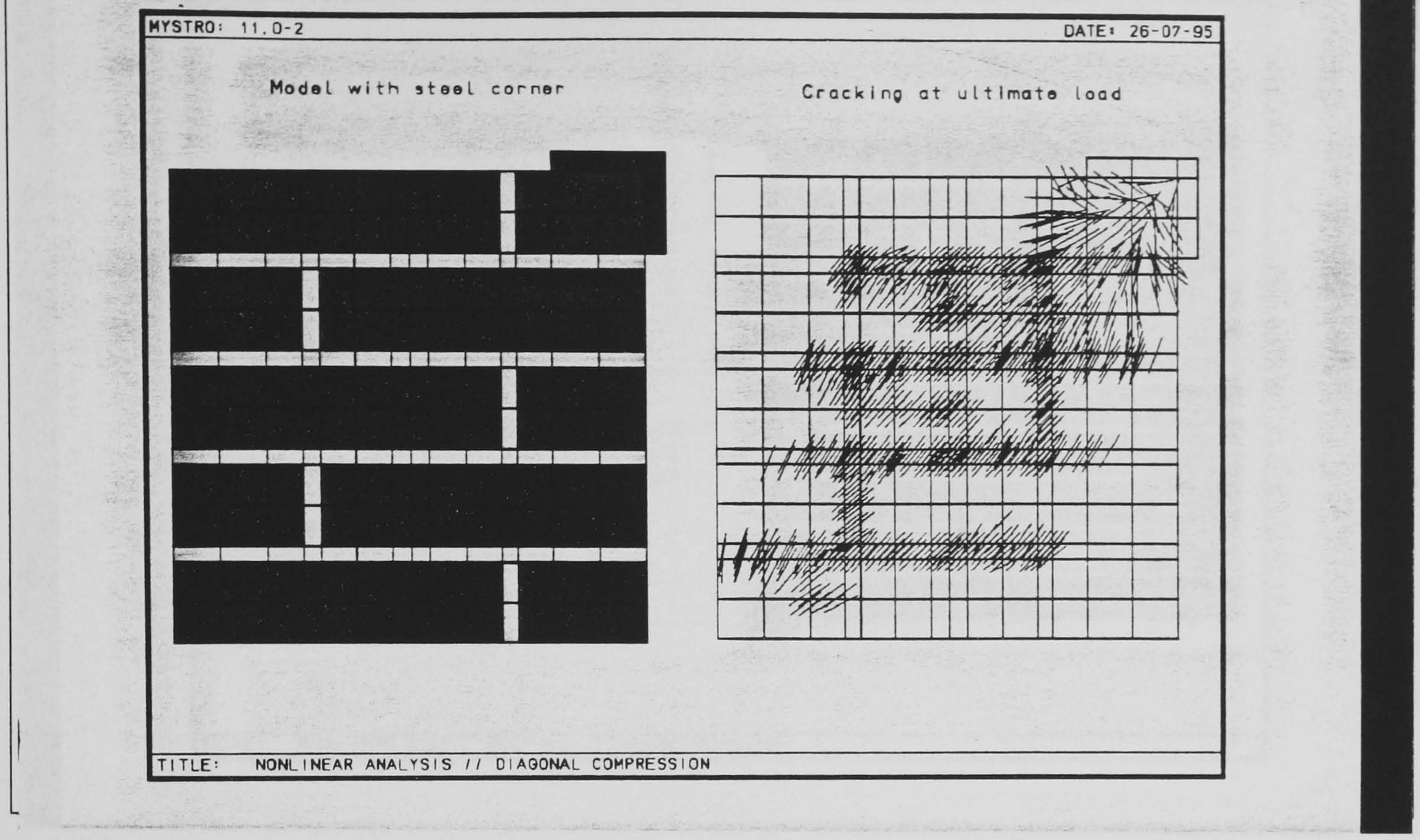

Figure 6.5 F.E. mesh of masonry wallette (with steel corner) and cracking pattern

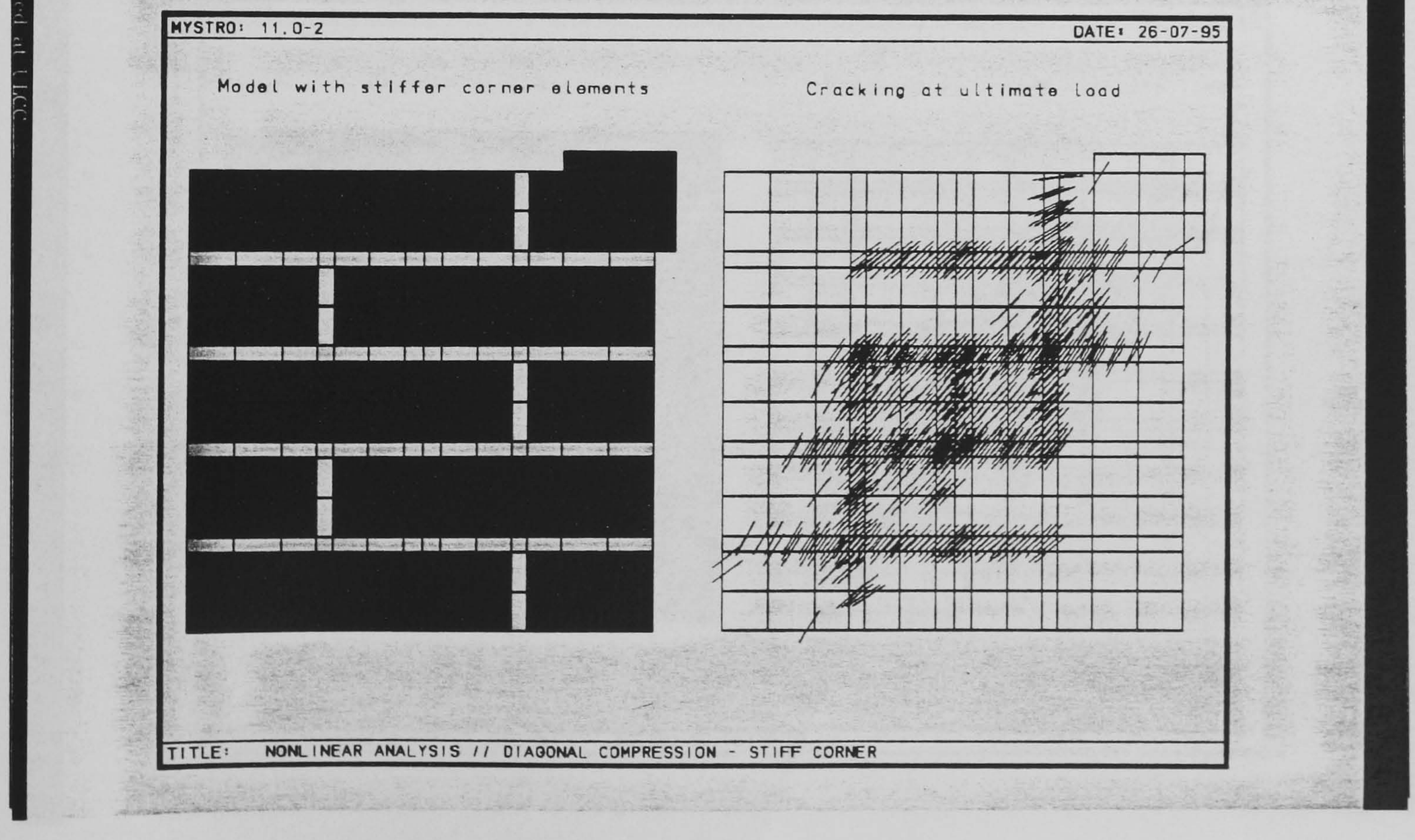

Figure 6.6 Masonry wallette (stiffer corner elements) and cracking pattern

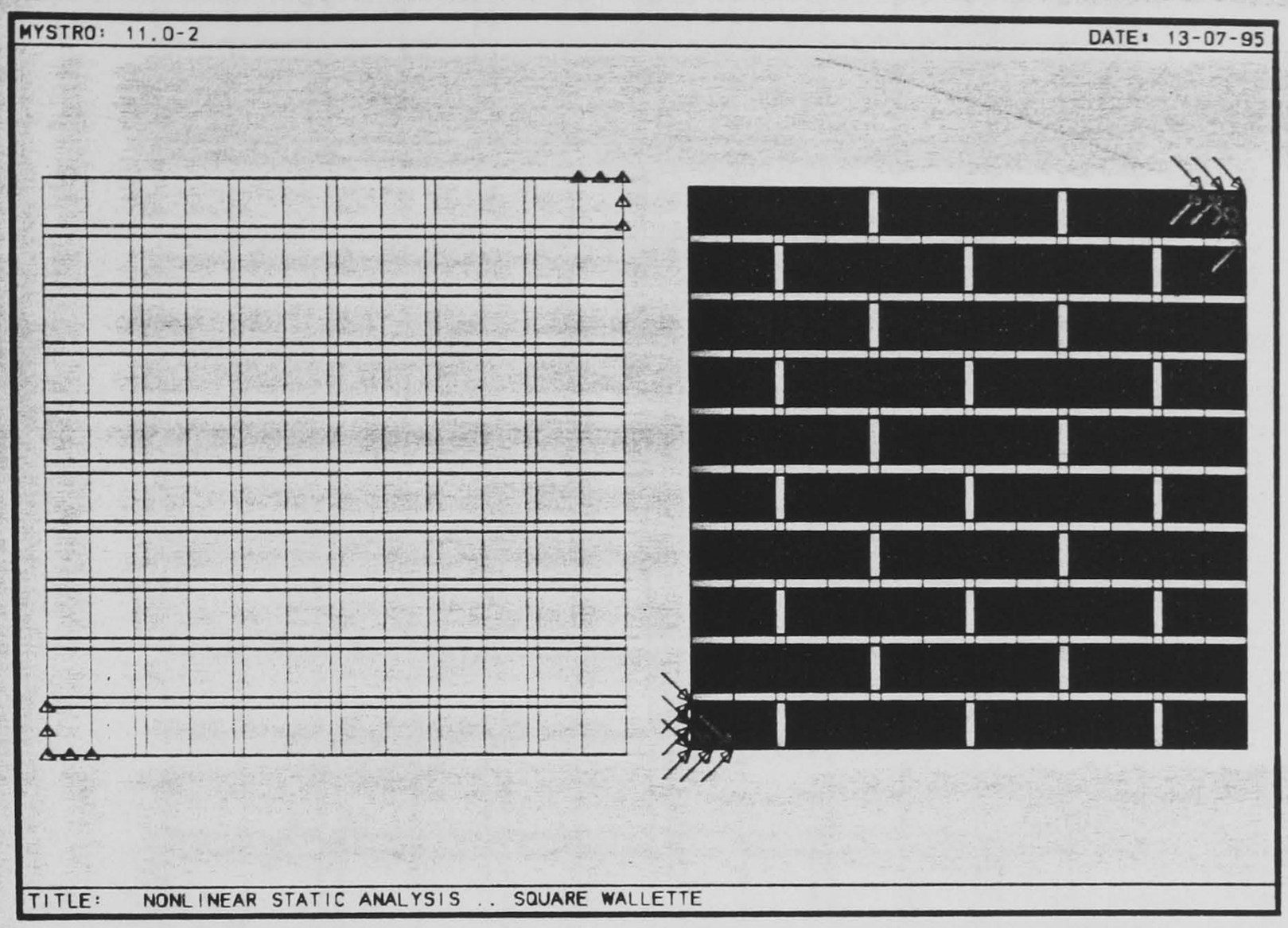

Figure 6.7 Masonry wallette F.E. mesh and boundary conditions (larger model)

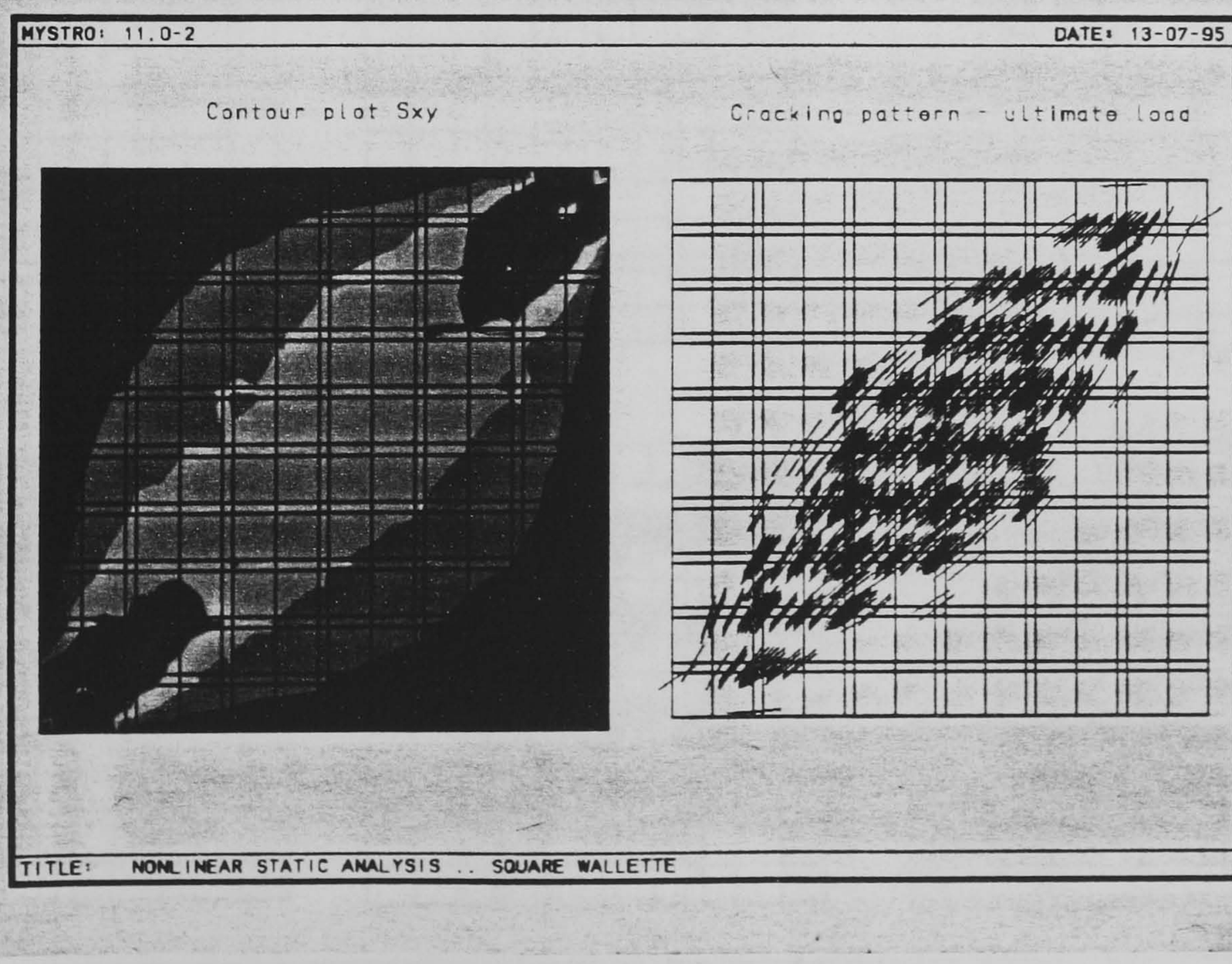

Figure 6.8 Stress distribution and cracking under in-plane diagonal compression

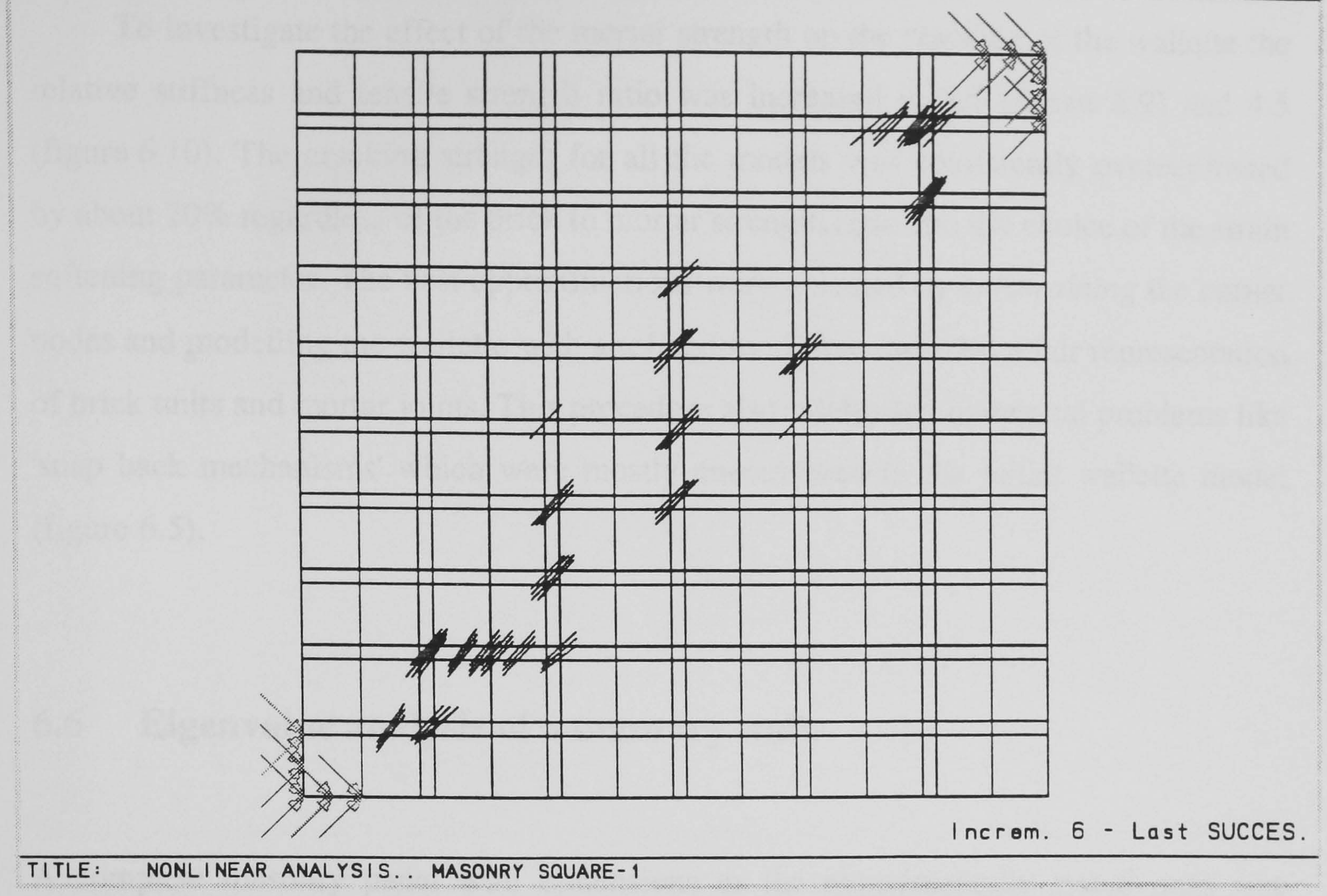

Figure 6.9 Cracking pattern (brick f_t / mortar f_t = 3.5)

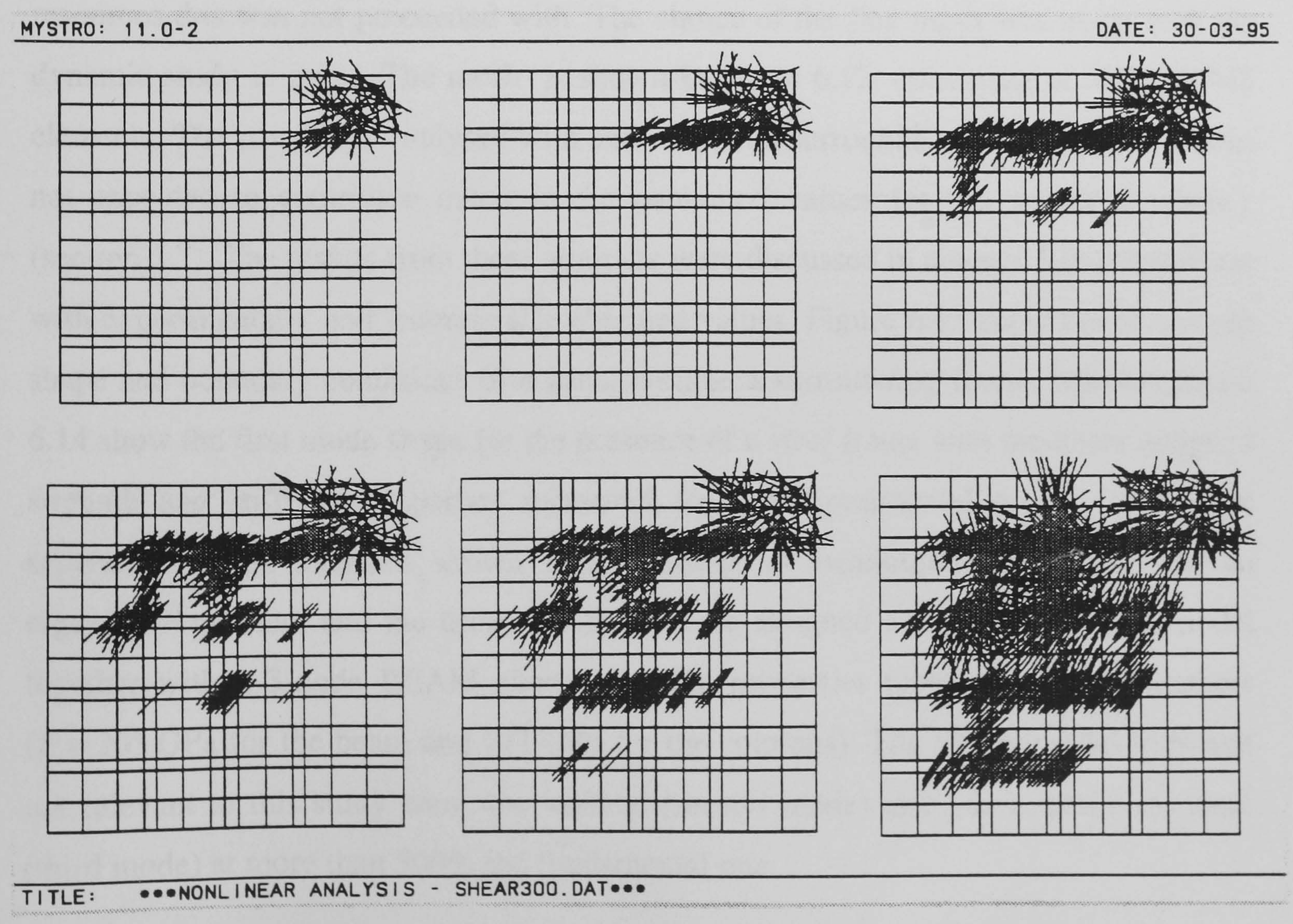

Figure 6.10 Cracking pattern (brick f_t / mortar f_t = 4.5)

To investigate the effect of the mortar strength on the cracking of the wallette the relative stiffness and tensile strength ratio was increased to 3.5 (figure 6.9) and 4.5 (figure 6.10). The cracking strength for all the models was consistently overestimated by about 20% regardless of the brick to mortar strength ratio and the choice of the strain softening parameter. The best approximations were obtained by *constraining* the corner nodes and modelling the wallette with a refined mesh that included a fair representation of brick units and mortar joints. This procedure also minimised numerical problems like 'snap back mechanisms' which were mostly encountered in the initial wallette model (figure 6.5).

6.6 Eigenvalue analysis of a masonry wall.

A complete masonry panel with dimensions as the experimentally tested ones was analysed to obtain the natural frequency and mode shapes (figure 6.11). Initially the model was prepared for a time-history dynamic analysis study but due to limited resources this was not proceeded with. The choice of the fine mesh was made with the dynamic study in mind. The mesh is shown in figure 6.12, consisting of 3025 QPM8 elements. The panel was analysed with and without a surrounding steel frame, as it was not expected to contribute much to the computed values for the natural frequency (section 5.7). The results from these analyses were discussed in chapter 5 in comparison with experimentally and theoretically obtained values. Figure 6.13 show the first mode shape and boundary conditions of a panel without a surrounding frame, whereas figure 6.14 show the first mode shape for the presence of a steel frame with members assigned strength and stiffness properties measured for the experimental set-up frame. The separation at the interface shown in figure 6.14 is meaningless since this was an eigenvalue problem and the frame members were assigned a different material model together with a 3-node BEAM element having properties typical for steel members (E_s= 205 GPa for the beam and 241 GPa for the columns). The higher modes although not relevant to this study were one vertical (second mode) and one in-plane torsional (third mode) at more than 300% the fundamental one.

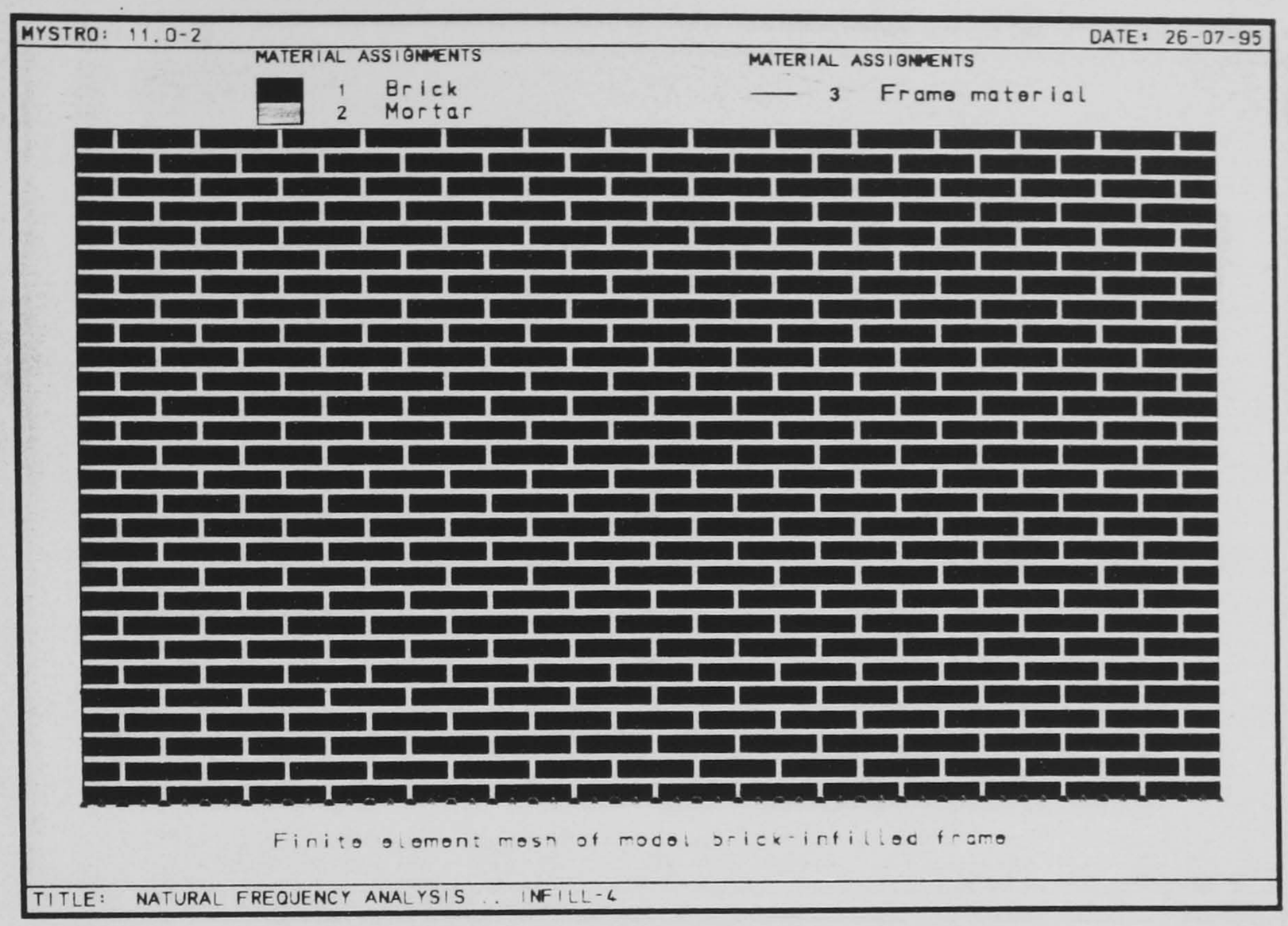

Figure 6.11 Masonry panel finite element model and material assignment

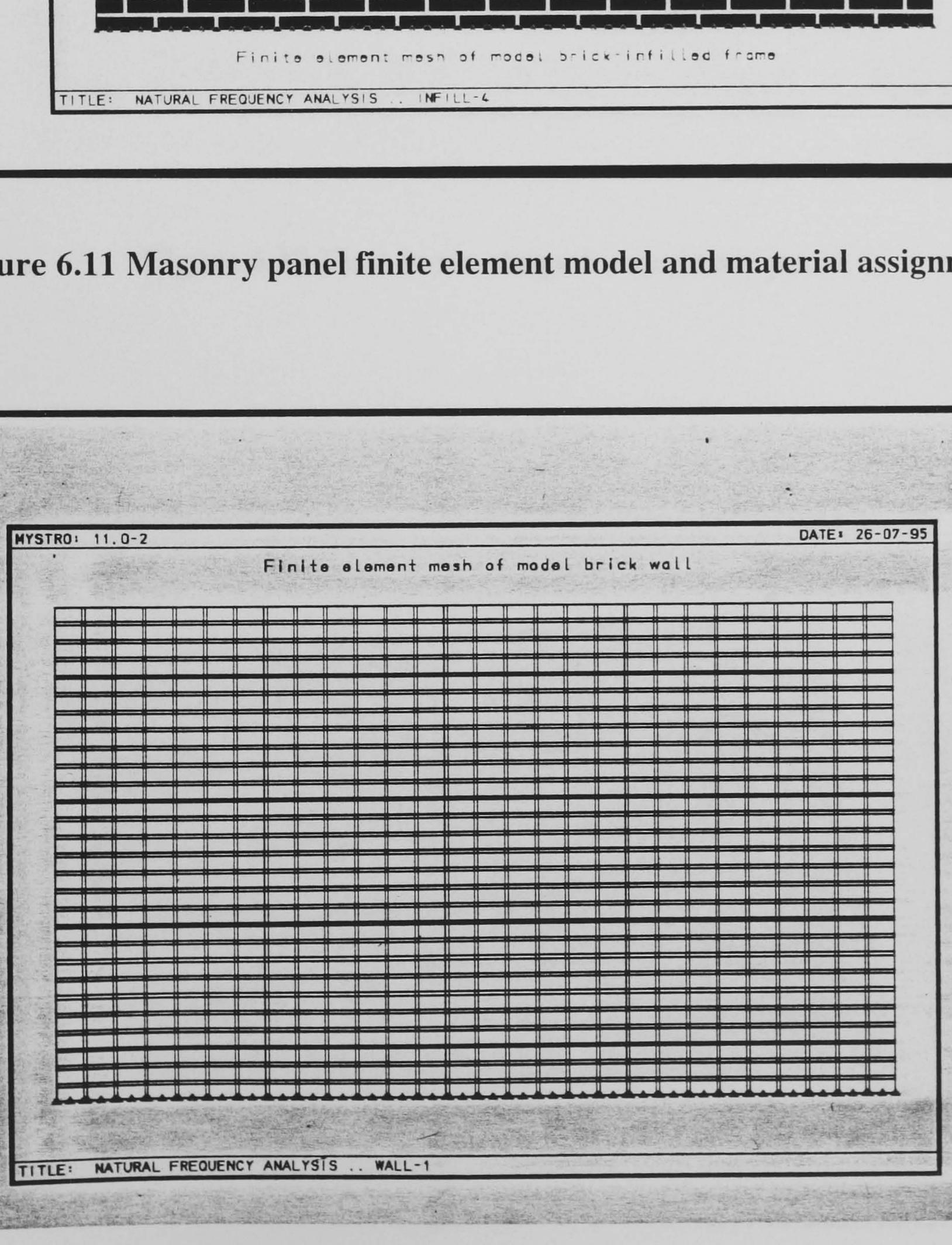

Figure 6.12 Finite element mesh for masonry panel

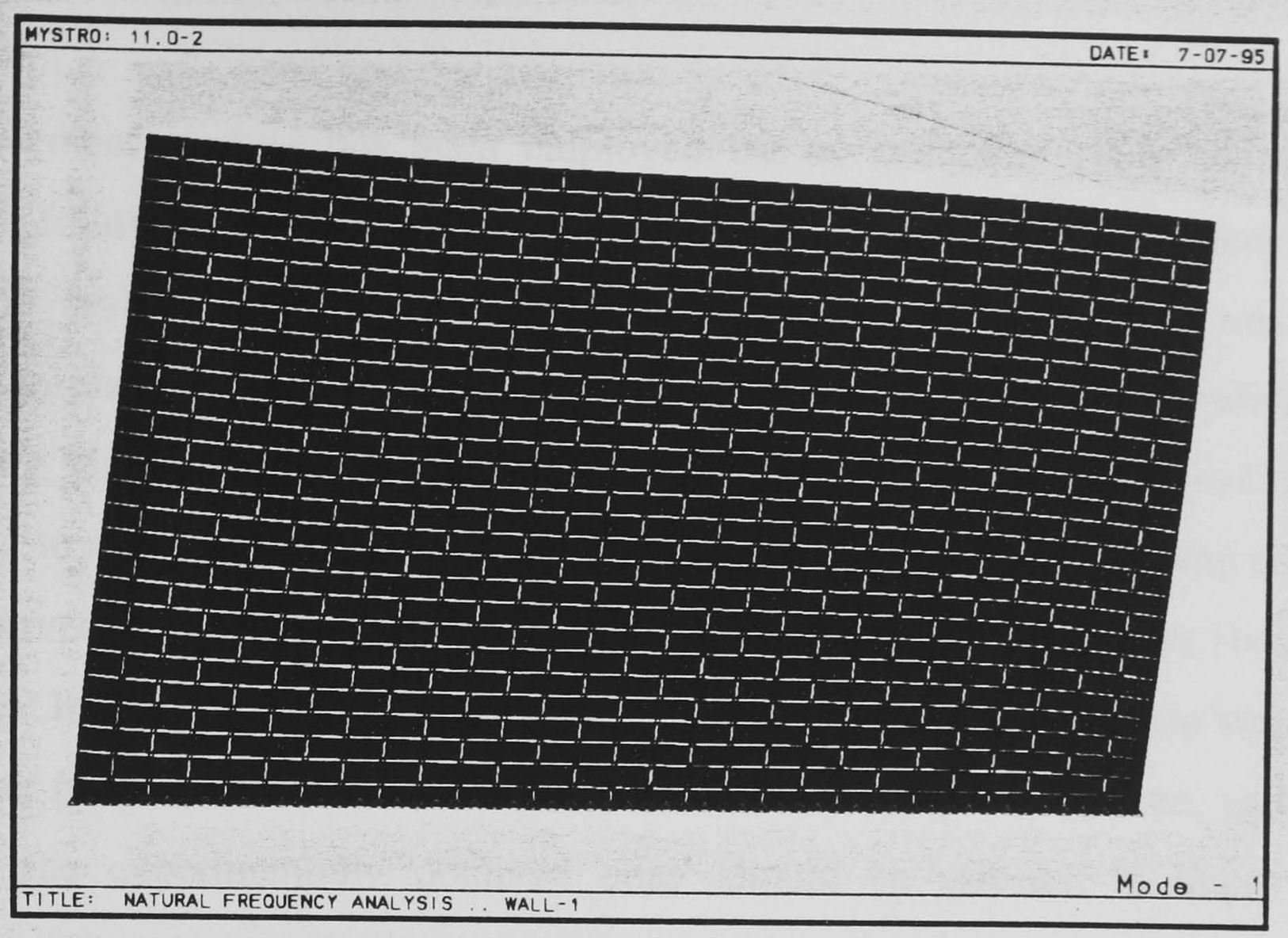

Figure 6.13 First mode shape for masonry panel

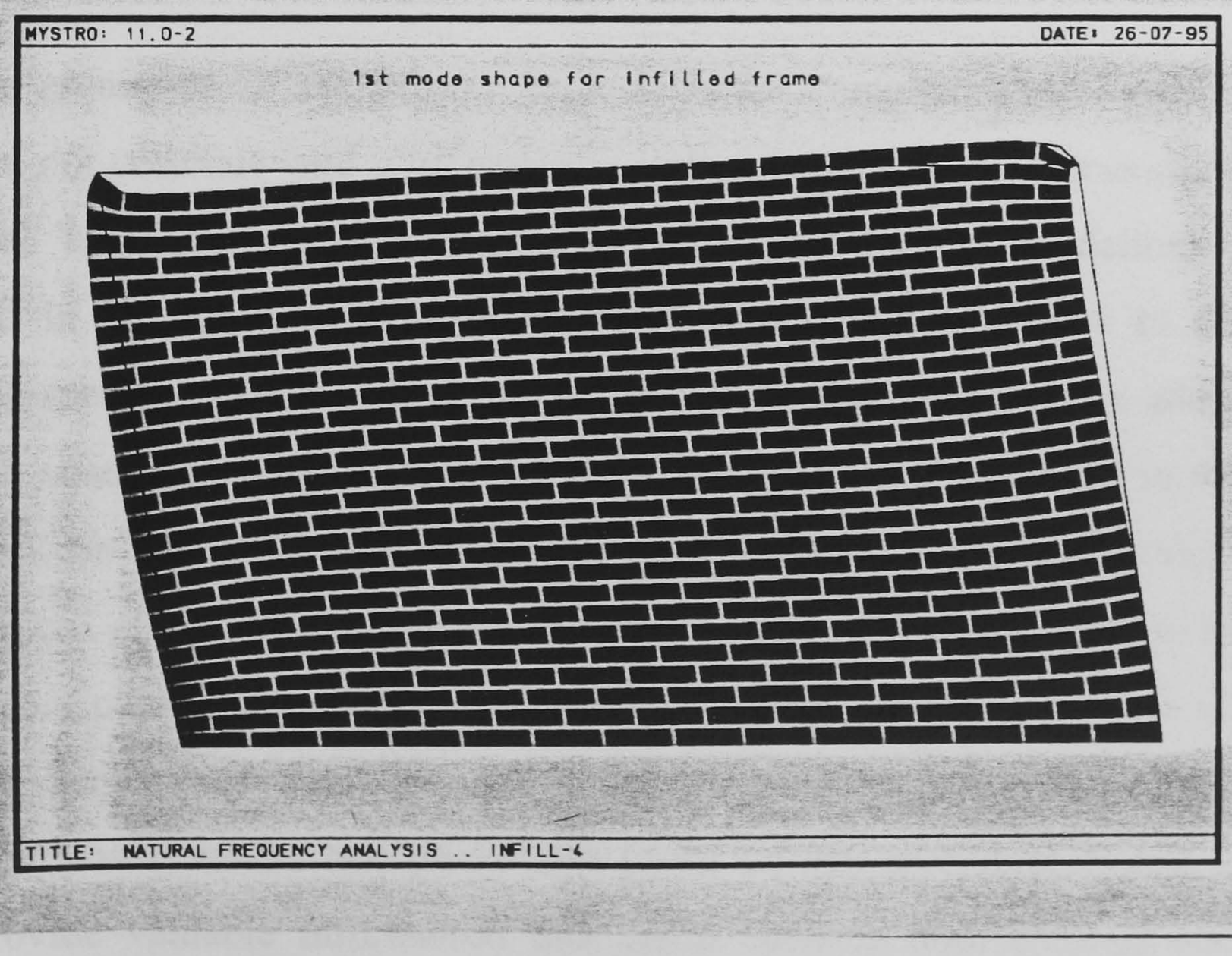

Figure 6.14 First mode shape for masonry infill panel

6.7 Conclusions.

The finite element method has been employed for an analytical study of masonry assemblages, following an extensive experimental investigation. A stack bond prism and a square wallette have been modelled under static loading conditions using non-linear two-phase models. Bricks and mortar joints have been treated individually by prescribing separate values for their mechanical properties whereas a perfect bond was assumed to exist at the interface. The models successfully simulated the cracking patterns observed experimentally but overestimated the ultimate strength by about 20% in most cases. In particular the wallette model proved that the mortar tensile strength is the governing parameter in the biaxial behaviour of the composite system, and lower values than the experimentally obtained ones' should be selected to improve the solution. The concrete constitutive material model incorporated into LUSAS can be used for modelling masonry by fine-tuning the parameters that describe its behaviour. Inclusion of the *shear-retention* and *strain-softening* factors in the material formulation can be advantageously used in masonry modelling. For analytical studies that incorporate interface elements with friction prescribed properties, these factors can refine and improve the solution and this should be investigated further.

The prediction of the natural frequencies for complete panels analysed in this study, did not correlate well with experimentally obtained values. Considering that the theoretical calculations exhibited similar discrepancies, the modelling should as suggested in chapter 5 be performed incorporating reduced values in the material properties specifications to allow for flaws and shrinkage cracking in addition to the low value observed for the shear modulus which was not be included in the analysis. The model can be implemented for dynamic time history analysis provided sufficient computational resources are available. Enough proof exists in literature to recommend that the two-phase modelling procedure investigated in this study be adopted for analytical calculations based on finite element methods. Although best suited for research purposes, results and predictions based on this procedure should in the near future provide valuable information that could enhance both analysis and physical testing.

Chapter 7

Concluding remarks and recommendations for further research

7.1 Summary of remarks and conclusions.

The literature review revealed a great variability with regards to the testing methods, choice of boundary conditions, modelling parameters and panel dimensions. There were numerous cases where simplifications were imposed due to the difficulties associated with small scale physical modelling and often important parameters such as the aspect ratio, mortar joint thickness and simulation of the working stresses were sacrificed or not accounted for to allow other parameters to be investigated in greater detail. Some of these limitations were addressed in this thesis during both the static and dynamic testing stages. A summary of the conclusions drawn from the complete course of this study is given below followed by recommendations for further research in the light of findings from the present investigation.

1. The first stage of this work was successful in producing a 1:4 scale moulded brick unit using easily available materials. The mechanical properties were obtained using scaled down prototype testing procedures to maintain consistency between basic tests and panel tests and to minimise scale effects. The advantage of moulding the units and mortar was evident with respect to the control specimens that were prepared to obtain the strength and stiffness properties with techniques adopted from concrete technology. This eliminated the need to test the units themselves which at this scale would be difficult if not impossible.

2. Stress-strain relationships were obtained tracing the complete response including the descending strain softening region. The non-linear behaviour was confirmed for bricks, mortar and masonry and with displacement control a descending branch for masonry under compressive load was measured, with maximum strain recorded at about 2 to 4 times the value at ultimate load.

3. Results from the measurement of the modulus of rigidity (shear modulus) using both the ASTM and RILEM test set-up, show that the currently assumed value that is related to the modulus of elasticity is overestimated by about 40%. This fact has also been reported by other researchers and relates to the anisotropy of the material that occurs under biaxial stress. This in turn will tend to overestimate the in-plane stiffness of a masonry section for static and dynamic property identification.

4. The importance of the interface bond strength between the brick units and mortar has long been recognised particularly for masonry systems subjected to lateral loads. A simple test set-up was used and confirmed for the model system as with the prototype, that the water absorption characteristic of the units is the most influential parameter and its inclusion in any prediction for the shear strength of a masonry system should be considered in detail.

5. For masonry consisting of two materials that are significantly different with respect to their constituent strength properties, the tensile strength of the mortar will predominate and dictate the behaviour, cracking pattern and mode of failure.

6. A simple shaking table facility that can introduce sinusoidally-varying excitations was constructed and proved adequate for subjecting the author's model structures to the time deformation cycles experienced by an infill panel during an earthquake. Since earthquakes are probabilistic events it is believed that exact simulation of an actual ground loading history is irrelevant. The frequency content, time duration and load reversal of the applied ground motion will produce results which will help in the understanding of the behaviour of any structural assemblage provided

careful planning and an appreciation of the limitations is exercised and acknowledged.

7. Six low aspect (ratio 1.7 - L/H), masonry panels were tested on a shaking table. The panels were set within a steel frame and additional loading was introduced to provide a constant axial force representing approximately 15% of the panel's ultimate compressive strength. The set-up was designed in such a way as to inhibit flexural failure modes but the level of the axial forces was chosen so as to allow horizontal cracking to occur if required but not to completely dominate the behaviour and collapse.

8. The experimental determination of the natural frequency shows differences of about 48% and 75% with theoretically and analytically obtained values respectively. This was attributed to the overestimation of the panel uncracked lateral stiffness. Although the experimentally obtained values for the strength and stiffness properties were used in the shear-beam model equation, the error was too high indicating the limitations of this procedure. The finite element prediction relies on the individual material properties for bricks and mortar and not the properties for the complete masonry system. Shrinkage micro-cracking, flaws in the brick units, workmanship relating to the mortar placing and the anisotropy of masonry are difficult to assess and quantify in order to accurately predict the dynamic properties. This fact must occur probably to an even greater extent, in full scale masonry panels and a reduction factor should be applied to the real analysis which involves predictions for the fundamental natural frequency of masonry systems. Model tests of the type carried out by the author, can provide an adequate estimate of these reduction factors that should be applied to prototype prediction.

9. One panel exhibited typical corner crushing failure mode and subsequent loss of the compression strut action. This behaviour was attributed to the high compressive and shear strength of the whole masonry assembly in this test. A similarly strong panel but with a lower interface bond strength cracked in the central area, in a typical cross-diagonal mode after subjecting it to the same intensity of the applied

ground motion. The test terminated while the panel was still in a 'service state' condition.

10. Three other panels collapsed after the cross (X) diagonal cracks spread to cover the full area of the panel. The pattern consisted of one main diagonal which was augmented by secondary diagonal cracks as it became unable to carry the main stress pattern as larger magnitudes of lateral load were applied. For load reversals, crack opening and closing was observed for several subsequent cycles. Once diagonal cracking had occurred, sliding of the sections along the crack interface was observed, resulting in lateral drift of about 4 times the drift at first cracking. The important property of ductility was observed in selected tests and was clearly demonstrated by the form of the developing hysteresis loops as damaged progressed. The final phases showed the loops migrating to larger horizontal displacements with each cycle. In the final sixth test, this progress towards collapse was controlled by lateral restraint from the external confining system holding the wall in-plane throughout.

11. The effect of the low axial force was to increase friction both in the elastic and post-cracking phases and to a lesser extent the shear strength, while still able to provide confinement with respect to out-of-plane collapse. It did however result in explosive failure modes once the damage was sufficient to impair local stability. This aspect was also part of the investigation carried out in the sixth panel which was externally reinforced. This lateral confinement spread the otherwise unstable local damage and eventually resulted in predominantly vertical splitting which separated the panel into vertical (i.e. columnar) segments. This triaxial state of stress imposed on the panel by the horizontal constraint and the axial force maintained a form of in-plane integrity which could have major contribution to high damage prototype conditions.

12. Analytical investigations of masonry systems have only recently begun to emerge in the technical literature and the uncertainties relating to the calibration of constitutive relations based on experimental data are recognised. Similarity of

cracking under static loads have been demonstrated during this course of study, by using a commercially available program based on a non-linear concrete model with modified mechanical properties. The ultimate strength predictions however, were not in close enough agreement to warrant departure from further experimental testing though with sensible modification to the input parameters that control the material behaviour, this numerical the two-phase modelling procedure looks very promising.

7.2 Recommendations for further research.

1. The experimentally obtained shear strength of masonry using square wallettes and following the procedures described earlier, should be experimentally investigated in greater detail. Overestimation of the shear strength and modulus of rigidity resulting partly from the uncertain boundary conditions prescribed for this test set-up, are a major cause of concern since the calculation of a number of static and dynamic fundamental material properties is based on this experimental estimation of the shear modulus.

2. Parametric studies possibly using the shear box set-up, should be conducted to establish a relationship between the interface bond strength to the masonry shear strength with respect to the constituent material properties (and in particular water absorption characteristics) and to the level of axial compressive forces.

3. Shrinkage micro-cracking appears to be an important characteristic of models and certainly full scale masonry panels. It needs to be reduced or even eliminated for panels cured under humidity control in a properly designed and operated fog room. Besides providing a better understanding of its contribution to the overall behaviour, this would also allow a comparison to be made with natural frequency measurements and subsequently the observed discrepancies mentioned before could be identified to a greater degree. Considering that an overestimation of the natural frequency of a masonry panel or structure in this respect, could amount to

highly erroneous predictions regarding the response to real seismic forces, its importance cannot be overemphasised.

4. Lateral restraint has been shown to be effective in increasing ductility and hysteretic behaviour. Horizontal reinforcement has also been shown to improve these properties. Model tests incorporating reinforcement anchored in the mortar should be investigated for comparison. A model perforated unit has also been produced in this study and with the moulds being easily adaptable, these can be mass produced and should be used for investigating vertical anchoring of the reinforcement to the brick units through the holes rather than the mortar joints.

5. The wall bed and loading frame are able to accept double-leaf masonry panels. These should be investigated to observe the response, interaction and behaviour of complex bond patterns.

6. The vertical confinement supplied by the prestressing set-up can be used to study out-of-plane behaviour and stability using the same panels as investigated in this thesis. A lockable horizontal roller-hinging mechanism can be incorporated to the base of the panel at the underside of the steel beam that would allow a 90^0 rotation of the panel from an in-plane to an out-of-plane position with respect to the direction of the applied ground motion. This would allow an in-plane test to be followed by an out-of plane testing phase or vice-versa without the need for adapting the table-platform driving mechanism. The out-of-plane stability should be studied for confined panels following cracking and damage incurred during in-plane excitations.

7. External reinforcing techniques using wire meshes have repeatedly proven that cracked masonry can be safely contained, exhibiting excellent ductility and hysteretic behaviour. Although the perspex used in this study for one side of the panel was adopted more for reasons of visual clarity to observe cracking formation, the influence of the rectangular shape and arrangement of the sections should be

further examined regardless of the material used. The anchoring of such reinforcement is usually done by pinning it through the bricks or mortar at the joints but there is evidence to suggest that when the two sides are connected tightly together as in this case with threaded rod, this can further enhance the lateral confinement.

8. The analytical simulations performed pave the way for further and more complex analyses to be conducted, based on the parametric studies and model calibration which resulted in a set of values for the basic material properties that can aid in the modelling of masonry systems using the non-linear constitutive concrete model. Non-linear dynamic analyses are also possible and to the knowledge of the author only two similar studies have ever being reported, using the previously described two-phase idealisation procedure. However such work would be more applicable to a project dedicated entirely to computational work.

7.3 Concluding comments regarding the design process.

Although infill panels are extensively used in many countries around the world, no clear guidelines exist to assist practising structural engineers. Furthermore there is a growing number of experimental evidence to indicate that properly designed infill panels can positively influence the seismic resistant capacity of steel and reinforced concrete framed structures. One of the most important findings presented in this thesis, cast doubt over current code procedures for the determination of the dynamic properties of masonry walls, as experimental data proved that the fundamental natural frequency computed using such theoretical or even analytical equations is greatly overestimated. This can have serious design implications, considering the number of masonry panels that are incorporated as internal and external partitions in an ordinary medium rise building. The energy dissipation capacity of masonry infills subjected to dynamic ground excitations, was clearly demonstrated and attributed to cracking and hysteretic damping. Further research is urgently needed to produce simple guidelines that would allow infill panels to be designed considering their inelastic and ultimate strength

behaviour. Such guidelines need not only be applied for newly built structures but also for retrofitting existing ones and even for strengthening historical buildings. It should be more appropriate perhaps to consider some form of internal or external reinforcement in cases where cost-effective design is not a primary target. A novel form of external reinforcement was investigated as part of the experimental work carried out during this research work and involved tying a wire mesh on a masonry infill panel effectively introducing a form of lateral confinement. As a result, the energy dissipation capacity together with the cracking and ultimate strength were substantially increased, to a level that should undoubtedly warrant further experimental research.

7.4 Closure.

Similarity between masonry models and full-scale structures or structural assemblages can be relied upon when it successfully reproduces the cracking patterns and failure modes of full scale systems under similar loading conditions. This has been successfully demonstrated and is documented in the numerous photographs presented in this thesis which provide and supplement the quantitative evidence from the experimental investigation. The visual recording of the crack formation and propagation should also help in the understanding of the complex behaviour of unreinforced masonry panels subjected to horizontal cyclic loading. Once the contribution of the infill panels to the energy dissipation capacity of the surrounding frame can be assessed, procedures can be formulated to incorporate these into an original or retrofitting design process by allowing the frame members and in particular the side columns to horizontally deform elastically and transfer the lateral loads to the panel in the form of shear stresses through the compression strut mechanism. Similarities of this approach to the *capacity design* concept are apparent since both are aimed at protecting the load-bearing elements from failure and collapse by allowing secondary elements to absorb the seismic induced energy through inelastic deformations. To this respect a masonry panel can be interpreted as an intentionally introduced *'energy dissipating structural element'*, whose behaviour, cracking and ultimate failure, is anticipated and accounted for during the design and detailing process.

References

1. Sabnis G. M., Harris H. G., White R. N., Mirza M. S., "Structural modeling and experimental techniques", published by Prentice-Hall, Inc., Englewood Cliffs, 1983.

2. Moncarz P. D., Krawinkler H., "Theory and application of experimental model analysis in earthquake engineering", Report No. 50, The John A. Blume Earthquake Engineering Centre, Stanford University, 1981.

3. Ady N., Carpenter J.E., "Models for concrete structures-Bibliography", *Models for Concrete Structures, A.C.I. Publication SP-24,* Detroit Michigan 1970.

4. Sabnis G. M., White R. N., "A gypsum mortar for small scale models", *A.C.I. Structural Journal*, p. 767-774, November 1967.

5. Aldridge W., Breen J., "Useful techniques in direct modelling of reinforced concrete structures", *Models for Concrete Structures, A.C.I. Publication SP-24,* Detroit Michigan 1970.

6. Harris H. G., Sabnis G. M., White R. N., "Reinforcement for small scale direct models of concrete structures", *Models for Concrete Structures, A.C.I. Publication SP-24,* Detroit Michigan 1970.

7. Noor F. A., "Recent developments in modelling materials", *Small Scale Modelling of Concrete Structures,* edited by F. A. Noor and L. F. Boswell, Elsevier Science Publishers, London 1992.

8. Swamy R. N., Falih F. M., "Development of a small aggregate concrete for structural similitude of slab column connections", *Design of Concrete Structures : the use of Model Analysis,* edited by J. Clarke, F. Garas, and G. Armer, Elsevier Applied Science Publishers, London, 1985.

9. Noor F. A., "Modelling the stress-strain relationship of structural concrete", *Magazine Of Concrete Research, Vol. 34, No. 118,* 1982.

10. Müller R. K., "Microconcrete for structural model analysis", *Design of Concrete Structures : the use of Model Analysis,* edited by J. Clarke, F. Garas, and G. Armer, Elsevier Applied Science Publishers, London, 1985.

11. Clough R. W., Niwa A., "Earthquake simulator research on arch dam models", *Dynamic Modelling of Concrete Structures, A.C.I. Publication SP-73,* edited by H. G. Harris, Detroit Michigan, 1982.

12. Vogt H., "Considerations and investigations on the basic principle of the model tests in brickwork and masonry structures", Library Communication No. 932, British Research Station, Garston, 1956.

13. Hendry A. W., Murthy C. K., "Comparative tests on 1:3 and 1:6 scale model brickwork piers and walls", *Proceedings of the British Ceramic Society, Vol. 4,* 1965.

14. Murthy C. K., Hendry A. W., "Model experiments in load bearing brickwork", *Building Science, Vol. 1,* Pergamon Press, London, 1966.

15. Sinha B. P., "Model studies related to load bearing brickwork", *PhD Thesis,* University of Edinburgh, 1967.

16. Hendry A. W., Sinha B. P., "Shear tests on full scale single storey brickwork structures subjected to precompression", *Civil Engineering Published Works, Vol. 66,* 1971.

17. Sinha B. P., Hendry A. W., "Compressive strength of axially loaded brick walls stiffened along their vertical edges", *Proceedings of the Fifth International Brick Masonry Conference,* Washington, 1979.

18. Sinha B. P., Maurenbrecher A. H. P., Hendry A. W., "Model and full scale tests on a five storey cross wall structure under lateral loading", *Proceedings of the Second International Brick Masonry Conference,* Stoke-on-Trent, 1970.

19. Kadir M. R. A., "The structural behaviour of masonry infill panels in framed structures", *PhD Thesis,* University of Edinburgh, 1974.

20. Tomazevic M., "Dynamic modelling of masonry buildings: storey mechanism model as a simple alternative", *Earthquake Engineering and Structural Dynamics, Vol. 15,* 1987.

21. Tomazevic M., Modena C., "Seismic behaviour of masonry buildings with a mixed structural system: earthquake simulator study of three-storeyed building systems", *European Earthquake Engineering , Vol. 1,* 1989.

22. Modena C., Tomazevic M., "A research program on the seismic behaviour of modern masonry buildings", *Proceedings of the Ninth European Conference on Earthquake Engineering, Vol. 5,* Moscow, 1990.

23. Tomazevic M., Modena C., "The effect of reinforcement on the seismic behaviour of masonry buildings with mixed structural system: an experimental study", *Proceedings of the Ninth European Conference on Earthquake Engineering, Vol. 5,* Moscow, 1990.

24. Tomazevic M., Modena C., Velechovsky T., "Seismic behaviour of mixed structural systems with peripheral masonry walls and internal r.c. columns: an earthquake simulator study", *Proceedings of the Fifth North American Masonry Conference, Vol. 1,* University of Illinois at Urbana-Champaign, 1990.

25. Tomazevic M., Weiss P., "A rational experimentally based method for the verification of earthquake resistance of masonry buildings", *Proceedings of the Fourth U.S. National Conference on Earthquake Engineering, Vol. 2,* Palm Springs California, 1990.

26. Tomazevic M., Sheppard P., "Mathematical modelling of masonry buildings for earthquake resistance analysis", *Engineering Aspects of Earthquake Phenomena,* edited by A. Koridze, 1986.

27. Tomazevic M., Velechovsky T., "Some aspects of testing small scale masonry building models on simple earthquake simulators", *Earthquake Engineering and Structural Dynamics, Vol. 21,* 1992.

28. Tomazevic M., Weiss P., Velechovsky T., "The influence of rigidity of floors on the seismic behaviour of old stone-masonry buildings", *European Earthquake Engineering , Vol. 3,* 1991.

29. Tomazevic M., Lutman M., Weiss P., "The seismic resistance of historical urban buildings and the interventions in their floor systems: an experimental study", *Proceedings of the Sixth North American Masonry Conference, Vol. 2,* Drexel University, Philadelphia, Pennsylvania, 1993.

30. Tomazevic M., Lutman M., Velechovsky T., "The influence of lateral load time-history on the behaviour of reinforced-masonry walls failing in shear", *Proceedings of the Sixth North American Masonry Conference, Vol. 2,* Drexel University, Philadelphia, Pennsylvania, 1993.

31. Benedetti D., Castoldi A., "Dynamic and static experimental analysis of stone, masonry buildings", *Proceedings of the Seventh European Conference on Earthquake Engineering, Vol. 5,* Athens Greece, 1982.

32. Manos G.C., Mpoufidis D., Demosthenous M., Triamataki M., "Influence of masonry infill panels on the response of r.c. structures subjected to lateral loads",

Proceedings of the Fifth North American Masonry Conference, Vol. 1, University of Illinois at Urbana-Champaign, 1990.

33. Manos G.C., Mpoufidis D., Demosthenous M., "Experimental and analytical study of the response of a two storey r.c. scale model structure to simulated earthquake ground motions", *Proceedings of the Ninth European Conference on Earthquake Engineering, Vol. 5,* Moscow, 1990.

34. Manos G.C., Yasin B., Valiasis T., "Small scale model simulation of the cyclic behaviour of infill brick panels", *Proceedings of the Sixth North American Masonry Conference, Vol. 1,* Drexel University, Philadelphia, Pennsylvania, 1993.

35. Valiasis T., Stylianidis K., "Masonry infilled r.c. frames under horizontal loading: experimental results", *European Earthquake Engineering, Vol. 3,* 1989.

36. Manos G.C., Triamataki M., Demosthenous M., Yasin B., "Equivalent diagonal strut simulation of the influence of masonry infills on the seismic response of r.c. framed structures", *Proceedings of the Sixth North American Masonry Conference, Vol. 1,* Drexel University, Philadelphia, Pennsylvania, 1993.

37. Benjamin J. R., Williams H. A., "The behaviour of one story brick shear walls", *ASCE, Journal of the Structural Division, Vol. 84, no. ST 4,* 1958.

38. Yorulmaz M., Sozen M. A., "Behaviour of single-storey reinforced concrete frames with filler walls", from S. Sahlin, *"Structural Masonry"*, published by Prentice-Hall Inc. New Jersey, 1971.

39. Harris H. G., Besica I.J., "Direct small scale modelling of concrete masonry", *Proceedings of Symposium on Advances in Civil Engineering Mechanics, EMD-ASCE,* New York, 1977.

40. Hamid A. A., Abboud B. E., Harris H. G., "Direct modelling of concrete block masonry under axial compression", *Masonry : Research, Application and Problems, ASTM STP 871,* edited by J. C. Grogan and J. T. Conway, Philadelphia, 1985.

41. Hamid A. A., Abboud B. E., "Direct modelling of concrete block masonry under shear and in-plane tension", *Journal of Testing and Evaluation, JETVA Vol. 14, No. 2,* March 1986.

42. Abboud B. E., Hamid A. A., Harris H. G., "Further investigation on the use of direct small scale modelling of concrete block masonry", *Proceedings of the Fourth Canadian Masonry Symposium, Vol. 1,* University of New Brunswick, Fredericton, Canada, 1986.

43. Abboud B. E., Hamid A. A., Harris H. G., "Small-scale modelling of concrete block masonry structures", *A.C.I. Structural Journal, Vol. 87, No. 2*, 1990.

44. Abboud B. E., Hamid A. A., "Behaviour of model concrete masonry slender walls under out-of-plane lateral loads", *Proceedings of the Fifth North American Masonry Conference, Vol. 1,* University of Illinois at Urbana-Champaign, 1990.

45. Larbi A., Harris H. G., "Seismic performance of low aspect ratio reinforced block masonry shear walls", *Proceedings of the Fourth U.S. National Conference on Earthquake Engineering, Vol. 2,* Palm Springs, California, 1990

46. Larbi A., Harris H. G., "Seismic behaviour of reinforced block masonry shear walls using 1/3 scale direct models", *Proceedings of the Fifth North American Masonry Conference, Vol. 1,* University of Illinois at Urbana-Champaign, 1990.

47. Ghanem G. M., Salama A. E., Elmagd S. A., Hamid A. A., "Effect of axial compression on the behaviour of partially reinforced masonry shear walls", *Proceedings of the Sixth North American Masonry Conference, Vol. 1,* Drexel University, Philadelphia, Pennsylvania, 1993.

48. Harris H. G., Balouz G. R., Kopatz K. W., "Preliminary studies in seismic retrofitting of lightly reinforced concrete frames using masonry infills", *Proceedings of the Sixth North American Masonry Conference, Vol. 1,* Drexel University, Philadelphia, Pennsylvania, 1993.

49. Noland J. L., "1990 Status Report: U.S. Co-ordinated Program or Masonry Building Research: Sixth Year Status", *Proceedings of the Fifth North American Masonry Conference, Vol. 1,* University of Illinois at Urbana-Champaign, 1990.

50. Noland J. L., "U.S. Co-ordinated Program or Masonry Building Research: Sixth Year Status", *Proceedings of the 23rd Joint Meeting on Wind and Seismic Effects,* U.S. Department of Commerce, NIST, 1991.

51. Abrams D. P., Paulson T. J., Colunga A. T., "Aspects of response for masonry building structures", *Proceedings of the Fourth U.S. National Conference on Earthquake Engineering, Vol. 2,* Palm Springs, California, 1990

52. Abrams D. P., Paulson T. J., "Perceptions and observations of seismic response for reinforced masonry building structures" *Proceedings of the Fifth North American Masonry Conference, Vol. 1,* University of Illinois at Urbana-Champaign, 1990.

53. Abrams D. P., Paulson T. J., "Modelling earthquake response of concrete masonry building structures", *A.C.I. Structural Journal, Vol. 88, No. 4,* 1991.

54. Abrams D. P., "Strength and behaviour of unreinforced masonry elements", *Proceedings of the Tenth World Conference on Earthquake Engineering, Vol. 6,* Madrid, Spain, 1992.

55. Maidstone R. J., "On the strengths and stiffnesses of infilled frames", *Proceedings of the Institution of Civil Engineers, Supplementary Volume,* 1971.

56. Klinger R. E., Bertero V. V., "Earthquake resistance of infilled frames", *Proceedings, ASCE, Journal of the Structural Division, Vol. 104, ST6,* 1978.

57. Brokken S. T., Bertero V. V., "Studies on effects of infills in seismic resistant R/C construction", *Report No. UCB/EERC-81/12, Earthquake Engineering Research Centre, University of California, Berkeley,* 1981.

58. Page A. W., "The biaxial compressive strength of brick masonry", *Proceedings of the Institution of Civil Engineers, Part 2, Vol. 71,* 1981.

59. Dhanasekar M., Page A. W., Kleeman P. W., "The failure of brick masonry under biaxial stresses", *Proceedings of the Institution of Civil Engineers, Part 2, Vol. 79,* 1985.

60. Dhanasekar M., Page A. W., Kleeman P. W., "The behaviour of brick masonry under biaxial stress with particular reference to infilled frames", *Proceedings of the Seventh International Brick Masonry Conference, Vol. 2, Melbourne, Australia,* 1985.

61. Dhanasekar M., Page A. W., "The influence of brick masonry infill properties on the behaviour of infilled frames", *Proceedings of the Institution of Civil Engineers, Part 2, Vol. 81,* 1986.

62. Dawe J. L., Shriver A. B., Sofocleous C., "Masonry infilled frames subjected to dynamic load", *Canadian Journal of Civil Engineering, Vol. 16,* 1989.

63. Liauw T. C., Kwan A. K. H., "Experimental study of shear wall and infilled frame on shake table", *Proceedings of the Tenth World Conference on Earthquake Engineering, Vol. 5,* Madrid, Spain, 1992.

64. Jurukovski D., Krstevska L., Alessi R., Diotallevi P. P., Merli M., Zarri F., "Shaking table tests of three four-storey brick masonry models: Original and

strengthened by R/C core and R/C jackets", *Proceedings of the Tenth World Conference on Earthquake Engineering, Vol. 5,* Madrid, Spain, 1992.

65. Alessi R., Diotallevi P. P., Jurukovski D., Petkovski M., Tashkov L., Zarri F., "Shaking table test of reduced scale model of brick masonry buildings", *Proceedings of the Ninth European Conference on Earthquake Engineering, Vol. 5,* Moscow, 1990.

66. Francis A. J., Horman C. B., Jerrems L. E., "The effect of joint thickness and other factors on the compressive strength of brickwork", *Proceedings of the Second International Brick masonry Conference,* Stoke-on-Trent, 1970.

67. Atkinson R. H., Noland J. L., "A proposed failure theory for brick masonry in compression", *Proceedings of the Third Canadian Masonry Symposium,* Edmonton, Canada, 1983.

68. McNary W. S., Abrams D. P., "Mechanics of masonry in compression", *ASCE, Journal of Structural Engineering, Vol. 111, No. 4,* 1985.

69. Ali M. M., "Discussion on paper by McNary and Abrams [Ref. 68]", *ASCE, Journal of Structural Engineering, Vol. , No. ,* 1985

70. Hilsdorf H. K., "Investigation into the failure mechanism of brick masonry loaded in axial compression", *Proceedings of International Conference on Masonry Structural Systems,* Texas, 1967.

71. Khoo C. L., Hendry A. W., "A failure criterion for brickwork under axial compression", *Proceedings of the Third International Brick Masonry Conference,* Essen, Germany, 1973.

72. Stafford-Smith B., "Behaviour of square infilled frames", *Proceedings ASCE, Journal of the Structural Division, Vol. 92, ST1,* 1966.

73. Stafford-Smith B., Carter C., "A method of analysis for infilled frames", *Proceedings of the Institution of Civil Engineers, Vol. 44,* 1969.

74. Smolira M., "Analysis of infilled shear walls", *Proceedings of the Institution of Civil Engineers, Vol. 55, Part 2,* 1973.

75. Stafford-Smith B., Riddington J. R., "The design of masonry infilled steel frames for bracing structures", *The Structural Engineer, Vol. 56B, No. 1,* 1978.

76. Riddington J. R., Stafford-Smith B., "Analysis of infilled frames subject to racking with design recommendations", *The Structural Engineer, Vol. 55, No. 6,* 1977.

77. Thiruvengadam V., "On the natural frequencies of infilled frames", *Earthquake Engineering and Structural Dynamics, Vol. 13,* 1985.

78. Drysdale R. G., Hamid A. A., Baker L. R., "Masonry structures-Behaviour and Design", published by Prentice-Hall Inc., New Jersey, 1994.

79. Wood R. H., "Plasticity, composite action and collapse of reinforced shear wall panels in frames", *Proceedings of the Institution of Civil Engineers, Part 2, Vol. 65,* 1978.

80. Liauw T. C., Kwan A. K. H., "Plastic theory of non-integral infilled frames", *Proceedings of the Institution of Civil Engineers, Part 2, Vol. 75,* 1983.

81. "BS 5628: 1985, Use of Masonry - Part 3 : materials and components, design and workmanship", *British Standards Institution*, 1985.

82. **a -** "BS 3921: 1985, Clay bricks", *British Standards Institution*, 1985.

b - "BS 4551: 1980, Methods of testing mortars, screeds and plasters", *British Standards Institution*, 1980.

83. American Society for Testing and Materials (1978), "ASTM C 270-73, Standard specification for mortar for unit masonry", *ASTM Standards in Building Codes, Vol. 1,* 1978.

84. American Society for Testing and Materials (1978), "ASTM C 67-78, Standard methods of sampling and testing brick and structural clay tile", *ASTM Standards in Building Codes, Vol. 1,* 1978.

85. **a -** American Society for Testing and Materials (1978), "ASTM C 109-77, Standard test method for compressive strength of hydraulic cement mortars (using 50-mm cube specimens)", *ASTM Standards in Building Codes, Vol. 1,* 1978.

b - American Society for Testing and Materials (1985), "ASTM C 190-85, Standard test method for tensile strength of hydraulic cement mortars", *ASTM Standards in Building Codes*, 1985.

86. American Society for Testing and Materials (1978), "ASTM E 447-74, Standard test methods for compressive strength of masonry prisms", *ASTM Standards in Building Codes, Vol. 1,* 1978.

87. American Society for Testing and Materials (1978), "ASTM E 518-76, Standard test methods for flexural bond strength of masonry", *ASTM Standards in Building Codes, Vol. 1,* 1978.

88. American Society for Testing and Materials (1978), "ASTM E 519-74, Standard test method for diagonal tension (shear) in masonry assemblages", *ASTM Standards in Building Codes, Vol. 1,* 1978.

89. "RILEM Technical recommendations for the testing and use of construction materials", *International Union of Testing and Research Laboratories for Materials and Structures*, published by E & FN Spon, London, 1994.

90. Mayes R. L., Clough R. W., "A literature survey - compressive, tensile, bond and shear strength of masonry" Report No. EERC 75-15, Earthquake Engineering Research Centre, University of California, Berkeley, 1975.

91. Hendry A. W., Sinha B. P., Davies S. R., "Load bearing brickwork design", published by Ellis Horwood Ltd., 1987.

92. Chiostrini S., Vignoli A., "Application of a numerical method to study masonry panels with various geometry under seismic loads" *Proceedings of the International Conference on Structural Studies, Repairs and Maintenance of Historical Buildings, STREMA*, Florence 1989.

93. Saadeghvaziri M. A., Mehta S. S., "An analytical model for urm structures", *Proceedings of the Sixth North American Masonry Conference, Vol. 1,* Drexel University, Philadelphia, Pennsylvania, 1993.

94. Rots J. G., Lourenco P. B., "Fracture simulations of masonry using non-linear interface elements", *Proceedings of the Sixth North American Masonry Conference, Vol. 2,* Drexel University, Philadelphia, Pennsylvania, 1993.

95. Vermeltfoort A. T., Raijmakers T. M., Janssen H. J., "Shear tests on masonry walls ", *Proceedings of the Sixth North American Masonry Conference, Vol. 2,* Drexel University, Philadelphia, Pennsylvania, 1993.

96. Vermeltfoort A. T., Pluijm R. van der, "Shear and deformation properties of masonry to be used in computer calculations ", *Proceedings of the Ninth International Brick Masonry Conference,* Berlin, 1991.

97. Molyneaux T. C. K., "Vehicle impact on masonry parapets", *SECED Newsletter, Vol. 9, No. 1*, 1995.

98. Cerioni R., Brighenti R., Donida G., "Use of incompatible displacement modes in a finite element model to analyse the dynamic behaviour of unreinforced masonry panels", *Computers and Structures, Vol. 57, No. 1*, 1995.

99. Combescure D., Pegon P., Anthoine A., "Modelling of the in-plane behaviour of masonry infilled frames", *Proceedings of the Fifth SECED Conference on European Seismic Design Practice*, Chester, 1995.

100. "LABTECH NOTEBOOK User Manual", Labtech Technologies Corp., MS-DOS version 4.3.3, 1985.

101. "The Handbook of personal computer instrumentation", (commercial brochure), Intelligent Instrumentation, Inc., U.S.A., 1994.

102. Dally J. W., Riley W. F., McConnell K. G., "Instrumentation for engineering measurements", published by John Wiley & Sons, Inc., U.S.A., 1984.

103. Tassios T. P., "Masonry infill and r.c. walls under cyclic actions: State-of-the-art report", CIB Symposium on Wall Structures, Warsaw, 1984.

104. Hendry, A.W. "Structural masonry", published by Macmillan Education Ltd., London, 1990.

105. Wolde-Tinsae A., Atkinson R. H., Hamid A. A., "State-of-the-art: modulus of elasticity of masonry", *Proceedings of the Sixth North American Masonry Conference, Vol. 2,* Drexel University, Philadelphia, Pennsylvania, 1993.

106. Riddington J. R., Ghazali M. Z., "Hypothesis for shear failure in masonry joints", *Proceedings of the Institution of Civil Engineers, Part 2, Volume 89,* 1990.

107. Manfedi G., Mazzolani S., "Review of existing testing of masonry structures subjected to horizontal loads", *Proceedings of the Tenth World Conference on Earthquake Engineering, Vol. 6,* Madrid, Spain, 1992.

108. Paz M., "International handbook of earthquake engineering : Codes, programs and examples", published by Chapman and Hall, Inc., 1994.

109. Moghaddam H. A., Dowling P. J., "The state of the art in infilled frames", *ESEE Research Report, No. 87-2,* Imperial College of Science and Technology, 1987.

110. Mersereau R. M., Smith M. J. T., "Digital filtering : a computer laboratory textbook", published by John Wiley & Sons, Inc., 1994.

111. Bruneau M., "Seismic evaluation of unreinforced masonry buildings - A state-of-the-art report", *Canadian Journal of Civil Engineering, Vol. 21,* 1994.

112. Scaletti H., Chariarse V. Cuadra C., Cuadros G., "Pseudo dynamic tests of confined masonry buildings", *Proceedings of the Tenth World Conference on Earthquake Engineering, Vol. 6,* Madrid, Spain, 1992.

113. LUSAS Theory Manual - v.10.0, User Manual - v.11.0, Element library - v.11.0, MYSTRO User Manual - v.11.0, Finite Element Analysis Ltd., U.K.

114. Crisfield M. A., "Non-linear finite elements analysis of solids and structures", Volume 1, published by John Wiley & Sons Ltd., 1991.

115. Bell A., Finite Element Analysis Ltd., *Personal Communication.*

116. Hinton E., Owen R., "Computational modelling of reinforced concrete structures", published by Pineridge Press, Swansea, 1986.

Appendix A

A.1 Digital signal processing and filter details.

EIGEN.FIL | Rectangular window - linear phase - low pass filter
h[n1]..[n32]
SEQUENCE VALUES
0.0123632368414928855
0.0205575934096104557
0.0230704014664837587
0.0182041787960587238
0.0063122859796239496 1
-0.0100037468725634928
-0.0263017913871216556
-0.0372544944388094115
-0.0379423968319176283
-0.0251699113578942764
0.0015366354209849393 5
0.0395262396757125808
0.0833536770291477269
0.1258000935243938 91
0.1593644433635803 55
0.1778814308593745 23
0.1778814308593745 23
0.1593644433635803 55
0.1258000935243938 91
0.0833536770291477269
0.0395262396757125808
0.0015366354209849393 5
-0.0251699113578942764
-0.0379423968319176283
-0.0372544944388094115
-0.0263017913871216556
-0.0100037468725634928
0.0063122859796239496 1
0.0182041787960587238
0.0230704014664837587
0.0205575934096104557
0.0123632368414928855

Filter function : **y[n] = x[n] * h[n]**

where : y[n] is the filtered output signal

x[n] is the signal input file

h[n] is the filter sequence

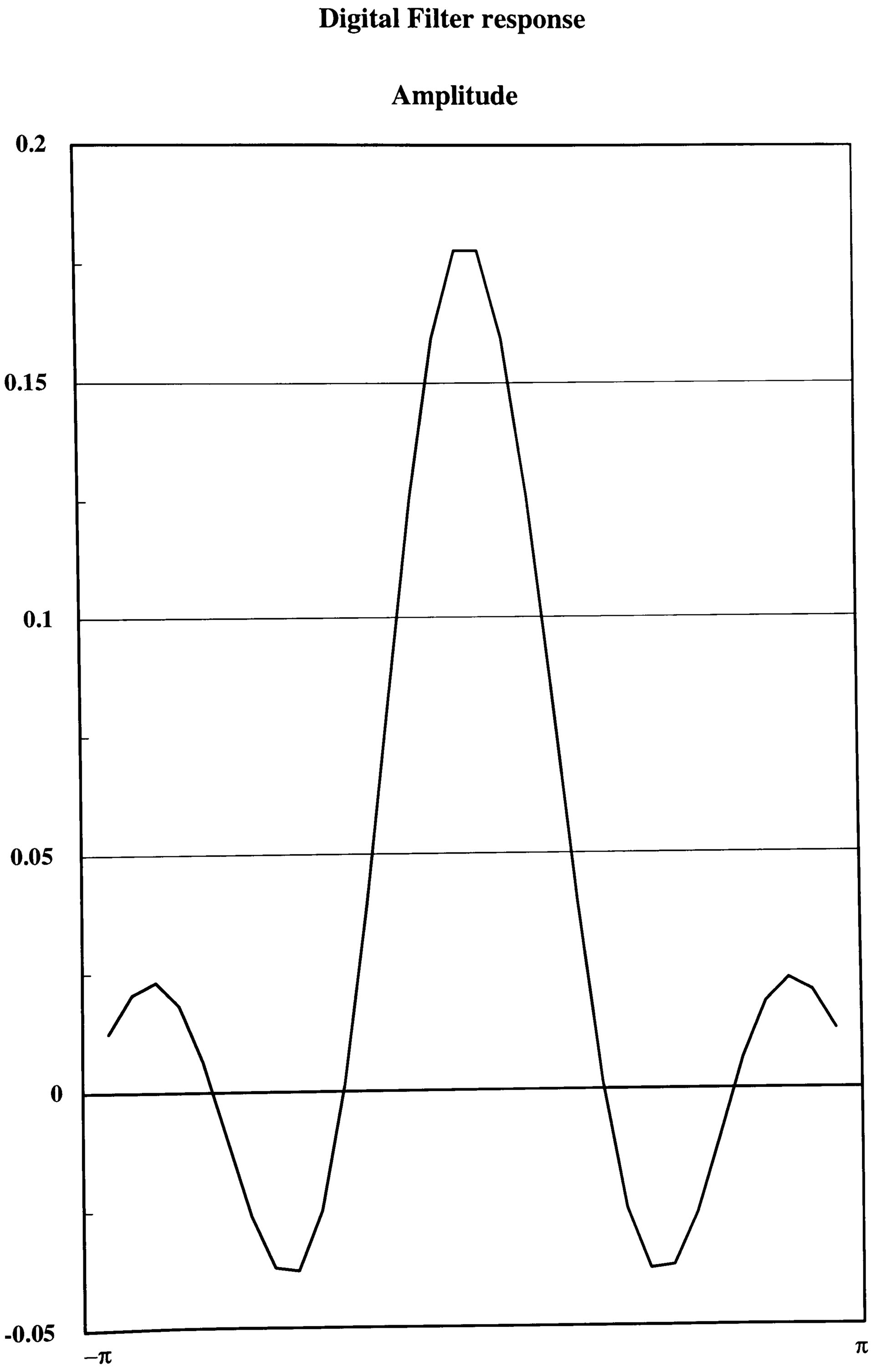

Figure A.1 EIGEN.FIL frequency repsonse

FFT - Real Part

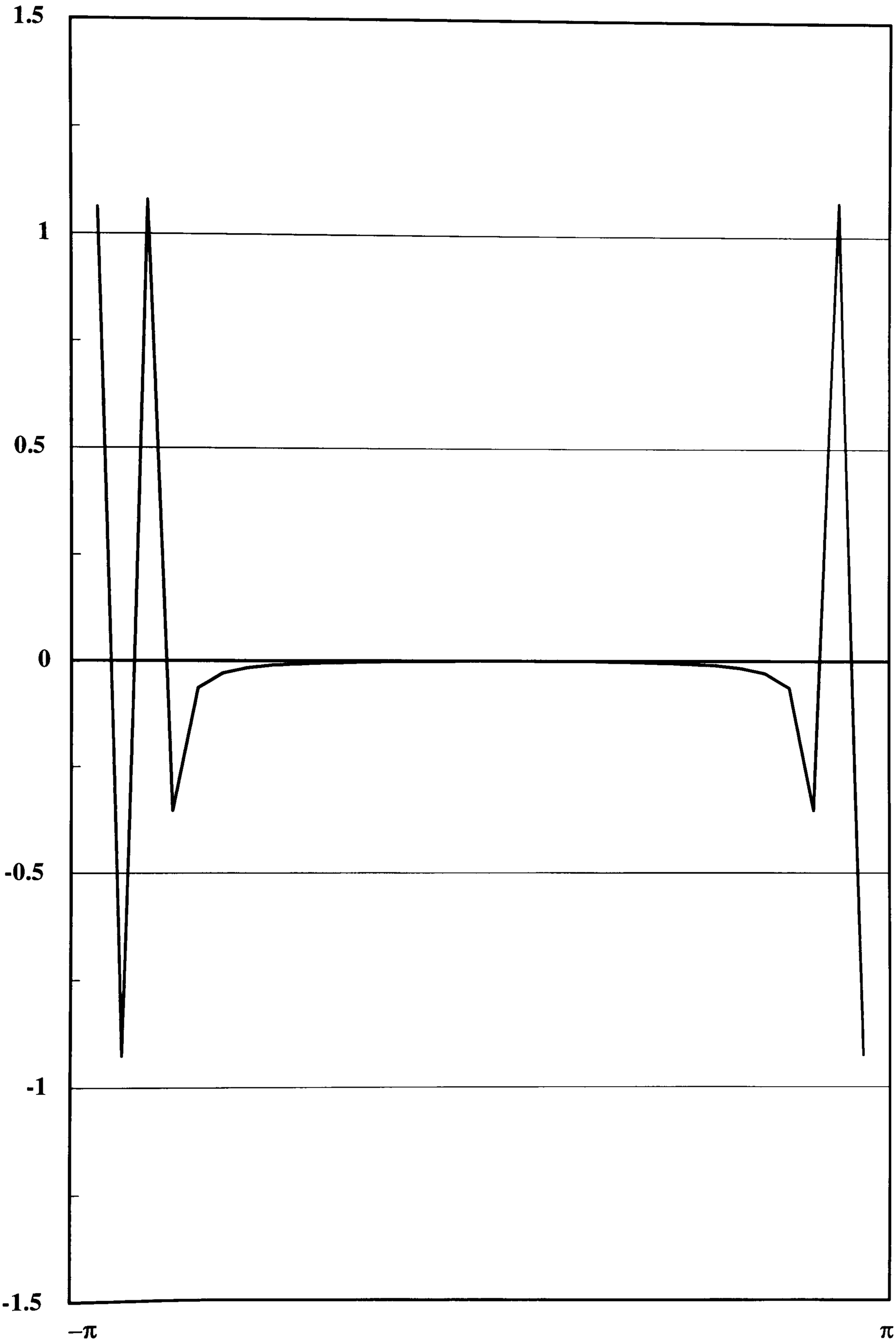

Figure A.2 FFT of digital signal (real part)

FFT - Imaginary Part

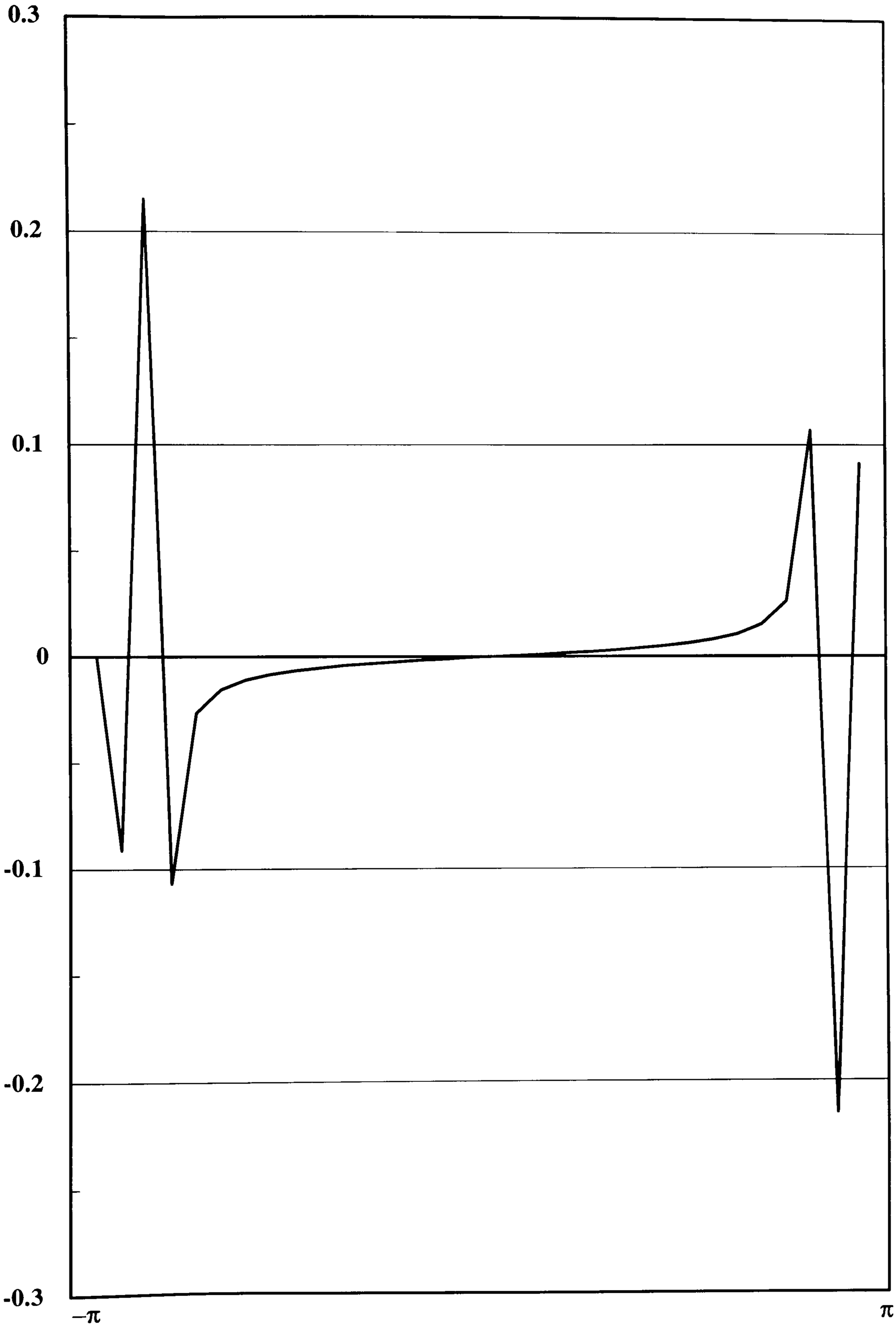

Figure A.3 FFT of digital signal (imaginary part)

A.2 Calibration chart for prestressing springs.

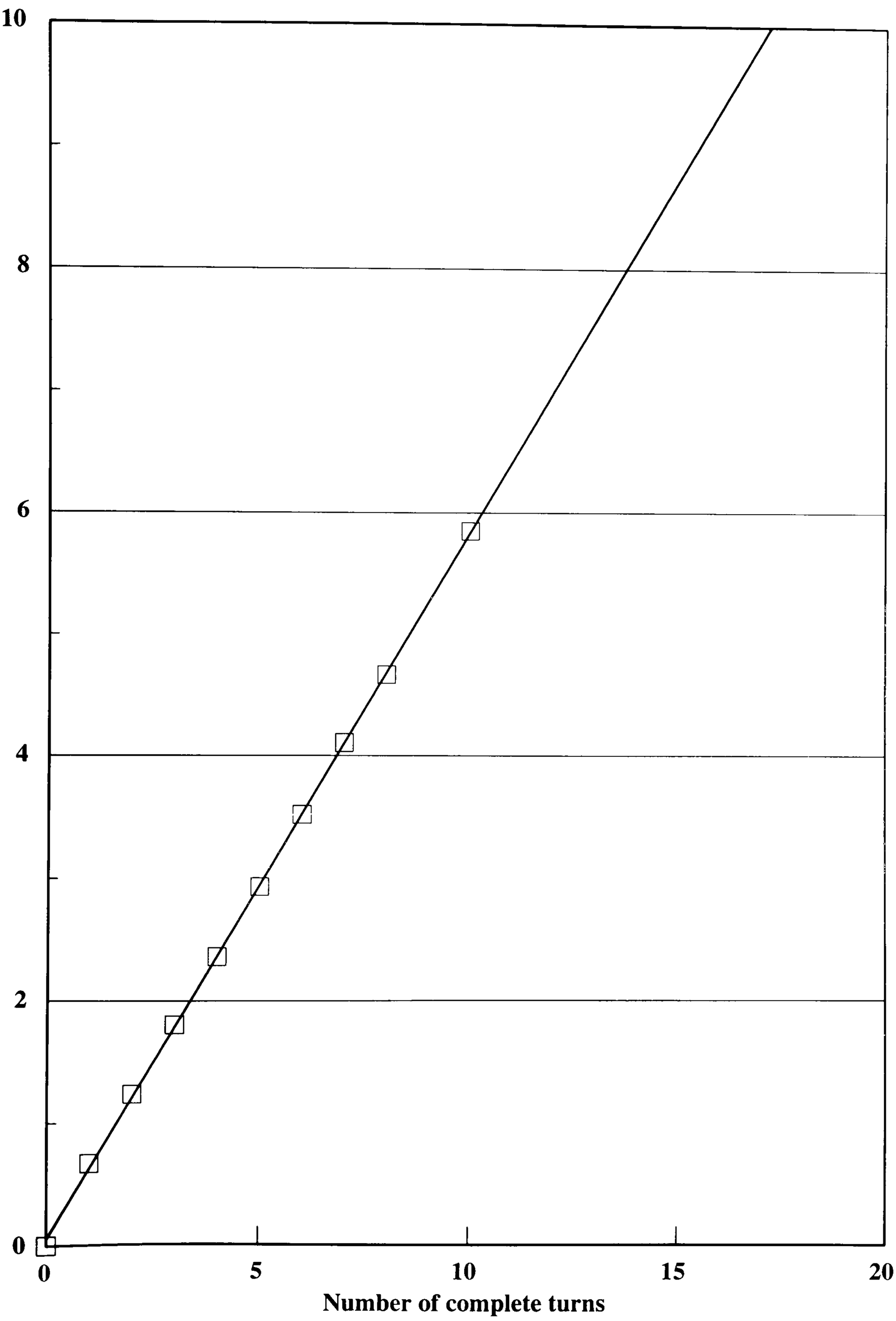

Figure A.4 Calibration chart (relates to total prestressing axial force)

Appendix B

B.1 Masonry 5-course prism LUSAS data input file.

```
PROBLEM TITLE   NONLINEAR STATIC ANALYSIS - Uniaxial Compression  - PRISM11B.DAT
UNITS N mm
OPTION  18 26 27 44 49 55 62 164
QPM8   ELEMENT TOPOLOGY
FIRST  1   1  2  3  20 37 36 35 18
INC      1    2  2  2  2  2  2  2  2    8
INC      8   34 34 34 34 34 34 34 34   14
SOLUTION ORDER AUTOMATIC
NODE COORDINATES
FIRST  1      0       0
INC    1    3.175     0     17
FIRST  18     0      3.175
INC    1    3.175     0     17
FIRST  35     0      6.350
INC    1    3.175     0     17
FIRST  52     0      9.525
INC    1    3.175     0     17
FIRST  69     0      12.70
INC    1    3.175     0     17
FIRST  86     0      13.95
INC    1    3.175     0     17
FIRST  103    0      15.20
INC    1    3.175     0     17
FIRST  120    0      18.375
INC    1    3.175     0     17
FIRST  137    0      21.55
INC    1    3.175     0     17
FIRST  154    0      24.725
INC    1    3.175     0     17
FIRST  171    0      27.90
INC    1    3.175     0     17
FIRST  188    0      29.15
INC    1    3.175     0     17
FIRST  205    0      30.40
INC    1    3.175     0     17
FIRST  222    0      33.575
INC    1    3.175     0     17
FIRST  239    0      36.75
INC    1    3.175     0     17
FIRST  256    0      39.925
INC    1    3.175     0     17
FIRST  273    0      43.10
INC    1    3.175     0     17
FIRST  290    0      44.35
INC    1    3.175     0     17
FIRST  307    0      45.60
```

```
INC    1    3.175     0    17
FIRST  324    0     48.775
INC    1    3.175     0    17
FIRST  341    0     51.95
INC    1    3.175     0    17
FIRST  358    0     55.125
INC    1    3.175     0    17
FIRST  375    0     58.30
INC    1    3.175     0    17
FIRST  392    0     59.55
INC    1    3.175     0    17
FIRST  409    0     60.80
INC    1    3.175     0    17
FIRST  426    0     63.975
INC    1    3.175     0    17
FIRST  443    0     67.15
INC    1    3.175     0    17
FIRST  460    0     70.325
INC    1    3.175     0    17
FIRST  477    0     73.50
INC    1    3.175     0    17
C  ***Delete dummy central element nodes***
DELETE NODES  19  33   2
DELETE NODES  53  67   2
DELETE NODES  87  101  2
DELETE NODES  121 135  2
DELETE NODES  155 169  2
DELETE NODES  189 203  2
DELETE NODES  223 237  2
DELETE NODES  257 271  2
DELETE NODES  291 305  2
DELETE NODES  325 339  2
DELETE NODES  359 373  2
DELETE NODES  393 407  2
DELETE NODES  427 441  2
DELETE NODES  461 475  2
C  ***Element thickness  25.6 mm***
QPM8 GEOMETRIC PROPERTIES
1   25.6  25.6  25.6  25.6  25.6  25.6  25.6  25.6
GEOMETRIC ASSIGNMENTS
1  112  1    1
C  ***Brick properties***
MATERIAL PROPERTIES NONLINEAR 24
1   3000  0.17    5.0    0.1   0.30    5
C  ***Mortar properties***
MATERIAL PROPERTIES NONLINEAR 24
2   1700   0.10   2.0    0.2   0.12    5
MATERIAL ASSIGNMENTS
1   16   1    1
17  24   1    2
25  40   1    1
41  48   1    2
49  64   1    1
65  72   1    2
73  88   1    1
89  96   1    2
97  112  1    1
SUPPORT NODES
```

```
1   17   1      R  R
477  493   1    R  R
LOAD CASE  TITLE   "PDSP Compressive vertical  total=0.20mm over 50 increments"
PDSP  2
477  493   1    0.00   -0.20
ELEMENT OUTPUT
9   97   8   2
NODE OUTPUT
477  493   1    3
NONLINEAR CONTROL
INCREMENTATION  0.02      0      0
ITERATIONS  20     D       D
CONVERGENCE   0      0        D       D
OUTPUT     0        1        1        0        0
TERMINATION    1
END
```

B.2 Masonry square wallette LUSAS data input file.

```
PROBLEM TITLE    NONLINEAR STATIC ANALYSIS  - Diagonal Compression - SHEAR4X.DAT
UNITS N mm
OPTION  18 26 27 44 55 62 115 139
QPM8   ELEMENT TOPOLOGY
FIRST   1    1    2    3    32    61    60    59   30
INC      1     2    2    2    2     2     2     2    2     14
INC     14   58   58   58   58    58    58    58   58    14
QPM4   ELEMENT TOPOLOGY
197  837 839 843 842
198  839 841 844 843
199  841 846 845 844
200  783 847 846 841
201  725 848 847 783
SOLUTION ORDER AUTOMATIC
NODE COORDINATES
1      0.00     0.00
29     73.5     0.00
SPACING
1     29    2    7.35 7.35 5.5 2.5 5.5 5.7 2.85 2.85 5.7 5.5 2.5 5.5 7.35 7.35
NODE COORDINATES
30     0.00     3.175
58     73.5     3.175
SPACING
30    58    2    7.35 7.35 5.5 2.5 5.5 5.7 2.85 2.85 5.7 5.5 2.5 5.5 7.35 7.35
NODE COORDINATES
59     0.00     6.35
87     73.5     6.35
SPACING
59    87    2    7.35 7.35 5.5 2.5 5.5 5.7 2.85 2.85 5.7 5.5 2.5 5.5 7.35 7.35
NODE COORDINATES
88     0.00     9.525
116    73.5     9.525
SPACING
88   116    2   7.35 7.35 5.5 2.5 5.5 5.7 2.85 2.85 5.7 5.5 2.5 5.5 7.35 7.35
NODE COORDINATES
117    0.00     12.7
```

145 73.5 12.7
SPACING
117 145 2 7.35 7.35 5.5 2.5 5.5 5.7 2.85 2.85 5.7 5.5 2.5 5.5 7.35 7.35
NODE COORDINATES
146 0.00 13.95
174 73.5 13.95
SPACING
146 174 2 7.35 7.35 5.5 2.5 5.5 5.7 2.85 2.85 5.7 5.5 2.5 5.5 7.35 7.35
NODE COORDINATES
175 0.00 15.2
203 73.5 15.2
SPACING
175 203 2 7.35 7.35 5.5 2.5 5.5 5.7 2.85 2.85 5.7 5.5 2.5 5.5 7.35 7.35
NODE COORDINATES
204 0.00 18.375
232 73.5 18.375
SPACING
204 232 2 7.35 7.35 5.5 2.5 5.5 5.7 2.85 2.85 5.7 5.5 2.5 5.5 7.35 7.35
NODE COORDINATES
233 0.00 21.55
261 73.5 21.55
SPACING
233 261 2 7.35 7.35 5.5 2.5 5.5 5.7 2.85 2.85 5.7 5.5 2.5 5.5 7.35 7.35
NODE COORDINATES
262 0.00 24.725
290 73.5 24.725
SPACING
262 290 2 7.35 7.35 5.5 2.5 5.5 5.7 2.85 2.85 5.7 5.5 2.5 5.5 7.35 7.35
NODE COORDINATES
291 0.00 27.9
319 73.5 27.9
SPACING
291 319 2 7.35 7.35 5.5 2.5 5.5 5.7 2.85 2.85 5.7 5.5 2.5 5.5 7.35 7.35
NODE COORDINATES
320 0.00 29.15
348 73.5 29.15
SPACING
320 348 2 7.35 7.35 5.5 2.5 5.5 5.7 2.85 2.85 5.7 5.5 2.5 5.5 7.35 7.35
NODE COORDINATES
349 0.00 30.4
377 73.5 30.4
SPACING
349 377 2 7.35 7.35 5.5 2.5 5.5 5.7 2.85 2.85 5.7 5.5 2.5 5.5 7.35 7.35
NODE COORDINATES
378 0.00 33.575
406 73.5 33.575
SPACING
378 406 2 7.35 7.35 5.5 2.5 5.5 5.7 2.85 2.85 5.7 5.5 2.5 5.5 7.35 7.35
NODE COORDINATES
407 0.00 36.75
435 73.5 36.75
SPACING
407 435 2 7.35 7.35 5.5 2.5 5.5 5.7 2.85 2.85 5.7 5.5 2.5 5.5 7.35 7.35
NODE COORDINATES
436 0.00 39.925
464 73.5 39.925
SPACING
436 464 2 7.35 7.35 5.5 2.5 5.5 5.7 2.85 2.85 5.7 5.5 2.5 5.5 7.35 7.35

```
NODE COORDINATES
465  0.00   43.1
493  73.5   43.1
SPACING
465 493  2  7.35 7.35 5.5 2.5 5.5 5.7 2.85 2.85 5.7 5.5 2.5 5.5 7.35 7.35
NODE COORDINATES
494  0.00   44.35
522  73.5   44.35
SPACING
494 522  2  7.35 7.35 5.5 2.5 5.5 5.7 2.85 2.85 5.7 5.5 2.5 5.5 7.35 7.35
NODE COORDINATES
523  0.00   45.6
551  73.5   45.6
SPACING
523 551  2  7.35 7.35 5.5 2.5 5.5 5.7 2.85 2.85 5.7 5.5 2.5 5.5 7.35 7.35
NODE COORDINATES
552  0.00   48.775
580  73.5   48.775
SPACING
552 580  2  7.35 7.35 5.5 2.5 5.5 5.7 2.85 2.85 5.7 5.5 2.5 5.5 7.35 7.35
NODE COORDINATES
581  0.00   51.95
609  73.5   51.95
SPACING
581 609  2  7.35 7.35 5.5 2.5 5.5 5.7 2.85 2.85 5.7 5.5 2.5 5.5 7.35 7.35
NODE COORDINATES
610  0.00   55.125
638  73.5   55.125
SPACING
610 638  2  7.35 7.35 5.5 2.5 5.5 5.7 2.85 2.85 5.7 5.5 2.5 5.5 7.35 7.35
NODE COORDINATES
639  0.00   58.3
667  73.5   58.3
SPACING
639 667  2  7.35 7.35 5.5 2.5 5.5 5.7 2.85 2.85 5.7 5.5 2.5 5.5 7.35 7.35
NODE COORDINATES
668  0.00   59.55
696  73.5   59.55
SPACING
668 696  2  7.35 7.35 5.5 2.5 5.5 5.7 2.85 2.85 5.7 5.5 2.5 5.5 7.35 7.35
NODE COORDINATES
697  0.00   60.8
725  73.5   60.8
SPACING
697 725  2  7.35 7.35 5.5 2.5 5.5 5.7 2.85 2.85 5.7 5.5 2.5 5.5 7.35 7.35
NODE COORDINATES
726  0.00   63.975
754  73.5   63.975
SPACING
726 754  2  7.35 7.35 5.5 2.5 5.5 5.7 2.85 2.85 5.7 5.5 2.5 5.5 7.35 7.35
NODE COORDINATES
755  0.00   67.15
783  73.5   67.15
SPACING
755 783  2  7.35 7.35 5.5 2.5 5.5 5.7 2.85 2.85 5.7 5.5 2.5 5.5 7.35 7.35
NODE COORDINATES
784  0.00   70.325
812  73.5   70.325
```

SPACING
784 812 2 7.35 7.35 5.5 2.5 5.5 5.7 2.85 2.85 5.7 5.5 2.5 5.5 7.35 7.35
NODE COORDINATES
813 0.00 73.5
841 73.5 73.5
SPACING
813 841 2 7.35 7.35 5.5 2.5 5.5 5.7 2.85 2.85 5.7 5.5 2.5 5.5 7.35 7.35
NODE COORDINATES
2 3.675 0.00
28 69.825 0.00
SPACING
2 28 2 7.35 6.425 4 4 5.6 4.275 2.85 4.275 5.6 4 4 6.425 7.35
NODE COORDINATES
31 3.675 3.175
57 69.825 3.175
SPACING
31 57 2 7.35 6.425 4 4 5.6 4.275 2.85 4.275 5.6 4 4 6.425 7.35
NODE COORDINATES
60 3.675 6.35
86 69.825 6.35
SPACING
60 86 2 7.35 6.425 4 4 5.6 4.275 2.85 4.275 5.6 4 4 6.425 7.35
NODE COORDINATES
89 3.675 9.525
115 69.825 9.525
SPACING
89 115 2 7.35 6.425 4 4 5.6 4.275 2.85 4.275 5.6 4 4 6.425 7.35
NODE COORDINATES
118 3.675 12.7
144 69.825 12.7
SPACING
118 144 2 7.35 6.425 4 4 5.6 4.275 2.85 4.275 5.6 4 4 6.425 7.35
NODE COORDINATES
147 3.675 13.95
173 69.825 13.95
SPACING
147 173 2 7.35 6.425 4 4 5.6 4.275 2.85 4.275 5.6 4 4 6.425 7.35
NODE COORDINATES
176 3.675 15.2
202 69.825 15.2
SPACING
176 202 2 7.35 6.425 4 4 5.6 4.275 2.85 4.275 5.6 4 4 6.425 7.35
NODE COORDINATES
205 3.675 18.375
231 69.825 18.375
SPACING
205 231 2 7.35 6.425 4 4 5.6 4.275 2.85 4.275 5.6 4 4 6.425 7.35
NODE COORDINATES
234 3.675 21.55
260 69.825 21.55
SPACING
234 260 2 7.35 6.425 4 4 5.6 4.275 2.85 4.275 5.6 4 4 6.425 7.35
NODE COORDINATES
263 3.675 24.725
289 69.825 24.725
SPACING
263 289 2 7.35 6.425 4 4 5.6 4.275 2.85 4.275 5.6 4 4 6.425 7.35
NODE COORDINATES

292 3.675 27.9
318 69.825 27.9
SPACING
292 318 2 7.35 6.425 4 4 5.6 4.275 2.85 4.275 5.6 4 4 6.425 7.35
NODE COORDINATES
321 3.675 29.15
347 69.825 29.15
SPACING
321 347 2 7.35 6.425 4 4 5.6 4.275 2.85 4.275 5.6 4 4 6.425 7.35
NODE COORDINATES
350 3.675 30.4
376 69.825 30.4
SPACING
350 376 2 7.35 6.425 4 4 5.6 4.275 2.85 4.275 5.6 4 4 6.425 7.35
NODE COORDINATES
379 3.675 33.575
405 69.825 33.575
SPACING
379 405 2 7.35 6.425 4 4 5.6 4.275 2.85 4.275 5.6 4 4 6.425 7.35
NODE COORDINATES
408 3.675 36.75
434 69.825 36.75
SPACING
408 434 2 7.35 6.425 4 4 5.6 4.275 2.85 4.275 5.6 4 4 6.425 7.35
NODE COORDINATES
437 3.675 39.925
463 69.825 39.925
SPACING
437 463 2 7.35 6.425 4 4 5.6 4.275 2.85 4.275 5.6 4 4 6.425 7.35
NODE COORDINATES
466 3.675 43.1
492 69.825 43.1
SPACING
466 492 2 7.35 6.425 4 4 5.6 4.275 2.85 4.275 5.6 4 4 6.425 7.35
NODE COORDINATES
495 3.675 44.35
521 69.825 44.35
SPACING
495 521 2 7.35 6.425 4 4 5.6 4.275 2.85 4.275 5.6 4 4 6.425 7.35
NODE COORDINATES
524 3.675 45.6
550 69.825 45.6
SPACING
524 550 2 7.35 6.425 4 4 5.6 4.275 2.85 4.275 5.6 4 4 6.425 7.35
NODE COORDINATES
553 3.675 48.775
579 69.825 48.775
SPACING
553 579 2 7.35 6.425 4 4 5.6 4.275 2.85 4.275 5.6 4 4 6.425 7.35
NODE COORDINATES
582 3.675 51.95
608 69.825 51.95
SPACING
582 608 2 7.35 6.425 4 4 5.6 4.275 2.85 4.275 5.6 4 4 6.425 7.35
NODE COORDINATES
611 3.675 55.125
637 69.825 55.125
SPACING

611 637 2 7.35 6.425 4 4 5.6 4.275 2.85 4.275 5.6 4 4 6.425 7.35
NODE COORDINATES
640 3.675 58.3
666 69.825 58.3
SPACING
640 666 2 7.35 6.425 4 4 5.6 4.275 2.85 4.275 5.6 4 4 6.425 7.35
NODE COORDINATES
669 3.675 59.55
695 69.825 59.55
SPACING
669 695 2 7.35 6.425 4 4 5.6 4.275 2.85 4.275 5.6 4 4 6.425 7.35
NODE COORDINATES
698 3.675 60.8
724 69.825 60.8
SPACING
698 724 2 7.35 6.425 4 4 5.6 4.275 2.85 4.275 5.6 4 4 6.425 7.35
NODE COORDINATES
727 3.675 63.975
753 69.825 63.975
SPACING
727 753 2 7.35 6.425 4 4 5.6 4.275 2.85 4.275 5.6 4 4 6.425 7.35
NODE COORDINATES
756 3.675 67.15
782 69.825 67.15
SPACING
756 782 2 7.35 6.425 4 4 5.6 4.275 2.85 4.275 5.6 4 4 6.425 7.35
NODE COORDINATES
785 3.675 70.325
811 69.825 70.325
SPACING
785 811 2 7.35 6.425 4 4 5.6 4.275 2.85 4.275 5.6 4 4 6.425 7.35
NODE COORDINATES
814 3.675 73.5
840 69.825 73.5
SPACING
814 840 2 7.35 6.425 4 4 5.6 4.275 2.85 4.275 5.6 4 4 6.425 7.35
842 58.80 76.675
843 66.15 76.675
844 73.50 76.675
845 76.675 76.675
846 76.675 73.50
847 76.675 67.15
848 76.675 60.80
DELETE NODES 31 57 2
DELETE NODES 89 115 2
DELETE NODES 147 173 2
DELETE NODES 205 231 2
DELETE NODES 263 289 2
DELETE NODES 321 347 2
DELETE NODES 379 405 2
DELETE NODES 437 463 2
DELETE NODES 495 521 2
DELETE NODES 553 579 2
DELETE NODES 611 637 2
DELETE NODES 669 695 2
DELETE NODES 727 753 2
DELETE NODES 785 811 2
QPM8 GEOMETRIC PROPERTIES

```
 1   25.6  25.6  25.6  25.6  25.6  25.6  25.6  25.6
 QPM4  GEOMETRIC PROPERTIES
2   25.6  25.6  25.6  25.6
GEOMETRIC ASSIGNMENTS
1   196  1    1
197  201  1    2
C          ***Brick properties***
MATERIAL PROPERTIES NONLINEAR 24
1   3500  0.17  6.0    0.1    0.40   0.0001   5
C          ***Mortar properties***
MATERIAL PROPERTIES NONLINEAR 24
2   800  0.10    1.5    0.1    0.18   0.0001   5
C          ***Steel corner shoe properties***
MATERIAL PROPERTIES
3   200.0E3   0.3
MATERIAL ASSIGNMENTS
1   2    1    1
3   10   1    1
11   11   0    2
12   14   1    1
15   15   0    1
16   24   1    1
25   25   0    2
26   28   1    1
29   42   1    2
43   45   1    1
46   46   0    2
47   59   1    1
60   60   0    2
61   70   1    1
71   84   1    2
85   94   1    1
95   95   0    2
96   108   1    1
109  109   0    2
110  112   1    1
113  126   1    2
127  129   1    1
130  130   0    2
131  143   1    1
144  144   0    2
145  154   1    1
155  168   1    2
169  178   1    1
179  179   0    2
180  181   1    1
182  182   0    1
183  192   1    1
193  193   0    2
194  194   0    1
195  196   1    1
197  201   1    3
CARTESIAN SETS MATRIX
1   0.7071067812  -0.7071067812  0.7071067812  0.7071067812
TRANSFORMED FREEDOMS
1   848  1    1
SUPPORT NODES
1   3    1        R  R
```

```
30  30   0     R  R
59  59   0     R  R
837 841  1     R  F
812 812  0     R  F
783 783  0     R  F
754 754  0     R  F
725 725  0     R  F
842 848  1     R  R
LOAD CASE TITLE     "Diagonal compression total=0.30mm over 50 increments"
PDSP  2
845 845  0     0.00   -0.30
ELEMENT OUTPUT
1   196  1     0
NODE OUTPUT
421 421  0     0
NONLINEAR CONTROL
INCREMENTATION  0.02      0      1      4     0      0      0
ITERATIONS  20     4      0.5
NR
FIRST MNR
INC  20
CONVERGENCE   0      0       5       5       0
OUTPUT    20       50        1       0      0
TERMINATION   1
END
```

B.3 Square wallette (finer mesh) LUSAS input data file.

```
PROBLEM TITLE     NONLINEAR ANALYSIS  - Diagonal Compression  - ALT20M.DAT
UNITS N mm
OPTION  18 26 27 44 55 62 115 139
QPM8   ELEMENT TOPOLOGY
FIRST  1     1  2   3   38  73  72  71  36
INC    1     2  2   2   2   2   2   2   2    17
INC    17   70  70  70  70  70  70  70  70   19
SOLUTION ORDER AUTOMATIC
NODE COORDINATES
1       0.0     0.0
2       6.0     0.0
3       12.0    0.0
4       18.0    0.0
5       24.0    0.0
6       25.5    0.0
7       27.0    0.0
8       33.0    0.0
9       39.0    0.0
10      45.0    0.0
11      51.0    0.0
12      52.5    0.0
13      54.0    0.0
14      60.0    0.0
15      66.0    0.0
16      72.0    0.0
17      78.0    0.0
18      79.5    0.0
```

```
19      81.0   0.0
20      87.0   0.0
21      93.0   0.0
22      99.0   0.0
23     105.0   0.0
24     106.5   0.0
25     108.0   0.0
26     114.0   0.0
27     120.0   0.0
28     126.0   0.0
29     132.0   0.0
30     133.5   0.0
31     135.0   0.0
32     141.0   0.0
33     147.0   0.0
34     153.0   0.0
35     159.0   0.0
1331     0.0 159.0
1332     6.0 159.0
1333    12.0 159.0
1334    18.0 159.0
1335    24.0 159.0
1336    25.5 159.0
1337    27.0 159.0
1338    33.0 159.0
1339    39.0 159.0
1340    45.0 159.0
1341    51.0 159.0
1342    52.5 159.0
1343    54.0 159.0
1344    60.0 159.0
1345    66.0 159.0
1346    72.0 159.0
1347    78.0 159.0
1348    79.5 159.0
1349    81.0 159.0
1350    87.0 159.0
1351    93.0 159.0
1352    99.0 159.0
1353   105.0 159.0
1354   106.5 159.0
1355   108.0 159.0
1356   114.0 159.0
1357   120.0 159.0
1358   126.0 159.0
1359   132.0 159.0
1360   133.5 159.0
1361   135.0 159.0
1362   141.0 159.0
1363   147.0 159.0
1364   153.0 159.0
1365   159.0 159.0
SPACING
1 1331 35     2*6.6 2*1.5  2*6.6 2*1.5  2*6.6 2*1.5  2*6.6 2*1.5 ...
          2*6.6 2*1.5  2*6.6 2*1.5  2*6.6 2*1.5  2*6.6 2*1.5 ...
          2*6.6 2*1.5  2*6.6
SPACING
2 1332 35     2*6.6 2*1.5  2*6.6 2*1.5  2*6.6 2*1.5  2*6.6 2*1.5 ...
```

2*6.6 2*1.5 2*6.6 2*1.5 2*6.6 2*1.5 2*6.6 2*1.5 ...
2*6.6 2*1.5 2*6.6
SPACING
3 1333 35 2*6.6 2*1.5 2*6.6 2*1.5 2*6.6 2*1.5 2*6.6 2*1.5 ...
2*6.6 2*1.5 2*6.6 2*1.5 2*6.6 2*1.5 2*6.6 2*1.5 ...
2*6.6 2*1.5 2*6.6
SPACING
4 1334 35 2*6.6 2*1.5 2*6.6 2*1.5 2*6.6 2*1.5 2*6.6 2*1.5 ...
2*6.6 2*1.5 2*6.6 2*1.5 2*6.6 2*1.5 2*6.6 2*1.5 ...
2*6.6 2*1.5 2*6.6
SPACING
5 1335 35 2*6.6 2*1.5 2*6.6 2*1.5 2*6.6 2*1.5 2*6.6 2*1.5 ...
2*6.6 2*1.5 2*6.6 2*1.5 2*6.6 2*1.5 2*6.6 2*1.5 ...
2*6.6 2*1.5 2*6.6
SPACING
6 1336 35 2*6.6 2*1.5 2*6.6 2*1.5 2*6.6 2*1.5 2*6.6 2*1.5 ...
2*6.6 2*1.5 2*6.6 2*1.5 2*6.6 2*1.5 2*6.6 2*1.5 ...
2*6.6 2*1.5 2*6.6
SPACING
7 1337 35 2*6.6 2*1.5 2*6.6 2*1.5 2*6.6 2*1.5 2*6.6 2*1.5 ...
2*6.6 2*1.5 2*6.6 2*1.5 2*6.6 2*1.5 2*6.6 2*1.5 ...
2*6.6 2*1.5 2*6.6
SPACING
8 1338 35 2*6.6 2*1.5 2*6.6 2*1.5 2*6.6 2*1.5 2*6.6 2*1.5 ...
2*6.6 2*1.5 2*6.6 2*1.5 2*6.6 2*1.5 2*6.6 2*1.5 ...
2*6.6 2*1.5 2*6.6
SPACING
9 1339 35 2*6.6 2*1.5 2*6.6 2*1.5 2*6.6 2*1.5 2*6.6 2*1.5 ...
2*6.6 2*1.5 2*6.6 2*1.5 2*6.6 2*1.5 2*6.6 2*1.5 ...
2*6.6 2*1.5 2*6.6
SPACING
10 1340 35 2*6.6 2*1.5 2*6.6 2*1.5 2*6.6 2*1.5 2*6.6 2*1.5 ...
2*6.6 2*1.5 2*6.6 2*1.5 2*6.6 2*1.5 2*6.6 2*1.5 ...
2*6.6 2*1.5 2*6.6
SPACING
11 1341 35 2*6.6 2*1.5 2*6.6 2*1.5 2*6.6 2*1.5 2*6.6 2*1.5 ...
2*6.6 2*1.5 2*6.6 2*1.5 2*6.6 2*1.5 2*6.6 2*1.5 ...
2*6.6 2*1.5 2*6.6
SPACING
12 1342 35 2*6.6 2*1.5 2*6.6 2*1.5 2*6.6 2*1.5 2*6.6 2*1.5 ...
2*6.6 2*1.5 2*6.6 2*1.5 2*6.6 2*1.5 2*6.6 2*1.5 ...
2*6.6 2*1.5 2*6.6
SPACING
13 1343 35 2*6.6 2*1.5 2*6.6 2*1.5 2*6.6 2*1.5 2*6.6 2*1.5 ...
2*6.6 2*1.5 2*6.6 2*1.5 2*6.6 2*1.5 2*6.6 2*1.5 ...
2*6.6 2*1.5 2*6.6
SPACING
14 1344 35 2*6.6 2*1.5 2*6.6 2*1.5 2*6.6 2*1.5 2*6.6 2*1.5 ...
2*6.6 2*1.5 2*6.6 2*1.5 2*6.6 2*1.5 2*6.6 2*1.5 ...
2*6.6 2*1.5 2*6.6
SPACING
15 1345 35 2*6.6 2*1.5 2*6.6 2*1.5 2*6.6 2*1.5 2*6.6 2*1.5 ...
2*6.6 2*1.5 2*6.6 2*1.5 2*6.6 2*1.5 2*6.6 2*1.5 ...
2*6.6 2*1.5 2*6.6
SPACING
16 1346 35 2*6.6 2*1.5 2*6.6 2*1.5 2*6.6 2*1.5 2*6.6 2*1.5 ...
2*6.6 2*1.5 2*6.6 2*1.5 2*6.6 2*1.5 2*6.6 2*1.5 ...
2*6.6 2*1.5 2*6.6

```
SPACING
17 1347 35     2*6.6 2*1.5  2*6.6 2*1.5  2*6.6 2*1.5  2*6.6 2*1.5 ...
           2*6.6 2*1.5  2*6.6 2*1.5  2*6.6 2*1.5  2*6.6 2*1.5 ...
           2*6.6 2*1.5  2*6.6
SPACING
18 1348 35     2*6.6 2*1.5  2*6.6 2*1.5  2*6.6 2*1.5  2*6.6 2*1.5 ...
           2*6.6 2*1.5  2*6.6 2*1.5  2*6.6 2*1.5  2*6.6 2*1.5 ...
           2*6.6 2*1.5  2*6.6
SPACING
19 1349 35     2*6.6 2*1.5  2*6.6 2*1.5  2*6.6 2*1.5  2*6.6 2*1.5 ...
           2*6.6 2*1.5  2*6.6 2*1.5  2*6.6 2*1.5  2*6.6 2*1.5 ...
           2*6.6 2*1.5  2*6.6
SPACING
20 1350 35     2*6.6 2*1.5  2*6.6 2*1.5  2*6.6 2*1.5  2*6.6 2*1.5 ...
           2*6.6 2*1.5  2*6.6 2*1.5  2*6.6 2*1.5  2*6.6 2*1.5 ...
           2*6.6 2*1.5  2*6.6
SPACING
21 1351 35     2*6.6 2*1.5  2*6.6 2*1.5  2*6.6 2*1.5  2*6.6 2*1.5 ...
           2*6.6 2*1.5  2*6.6 2*1.5  2*6.6 2*1.5  2*6.6 2*1.5 ...
           2*6.6 2*1.5  2*6.6
SPACING
22 1352 35     2*6.6 2*1.5  2*6.6 2*1.5  2*6.6 2*1.5  2*6.6 2*1.5 ...
           2*6.6 2*1.5  2*6.6 2*1.5  2*6.6 2*1.5  2*6.6 2*1.5 ...
           2*6.6 2*1.5  2*6.6
SPACING
23 1353 35     2*6.6 2*1.5  2*6.6 2*1.5  2*6.6 2*1.5  2*6.6 2*1.5 ...
           2*6.6 2*1.5  2*6.6 2*1.5  2*6.6 2*1.5  2*6.6 2*1.5 ...
           2*6.6 2*1.5  2*6.6
SPACING
24 1354 35     2*6.6 2*1.5  2*6.6 2*1.5  2*6.6 2*1.5  2*6.6 2*1.5 ...
           2*6.6 2*1.5  2*6.6 2*1.5  2*6.6 2*1.5  2*6.6 2*1.5 ...
           2*6.6 2*1.5  2*6.6
SPACING
25 1355 35     2*6.6 2*1.5  2*6.6 2*1.5  2*6.6 2*1.5  2*6.6 2*1.5 ...
           2*6.6 2*1.5  2*6.6 2*1.5  2*6.6 2*1.5  2*6.6 2*1.5 ...
           2*6.6 2*1.5  2*6.6
SPACING
26 1356 35     2*6.6 2*1.5  2*6.6 2*1.5  2*6.6 2*1.5  2*6.6 2*1.5 ...
           2*6.6 2*1.5  2*6.6 2*1.5  2*6.6 2*1.5  2*6.6 2*1.5 ...
           2*6.6 2*1.5  2*6.6
SPACING
27 1357 35     2*6.6 2*1.5  2*6.6 2*1.5  2*6.6 2*1.5  2*6.6 2*1.5 ...
           2*6.6 2*1.5  2*6.6 2*1.5  2*6.6 2*1.5  2*6.6 2*1.5 ...
           2*6.6 2*1.5  2*6.6
SPACING
28 1358 35     2*6.6 2*1.5  2*6.6 2*1.5  2*6.6 2*1.5  2*6.6 2*1.5 ...
           2*6.6 2*1.5  2*6.6 2*1.5  2*6.6 2*1.5  2*6.6 2*1.5 ...
           2*6.6 2*1.5  2*6.6
SPACING
29 1359 35     2*6.6 2*1.5  2*6.6 2*1.5  2*6.6 2*1.5  2*6.6 2*1.5 ...
           2*6.6 2*1.5  2*6.6 2*1.5  2*6.6 2*1.5  2*6.6 2*1.5 ...
           2*6.6 2*1.5  2*6.6
SPACING
30 1360 35     2*6.6 2*1.5  2*6.6 2*1.5  2*6.6 2*1.5  2*6.6 2*1.5 ...
           2*6.6 2*1.5  2*6.6 2*1.5  2*6.6 2*1.5  2*6.6 2*1.5 ...
           2*6.6 2*1.5  2*6.6
SPACING
31 1361 35     2*6.6 2*1.5  2*6.6 2*1.5  2*6.6 2*1.5  2*6.6 2*1.5 ...
```

```
          2*6.6 2*1.5  2*6.6 2*1.5  2*6.6 2*1.5  2*6.6 2*1.5 ...
          2*6.6 2*1.5  2*6.6
SPACING
32 1362 35    2*6.6 2*1.5  2*6.6 2*1.5  2*6.6 2*1.5  2*6.6 2*1.5 ...
          2*6.6 2*1.5  2*6.6 2*1.5  2*6.6 2*1.5  2*6.6 2*1.5 ...
          2*6.6 2*1.5  2*6.6
SPACING
33 1363 35    2*6.6 2*1.5  2*6.6 2*1.5  2*6.6 2*1.5  2*6.6 2*1.5 ...
          2*6.6 2*1.5  2*6.6 2*1.5  2*6.6 2*1.5  2*6.6 2*1.5 ...
          2*6.6 2*1.5  2*6.6
SPACING
34 1364 35    2*6.6 2*1.5  2*6.6 2*1.5  2*6.6 2*1.5  2*6.6 2*1.5 ...
          2*6.6 2*1.5  2*6.6 2*1.5  2*6.6 2*1.5  2*6.6 2*1.5 ...
          2*6.6 2*1.5  2*6.6
SPACING
35 1365 35    2*6.6 2*1.5  2*6.6 2*1.5  2*6.6 2*1.5  2*6.6 2*1.5 ...
          2*6.6 2*1.5  2*6.6 2*1.5  2*6.6 2*1.5  2*6.6 2*1.5 ...
          2*6.6 2*1.5  2*6.6
DELETE NODES  37   69   2
DELETE NODES  107  139  2
DELETE NODES  177  209  2
DELETE NODES  247  279  2
DELETE NODES  317  349  2
DELETE NODES  387  419  2
DELETE NODES  457  489  2
DELETE NODES  527  559  2
DELETE NODES  597  629  2
DELETE NODES  667  699  2
DELETE NODES  737  769  2
DELETE NODES  807  839  2
DELETE NODES  877  909  2
DELETE NODES  947  979  2
DELETE NODES  1017 1049 2
DELETE NODES  1087 1119 2
DELETE NODES  1157 1189 2
DELETE NODES  1227 1259 2
DELETE NODES  1297 1329 2
QPM8  GEOMETRIC PROPERTIES
1   25.6  25.6  25.6  25.6  25.6  25.6  25.6  25.6
GEOMETRIC ASSIGNMENTS
1  323  1   1
C          ***Brick properties***
MATERIAL PROPERTIES NONLINEAR 24
1   3000  0.14  6.0   0.3   0.20   0.0001   10
C          ***Mortar properties***
MATERIAL PROPERTIES NONLINEAR 24
2   1200  0.12   2.0   0.3   0.40   0.0001   10
MATERIAL ASSIGNMENTS
1 2 1  1
3 3 0  2
4 8 1  1
9 9 0  2
10 14 1  1
15 15 0  2
16 17 1  1
18 34 1  2
35 39 1  1
40 40 0  2
```

41 45 1 1
46 46 0 2
47 51 1 1
52 68 1 2
69 70 1 1
71 71 0 2
72 76 1 1
77 77 0 2
78 82 1 1
83 83 0 2
84 85 1 1
86 102 1 2
103 107 1 1
108 108 0 2
109 113 1 1
114 114 0 2
115 119 1 1
120 136 1 2
137 138 1 1
139 139 0 2
140 144 1 1
145 145 0 2
146 150 1 1
151 151 0 2
152 153 1 1
154 170 1 2
171 175 1 1
176 176 0 2
177 181 1 1
182 182 0 2
183 187 1 1
188 204 1 2
205 206 1 1
207 207 0 2
208 212 1 1
213 213 0 2
214 218 1 1
219 219 0 2
220 221 1 1
222 238 1 2
239 243 1 1
244 244 0 2
245 249 1 1
250 250 0 2
251 255 1 1
256 272 1 2
273 274 1 1
275 275 0 2
276 280 1 1
281 281 0 2
282 286 1 1
287 287 0 2
288 289 1 1
290 306 1 2
307 311 1 1
312 312 0 2
313 317 1 1
318 318 0 2

```
319 323 1  1
CARTESIAN SETS MATRIX
1  0.7071067812  -0.7071067812  0.7071067812  0.7071067812
TRANSFORMED FREEDOMS
1  1365  1   1
SUPPORT NODES
1     3     1     R  R
36    71     35    R  R
1363  1365   1     R  R
1295  1330   35    R  R
LOAD CASE TITLE  "Diagonal compression 0.50mm / 50 increments"
PDSP  2
1363   1365   1      0.00   -0.11
1295   1330   35     0.00   -0.11
ELEMENT OUTPUT
1    323    1     0
NODE OUTPUT
1365  1365  0     3
NONLINEAR CONTROL
INCREMENTATION  0.02       0      1      4     0       0       0
ITERATIONS  20     4      0.5
NR
FIRST MNR
INC  20
CONVERGENCE   0       0        5        5        0
OUTPUT    20        6         1         0       0
TERMINATION    1
END
```

B.4 Infill panel LUSAS data input file (eigenvalue analysis).

```
PROBLEM TITLE    NATURAL FREQUENCY ANALYSIS  - INFILL5R.DAT
UNITS N mm Kg
OPTION  18 26 27 44 55 62 115 139
QPM8   ELEMENT TOPOLOGY
FIRST   1     1   2   3   114  225  224  223  112
INC     1     2   2   2   2    2    2    2    2     55
INC     55    222 222 222 222  222  222  222  222   55
BEAM   ELEMENT TOPOLOGY
3026    1       12211
3027    12211   12321
3028    12321   111
SOLUTION ORDER AUTOMATIC
NODE COORDINATES
1       0       0
61      405     0
111     753     0
7105    0       256
7106    12      256
7107    24      256
7108    25.5    256
7109    27      256
7110    39      256
7111    51      256
```

7112 52.5 256
7113 54 256
7114 66 256
7115 78 256
7116 79.5 256
7117 81 256
7118 93 256
7119 105 256
7120 106.5 256
7121 108 256
7122 120 256
7123 132 256
7124 133.5 256
7125 135 256
7126 147 256
7127 159 256
7128 160.5 256
7129 162 256
7130 174 256
7131 186 256
7132 187.5 256
7133 189 256
7134 201 256
7135 213 256
7136 214.5 256
7137 216 256
7138 228 256
7139 240 256
7140 241.5 256
7141 243 256
7142 255 256
7143 267 256
7144 268.5 256
7145 270 256
7146 282 256
7147 294 256
7148 295.5 256
7149 297 256
7150 309 256
7151 321 256
7152 322.5 256
7153 324 256
7154 336 256
7155 348 256
7156 349.5 256
7157 351 256
7158 363 256
7159 375 256
7160 376.5 256
7161 378 256
7162 390 256
7163 402 256
7164 403.5 256
7165 405 256
7166 417 256
7167 429 256
7168 430.5 256
7169 432 256

```
7170   444    256
7171   456    256
7172   457.5  256
7173   459    256
7174   471    256
7175   483    256
7176   484.5  256
7177   486    256
7178   498    256
7179   510    256
7180   511.5  256
7181   513    256
7182   525    256
7183   537    256
7184   538.5  256
7185   540    256
7186   552    256
7187   564    256
7188   565.5  256
7189   567    256
7190   579    256
7191   591    256
7192   592.5  256
7193   594    256
7194   606    256
7195   618    256
7196   619.5  256
7197   621    256
7198   633    256
7199   645    256
7200   646.5  256
7201   648    256
7202   660    256
7203   672    256
7204   673.5  256
7205   675    256
7206   687    256
7207   699    256
7208   700.5  256
7209   702    256
7210   714    256
7211   726    256
7212   727.5  256
7213   729    256
7214   741    256
7215   753    256
12211   0.000    445.0
12271   405.0    445.0
12321   753.0    445.0
C ***Node generation split in two parts due to system overload**
SPACING
1  61  1  2*12 2*1.5 2*12 2*1.5 2*12 2*1.5 2*12 2*1.5 2*12 2*1.5 ...
           2*12 2*1.5 2*12 2*1.5 2*12 2*1.5 2*12 2*1.5 2*12 2*1.5 ...
           2*12 2*1.5 2*12 2*1.5 2*12 2*1.5 2*12 2*1.5 2*12 2*1.5
61 111 1  2*12 2*1.5 2*12 2*1.5 2*12 2*1.5 2*12 2*1.5 2*12 2*1.5 ...
           2*12 2*1.5 2*12 2*1.5 2*12 2*1.5 2*12 2*1.5 2*12 2*1.5 ...
           2*12 2*1.5 2*12 2*1.5 2*12
12211 12271 1  2*12 2*1.5 2*12 2*1.5 2*12 2*1.5 2*12 2*1.5 2*12 2*1.5 ...
```

```
                2*12 2*1.5 2*12 2*1.5 2*12 2*1.5 2*12 2*1.5 2*12 2*1.5 ...
                2*12 2*1.5 2*12 2*1.5 2*12 2*1.5 2*12 2*1.5 2*12 2*1.5
12271 12321 1  2*12 2*1.5 2*12 2*1.5 2*12 2*1.5 2*12 2*1.5 2*12 2*1.5 ...
                2*12 2*1.5 2*12 2*1.5 2*12 2*1.5 2*12 2*1.5 2*12 2*1.5 ...
                2*12 2*1.5 2*12 2*1.5 2*12
SPACING
1 7105 111 2*6.5 2*1.5 2*6.5 2*1.5 2*6.5 2*1.5 2*6.5 2*1.5 ...
                2*6.5 2*1.5 2*6.5 2*1.5 2*6.5 2*1.5 2*6.5 2*1.5 ...
                2*6.5 2*1.5 2*6.5 2*1.5 2*6.5 2*1.5 2*6.5 2*1.5 ...
                2*6.5 2*1.5 2*6.5 2*1.5 2*6.5 2*1.5 2*6.5 2*1.5
7105 12211 111 2*6.5 2*1.5 2*6.5 2*1.5 2*6.5 2*1.5 2*6.5 2*1.5 ...
                2*6.5 2*1.5 2*6.5 2*1.5 2*6.5 2*1.5 2*6.5 2*1.5 ...
                2*6.5 2*1.5 2*6.5 2*1.5 2*6.5 2*1.5 2*6.5
2 7106 111 2*6.5 2*1.5 2*6.5 2*1.5 2*6.5 2*1.5 2*6.5 2*1.5 ...
                2*6.5 2*1.5 2*6.5 2*1.5 2*6.5 2*1.5 2*6.5 2*1.5 ...
                2*6.5 2*1.5 2*6.5 2*1.5 2*6.5 2*1.5 2*6.5 2*1.5 ...
                2*6.5 2*1.5 2*6.5 2*1.5 2*6.5 2*1.5 2*6.5 2*1.5
7106 12212 111 2*6.5 2*1.5 2*6.5 2*1.5 2*6.5 2*1.5 2*6.5 2*1.5 ...
                2*6.5 2*1.5 2*6.5 2*1.5 2*6.5 2*1.5 2*6.5 2*1.5 ...
                2*6.5 2*1.5 2*6.5 2*1.5 2*6.5 2*1.5 2*6.5
3 7107 111 2*6.5 2*1.5 2*6.5 2*1.5 2*6.5 2*1.5 2*6.5 2*1.5 ...
                2*6.5 2*1.5 2*6.5 2*1.5 2*6.5 2*1.5 2*6.5 2*1.5 ...
                2*6.5 2*1.5 2*6.5 2*1.5 2*6.5 2*1.5 2*6.5 2*1.5 ...
                2*6.5 2*1.5 2*6.5 2*1.5 2*6.5 2*1.5 2*6.5 2*1.5
7107 12213 111 2*6.5 2*1.5 2*6.5 2*1.5 2*6.5 2*1.5 2*6.5 2*1.5 ...
                2*6.5 2*1.5 2*6.5 2*1.5 2*6.5 2*1.5 2*6.5 2*1.5 ...
                2*6.5 2*1.5 2*6.5 2*1.5 2*6.5 2*1.5 2*6.5
4 7108 111 2*6.5 2*1.5 2*6.5 2*1.5 2*6.5 2*1.5 2*6.5 2*1.5 ...
                2*6.5 2*1.5 2*6.5 2*1.5 2*6.5 2*1.5 2*6.5 2*1.5 ...
                2*6.5 2*1.5 2*6.5 2*1.5 2*6.5 2*1.5 2*6.5 2*1.5 ...
                2*6.5 2*1.5 2*6.5 2*1.5 2*6.5 2*1.5 2*6.5 2*1.5
7108 12214 111 2*6.5 2*1.5 2*6.5 2*1.5 2*6.5 2*1.5 2*6.5 2*1.5 ...
                2*6.5 2*1.5 2*6.5 2*1.5 2*6.5 2*1.5 2*6.5 2*1.5 ...
                2*6.5 2*1.5 2*6.5 2*1.5 2*6.5 2*1.5 2*6.5
5 7109 111 2*6.5 2*1.5 2*6.5 2*1.5 2*6.5 2*1.5 2*6.5 2*1.5 ...
                2*6.5 2*1.5 2*6.5 2*1.5 2*6.5 2*1.5 2*6.5 2*1.5 ...
                2*6.5 2*1.5 2*6.5 2*1.5 2*6.5 2*1.5 2*6.5 2*1.5 ...
                2*6.5 2*1.5 2*6.5 2*1.5 2*6.5 2*1.5 2*6.5 2*1.5
7109 12215 111 2*6.5 2*1.5 2*6.5 2*1.5 2*6.5 2*1.5 2*6.5 2*1.5 ...
                2*6.5 2*1.5 2*6.5 2*1.5 2*6.5 2*1.5 2*6.5 2*1.5 ...
                2*6.5 2*1.5 2*6.5 2*1.5 2*6.5 2*1.5 2*6.5
6 7110 111 2*6.5 2*1.5 2*6.5 2*1.5 2*6.5 2*1.5 2*6.5 2*1.5 ...
                2*6.5 2*1.5 2*6.5 2*1.5 2*6.5 2*1.5 2*6.5 2*1.5 ...
                2*6.5 2*1.5 2*6.5 2*1.5 2*6.5 2*1.5 2*6.5 2*1.5 ...
                2*6.5 2*1.5 2*6.5 2*1.5 2*6.5 2*1.5 2*6.5 2*1.5
7110 12216 111 2*6.5 2*1.5 2*6.5 2*1.5 2*6.5 2*1.5 2*6.5 2*1.5 ...
                2*6.5 2*1.5 2*6.5 2*1.5 2*6.5 2*1.5 2*6.5 2*1.5 ...
                2*6.5 2*1.5 2*6.5 2*1.5 2*6.5 2*1.5 2*6.5
7 7111 111 2*6.5 2*1.5 2*6.5 2*1.5 2*6.5 2*1.5 2*6.5 2*1.5 ...
                2*6.5 2*1.5 2*6.5 2*1.5 2*6.5 2*1.5 2*6.5 2*1.5 ...
                2*6.5 2*1.5 2*6.5 2*1.5 2*6.5 2*1.5 2*6.5 2*1.5 ...
                2*6.5 2*1.5 2*6.5 2*1.5 2*6.5 2*1.5 2*6.5 2*1.5
7111 12217 111 2*6.5 2*1.5 2*6.5 2*1.5 2*6.5 2*1.5 2*6.5 2*1.5 ...
                2*6.5 2*1.5 2*6.5 2*1.5 2*6.5 2*1.5 2*6.5 2*1.5 ...
                2*6.5 2*1.5 2*6.5 2*1.5 2*6.5 2*1.5 2*6.5
8 7112 111 2*6.5 2*1.5 2*6.5 2*1.5 2*6.5 2*1.5 2*6.5 2*1.5 ...
                2*6.5 2*1.5 2*6.5 2*1.5 2*6.5 2*1.5 2*6.5 2*1.5 ...
                2*6.5 2*1.5 2*6.5 2*1.5 2*6.5 2*1.5 2*6.5 2*1.5 ...
```

2*6.5 2*1.5 2*6.5 2*1.5 2*6.5 2*1.5 2*6.5 2*1.5
7112 12218 111 2*6.5 2*1.5 2*6.5 2*1.5 2*6.5 2*1.5 2*6.5 2*1.5 ...
2*6.5 2*1.5 2*6.5 2*1.5 2*6.5 2*1.5 2*6.5 2*1.5 ...
2*6.5 2*1.5 2*6.5 2*1.5 2*6.5 2*1.5 2*6.5
9 7113 111 2*6.5 2*1.5 2*6.5 2*1.5 2*6.5 2*1.5 2*6.5 2*1.5 ...
2*6.5 2*1.5 2*6.5 2*1.5 2*6.5 2*1.5 2*6.5 2*1.5 ...
2*6.5 2*1.5 2*6.5 2*1.5 2*6.5 2*1.5 2*6.5 2*1.5 ...
2*6.5 2*1.5 2*6.5 2*1.5 2*6.5 2*1.5 2*6.5 2*1.5
7113 12219 111 2*6.5 2*1.5 2*6.5 2*1.5 2*6.5 2*1.5 2*6.5 2*1.5 ...
2*6.5 2*1.5 2*6.5 2*1.5 2*6.5 2*1.5 2*6.5 2*1.5 ...
2*6.5 2*1.5 2*6.5 2*1.5 2*6.5 2*1.5 2*6.5
10 7114 111 2*6.5 2*1.5 2*6.5 2*1.5 2*6.5 2*1.5 2*6.5 2*1.5 ...
2*6.5 2*1.5 2*6.5 2*1.5 2*6.5 2*1.5 2*6.5 2*1.5 ...
2*6.5 2*1.5 2*6.5 2*1.5 2*6.5 2*1.5 2*6.5 2*1.5
7114 12220 111 2*6.5 2*1.5 2*6.5 2*1.5 2*6.5 2*1.5 2*6.5 2*1.5 ...
2*6.5 2*1.5 2*6.5 2*1.5 2*6.5 2*1.5 2*6.5 2*1.5 ...
2*6.5 2*1.5 2*6.5 2*1.5 2*6.5 2*1.5 2*6.5
11 7115 111 2*6.5 2*1.5 2*6.5 2*1.5 2*6.5 2*1.5 2*6.5 2*1.5 ...
2*6.5 2*1.5 2*6.5 2*1.5 2*6.5 2*1.5 2*6.5 2*1.5 ...
2*6.5 2*1.5 2*6.5 2*1.5 2*6.5 2*1.5 2*6.5 2*1.5 ...
2*6.5 2*1.5 2*6.5 2*1.5 2*6.5 2*1.5 2*6.5 2*1.5
7115 12221 111 2*6.5 2*1.5 2*6.5 2*1.5 2*6.5 2*1.5 2*6.5 2*1.5 ...
2*6.5 2*1.5 2*6.5 2*1.5 2*6.5 2*1.5 2*6.5 2*1.5 ...
2*6.5 2*1.5 2*6.5 2*1.5 2*6.5 2*1.5 2*6.5
12 7116 111 2*6.5 2*1.5 2*6.5 2*1.5 2*6.5 2*1.5 2*6.5 2*1.5 ...
2*6.5 2*1.5 2*6.5 2*1.5 2*6.5 2*1.5 2*6.5 2*1.5 ...
2*6.5 2*1.5 2*6.5 2*1.5 2*6.5 2*1.5 2*6.5 2*1.5 ...
2*6.5 2*1.5 2*6.5 2*1.5 2*6.5 2*1.5 2*6.5 2*1.5
7116 12222 111 2*6.5 2*1.5 2*6.5 2*1.5 2*6.5 2*1.5 2*6.5 2*1.5 ...
2*6.5 2*1.5 2*6.5 2*1.5 2*6.5 2*1.5 2*6.5 2*1.5 ...
2*6.5 2*1.5 2*6.5 2*1.5 2*6.5 2*1.5 2*6.5
13 7117 111 2*6.5 2*1.5 2*6.5 2*1.5 2*6.5 2*1.5 2*6.5 2*1.5 ...
2*6.5 2*1.5 2*6.5 2*1.5 2*6.5 2*1.5 2*6.5 2*1.5 ...
2*6.5 2*1.5 2*6.5 2*1.5 2*6.5 2*1.5 2*6.5 2*1.5 ...
2*6.5 2*1.5 2*6.5 2*1.5 2*6.5 2*1.5 2*6.5 2*1.5
7117 12223 111 2*6.5 2*1.5 2*6.5 2*1.5 2*6.5 2*1.5 2*6.5 2*1.5 ...
2*6.5 2*1.5 2*6.5 2*1.5 2*6.5 2*1.5 2*6.5 2*1.5 ...
2*6.5 2*1.5 2*6.5 2*1.5 2*6.5 2*1.5 2*6.5
14 7118 111 2*6.5 2*1.5 2*6.5 2*1.5 2*6.5 2*1.5 2*6.5 2*1.5 ...
2*6.5 2*1.5 2*6.5 2*1.5 2*6.5 2*1.5 2*6.5 2*1.5 ...
2*6.5 2*1.5 2*6.5 2*1.5 2*6.5 2*1.5 2*6.5 2*1.5 ...
2*6.5 2*1.5 2*6.5 2*1.5 2*6.5 2*1.5 2*6.5 2*1.5
7118 12224 111 2*6.5 2*1.5 2*6.5 2*1.5 2*6.5 2*1.5 2*6.5 2*1.5 ...
2*6.5 2*1.5 2*6.5 2*1.5 2*6.5 2*1.5 2*6.5 2*1.5 ...
2*6.5 2*1.5 2*6.5 2*1.5 2*6.5 2*1.5 2*6.5
15 7119 111 2*6.5 2*1.5 2*6.5 2*1.5 2*6.5 2*1.5 2*6.5 2*1.5 ...
2*6.5 2*1.5 2*6.5 2*1.5 2*6.5 2*1.5 2*6.5 2*1.5 ...
2*6.5 2*1.5 2*6.5 2*1.5 2*6.5 2*1.5 2*6.5 2*1.5
7119 12225 111 2*6.5 2*1.5 2*6.5 2*1.5 2*6.5 2*1.5 2*6.5 2*1.5 ...
2*6.5 2*1.5 2*6.5 2*1.5 2*6.5 2*1.5 2*6.5 2*1.5 ...
2*6.5 2*1.5 2*6.5 2*1.5 2*6.5 2*1.5 2*6.5
16 7120 111 2*6.5 2*1.5 2*6.5 2*1.5 2*6.5 2*1.5 2*6.5 2*1.5 ...
2*6.5 2*1.5 2*6.5 2*1.5 2*6.5 2*1.5 2*6.5 2*1.5 ...
2*6.5 2*1.5 2*6.5 2*1.5 2*6.5 2*1.5 2*6.5 2*1.5 ...
2*6.5 2*1.5 2*6.5 2*1.5 2*6.5 2*1.5 2*6.5 2*1.5
7120 12226 111 2*6.5 2*1.5 2*6.5 2*1.5 2*6.5 2*1.5 2*6.5 2*1.5 ...

2*6.5 2*1.5 2*6.5 2*1.5 2*6.5 2*1.5 2*6.5 2*1.5 ...
2*6.5 2*1.5 2*6.5 2*1.5 2*6.5 2*1.5 2*6.5
17 7121 111 2*6.5 2*1.5 2*6.5 2*1.5 2*6.5 2*1.5 2*6.5 2*1.5 ...
2*6.5 2*1.5 2*6.5 2*1.5 2*6.5 2*1.5 2*6.5 2*1.5 ...
2*6.5 2*1.5 2*6.5 2*1.5 2*6.5 2*1.5 2*6.5 2*1.5 ...
2*6.5 2*1.5 2*6.5 2*1.5 2*6.5 2*1.5 2*6.5 2*1.5
7121 12227 111 2*6.5 2*1.5 2*6.5 2*1.5 2*6.5 2*1.5 2*6.5 2*1.5 ...
2*6.5 2*1.5 2*6.5 2*1.5 2*6.5 2*1.5 2*6.5 2*1.5 ...
2*6.5 2*1.5 2*6.5 2*1.5 2*6.5 2*1.5 2*6.5
18 7122 111 2*6.5 2*1.5 2*6.5 2*1.5 2*6.5 2*1.5 2*6.5 2*1.5 ...
2*6.5 2*1.5 2*6.5 2*1.5 2*6.5 2*1.5 2*6.5 2*1.5 ...
2*6.5 2*1.5 2*6.5 2*1.5 2*6.5 2*1.5 2*6.5 2*1.5 ...
2*6.5 2*1.5 2*6.5 2*1.5 2*6.5 2*1.5 2*6.5 2*1.5
7122 12228 111 2*6.5 2*1.5 2*6.5 2*1.5 2*6.5 2*1.5 2*6.5 2*1.5 ...
2*6.5 2*1.5 2*6.5 2*1.5 2*6.5 2*1.5 2*6.5 2*1.5 ...
2*6.5 2*1.5 2*6.5 2*1.5 2*6.5 2*1.5 2*6.5
19 7123 111 2*6.5 2*1.5 2*6.5 2*1.5 2*6.5 2*1.5 2*6.5 2*1.5 ...
2*6.5 2*1.5 2*6.5 2*1.5 2*6.5 2*1.5 2*6.5 2*1.5 ...
2*6.5 2*1.5 2*6.5 2*1.5 2*6.5 2*1.5 2*6.5 2*1.5 ...
2*6.5 2*1.5 2*6.5 2*1.5 2*6.5 2*1.5 2*6.5 2*1.5
7123 12229 111 2*6.5 2*1.5 2*6.5 2*1.5 2*6.5 2*1.5 2*6.5 2*1.5 ...
2*6.5 2*1.5 2*6.5 2*1.5 2*6.5 2*1.5 2*6.5 2*1.5 ...
2*6.5 2*1.5 2*6.5 2*1.5 2*6.5 2*1.5 2*6.5
20 7124 111 2*6.5 2*1.5 2*6.5 2*1.5 2*6.5 2*1.5 2*6.5 2*1.5 ...
2*6.5 2*1.5 2*6.5 2*1.5 2*6.5 2*1.5 2*6.5 2*1.5 ...
2*6.5 2*1.5 2*6.5 2*1.5 2*6.5 2*1.5 2*6.5 2*1.5 ...
2*6.5 2*1.5 2*6.5 2*1.5 2*6.5 2*1.5 2*6.5 2*1.5
7124 12230 111 2*6.5 2*1.5 2*6.5 2*1.5 2*6.5 2*1.5 2*6.5 2*1.5 ...
2*6.5 2*1.5 2*6.5 2*1.5 2*6.5 2*1.5 2*6.5 2*1.5 ...
2*6.5 2*1.5 2*6.5 2*1.5 2*6.5 2*1.5 2*6.5
21 7125 111 2*6.5 2*1.5 2*6.5 2*1.5 2*6.5 2*1.5 2*6.5 2*1.5 ...
2*6.5 2*1.5 2*6.5 2*1.5 2*6.5 2*1.5 2*6.5 2*1.5 ...
2*6.5 2*1.5 2*6.5 2*1.5 2*6.5 2*1.5 2*6.5 2*1.5 ...
2*6.5 2*1.5 2*6.5 2*1.5 2*6.5 2*1.5 2*6.5 2*1.5
7125 12231 111 2*6.5 2*1.5 2*6.5 2*1.5 2*6.5 2*1.5 2*6.5 2*1.5 ...
2*6.5 2*1.5 2*6.5 2*1.5 2*6.5 2*1.5 2*6.5 2*1.5 ...
2*6.5 2*1.5 2*6.5 2*1.5 2*6.5 2*1.5 2*6.5
22 7126 111 2*6.5 2*1.5 2*6.5 2*1.5 2*6.5 2*1.5 2*6.5 2*1.5 ...
2*6.5 2*1.5 2*6.5 2*1.5 2*6.5 2*1.5 2*6.5 2*1.5 ...
2*6.5 2*1.5 2*6.5 2*1.5 2*6.5 2*1.5 2*6.5 2*1.5 ...
2*6.5 2*1.5 2*6.5 2*1.5 2*6.5 2*1.5 2*6.5 2*1.5
7126 12232 111 2*6.5 2*1.5 2*6.5 2*1.5 2*6.5 2*1.5 2*6.5 2*1.5 ...
2*6.5 2*1.5 2*6.5 2*1.5 2*6.5 2*1.5 2*6.5 2*1.5 ...
2*6.5 2*1.5 2*6.5 2*1.5 2*6.5 2*1.5 2*6.5
23 7127 111 2*6.5 2*1.5 2*6.5 2*1.5 2*6.5 2*1.5 2*6.5 2*1.5 ...
2*6.5 2*1.5 2*6.5 2*1.5 2*6.5 2*1.5 2*6.5 2*1.5 ...
2*6.5 2*1.5 2*6.5 2*1.5 2*6.5 2*1.5 2*6.5 2*1.5 ...
2*6.5 2*1.5 2*6.5 2*1.5 2*6.5 2*1.5 2*6.5 2*1.5
7127 12233 111 2*6.5 2*1.5 2*6.5 2*1.5 2*6.5 2*1.5 2*6.5 2*1.5 ...
2*6.5 2*1.5 2*6.5 2*1.5 2*6.5 2*1.5 2*6.5 2*1.5 ...
2*6.5 2*1.5 2*6.5 2*1.5 2*6.5 2*1.5 2*6.5
24 7128 111 2*6.5 2*1.5 2*6.5 2*1.5 2*6.5 2*1.5 2*6.5 2*1.5 ...
2*6.5 2*1.5 2*6.5 2*1.5 2*6.5 2*1.5 2*6.5 2*1.5 ...
2*6.5 2*1.5 2*6.5 2*1.5 2*6.5 2*1.5 2*6.5 2*1.5 ...
2*6.5 2*1.5 2*6.5 2*1.5 2*6.5 2*1.5 2*6.5 2*1.5
7128 12234 111 2*6.5 2*1.5 2*6.5 2*1.5 2*6.5 2*1.5 2*6.5 2*1.5 ...
2*6.5 2*1.5 2*6.5 2*1.5 2*6.5 2*1.5 2*6.5 2*1.5 ...
2*6.5 2*1.5 2*6.5 2*1.5 2*6.5 2*1.5 2*6.5

25 7129 111 2*6.5 2*1.5 2*6.5 2*1.5 2*6.5 2*1.5 2*6.5 2*1.5 ...
2*6.5 2*1.5 2*6.5 2*1.5 2*6.5 2*1.5 2*6.5 2*1.5 ...
2*6.5 2*1.5 2*6.5 2*1.5 2*6.5 2*1.5 2*6.5 2*1.5 ...
2*6.5 2*1.5 2*6.5 2*1.5 2*6.5 2*1.5 2*6.5 2*1.5
7129 12235 111 2*6.5 2*1.5 2*6.5 2*1.5 2*6.5 2*1.5 2*6.5 2*1.5 ...
2*6.5 2*1.5 2*6.5 2*1.5 2*6.5 2*1.5 2*6.5 2*1.5 ...
2*6.5 2*1.5 2*6.5 2*1.5 2*6.5 2*1.5 2*6.5
26 7130 111 2*6.5 2*1.5 2*6.5 2*1.5 2*6.5 2*1.5 2*6.5 2*1.5 ...
2*6.5 2*1.5 2*6.5 2*1.5 2*6.5 2*1.5 2*6.5 2*1.5 ...
2*6.5 2*1.5 2*6.5 2*1.5 2*6.5 2*1.5 2*6.5 2*1.5 ...
2*6.5 2*1.5 2*6.5 2*1.5 2*6.5 2*1.5 2*6.5 2*1.5
7130 12236 111 2*6.5 2*1.5 2*6.5 2*1.5 2*6.5 2*1.5 2*6.5 2*1.5 ...
2*6.5 2*1.5 2*6.5 2*1.5 2*6.5 2*1.5 2*6.5 2*1.5 ...
2*6.5 2*1.5 2*6.5 2*1.5 2*6.5 2*1.5 2*6.5
27 7131 111 2*6.5 2*1.5 2*6.5 2*1.5 2*6.5 2*1.5 2*6.5 2*1.5 ...
2*6.5 2*1.5 2*6.5 2*1.5 2*6.5 2*1.5 2*6.5 2*1.5 ...
2*6.5 2*1.5 2*6.5 2*1.5 2*6.5 2*1.5 2*6.5 2*1.5 ...
2*6.5 2*1.5 2*6.5 2*1.5 2*6.5 2*1.5 2*6.5 2*1.5
7131 12237 111 2*6.5 2*1.5 2*6.5 2*1.5 2*6.5 2*1.5 2*6.5 2*1.5 ...
2*6.5 2*1.5 2*6.5 2*1.5 2*6.5 2*1.5 2*6.5 2*1.5 ...
2*6.5 2*1.5 2*6.5 2*1.5 2*6.5 2*1.5 2*6.5
28 7132 111 2*6.5 2*1.5 2*6.5 2*1.5 2*6.5 2*1.5 2*6.5 2*1.5 ...
2*6.5 2*1.5 2*6.5 2*1.5 2*6.5 2*1.5 2*6.5 2*1.5 ...
2*6.5 2*1.5 2*6.5 2*1.5 2*6.5 2*1.5 2*6.5 2*1.5 ...
2*6.5 2*1.5 2*6.5 2*1.5 2*6.5 2*1.5 2*6.5 2*1.5
7132 12238 111 2*6.5 2*1.5 2*6.5 2*1.5 2*6.5 2*1.5 2*6.5 2*1.5 ...
2*6.5 2*1.5 2*6.5 2*1.5 2*6.5 2*1.5 2*6.5 2*1.5 ...
2*6.5 2*1.5 2*6.5 2*1.5 2*6.5 2*1.5 2*6.5
29 7133 111 2*6.5 2*1.5 2*6.5 2*1.5 2*6.5 2*1.5 2*6.5 2*1.5 ...
2*6.5 2*1.5 2*6.5 2*1.5 2*6.5 2*1.5 2*6.5 2*1.5 ...
2*6.5 2*1.5 2*6.5 2*1.5 2*6.5 2*1.5 2*6.5 2*1.5
7133 12239 111 2*6.5 2*1.5 2*6.5 2*1.5 2*6.5 2*1.5 2*6.5 2*1.5 ...
2*6.5 2*1.5 2*6.5 2*1.5 2*6.5 2*1.5 2*6.5 2*1.5 ...
2*6.5 2*1.5 2*6.5 2*1.5 2*6.5 2*1.5 2*6.5
30 7134 111 2*6.5 2*1.5 2*6.5 2*1.5 2*6.5 2*1.5 2*6.5 2*1.5 ...
2*6.5 2*1.5 2*6.5 2*1.5 2*6.5 2*1.5 2*6.5 2*1.5 ...
2*6.5 2*1.5 2*6.5 2*1.5 2*6.5 2*1.5 2*6.5 2*1.5 ...
2*6.5 2*1.5 2*6.5 2*1.5 2*6.5 2*1.5 2*6.5 2*1.5
7134 12240 111 2*6.5 2*1.5 2*6.5 2*1.5 2*6.5 2*1.5 2*6.5 2*1.5 ...
2*6.5 2*1.5 2*6.5 2*1.5 2*6.5 2*1.5 2*6.5 2*1.5 ...
2*6.5 2*1.5 2*6.5 2*1.5 2*6.5 2*1.5 2*6.5
31 7135 111 2*6.5 2*1.5 2*6.5 2*1.5 2*6.5 2*1.5 2*6.5 2*1.5 ...
2*6.5 2*1.5 2*6.5 2*1.5 2*6.5 2*1.5 2*6.5 2*1.5 ...
2*6.5 2*1.5 2*6.5 2*1.5 2*6.5 2*1.5 2*6.5 2*1.5 ...
2*6.5 2*1.5 2*6.5 2*1.5 2*6.5 2*1.5 2*6.5 2*1.5
7135 12241 111 2*6.5 2*1.5 2*6.5 2*1.5 2*6.5 2*1.5 2*6.5 2*1.5 ...
2*6.5 2*1.5 2*6.5 2*1.5 2*6.5 2*1.5 2*6.5 2*1.5 ...
2*6.5 2*1.5 2*6.5 2*1.5 2*6.5 2*1.5 2*6.5
32 7136 111 2*6.5 2*1.5 2*6.5 2*1.5 2*6.5 2*1.5 2*6.5 2*1.5 ...
2*6.5 2*1.5 2*6.5 2*1.5 2*6.5 2*1.5 2*6.5 2*1.5 ...
2*6.5 2*1.5 2*6.5 2*1.5 2*6.5 2*1.5 2*6.5 2*1.5 ...
2*6.5 2*1.5 2*6.5 2*1.5 2*6.5 2*1.5 2*6.5 2*1.5
7136 12242 111 2*6.5 2*1.5 2*6.5 2*1.5 2*6.5 2*1.5 2*6.5 2*1.5 ...
2*6.5 2*1.5 2*6.5 2*1.5 2*6.5 2*1.5 2*6.5 2*1.5 ...
2*6.5 2*1.5 2*6.5 2*1.5 2*6.5 2*1.5 2*6.5
33 7137 111 2*6.5 2*1.5 2*6.5 2*1.5 2*6.5 2*1.5 2*6.5 2*1.5 ...
2*6.5 2*1.5 2*6.5 2*1.5 2*6.5 2*1.5 2*6.5 2*1.5 ...

2*6.5 2*1.5 2*6.5 2*1.5 2*6.5 2*1.5 2*6.5 2*1.5 ...
2*6.5 2*1.5 2*6.5 2*1.5 2*6.5 2*1.5 2*6.5 2*1.5
7137 12243 111 2*6.5 2*1.5 2*6.5 2*1.5 2*6.5 2*1.5 2*6.5 2*1.5 ...
2*6.5 2*1.5 2*6.5 2*1.5 2*6.5 2*1.5 2*6.5 2*1.5 ...
2*6.5 2*1.5 2*6.5 2*1.5 2*6.5 2*1.5 2*6.5
34 7138 111 2*6.5 2*1.5 2*6.5 2*1.5 2*6.5 2*1.5 2*6.5 2*1.5 ...
2*6.5 2*1.5 2*6.5 2*1.5 2*6.5 2*1.5 2*6.5 2*1.5 ...
2*6.5 2*1.5 2*6.5 2*1.5 2*6.5 2*1.5 2*6.5 2*1.5 ...
2*6.5 2*1.5 2*6.5 2*1.5 2*6.5 2*1.5 2*6.5 2*1.5
7138 12244 111 2*6.5 2*1.5 2*6.5 2*1.5 2*6.5 2*1.5 2*6.5 2*1.5 ...
2*6.5 2*1.5 2*6.5 2*1.5 2*6.5 2*1.5 2*6.5 2*1.5 ...
2*6.5 2*1.5 2*6.5 2*1.5 2*6.5 2*1.5 2*6.5
35 7139 111 2*6.5 2*1.5 2*6.5 2*1.5 2*6.5 2*1.5 2*6.5 2*1.5 ...
2*6.5 2*1.5 2*6.5 2*1.5 2*6.5 2*1.5 2*6.5 2*1.5 ...
2*6.5 2*1.5 2*6.5 2*1.5 2*6.5 2*1.5 2*6.5 2*1.5 ...
2*6.5 2*1.5 2*6.5 2*1.5 2*6.5 2*1.5 2*6.5 2*1.5
7139 12245 111 2*6.5 2*1.5 2*6.5 2*1.5 2*6.5 2*1.5 2*6.5 2*1.5 ...
2*6.5 2*1.5 2*6.5 2*1.5 2*6.5 2*1.5 2*6.5 2*1.5 ...
2*6.5 2*1.5 2*6.5 2*1.5 2*6.5 2*1.5 2*6.5
36 7140 111 2*6.5 2*1.5 2*6.5 2*1.5 2*6.5 2*1.5 2*6.5 2*1.5 ...
2*6.5 2*1.5 2*6.5 2*1.5 2*6.5 2*1.5 2*6.5 2*1.5 ...
2*6.5 2*1.5 2*6.5 2*1.5 2*6.5 2*1.5 2*6.5 2*1.5 ...
2*6.5 2*1.5 2*6.5 2*1.5 2*6.5 2*1.5 2*6.5 2*1.5
7140 12246 111 2*6.5 2*1.5 2*6.5 2*1.5 2*6.5 2*1.5 2*6.5 2*1.5 ...
2*6.5 2*1.5 2*6.5 2*1.5 2*6.5 2*1.5 2*6.5 2*1.5 ...
2*6.5 2*1.5 2*6.5 2*1.5 2*6.5 2*1.5 2*6.5
37 7141 111 2*6.5 2*1.5 2*6.5 2*1.5 2*6.5 2*1.5 2*6.5 2*1.5 ...
2*6.5 2*1.5 2*6.5 2*1.5 2*6.5 2*1.5 2*6.5 2*1.5 ...
2*6.5 2*1.5 2*6.5 2*1.5 2*6.5 2*1.5 2*6.5 2*1.5 ...
2*6.5 2*1.5 2*6.5 2*1.5 2*6.5 2*1.5 2*6.5 2*1.5
7141 12247 111 2*6.5 2*1.5 2*6.5 2*1.5 2*6.5 2*1.5 2*6.5 2*1.5 ...
2*6.5 2*1.5 2*6.5 2*1.5 2*6.5 2*1.5 2*6.5 2*1.5 ...
2*6.5 2*1.5 2*6.5 2*1.5 2*6.5 2*1.5 2*6.5
38 7142 111 2*6.5 2*1.5 2*6.5 2*1.5 2*6.5 2*1.5 2*6.5 2*1.5 ...
2*6.5 2*1.5 2*6.5 2*1.5 2*6.5 2*1.5 2*6.5 2*1.5 ...
2*6.5 2*1.5 2*6.5 2*1.5 2*6.5 2*1.5 2*6.5 2*1.5 ...
2*6.5 2*1.5 2*6.5 2*1.5 2*6.5 2*1.5 2*6.5 2*1.5
7142 12248 111 2*6.5 2*1.5 2*6.5 2*1.5 2*6.5 2*1.5 2*6.5 2*1.5 ...
2*6.5 2*1.5 2*6.5 2*1.5 2*6.5 2*1.5 2*6.5 2*1.5 ...
2*6.5 2*1.5 2*6.5 2*1.5 2*6.5 2*1.5 2*6.5
39 7143 111 2*6.5 2*1.5 2*6.5 2*1.5 2*6.5 2*1.5 2*6.5 2*1.5 ...
2*6.5 2*1.5 2*6.5 2*1.5 2*6.5 2*1.5 2*6.5 2*1.5 ...
2*6.5 2*1.5 2*6.5 2*1.5 2*6.5 2*1.5 2*6.5 2*1.5 ...
2*6.5 2*1.5 2*6.5 2*1.5 2*6.5 2*1.5 2*6.5 2*1.5
7143 12249 111 2*6.5 2*1.5 2*6.5 2*1.5 2*6.5 2*1.5 2*6.5 2*1.5 ...
2*6.5 2*1.5 2*6.5 2*1.5 2*6.5 2*1.5 2*6.5 2*1.5 ...
2*6.5 2*1.5 2*6.5 2*1.5 2*6.5 2*1.5 2*6.5
40 7144 111 2*6.5 2*1.5 2*6.5 2*1.5 2*6.5 2*1.5 2*6.5 2*1.5 ...
2*6.5 2*1.5 2*6.5 2*1.5 2*6.5 2*1.5 2*6.5 2*1.5 ...
2*6.5 2*1.5 2*6.5 2*1.5 2*6.5 2*1.5 2*6.5 2*1.5 ...
2*6.5 2*1.5 2*6.5 2*1.5 2*6.5 2*1.5 2*6.5 2*1.5
7144 12250 111 2*6.5 2*1.5 2*6.5 2*1.5 2*6.5 2*1.5 2*6.5 2*1.5 ...
2*6.5 2*1.5 2*6.5 2*1.5 2*6.5 2*1.5 2*6.5 2*1.5 ...
2*6.5 2*1.5 2*6.5 2*1.5 2*6.5 2*1.5 2*6.5
41 7145 111 2*6.5 2*1.5 2*6.5 2*1.5 2*6.5 2*1.5 2*6.5 2*1.5 ...
2*6.5 2*1.5 2*6.5 2*1.5 2*6.5 2*1.5 2*6.5 2*1.5 ...
2*6.5 2*1.5 2*6.5 2*1.5 2*6.5 2*1.5 2*6.5 2*1.5 ...
2*6.5 2*1.5 2*6.5 2*1.5 2*6.5 2*1.5 2*6.5 2*1.5

7145 12251 111 2*6.5 2*1.5 2*6.5 2*1.5 2*6.5 2*1.5 2*6.5 2*1.5 ...
2*6.5 2*1.5 2*6.5 2*1.5 2*6.5 2*1.5 2*6.5 2*1.5 ...
2*6.5 2*1.5 2*6.5 2*1.5 2*6.5 2*1.5 2*6.5
42 7146 111 2*6.5 2*1.5 2*6.5 2*1.5 2*6.5 2*1.5 2*6.5 2*1.5 ...
2*6.5 2*1.5 2*6.5 2*1.5 2*6.5 2*1.5 2*6.5 2*1.5 ...
2*6.5 2*1.5 2*6.5 2*1.5 2*6.5 2*1.5 2*6.5 2*1.5 ...
2*6.5 2*1.5 2*6.5 2*1.5 2*6.5 2*1.5 2*6.5 2*1.5
7146 12252 111 2*6.5 2*1.5 2*6.5 2*1.5 2*6.5 2*1.5 2*6.5 2*1.5 ...
2*6.5 2*1.5 2*6.5 2*1.5 2*6.5 2*1.5 2*6.5 2*1.5 ...
2*6.5 2*1.5 2*6.5 2*1.5 2*6.5 2*1.5 2*6.5
43 7147 111 2*6.5 2*1.5 2*6.5 2*1.5 2*6.5 2*1.5 2*6.5 2*1.5 ...
2*6.5 2*1.5 2*6.5 2*1.5 2*6.5 2*1.5 2*6.5 2*1.5 ...
2*6.5 2*1.5 2*6.5 2*1.5 2*6.5 2*1.5 2*6.5 2*1.5
7147 12253 111 2*6.5 2*1.5 2*6.5 2*1.5 2*6.5 2*1.5 2*6.5 2*1.5 ...
2*6.5 2*1.5 2*6.5 2*1.5 2*6.5 2*1.5 2*6.5 2*1.5 ...
2*6.5 2*1.5 2*6.5 2*1.5 2*6.5 2*1.5 2*6.5
44 7148 111 2*6.5 2*1.5 2*6.5 2*1.5 2*6.5 2*1.5 2*6.5 2*1.5 ...
2*6.5 2*1.5 2*6.5 2*1.5 2*6.5 2*1.5 2*6.5 2*1.5 ...
2*6.5 2*1.5 2*6.5 2*1.5 2*6.5 2*1.5 2*6.5 2*1.5 ...
2*6.5 2*1.5 2*6.5 2*1.5 2*6.5 2*1.5 2*6.5 2*1.5
7148 12254 111 2*6.5 2*1.5 2*6.5 2*1.5 2*6.5 2*1.5 2*6.5 2*1.5 ...
2*6.5 2*1.5 2*6.5 2*1.5 2*6.5 2*1.5 2*6.5 2*1.5 ...
2*6.5 2*1.5 2*6.5 2*1.5 2*6.5 2*1.5 2*6.5
45 7149 111 2*6.5 2*1.5 2*6.5 2*1.5 2*6.5 2*1.5 2*6.5 2*1.5 ...
2*6.5 2*1.5 2*6.5 2*1.5 2*6.5 2*1.5 2*6.5 2*1.5 ...
2*6.5 2*1.5 2*6.5 2*1.5 2*6.5 2*1.5 2*6.5 2*1.5 ...
2*6.5 2*1.5 2*6.5 2*1.5 2*6.5 2*1.5 2*6.5 2*1.5
7149 12255 111 2*6.5 2*1.5 2*6.5 2*1.5 2*6.5 2*1.5 2*6.5 2*1.5 ...
2*6.5 2*1.5 2*6.5 2*1.5 2*6.5 2*1.5 2*6.5 2*1.5 ...
2*6.5 2*1.5 2*6.5 2*1.5 2*6.5 2*1.5 2*6.5
46 7150 111 2*6.5 2*1.5 2*6.5 2*1.5 2*6.5 2*1.5 2*6.5 2*1.5 ...
2*6.5 2*1.5 2*6.5 2*1.5 2*6.5 2*1.5 2*6.5 2*1.5 ...
2*6.5 2*1.5 2*6.5 2*1.5 2*6.5 2*1.5 2*6.5 2*1.5 ...
2*6.5 2*1.5 2*6.5 2*1.5 2*6.5 2*1.5 2*6.5 2*1.5
7150 12256 111 2*6.5 2*1.5 2*6.5 2*1.5 2*6.5 2*1.5 2*6.5 2*1.5 ...
2*6.5 2*1.5 2*6.5 2*1.5 2*6.5 2*1.5 2*6.5 2*1.5 ...
2*6.5 2*1.5 2*6.5 2*1.5 2*6.5 2*1.5 2*6.5
47 7151 111 2*6.5 2*1.5 2*6.5 2*1.5 2*6.5 2*1.5 2*6.5 2*1.5 ...
2*6.5 2*1.5 2*6.5 2*1.5 2*6.5 2*1.5 2*6.5 2*1.5 ...
2*6.5 2*1.5 2*6.5 2*1.5 2*6.5 2*1.5 2*6.5 2*1.5 ...
2*6.5 2*1.5 2*6.5 2*1.5 2*6.5 2*1.5 2*6.5 2*1.5
7151 12257 111 2*6.5 2*1.5 2*6.5 2*1.5 2*6.5 2*1.5 2*6.5 2*1.5 ...
2*6.5 2*1.5 2*6.5 2*1.5 2*6.5 2*1.5 2*6.5 2*1.5 ...
2*6.5 2*1.5 2*6.5 2*1.5 2*6.5 2*1.5 2*6.5
48 7152 111 2*6.5 2*1.5 2*6.5 2*1.5 2*6.5 2*1.5 2*6.5 2*1.5 ...
2*6.5 2*1.5 2*6.5 2*1.5 2*6.5 2*1.5 2*6.5 2*1.5 ...
2*6.5 2*1.5 2*6.5 2*1.5 2*6.5 2*1.5 2*6.5 2*1.5
7152 12258 111 2*6.5 2*1.5 2*6.5 2*1.5 2*6.5 2*1.5 2*6.5 2*1.5 ...
2*6.5 2*1.5 2*6.5 2*1.5 2*6.5 2*1.5 2*6.5 2*1.5 ...
2*6.5 2*1.5 2*6.5 2*1.5 2*6.5 2*1.5 2*6.5
49 7153 111 2*6.5 2*1.5 2*6.5 2*1.5 2*6.5 2*1.5 2*6.5 2*1.5 ...
2*6.5 2*1.5 2*6.5 2*1.5 2*6.5 2*1.5 2*6.5 2*1.5 ...
2*6.5 2*1.5 2*6.5 2*1.5 2*6.5 2*1.5 2*6.5 2*1.5 ...
2*6.5 2*1.5 2*6.5 2*1.5 2*6.5 2*1.5 2*6.5 2*1.5
7153 12259 111 2*6.5 2*1.5 2*6.5 2*1.5 2*6.5 2*1.5 2*6.5 2*1.5 ...
2*6.5 2*1.5 2*6.5 2*1.5 2*6.5 2*1.5 2*6.5 2*1.5 ...

2*6.5 2*1.5 2*6.5 2*1.5 2*6.5 2*1.5 2*6.5
50 7154 111 2*6.5 2*1.5 2*6.5 2*1.5 2*6.5 2*1.5 2*6.5 2*1.5 ...
2*6.5 2*1.5 2*6.5 2*1.5 2*6.5 2*1.5 2*6.5 2*1.5 ...
2*6.5 2*1.5 2*6.5 2*1.5 2*6.5 2*1.5 2*6.5 2*1.5 ...
2*6.5 2*1.5 2*6.5 2*1.5 2*6.5 2*1.5 2*6.5 2*1.5
7154 12260 111 2*6.5 2*1.5 2*6.5 2*1.5 2*6.5 2*1.5 2*6.5 2*1.5 ...
2*6.5 2*1.5 2*6.5 2*1.5 2*6.5 2*1.5 2*6.5 2*1.5 ...
2*6.5 2*1.5 2*6.5 2*1.5 2*6.5 2*1.5 2*6.5
51 7155 111 2*6.5 2*1.5 2*6.5 2*1.5 2*6.5 2*1.5 2*6.5 2*1.5 ...
2*6.5 2*1.5 2*6.5 2*1.5 2*6.5 2*1.5 2*6.5 2*1.5 ...
2*6.5 2*1.5 2*6.5 2*1.5 2*6.5 2*1.5 2*6.5 2*1.5 ...
2*6.5 2*1.5 2*6.5 2*1.5 2*6.5 2*1.5 2*6.5 2*1.5
7155 12261 111 2*6.5 2*1.5 2*6.5 2*1.5 2*6.5 2*1.5 2*6.5 2*1.5 ...
2*6.5 2*1.5 2*6.5 2*1.5 2*6.5 2*1.5 2*6.5 2*1.5 ...
2*6.5 2*1.5 2*6.5 2*1.5 2*6.5 2*1.5 2*6.5
52 7156 111 2*6.5 2*1.5 2*6.5 2*1.5 2*6.5 2*1.5 2*6.5 2*1.5 ...
2*6.5 2*1.5 2*6.5 2*1.5 2*6.5 2*1.5 2*6.5 2*1.5 ...
2*6.5 2*1.5 2*6.5 2*1.5 2*6.5 2*1.5 2*6.5 2*1.5 ...
2*6.5 2*1.5 2*6.5 2*1.5 2*6.5 2*1.5 2*6.5 2*1.5
7156 12262 111 2*6.5 2*1.5 2*6.5 2*1.5 2*6.5 2*1.5 2*6.5 2*1.5 ...
2*6.5 2*1.5 2*6.5 2*1.5 2*6.5 2*1.5 2*6.5 2*1.5 ...
2*6.5 2*1.5 2*6.5 2*1.5 2*6.5 2*1.5 2*6.5
53 7157 111 2*6.5 2*1.5 2*6.5 2*1.5 2*6.5 2*1.5 2*6.5 2*1.5 ...
2*6.5 2*1.5 2*6.5 2*1.5 2*6.5 2*1.5 2*6.5 2*1.5 ...
2*6.5 2*1.5 2*6.5 2*1.5 2*6.5 2*1.5 2*6.5 2*1.5 ...
2*6.5 2*1.5 2*6.5 2*1.5 2*6.5 2*1.5 2*6.5 2*1.5
7157 12263 111 2*6.5 2*1.5 2*6.5 2*1.5 2*6.5 2*1.5 2*6.5 2*1.5 ...
2*6.5 2*1.5 2*6.5 2*1.5 2*6.5 2*1.5 2*6.5 2*1.5 ...
2*6.5 2*1.5 2*6.5 2*1.5 2*6.5 2*1.5 2*6.5
54 7158 111 2*6.5 2*1.5 2*6.5 2*1.5 2*6.5 2*1.5 2*6.5 2*1.5 ...
2*6.5 2*1.5 2*6.5 2*1.5 2*6.5 2*1.5 2*6.5 2*1.5 ...
2*6.5 2*1.5 2*6.5 2*1.5 2*6.5 2*1.5 2*6.5 2*1.5 ...
2*6.5 2*1.5 2*6.5 2*1.5 2*6.5 2*1.5 2*6.5 2*1.5
7158 12264 111 2*6.5 2*1.5 2*6.5 2*1.5 2*6.5 2*1.5 2*6.5 2*1.5 ...
2*6.5 2*1.5 2*6.5 2*1.5 2*6.5 2*1.5 2*6.5 2*1.5 ...
2*6.5 2*1.5 2*6.5 2*1.5 2*6.5 2*1.5 2*6.5
55 7159 111 2*6.5 2*1.5 2*6.5 2*1.5 2*6.5 2*1.5 2*6.5 2*1.5 ...
2*6.5 2*1.5 2*6.5 2*1.5 2*6.5 2*1.5 2*6.5 2*1.5 ...
2*6.5 2*1.5 2*6.5 2*1.5 2*6.5 2*1.5 2*6.5 2*1.5 ...
2*6.5 2*1.5 2*6.5 2*1.5 2*6.5 2*1.5 2*6.5 2*1.5
7159 12265 111 2*6.5 2*1.5 2*6.5 2*1.5 2*6.5 2*1.5 2*6.5 2*1.5 ...
2*6.5 2*1.5 2*6.5 2*1.5 2*6.5 2*1.5 2*6.5 2*1.5 ...
2*6.5 2*1.5 2*6.5 2*1.5 2*6.5 2*1.5 2*6.5
56 7160 111 2*6.5 2*1.5 2*6.5 2*1.5 2*6.5 2*1.5 2*6.5 2*1.5 ...
2*6.5 2*1.5 2*6.5 2*1.5 2*6.5 2*1.5 2*6.5 2*1.5 ...
2*6.5 2*1.5 2*6.5 2*1.5 2*6.5 2*1.5 2*6.5 2*1.5 ...
2*6.5 2*1.5 2*6.5 2*1.5 2*6.5 2*1.5 2*6.5 2*1.5
7160 12266 111 2*6.5 2*1.5 2*6.5 2*1.5 2*6.5 2*1.5 2*6.5 2*1.5 ...
2*6.5 2*1.5 2*6.5 2*1.5 2*6.5 2*1.5 2*6.5 2*1.5 ...
2*6.5 2*1.5 2*6.5 2*1.5 2*6.5 2*1.5 2*6.5
57 7161 111 2*6.5 2*1.5 2*6.5 2*1.5 2*6.5 2*1.5 2*6.5 2*1.5 ...
2*6.5 2*1.5 2*6.5 2*1.5 2*6.5 2*1.5 2*6.5 2*1.5 ...
2*6.5 2*1.5 2*6.5 2*1.5 2*6.5 2*1.5 2*6.5 2*1.5 ...
2*6.5 2*1.5 2*6.5 2*1.5 2*6.5 2*1.5 2*6.5 2*1.5
7161 12267 111 2*6.5 2*1.5 2*6.5 2*1.5 2*6.5 2*1.5 2*6.5 2*1.5 ...
2*6.5 2*1.5 2*6.5 2*1.5 2*6.5 2*1.5 2*6.5 2*1.5 ...
2*6.5 2*1.5 2*6.5 2*1.5 2*6.5 2*1.5 2*6.5
58 7162 111 2*6.5 2*1.5 2*6.5 2*1.5 2*6.5 2*1.5 2*6.5 2*1.5 ...

2*6.5 2*1.5 2*6.5 2*1.5 2*6.5 2*1.5 2*6.5 2*1.5 ...
2*6.5 2*1.5 2*6.5 2*1.5 2*6.5 2*1.5 2*6.5 2*1.5 ...
2*6.5 2*1.5 2*6.5 2*1.5 2*6.5 2*1.5 2*6.5 2*1.5
7162 12268 111 2*6.5 2*1.5 2*6.5 2*1.5 2*6.5 2*1.5 2*6.5 2*1.5 ...
2*6.5 2*1.5 2*6.5 2*1.5 2*6.5 2*1.5 2*6.5 2*1.5 ...
2*6.5 2*1.5 2*6.5 2*1.5 2*6.5 2*1.5 2*6.5
59 7163 111 2*6.5 2*1.5 2*6.5 2*1.5 2*6.5 2*1.5 2*6.5 2*1.5 ...
2*6.5 2*1.5 2*6.5 2*1.5 2*6.5 2*1.5 2*6.5 2*1.5 ...
2*6.5 2*1.5 2*6.5 2*1.5 2*6.5 2*1.5 2*6.5 2*1.5 ...
2*6.5 2*1.5 2*6.5 2*1.5 2*6.5 2*1.5 2*6.5 2*1.5
7163 12269 111 2*6.5 2*1.5 2*6.5 2*1.5 2*6.5 2*1.5 2*6.5 2*1.5 ...
2*6.5 2*1.5 2*6.5 2*1.5 2*6.5 2*1.5 2*6.5 2*1.5 ...
2*6.5 2*1.5 2*6.5 2*1.5 2*6.5 2*1.5 2*6.5
60 7164 111 2*6.5 2*1.5 2*6.5 2*1.5 2*6.5 2*1.5 2*6.5 2*1.5 ...
2*6.5 2*1.5 2*6.5 2*1.5 2*6.5 2*1.5 2*6.5 2*1.5 ...
2*6.5 2*1.5 2*6.5 2*1.5 2*6.5 2*1.5 2*6.5 2*1.5 ...
2*6.5 2*1.5 2*6.5 2*1.5 2*6.5 2*1.5 2*6.5 2*1.5
7164 12270 111 2*6.5 2*1.5 2*6.5 2*1.5 2*6.5 2*1.5 2*6.5 2*1.5 ...
2*6.5 2*1.5 2*6.5 2*1.5 2*6.5 2*1.5 2*6.5 2*1.5 ...
2*6.5 2*1.5 2*6.5 2*1.5 2*6.5 2*1.5 2*6.5
61 7165 111 2*6.5 2*1.5 2*6.5 2*1.5 2*6.5 2*1.5 2*6.5 2*1.5 ...
2*6.5 2*1.5 2*6.5 2*1.5 2*6.5 2*1.5 2*6.5 2*1.5 ...
2*6.5 2*1.5 2*6.5 2*1.5 2*6.5 2*1.5 2*6.5 2*1.5 ...
2*6.5 2*1.5 2*6.5 2*1.5 2*6.5 2*1.5 2*6.5 2*1.5
7165 12271 111 2*6.5 2*1.5 2*6.5 2*1.5 2*6.5 2*1.5 2*6.5 2*1.5 ...
2*6.5 2*1.5 2*6.5 2*1.5 2*6.5 2*1.5 2*6.5 2*1.5 ...
2*6.5 2*1.5 2*6.5 2*1.5 2*6.5 2*1.5 2*6.5
62 7166 111 2*6.5 2*1.5 2*6.5 2*1.5 2*6.5 2*1.5 2*6.5 2*1.5 ...
2*6.5 2*1.5 2*6.5 2*1.5 2*6.5 2*1.5 2*6.5 2*1.5 ...
2*6.5 2*1.5 2*6.5 2*1.5 2*6.5 2*1.5 2*6.5 2*1.5 ...
2*6.5 2*1.5 2*6.5 2*1.5 2*6.5 2*1.5 2*6.5 2*1.5
7166 12272 111 2*6.5 2*1.5 2*6.5 2*1.5 2*6.5 2*1.5 2*6.5 2*1.5 ...
2*6.5 2*1.5 2*6.5 2*1.5 2*6.5 2*1.5 2*6.5 2*1.5 ...
2*6.5 2*1.5 2*6.5 2*1.5 2*6.5 2*1.5 2*6.5
63 7167 111 2*6.5 2*1.5 2*6.5 2*1.5 2*6.5 2*1.5 2*6.5 2*1.5 ...
2*6.5 2*1.5 2*6.5 2*1.5 2*6.5 2*1.5 2*6.5 2*1.5 ...
2*6.5 2*1.5 2*6.5 2*1.5 2*6.5 2*1.5 2*6.5 2*1.5 ...
2*6.5 2*1.5 2*6.5 2*1.5 2*6.5 2*1.5 2*6.5 2*1.5
7167 12273 111 2*6.5 2*1.5 2*6.5 2*1.5 2*6.5 2*1.5 2*6.5 2*1.5 ...
2*6.5 2*1.5 2*6.5 2*1.5 2*6.5 2*1.5 2*6.5 2*1.5 ...
2*6.5 2*1.5 2*6.5 2*1.5 2*6.5 2*1.5 2*6.5
64 7168 111 2*6.5 2*1.5 2*6.5 2*1.5 2*6.5 2*1.5 2*6.5 2*1.5 ...
2*6.5 2*1.5 2*6.5 2*1.5 2*6.5 2*1.5 2*6.5 2*1.5 ...
2*6.5 2*1.5 2*6.5 2*1.5 2*6.5 2*1.5 2*6.5 2*1.5 ...
2*6.5 2*1.5 2*6.5 2*1.5 2*6.5 2*1.5 2*6.5 2*1.5
7168 12274 111 2*6.5 2*1.5 2*6.5 2*1.5 2*6.5 2*1.5 2*6.5 2*1.5 ...
2*6.5 2*1.5 2*6.5 2*1.5 2*6.5 2*1.5 2*6.5 2*1.5 ...
2*6.5 2*1.5 2*6.5 2*1.5 2*6.5 2*1.5 2*6.5
65 7169 111 2*6.5 2*1.5 2*6.5 2*1.5 2*6.5 2*1.5 2*6.5 2*1.5 ...
2*6.5 2*1.5 2*6.5 2*1.5 2*6.5 2*1.5 2*6.5 2*1.5 ...
2*6.5 2*1.5 2*6.5 2*1.5 2*6.5 2*1.5 2*6.5 2*1.5 ...
2*6.5 2*1.5 2*6.5 2*1.5 2*6.5 2*1.5 2*6.5 2*1.5
7169 12275 111 2*6.5 2*1.5 2*6.5 2*1.5 2*6.5 2*1.5 2*6.5 2*1.5 ...
2*6.5 2*1.5 2*6.5 2*1.5 2*6.5 2*1.5 2*6.5 2*1.5 ...
2*6.5 2*1.5 2*6.5 2*1.5 2*6.5 2*1.5 2*6.5
66 7170 111 2*6.5 2*1.5 2*6.5 2*1.5 2*6.5 2*1.5 2*6.5 2*1.5 ...
2*6.5 2*1.5 2*6.5 2*1.5 2*6.5 2*1.5 2*6.5 2*1.5 ...
2*6.5 2*1.5 2*6.5 2*1.5 2*6.5 2*1.5 2*6.5 2*1.5 ...

2*6.5 2*1.5 2*6.5 2*1.5 2*6.5 2*1.5 2*6.5 2*1.5
7170 12276 111 2*6.5 2*1.5 2*6.5 2*1.5 2*6.5 2*1.5 2*6.5 2*1.5 ...
2*6.5 2*1.5 2*6.5 2*1.5 2*6.5 2*1.5 2*6.5 2*1.5 ...
2*6.5 2*1.5 2*6.5 2*1.5 2*6.5 2*1.5 2*6.5
67 7171 111 2*6.5 2*1.5 2*6.5 2*1.5 2*6.5 2*1.5 2*6.5 2*1.5 ...
2*6.5 2*1.5 2*6.5 2*1.5 2*6.5 2*1.5 2*6.5 2*1.5 ...
2*6.5 2*1.5 2*6.5 2*1.5 2*6.5 2*1.5 2*6.5 2*1.5 ...
2*6.5 2*1.5 2*6.5 2*1.5 2*6.5 2*1.5 2*6.5 2*1.5
7171 12277 111 2*6.5 2*1.5 2*6.5 2*1.5 2*6.5 2*1.5 2*6.5 2*1.5 ...
2*6.5 2*1.5 2*6.5 2*1.5 2*6.5 2*1.5 2*6.5 2*1.5 ...
2*6.5 2*1.5 2*6.5 2*1.5 2*6.5 2*1.5 2*6.5
68 7172 111 2*6.5 2*1.5 2*6.5 2*1.5 2*6.5 2*1.5 2*6.5 2*1.5 ...
2*6.5 2*1.5 2*6.5 2*1.5 2*6.5 2*1.5 2*6.5 2*1.5 ...
2*6.5 2*1.5 2*6.5 2*1.5 2*6.5 2*1.5 2*6.5 2*1.5
7172 12278 111 2*6.5 2*1.5 2*6.5 2*1.5 2*6.5 2*1.5 2*6.5 2*1.5 ...
2*6.5 2*1.5 2*6.5 2*1.5 2*6.5 2*1.5 2*6.5 2*1.5 ...
2*6.5 2*1.5 2*6.5 2*1.5 2*6.5 2*1.5 2*6.5
69 7173 111 2*6.5 2*1.5 2*6.5 2*1.5 2*6.5 2*1.5 2*6.5 2*1.5 ...
2*6.5 2*1.5 2*6.5 2*1.5 2*6.5 2*1.5 2*6.5 2*1.5 ...
2*6.5 2*1.5 2*6.5 2*1.5 2*6.5 2*1.5 2*6.5 2*1.5 ...
2*6.5 2*1.5 2*6.5 2*1.5 2*6.5 2*1.5 2*6.5 2*1.5
7173 12279 111 2*6.5 2*1.5 2*6.5 2*1.5 2*6.5 2*1.5 2*6.5 2*1.5 ...
2*6.5 2*1.5 2*6.5 2*1.5 2*6.5 2*1.5 2*6.5 2*1.5 ...
2*6.5 2*1.5 2*6.5 2*1.5 2*6.5 2*1.5 2*6.5
70 7174 111 2*6.5 2*1.5 2*6.5 2*1.5 2*6.5 2*1.5 2*6.5 2*1.5 ...
2*6.5 2*1.5 2*6.5 2*1.5 2*6.5 2*1.5 2*6.5 2*1.5 ...
2*6.5 2*1.5 2*6.5 2*1.5 2*6.5 2*1.5 2*6.5 2*1.5 ...
2*6.5 2*1.5 2*6.5 2*1.5 2*6.5 2*1.5 2*6.5 2*1.5
7174 12280 111 2*6.5 2*1.5 2*6.5 2*1.5 2*6.5 2*1.5 2*6.5 2*1.5 ...
2*6.5 2*1.5 2*6.5 2*1.5 2*6.5 2*1.5 2*6.5 2*1.5 ...
2*6.5 2*1.5 2*6.5 2*1.5 2*6.5 2*1.5 2*6.5
71 7175 111 2*6.5 2*1.5 2*6.5 2*1.5 2*6.5 2*1.5 2*6.5 2*1.5 ...
2*6.5 2*1.5 2*6.5 2*1.5 2*6.5 2*1.5 2*6.5 2*1.5 ...
2*6.5 2*1.5 2*6.5 2*1.5 2*6.5 2*1.5 2*6.5 2*1.5 ...
2*6.5 2*1.5 2*6.5 2*1.5 2*6.5 2*1.5 2*6.5 2*1.5
7175 12281 111 2*6.5 2*1.5 2*6.5 2*1.5 2*6.5 2*1.5 2*6.5 2*1.5 ...
2*6.5 2*1.5 2*6.5 2*1.5 2*6.5 2*1.5 2*6.5 2*1.5 ...
2*6.5 2*1.5 2*6.5 2*1.5 2*6.5 2*1.5 2*6.5
72 7176 111 2*6.5 2*1.5 2*6.5 2*1.5 2*6.5 2*1.5 2*6.5 2*1.5 ...
2*6.5 2*1.5 2*6.5 2*1.5 2*6.5 2*1.5 2*6.5 2*1.5 ...
2*6.5 2*1.5 2*6.5 2*1.5 2*6.5 2*1.5 2*6.5 2*1.5 ...
2*6.5 2*1.5 2*6.5 2*1.5 2*6.5 2*1.5 2*6.5 2*1.5
7176 12282 111 2*6.5 2*1.5 2*6.5 2*1.5 2*6.5 2*1.5 2*6.5 2*1.5 ...
2*6.5 2*1.5 2*6.5 2*1.5 2*6.5 2*1.5 2*6.5 2*1.5 ...
2*6.5 2*1.5 2*6.5 2*1.5 2*6.5 2*1.5 2*6.5
73 7177 111 2*6.5 2*1.5 2*6.5 2*1.5 2*6.5 2*1.5 2*6.5 2*1.5 ...
2*6.5 2*1.5 2*6.5 2*1.5 2*6.5 2*1.5 2*6.5 2*1.5 ...
2*6.5 2*1.5 2*6.5 2*1.5 2*6.5 2*1.5 2*6.5 2*1.5
7177 12283 111 2*6.5 2*1.5 2*6.5 2*1.5 2*6.5 2*1.5 2*6.5 2*1.5 ...
2*6.5 2*1.5 2*6.5 2*1.5 2*6.5 2*1.5 2*6.5 2*1.5 ...
2*6.5 2*1.5 2*6.5 2*1.5 2*6.5 2*1.5 2*6.5
74 7178 111 2*6.5 2*1.5 2*6.5 2*1.5 2*6.5 2*1.5 2*6.5 2*1.5 ...
2*6.5 2*1.5 2*6.5 2*1.5 2*6.5 2*1.5 2*6.5 2*1.5 ...
2*6.5 2*1.5 2*6.5 2*1.5 2*6.5 2*1.5 2*6.5 2*1.5 ...
2*6.5 2*1.5 2*6.5 2*1.5 2*6.5 2*1.5 2*6.5 2*1.5
7178 12284 111 2*6.5 2*1.5 2*6.5 2*1.5 2*6.5 2*1.5 2*6.5 2*1.5 ...

2*6.5 2*1.5 2*6.5 2*1.5 2*6.5 2*1.5 2*6.5 2*1.5 ...
2*6.5 2*1.5 2*6.5 2*1.5 2*6.5 2*1.5 2*6.5
75 7179 111 2*6.5 2*1.5 2*6.5 2*1.5 2*6.5 2*1.5 2*6.5 2*1.5 ...
2*6.5 2*1.5 2*6.5 2*1.5 2*6.5 2*1.5 2*6.5 2*1.5 ...
2*6.5 2*1.5 2*6.5 2*1.5 2*6.5 2*1.5 2*6.5 2*1.5 ...
2*6.5 2*1.5 2*6.5 2*1.5 2*6.5 2*1.5 2*6.5 2*1.5
7179 12285 111 2*6.5 2*1.5 2*6.5 2*1.5 2*6.5 2*1.5 2*6.5 2*1.5 ...
2*6.5 2*1.5 2*6.5 2*1.5 2*6.5 2*1.5 2*6.5 2*1.5 ...
2*6.5 2*1.5 2*6.5 2*1.5 2*6.5 2*1.5 2*6.5
76 7180 111 2*6.5 2*1.5 2*6.5 2*1.5 2*6.5 2*1.5 2*6.5 2*1.5 ...
2*6.5 2*1.5 2*6.5 2*1.5 2*6.5 2*1.5 2*6.5 2*1.5 ...
2*6.5 2*1.5 2*6.5 2*1.5 2*6.5 2*1.5 2*6.5 2*1.5 ...
2*6.5 2*1.5 2*6.5 2*1.5 2*6.5 2*1.5 2*6.5 2*1.5
7180 12286 111 2*6.5 2*1.5 2*6.5 2*1.5 2*6.5 2*1.5 2*6.5 2*1.5 ...
2*6.5 2*1.5 2*6.5 2*1.5 2*6.5 2*1.5 2*6.5 2*1.5 ...
2*6.5 2*1.5 2*6.5 2*1.5 2*6.5 2*1.5 2*6.5
77 7181 111 2*6.5 2*1.5 2*6.5 2*1.5 2*6.5 2*1.5 2*6.5 2*1.5 ...
2*6.5 2*1.5 2*6.5 2*1.5 2*6.5 2*1.5 2*6.5 2*1.5 ...
2*6.5 2*1.5 2*6.5 2*1.5 2*6.5 2*1.5 2*6.5 2*1.5 ...
2*6.5 2*1.5 2*6.5 2*1.5 2*6.5 2*1.5 2*6.5 2*1.5
7181 12287 111 2*6.5 2*1.5 2*6.5 2*1.5 2*6.5 2*1.5 2*6.5 2*1.5 ...
2*6.5 2*1.5 2*6.5 2*1.5 2*6.5 2*1.5 2*6.5 2*1.5 ...
2*6.5 2*1.5 2*6.5 2*1.5 2*6.5 2*1.5 2*6.5
78 7182 111 2*6.5 2*1.5 2*6.5 2*1.5 2*6.5 2*1.5 2*6.5 2*1.5 ...
2*6.5 2*1.5 2*6.5 2*1.5 2*6.5 2*1.5 2*6.5 2*1.5 ...
2*6.5 2*1.5 2*6.5 2*1.5 2*6.5 2*1.5 2*6.5 2*1.5 ...
2*6.5 2*1.5 2*6.5 2*1.5 2*6.5 2*1.5 2*6.5 2*1.5
7182 12288 111 2*6.5 2*1.5 2*6.5 2*1.5 2*6.5 2*1.5 2*6.5 2*1.5 ...
2*6.5 2*1.5 2*6.5 2*1.5 2*6.5 2*1.5 2*6.5 2*1.5 ...
2*6.5 2*1.5 2*6.5 2*1.5 2*6.5 2*1.5 2*6.5
79 7183 111 2*6.5 2*1.5 2*6.5 2*1.5 2*6.5 2*1.5 2*6.5 2*1.5 ...
2*6.5 2*1.5 2*6.5 2*1.5 2*6.5 2*1.5 2*6.5 2*1.5 ...
2*6.5 2*1.5 2*6.5 2*1.5 2*6.5 2*1.5 2*6.5 2*1.5 ...
2*6.5 2*1.5 2*6.5 2*1.5 2*6.5 2*1.5 2*6.5 2*1.5
7183 12289 111 2*6.5 2*1.5 2*6.5 2*1.5 2*6.5 2*1.5 2*6.5 2*1.5 ...
2*6.5 2*1.5 2*6.5 2*1.5 2*6.5 2*1.5 2*6.5 2*1.5 ...
2*6.5 2*1.5 2*6.5 2*1.5 2*6.5 2*1.5 2*6.5
80 7184 111 2*6.5 2*1.5 2*6.5 2*1.5 2*6.5 2*1.5 2*6.5 2*1.5 ...
2*6.5 2*1.5 2*6.5 2*1.5 2*6.5 2*1.5 2*6.5 2*1.5 ...
2*6.5 2*1.5 2*6.5 2*1.5 2*6.5 2*1.5 2*6.5 2*1.5 ...
2*6.5 2*1.5 2*6.5 2*1.5 2*6.5 2*1.5 2*6.5 2*1.5
7184 12290 111 2*6.5 2*1.5 2*6.5 2*1.5 2*6.5 2*1.5 2*6.5 2*1.5 ...
2*6.5 2*1.5 2*6.5 2*1.5 2*6.5 2*1.5 2*6.5 2*1.5 ...
2*6.5 2*1.5 2*6.5 2*1.5 2*6.5 2*1.5 2*6.5
81 7185 111 2*6.5 2*1.5 2*6.5 2*1.5 2*6.5 2*1.5 2*6.5 2*1.5 ...
2*6.5 2*1.5 2*6.5 2*1.5 2*6.5 2*1.5 2*6.5 2*1.5 ...
2*6.5 2*1.5 2*6.5 2*1.5 2*6.5 2*1.5 2*6.5 2*1.5 ...
2*6.5 2*1.5 2*6.5 2*1.5 2*6.5 2*1.5 2*6.5 2*1.5
7185 12291 111 2*6.5 2*1.5 2*6.5 2*1.5 2*6.5 2*1.5 2*6.5 2*1.5 ...
2*6.5 2*1.5 2*6.5 2*1.5 2*6.5 2*1.5 2*6.5 2*1.5 ...
2*6.5 2*1.5 2*6.5 2*1.5 2*6.5 2*1.5 2*6.5
82 7186 111 2*6.5 2*1.5 2*6.5 2*1.5 2*6.5 2*1.5 2*6.5 2*1.5 ...
2*6.5 2*1.5 2*6.5 2*1.5 2*6.5 2*1.5 2*6.5 2*1.5 ...
2*6.5 2*1.5 2*6.5 2*1.5 2*6.5 2*1.5 2*6.5 2*1.5 ...
2*6.5 2*1.5 2*6.5 2*1.5 2*6.5 2*1.5 2*6.5 2*1.5
7186 12292 111 2*6.5 2*1.5 2*6.5 2*1.5 2*6.5 2*1.5 2*6.5 2*1.5 ...
2*6.5 2*1.5 2*6.5 2*1.5 2*6.5 2*1.5 2*6.5 2*1.5 ...
2*6.5 2*1.5 2*6.5 2*1.5 2*6.5 2*1.5 2*6.5

83 7187 111 2*6.5 2*1.5 2*6.5 2*1.5 2*6.5 2*1.5 2*6.5 2*1.5 ...
2*6.5 2*1.5 2*6.5 2*1.5 2*6.5 2*1.5 2*6.5 2*1.5 ...
2*6.5 2*1.5 2*6.5 2*1.5 2*6.5 2*1.5 2*6.5 2*1.5 ...
2*6.5 2*1.5 2*6.5 2*1.5 2*6.5 2*1.5 2*6.5 2*1.5
7187 12293 111 2*6.5 2*1.5 2*6.5 2*1.5 2*6.5 2*1.5 2*6.5 2*1.5 ...
2*6.5 2*1.5 2*6.5 2*1.5 2*6.5 2*1.5 2*6.5 2*1.5 ...
2*6.5 2*1.5 2*6.5 2*1.5 2*6.5 2*1.5 2*6.5
84 7188 111 2*6.5 2*1.5 2*6.5 2*1.5 2*6.5 2*1.5 2*6.5 2*1.5 ...
2*6.5 2*1.5 2*6.5 2*1.5 2*6.5 2*1.5 2*6.5 2*1.5 ...
2*6.5 2*1.5 2*6.5 2*1.5 2*6.5 2*1.5 2*6.5 2*1.5 ...
2*6.5 2*1.5 2*6.5 2*1.5 2*6.5 2*1.5 2*6.5 2*1.5
7188 12294 111 2*6.5 2*1.5 2*6.5 2*1.5 2*6.5 2*1.5 2*6.5 2*1.5 ...
2*6.5 2*1.5 2*6.5 2*1.5 2*6.5 2*1.5 2*6.5 2*1.5 ...
2*6.5 2*1.5 2*6.5 2*1.5 2*6.5 2*1.5 2*6.5
85 7189 111 2*6.5 2*1.5 2*6.5 2*1.5 2*6.5 2*1.5 2*6.5 2*1.5 ...
2*6.5 2*1.5 2*6.5 2*1.5 2*6.5 2*1.5 2*6.5 2*1.5 ...
2*6.5 2*1.5 2*6.5 2*1.5 2*6.5 2*1.5 2*6.5 2*1.5 ...
2*6.5 2*1.5 2*6.5 2*1.5 2*6.5 2*1.5 2*6.5 2*1.5
7189 12295 111 2*6.5 2*1.5 2*6.5 2*1.5 2*6.5 2*1.5 2*6.5 2*1.5 ...
2*6.5 2*1.5 2*6.5 2*1.5 2*6.5 2*1.5 2*6.5 2*1.5 ...
2*6.5 2*1.5 2*6.5 2*1.5 2*6.5 2*1.5 2*6.5
86 7190 111 2*6.5 2*1.5 2*6.5 2*1.5 2*6.5 2*1.5 2*6.5 2*1.5 ...
2*6.5 2*1.5 2*6.5 2*1.5 2*6.5 2*1.5 2*6.5 2*1.5 ...
2*6.5 2*1.5 2*6.5 2*1.5 2*6.5 2*1.5 2*6.5 2*1.5 ...
2*6.5 2*1.5 2*6.5 2*1.5 2*6.5 2*1.5 2*6.5 2*1.5
7190 12296 111 2*6.5 2*1.5 2*6.5 2*1.5 2*6.5 2*1.5 2*6.5 2*1.5 ...
2*6.5 2*1.5 2*6.5 2*1.5 2*6.5 2*1.5 2*6.5 2*1.5 ...
2*6.5 2*1.5 2*6.5 2*1.5 2*6.5 2*1.5 2*6.5
87 7191 111 2*6.5 2*1.5 2*6.5 2*1.5 2*6.5 2*1.5 2*6.5 2*1.5 ...
2*6.5 2*1.5 2*6.5 2*1.5 2*6.5 2*1.5 2*6.5 2*1.5 ...
2*6.5 2*1.5 2*6.5 2*1.5 2*6.5 2*1.5 2*6.5 2*1.5
7191 12297 111 2*6.5 2*1.5 2*6.5 2*1.5 2*6.5 2*1.5 2*6.5 2*1.5 ...
2*6.5 2*1.5 2*6.5 2*1.5 2*6.5 2*1.5 2*6.5 2*1.5 ...
2*6.5 2*1.5 2*6.5 2*1.5 2*6.5 2*1.5 2*6.5
88 7192 111 2*6.5 2*1.5 2*6.5 2*1.5 2*6.5 2*1.5 2*6.5 2*1.5 ...
2*6.5 2*1.5 2*6.5 2*1.5 2*6.5 2*1.5 2*6.5 2*1.5 ...
2*6.5 2*1.5 2*6.5 2*1.5 2*6.5 2*1.5 2*6.5 2*1.5 ...
2*6.5 2*1.5 2*6.5 2*1.5 2*6.5 2*1.5 2*6.5 2*1.5
7192 12298 111 2*6.5 2*1.5 2*6.5 2*1.5 2*6.5 2*1.5 2*6.5 2*1.5 ...
2*6.5 2*1.5 2*6.5 2*1.5 2*6.5 2*1.5 2*6.5 2*1.5 ...
2*6.5 2*1.5 2*6.5 2*1.5 2*6.5 2*1.5 2*6.5
89 7193 111 2*6.5 2*1.5 2*6.5 2*1.5 2*6.5 2*1.5 2*6.5 2*1.5 ...
2*6.5 2*1.5 2*6.5 2*1.5 2*6.5 2*1.5 2*6.5 2*1.5 ...
2*6.5 2*1.5 2*6.5 2*1.5 2*6.5 2*1.5 2*6.5 2*1.5 ...
2*6.5 2*1.5 2*6.5 2*1.5 2*6.5 2*1.5 2*6.5 2*1.5
7193 12299 111 2*6.5 2*1.5 2*6.5 2*1.5 2*6.5 2*1.5 2*6.5 2*1.5 ...
2*6.5 2*1.5 2*6.5 2*1.5 2*6.5 2*1.5 2*6.5 2*1.5 ...
2*6.5 2*1.5 2*6.5 2*1.5 2*6.5 2*1.5 2*6.5
90 7194 111 2*6.5 2*1.5 2*6.5 2*1.5 2*6.5 2*1.5 2*6.5 2*1.5 ...
2*6.5 2*1.5 2*6.5 2*1.5 2*6.5 2*1.5 2*6.5 2*1.5 ...
2*6.5 2*1.5 2*6.5 2*1.5 2*6.5 2*1.5 2*6.5 2*1.5 ...
2*6.5 2*1.5 2*6.5 2*1.5 2*6.5 2*1.5 2*6.5 2*1.5
7194 12300 111 2*6.5 2*1.5 2*6.5 2*1.5 2*6.5 2*1.5 2*6.5 2*1.5 ...
2*6.5 2*1.5 2*6.5 2*1.5 2*6.5 2*1.5 2*6.5 2*1.5 ...
2*6.5 2*1.5 2*6.5 2*1.5 2*6.5 2*1.5 2*6.5
91 7195 111 2*6.5 2*1.5 2*6.5 2*1.5 2*6.5 2*1.5 2*6.5 2*1.5 ...
2*6.5 2*1.5 2*6.5 2*1.5 2*6.5 2*1.5 2*6.5 2*1.5 ...

2*6.5 2*1.5 2*6.5 2*1.5 2*6.5 2*1.5 2*6.5 2*1.5 ...
2*6.5 2*1.5 2*6.5 2*1.5 2*6.5 2*1.5 2*6.5 2*1.5
7195 12301 111 2*6.5 2*1.5 2*6.5 2*1.5 2*6.5 2*1.5 2*6.5 2*1.5 ...
2*6.5 2*1.5 2*6.5 2*1.5 2*6.5 2*1.5 2*6.5 2*1.5 ...
2*6.5 2*1.5 2*6.5 2*1.5 2*6.5 2*1.5 2*6.5
92 7196 111 2*6.5 2*1.5 2*6.5 2*1.5 2*6.5 2*1.5 2*6.5 2*1.5 ...
2*6.5 2*1.5 2*6.5 2*1.5 2*6.5 2*1.5 2*6.5 2*1.5 ...
2*6.5 2*1.5 2*6.5 2*1.5 2*6.5 2*1.5 2*6.5 2*1.5 ...
2*6.5 2*1.5 2*6.5 2*1.5 2*6.5 2*1.5 2*6.5 2*1.5
7196 12302 111 2*6.5 2*1.5 2*6.5 2*1.5 2*6.5 2*1.5 2*6.5 2*1.5 ...
2*6.5 2*1.5 2*6.5 2*1.5 2*6.5 2*1.5 2*6.5 2*1.5 ...
2*6.5 2*1.5 2*6.5 2*1.5 2*6.5 2*1.5 2*6.5
93 7197 111 2*6.5 2*1.5 2*6.5 2*1.5 2*6.5 2*1.5 2*6.5 2*1.5 ...
2*6.5 2*1.5 2*6.5 2*1.5 2*6.5 2*1.5 2*6.5 2*1.5 ...
2*6.5 2*1.5 2*6.5 2*1.5 2*6.5 2*1.5 2*6.5 2*1.5 ...
2*6.5 2*1.5 2*6.5 2*1.5 2*6.5 2*1.5 2*6.5 2*1.5
7197 12303 111 2*6.5 2*1.5 2*6.5 2*1.5 2*6.5 2*1.5 2*6.5 2*1.5 ...
2*6.5 2*1.5 2*6.5 2*1.5 2*6.5 2*1.5 2*6.5 2*1.5 ...
2*6.5 2*1.5 2*6.5 2*1.5 2*6.5 2*1.5 2*6.5
94 7198 111 2*6.5 2*1.5 2*6.5 2*1.5 2*6.5 2*1.5 2*6.5 2*1.5 ...
2*6.5 2*1.5 2*6.5 2*1.5 2*6.5 2*1.5 2*6.5 2*1.5 ...
2*6.5 2*1.5 2*6.5 2*1.5 2*6.5 2*1.5 2*6.5 2*1.5 ...
2*6.5 2*1.5 2*6.5 2*1.5 2*6.5 2*1.5 2*6.5 2*1.5
7198 12304 111 2*6.5 2*1.5 2*6.5 2*1.5 2*6.5 2*1.5 2*6.5 2*1.5 ...
2*6.5 2*1.5 2*6.5 2*1.5 2*6.5 2*1.5 2*6.5 2*1.5 ...
2*6.5 2*1.5 2*6.5 2*1.5 2*6.5 2*1.5 2*6.5
95 7199 111 2*6.5 2*1.5 2*6.5 2*1.5 2*6.5 2*1.5 2*6.5 2*1.5 ...
2*6.5 2*1.5 2*6.5 2*1.5 2*6.5 2*1.5 2*6.5 2*1.5 ...
2*6.5 2*1.5 2*6.5 2*1.5 2*6.5 2*1.5 2*6.5 2*1.5 ...
2*6.5 2*1.5 2*6.5 2*1.5 2*6.5 2*1.5 2*6.5 2*1.5
7199 12305 111 2*6.5 2*1.5 2*6.5 2*1.5 2*6.5 2*1.5 2*6.5 2*1.5 ...
2*6.5 2*1.5 2*6.5 2*1.5 2*6.5 2*1.5 2*6.5 2*1.5 ...
2*6.5 2*1.5 2*6.5 2*1.5 2*6.5 2*1.5 2*6.5
96 7200 111 2*6.5 2*1.5 2*6.5 2*1.5 2*6.5 2*1.5 2*6.5 2*1.5 ...
2*6.5 2*1.5 2*6.5 2*1.5 2*6.5 2*1.5 2*6.5 2*1.5 ...
2*6.5 2*1.5 2*6.5 2*1.5 2*6.5 2*1.5 2*6.5 2*1.5 ...
2*6.5 2*1.5 2*6.5 2*1.5 2*6.5 2*1.5 2*6.5 2*1.5
7200 12306 111 2*6.5 2*1.5 2*6.5 2*1.5 2*6.5 2*1.5 2*6.5 2*1.5 ...
2*6.5 2*1.5 2*6.5 2*1.5 2*6.5 2*1.5 2*6.5 2*1.5 ...
2*6.5 2*1.5 2*6.5 2*1.5 2*6.5 2*1.5 2*6.5
97 7201 111 2*6.5 2*1.5 2*6.5 2*1.5 2*6.5 2*1.5 2*6.5 2*1.5 ...
2*6.5 2*1.5 2*6.5 2*1.5 2*6.5 2*1.5 2*6.5 2*1.5 ...
2*6.5 2*1.5 2*6.5 2*1.5 2*6.5 2*1.5 2*6.5 2*1.5 ...
2*6.5 2*1.5 2*6.5 2*1.5 2*6.5 2*1.5 2*6.5 2*1.5
7201 12307 111 2*6.5 2*1.5 2*6.5 2*1.5 2*6.5 2*1.5 2*6.5 2*1.5 ...
2*6.5 2*1.5 2*6.5 2*1.5 2*6.5 2*1.5 2*6.5 2*1.5 ...
2*6.5 2*1.5 2*6.5 2*1.5 2*6.5 2*1.5 2*6.5
98 7202 111 2*6.5 2*1.5 2*6.5 2*1.5 2*6.5 2*1.5 2*6.5 2*1.5 ...
2*6.5 2*1.5 2*6.5 2*1.5 2*6.5 2*1.5 2*6.5 2*1.5 ...
2*6.5 2*1.5 2*6.5 2*1.5 2*6.5 2*1.5 2*6.5 2*1.5 ...
2*6.5 2*1.5 2*6.5 2*1.5 2*6.5 2*1.5 2*6.5 2*1.5
7202 12308 111 2*6.5 2*1.5 2*6.5 2*1.5 2*6.5 2*1.5 2*6.5 2*1.5 ...
2*6.5 2*1.5 2*6.5 2*1.5 2*6.5 2*1.5 2*6.5 2*1.5 ...
2*6.5 2*1.5 2*6.5 2*1.5 2*6.5 2*1.5 2*6.5
99 7203 111 2*6.5 2*1.5 2*6.5 2*1.5 2*6.5 2*1.5 2*6.5 2*1.5 ...
2*6.5 2*1.5 2*6.5 2*1.5 2*6.5 2*1.5 2*6.5 2*1.5 ...
2*6.5 2*1.5 2*6.5 2*1.5 2*6.5 2*1.5 2*6.5 2*1.5 ...
2*6.5 2*1.5 2*6.5 2*1.5 2*6.5 2*1.5 2*6.5 2*1.5

7203 12309 111 2*6.5 2*1.5 2*6.5 2*1.5 2*6.5 2*1.5 2*6.5 2*1.5 ...
2*6.5 2*1.5 2*6.5 2*1.5 2*6.5 2*1.5 2*6.5 2*1.5 ...
2*6.5 2*1.5 2*6.5 2*1.5 2*6.5 2*1.5 2*6.5
100 7204 111 2*6.5 2*1.5 2*6.5 2*1.5 2*6.5 2*1.5 2*6.5 2*1.5 ...
2*6.5 2*1.5 2*6.5 2*1.5 2*6.5 2*1.5 2*6.5 2*1.5 ...
2*6.5 2*1.5 2*6.5 2*1.5 2*6.5 2*1.5 2*6.5 2*1.5 ...
2*6.5 2*1.5 2*6.5 2*1.5 2*6.5 2*1.5 2*6.5 2*1.5
7204 12310 111 2*6.5 2*1.5 2*6.5 2*1.5 2*6.5 2*1.5 2*6.5 2*1.5 ...
2*6.5 2*1.5 2*6.5 2*1.5 2*6.5 2*1.5 2*6.5 2*1.5 ...
2*6.5 2*1.5 2*6.5 2*1.5 2*6.5 2*1.5 2*6.5
101 7205 111 2*6.5 2*1.5 2*6.5 2*1.5 2*6.5 2*1.5 2*6.5 2*1.5 ...
2*6.5 2*1.5 2*6.5 2*1.5 2*6.5 2*1.5 2*6.5 2*1.5 ...
2*6.5 2*1.5 2*6.5 2*1.5 2*6.5 2*1.5 2*6.5 2*1.5
7205 12311 111 2*6.5 2*1.5 2*6.5 2*1.5 2*6.5 2*1.5 2*6.5 2*1.5 ...
2*6.5 2*1.5 2*6.5 2*1.5 2*6.5 2*1.5 2*6.5 2*1.5 ...
2*6.5 2*1.5 2*6.5 2*1.5 2*6.5 2*1.5 2*6.5
102 7206 111 2*6.5 2*1.5 2*6.5 2*1.5 2*6.5 2*1.5 2*6.5 2*1.5 ...
2*6.5 2*1.5 2*6.5 2*1.5 2*6.5 2*1.5 2*6.5 2*1.5 ...
2*6.5 2*1.5 2*6.5 2*1.5 2*6.5 2*1.5 2*6.5 2*1.5 ...
2*6.5 2*1.5 2*6.5 2*1.5 2*6.5 2*1.5 2*6.5 2*1.5
7206 12312 111 2*6.5 2*1.5 2*6.5 2*1.5 2*6.5 2*1.5 2*6.5 2*1.5 ...
2*6.5 2*1.5 2*6.5 2*1.5 2*6.5 2*1.5 2*6.5 2*1.5 ...
2*6.5 2*1.5 2*6.5 2*1.5 2*6.5 2*1.5 2*6.5
103 7207 111 2*6.5 2*1.5 2*6.5 2*1.5 2*6.5 2*1.5 2*6.5 2*1.5 ...
2*6.5 2*1.5 2*6.5 2*1.5 2*6.5 2*1.5 2*6.5 2*1.5 ...
2*6.5 2*1.5 2*6.5 2*1.5 2*6.5 2*1.5 2*6.5 2*1.5 ...
2*6.5 2*1.5 2*6.5 2*1.5 2*6.5 2*1.5 2*6.5 2*1.5
7207 12313 111 2*6.5 2*1.5 2*6.5 2*1.5 2*6.5 2*1.5 2*6.5 2*1.5 ...
2*6.5 2*1.5 2*6.5 2*1.5 2*6.5 2*1.5 2*6.5 2*1.5 ...
2*6.5 2*1.5 2*6.5 2*1.5 2*6.5 2*1.5 2*6.5
104 7208 111 2*6.5 2*1.5 2*6.5 2*1.5 2*6.5 2*1.5 2*6.5 2*1.5 ...
2*6.5 2*1.5 2*6.5 2*1.5 2*6.5 2*1.5 2*6.5 2*1.5 ...
2*6.5 2*1.5 2*6.5 2*1.5 2*6.5 2*1.5 2*6.5 2*1.5 ...
2*6.5 2*1.5 2*6.5 2*1.5 2*6.5 2*1.5 2*6.5 2*1.5
7208 12314 111 2*6.5 2*1.5 2*6.5 2*1.5 2*6.5 2*1.5 2*6.5 2*1.5 ...
2*6.5 2*1.5 2*6.5 2*1.5 2*6.5 2*1.5 2*6.5 2*1.5 ...
2*6.5 2*1.5 2*6.5 2*1.5 2*6.5 2*1.5 2*6.5
105 7209 111 2*6.5 2*1.5 2*6.5 2*1.5 2*6.5 2*1.5 2*6.5 2*1.5 ...
2*6.5 2*1.5 2*6.5 2*1.5 2*6.5 2*1.5 2*6.5 2*1.5 ...
2*6.5 2*1.5 2*6.5 2*1.5 2*6.5 2*1.5 2*6.5 2*1.5 ...
2*6.5 2*1.5 2*6.5 2*1.5 2*6.5 2*1.5 2*6.5 2*1.5
7209 12315 111 2*6.5 2*1.5 2*6.5 2*1.5 2*6.5 2*1.5 2*6.5 2*1.5 ...
2*6.5 2*1.5 2*6.5 2*1.5 2*6.5 2*1.5 2*6.5 2*1.5 ...
2*6.5 2*1.5 2*6.5 2*1.5 2*6.5 2*1.5 2*6.5
106 7210 111 2*6.5 2*1.5 2*6.5 2*1.5 2*6.5 2*1.5 2*6.5 2*1.5 ...
2*6.5 2*1.5 2*6.5 2*1.5 2*6.5 2*1.5 2*6.5 2*1.5 ...
2*6.5 2*1.5 2*6.5 2*1.5 2*6.5 2*1.5 2*6.5 2*1.5 ...
2*6.5 2*1.5 2*6.5 2*1.5 2*6.5 2*1.5 2*6.5 2*1.5
7210 12316 111 2*6.5 2*1.5 2*6.5 2*1.5 2*6.5 2*1.5 2*6.5 2*1.5 ...
2*6.5 2*1.5 2*6.5 2*1.5 2*6.5 2*1.5 2*6.5 2*1.5 ...
2*6.5 2*1.5 2*6.5 2*1.5 2*6.5 2*1.5 2*6.5
107 7211 111 2*6.5 2*1.5 2*6.5 2*1.5 2*6.5 2*1.5 2*6.5 2*1.5 ...
2*6.5 2*1.5 2*6.5 2*1.5 2*6.5 2*1.5 2*6.5 2*1.5 ...
2*6.5 2*1.5 2*6.5 2*1.5 2*6.5 2*1.5 2*6.5 2*1.5 ...
2*6.5 2*1.5 2*6.5 2*1.5 2*6.5 2*1.5 2*6.5 2*1.5
7211 12317 111 2*6.5 2*1.5 2*6.5 2*1.5 2*6.5 2*1.5 2*6.5 2*1.5 ...
2*6.5 2*1.5 2*6.5 2*1.5 2*6.5 2*1.5 2*6.5 2*1.5 ...

```
                2*6.5 2*1.5 2*6.5 2*1.5 2*6.5 2*1.5 2*6.5
108 7212 111 2*6.5 2*1.5 2*6.5 2*1.5 2*6.5 2*1.5 2*6.5 2*1.5 ...
                2*6.5 2*1.5 2*6.5 2*1.5 2*6.5 2*1.5 2*6.5 2*1.5 ...
                2*6.5 2*1.5 2*6.5 2*1.5 2*6.5 2*1.5 2*6.5 2*1.5 ...
                2*6.5 2*1.5 2*6.5 2*1.5 2*6.5 2*1.5 2*6.5 2*1.5
7212 12318 111 2*6.5 2*1.5 2*6.5 2*1.5 2*6.5 2*1.5 2*6.5 2*1.5 ...
                2*6.5 2*1.5 2*6.5 2*1.5 2*6.5 2*1.5 2*6.5 2*1.5 ...
                2*6.5 2*1.5 2*6.5 2*1.5 2*6.5 2*1.5 2*6.5
109 7213 111 2*6.5 2*1.5 2*6.5 2*1.5 2*6.5 2*1.5 2*6.5 2*1.5 ...
                2*6.5 2*1.5 2*6.5 2*1.5 2*6.5 2*1.5 2*6.5 2*1.5 ...
                2*6.5 2*1.5 2*6.5 2*1.5 2*6.5 2*1.5 2*6.5 2*1.5 ...
                2*6.5 2*1.5 2*6.5 2*1.5 2*6.5 2*1.5 2*6.5 2*1.5
7213 12319 111 2*6.5 2*1.5 2*6.5 2*1.5 2*6.5 2*1.5 2*6.5 2*1.5 ...
                2*6.5 2*1.5 2*6.5 2*1.5 2*6.5 2*1.5 2*6.5 2*1.5 ...
                2*6.5 2*1.5 2*6.5 2*1.5 2*6.5 2*1.5 2*6.5
110 7214 111 2*6.5 2*1.5 2*6.5 2*1.5 2*6.5 2*1.5 2*6.5 2*1.5 ...
                2*6.5 2*1.5 2*6.5 2*1.5 2*6.5 2*1.5 2*6.5 2*1.5 ...
                2*6.5 2*1.5 2*6.5 2*1.5 2*6.5 2*1.5 2*6.5 2*1.5 ...
                2*6.5 2*1.5 2*6.5 2*1.5 2*6.5 2*1.5 2*6.5 2*1.5
7214 12320 111 2*6.5 2*1.5 2*6.5 2*1.5 2*6.5 2*1.5 2*6.5 2*1.5 ...
                2*6.5 2*1.5 2*6.5 2*1.5 2*6.5 2*1.5 2*6.5 2*1.5 ...
                2*6.5 2*1.5 2*6.5 2*1.5 2*6.5 2*1.5 2*6.5
111 7215 111 2*6.5 2*1.5 2*6.5 2*1.5 2*6.5 2*1.5 2*6.5 2*1.5 ...
                2*6.5 2*1.5 2*6.5 2*1.5 2*6.5 2*1.5 2*6.5 2*1.5 ...
                2*6.5 2*1.5 2*6.5 2*1.5 2*6.5 2*1.5 2*6.5 2*1.5 ...
                2*6.5 2*1.5 2*6.5 2*1.5 2*6.5 2*1.5 2*6.5 2*1.5
7215 12321 111 2*6.5 2*1.5 2*6.5 2*1.5 2*6.5 2*1.5 2*6.5 2*1.5 ...
                2*6.5 2*1.5 2*6.5 2*1.5 2*6.5 2*1.5 2*6.5 2*1.5 ...
                2*6.5 2*1.5 2*6.5 2*1.5 2*6.5 2*1.5 2*6.5
DELETE NODES  113    221   2
DELETE NODES  335    443   2
DELETE NODES  557    665   2
DELETE NODES  779    887   2
DELETE NODES  1001   1109  2
DELETE NODES  1223   1331  2
DELETE NODES  1445   1553  2
DELETE NODES  1667   1775  2
DELETE NODES  1889   1997  2
DELETE NODES  2111   2219  2
DELETE NODES  2333   2441  2
DELETE NODES  2555   2663  2
DELETE NODES  2777   2885  2
DELETE NODES  2999   3107  2
DELETE NODES  3221   3329  2
DELETE NODES  3443   3551  2
DELETE NODES  3665   3773  2
DELETE NODES  3887   3995  2
DELETE NODES  4109   4217  2
DELETE NODES  4331   4439  2
DELETE NODES  4553   4661  2
DELETE NODES  4775   4883  2
DELETE NODES  4997   5105  2
DELETE NODES  5219   5327  2
DELETE NODES  5441   5549  2
DELETE NODES  5663   5771  2
DELETE NODES  5885   5993  2
DELETE NODES  6107   6215  2
DELETE NODES  6329   6437  2
```

```
DELETE NODES  6551   6659   2
DELETE NODES  6773   6881   2
DELETE NODES  6995   7103   2
DELETE NODES  7217   7325   2
DELETE NODES  7439   7547   2
DELETE NODES  7661   7769   2
DELETE NODES  7883   7991   2
DELETE NODES  8105   8213   2
DELETE NODES  8327   8435   2
DELETE NODES  8549   8657   2
DELETE NODES  8771   8879   2
DELETE NODES  8993   9101   2
DELETE NODES  9215   9323   2
DELETE NODES  9437   9545   2
DELETE NODES  9659   9767   2
DELETE NODES  9881   9989   2
DELETE NODES  10103  10211  2
DELETE NODES  10325  10433  2
DELETE NODES  10547  10655  2
DELETE NODES  10769  10877  2
DELETE NODES  10991  11099  2
DELETE NODES  11213  11321  2
DELETE NODES  11435  11543  2
DELETE NODES  11657  11765  2
DELETE NODES  11879  11987  2
DELETE NODES  12101  12209  2
QPM8  GEOMETRIC PROPERTIES
1  25.6  25.6  25.6  25.6  25.6  25.6  25.6  25.6
BEAM  GEOMETRIC PROPERTIES
2  125.235  255.714  125000
3  762      57150    762000
GEOMETRIC ASSIGNMENTS
1    3025   1   1
3026 3028   2   2
3027 3027   0   3
MATERIAL PROPERTIES
1     5000  0.15  32000E-12
2     3200  0.15  2200E-12
3   240000  0.30  7800E-12
4   205000  0.30  7800E-12
MATERIAL ASSIGNMENTS
3026   3028   2     3
3027   3027   0     4
1      3      1     1
221    223    1     1
441    443    1     1
661    663    1     1
881    883    1     1
1101   1103   1     1
1321   1323   1     1
1541   1543   1     1
1761   1763   1     1
1981   1983   1     1
2201   2203   1     1
2421   2423   1     1
2641   2643   1     1
2861   2863   1     1
5      7      1     1
```

225	227	1	1
445	447	1	1
665	667	1	1
885	887	1	1
1105	1107	1	1
1325	1327	1	1
1545	1547	1	1
1765	1767	1	1
1985	1987	1	1
2205	2207	1	1
2425	2427	1	1
2645	2647	1	1
2865	2867	1	1
9	11	1	1
229	231	1	1
449	451	1	1
669	671	1	1
889	891	1	1
1109	1111	1	1
1329	1331	1	1
1549	1551	1	1
1769	1771	1	1
1989	1991	1	1
2209	2211	1	1
2429	2431	1	1
2649	2651	1	1
2869	2871	1	1
13	15	1	1
233	235	1	1
453	455	1	1
673	675	1	1
893	895	1	1
1113	1115	1	1
1333	1335	1	1
1553	1555	1	1
1773	1775	1	1
1993	1995	1	1
2213	2215	1	1
2433	2435	1	1
2653	2655	1	1
2873	2875	1	1
17	19	1	1
237	239	1	1
457	459	1	1
677	679	1	1
897	899	1	1
1117	1119	1	1
1337	1339	1	1
1557	1559	1	1
1777	1779	1	1
1997	1999	1	1
2217	2219	1	1
2437	2439	1	1
2657	2659	1	1
2877	2879	1	1
21	23	1	1
241	243	1	1
461	463	1	1

681	683	1	1
901	903	1	1
1121	1123	1	1
1341	1343	1	1
1561	1563	1	1
1781	1783	1	1
2001	2003	1	1
2221	2223	1	1
2441	2443	1	1
2661	2663	1	1
2881	2883	1	1
25	27	1	1
245	247	1	1
465	467	1	1
685	687	1	1
905	907	1	1
1125	1127	1	1
1345	1347	1	1
1565	1567	1	1
1785	1787	1	1
2005	2007	1	1
2225	2227	1	1
2445	2447	1	1
2665	2667	1	1
2885	2887	1	1
29	31	1	1
249	251	1	1
469	471	1	1
689	691	1	1
909	911	1	1
1129	1131	1	1
1349	1351	1	1
1569	1571	1	1
1789	1791	1	1
2009	2011	1	1
2229	2231	1	1
2449	2451	1	1
2669	2671	1	1
2889	2891	1	1
33	35	1	1
253	255	1	1
473	475	1	1
693	695	1	1
913	915	1	1
1133	1135	1	1
1353	1355	1	1
1573	1575	1	1
1793	1795	1	1
2013	2015	1	1
2233	2235	1	1
2453	2455	1	1
2673	2675	1	1
2893	2895	1	1
37	39	1	1
257	259	1	1
477	479	1	1
697	699	1	1
917	919	1	1

1137	1139	1	1
1357	1359	1	1
1577	1579	1	1
1797	1799	1	1
2017	2019	1	1
2237	2239	1	1
2457	2459	1	1
2677	2679	1	1
2897	2899	1	1
41	43	1	1
261	263	1	1
481	483	1	1
701	703	1	1
921	923	1	1
1141	1143	1	1
1361	1363	1	1
1581	1583	1	1
1801	1803	1	1
2021	2023	1	1
2241	2243	1	1
2461	2463	1	1
2681	2683	1	1
2901	2903	1	1
45	47	1	1
265	267	1	1
485	487	1	1
705	707	1	1
925	927	1	1
1145	1147	1	1
1365	1367	1	1
1585	1587	1	1
1805	1807	1	1
2025	2027	1	1
2245	2247	1	1
2465	2467	1	1
2685	2687	1	1
2905	2907	1	1
49	51	1	1
269	271	1	1
489	491	1	1
709	711	1	1
929	931	1	1
1149	1151	1	1
1369	1371	1	1
1589	1591	1	1
1809	1811	1	1
2029	2031	1	1
2249	2251	1	1
2469	2471	1	1
2689	2691	1	1
2909	2911	1	1
53	55	1	1
273	275	1	1
493	495	1	1
713	715	1	1
933	935	1	1
1153	1155	1	1
1373	1375	1	1

1593	1595	1	1
1813	1815	1	1
2033	2035	1	1
2253	2255	1	1
2473	2475	1	1
2693	2695	1	1
2913	2915	1	1
111	111	0	1
331	331	0	1
551	551	0	1
771	771	0	1
991	991	0	1
1211	1211	0	1
1431	1431	0	1
1651	1651	0	1
1871	1871	0	1
2091	2091	0	1
2311	2311	0	1
2531	2531	0	1
2751	2751	0	1
2971	2971	0	1
113	115	1	1
333	335	1	1
553	555	1	1
773	775	1	1
993	995	1	1
1213	1215	1	1
1433	1435	1	1
1653	1655	1	1
1873	1875	1	1
2093	2095	1	1
2313	2315	1	1
2533	2535	1	1
2753	2755	1	1
2973	2975	1	1
117	119	1	1
337	339	1	1
557	559	1	1
777	779	1	1
997	999	1	1
1217	1219	1	1
1437	1439	1	1
1657	1659	1	1
1877	1879	1	1
2097	2099	1	1
2317	2319	1	1
2537	2539	1	1
2757	2759	1	1
2977	2979	1	1
121	123	1	1
341	343	1	1
561	563	1	1
781	783	1	1
1001	1003	1	1
1221	1223	1	1
1441	1443	1	1
1661	1663	1	1
1881	1883	1	1

2101	2103	1	1
2321	2323	1	1
2541	2543	1	1
2761	2763	1	1
2981	2983	1	1
125	127	1	1
345	347	1	1
565	567	1	1
785	787	1	1
1005	1007	1	1
1225	1227	1	1
1445	1447	1	1
1665	1667	1	1
1885	1887	1	1
2105	2107	1	1
2325	2327	1	1
2545	2547	1	1
2765	2767	1	1
2985	2987	1	1
129	131	1	1
349	351	1	1
569	571	1	1
789	791	1	1
1009	1011	1	1
1229	1231	1	1
1449	1451	1	1
1669	1671	1	1
1889	1891	1	1
2109	2111	1	1
2329	2331	1	1
2549	2551	1	1
2769	2771	1	1
2989	2991	1	1
133	135	1	1
353	355	1	1
573	575	1	1
793	795	1	1
1013	1015	1	1
1233	1235	1	1
1453	1455	1	1
1673	1675	1	1
1893	1895	1	1
2113	2115	1	1
2333	2335	1	1
2553	2555	1	1
2773	2775	1	1
2993	2995	1	1
137	139	1	1
357	359	1	1
577	579	1	1
797	799	1	1
1017	1019	1	1
1237	1239	1	1
1457	1459	1	1
1677	1679	1	1
1897	1899	1	1
2117	2119	1	1
2337	2339	1	1

2557	2559	1	1
2777	2779	1	1
2997	2999	1	1
141	143	1	1
361	363	1	1
581	583	1	1
801	803	1	1
1021	1023	1	1
1241	1243	1	1
1461	1463	1	1
1681	1683	1	1
1901	1903	1	1
2121	2123	1	1
2341	2343	1	1
2561	2563	1	1
2781	2783	1	1
3001	3003	1	1
145	147	1	1
365	367	1	1
585	587	1	1
805	807	1	1
1025	1027	1	1
1245	1247	1	1
1465	1467	1	1
1685	1687	1	1
1905	1907	1	1
2125	2127	1	1
2345	2347	1	1
2565	2567	1	1
2785	2787	1	1
3005	3007	1	1
149	151	1	1
369	371	1	1
589	591	1	1
809	811	1	1
1029	1031	1	1
1249	1251	1	1
1469	1471	1	1
1689	1691	1	1
1909	1911	1	1
2129	2131	1	1
2349	2351	1	1
2569	2571	1	1
2789	2791	1	1
3009	3011	1	1
153	155	1	1
373	375	1	1
593	595	1	1
813	815	1	1
1033	1035	1	1
1253	1255	1	1
1473	1475	1	1
1693	1695	1	1
1913	1915	1	1
2133	2135	1	1
2353	2355	1	1
2573	2575	1	1
2793	2795	1	1

3013	3015	1	1
157	159	1	1
377	379	1	1
597	599	1	1
817	819	1	1
1037	1039	1	1
1257	1259	1	1
1477	1479	1	1
1697	1699	1	1
1917	1919	1	1
2137	2139	1	1
2357	2359	1	1
2577	2579	1	1
2797	2799	1	1
3017	3019	1	1
161	163	1	1
381	383	1	1
601	603	1	1
821	823	1	1
1041	1043	1	1
1261	1263	1	1
1481	1483	1	1
1701	1703	1	1
1921	1923	1	1
2141	2143	1	1
2361	2363	1	1
2581	2583	1	1
2801	2803	1	1
3021	3023	1	1
165	165	0	1
385	385	0	1
605	605	0	1
825	825	0	1
1045	1045	0	1
1265	1265	0	1
1485	1485	0	1
1705	1705	0	1
1925	1925	0	1
2145	2145	0	1
2365	2365	0	1
2585	2585	0	1
2805	2805	0	1
3025	3025	0	1
4	52	4	2
224	272	4	2
444	492	4	2
664	712	4	2
884	932	4	2
1104	1152	4	2
1324	1372	4	2
1544	1592	4	2
1764	1812	4	2
1984	2032	4	2
2204	2252	4	2
2424	2472	4	2
2644	2692	4	2
2864	2912	4	2
56	110	1	2

```
166    220     1     2
276    330     1     2
386    440     1     2
496    550     1     2
606    660     1     2
716    770     1     2
826    880     1     2
936    990     1     2
1046   1100    1     2
1156   1210    1     2
1266   1320    1     2
1376   1430    1     2
1486   1540    1     2
1596   1650    1     2
1706   1760    1     2
1816   1870    1     2
1926   1980    1     2
2036   2090    1     2
2146   2200    1     2
2256   2310    1     2
2366   2420    1     2
2476   2530    1     2
2586   2640    1     2
2696   2750    1     2
2806   2860    1     2
2916   2970    1     2
112    164     4     2
332    384     4     2
552    604     4     2
772    824     4     2
992    1044    4     2
1212   1264    4     2
1432   1484    4     2
1652   1704    4     2
1872   1924    4     2
2092   2144    4     2
2312   2364    4     2
2532   2584    4     2
2752   2804    4     2
2972   3024    4     2
SUPPORT NODES
1  111  1    R  R  R
ELEMENT OUTPUT
1  3025  1   3
NODE OUTPUT
12211  12211  0  3
1  12321       1  1
EIGENVALUE CONTROL
CONSTANTS 2 D D 1 D D D D
PLOT FILE
END
```